

# TELEMAC-2D

## Validation Manual

Version v8p3  
December 6, 2021



# Contents

|            |   |           |
|------------|---|-----------|
| <b>1</b>   | <b>Algae 2D Coupling (2Dcoupling_algae)</b> | <b>18</b> |
| <b>1.1</b> | <b>Purpose</b>                              | <b>18</b> |
| <b>1.2</b> | <b>Description</b>                          | <b>18</b> |
| <b>1.3</b> | <b>Results</b>                              | <b>19</b> |
| <b>2</b>   | <b>Flow around a cylinder (Negretti2D)</b>  | <b>21</b> |
| <b>2.1</b> | <b>Description</b>                          | <b>21</b> |
| 2.1.1      | Initial and boundary conditions             | 21        |
| 2.1.2      | Mesh and numerical parameters               | 21        |
| 2.1.3      | Physical parameters                         | 21        |
| <b>2.2</b> | <b>Results</b>                              | <b>22</b> |
| <b>2.3</b> | <b>Conclusions</b>                          | <b>23</b> |
| <b>3</b>   | <b>Balzano</b>                              | <b>24</b> |
| <b>3.1</b> | <b>Purpose</b>                              | <b>24</b> |
| <b>3.2</b> | <b>Description</b>                          | <b>24</b> |
| 3.2.1      | Geometry and mesh                           | 24        |
| 3.2.2      | Bathymetry                                  | 24        |
| 3.2.3      | Initial conditions                          | 25        |
| 3.2.4      | Boundary conditions                         | 25        |
| 3.2.5      | Analytical solution at equilibrium          | 25        |
| 3.2.6      | Physical parameters                         | 25        |
| 3.2.7      | Numerical parameters                        | 26        |
| <b>3.3</b> | <b>Results</b>                              | <b>26</b> |
| 3.3.1      | First observation                           | 26        |
| 3.3.2      | Computation time                            | 26        |
| 3.3.3      | Comparison of schemes                       | 27        |
| 3.3.4      | Positivity of the water depth               | 28        |
| 3.3.5      | Mass balance                                | 29        |
| 3.3.6      | Energy balance                              | 29        |
| <b>3.4</b> | <b>Conclusion</b>                           | <b>30</b> |

|            |  |           |
|------------|--|-----------|
| <b>4</b>   | <b>Wave driven currents (bj78)</b>                     | <b>31</b> |
| <b>4.1</b> | <b>Description</b>                                     | <b>31</b> |
| 4.1.1      | Initial and boundary conditions . . . . .              | 31        |
| 4.1.2      | Mesh and numerical parameters . . . . .                | 32        |
| 4.1.3      | Physical parameters . . . . .                          | 32        |
| <b>4.2</b> | <b>Results</b>   | <b>32</b> |
| <b>4.3</b> | <b>Conclusion</b>                                      | <b>33</b> |
| <b>5</b>   | <b>Breach</b>  | <b>34</b> |
| <b>5.1</b> | <b>Purpose</b>   | <b>34</b> |
| <b>6</b>   | <b>Diffraction by semi-infinite breakwater (break)</b> | <b>35</b> |
| <b>6.1</b> | <b>Purpose</b>   | <b>35</b> |
| <b>6.2</b> | <b>Description</b>                                     | <b>35</b> |
| 6.2.1      | Numerical and physical parameters . . . . .            | 35        |
| 6.2.2      | Boundary conditions . . . . .                          | 36        |
| <b>6.3</b> | <b>Results</b>   | <b>36</b> |
| <b>6.4</b> | <b>Conclusion</b>                                      | <b>37</b> |
| <b>7</b>   | <b>Bridge</b>  | <b>38</b> |
| <b>7.1</b> | <b>Purpose</b>   | <b>38</b> |
| <b>7.2</b> | <b>Description</b>                                     | <b>38</b> |
| 7.2.1      | Geometry and mesh . . . . .                            | 38        |
| 7.2.2      | Boundaries . . . . .                                   | 38        |
| 7.2.3      | Physical Parameters . . . . .                          | 39        |
| 7.2.4      | Numerical Parameters . . . . .                         | 39        |
| <b>7.3</b> | <b>Results</b>   | <b>40</b> |
| <b>7.4</b> | <b>Conclusions</b>                                     | <b>40</b> |
| <b>7.5</b> | <b>Figures</b>   | <b>41</b> |
| <b>8</b>   | <b>Flow over a bump (bump)</b>                         | <b>45</b> |
| <b>8.1</b> | <b>Purpose</b>   | <b>45</b> |
| <b>8.2</b> | <b>Description</b>                                     | <b>45</b> |
| 8.2.1      | Analytical solution . . . . .                          | 45        |
| 8.2.2      | Geometry and mesh . . . . .                            | 46        |
| 8.2.3      | Bathymetry . . . . .                                   | 46        |
| 8.2.4      | Initial and boundary conditions . . . . .              | 47        |
| 8.2.5      | Physical parameters . . . . .                          | 47        |
| 8.2.6      | Numerical parameters . . . . .                         | 47        |
| <b>8.3</b> | <b>Results</b>   | <b>48</b> |
| 8.3.1      | Computation time . . . . .                             | 48        |
| 8.3.2      | First observation . . . . .                            | 49        |

|             |   |           |
|-------------|---|-----------|
| 8.3.3       | Comparison of schemes . . . . .                         | 50        |
| 8.3.4       | Accuracy . . . . .                                      | 51        |
| 8.3.5       | Convergence in the subcritical case . . . . .           | 52        |
| 8.3.6       | Convergence in the critical case . . . . .              | 56        |
| <b>8.4</b>  | <b>Conclusion</b>                                       | <b>59</b> |
| <b>9</b>    | <b>Flow driven by a stage-discharge curve (canal)</b>   | <b>60</b> |
| <b>9.1</b>  | <b>Description</b>                                      | <b>60</b> |
| 9.1.1       | Initial and boundary conditions . . . . .               | 60        |
| 9.1.2       | Mesh and numerical parameters . . . . .                 | 61        |
| <b>9.2</b>  | <b>Results</b>  | <b>61</b> |
| <b>9.3</b>  | <b>Conclusion</b>                                       | <b>62</b> |
| <b>10</b>   | <b>Algae transport in a canal (canal_algae)</b>         | <b>63</b> |
| <b>10.1</b> | <b>Purpose</b>  | <b>63</b> |
| <b>10.2</b> | <b>Description</b>                                      | <b>63</b> |
| 10.2.1      | Geometry and mesh . . . . .                             | 65        |
| 10.2.2      | Numerical parameters . . . . .                          | 65        |
| <b>10.3</b> | <b>Results</b>  | <b>66</b> |
| 10.3.1      | Explanation of the results . . . . .                    | 66        |
| 10.3.2      | Simulation results . . . . .                            | 67        |
| <b>11</b>   | <b>Algae transport in a canal 2 (canal_algae)</b>       | <b>71</b> |
| <b>11.1</b> | <b>Purpose</b>  | <b>71</b> |
| <b>11.2</b> | <b>Description of the test case</b>                     | <b>71</b> |
| <b>11.3</b> | <b>Results</b>  | <b>72</b> |
| <b>12</b>   | <b>Flow in a channel with a cavity (cavity)</b>         | <b>74</b> |
| <b>12.1</b> | <b>Purpose</b>  | <b>74</b> |
| <b>12.2</b> | <b>Approach</b>   | <b>74</b> |
| 12.2.1      | Geometry and mesh . . . . .                             | 74        |
| 12.2.2      | Boundaries . . . . .                                    | 76        |
| 12.2.3      | Physical parameters . . . . .                           | 76        |
| 12.2.4      | Numerical parameters . . . . .                          | 76        |
| <b>12.3</b> | <b>Results</b>  | <b>76</b> |
| <b>12.4</b> | <b>Conclusions</b>                                      | <b>76</b> |
| <b>13</b>   | <b>Advection of tracers with a rotating cone (cone)</b> | <b>80</b> |
| <b>13.1</b> | <b>Purpose</b>  | <b>80</b> |
| <b>13.2</b> | <b>Description</b>                                      | <b>80</b> |
| 13.2.1      | Geometry and mesh . . . . .                             | 80        |
| 13.2.2      | Initial condition . . . . .                             | 81        |

|             |   |           |
|-------------|---|-----------|
| 13.2.3      | Analytical solution . . . . .   | 81        |
| 13.2.4      | Physical parameters . . . . .   | 81        |
| 13.2.5      | Numerical parameters . . . . .  | 81        |
| <b>13.3</b> | <b>Results</b>  | <b>81</b> |
| 13.3.1      | Comparison of schemes . . . . .   | 81        |
| 13.3.2      | Maximum principle . . . . .   | 84        |
| 13.3.3      | Accuracy . . . . .  | 84        |
| 13.3.4      | Convergence . . . . .   | 85        |
| <b>13.4</b> | <b>Conclusion</b>   | <b>87</b> |
| <b>14</b>   | <b>Diffusion of tracers in 2D (cone_diffusion) . . . . .</b>                  | <b>88</b> |
| <b>14.1</b> | <b>Purpose</b>  | <b>88</b> |
| <b>14.2</b> | <b>Description</b>  | <b>88</b> |
| 14.2.1      | Geometry and mesh . . . . .   | 88        |
| 14.2.2      | Initial condition . . . . .   | 88        |
| 14.2.3      | Boundary conditions . . . . .   | 88        |
| 14.2.4      | Physical parameters . . . . .   | 89        |
| 14.2.5      | Numerical parameters . . . . .  | 90        |
| <b>14.3</b> | <b>Results</b>  | <b>90</b> |
| 14.3.1      | Computation time . . . . .  | 90        |
| 14.3.2      | Comparison of diffusion schemes . . . . .                                     | 90        |
| <b>14.4</b> | <b>Conclusion</b>   | <b>91</b> |
| <b>15</b>   | <b>Flow at a river confluence (confluence) . . . . .</b>                      | <b>93</b> |
| <b>15.1</b> | <b>Purpose</b>  | <b>93</b> |
| <b>15.2</b> | <b>Description</b>  | <b>93</b> |
| 15.2.1      | Geometry and Mesh . . . . .   | 93        |
| 15.2.2      | Bathymetry . . . . .  | 94        |
| 15.2.3      | Initial condition . . . . .   | 94        |
| 15.2.4      | Boundary Conditions . . . . .   | 94        |
| 15.2.5      | Physical parameters . . . . .   | 94        |
| 15.2.6      | Numerical parameters . . . . .  | 94        |
| <b>15.3</b> | <b>Results</b>  | <b>95</b> |
| <b>15.4</b> | <b>Conclusions</b>  | <b>96</b> |
| <b>16</b>   | <b>Propagation of a wave over a conical island (conical_island) . . . . .</b> | <b>97</b> |
| <b>16.1</b> | <b>Purpose</b>  | <b>97</b> |
| <b>16.2</b> | <b>Description</b>  | <b>97</b> |
| 16.2.1      | Geometry and mesh . . . . .   | 97        |
| 16.2.2      | Boundaries . . . . .  | 98        |
| 16.2.3      | Physical Parameters . . . . .   | 99        |
| 16.2.4      | Numerical parameters . . . . .  | 99        |
| <b>16.3</b> | <b>Results</b>  | <b>99</b> |

|           |  |            |
|-----------|--|------------|
| <b>17</b> | <b>convergence</b>   | <b>102</b> |
| <b>18</b> | <b>Transient flood flow in the valley of river Culm (culm)</b> | <b>103</b> |
| 18.1      | <b>Purpose</b>   | <b>103</b> |
| 18.1.1    | Approach . . . . .   | 103        |
| 18.2      | <b>Description</b>   | <b>103</b> |
| 18.2.1    | Geometry and mesh . . . . .                                    | 103        |
| 18.2.2    | Boundaries . . . . .   | 103        |
| 18.2.3    | Physical parameters . . . . .                                  | 105        |
| 18.2.4    | Numerical parameters . . . . .                                 | 105        |
| 18.3      | <b>Results</b>   | <b>105</b> |
| 18.4      | <b>Conclusion</b>  | <b>107</b> |
| <b>19</b> | <b>Dambreak: Ritter and Stoker</b>                             | <b>108</b> |
| 19.1      | <b>Purpose</b>   | <b>108</b> |
| 19.2      | <b>Description</b>   | <b>108</b> |
| 19.2.1    | Geometry and mesh . . . . .                                    | 108        |
| 19.2.2    | Initial conditions . . . . .                                   | 108        |
| 19.2.3    | Analytical solutions . . . . .                                 | 109        |
| 19.2.4    | Boundary conditions . . . . .                                  | 110        |
| 19.2.5    | Physical parameters . . . . .                                  | 110        |
| 19.2.6    | Numerical parameters . . . . .                                 | 110        |
| 19.3      | <b>Results for Ritter</b>                                      | <b>110</b> |
| 19.3.1    | Computation time . . . . .                                     | 110        |
| 19.3.2    | First observation . . . . .                                    | 111        |
| 19.3.3    | Comparison of schemes . . . . .                                | 111        |
| 19.3.4    | Accuracy . . . . .   | 112        |
| 19.3.5    | Positivity of the water depth . . . . .                        | 114        |
| 19.3.6    | Mass balance . . . . .   | 114        |
| 19.3.7    | Energy balance . . . . .                                       | 114        |
| 19.4      | <b>Results for Stoker</b>                                      | <b>116</b> |
| 19.4.1    | Computation time . . . . .                                     | 116        |
| 19.4.2    | First observation . . . . .                                    | 116        |
| 19.4.3    | Comparison of schemes . . . . .                                | 116        |
| 19.4.4    | Accuracy . . . . .   | 117        |
| 19.4.5    | Positivity of the water depth . . . . .                        | 118        |
| 19.4.6    | Mass balance . . . . .   | 119        |
| 19.4.7    | Energy balance . . . . .                                       | 119        |
| 19.5      | <b>Conclusions</b>   | <b>120</b> |
| 19.6      | <b>Reference</b>   | <b>120</b> |
| <b>20</b> | <b>One way chaining with DELWAQ (delwaq)</b>                   | <b>121</b> |
| 20.1      | <b>Description</b>   | <b>121</b> |
| 20.1.1    | Initial and boundary conditions . . . . .                      | 121        |
| 20.1.2    | Mesh and numerical parameters . . . . .                        | 122        |

|             |  |            |
|-------------|--|------------|
| 20.1.3      | Physical parameters .....                        | 122        |
| <b>20.2</b> | <b>Results</b>                                   | <b>122</b> |
| <b>20.3</b> | <b>Conclusion</b>                                | <b>124</b> |
| <b>21</b>   | <b>Flow over a breakwater (digue) .....</b>      | <b>125</b> |
| <b>21.1</b> | <b>Purpose</b>                                   | <b>125</b> |
| 21.1.1      | Approach .....                                   | 125        |
| <b>21.2</b> | <b>Description</b>                               | <b>126</b> |
| 21.2.1      | Geometry and mesh .....                          | 126        |
| 21.2.2      | Boundaries .....                                 | 126        |
| 21.2.3      | Physical parameters .....                        | 127        |
| 21.2.4      | Numerical parameters .....                       | 127        |
| <b>21.3</b> | <b>Results</b>                                   | <b>127</b> |
| <b>21.4</b> | <b>Conclusions</b>                               | <b>128</b> |
| <b>22</b>   | <b>donau .....</b>                               | <b>129</b> |
| <b>22.1</b> | <b>Purpose</b>                                   | <b>129</b> |
| <b>22.2</b> | <b>Description</b>                               | <b>129</b> |
| 22.2.1      | Geometry and mesh .....                          | 129        |
| 22.2.2      | Initial condition .....                          | 130        |
| 22.2.3      | Boundary conditions .....                        | 130        |
| 22.2.4      | Physical parameters .....                        | 131        |
| 22.2.5      | Numerical parameters .....                       | 132        |
| <b>22.3</b> | <b>Results</b>                                   | <b>132</b> |
| <b>22.4</b> | <b>Conclusion</b>                                | <b>132</b> |
| <b>23</b>   | <b>Drag force in a channel (dragforce) .....</b> | <b>136</b> |
| <b>23.1</b> | <b>Description</b>                               | <b>136</b> |
| 23.1.1      | Initial and boundary conditions .....            | 136        |
| 23.1.2      | Mesh and numerical parameters .....              | 136        |
| 23.1.3      | Physical parameters .....                        | 137        |
| <b>23.2</b> | <b>Results</b>                                   | <b>137</b> |
| <b>23.3</b> | <b>Conclusions</b>                               | <b>137</b> |
| <b>24</b>   | <b>Parameter estimation (estimation) .....</b>   | <b>138</b> |
| <b>24.1</b> | <b>Description</b>                               | <b>138</b> |
| 24.1.1      | Initial and boundary conditions .....            | 138        |
| 24.1.2      | Mesh and numerical parameters .....              | 138        |
| 24.1.3      | Physical parameters .....                        | 139        |
| <b>24.2</b> | <b>Conclusions</b>                               | <b>139</b> |

|           |   |            |
|-----------|---|------------|
| <b>25</b> | <b>Particle transport (fleuteurs)</b>                       | <b>140</b> |
| 25.1      | Description   | 140        |
| 25.1.1    | Initial and boundary conditions . . . . .                   | 140        |
| 25.1.2    | Mesh and numerical parameters . . . . .                     | 140        |
| 25.1.3    | Physical parameters . . . . .                               | 141        |
| 25.2      | Results   | 141        |
| <b>26</b> | <b>Flume with tracers (flume_tracer)</b>                    | <b>143</b> |
| 26.1      | Purpose   | 143        |
| 26.2      | Description   | 143        |
| 26.2.1    | Geometry and mesh . . . . .                                 | 143        |
| 26.2.2    | Initial condition . . . . .                                 | 143        |
| 26.2.3    | Analytical solution . . . . .                               | 143        |
| 26.2.4    | Physical parameters . . . . .                               | 144        |
| 26.2.5    | Numerical parameters . . . . .                              | 144        |
| 26.3      | Results   | 144        |
| 26.3.1    | Computation time . . . . .                                  | 144        |
| 26.3.2    | Comparison of schemes . . . . .                             | 144        |
| 26.3.3    | Convergence . . . . .                                       | 146        |
| 26.4      | Conclusion  | 146        |
| <b>27</b> | <b>Flow in a channel with slope and friction (friction)</b> | <b>149</b> |
| 27.1      | Description   | 149        |
| 27.1.1    | Initial and boundary conditions . . . . .                   | 149        |
| 27.1.2    | Mesh and numerical parameters . . . . .                     | 149        |
| 27.1.3    | Physical parameters . . . . .                               | 150        |
| 27.2      | Results   | 150        |
| 27.3      | Conclusions   | 151        |
| <b>28</b> | <b>Gaussian water surface (gouttedo)</b>                    | <b>152</b> |
| 28.1      | Purpose   | 152        |
| 28.2      | Description of the problem                                  | 152        |
| 28.2.1    | Geometry and mesh . . . . .                                 | 152        |
| 28.2.2    | Initial conditions . . . . .                                | 153        |
| 28.2.3    | Boundary conditions . . . . .                               | 153        |
| 28.2.4    | Physical parameters . . . . .                               | 153        |
| 28.2.5    | Numerical parameters . . . . .                              | 153        |
| 28.3      | Results with solid walls                                    | 154        |
| 28.4      | Results with Thompson boundary conditions                   | 155        |
| 28.5      | Conclusions   | 157        |

|             |  |            |
|-------------|--|------------|
| <b>29</b>   | <b>init</b>  | <b>158</b> |
| <b>29.1</b> | <b>Description</b>   | <b>158</b> |
| 29.1.1      | Initial and boundary conditions . . . . .  | 158        |
| 29.1.2      | Mesh and numerical parameters . . . . .  | 159        |
| 29.1.3      | Physical parameters . . . . .  | 159        |
| <b>29.2</b> | <b>Results</b>   | <b>160</b> |
| <b>30</b>   | <b>Transformation of the M2 tide constituent along the western European Continental shelf (m2wave)</b> | <b>164</b> |
| <b>30.1</b> | <b>Purpose</b>   | <b>164</b> |
| <b>30.2</b> | <b>Description</b>   | <b>164</b> |
| 30.2.1      | Approach . . . . .   | 164        |
| 30.2.2      | Geometry and mesh . . . . .  | 164        |
| 30.2.3      | Boundaries . . . . .   | 164        |
| 30.2.4      | Bottom . . . . .   | 164        |
| 30.2.5      | Numerical parameters . . . . .   | 165        |
| <b>30.3</b> | <b>Results</b>   | <b>166</b> |
| <b>31</b>   | <b>Malpasset dambreak (malpasset)</b>  | <b>168</b> |
| <b>31.1</b> | <b>Purpose</b>   | <b>168</b> |
| <b>31.2</b> | <b>Description</b>   | <b>168</b> |
| 31.2.1      | Geometry and mesh . . . . .  | 168        |
| 31.2.2      | Bathymetry . . . . .   | 170        |
| 31.2.3      | Reference data . . . . .   | 170        |
| 31.2.4      | Initial conditions . . . . .   | 171        |
| 31.2.5      | Boundary conditions . . . . .  | 171        |
| 31.2.6      | Physical parameters . . . . .  | 171        |
| 31.2.7      | Numerical parameters . . . . .   | 171        |
| <b>31.3</b> | <b>Results</b>   | <b>172</b> |
| 31.3.1      | First observations - regular mesh . . . . .  | 172        |
| 31.3.2      | First observations - fine mesh . . . . .   | 173        |
| 31.3.3      | Computation time . . . . .   | 174        |
| 31.3.4      | Comparison of schemes . . . . .  | 174        |
| 31.3.5      | Accuracy of the water depth . . . . .  | 178        |
| 31.3.6      | Accuracy of the wave propagation . . . . .   | 179        |
| 31.3.7      | Comparison on profiles . . . . .   | 179        |
| 31.3.8      | Positivity of the water depth . . . . .  | 180        |
| 31.3.9      | Mass conservation . . . . .  | 180        |
| <b>31.4</b> | <b>Conclusion</b>  | <b>181</b> |
| <b>32</b>   | <b>Tidal flow in the Mersey estuary (mersey)</b>   | <b>182</b> |
| <b>32.1</b> | <b>Purpose</b>   | <b>182</b> |
| 32.1.1      | Approach . . . . .   | 182        |

|   |            |
|---|------------|
| <b>32.2 Description</b>   | <b>182</b> |
| 32.2.1 Geometry and mesh . . . . .                                      | 182        |
| 32.2.2 Boundaries . . . . .   | 182        |
| 32.2.3 Bottom . . . . .   | 182        |
| 32.2.4 Physical parameters . . . . .                                    | 183        |
| 32.2.5 Numerical parameters . . . . .                                   | 183        |
| <b>32.3 Results</b>   | <b>184</b> |
| <br><b>33 Monai Valley experiment (monai_valley) . . . . .</b>          | <b>187</b> |
| <b>33.1 Purpose</b>   | <b>187</b> |
| <b>33.2 Description</b>   | <b>187</b> |
| 33.2.1 Mesh and geometry . . . . .                                      | 187        |
| 33.2.2 Boundary . . . . .   | 188        |
| 33.2.3 Physical parameters . . . . .                                    | 189        |
| 33.2.4 Numerical parameters . . . . .                                   | 189        |
| <b>33.3 Results</b>   | <b>189</b> |
| <br><b>34 Non-Newtonian model (nn_newt) . . . . .</b>                   | <b>191</b> |
| <b>34.1 Purpose</b>   | <b>191</b> |
| <b>34.2 Theoretical background</b>                                      | <b>191</b> |
| 34.2.1 Bingham model . . . . .  | 191        |
| 34.2.2 Herschel-Bulkley model . . . . .                                 | 192        |
| 34.2.3 Pseudo biphasic model . . . . .                                  | 192        |
| <b>34.3 Dambreak test case</b>  | <b>193</b> |
| 34.3.1 Description . . . . .  | 193        |
| 34.3.2 Theoretical solution . . . . .                                   | 193        |
| 34.3.3 Geometry and mesh . . . . .                                      | 193        |
| 34.3.4 Initial and boundary conditions . . . . .                        | 193        |
| 34.3.5 Physical parameters . . . . .                                    | 193        |
| 34.3.6 Numerical parameters . . . . .                                   | 193        |
| 34.3.7 Results . . . . .  | 194        |
| <b>34.4 Pseudo biphasic</b>   | <b>195</b> |
| 34.4.1 Description . . . . .  | 195        |
| 34.4.2 Geometry and mesh . . . . .                                      | 195        |
| 34.4.3 Initial and boundary conditions . . . . .                        | 195        |
| 34.4.4 Physical parameters . . . . .                                    | 195        |
| 34.4.5 Numerical parameters . . . . .                                   | 196        |
| 34.4.6 Results . . . . .  | 196        |
| <b>34.5 Conclusion</b>  | <b>196</b> |
| <br><b>35 Tsunami generation with the Okada model (okada) . . . . .</b> | <b>198</b> |
| <b>35.1 Purpose</b>   | <b>198</b> |
| <b>35.2 Description</b>   | <b>198</b> |
| 35.2.1 Geometry and Mesh . . . . .                                      | 198        |
| 35.2.2 Parameters . . . . .   | 198        |

|             |  |            |
|-------------|--|------------|
| <b>35.3</b> | <b>Results</b>   | <b>199</b> |
| <b>35.4</b> | <b>Conclusion</b>  | <b>199</b> |
| <b>36</b>   | <b>Flow in a channel with 2 bridge piers (pildepon) . . . . .</b>            | <b>201</b> |
| <b>36.1</b> | <b>Purpose</b>   | <b>201</b> |
| <b>36.2</b> | <b>Description</b>   | <b>201</b> |
| 36.2.1      | Geometry . . . . .   | 201        |
| 36.2.2      | Mesh and Bathymetry . . . . .  | 201        |
| 36.2.3      | Initial condition . . . . .  | 202        |
| 36.2.4      | Boundary conditions . . . . .  | 202        |
| 36.2.5      | Computation of the Strouhal number . . . . .                                 | 202        |
| 36.2.6      | Physical parameters . . . . .  | 203        |
| 36.2.7      | Numerical parameters . . . . .   | 203        |
| <b>36.3</b> | <b>Results</b>   | <b>203</b> |
| 36.3.1      | First observation . . . . .  | 203        |
| 36.3.2      | Comparison of numerical schemes . . . . .                                    | 204        |
| 36.3.3      | Computation of the Strouhal number . . . . .                                 | 205        |
| 36.3.4      | Mass balance . . . . .   | 206        |
| <b>37</b>   | <b>Infiltration with the SCS-Curve Number runoff model (pluie) . . . 207</b> |            |
| <b>37.1</b> | <b>Purpose</b>   | <b>207</b> |
| <b>37.2</b> | <b>Theoretical background</b>  | <b>207</b> |
| <b>37.3</b> | <b>Description</b>   | <b>208</b> |
| 37.3.1      | Geometry and mesh . . . . .  | 208        |
| 37.3.2      | Bathymetry . . . . .   | 208        |
| 37.3.3      | Initial and boundary conditions . . . . .                                    | 208        |
| 37.3.4      | Physical parameters . . . . .  | 208        |
| <b>37.4</b> | <b>Results</b>   | <b>209</b> |
| <b>37.5</b> | <b>Conclusion</b>  | <b>209</b> |
| <b>38</b>   | <b>Porosity (porosite) . . . . .</b>   | <b>210</b> |
| <b>38.1</b> | <b>Description</b>   | <b>210</b> |
| 38.1.1      | Initial and boundary conditions . . . . .                                    | 210        |
| 38.1.2      | Mesh and numerical parameters . . . . .                                      | 210        |
| 38.1.3      | Physical parameters . . . . .  | 211        |
| <b>38.2</b> | <b>Results</b>   | <b>211</b> |
| <b>38.3</b> | <b>Conclusions</b>   | <b>211</b> |
| <b>39</b>   | <b>Rain runoff and hydrostatic reconstruction (rain_runoff) . . . . .</b>    | <b>212</b> |
| <b>39.1</b> | <b>Purpose</b>   | <b>212</b> |
| <b>39.2</b> | <b>Description</b>   | <b>212</b> |
| 39.2.1      | Analytical solution . . . . .  | 212        |
| 39.2.2      | Experimental data . . . . .  | 213        |

|             |   |            |
|-------------|---|------------|
| 39.2.3      | Geometry and mesh . . . . .   | 213        |
| 39.2.4      | Bathymetry . . . . .  | 213        |
| 39.2.5      | Initial and boundary conditions . . . . .   | 214        |
| 39.2.6      | Physical parameters . . . . .   | 215        |
| 39.2.7      | Numerical parameters . . . . .  | 215        |
| <b>39.3</b> | <b>Results</b>  | <b>215</b> |
| <b>40</b>   | <b>riogrande . . . . .</b>  | <b>217</b> |
| <b>40.1</b> | <b>Description</b>  | <b>217</b> |
| 40.1.1      | Initial and boundary conditions . . . . .   | 217        |
| 40.1.2      | Mesh and numerical parameters . . . . .   | 218        |
| 40.1.3      | Physical parameters . . . . .   | 219        |
| <b>40.2</b> | <b>Results</b>  | <b>219</b> |
| <b>40.3</b> | <b>Conclusion</b>   | <b>219</b> |
| <b>41</b>   | <b>Oil spill artificial river experiments (riv_art) . . . . .</b>                 | <b>220</b> |
| <b>41.1</b> | <b>Purpose</b>  | <b>220</b> |
| <b>41.2</b> | <b>Description</b>  | <b>221</b> |
| 41.3        | Result  | 221        |
| <b>42</b>   | <b>Secondary flow correction (seccurrents) . . . . .</b>                          | <b>223</b> |
| <b>42.1</b> | <b>Purpose</b>  | <b>223</b> |
| <b>42.2</b> | <b>Description</b>  | <b>223</b> |
| 42.2.1      | Boundary Conditions . . . . .   | 224        |
| 42.2.2      | Mesh and numerical/physical parameters . . . . .                                  | 224        |
| <b>42.3</b> | <b>Results</b>  | <b>225</b> |
| <b>43</b>   | <b>Seiche . . . . .</b>   | <b>226</b> |
| <b>43.1</b> | <b>Purpose</b>  | <b>226</b> |
| <b>43.2</b> | <b>Description</b>  | <b>226</b> |
| 43.2.1      | Initial conditions . . . . .  | 226        |
| <b>43.3</b> | <b>Reference</b>  | <b>227</b> |
| <b>43.4</b> | <b>Results</b>  | <b>227</b> |
| <b>43.5</b> | <b>Conclusion</b>   | <b>227</b> |
| <b>44</b>   | <b>Shape file to define bathymetry (shapeTXT) . . . . .</b>                       | <b>228</b> |
| <b>44.1</b> | <b>Purpose</b>  | <b>228</b> |
| <b>44.2</b> | <b>Results</b>  | <b>228</b> |
| <b>45</b>   | <b>Wave refraction and diffraction around a circular island (shoal) . . . . .</b> | <b>229</b> |
| <b>45.1</b> | <b>Purpose</b>  | <b>229</b> |

|             |   |            |
|-------------|---|------------|
| <b>45.2</b> | <b>Description</b>  | <b>229</b> |
| 45.2.1      | Numerical and physical parameters . . . . .               | 229        |
| <b>45.3</b> | <b>Results</b>  | <b>229</b> |
| <b>46</b>   | <b>Culvert modelling (siphon)</b> . . . . .               | <b>232</b> |
| <b>46.1</b> | <b>Purpose</b>  | <b>232</b> |
| <b>46.2</b> | <b>Description</b>  | <b>232</b> |
| 46.2.1      | Geometry and mesh . . . . .                               | 232        |
| 46.2.2      | Boundaries . . . . .                                      | 232        |
| 46.2.3      | Physical Parameters . . . . .                             | 232        |
| 46.2.4      | Numerical Parameters . . . . .                            | 233        |
| <b>46.3</b> | <b>Results</b>  | <b>233</b> |
| <b>46.4</b> | <b>Conclusions</b>  | <b>233</b> |
| <b>46.5</b> | <b>Figures</b>  | <b>233</b> |
| <b>47</b>   | <b>swash_solution</b> . . . . .                           | <b>239</b> |
| <b>47.1</b> | <b>Description</b>  | <b>239</b> |
| 47.1.1      | Geometry and mesh . . . . .                               | 239        |
| 47.1.2      | Boundaries . . . . .                                      | 240        |
| 47.1.3      | Physical parameters . . . . .                             | 240        |
| 47.1.4      | Numerical parameters . . . . .                            | 240        |
| <b>47.2</b> | <b>Results</b>  | <b>241</b> |
| <b>48</b>   | <b>Solitary wave run-up (tests_channel)</b> . . . . .     | <b>244</b> |
| <b>48.1</b> | <b>Purpose</b>  | <b>244</b> |
| <b>48.2</b> | <b>Description</b>  | <b>244</b> |
| 48.2.1      | Geometry and mesh . . . . .                               | 244        |
| 48.2.2      | Boundaries . . . . .                                      | 245        |
| 48.2.3      | Numerical parameters . . . . .                            | 245        |
| <b>48.3</b> | <b>Results</b>  | <b>245</b> |
| 48.3.1      | Case 1 . . . . .  | 245        |
| 48.3.2      | Case 2 . . . . .  | 246        |
| 48.3.3      | Case 3 . . . . .  | 246        |
| <b>48.4</b> | <b>Conclusion</b>   | <b>248</b> |
| <b>49</b>   | <b>Wet and dry moving transitions (thacker)</b> . . . . . | <b>249</b> |
| <b>49.1</b> | <b>Purpose</b>  | <b>249</b> |
| <b>49.2</b> | <b>Description</b>  | <b>249</b> |
| 49.2.1      | Thacker analytical solutions . . . . .                    | 249        |
| 49.2.2      | Geometry, mesh and bathymetry . . . . .                   | 250        |
| 49.2.3      | Initial conditions . . . . .                              | 250        |
| 49.2.4      | Boundary conditions . . . . .                             | 250        |
| 49.2.5      | Physical parameters . . . . .                             | 250        |

|             |  |            |
|-------------|--|------------|
| 49.2.6      | Numerical parameters . . . . .   | 251        |
| <b>49.3</b> | <b>Results - Rotation of a planar surface in a parabolic bowl</b>                    | <b>251</b> |
| 49.3.1      | First observation . . . . .  | 251        |
| 49.3.2      | Computation time . . . . .   | 252        |
| 49.3.3      | Comparison of schemes . . . . .  | 253        |
| 49.3.4      | Accuracy . . . . .   | 255        |
| 49.3.5      | Positivity of water depth . . . . .  | 256        |
| 49.3.6      | Mass balance . . . . .   | 256        |
| 49.3.7      | Energy balance . . . . .   | 257        |
| 49.3.8      | Convergence . . . . .  | 258        |
| <b>49.4</b> | <b>Results - Oscillation of a radially symmetrical paraboloid</b>                    | <b>261</b> |
| 49.4.1      | Computation time . . . . .   | 261        |
| 49.4.2      | Comparison of schemes . . . . .  | 261        |
| <b>49.5</b> | <b>Conclusion</b>  | <b>263</b> |
| <b>50</b>   | <b>Propagation of tide prescribed by boundary conditions (tide)</b>                  | <b>264</b> |
| <b>50.1</b> | <b>Purpose</b>   | <b>264</b> |
| <b>50.2</b> | <b>Description</b>   | <b>264</b> |
| 50.2.1      | Geometry and Mesh . . . . .  | 264        |
| 50.2.2      | Bathymetry . . . . .   | 265        |
| 50.2.3      | Initial conditions . . . . .   | 265        |
| 50.2.4      | Boundary conditions . . . . .  | 265        |
| 50.2.5      | Physical parameters . . . . .  | 266        |
| 50.2.6      | Numerical parameters . . . . .   | 266        |
| 50.2.7      | Comments . . . . .   | 266        |
| <b>50.3</b> | <b>Results</b>   | <b>266</b> |
| <b>50.4</b> | <b>Conclusion</b>  | <b>267</b> |
| <b>51</b>   | <b>Diffusion of tracers (tracer_diffusion)</b> . . . . .                             | <b>268</b> |
| <b>51.1</b> | <b>Purpose</b>   | <b>268</b> |
| <b>51.2</b> | <b>Description</b>   | <b>268</b> |
| 51.2.1      | Geometry and mesh . . . . .  | 268        |
| 51.2.2      | Initial condition . . . . .  | 268        |
| 51.2.3      | Boundary conditions . . . . .  | 269        |
| 51.2.4      | Physical parameters . . . . .  | 269        |
| 51.2.5      | Numerical parameters . . . . .   | 269        |
| <b>51.3</b> | <b>Results</b>   | <b>269</b> |
| 51.3.1      | Computation time . . . . .   | 269        |
| 51.3.2      | Comparison of diffusion schemes . . . . .  | 270        |
| <b>51.4</b> | <b>Conclusion</b>  | <b>271</b> |
| <b>52</b>   | <b>Convergence study for the diffusion of tracers (tracer_diffusion_convergence)</b> | <b>272</b> |
| <b>52.1</b> | <b>Purpose</b>   | <b>272</b> |

|  |            |
|--|------------|
| <b>52.2 Description</b>                            | <b>272</b> |
| 52.2.1 Geometry and mesh . . . . .                 | 272        |
| 52.2.2 Initial condition . . . . .                 | 272        |
| 52.2.3 Boundary conditions . . . . .               | 272        |
| 52.2.4 Physical parameters . . . . .               | 272        |
| 52.2.5 Numerical parameters . . . . .              | 273        |
| <b>52.3 Results</b>                                | <b>273</b> |
| 52.3.1 First observation . . . . .                 | 273        |
| 52.3.2 Computation time . . . . .                  | 274        |
| 52.3.3 Convergence . . . . .                       | 274        |
| <b>52.4 Conclusion</b>                             | <b>276</b> |
| <br>   |            |
| <b>53 triangular_shelf . . . . .</b>               | <b>277</b> |
| <b>53.1 Purpose</b>                                | <b>277</b> |
| <b>53.2 Description</b>                            | <b>277</b> |
| 53.2.1 Geometry and mesh . . . . .                 | 277        |
| 53.2.2 Boundaries . . . . .                        | 278        |
| 53.2.3 Physical parameters . . . . .               | 279        |
| 53.2.4 Numerical parameters . . . . .              | 279        |
| <b>53.3 Results</b>                                | <b>279</b> |
| <br>   |            |
| <b>54 Uncovering of a beach (vasque) . . . . .</b> | <b>281</b> |
| <b>54.1 Purpose</b>                                | <b>281</b> |
| <b>54.2 Description</b>                            | <b>281</b> |
| 54.2.1 Approach . . . . .                          | 281        |
| 54.2.2 Geometry and mesh . . . . .                 | 281        |
| 54.2.3 Boundaries . . . . .                        | 282        |
| 54.2.4 Bottom . . . . .                            | 282        |
| 54.2.5 Physical parameters . . . . .               | 282        |
| 54.2.6 Numerical parameters . . . . .              | 282        |
| <b>54.3 Results</b>                                | <b>283</b> |
| <b>54.4 Conclusion</b>                             | <b>283</b> |
| <br>   |            |
| <b>55 Vegetation laws (vegetation) . . . . .</b>   | <b>284</b> |
| <b>55.1 Purpose</b>                                | <b>284</b> |
| <b>55.2 Description</b>                            | <b>284</b> |
| 55.2.1 Geometry and mesh . . . . .                 | 284        |
| 55.2.2 Initial condition . . . . .                 | 284        |
| 55.2.3 Boundary conditions . . . . .               | 285        |
| 55.2.4 Physical parameters . . . . .               | 285        |
| 55.2.5 Numerical parameters . . . . .              | 286        |
| <b>55.3 Results</b>                                | <b>286</b> |
| <b>55.4 Conclusion</b>                             | <b>287</b> |

|             |   |            |
|-------------|---|------------|
| <b>56</b>   | <b>Propagation of waves in a channel (wave) .....</b> | <b>289</b> |
| <b>56.1</b> | <b>Purpose</b>  | <b>289</b> |
| <b>56.2</b> | <b>Description</b>                                    | <b>289</b> |
| 56.2.1      | Analytical solution .....                             | 289        |
| 56.2.2      | Geometry and mesh .....                               | 289        |
| 56.2.3      | Initial conditions .....                              | 290        |
| 56.2.4      | Boundary conditions .....                             | 290        |
| 56.2.5      | Physical parameters .....                             | 290        |
| 56.2.6      | Numerical parameters .....                            | 290        |
| <b>56.3</b> | <b>Results</b>  | <b>290</b> |
| <b>56.4</b> | <b>Conclusions</b>                                    | <b>292</b> |
| <b>57</b>   | <b>Weirs .....</b>                                    | <b>293</b> |
| <b>57.1</b> | <b>Purpose</b>  | <b>293</b> |
| <b>57.2</b> | <b>Description</b>                                    | <b>293</b> |
| <b>57.3</b> | <b>Option 1 - Horizontal weirs</b>                    | <b>293</b> |
| 57.3.1      | Geometry and mesh .....                               | 293        |
| 57.3.2      | Initial conditions .....                              | 294        |
| 57.3.3      | Boundary conditions .....                             | 294        |
| 57.3.4      | Physical parameters .....                             | 294        |
| 57.3.5      | Numerical parameters .....                            | 294        |
| 57.3.6      | Results .....   | 295        |
| <b>57.4</b> | <b>Option 2 - Generic weirs</b>                       | <b>296</b> |
| 57.4.1      | Geometry and mesh .....                               | 296        |
| 57.4.2      | Initial conditions .....                              | 299        |
| 57.4.3      | Boundary conditions .....                             | 299        |
| 57.4.4      | Physical parameters .....                             | 299        |
| 57.4.5      | Numerical parameters .....                            | 299        |
| 57.4.6      | Results .....   | 299        |
| <b>57.5</b> | <b>Conclusion</b>                                     | <b>302</b> |
| <b>58</b>   | <b>wesel .....</b>                                    | <b>303</b> |
| <b>58.1</b> | <b>Purpose</b>  | <b>303</b> |
| <b>58.2</b> | <b>Description</b>                                    | <b>303</b> |
| 58.2.1      | Geometry and mesh .....                               | 303        |
| 58.2.2      | Initial condition .....                               | 303        |
| 58.2.3      | Boundary conditions .....                             | 303        |
| 58.2.4      | Physical parameters .....                             | 303        |
| 58.2.5      | Numerical parameters .....                            | 304        |
| <b>58.3</b> | <b>Results</b>  | <b>305</b> |
| <b>58.4</b> | <b>Conclusion</b>                                     | <b>306</b> |

|             |  |            |
|-------------|--|------------|
| <b>59</b>   | <b>Flow in a channel submitted to wind (wind)</b>  | <b>308</b> |
| <b>59.1</b> | <b>Purpose</b>                                     | <b>308</b> |
| <b>59.2</b> | <b>Description</b>                                 | <b>308</b> |
| 59.2.1      | Analytical solution .....                          | 308        |
| 59.2.2      | Geometry and mesh .....                            | 308        |
| 59.2.3      | Initial conditions .....                           | 309        |
| 59.2.4      | Boundary conditions .....                          | 309        |
| 59.2.5      | Physical parameters .....                          | 309        |
| 59.2.6      | Numerical parameters .....                         | 309        |
| <b>59.3</b> | <b>Results</b>                                     | <b>310</b> |
| <b>59.4</b> | <b>Conclusion</b>                                  | <b>310</b> |
| <b>60</b>   | <b>Wind depending on time and space (wind_txy)</b> | <b>311</b> |
| <b>60.1</b> | <b>Purpose</b>                                     | <b>311</b> |
| <b>60.2</b> | <b>Description</b>                                 | <b>311</b> |
| 60.2.1      | Geometry and mesh .....                            | 311        |
| 60.2.2      | Initial conditions .....                           | 311        |
| 60.2.3      | Boundary conditions .....                          | 312        |
| 60.2.4      | Physical parameters .....                          | 312        |
| 60.2.5      | Numerical parameters .....                         | 312        |
| <b>60.3</b> | <b>Results</b>                                     | <b>312</b> |
| <b>60.4</b> | <b>Conclusion</b>                                  | <b>315</b> |
|             | <b>Bibliography .....</b>                          | <b>316</b> |

# 1. Algae 2D Coupling (2Dcoupling\_algae)

## 1.1 Purpose

The purpose of this example is to show that for a test with algae, the algae dislodgement can be defined as a function of bed wave orbital velocity taken from a coupled TOMAWAC run.

## 1.2 Description

This test case is based on the TOMAWAC test case **3Dcoupling**, which is turn based on the SISYPHE test case **littoral**. Details of the flows and waves can be found in the documentation for these test cases.

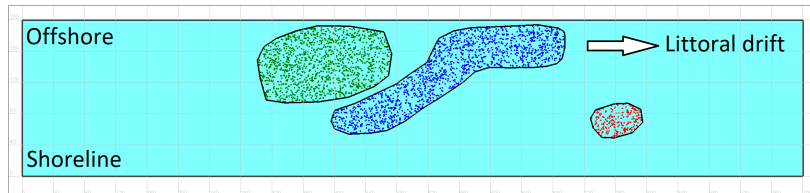


Figure 1.1: Initial algae distribution.

The initial algae distribution is defined using a polygon file, containing three polygons, which is specified using the keyword DROGUES INITIAL POSITIONING DATA FILE. The polygon file must be in the Blue Kenue i2s format. The central polygon defines algae with class 1. The left polygon defines algae with class 2. The right polygon defines algae with class 3.

For this test case, the keyword ALGAE RELEASE TYPE equals 2 for all 3 classes. This means an algae particle does not start to move until the wave orbital velocity at the bed exceeds a threshold value. This option only works if the TELEMAC-2D run is coupled with TOMAWAC and if TOMAWAC supplies the wave orbital velocity to the TELEMAC-2D run.

The threshold value of the wave orbital velocity varies with time, according to the equation:

$$OV_0 = OV_1 + (OV_2 - OV_1) \exp(-A \cdot T_{eff}), \quad (1.1)$$

$OV_1$ ,  $OV_2$  and  $A$  are specified in the steering file with the following keywords:

$OV_1 = \text{WAVE ORBITAL VELOCITY THRESHOLD FOR ALGAE } 1,$

$OV_2$  = WAVE ORBITAL VELOCITY THRESHOLD FOR ALGAE 2,

$A$  = RATE OF DEGRADATION FOR ALGAE.

$T_{eff}$  is an “effective time” relating to the cumulative wave forcing that has been experienced by each algae particle, defined by:  $T_{eff} = \sum OV.dt$ . This means that  $T_{eff}$  is the numerical integral of wave orbital velocity over time.

For this test,  $OV_1 = 0.5$  m/s for class 1, 0.7 m/s for class 2 and 0.4 m/s for class 3.  $A = 0.005$  for class 1 and class 2 and 0.01 for class 3.

### 1.3 Results

*Because of the turbulent particle movements the result on the reader’s machine may be slightly different to the results below, but it should be similar.*

Figure 1.2 to Figure 1.4 show the algae distribution after 3 s, 6 s and 9 s.

After 3 s, some of the central class 1 particles have been dislodged and have moved to the right. This is because  $OV_1$  is lower for the class 1 particles (blue) than the class 2 particles (green), which have not yet been dislodged. The class 3 particles (red) have not been dislodged yet because they are in a region of lower bed wave orbital velocity.

After 6 s, some of the class 2 particles have been dislodged. This is because the critical bed wave orbital velocity has become lower, according to the equation given above. In reality, the critical value would not change so quickly. This test case can to the critical value changing quickly in order to illustrate the principle.

After 9 s, the particles have moved further to the right and a wider band of particles have been dislodged. The class 3 particles have been dislodged and have moved to the left slightly.

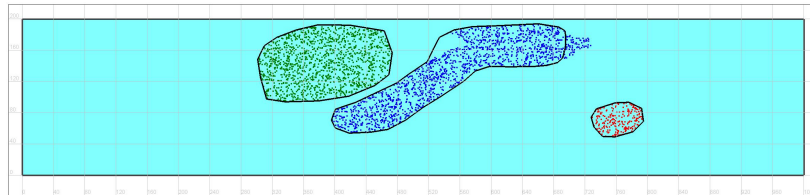


Figure 1.2: Algae distribution after 3 s.

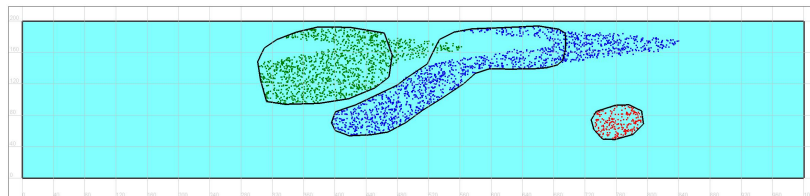


Figure 1.3: Algae distribution after 6 s.

The standard test case outputs the algae information as a Tecplot file. In this case the algae information is written to a file defined by the keyword ASCII DROGUES FILE. The default value of the DROGUES FILE FORMAT is TECPLOT. In order to output to a PCL file, give the

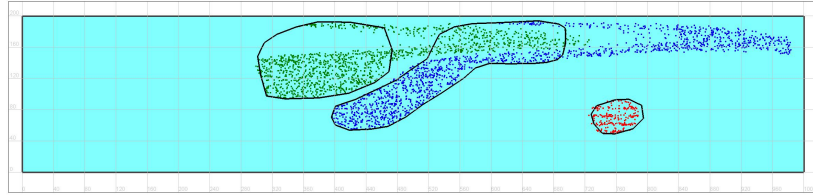


Figure 1.4: Algae distribution after 9 s.

output file name using the keyword `BINARY DROGUES FILE` and give the `DROGUES FILE FORMAT` as `BKBINPCL`. PCL files can be displayed using Blue Kenu.

This example outputs a text file called `polygon_particles.txt`. Output is written to the file every 10 s. The output relates to the three polygons that define the three initial regions of particles, as described above. For each time, the output file contains the time, and the number of initial particles that remain in each polygon and un-mobilised. Running of the test case should result in a text file identical to the `polygon_particles.txt` file.

For this test case example the random distribution of initial particles is fixed through lines 39 to 47 of the `CONDIN_DROGUES` subroutine. These lines ensure that the particles are initially located at the same place whenever the test case is run but should be commented out when running the code more generally.

## 2. Flow around a cylinder (Negretti2D)

### 2.1 Description

This example shows that TELEMAC-2D is able to simulate a flow around a cylinder with the Spalart-Allmaras turbulence model, in particular the impact of an obstacle on a channel flow. The configuration is a straight channel 20 m long and 8 m wide with a flat horizontal bottom without slope (at elevation -20 m) and a 2 m diameter cylinder inside the domain (its center is located at coordinates (0;0)).

#### 2.1.1 Initial and boundary conditions

The computation is initialised with a constant elevation equal to -18 m and no velocity. The boundary conditions are:

- For the solid walls, a Strickler law on channel banks is used for the velocities with friction coefficient equal to  $60 \text{ m}^{1/3}/\text{s}$ ,
- On the bottom, a Strickler law with friction coefficient equal to  $20 \text{ m}^{1/3}/\text{s}$  is prescribed,
- Upstream a flowrate equal to  $32 \text{ m}^3/\text{s}$  is prescribed from time = 10 s, linearly increasing from 0 to  $32 \text{ m}^3/\text{s}$  during the first 10 s,
- Downstream the water level is suggested to be equal to -18 m.

Thompson boundary conditions are used for both liquid boundaries.

#### 2.1.2 Mesh and numerical parameters

The mesh (Figure 2.1) is rather refined and is made of 33,598 triangular elements (17,178 nodes). It is a little bit more refined around the island.

The time step is 0.0125 s for a simulated period of 80 s.

To solve the advection, the NERD scheme is used for every variable (velocities and turbulent variable, = scheme 14). The conjugate gradient is used for solving the propagation step (option 1) with solver accuracy equal to  $10^{-16}$  and the implicitation coefficients for depth and velocities are both equal to 0.6.

#### 2.1.3 Physical parameters

The Spalart-Allmaras model is used for turbulence modelling (TURBULENCE MODEL = 6) with VELOCITY DIFFUSIVITY =  $10^{-3} \text{ m}^2/\text{s}$ .

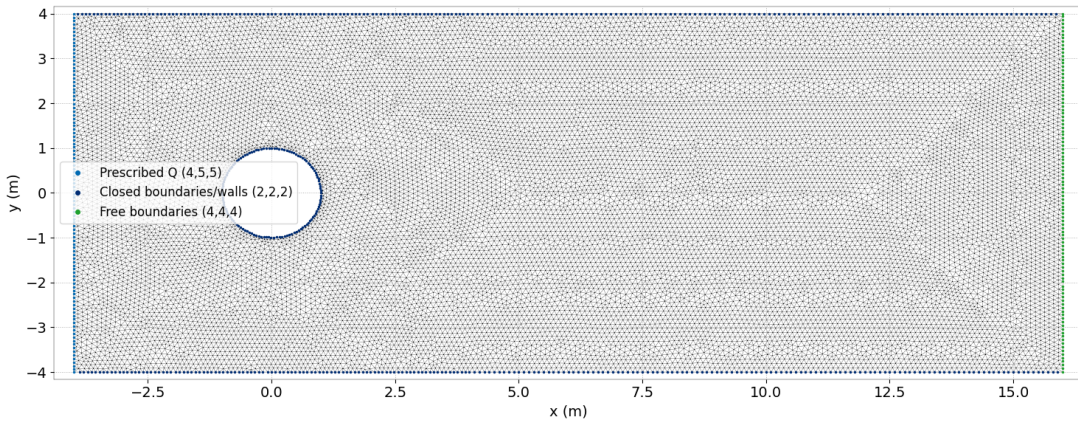


Figure 2.1: Horizontal mesh.

## 2.2 Results

The flow establishes a steady flow where the free surface is lightly higher in front of the cylinder and lower on the left and the right of the cylinder (in the direction of the flow), see Figure 2.2. Moreover, the velocity decreases in front of the cylinder and in its wake, but it increases when going around the cylinder on the left or the right, see Figures 2.3 and 2.4.

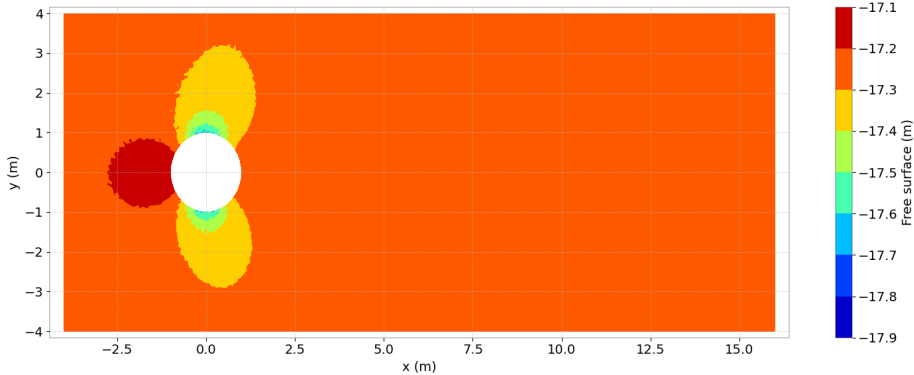


Figure 2.2: Free surface elevation at final time step.

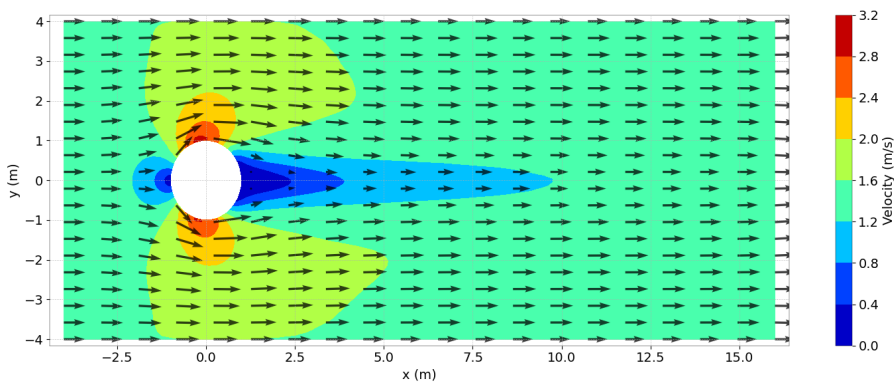


Figure 2.3: Magnitude of velocity at final time step with vectors.

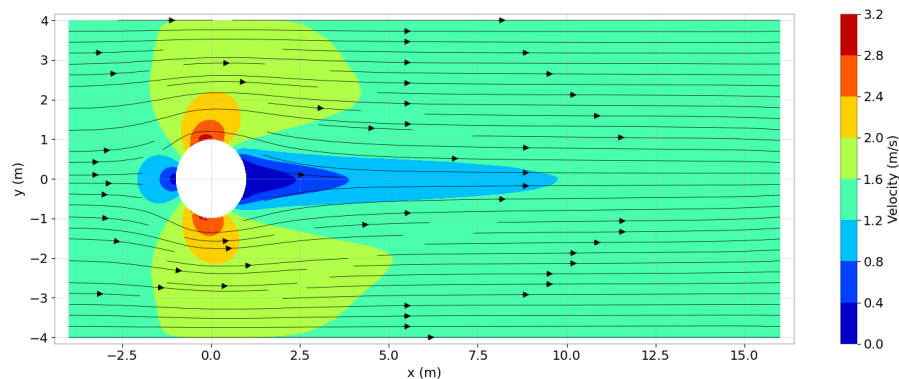


Figure 2.4: Magnitude of velocity at final time step with streamlines.

### 2.3 Conclusions

This example validates the Spalart-Allmaras turbulence model of TELEMAC-2D.

## 3. Balzano

### 3.1 Purpose

This test illustrates that TELEMAC-2D is able to simulate water retention in a bowed beach. It is also useful to check that the schemes are well-balanced and mass conservative in severe drying conditions.

### 3.2 Description

#### 3.2.1 Geometry and mesh

The computational domain is a  $13,800 \text{ m} \times 1,200 \text{ m}$  rectangular channel. A triangular non-structured mesh is constructed on this domain and contains 8,000 triangular elements and 4,161 nodes (cf. Figure 3.1).

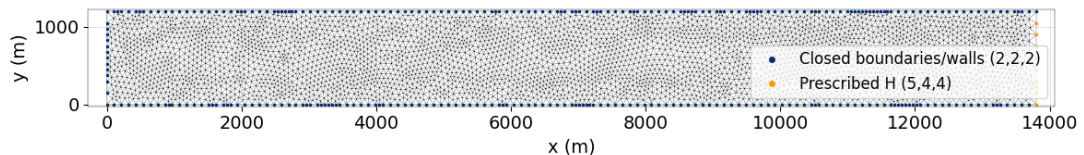


Figure 3.1: Geometry and mesh of the Balzano test case.

#### 3.2.2 Bathymetry

The channel is characterized by a uniform slope, going from maximum  $z = 0 \text{ m}$  at  $x = 0 \text{ m}$  to  $z = -5 \text{ m}$  at  $x = 13,800 \text{ m}$ , with a reservoir located at  $x = 4,800 \text{ m}$ . The bathymetry is defined in the **USER\_CORFON** subroutine as follows:

$$z(x) = \begin{cases} -\frac{x}{2760}, & x < 3600 \\ \frac{x}{2760} - \frac{60}{23}, & 3600 \leq x < 4800 \\ -\frac{x}{920} + \frac{100}{23}, & 4800 \leq x \leq 6000 \\ -\frac{x}{2760}, & x \geq 6000 \end{cases} \quad (3.1)$$

A 3D plot of the bathymetry can be found in Figure 3.2, as well as the profile of bathymetry along the  $x$  axis.

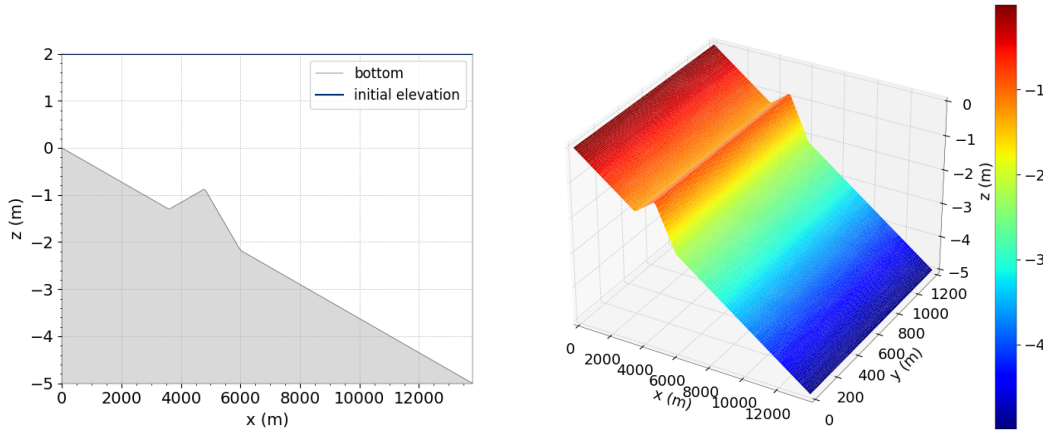


Figure 3.2: Bathymetry of the Balzano test case.

### 3.2.3 Initial conditions

At the beginning of the simulation the water is at rest (no velocities), with a constant free surface elevation equal to 2 m.

### 3.2.4 Boundary conditions

The boundaries are solid walls everywhere, except on the right-hand side boundary, which is a liquid boundary. There is no friction on the solid walls and a water level is prescribed at the liquid boundary, with a value of -2 m.

### 3.2.5 Analytical solution at equilibrium

Given the initial and boundary conditions, during the simulation the water level gradually decreases until it reaches the prescribed value of -2 m in the right-hand side part of the domain ( $x > 4,800$  m). In the left-hand side part of the domain ( $x < 4,800$  m), the water level gradually reaches the elevation  $z = -0.87$  m, which is the elevation of the bathymetry peak at  $x = 4,800$  m, and stabilizes. This is a severe drying scenario, and the stabilization of the free surface in both parts of the domain is a worthy result in itself. The analytical solution for the free surface at equilibrium is expressed as follows:

- -2 m in the right-hand side of the domain ( $x > 4,800$  m),
- -0.87 m in the left-hand side part of the domain ( $x < 4,800$  m).

### 3.2.6 Physical parameters

The physical characteristics of the case are the following:

- Seaside water depth  $H_0 = 3$  m,
- Characteristic length  $L = 13,800$  m,
- Characteristic slope defined by  $\tan(\alpha) = 3.6 \times 10^{-4}$  m,
- Galilei Number  $G_a = \frac{g \times L^3}{\nu} = 2.58 \times 10^{19}$  where  $\nu$  is the kinematic viscosity of water and  $g$  is the gravity acceleration.

The viscosity is set as constant and equal to 0 m<sup>2</sup>/s (VELOCITY DIFFUSIVITY = 0).

### 3.2.7 Numerical parameters

For this test case, duration is set to 70,000 s and several numerical schemes are confronted. The solver used is the conjugate gradient with an accuracy of  $10^{-4}$ . For finite element schemes the treatment of the linear system is set to wave equation (TREATMENT OF THE LINEAR SYSTEM = 2). The simulation parameters specific to each case are summed up in Table 3.1.

| Case | Name | Equations       | Elements for U,V & H | Advection scheme for velocities | Time-step / Desired Courant number |
|------|------|-----------------|----------------------|---------------------------------|------------------------------------|
| 1    | CHAR | Wave Eq. FE     | P1-P1                | characteristics                 | 5 s / -                            |
| 2    | NERD | Wave Eq. FE     | P1-P1                | edge-based N-scheme             | 5 s / -                            |
| 3    | ERIA | Wave Eq. FE     | P1-P1                | ERIA scheme                     | 5 s / -                            |
| 4    | KIN1 | Saint-Venant FV | -                    | kinetic order 1                 | - / 0.9                            |
| 5    | HLLC | Saint-Venant FV | -                    | HLLC order 1                    | - / 0.9                            |

Table 3.1: List of the simulation parameters used for the five cases.

## 3.3 Results

### 3.3.1 First observation

The water level in the reservoir gradually reaches the elevation -0.87 m. On the right side of the bump, an hydraulic jump forms as well as near the exit boundary until water level on the right-hand side of the domain stabilize around -2 m. The evolution of the free surface during the simulation is presented in Figure 3.3 with the kinetic scheme.

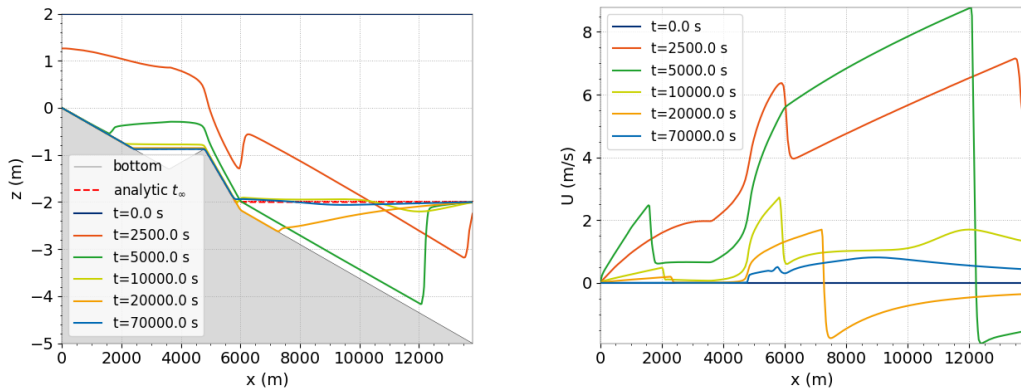


Figure 3.3: Free surface (left) and velocity (right) at different times with the first order kinetic scheme.

### 3.3.2 Computation time

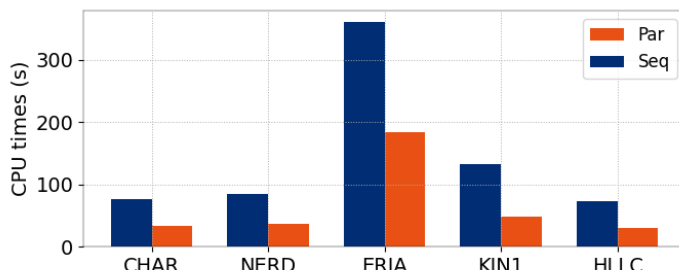


Figure 3.4: CPU times.

Simulation times for each of these cases with sequential and parallel runs (using 4 processors) are shown in Figure 3.4<sup>1</sup>.

### 3.3.3 Comparison of schemes

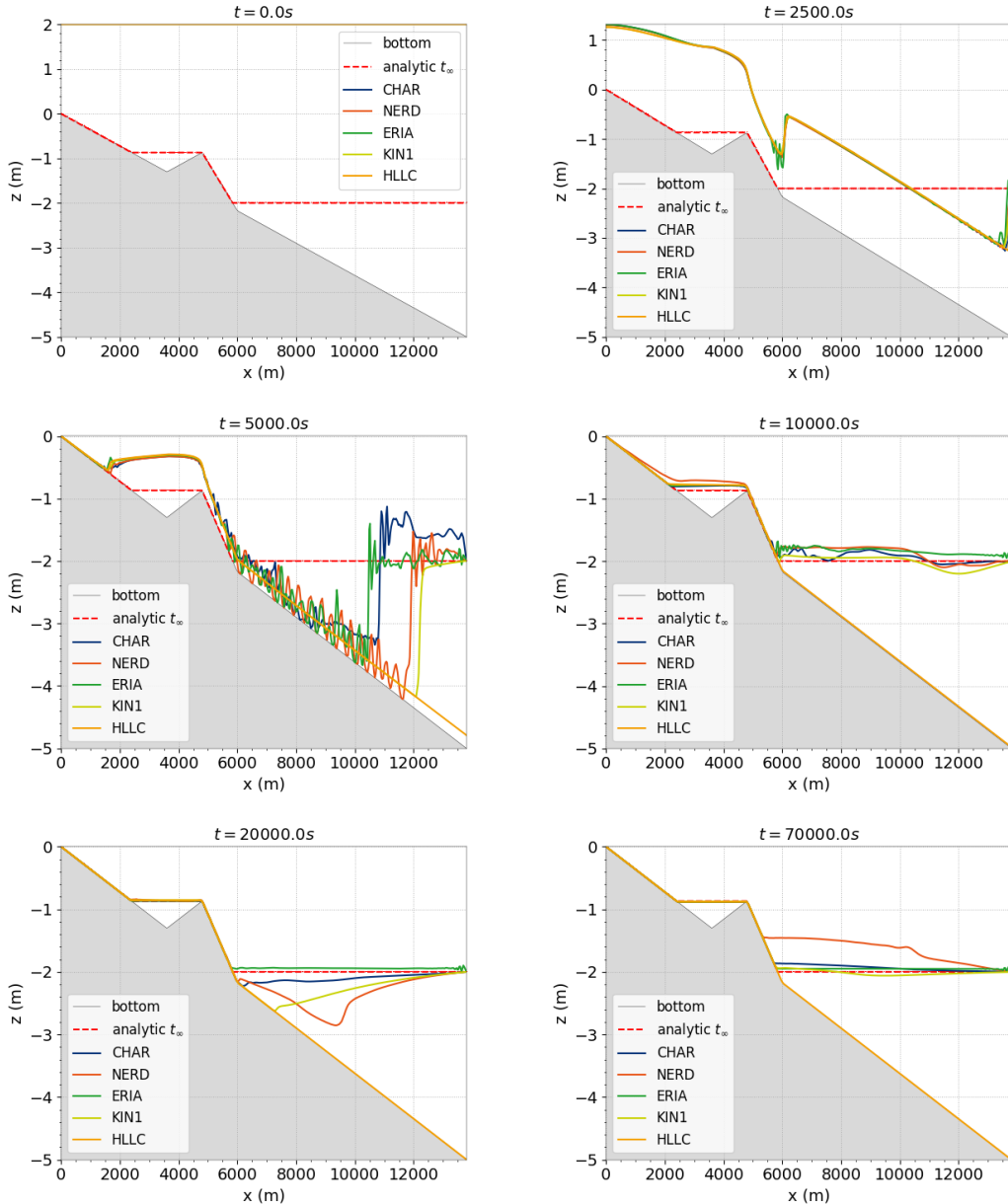


Figure 3.5: Free surface shape at different times in the Balzano case.

In this section, we compare the solution obtained with all the numerical schemes. In Figure 3.5 the evolution of the free surface is presented. Kinetic and HLLC schemes handle very well discontinuities and the jumps are well captured. CHAR, NERD and ERIA schemes are not able to capture the jumps with large time steps and numerical oscillations are visible when

---

<sup>1</sup>Keep in mind that these times are specific to the validation run and the type of processors that were used for this purpose.

the drying occurs. Once the hydraulic jump disappears the solutions are smoother and slowly converge towards equilibrium due to numerical diffusion.

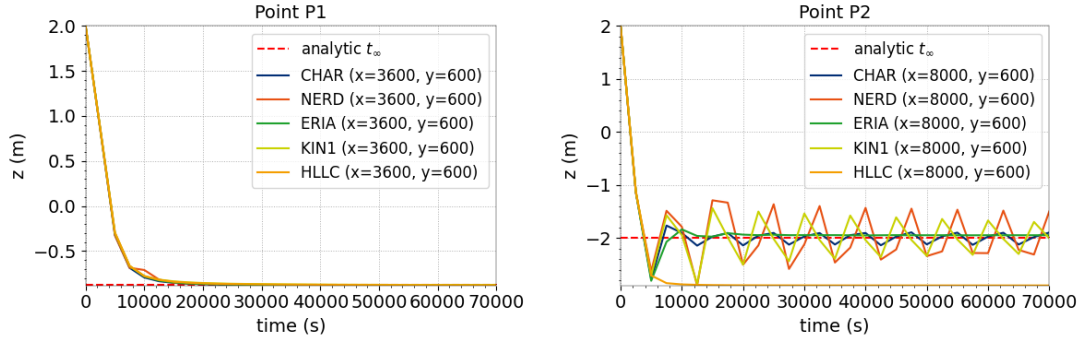


Figure 3.6: Evolution of the free surface elevation at points P1 and P2 for the five considered setups on the Balzano example.

We should observe a sinusoidal depletion of the right-hand side boundary level. The evolution of the water level at two different points, P1 ( $x = 3,600$  m,  $y = 600$  m) and P2 ( $x = 8,000$  m,  $y = 600$  m), located in the reservoir and at the right-hand side of the reservoir is plotted in Figure 3.6. For all the tested schemes, the asymptotic evolution in the reservoir is realized and is fast. On the right-hand side part of the domain, the water level abruptly falls at the beginning of the simulation, and later oscillates around the value -2 m, with a decreasing amplitude. In absence of friction and viscosity, the damping is slow and only comes from numerical diffusion.

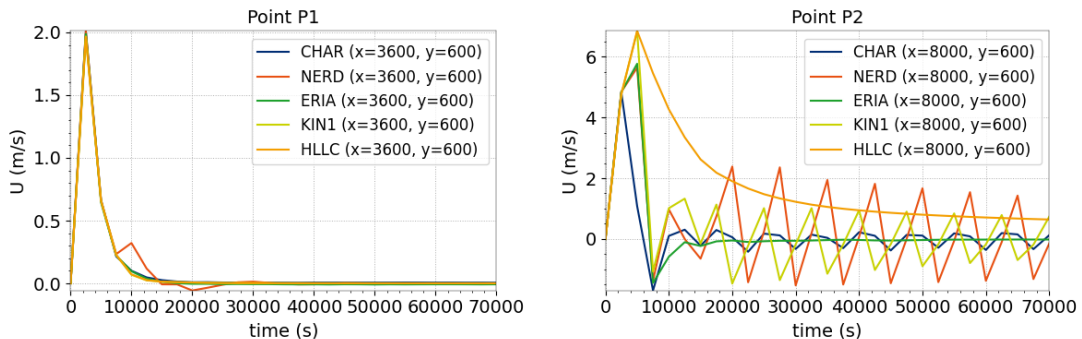


Figure 3.7: Evolution of the streamwise velocity using different schemes on the Balzano case.

Velocity values can also be compared in the reservoir (P1) and at the right-hand side of the channel (P2) in Figure 3.7. In the reservoir, there is an abrupt acceleration at the beginning of the simulation, followed by an abrupt deceleration, towards a permanent regime establishment (zero velocity). At the right-hand side of the channel, the same acceleration and deceleration phases are followed by an oscillation around a zero velocity for all schemes.

### 3.3.4 Positivity of the water depth

The minimum values of the water depth are checked during all simulation. Results are shown in Figure 3.8. In the case of finite volume schemes, positivity is ensured without additional treatment. With finite element schemes the positivity is ensured with a treatment of negative depths during simulation (TREATMENT OF NEGATIVE DEPTHS = 2 for characteristics and NERD and 3 for ERIA scheme).

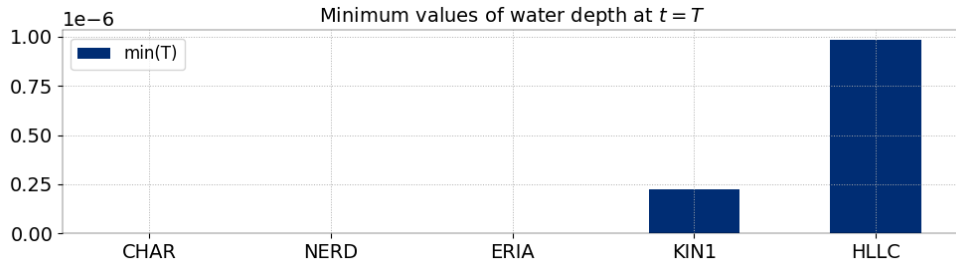


Figure 3.8: Minimum values of water depths.

### 3.3.5 Mass balance

Mass conservation can be checked by calculating the mass in the domain during time. The lost mass is calculated as  $M_{initial} - M_{final}$  and presented in Figure 3.9.

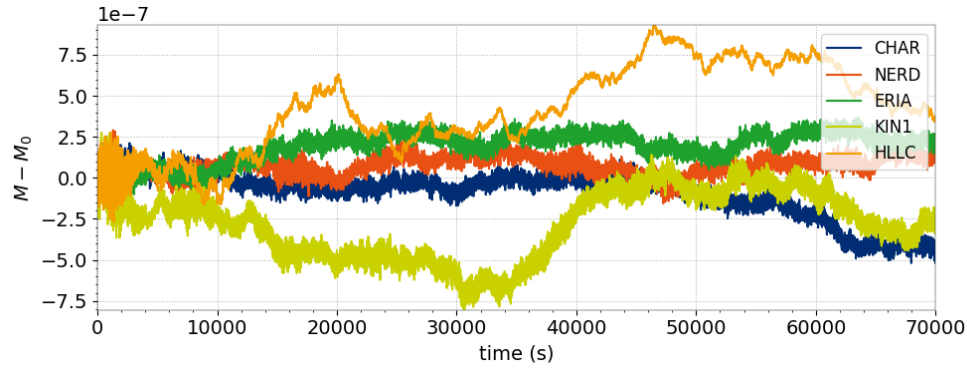


Figure 3.9: Balzano mass balance.

### 3.3.6 Energy balance

In this section, the conservation of the mean energy is checked. In fact, for the Saint-Venant equations, the quantity  $h \frac{\|U\|^2}{2} + g \frac{h^2}{2}$ , called mean or integrated energy, is conserved, where  $\|U\|$  is the Saint-Venant depth averaged velocity magnitude. The following quantities are studied:

- Integrated potential energy  $E_p = \int \int_{\Omega_{xy}} \rho_{water} g \frac{h^2}{2} dx dy$  where  $\Omega_{xy}$  is the 2D domain of simulation: Figure 3.10,
- Integrated kinetic energy  $E_c = \int \int_{\Omega_{xy}} \rho_{water} h \frac{\|U\|^2}{2} dx dy$ : Figure 3.11,
- Integrated mechanical energy  $E_m = E_p + E_c$ : Figure 3.12.

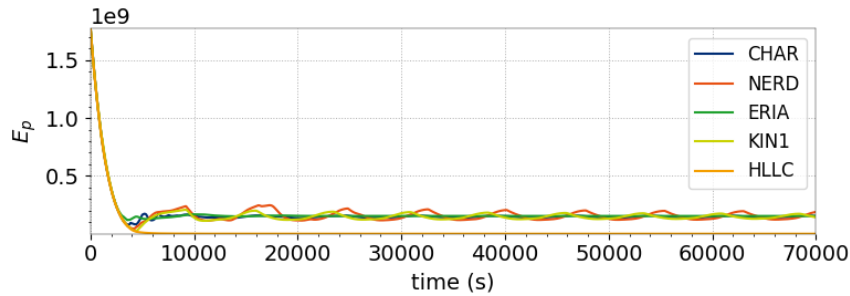


Figure 3.10: Potential energy evolution for all tested schemes on the Balzano case.

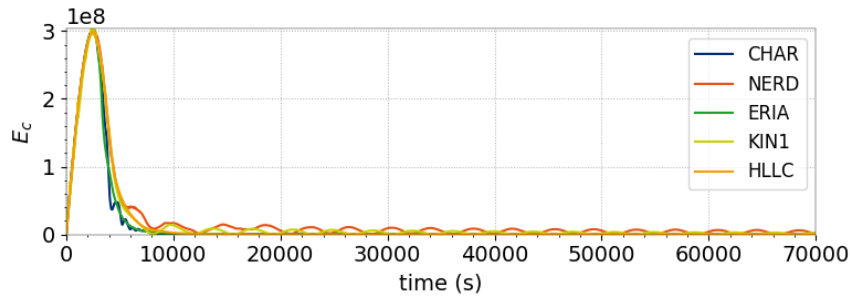


Figure 3.11: Kinetic energy evolution for all tested schemes on the Balzano case.

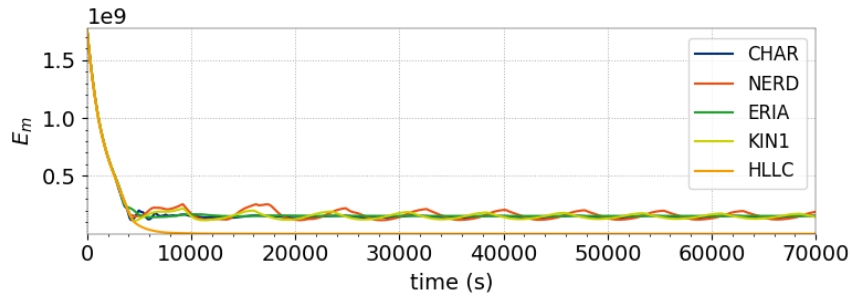


Figure 3.12: Mechanical energy evolution for all tested schemes on the Balzano case.

The potential energy evolution is directly linked to the evolution of the free surface as seen in Figure 3.6. In fact, there is a major loss of potential energy due to the abrupt decrease of water depth, and later oscillations around a constant value. The kinetic energy evolution visible in Figure 3.7 is, on the other hand, linked to the velocity variations.

### 3.4 Conclusion

This test case shows that TELEMAC-2D schemes are capable of simulating severe drying problems with some precautions regarding the choice of numerical parameters.

## 4. Wave driven currents (bj78)

### 4.1 Description

This test demonstrates the ability of TELEMAC-2D to model wave driven currents when chaining with a wave file.

The configuration is a 20.9 m long and 0.8 m wide channel with piecewise affine bottom (see Figures 4.1 and 4.2) defined by:

$$\left\{ \begin{array}{ll} \text{if } x < -5, & z_b = -0.616, \\ \text{if } -5 \leq x < 5, & z_b = -0.616 + 0.05(x+5), \\ \text{if } 5 \leq x < 9.4, & z_b = -0.116 - 0.025(x-5), \\ \text{if } x \geq 9.4, & z_b = -0.226 + 0.05(x-9.4), \\ & \text{and } z_b = \max(-0.04, z_b) \end{array} \right.$$

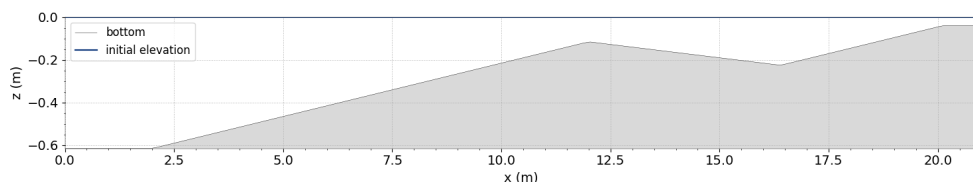


Figure 4.1: Bottom elevation and initial condition.

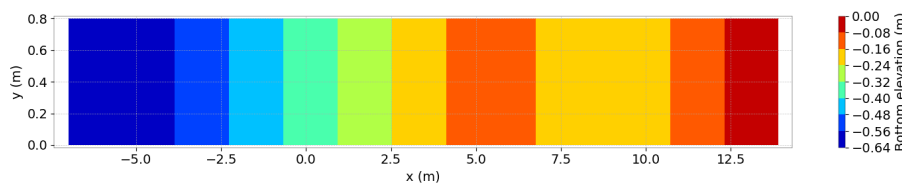


Figure 4.2: Bottom elevation.

#### 4.1.1 Initial and boundary conditions

The computation is initialised with a constant elevation equal to 0 m, no velocity.

The boundary conditions are:

- For the solid walls, a slip condition on channel banks is used for the velocities,
- On the bottom, a Strickler law with friction coefficient equal to  $45 \text{ m}^{1/3}/\text{s}$  is prescribed,
- Upstream conditions are let free for water depth and velocities. Thompson conditions are used to compute boundary conditions for this liquid boundary,
- Downstream is a solid wall with slip condition for velocities.

#### 4.1.2 Mesh and numerical parameters

The 2D mesh (Figure 4.3) is made of 1,394 triangular elements (842 nodes).

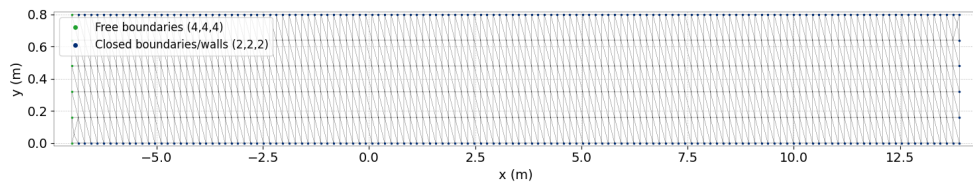


Figure 4.3: Horizontal mesh.

The time step is 0.05 s for a simulated period of 20 s.

To solve the advection, the PSI scheme (scheme 5) is used for the velocities. GMRES is used for solving the propagation step (option 7) and the implicitation coefficients for depth and velocities are let to default values.

#### 4.1.3 Physical parameters

A constant horizontal viscosity for velocity equal to  $0.001 \text{ m}^2/\text{s}$  is chosen.

Wave driven currents are taken into account by chaining TELEMAC-2D with a wave file.

## 4.2 Results

Figure 4.4 shows the free surface elevation at the end of the computation.

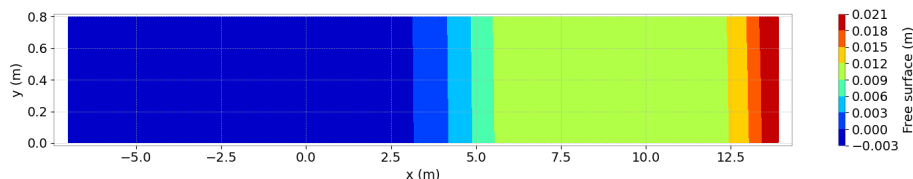


Figure 4.4: Free surface at final time step.

Figure 4.5 shows the free surface elevation evolution during the simulation at point of coordinates (10 ; 0.4).

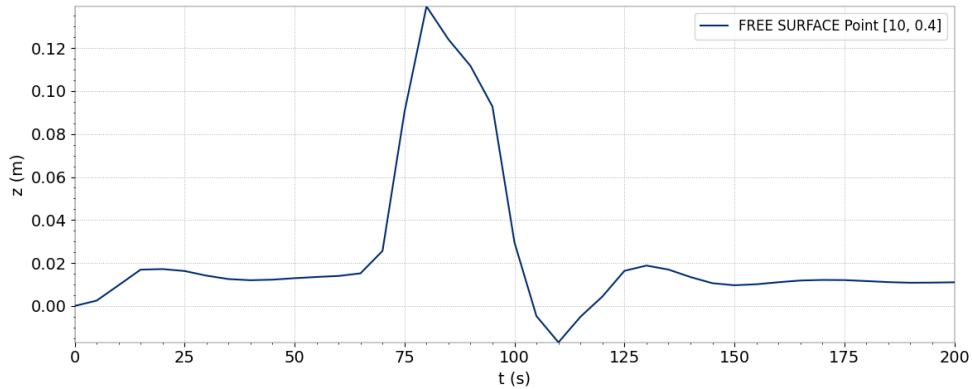


Figure 4.5: Free surface time series at point (10 ; 0.4).

Figure 4.6 shows free surface elevation cross sections along  $x$  for different times.

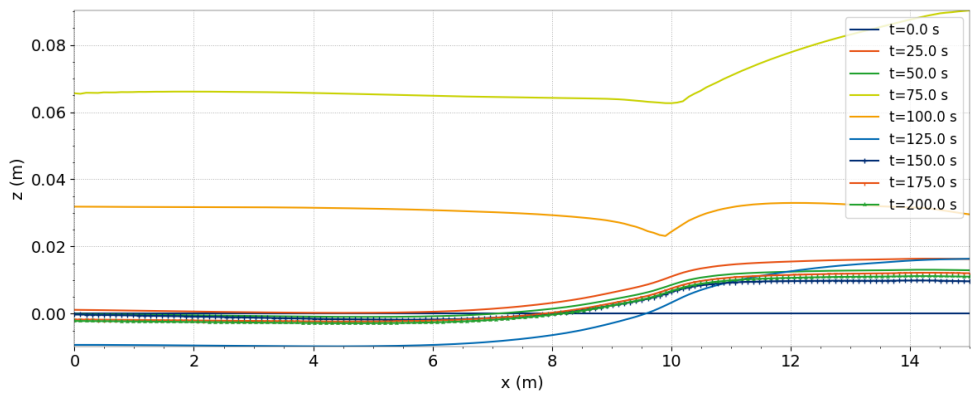


Figure 4.6: Free surface elevation cross section for different times.

### 4.3 Conclusion

TELEMAC-2D can be used to model wave driven currents when chaining with a wave file.

## 5. Breach

### 5.1 Purpose

The aim of this test is to model dykes breaching using different empirical laws and different option for breaching initiation, available in TELEMAC-2D. In particular, the following laws for breach widening are tested:

- Linear widening
- User-defined breach expansion formulations (linear widening in two steps)
- USBR formula (1988)
- Von Thun and Gillette formulas (1990)
- Verheij formula (2002): for sand and clay levees
- Verheij and Van der Knaap (2003) formula: for sand and clay levees
- Froehlich (2008) formula

## 6. Diffraction by semi-infinite breakwater (break)

### 6.1 Purpose

This case models wave diffraction occurring at the point of a semi-infinite breakwater [25]. This process is extremely important as tsunami waves travel a long way and is subject to diffraction around islands, headlands etc., and is subject to refraction wherever there are significant variations of water depth.

### 6.2 Description

This case is the analytical solution for a sinusoidal train of waves travelling north and diffracting around the tip of a semi-infinite breakwater along the positive  $x$ -axis as depicted in Figure 6.1.

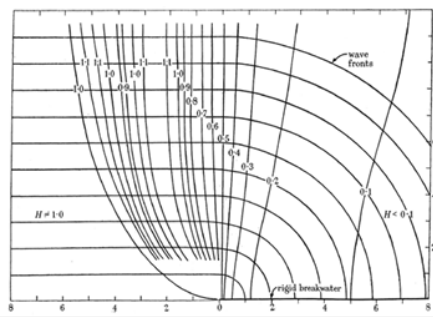


Figure 6.1: Wave fronts and contour lines of maximum wave heights in the lee of a breakwater. Waves are coming from the south.

The water depth is taken uniform so that the wave celerity is constant everywhere. The water depth is also taken sufficiently low that the wave length is greater than 20 times the water depth and so the shallow water wave equations are valid. The wave amplitude is also taken very small so as to minimise nonlinear effects.

#### 6.2.1 Numerical and physical parameters

The TELEMAC-2D flow model is run using the wave equation formulation and no friction or viscosity. The implicitation coefficients are taken as 0.501 (the model is second order accurate if implicitation = 0.5, but on the edge of instability as the scheme is unstable if implicitation < 0.5) and the free surface gradient compatibility is taken as 0.9 (recommended value).

### 6.2.2 Boundary conditions

The incident wave boundary condition (from the south) is taken as an absorbing wave paddle and the open exit boundaries (east, west and north) are all taken as absorbing boundaries using the Thompson boundary condition. The model extends south of the breakwater so that the tip of the breakwater is an internal point of the model grid and the boundary condition on the front and back face of the breakwater is a solid wall (100 % reflection condition).

Figure 6.2 shows the types of boundary conditions.

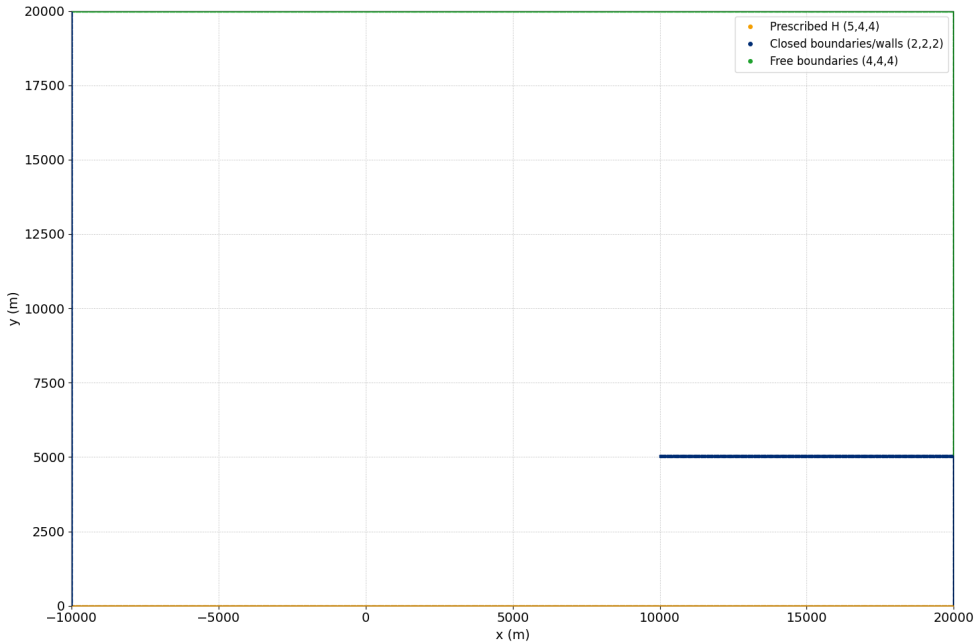


Figure 6.2: Boundary conditions types.

### 6.3 Results

In Figure 6.1 the  $y$  axis shows distance from the breakwater line non-dimensionalised by the wave length. Figure 6.3 shows a comparison between the wave amplitude from the model and the analytical solution along two lines parallel to and behind the breakwater at two and eight wavelengths.

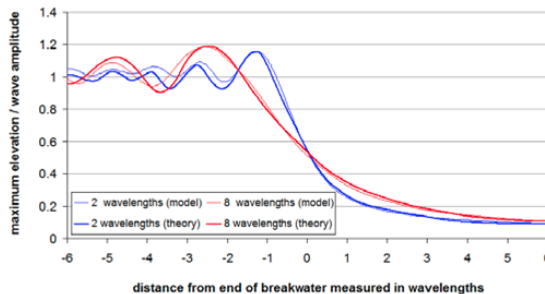


Figure 6.3: Wave amplitude along two lines parallel to and behind the breakwater at 2 and 8 wavelengths. Model (thin lines) and analytical (thick lines) solutions.

Free surface elevation and velocity magnitude at the end of the simulation can be seen in Figures

6.4 and 6.5.

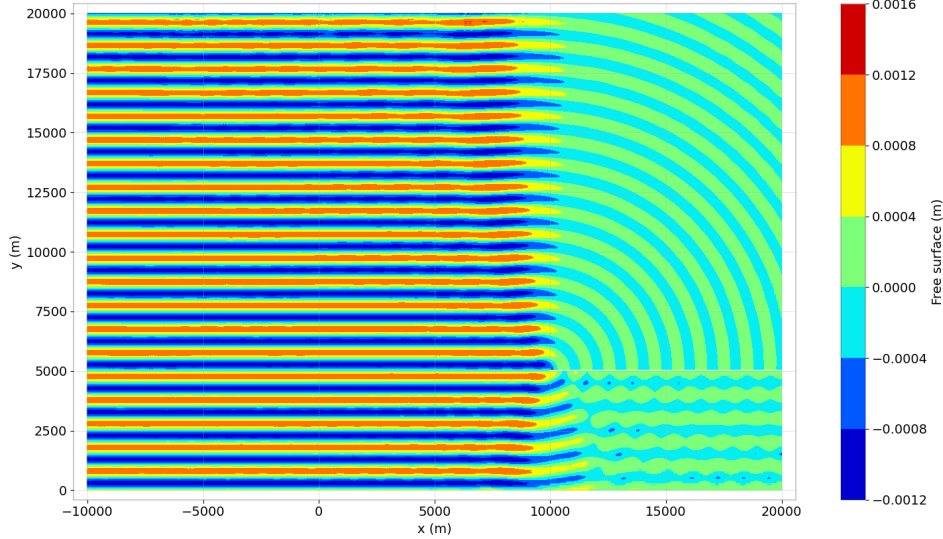


Figure 6.4: Free surface elevation at final time.

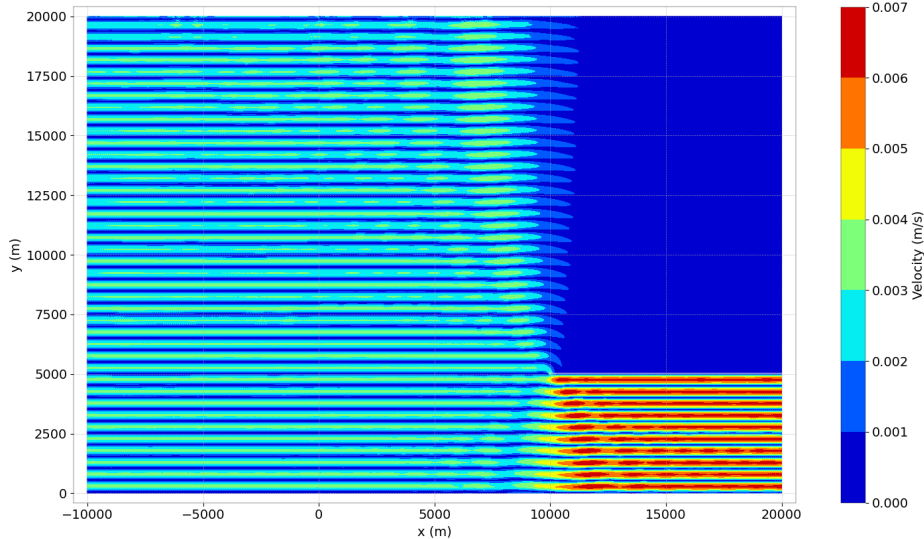


Figure 6.5: Velocity magnitude at final time.

## 6.4 Conclusion

The model gives a good representation of the reduction of the wave amplitude in the lee of the breakwater at two and eight wavelengths from the structure showing the diffraction process. The variation of the wave amplitude not in the lee is reasonable but rather less accurate.

## 7. Bridge

### 7.1 Purpose

This case is not properly saying a validation test case but more an example to demonstrate a possible solution for user to manage bridge in TELEMAC-2D.

### 7.2 Description

In this case, the choice is done to represent the bridge as an obstacle to the flow (like a dike in the river bed) where TELEMAC-2D will compute the overflowing discharge. Nevertheless, as the part of the discharge passing under the bridge is not negligible and also to allow the computation of the full hydrograph, the flow which passes under the bridge is taken in account by an internal singularity, under the form of a couple of source and sink nodes.

#### 7.2.1 Geometry and mesh

A river reach with its major bed of 1,000 m long is crossed by a road in the middle. At the location of the main channel and under the road, there are 2 rectangular tubes of 2.5 m width and 1.5 m height.

The mesh of the main channel and the road is regular ( $10 \times 10$  m). The rest of the mesh is computed without any constraint by Blue Kenue.

- 5,000 triangular elements,
- 2,626 nodes,
- Maximum size range: 16.36 m.

Figure 7.1 shows the mesh of the study.

#### 7.2.2 Boundaries

Lateral:

- Solid walls with slip condition on both lateral parts of the major bed,
- Imposed discharge upstream (left). The discharge varies in time: from 0 m<sup>3</sup>/s at the beginning, it increases to 20 m<sup>3</sup>/s and stays at this value between 100 s and 6,100 s. Then the discharge increases linearly to 120 m<sup>3</sup>/s at 6,600 s and stays at this value between

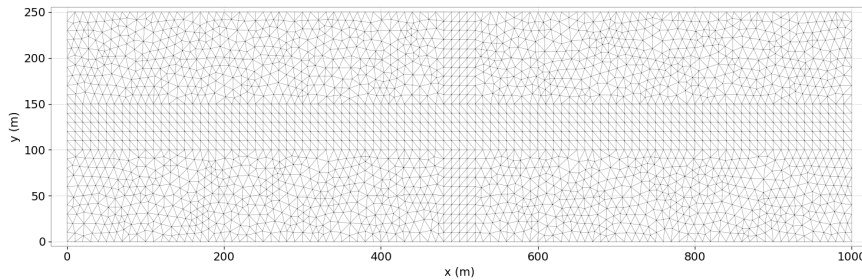


Figure 7.1: Mesh of the study.

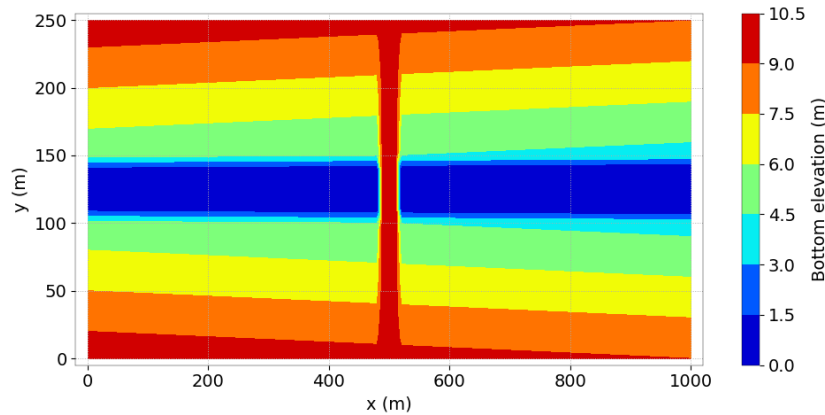


Figure 7.2: Topography of the model.

6,600 s and 17,600 s. After that, the discharge decreases to 20 m<sup>3</sup>/s and stays at this level for the rest of the simulation,

- Imposed water level downstream (right). The value of 3 m is imposed.

Bottom:

- Strickler formula with friction coefficient = 20 m<sup>1/3</sup>/s,
- Regular slope of 1 m along the model (between 1 and 0 for the main channel),
- The bank level is 5 m upstream and the major bed grow regularly from 5 to 10 m.

Figure 7.2 shows the bottom elevation.

### 7.2.3 Physical Parameters

Turbulence: Model of constant viscosity with velocity diffusivity = 1 m<sup>2</sup>/s.

### 7.2.4 Numerical Parameters

Type of advection:

- edge-based N-scheme on velocities (scheme #14,)
- conservative + modified SUPG on depth (mandatory),
- edge-based N-scheme on tracer (scheme #14).

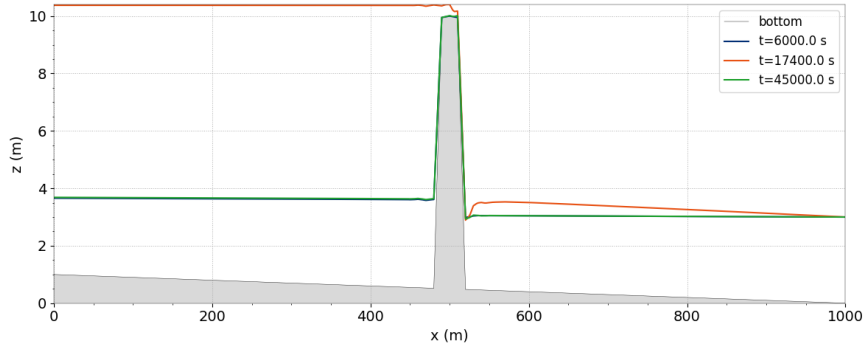


Figure 7.3: Free Surface profile along the channel.

Type of element:

- Linear triangle P1 for  $h$  and velocities.

Solver information:

- Conjugate gradient solver,
- Accuracy =  $10^{-8}$ .

Tracer:

- Initial concentrations : no tracer in the domain,
- Conjugate gradient solver (default value),
- Accuracy =  $10^{-10}$ .

Time data:

- Time step = 1 s.
- Simulation duration = 45,000 s.

### 7.3 Results

Figure 7.3 illustrates the results on a longitudinal profile located in the middle of the main channel at 3 significant time-steps

During the first part of the simulation (before 6,100 s), the flow stays in the minor bed as the culverts have sufficient capacities. Velocities are regular except locally at the location of culvert extremities. The tracer tends to an equilibrium in all the minor bed (see Figure 7.4).

With the increase of the discharge, the culverts reach a saturation and then the level upstream increases until the overflow appears and a new equilibrium exists. This is illustrated by results at 17,400 s (see Figure 7.5).

When the discharge decreases, there is a progressive diminution of the water lever upstream the dike. The simulation recover an equilibrium similar to the first one observed (see Figure 7.6).

### 7.4 Conclusions

Bridge in TELEMAC-2D could be taken in account by the combination of a local dike (which allows to represent the overflowing part) and some hydraulic structures which link the upstream and downstream of the dike.

**7.5 Figures**

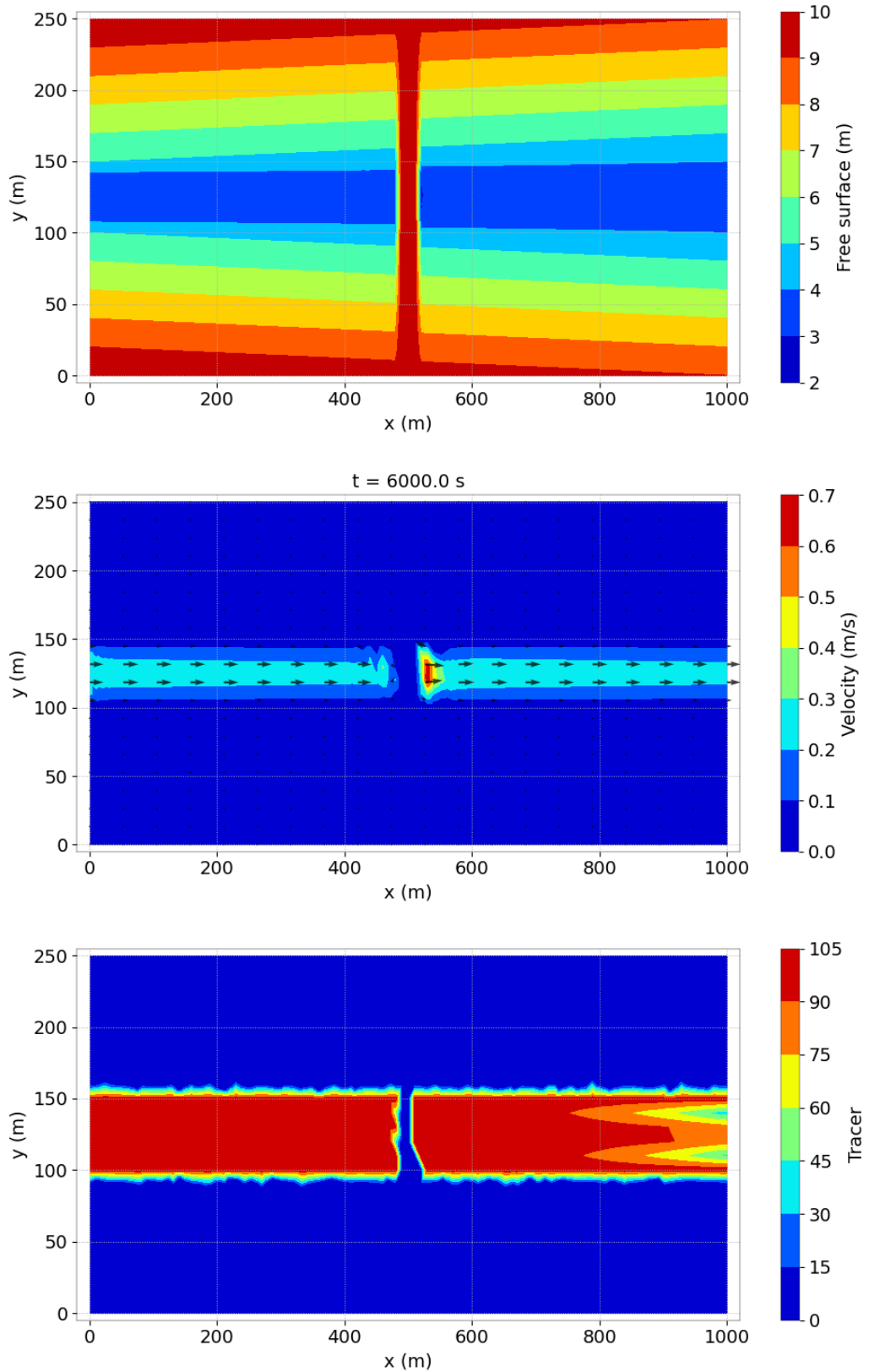


Figure 7.4: Map of the free surface elevation, the velocity and the tracer at  $t = 6,000$  s.

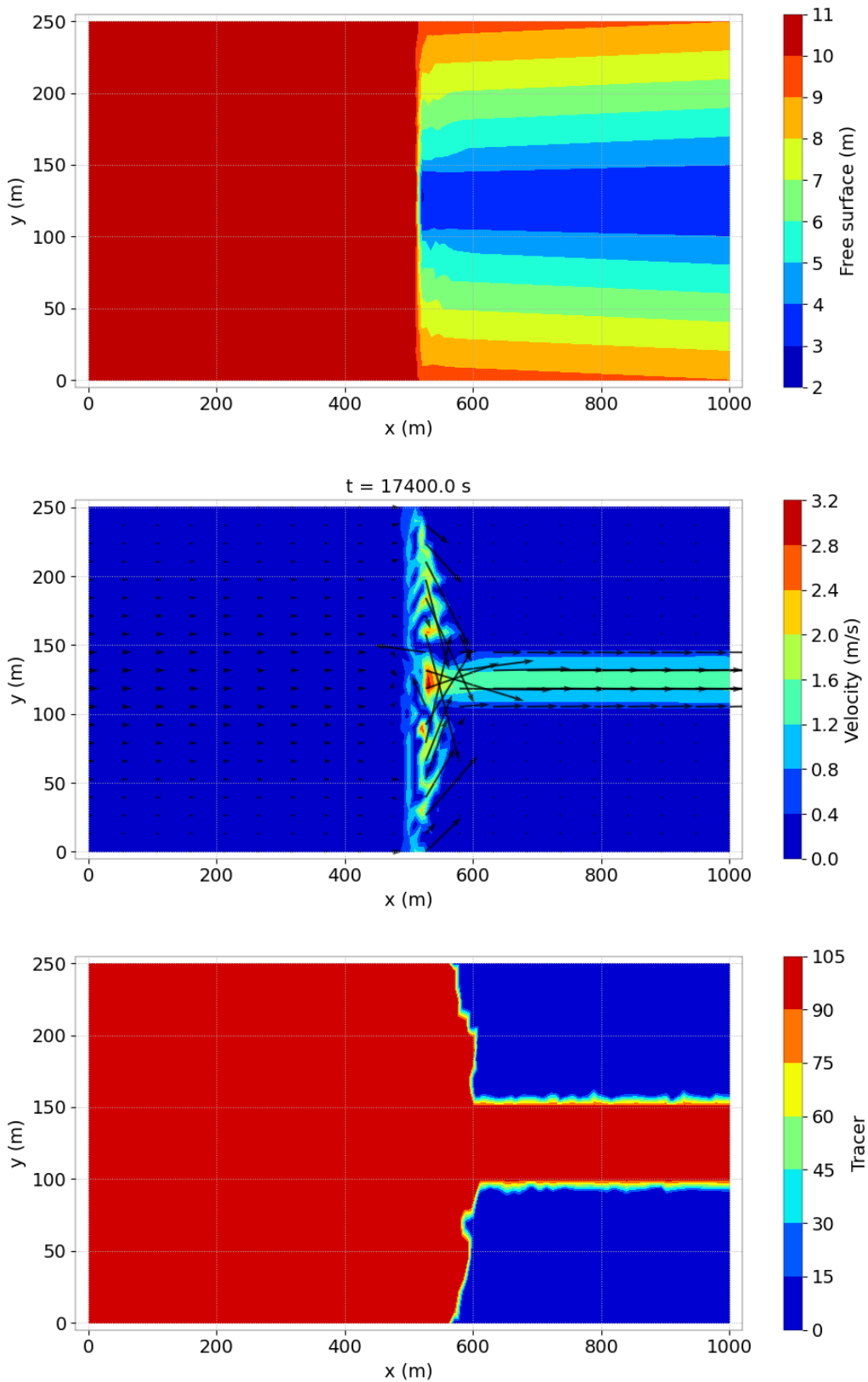


Figure 7.5: Map of the free surface elevation, the velocity and the tracer at  $t = 17,400$  s.

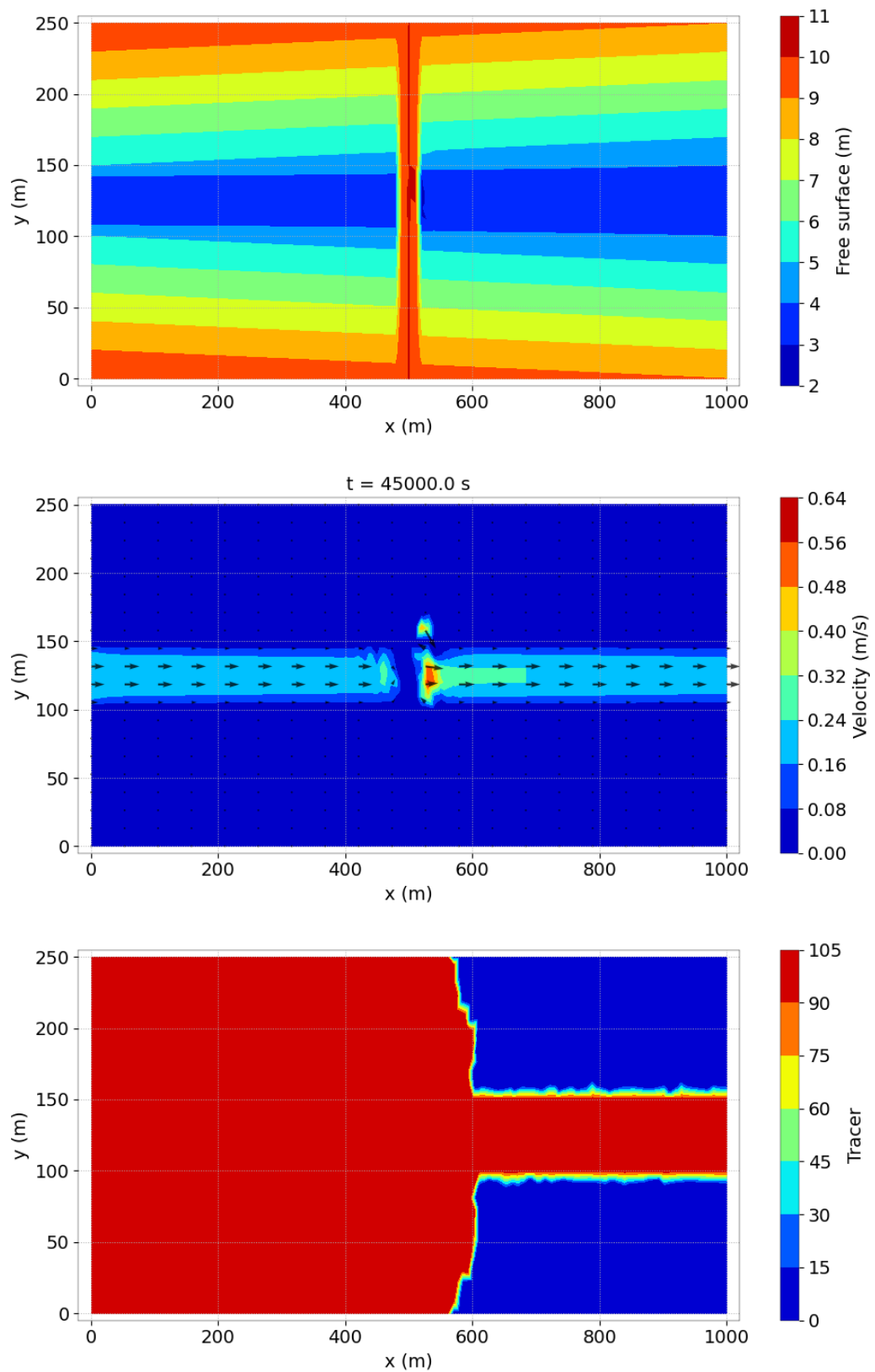


Figure 7.6: Map of the free surface elevation, the velocity and the tracer at  $t = 45,000$  s.

## 8. Flow over a bump (bump)

### 8.1 Purpose

This test case presents a flow over a bump on the bed with subcritical condition. It allows to show that TELEMAC-2D is able to correctly reproduce the hydrodynamic impact of a changing bed slopes, vertical flow contractions and expansions. Furthermore, it allows to have a good representation of flows computed in steady and transient flow regimes.

The solution produced by TELEMAC-2D in a frictionless channel presenting an idealised bump on the bottom is compared with the analytical solution to this problem. In this test case, all flow regimes i.e. subcritical, critical and transcritical are studied.

### 8.2 Description

#### 8.2.1 Analytical solution

From the strict hyperbolicity of the shallow water system, the flow over the bump can be characterized by a criticality condition. Depending on the value of the Froude number, the flow can either be subcritical (fluvial,  $Fr < 1$ ) or supercritical (torrential,  $Fr > 1$ ). Let us recall the definition of the Froude number:

$$Fr = \frac{|\mathbf{u}|}{\sqrt{gh}} \quad (8.1)$$

where  $|\mathbf{u}|$  is the norm of the depth averaged velocity and  $g$  is the gravitational acceleration. Another useful quantity in the case of a constant discharge  $q$  is the critical height defined by:

$$h_c = \left( \frac{q}{\sqrt{g}} \right)^{2/3} \quad (8.2)$$

The flow can either be subcritical if  $h > h_c$  or supercritical if  $h < h_c$ . In the case of a frictionless channel with a constant discharge  $q_0$ , the Bernoulli relation allows to express the water height in the channel at abscissa  $x$  by the relation:

$$\frac{q_0^2}{2gh(x)^2} + h(x) + z_b(x) = cst \quad (8.3)$$

with  $z_b$  the bottom elevation. Let us consider a channel of length  $L$ . From the Bernoulli relation, one can express the water depth as a solution of third degree equation, which depends on the the flow criticality:

- **Subcritical flow:**

$$h(x)^3 + \left( z_b(x) - \frac{q_0^2}{2gh(L)^2} - h(L) \right) h(x)^2 + \frac{q_0^2}{2g} = 0 \quad \forall x \in [0, L] \quad (8.4)$$

- **Critical flow:**

$$h(x)^3 + \left( z_b(x) - \frac{q_0^2}{2gh_c^2} - h_c - z_M \right) h(x)^2 + \frac{q_0^2}{2g} = 0 \quad \forall x \in [0, L] \quad (8.5)$$

with  $z_M = \max_{x \in [0, L]} z_b$ .

- **Transcritical flow:**

$$\begin{cases} h(x)^3 + \left( z_b(x) - \frac{q_0^2}{2gh_c^2} - h_c - z_M \right) h(x)^2 + \frac{q_0^2}{2g} = 0 & \text{for } x < x_{\text{shock}} \\ h(x)^3 + \left( z_b(x) - \frac{q_0^2}{2gh(L)^2} - h(L) \right) h(x)^2 + \frac{q_0^2}{2g} = 0 & \text{for } x > x_{\text{shock}} \\ q_0^2 \left( \frac{1}{h(x_{\text{shock}}^-)} - \frac{1}{h(x_{\text{shock}}^+)} \right) + \frac{g}{2} (h(x_{\text{shock}}^-)^2 - h(x_{\text{shock}}^+)^2) = 0 \end{cases} \quad (8.6)$$

### 8.2.2 Geometry and mesh

The geometry dimensions of the channel are 2 m wide and 20 m long. The mesh is regular along the channel. It is made up with quadrangles split into two triangles. It is composed of 1,280 triangular elements (729 nodes) and the size of triangles is about 0.25 m (see Figure 8.1).

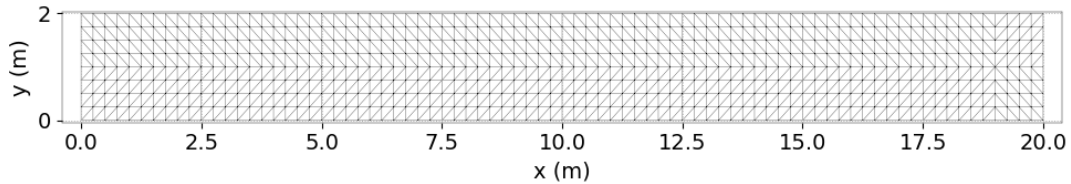


Figure 8.1: Mesh of the channel.

### 8.2.3 Bathymetry

The maximum elevation of the bump is 0.25 m (see Figure 8.2) with the bottom  $z_b$  described by the following equation:

$$z_b = 0.25 \exp\left(\frac{-(x-10)^2}{2}\right)$$

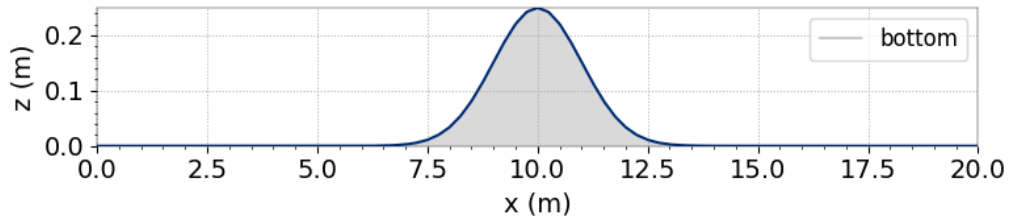


Figure 8.2: Bathymetry in the channel.

### 8.2.4 Initial and boundary conditions

The initial conditions are defined with analytical solution for both velocity and water depth to quickly achieve the steady state. The boundary conditions are defined as follows:

- **Subcritical flow:** At the channel entrance, the flow rate is  $Q = 1.5 \text{ m}^3\text{s}^{-1}$  (note that the discharge per unit length  $q_0 = Q/B$ ,  $B$  being the channel width). The flow rate  $Q$  is taken so that the  $q_0$  value is equal to the value  $\sqrt{gh}$  at the entrance. At the channel outlet, the free surface elevation is  $z_s = 0.8 \text{ m}$ .

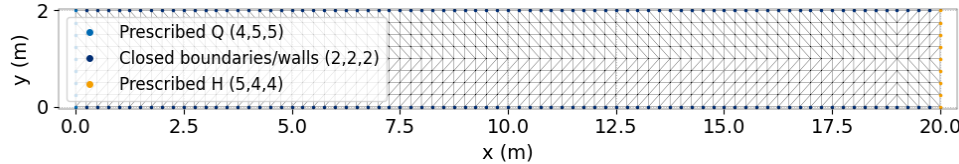


Figure 8.3: Boundary condition type for the subcritical case.

- **Critical flow:** At the channel entrance, the flow rate is  $Q = 0.3 \text{ m}^3\text{s}^{-1}$ . At the channel outlet, free velocity and free water level are imposed on the liquid boundary.

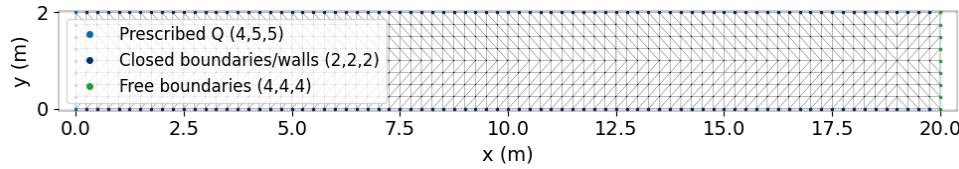


Figure 8.4: Boundary condition type for the critical case.

- **Transcritical flow:** At the channel entrance, the flow rate is  $Q = 0.45 \text{ m}^3\text{s}^{-1}$ . At the channel outlet, the free surface elevation is  $z_s = 0.35 \text{ m}$ .

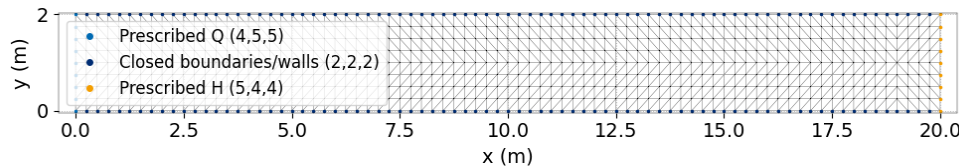


Figure 8.5: Boundary condition type for the transcritical case.

### 8.2.5 Physical parameters

No friction is taken into account on the bottom and on the lateral walls. Note that the horizontal viscosity turbulent is constant and equal to zero for all cases. However instead of prescribing a zero viscosity, no diffusion step could have been used (keyword DIFFUSION OF VELOCITY = NO).

### 8.2.6 Numerical parameters

TELEMAC-2D is run forward in time until a steady state flow is obtained. Several numerical schemes are tested. The parameters specific to each case are summed up in the Tables 8.1, 8.2, 8.3.

### Subcritical flow

| Case | Name | Equations       | Advection scheme for velocities | Time step / Desired Courant number |
|------|------|-----------------|---------------------------------|------------------------------------|
| 1    | CHAR | Wave Eq. FE     | Characteristics                 | 0.02 s / -                         |
| 2    | N    | Wave Eq. FE     | N-scheme                        | 0.02 s / -                         |
| 3    | PSI  | Wave Eq. FE     | PSI scheme                      | 0.02 s / -                         |
| 4    | LIPS | Wave Eq. FE     | PSI LIPS scheme                 | 0.02 s / -                         |
| 5    | NERD | Wave Eq. FE     | Edge based N-scheme             | 0.02 s / -                         |
| 6    | ERIA | Wave Eq. FE     | ERIA scheme                     | 0.02 s / -                         |
| 7    | ROE  | Saint-Venant FV | ROE order 1                     | - / 0.9                            |
| 8    | KIN1 | Saint-Venant FV | Kinetic order 1                 | - / 0.9                            |
| 9    | KIN2 | Saint-Venant FV | Kinetic order 2                 | - / 0.9                            |
| 10   | HLLC | Saint-Venant FV | HLLC order 1                    | - / 0.9                            |

Table 8.1: List of the simulation parameters used for the cases tested in the subcritical bump example.

### Critical flow

| Case | Name | Equations       | Advection scheme for velocities | Time step / Desired Courant number |
|------|------|-----------------|---------------------------------|------------------------------------|
| 1    | CHAR | Wave Eq. FE     | Characteristics                 | 0.02 s / -                         |
| 2    | N    | Wave Eq. FE     | N-scheme                        | 0.02 s / -                         |
| 3    | PSI  | Wave Eq. FE     | PSI scheme                      | 0.02 s / -                         |
| 4    | LIPS | Wave Eq. FE     | PSI LIPS scheme                 | 0.02 s / -                         |
| 5    | NERD | Wave Eq. FE     | Edge based N-scheme             | 0.005 s / -                        |
| 6    | ERIA | Wave Eq. FE     | ERIA scheme                     | 0.005 s / -                        |
| 7    | ROE  | Saint-Venant FV | ROE order 1                     | - / 0.9                            |
| 8    | KIN1 | Saint-Venant FV | Kinetic order 1                 | - / 0.9                            |
| 9    | KIN2 | Saint-Venant FV | Kinetic order 2                 | - / 0.9                            |
| 10   | HLLC | Saint-Venant FV | HLLC order 1                    | - / 0.9                            |

Table 8.2: List of the simulation parameters used for the cases tested in the critical bump example.

### Transcritical flow

| Case | Name | Equations       | Advection scheme for velocities | Time step / Desired Courant number |
|------|------|-----------------|---------------------------------|------------------------------------|
| 1    | CHAR | Wave Eq. FE     | Characteristics                 | 0.8 s / -                          |
| 2    | N    | Wave Eq. FE     | N-scheme                        | 0.7 s / -                          |
| 3    | PSI  | Wave Eq. FE     | PSI scheme                      | 0.7 s / -                          |
| 4    | LIPS | Wave Eq. FE     | PSI LIPS scheme                 | 0.7 s / -                          |
| 5    | NERD | Wave Eq. FE     | Edge based N-scheme             | 0.7 s / -                          |
| 6    | ERIA | Wave Eq. FE     | ERIA scheme                     | 0.7 s / -                          |
| 7    | ROE  | Saint-Venant FV | ROE order 1                     | - / 0.9                            |
| 8    | KIN1 | Saint-Venant FV | Kinetic order 1                 | - / 0.9                            |
| 9    | KIN2 | Saint-Venant FV | Kinetic order 2                 | - / 0.9                            |
| 10   | HLLC | Saint-Venant FV | HLLC order 1                    | - / 0.9                            |

Table 8.3: List of the simulation parameters used for the cases tested in the transcritical bump example.

## 8.3 Results

### 8.3.1 Computation time

Simulation times for each of these cases with sequential and parallel runs (using 4 processors) are shown in Figure 8.6.

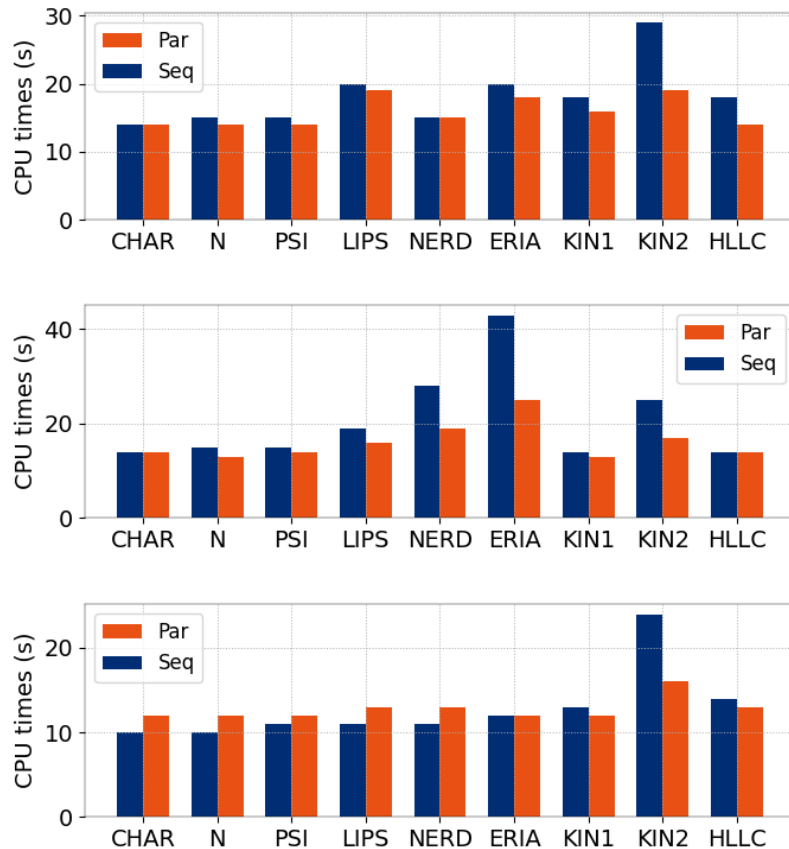


Figure 8.6: CPU times for subcritical, critical and transcritical flow with shock (from top to bottom).

### 8.3.2 First observation

In this test case, the numerical results are compared with the analytical solution, when the state flow is steady. Furthermore, the computed Froude number ( $Fr$ ) is also compared with the analytical solution. The solution produced by TELEMAC-2D is in close agreement with the analytical solution as shown in Figure 8.7.

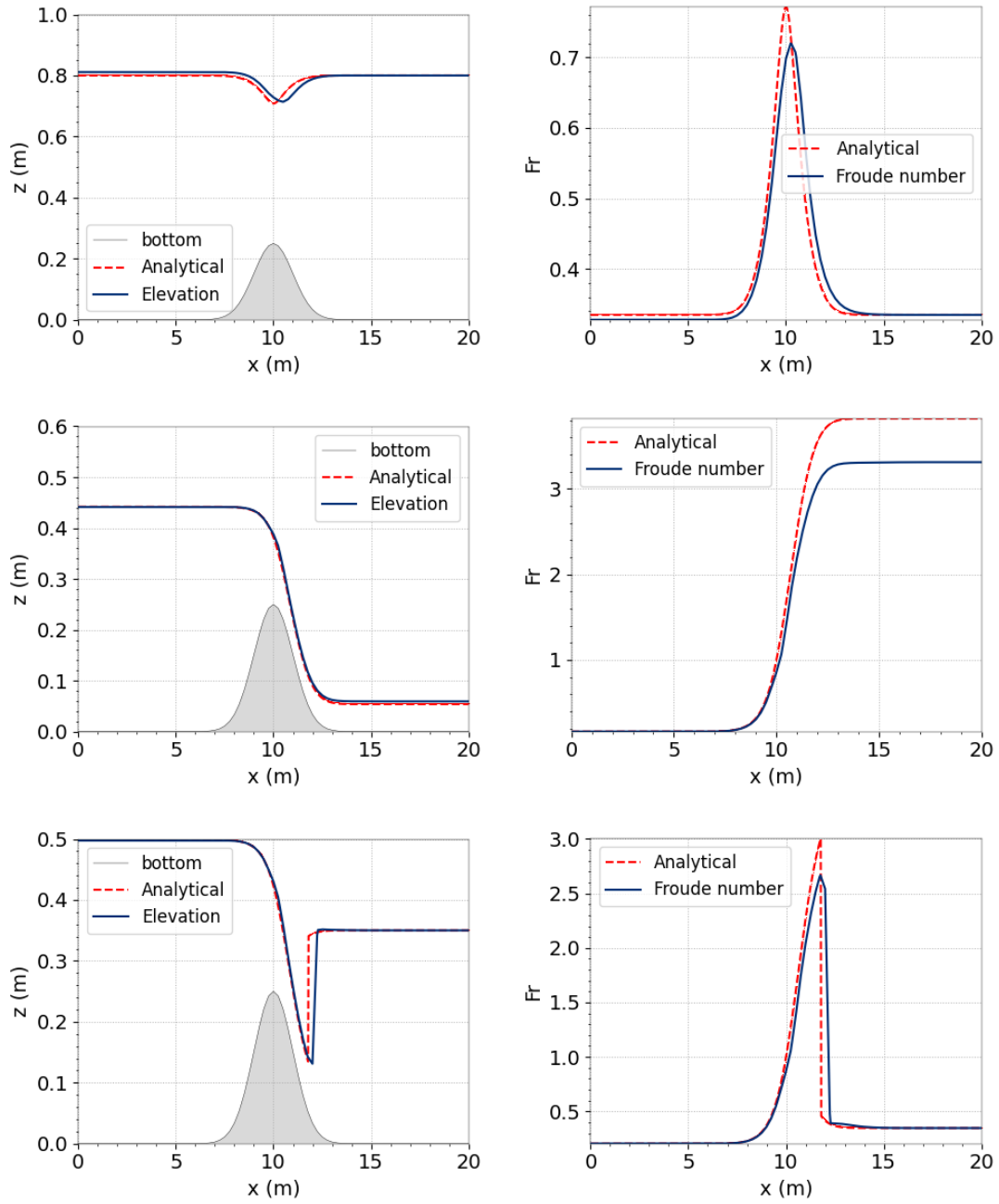


Figure 8.7: Comparison between analytical solution and TELEMAC-2D HLLC solution for subcritical, critical and transcritical flow with shock (from top to bottom).

### 8.3.3 Comparison of schemes

In Figure 8.8, results obtained with different numerical schemes are compared to the analytical solution at final time. For both critical and transcritical cases, numerical oscillations are visible for some schemes.

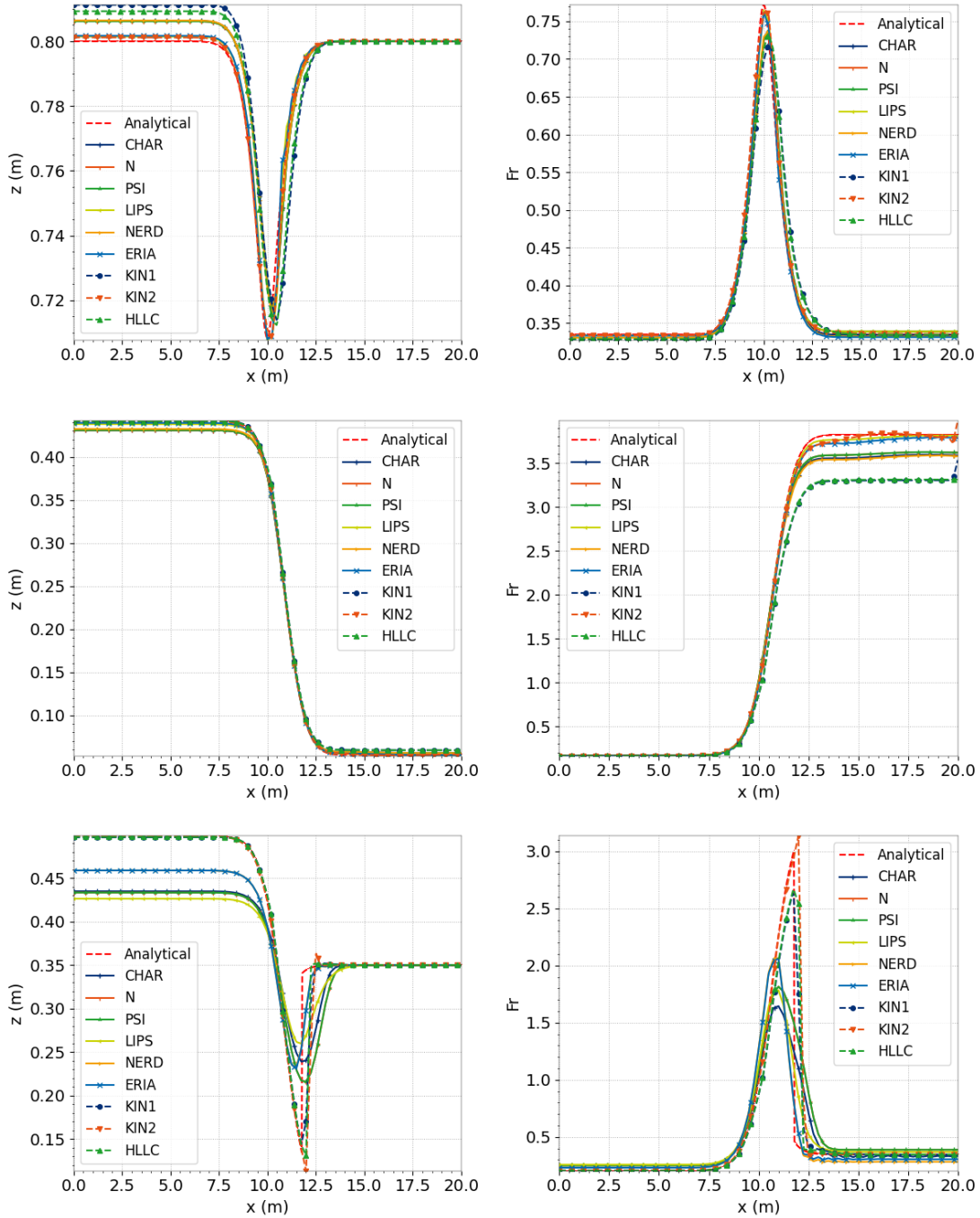


Figure 8.8: Comparison between analytical solution and various TELEMAC-2D numerical schemes for subcritical, critical and transcritical flow with shock (from top to bottom).

### 8.3.4 Accuracy

For a more quantitative comparison of schemes, the  $L^1$ ,  $L^2$  and  $L^\infty$  error norms of the water depth and velocity are calculated at final time. Results are presented in Figure 8.9.

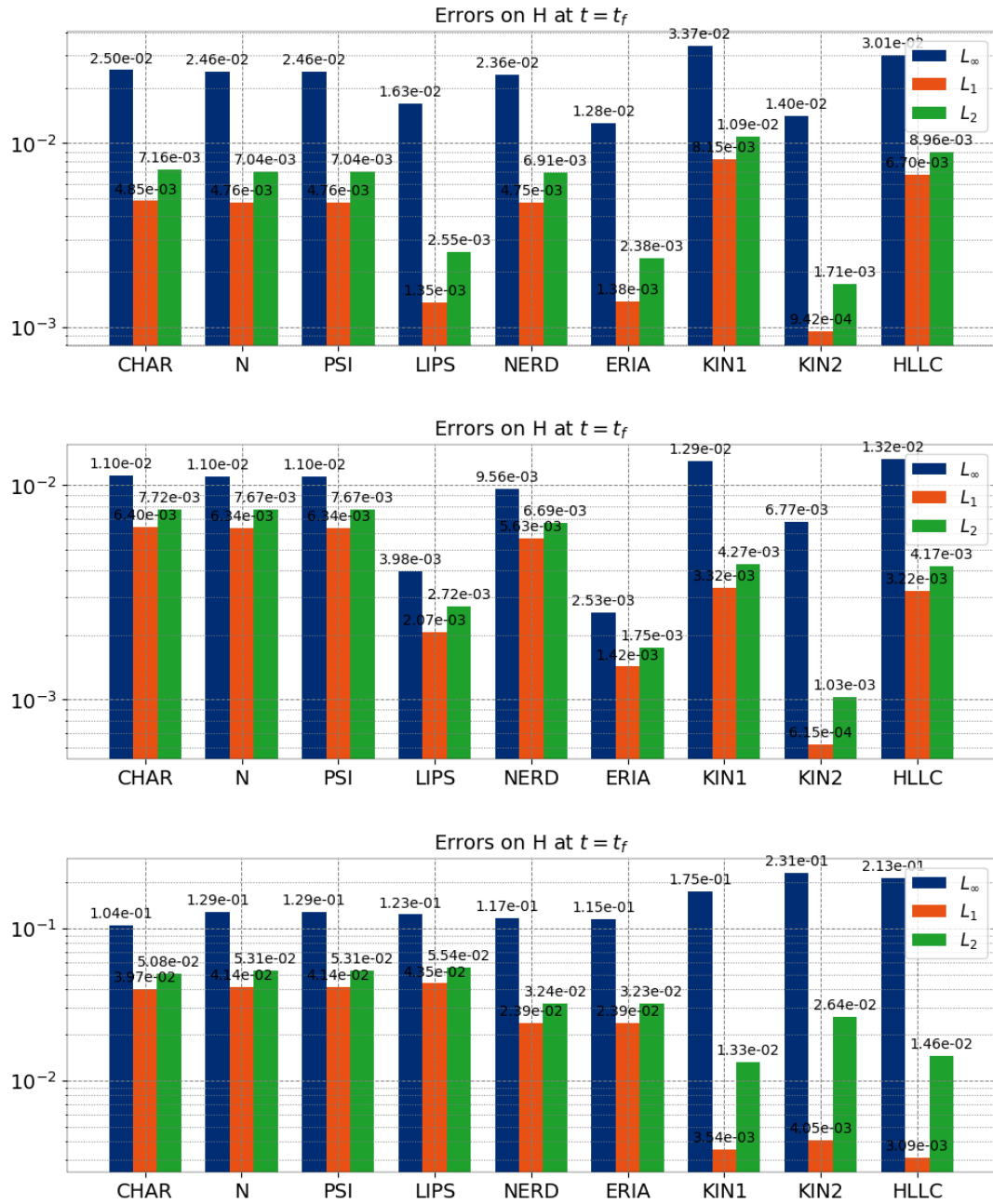


Figure 8.9: Errors at final time for subcritical, critical, transcritical (from top to bottom).

### 8.3.5 Convergence in the subcritical case

In this section, a mesh convergence is carried out for each numerical scheme on the subcritical test case. From a starting mesh with 160 elements, we divide by 4 each triangle recursively to generate new meshes. Meshes used in the convergence study are presented in Figure 8.10. Final time is set to  $t_f = 2$  min. With decreasing space step, we adjust time step to ensure a constant CFL for each mesh increment.

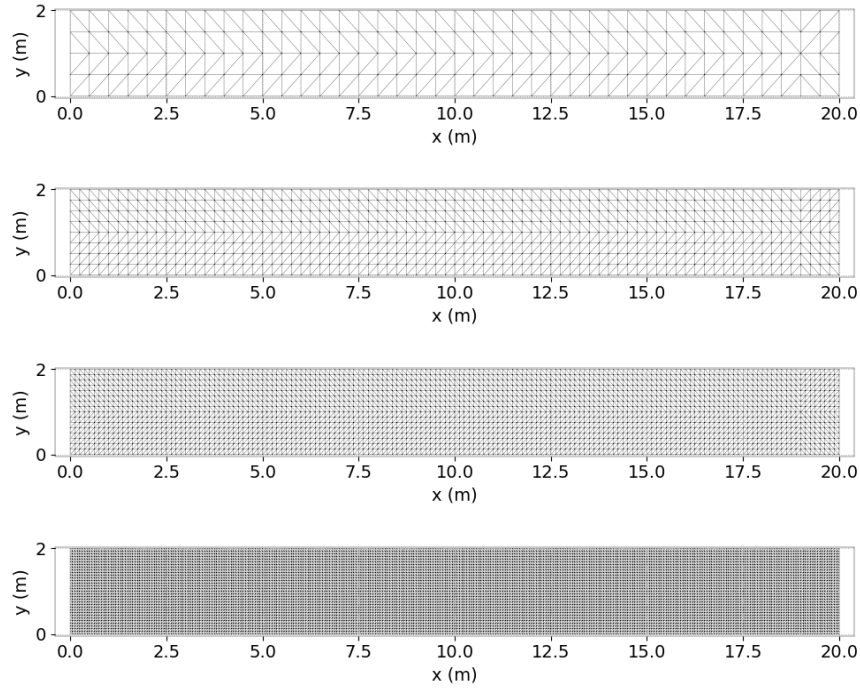


Figure 8.10: Meshes used in bump mesh convergence.

Errors in  $L^2$  norm for water depth are presented as functions of mesh discretization in Figure 8.11. In Figure 8.14, errors on H at final time and on the finest mesh are compared. On the next pages, convergence results are presented in  $L^1$ ,  $L^2$  and  $L^\infty$  norms for both water depth and velocity.

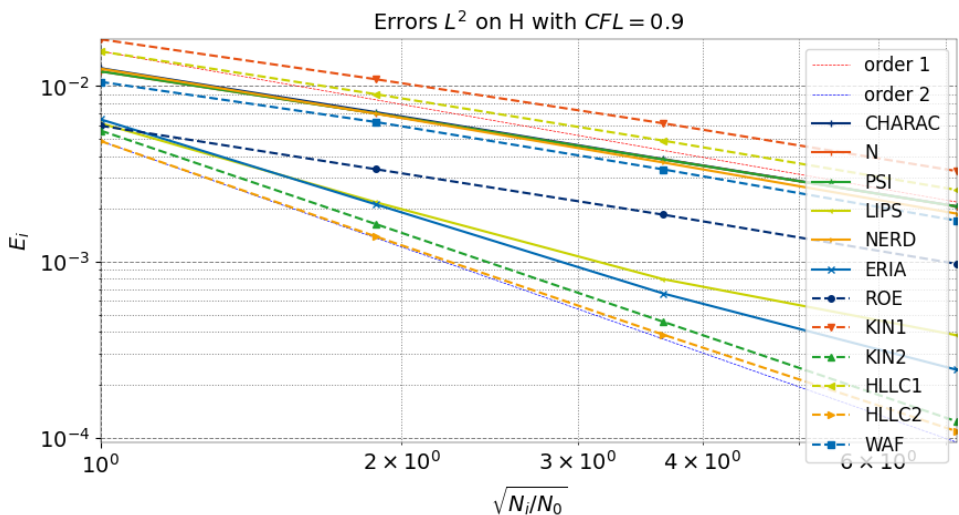


Figure 8.11: H convergence in  $L^2$  norm.

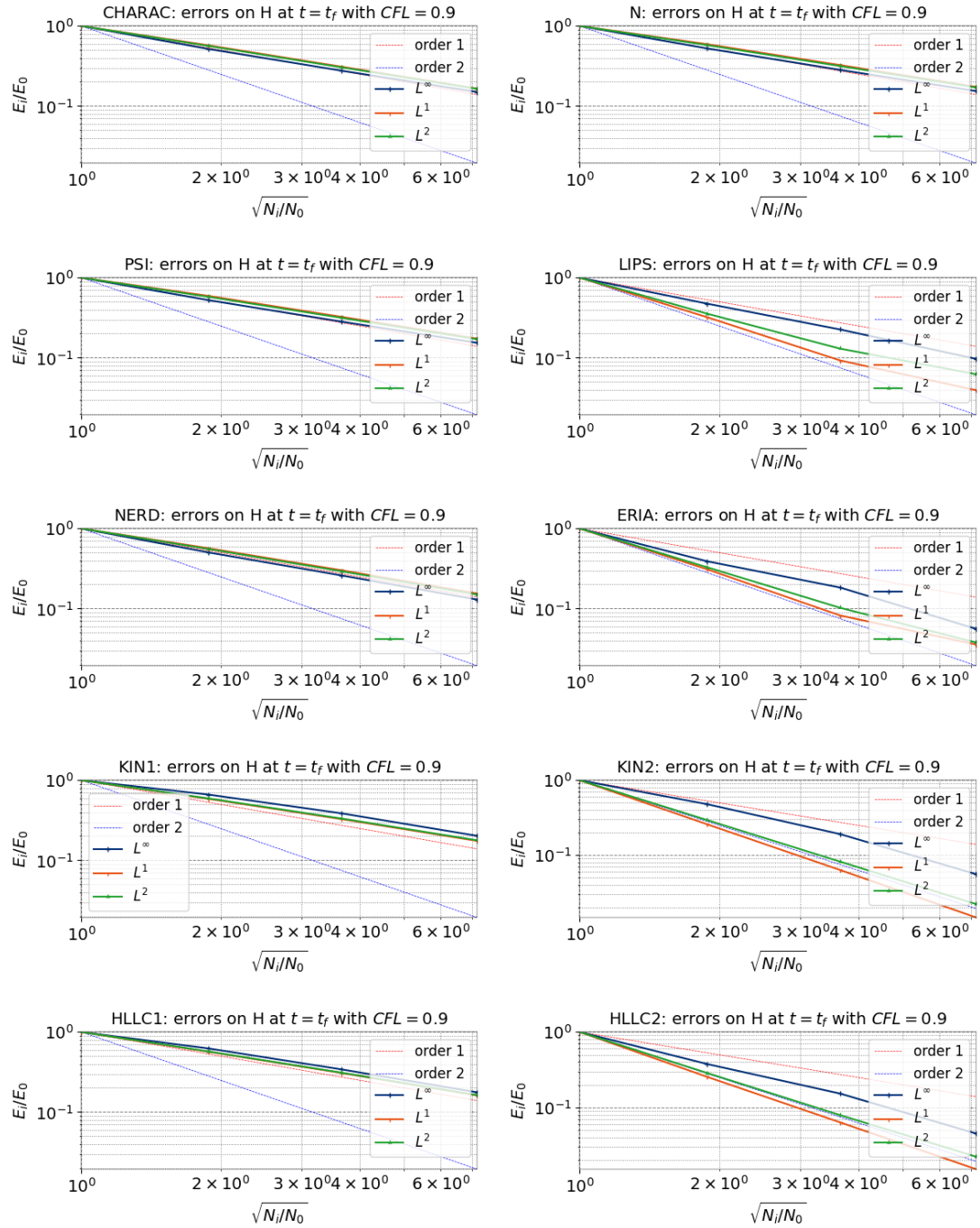


Figure 8.12: H convergence with different numerical schemes.

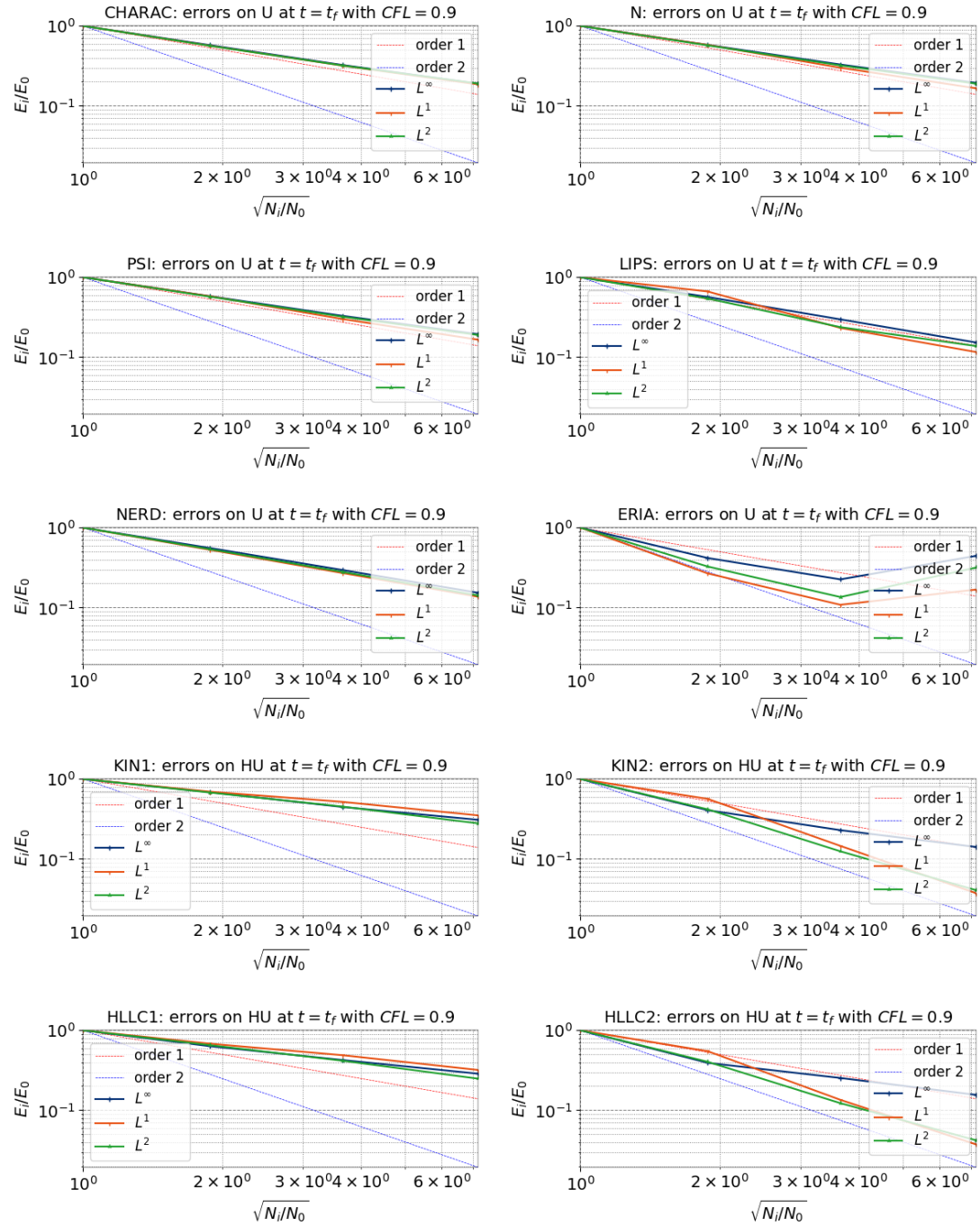


Figure 8.13: U convergence with different numerical schemes.

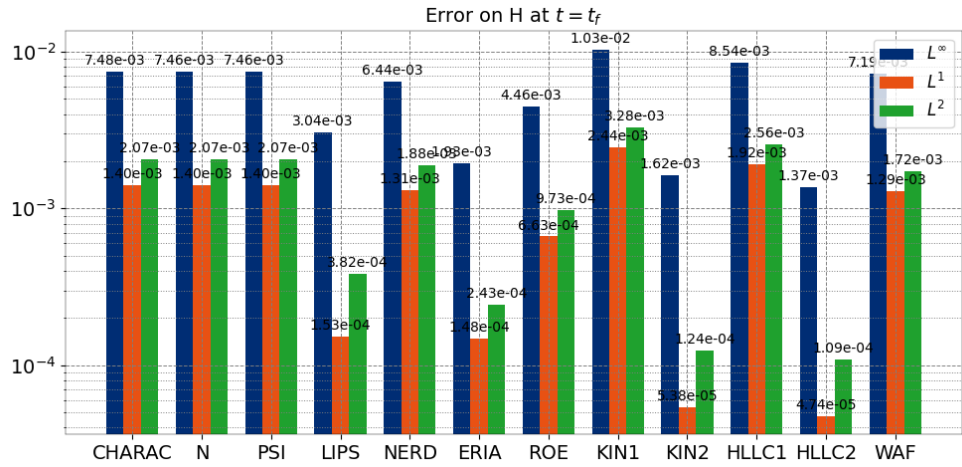
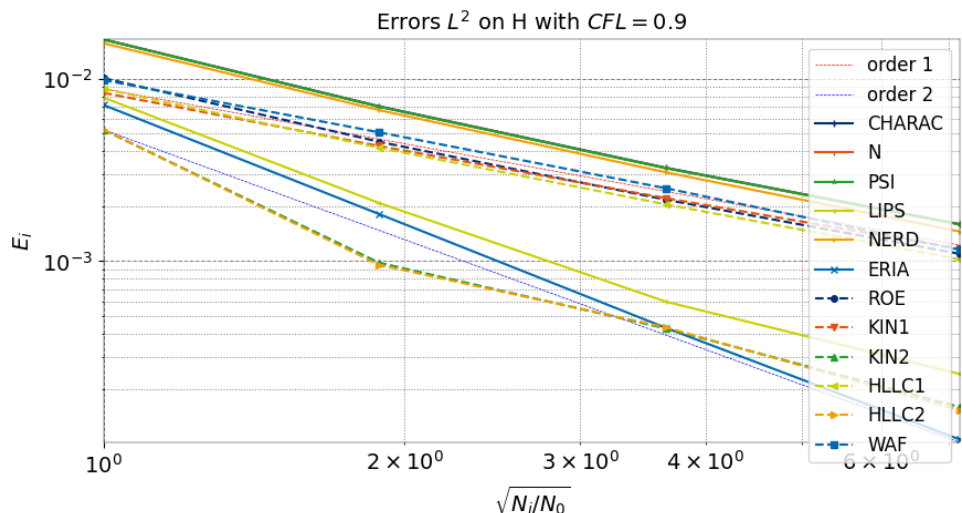


Figure 8.14: H errors on the finest mesh.

### 8.3.6 Convergence in the critical case

The same convergence study is carried out for the critical test case. Convergence of water depth in  $L^2$  norm for different numerical schemes are presented in Figure 8.15. On the next pages, convergence results for both velocity and water depth are presented in  $L^1$ ,  $L^2$  and  $L^\infty$  norms. Finally, errors at final time on the finest mesh are presented in Figure 8.18.

Figure 8.15: H convergence in  $L^2$  norm.

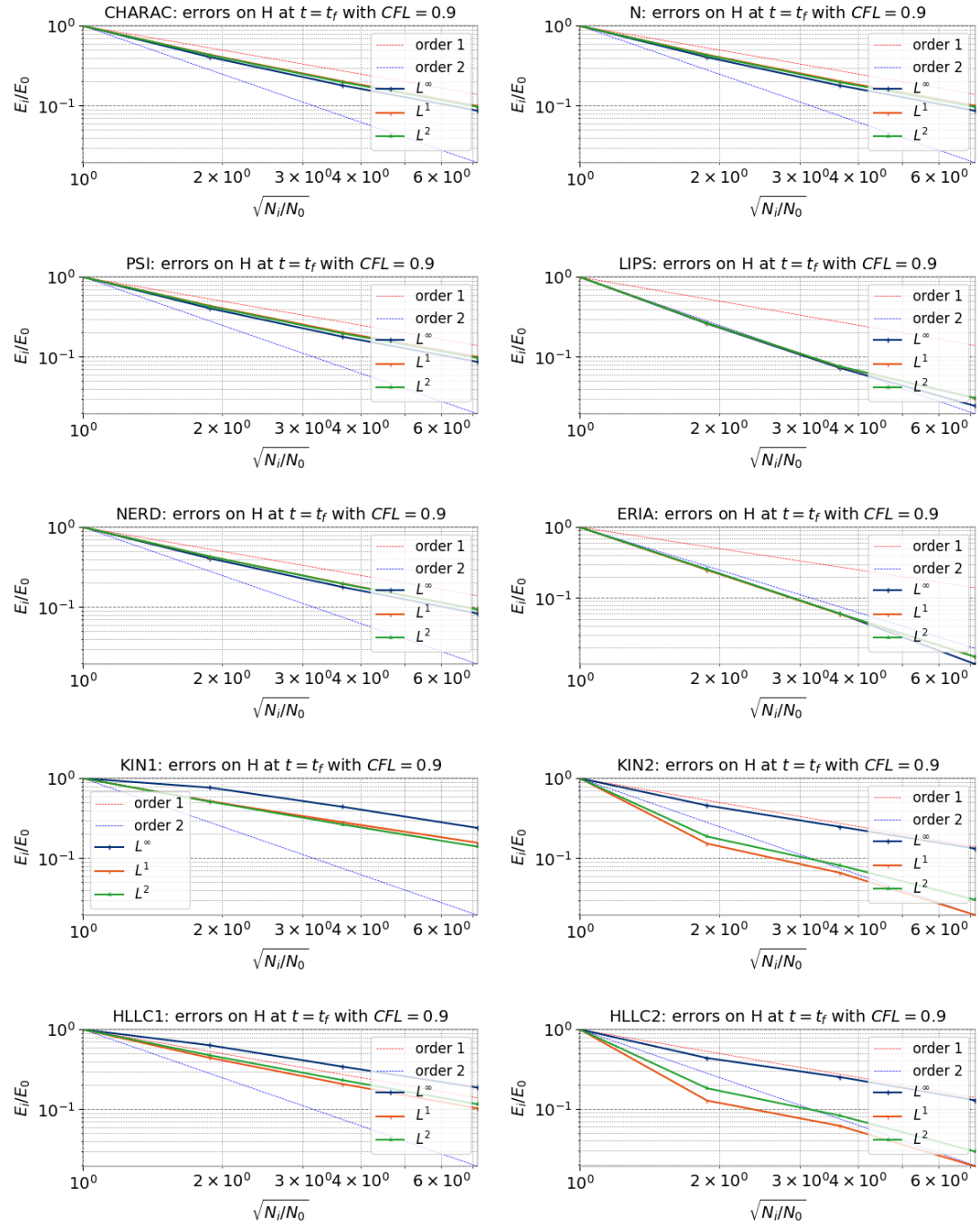


Figure 8.16: H convergence with different numerical schemes.

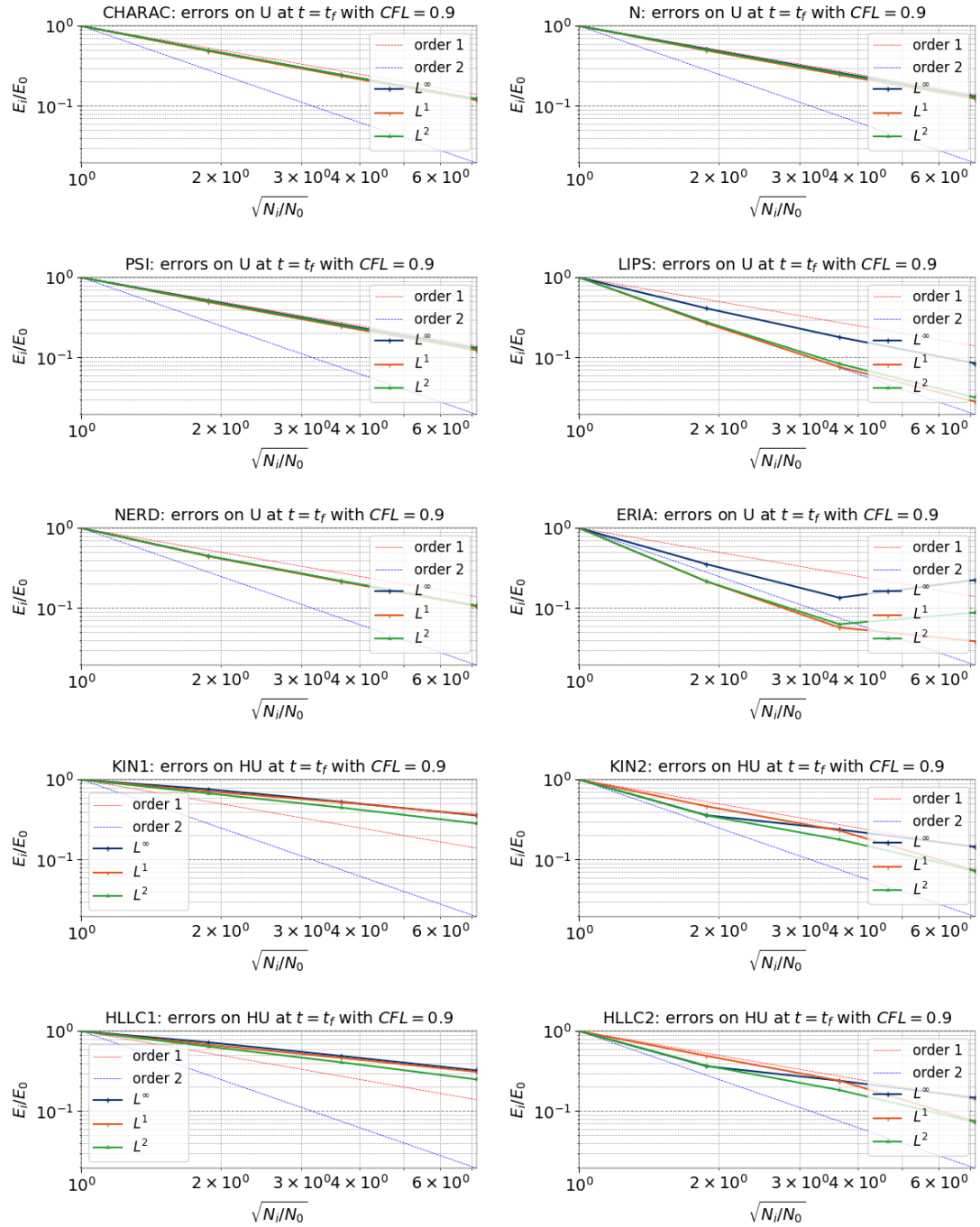


Figure 8.17: U convergence with different numerical schemes.

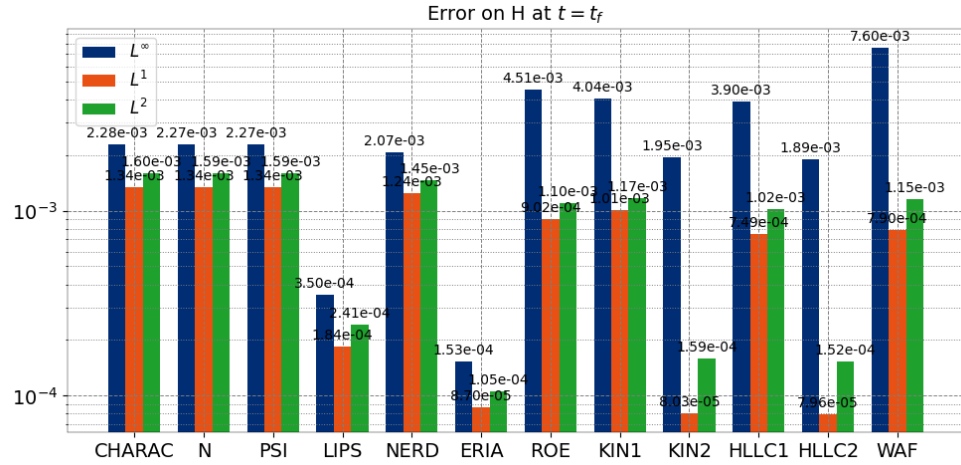


Figure 8.18: H errors on the finest mesh.

## 8.4 Conclusion

To conclude, this type of channel flow is adequately reproduced by TELEMAC-2D in either subcritical, transcritical or critical flow regimes.

## 9. Flow driven by a stage-discharge curve (canal)

### 9.1 Description

This example checks that TELEMAC-2D is able to deal with stage-discharge curves.

The chosen configuration is the same as the TELEMAC-3D example canal. This is a straight channel 500 m long and 100 m wide with a flat horizontal bottom without slope. Three different cases are studied:

- An initial computation with prescribed elevation at the exit and prescribed discharge at the entrance,
- A computation with prescribed discharge at the entrance and prescribed elevation using a stage-discharge curve  $Z = f(Q)$ ,
- A computation with prescribed elevation at the entrance and prescribed discharge using a stage-discharge curve  $Q = f(Z)$ .

In all cases, the flow establishes a steady flow where the free surface is influenced by the friction on the bottom.

#### 9.1.1 Initial and boundary conditions

The first computation is initialised with a constant elevation equal to 0.5 m and no velocity. The two last computations are initialised by a steady flow, the one computed by the first computation. See Figures 9.1 and 9.2.

The boundary conditions are:

- For the solid walls, a slip condition on channel banks is used for the velocities,
- On the bottom, Strickler law with friction coefficient equal to  $50 \text{ m}^{1/3} \cdot \text{s}^{-1}$  is prescribed,
- Upstream a flowrate equal to  $50 \text{ m}^3 \cdot \text{s}^{-1}$  is prescribed for the first and second computations. For the third computation, a flowrate is also prescribed but by giving a stage-discharge curve  $Q = f(Z)$ ,
- Downstream the water level is equal to 0.5 m for the first and third computations. For the second computation, elevation is also prescribed but by giving a stage-discharge curve  $Z = f(Q)$ .

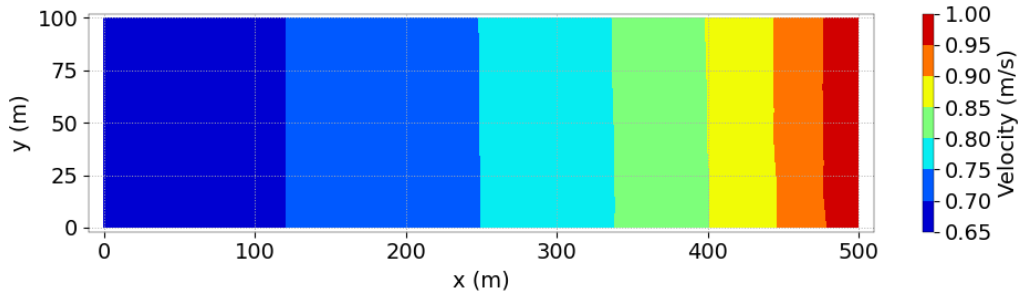


Figure 9.1: Horizontal velocity obtained at the steady state.

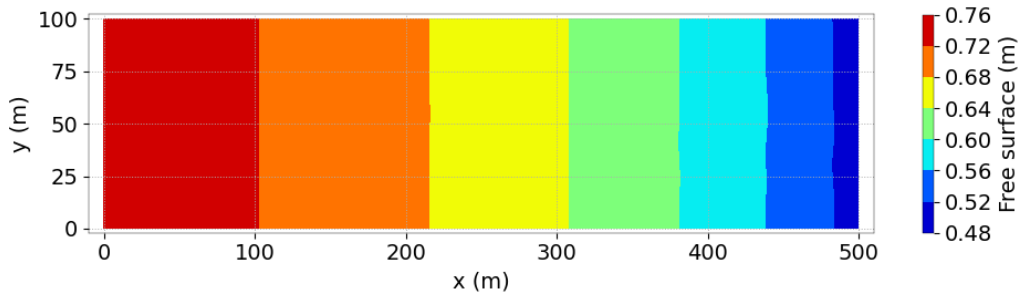


Figure 9.2: Free surface at the steady state.

### 9.1.2 Mesh and numerical parameters

The mesh (Figure 9.3) is made of 551 triangular elements (319 nodes).

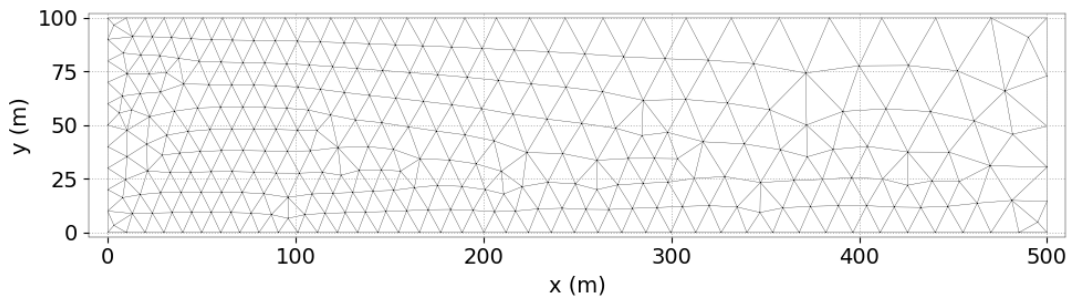


Figure 9.3: Horizontal mesh.

The time step is 2 s for a simulated period of 4,000 s for the initial 2D computation then 2,000 s more for the two computations with stage-discharge curves.

To solve the advection, the method of characteristics is used for the velocities (scheme 1). The conjugate gradient is used for solving the propagation step (option 1) and the implicitation coefficients for depth and velocities are respectively equal to 1 and 0.55.

## 9.2 Results

In Figure 9.4, the three free surface profiles corresponding to each simulation are compared. These three results are in good agreement. We can also observe that the flow is completely

symmetric without any influence of the space discretisation.

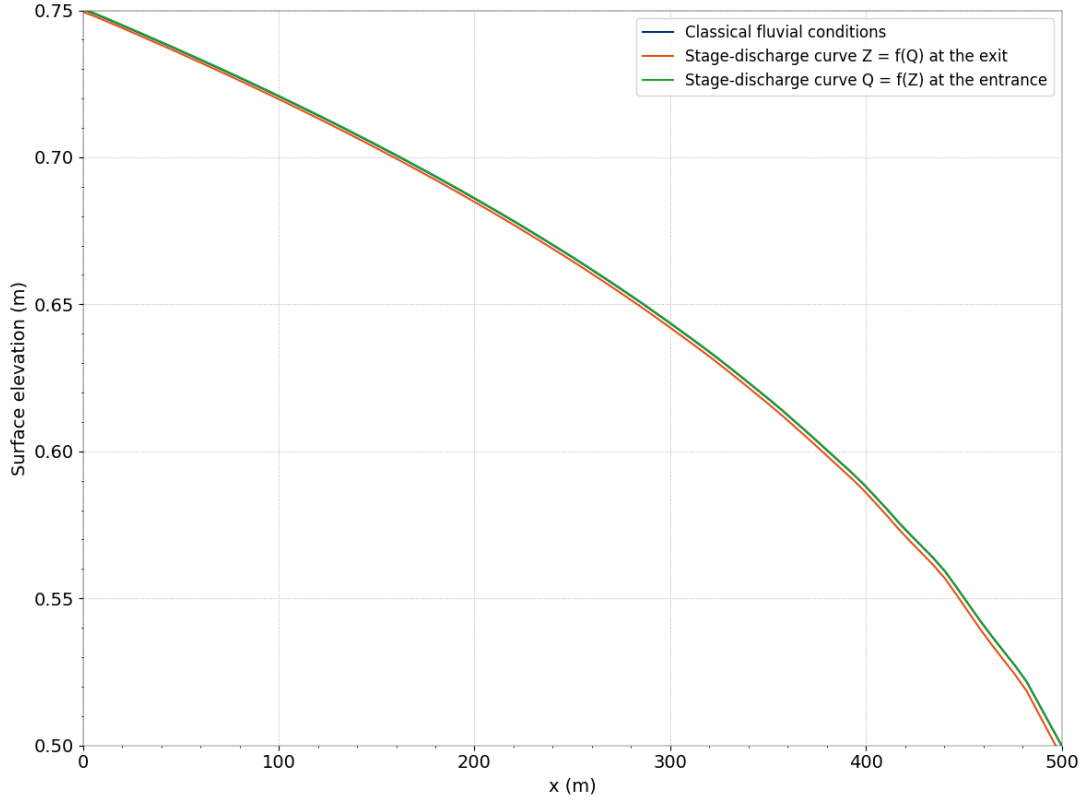


Figure 9.4: Comparison of the free surface profiles between the computations without or with stage-discharge curves.

### 9.3 Conclusion

To conclude, TELEMAC-2D is able to take into account stage-discharge curves.

## 10. Algae transport in a canal (canal\_algae)

### 10.1 Purpose

This test case validates the algae transport module in TELEMAC-2D, and it is a useful example for a user wanting to see how to make use of the particle positions and velocities.

In addition, there is a Python script (`convert_drogues_file_to_vtuConvertDat2Vtu.py`) used in the `vnv_canalalgae.py` validation script to convert the particle result file from a Tecplot format to a ParaView format.

### 10.2 Description

To validate the algae bloom transport model, the experiment presented in Joly [14] and Joly et al. [16] is modelled. More validation of the theory can also be found in Joly et al. [15]. The flow configuration of this experiment is that of partially obstructed open flat bed channel flow, which has the advantage of generating a large recirculation pattern downstream of the obstructing groyne. In this experiment a fluid with a density of  $1,000 \text{ kg/m}^3$  and a flow rate of  $0.5 \text{ m/s}$  is imposed in a  $2 \text{ m}$  wide channel which is obstructed by a groyne  $0.5 \text{ m}$  long and  $0.1 \text{ m}$  thick. The water depth is imposed to be  $0.3 \text{ m}$  before the flow arrives at the groyne. The groyne is constructed high enough to stop overtopping. The experimental setup is described in Figure 10.1, and the Reynolds number is thus  $10^6$ .

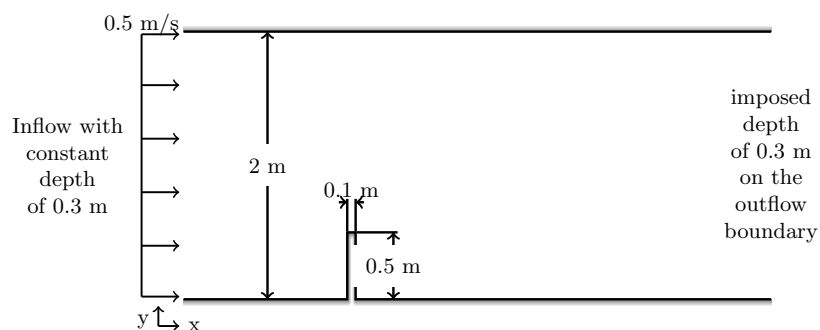


Figure 10.1: Experimental setup for a partially obstructed flat bed open channel flow (top view). In this experiment spherical particles are released to validate the algae transport of TELEMAC-2D.

The flow velocities are well modelled using TELEMAC-2D. In this case, the flow is modelled using a  $k-\varepsilon$  closure and it is validated against experimental measurements and another simulation performed with OpenFoam, which solves the two-dimensional Navier-Stokes equations with a  $k - \varepsilon$  closure using a finite volumes method. The horizontal fluid velocities are presented in Figure 10.2.

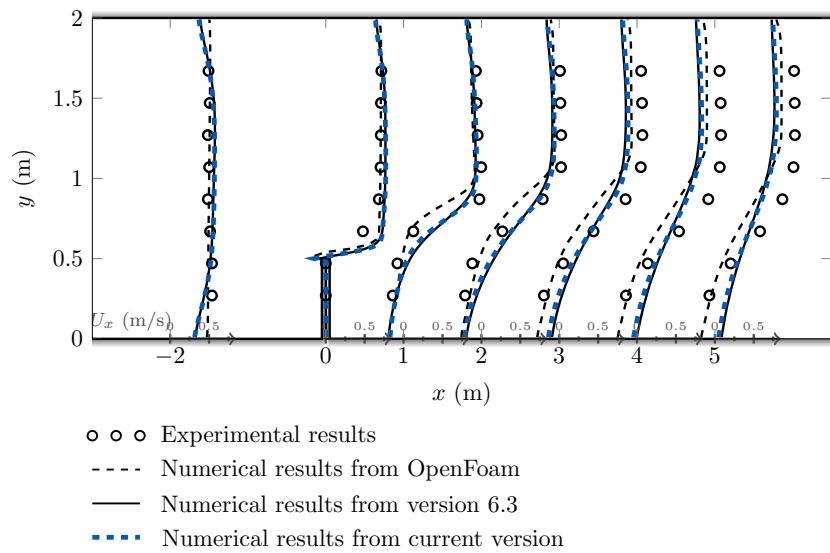


Figure 10.2: Profiles of the horizontal velocity plotted at different locations along the canal. The small axis marked on top of the  $x$ -axis represent the values of velocity magnitude.

Spheres 6 mm in diameter ( $D_s$ ) and of density  $\rho_s = 2,200 \text{ kg.m}^{-3}$  are released in the flow one at a time at fixed intervals (about 1 Hz). This is done to ensure that particles would not affect each other's motion. Several particles are released at different positions in the flow and the trajectories for these particles are recorded at different locations. The trajectories of these particles are measured with a camera that is placed above the flow so that the position of particles entering a window of measurement are recorded, see Figure 10.3. The process used to extract the trajectories is presented in Joly [14].

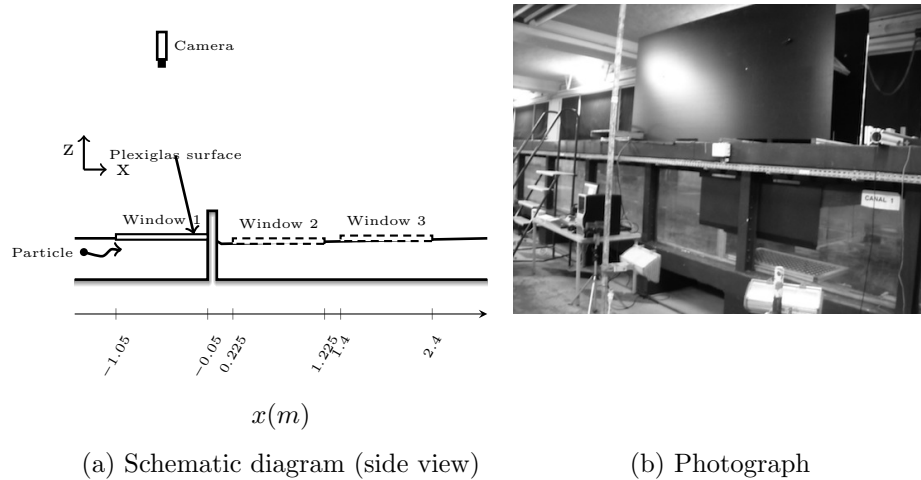


Figure 10.3: Experimental setup to record the particle trajectories.

### 10.2.1 Geometry and mesh

The mesh consists of the mesh has 36,996 nodes and 73,346 elements. The mesh elements size is about 0.1 m at the inflow, 0.015 m around the groyne and 0.3 m at the outflow. A picture of the mesh can be found in Figure 10.4.

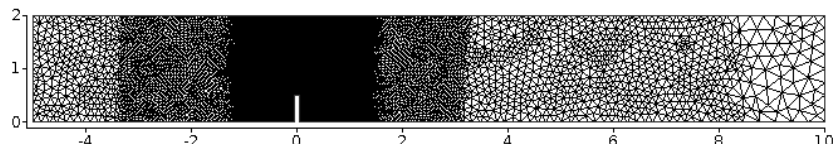


Figure 10.4: Mesh used to simulate the obstructed channel flow.

### 10.2.2 Numerical parameters

To help the simulation run faster, the computation is continued from a previous file, i.e. using the following keywords:

```
COMPUTATION CONTINUED = YES
PREVIOUS COMPUTATION FILE =
'./ini_canal_algae_en.slf'
INITIAL TIME SET TO ZERO = YES
```

In the simulations 1,000 spheres will be released with diameter 0.006 m and density  $2,200 \text{ kg.m}^{-3}$ . The following keywords activate the algae transport module and set these physical characteristics:

```
/-----
/                               ALGAE OPTIONS
/-----
MAXIMUM NUMBER OF DROGUES = 1000
PRINTOUT PERIOD FOR DROGUES = 40
ASCII DROGUES FILE = './alg_pos.dat'
ALGAE TRANSPORT MODEL = YES
DIAMETER OF ALGAE = 0.006
DENSITY OF ALGAE = 2200.0
ALGAE TYPE = 1
```

Finally, the particle defined by editing the user subroutine **USER\_FLOT**, and adding these lines of code:

```

IF (LT .EQ. 0) THEN
  DO I=1,NFLOT_MAX
    CALL ADD_PARTICLE (0.175D0,0.45D0,0.D0,I,NFLOT,
    &                               NFLOT_MAX,XFLOT,YFLOT,YFLOT,TAGFLO,
    &                               SHPFLO,SHPFLO,ELTFLO,ELTFLO,MESH,1,
    &                               0.D0,0.D0,0.D0,0.D0,0,0)
  END DO
ENDIF

```

## 10.3 Results

### 10.3.1 Explanation of the results

For this test case, the particles are released at position (0.175, 0.45) and recorded using window 2 (see Figure 10.3a). More results are presented in Joly [14].

To analyse the trajectories of the particles, the window of measurements is then divided into four quadrants. The number of particles entering each quadrant, and the time spent inside is recorded. The values are then non-dimensionnalised using the sum of all the quadrants, i.e.:

$$N_{res,Q_i} = \frac{N_{Q_i}}{\sum_j^4 N_{Q_j}}, \quad (10.1a)$$

$$T_{res,Q_i} = \frac{T_{Q_i}/\sum_j^4 T_{Q_j}}{N_{Q_i}/\sum_j^4 N_{Q_j}}, \quad (10.1b)$$

Where  $N_{res,Q_i}$  and  $T_{res,Q_i}$  represent the non-dimensionnalised proportion of particles and mean time of residence inside a quadrant  $Q_i$ .  $N_{Q_i}$  is the number of particles recorded in a quadrant and  $T_{Q_i}$  is the cumulative time spend by all the particles present in this quadrant.

This method of writing the results allows a comparison between numerical and experimental results, as during the experiment it is impossible to know if a particle that exited the window of measurement would re-enter it at a later time.

These results are plotted in Figures 10.6 and 10.7, where for each quadrant the value of interest is plotted along a line going from the inner most corner to the outer most corner. The length scales for these values are chosen in such a way that the maximum value is placed on the outer most corner. The points plotted for each quadrant are then linked together to form an area. An annotated description of the results is given in Figure 10.5.

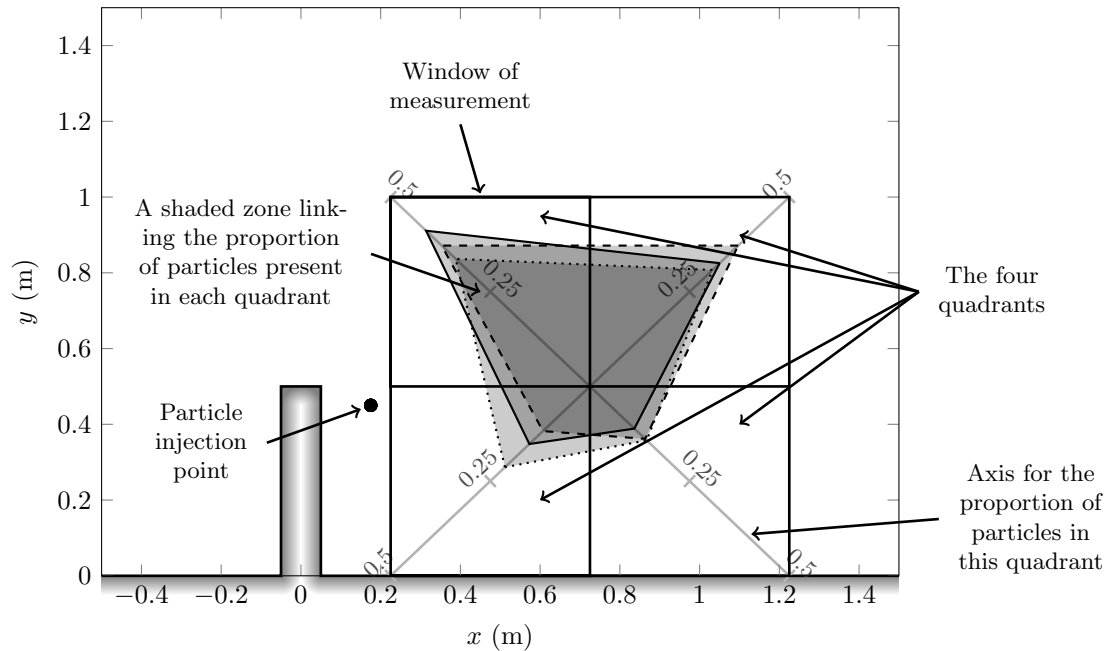
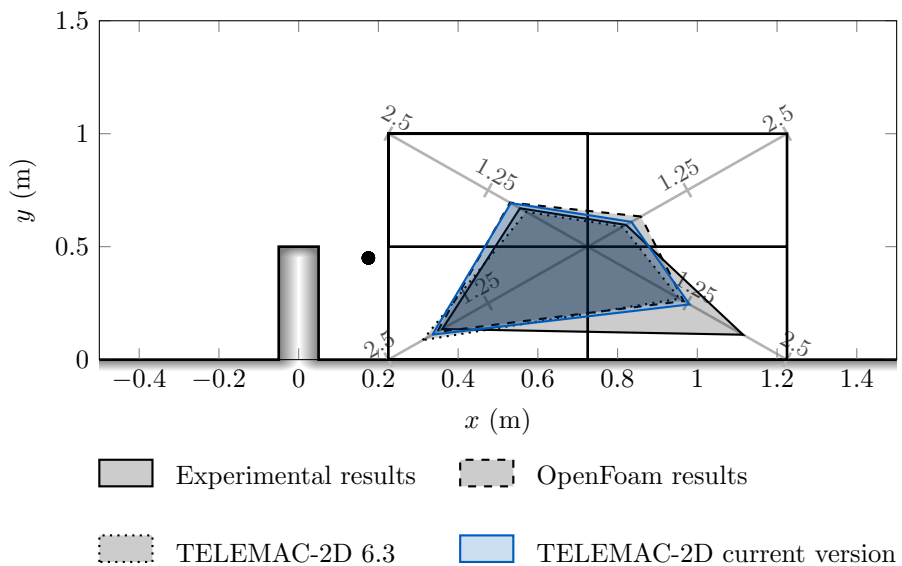
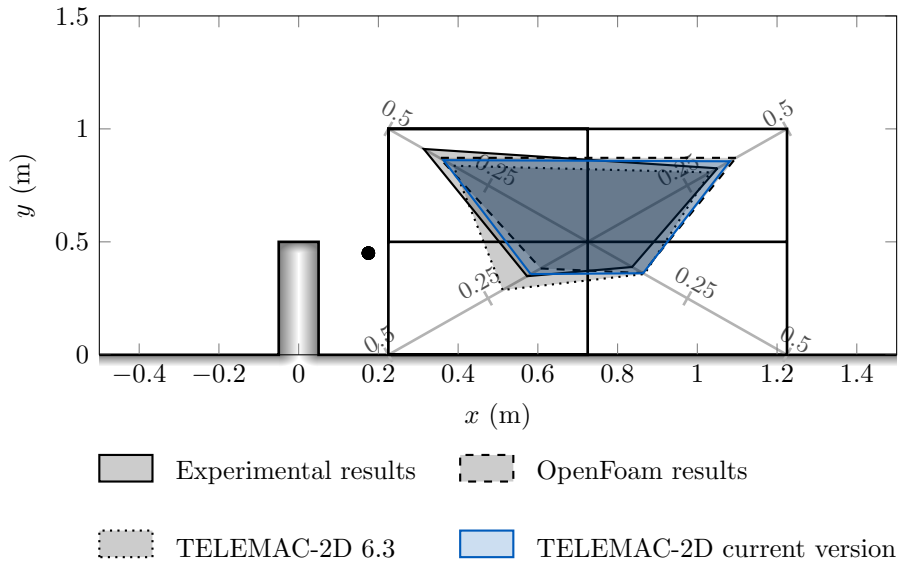


Figure 10.5: An annotated example to explain how the proportion of particles entering each quadrant of a window of measurement are presented.

The velocities of the particles are also analysed. To do so, profile plots are done of the properties of the particles crossing the line at  $x = 0.55$  m. These figures can be found in Figures 10.8 to 10.10.

### 10.3.2 Simulation results

The first result presented will be the proportion of particles entering a quadrant and their mean time of residence. These results will be compared to experimental results and results where the fluid velocities are simulated using OpenFoam. They are presented in Figures 10.6 and 10.7.



As can be seen from Figures 10.6 and 10.7, the **ALGAE\_TRANSP** module models accurately the position of spherical particles. There is only the mean time of residence of the bottom right corner which has noticeable differences, but this is also the case with the fluid velocities model using OpenFoam. This would suggest that the center of the recirculation pattern might be a bit off when modelled in TELEMAC-2D.

The next results will assess the ability of the model to predict the velocities of the particles released in the flow. In Figures 10.8 to 10.10 profiles will be shown of the fraction of particles crossing the section defined by  $x = 0.55$  m, as well as the horizontal and vertical velocities ( $V_x$

and  $V_y$ ).

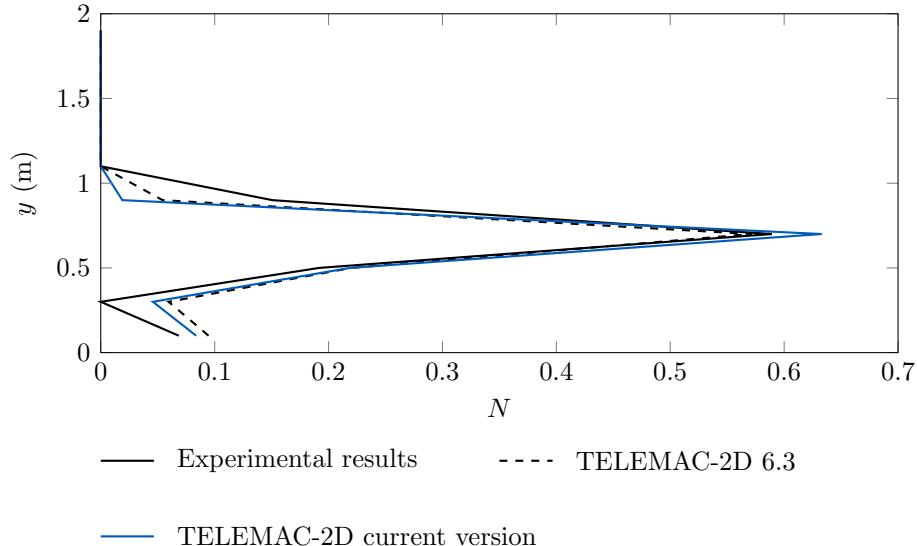


Figure 10.8: Partially obstructed channel flow: fraction of particles crossing the section defined by  $x = 0.55$  m.

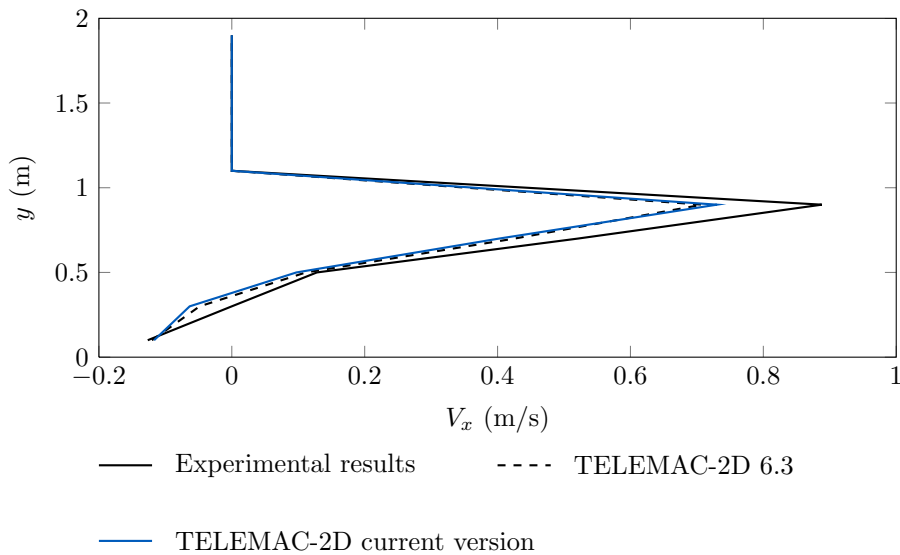


Figure 10.9: Partially obstructed channel flow: velocity along  $x$ -axis of particles crossing the section defined by  $x = 0.55$  m.

The results presented in Figures 10.8 to 10.10 show again that the module **ALGAE\_TRANSPI** models accurately the velocity. The only region of error would be for the vertical velocity near the solid boundaries, but this is probably linked to the previous mis-estimation of the center of the recirculation pattern in TELEMAC-2D. Furthermore the results are still independent of the number of processors used.

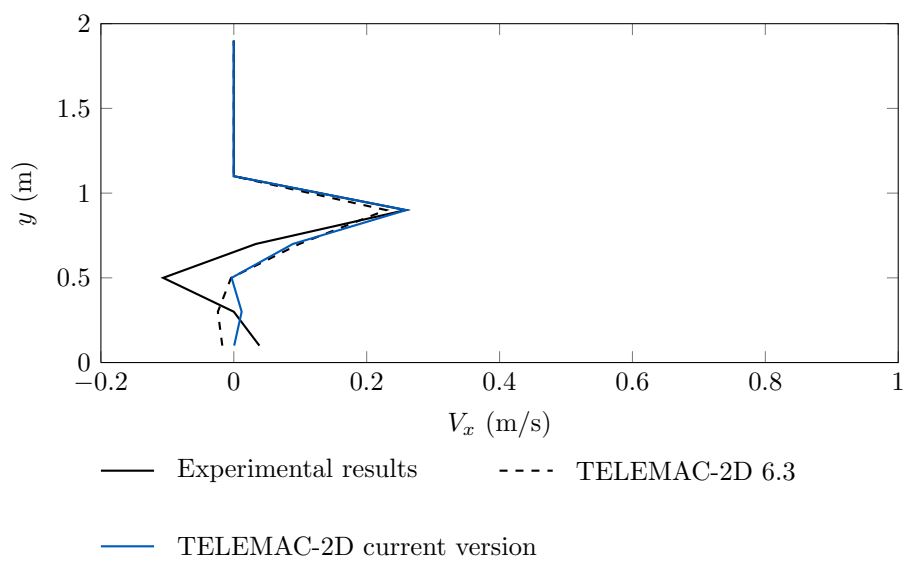


Figure 10.10: Partially obstructed channel flow: velocity along  $y$ -axis of particles crossing the section defined by  $x = 0.55$  m.

## 11. Algae transport in a canal 2 (canal\_algae)

### 11.1 Purpose

The purpose of this example is to show that the initial algae distribution for a test with algae can be defined in a number of different ways.

### 11.2 Description of the test case

This test case is based on the `canal_algae` test case. The only difference is the initial distribution of the algae. The details of the model can be found in the description for Algae Canal.

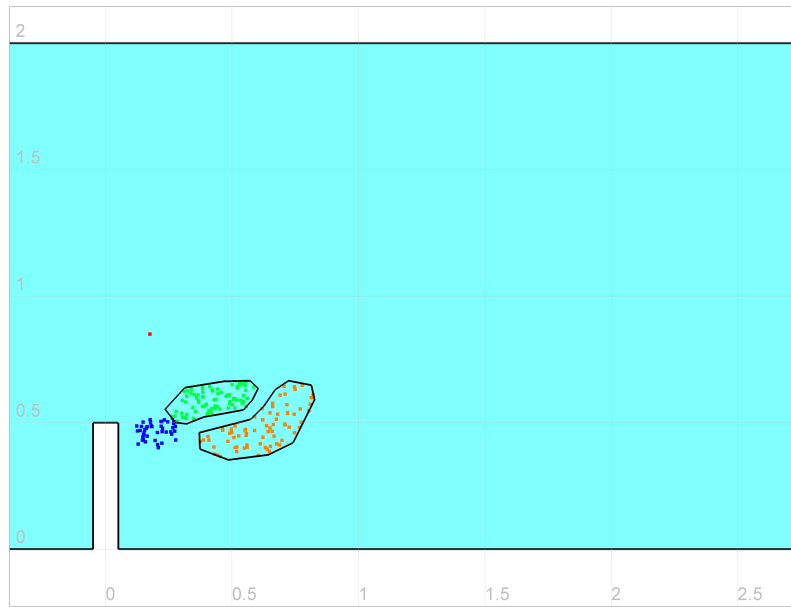


Figure 11.1: Initial algae distribution.

There are 500 algae particles at  $x = 0.175$  m,  $y = 0.45$  m. These are defined in the subroutine `USER_FLOT`, which uses the subroutine `ADD_PARTICLE` to add each algae particle. These are defined with class 4.

A second group of particles is defined using a polygon file, containing two polygons, which is specified using the keyword DROGUES INITIAL POSITIONING DATA FILE. The polygon file must be in the Blue Kenue i2s format. These two polygons are shown in Figure 11.1. The left polygon has defined some particles of class 2. The right polygon has defined some particles of class 3.

A third group of particles is defined using a variable called **DROGUES CLASSES** in the geometry file. In this case, there is an area close to the groyne where this variable is equal to 1. Elsewhere the variable is zero. This has resulted in a region of algae particles close to the groyne with class 1.

The keyword INITIAL DROGUES SAMPLING DENSITY gives the number of algae particles per unit area for a given class, for the cases where the algae is defined by polygons or the geometry file. In this case, the density is 2,000 for class 1 and class 2 particles and 1,000 for class 3 particles.

Figure 11.1 plots algae particles with class 1 as blue, class 2 as green, class 3 as orange and class 4 as red.

The keyword DURATION BEFORE ALGAE RELEASE gives the time of release (in seconds) for a given class. In this case the release times are 5 s for class 1, 10 s for class 2, 15 s for class 3 and 0 s for class 4.

### 11.3 Results

The algae distribution after 3 seconds, 12 seconds and 30 seconds (the end of the run) is shown in Figure 11.2 to Figure 11.4. By 30 seconds, most of the particles have left the domain through the right boundary.

*Because of the randomisation of the turbulent particle movements the result on the reader's machine may be slightly different to the results below, but it should be similar.*

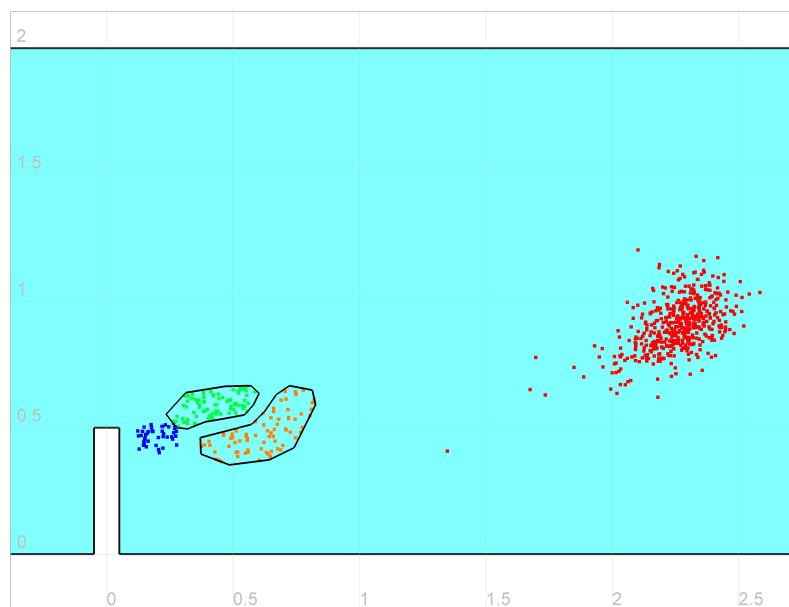


Figure 11.2: Algae distribution after 3 s.

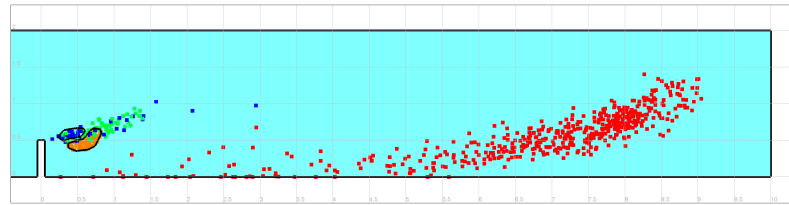


Figure 11.3: Algae distribution after 12 s.

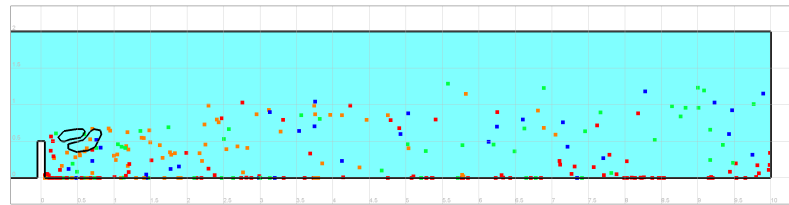


Figure 11.4: Algae distribution after 30 s.

The standard test case outputs the algae information as a Tecplot file. In this case, the algae information is written to a file defined by the keyword `ASCII DROGUES FILE`. The default value of the `DROGUES FILE FORMAT` is `TECPLOT`. In order to output to a PCL file, give the output file name using the keyword `BINARY DROGUES FILE` and give the `DROGUES FILE FORMAT` as `BKBINPCL`. PCL files can be displayed using Blue Kenue.

This example outputs a text file called `polygon_particles.txt`. Output is written to the file every 0.1 s. The output relates to four polygons that surround the four initial regions of particles, as described above. The first polygon surrounds the particles defined by the geometry file. Polygons 2 and 3 are illustrated in the previous figures. The fourth polygon surrounds the point with the initial 500 particles. For each time, the output file contains the time, and the number of initial particles that remain in the polygon and un-mobilised. Running of the test case should result in a text file identical to the `polygon_particles.txt` file.

For this test case example the random distribution of initial particles is fixed through lines 39 to 47 of the `CONDIN_DROGUES` subroutine. These lines ensure that the particles are initially located in the same place whenever the test case is run but should be commented out when running the code more generally.

## 12. Flow in a channel with a cavity (cavity)

### 12.1 Purpose

This test case is inspired from the paper from Faure (1995) [7] where the constant viscosity and  $k - \varepsilon$  turbulence models are compared to tests performed in a physical model. The Smagorinski model has been added to TELEMAC-2D after this comparison because it proved to be more efficient on this class of applications.

### 12.2 Approach

A 23 m long and 3 m wide channel is fed by a constant flow. The fluid is well-mixed over the 0.43 m depth: no stratification is present. On the left bank of the channel is located a harbour cavity. The cavity has a cross-section (perpendicular to the channel axis) terminating with a shallow beach having a mild slope (see Figure 12.1).

This three-dimensional configuration induces the formation of large size eddies. Bijvelds et al. [2] have shown that vortices induced in a similar harbour with constant depth are better reproduced with 3D simulation. In our case, a 2D simulation is possible since the beach where large size vortices are present is very shallow. The flow is typically unsteady although boundary conditions are steady. The Smagorinski turbulence model is tested on this configuration.

#### 12.2.1 Geometry and mesh

- Size of the model: channel = 23 m × 3 m, cavity = 6 m × 3 m,
- Water depth at rest = 0.43 m.

The mesh is dense, particularly in the cavity where the vortices take place and on the steep junction slope between the cavity and the beach. It is made up with quadrangles split into two triangles (see Figure 12.1).

- 8,160 triangular elements,
- 4,233 nodes,
- Size range: from 0.033 to 0.34 m.

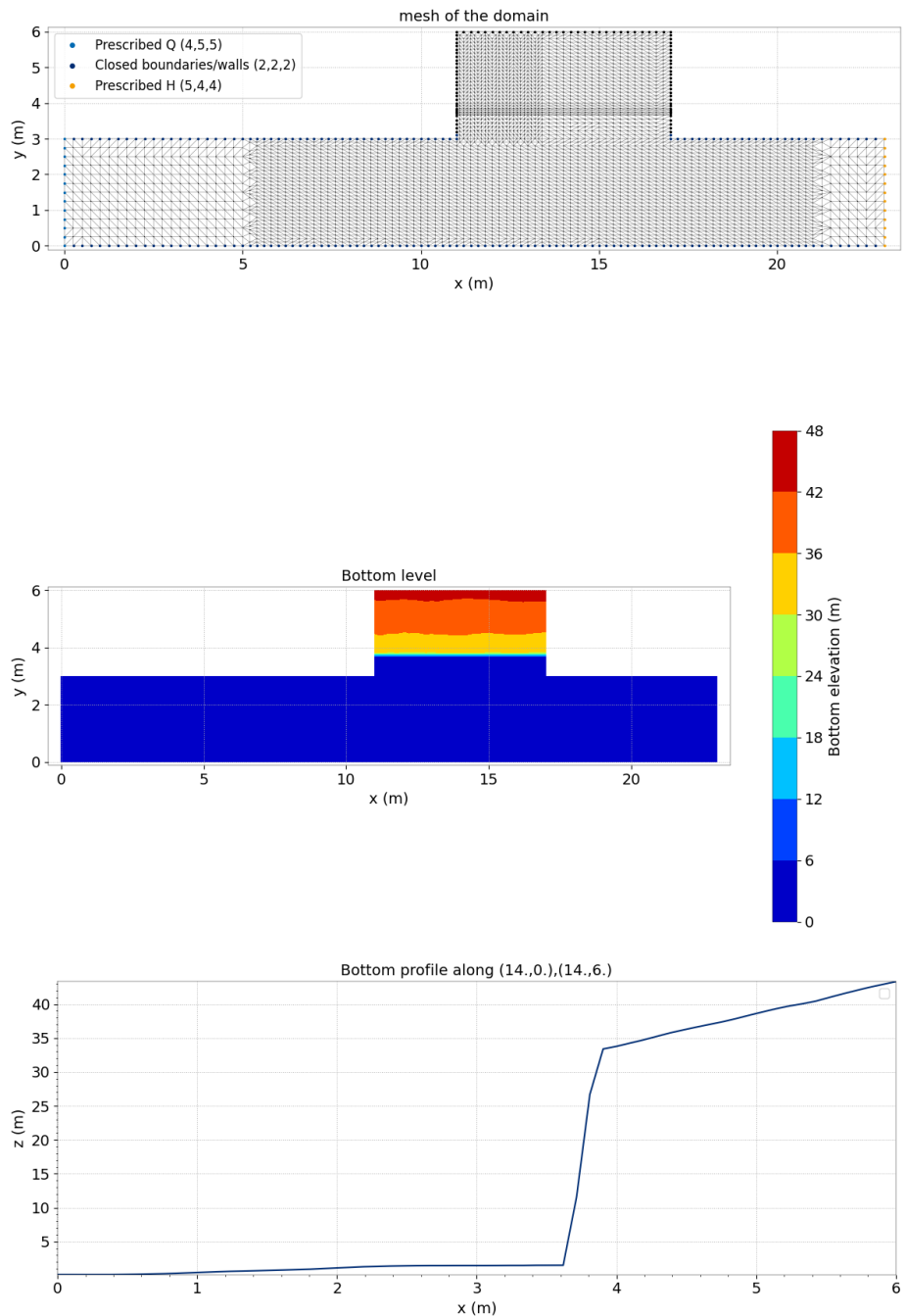


Figure 12.1: Mesh and topography.

### 12.2.2 Boundaries

- Channel entrance :  $Q = 0.155 \text{ m}^3/\text{s}$  imposed,
- Channel outlet:  $h = 0.445 \text{ m}$  imposed,
- Lateral boundaries: solid walls with slip condition in the channel and no-slip condition in the cavity (see Figure 12.1).

Bottom: In order to simulate small size bottom variations, the bed is uneven. Manning friction law with bottom roughness =  $0.015 \text{ s/m}^{1/3}$ . Bed isolines and a cross-section of the cavity are shown in Figure 12.1.

### 12.2.3 Physical parameters

Turbulence: Model of Smagorinski with coefficient of Smagorinski = 0.1.

### 12.2.4 Numerical parameters

Type of advection:

- Characteristics on velocities (scheme #1),
- Conservative + modified SUPG on depth (mandatory scheme).

Type of element: Quasi-bubble triangle for velocities and linear triangle (P1) for  $h$ .

- GMRES solver,
- Accuracy =  $10^{-3}$ ,
- Time data:
  - Time step = 0.2 s.
  - Simulation duration = 200 s.

## 12.3 Results

The velocity pattern and the free surface elevation in the cavity are shown in Figures 12.2. The flow is unsteady particularly in the cavity even though the boundary conditions are steady. Big and small eddies appear and move periodically in the cavity (see Figures 12.3 and 12.4). The period of big eddies is longer than the one of small eddies.

## 12.4 Conclusions

The phenomena observed on physical model are successfully reproduced by TELEMAC-2D with the Smagorinski model, although hydrodynamics are three dimensional in reality. In particular, the small and big eddies structures in the cavity are well represented.

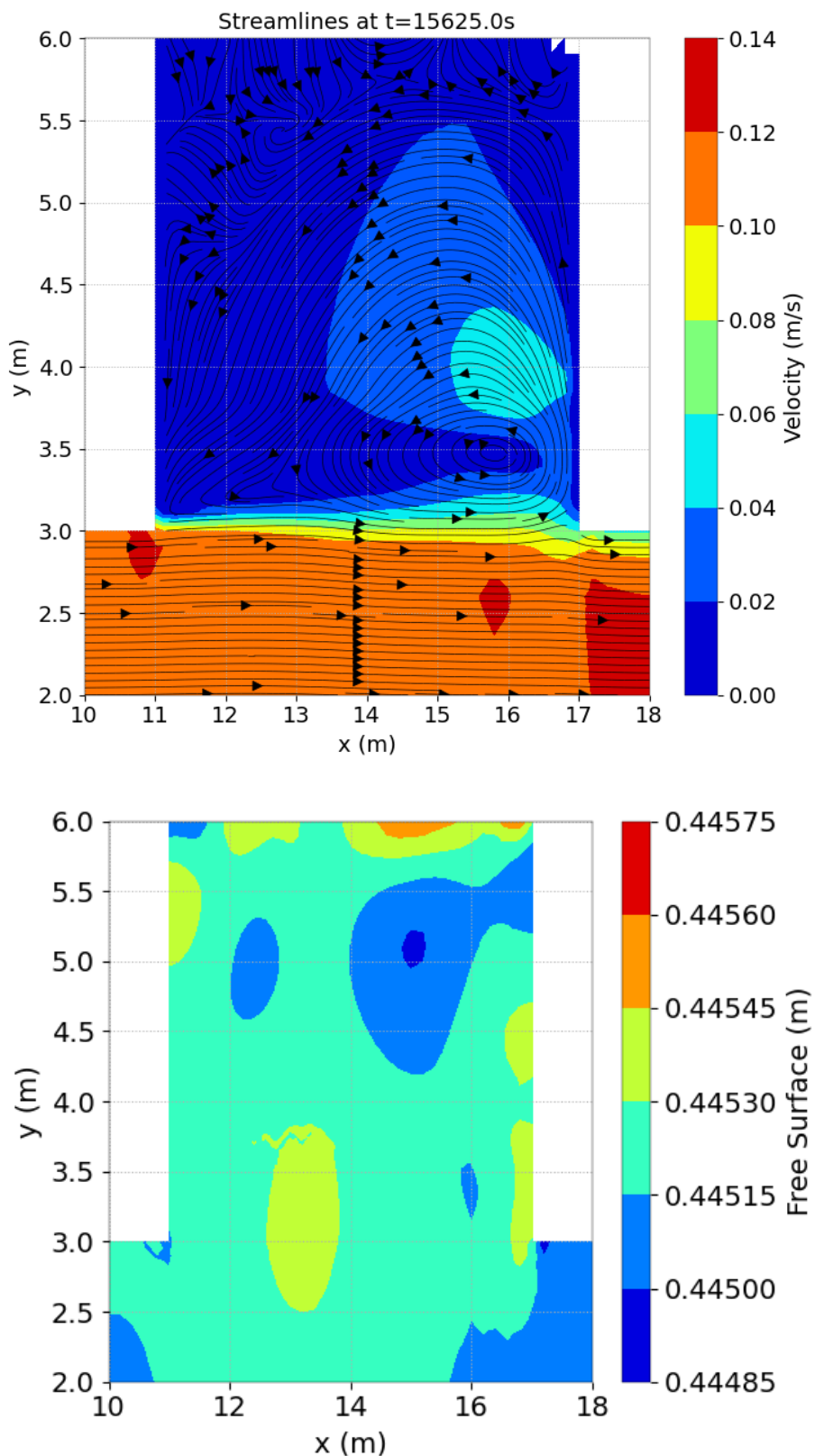


Figure 12.2: Velocity field and free surface in the cavity at time 15,625 s.

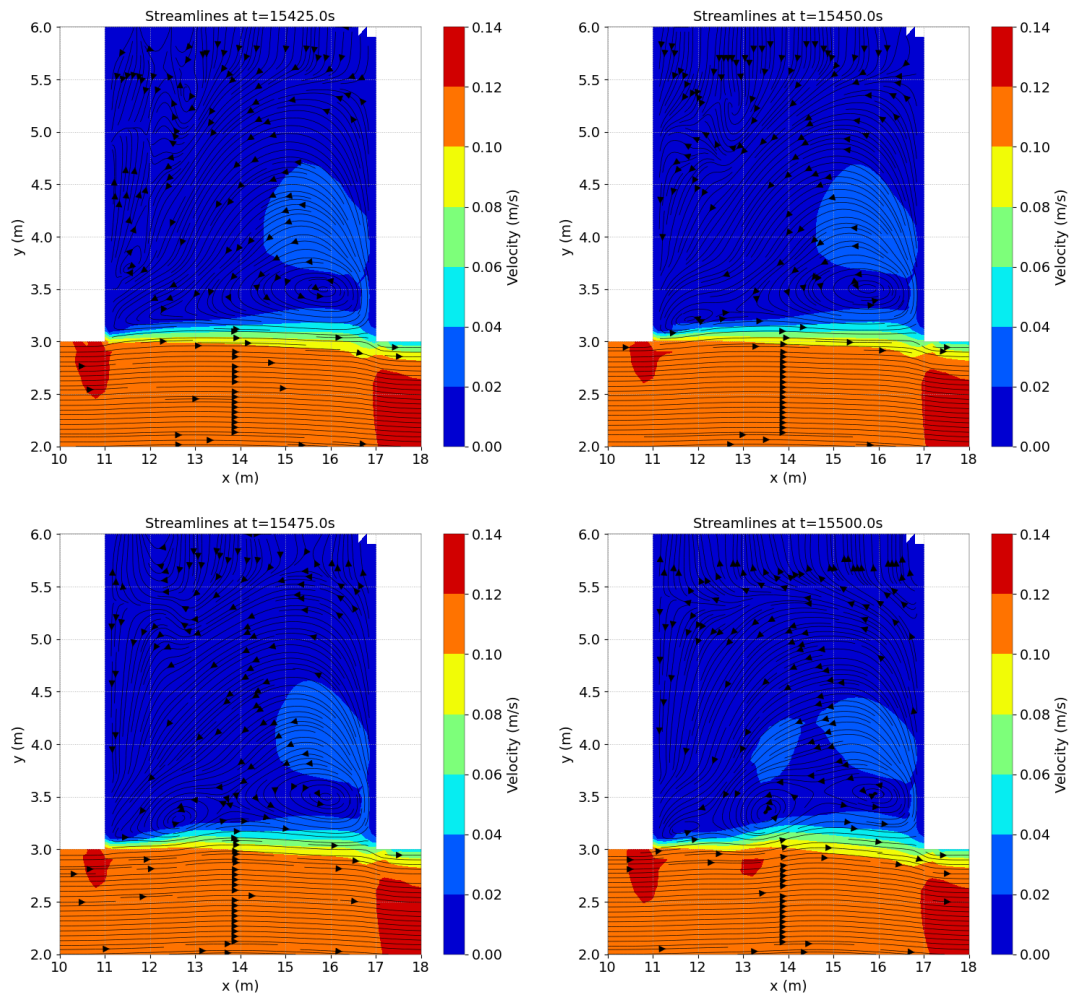


Figure 12.3: Evolution of the velocity field in time – Small eddy pattern.

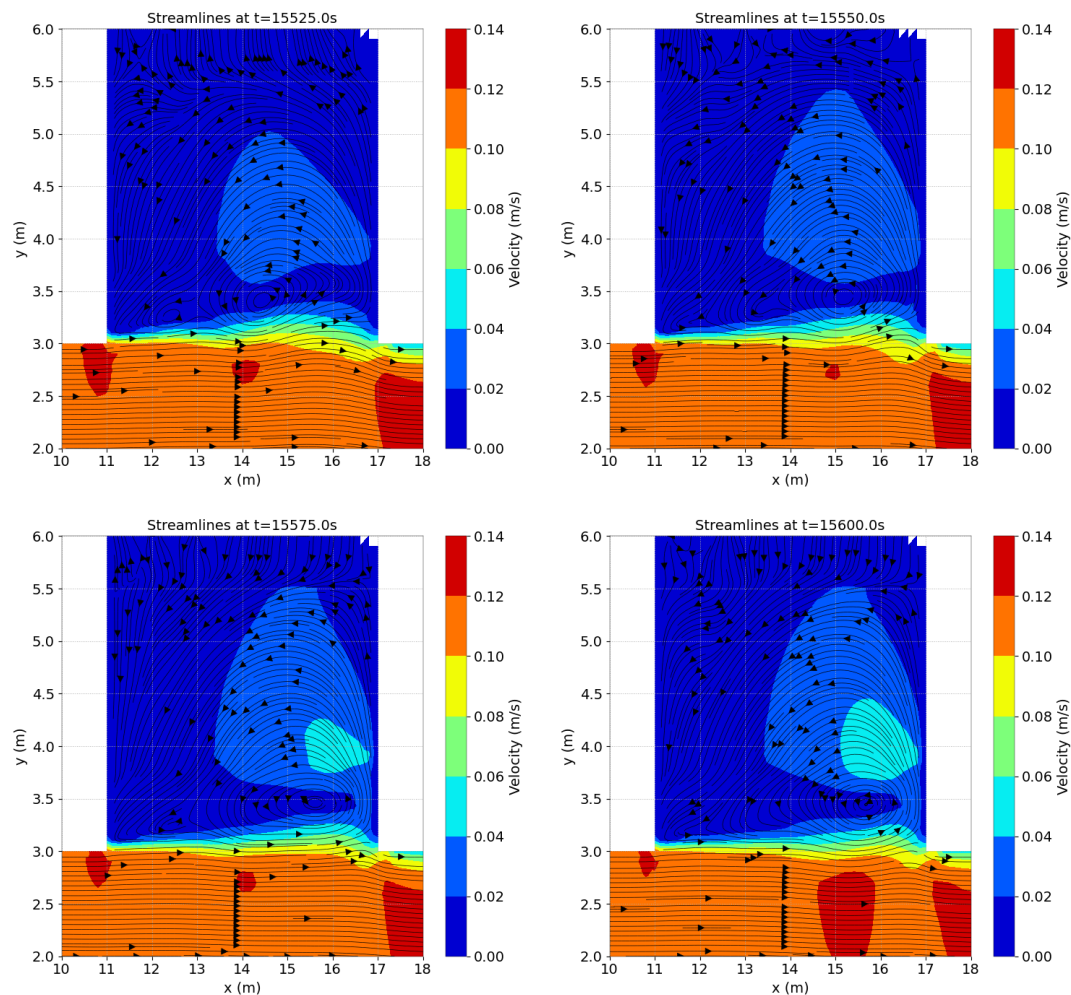


Figure 12.4: Evolution of the velocity field in time – Large eddy pattern.

## 13. Advection of tracers with a rotating cone (cone)

### 13.1 Purpose

This test shows the performance of the finite element advection schemes of TELEMAC-2D for passive scalar transport in a time dependent case. It shows the advection of a tracer (or any other passive scalar) in a square basin with flat frictionless bottom and with closed boundaries.

### 13.2 Description

#### 13.2.1 Geometry and mesh

The dimensions of the domain are  $[d \times d] = [20 \times 20]$  m<sup>2</sup>. The mesh is made from a regular grid from which all square are cut in half. The number of elements and nodes in the mesh are 20,000 and 10,201 respectively.

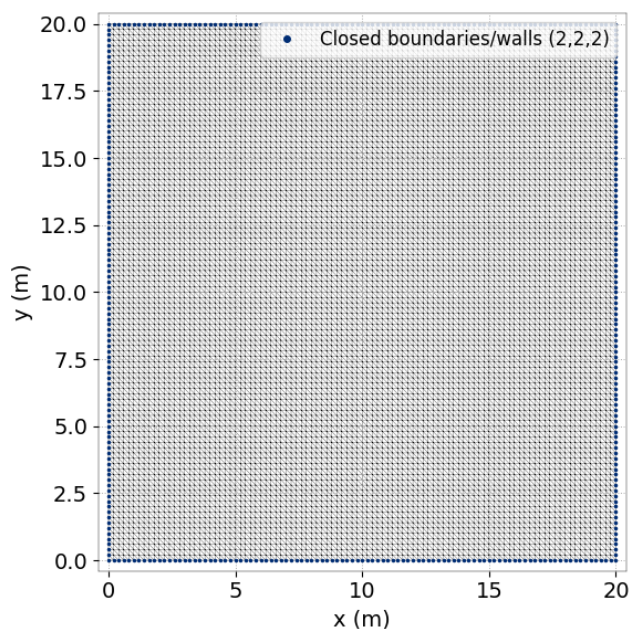


Figure 13.1: 2D domain and mesh of the cone test case.

### 13.2.2 Initial condition

The water depth is constant in time and in space, equal to 2 m. The velocity field is constant in time as well and is divergence free:

$$\mathbf{u} = \begin{cases} u(x, y) = -(y - y_0) \\ v(x, y) = (x - x_0) \end{cases}$$

With  $x_0 = 10$  m and  $y_0 = 10$  m. The initial value for the tracer is given by the Gaussian function off-centered 5 m to the right of  $(x_0, y_0)$ :

$$c^0(x, y) = e^{-\frac{1}{5}[(x-x_0-5)^2 + (y-y_0)^2]}.$$

### 13.2.3 Analytical solution

The tracer is described by a Gaussian function and is submitted to a rotating velocity field. After one period we expect that the tracer function has the same position and the same values as the initial condition (i.e. maximum value equal to 1 at the center). The analytical solution for the tracer  $c$  is given by:

$$c(x, y, t) = e^{-\frac{1}{5}[X^2 + Y^2]},$$

with:

$$\begin{cases} X = x - x_0 - R \cos(\omega t) \\ Y = y - y_0 - R \sin(\omega t) \end{cases}$$

where  $R = 5$  m.

### 13.2.4 Physical parameters

In this case the tracer advection equation is solved using fixed hydrodynamic conditions. No bottom friction is imposed and diffusivity of tracer is set to zero. Angular velocity of the rotating cone is equal to 1 rad.s<sup>-1</sup> which gives a rotation period equal to  $T = 2\pi$  (6.28 s).

### 13.2.5 Numerical parameters

The simulation time is set to one period of rotation. The time step is chosen in order to do the whole period in 64 steps, so it is equal to 0.098174771 s.

For tracers advection, all the numerical schemes available in TELEMAC-2D are tested. For weak characteristics, the number of Gauss points is set to 12. For distributive schemes, like predictor-corrector (PC) schemes (scheme 4 and 5 with options 2, 3) and locally implicit schemes (LIPS: scheme 4 and 5 with options 4), the number of corrections is set to 5, which is usually sufficient to converge to accurate results. For the locally implicit schemes (scheme 4 and 5 with option 4), the number of sub-steps is equal to 20.

## 13.3 Results

### 13.3.1 Comparison of schemes

The final contour maps after one rotation of the cone are plotted for each scheme in Figures 13.2 and 13.3. One dimensional profiles are also extracted from slice plane  $(x, y = 10, z)$  at  $t = T/2$  and  $t = T$  in Figure 13.4.

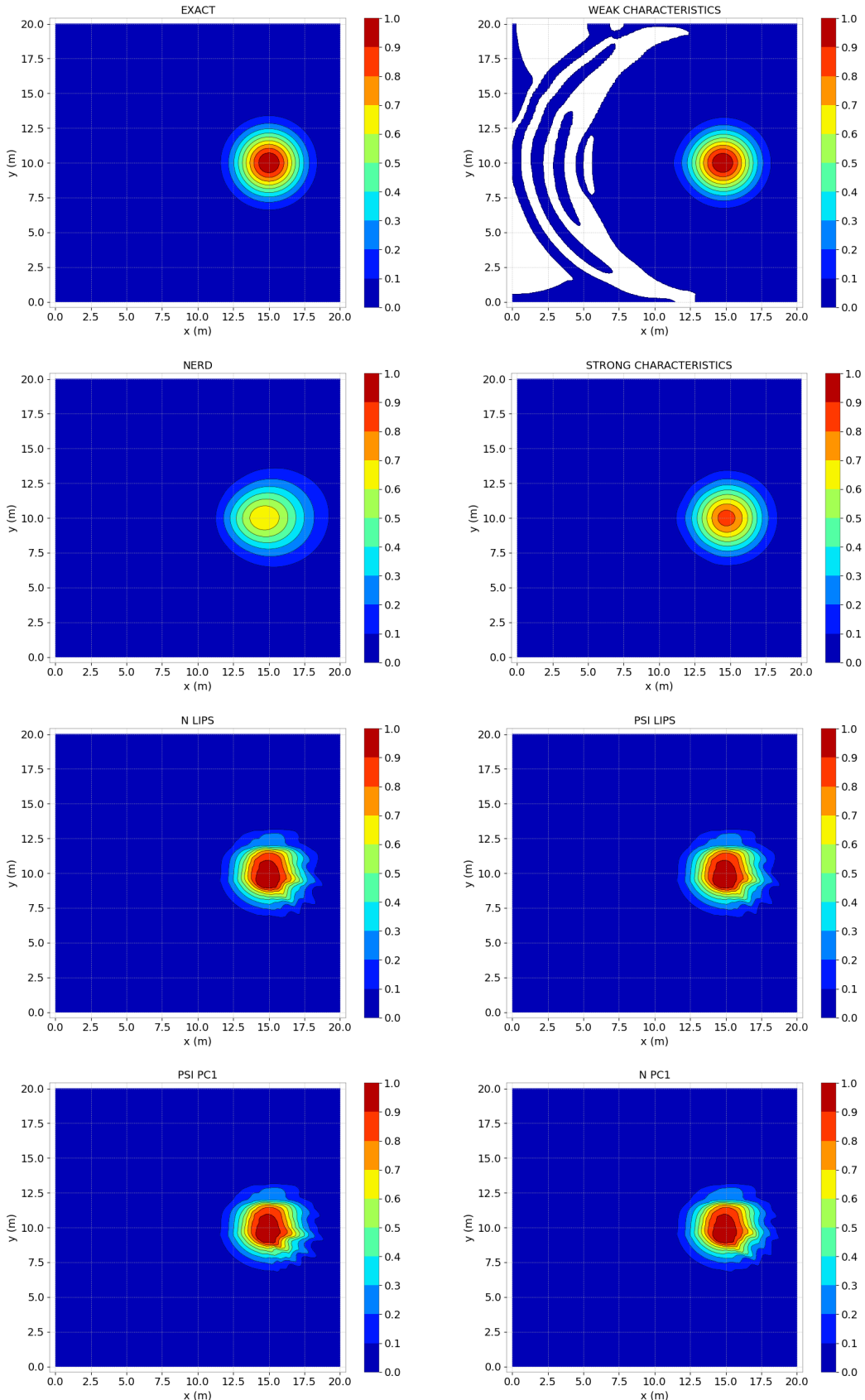


Figure 13.2: Cone test: contour maps of tracer after one period of rotation, for the advection schemes of TELEMAC-2D.

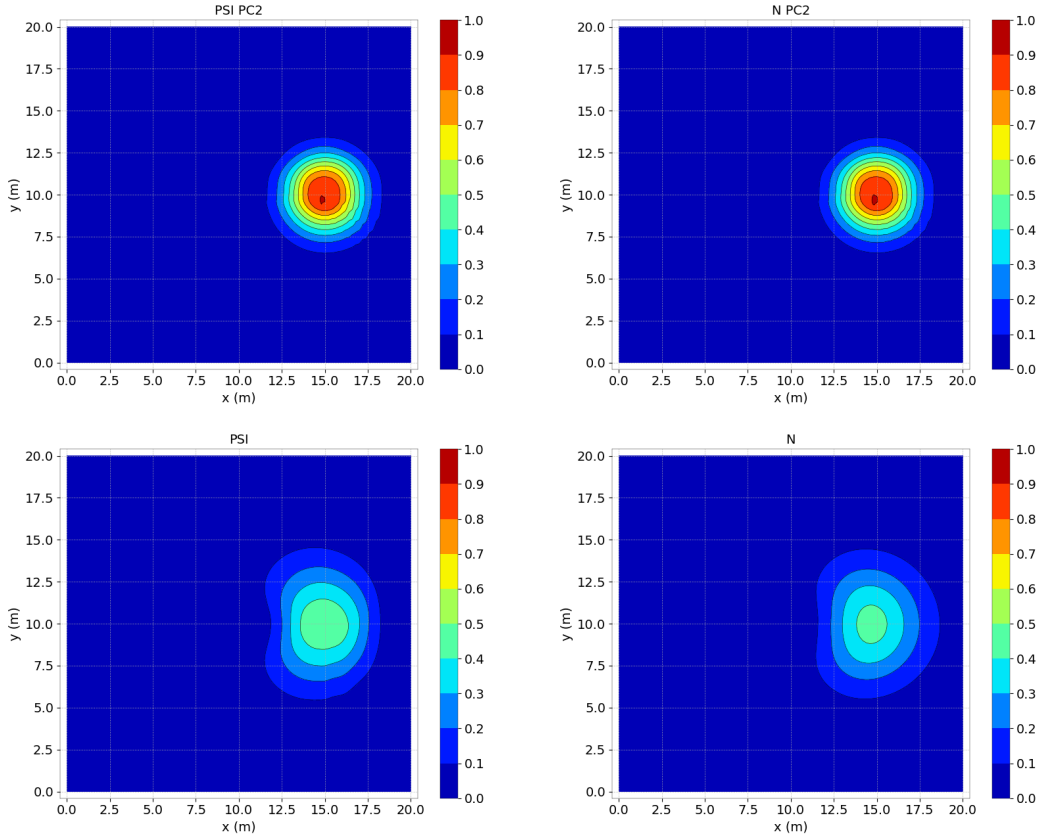


Figure 13.3: Cone test: contour maps of tracer after one period of rotation, for the advection schemes of TELEMAC-2D.

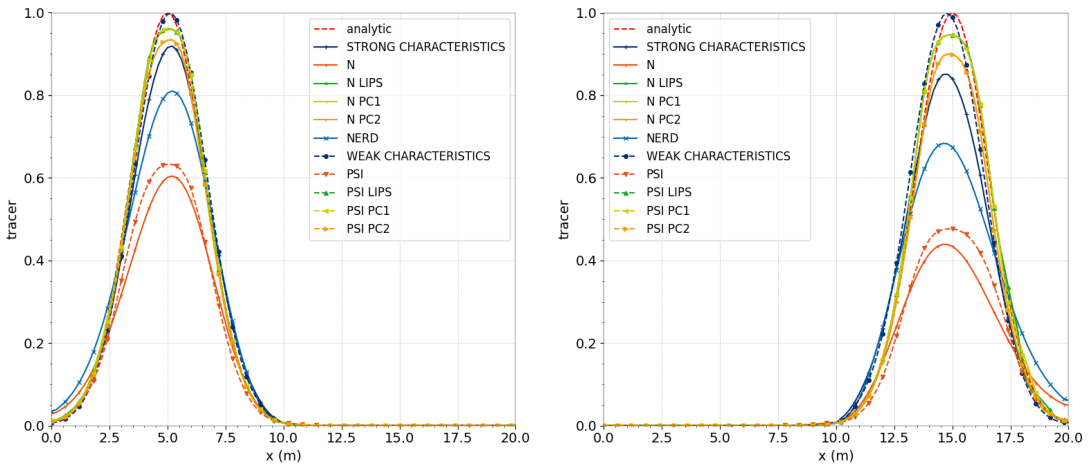


Figure 13.4: 1D solution along slice plane  $(x, z)$ ,  $y = 10$  m at  $t = T/2$  (left) and  $t = T$  (right).

### 13.3.2 Maximum principle

The minimum value of the Gaussian function is measured after one rotation. The maximum value is computed as well, in order to check the respect of the maximum principle (or monotonicity). Results are shown in Figures 13.5.

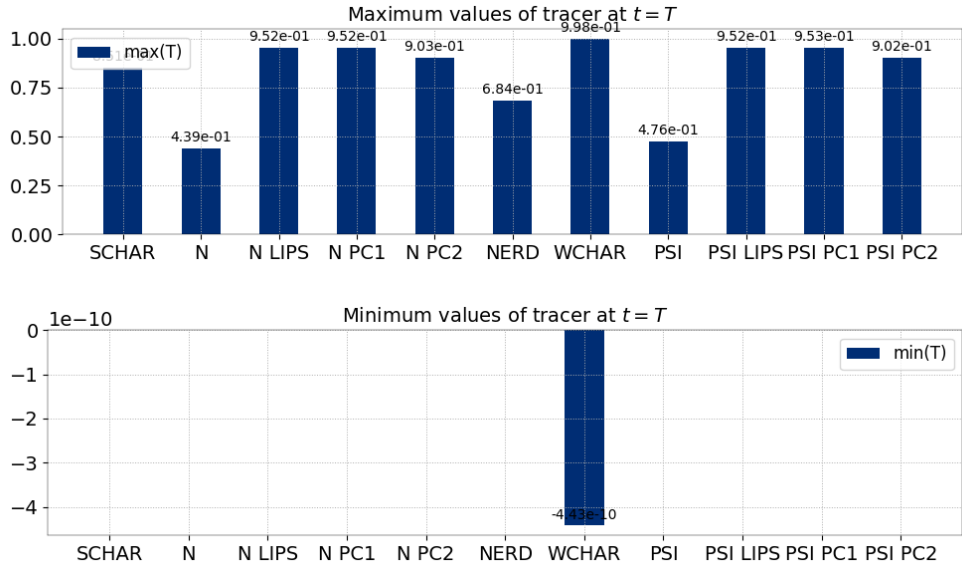


Figure 13.5: Maximum and minimum values of tracer after one rotation of the cone.

### 13.3.3 Accuracy

In order to evaluate the behaviour of the scheme, the error norms  $L^1, L^2, L^\infty$  are computed. Error norms are integrated over time to take into account the unsteady nature of the problem. The error norms integrated over time for one rotation of the cone are reported in Figure 13.9.

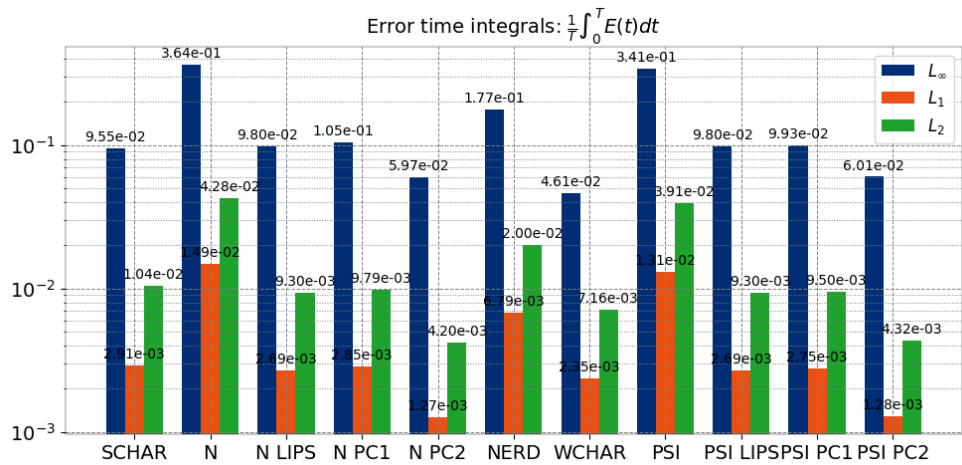


Figure 13.6: Error norms integrated over time for one rotation of the cone.

### 13.3.4 Convergence

To assess the accuracy of the schemes, computation of error on one mesh is not sufficient. In this section a mesh convergence is carried out for each numerical scheme. From a starting mesh with 441 points and 800 elements we divide by 4 each triangles recursively to generate new meshes. The first 4 meshes used in the convergence study are presented in Figure 49.16.

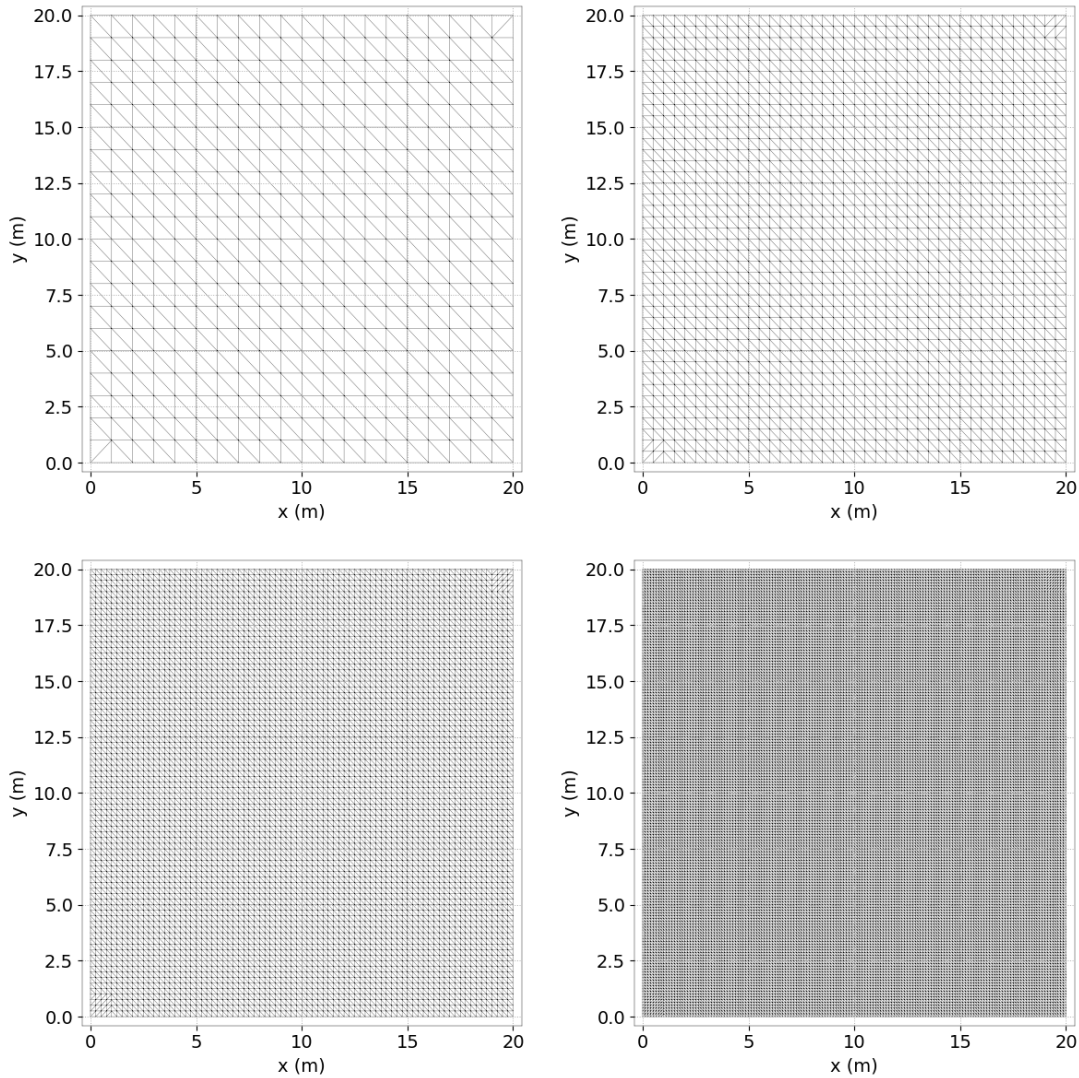


Figure 13.7: 2D Mesh used in cone mesh convergence.

Final time is set to  $t_f = T/4$ . Time step is set to ensure a constant CFL for each mesh increment. Strong characteristics, N and PSI schemes converge at first order with a slope slightly inferior to one. LIPS and predictor-corrector (PC) schemes as well as NERD have steeper slope of convergence comprised between one and two. Convergence slopes of error in  $L^1$ ,  $L^2$  and  $L^\infty$  norm at final time are plotted for each numerical scheme in Figure 13.8.

Convergence slopes in  $L^2$  norm are compared in Figure 13.9. Error with strong characteristics, N and PSI schemes are of the same magnitude as well as LIPS, PC, NERD. Errors on the finest mesh are presented in Figure 13.10.

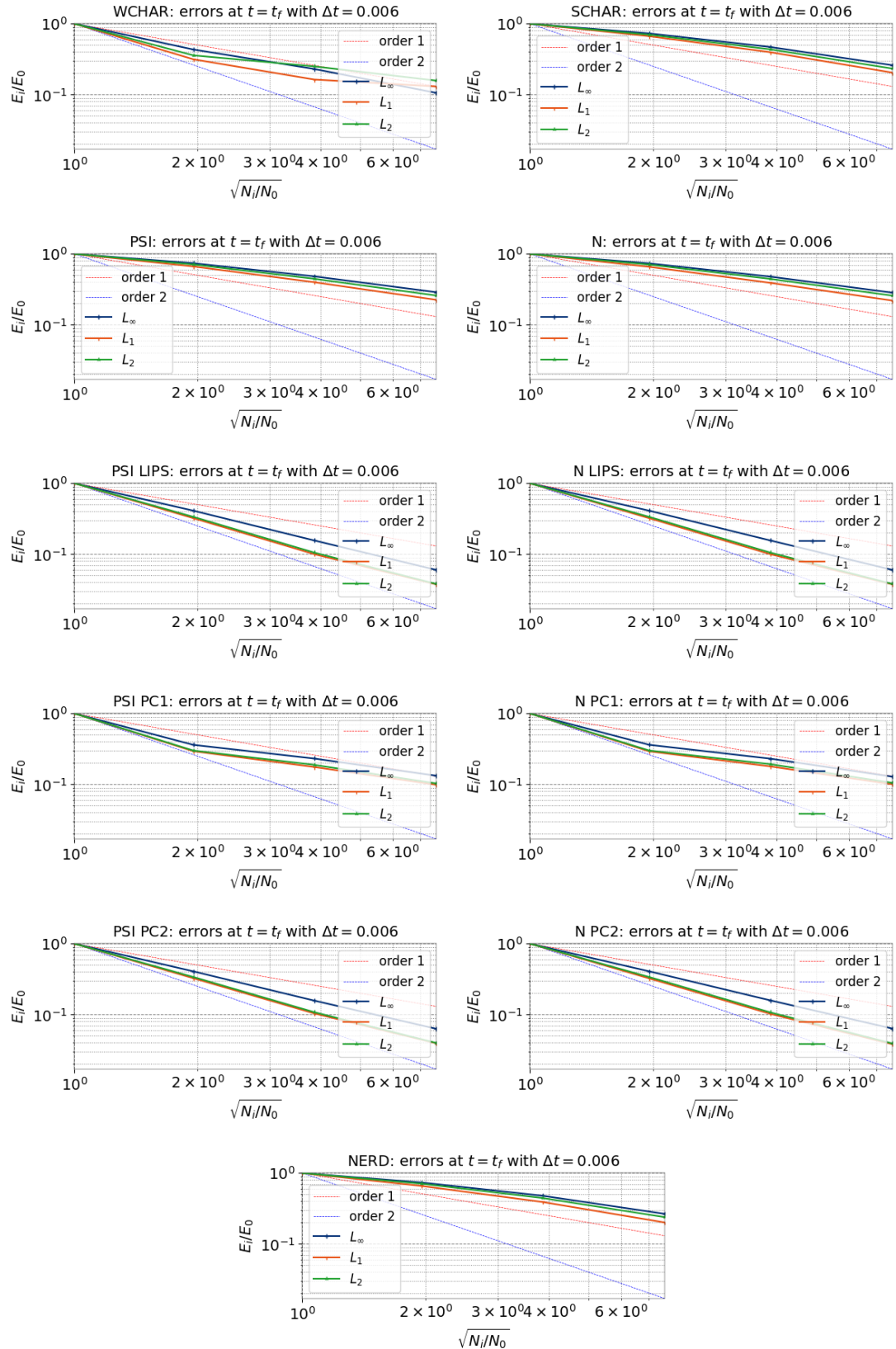


Figure 13.8: Mesh convergence of numerical schemes.

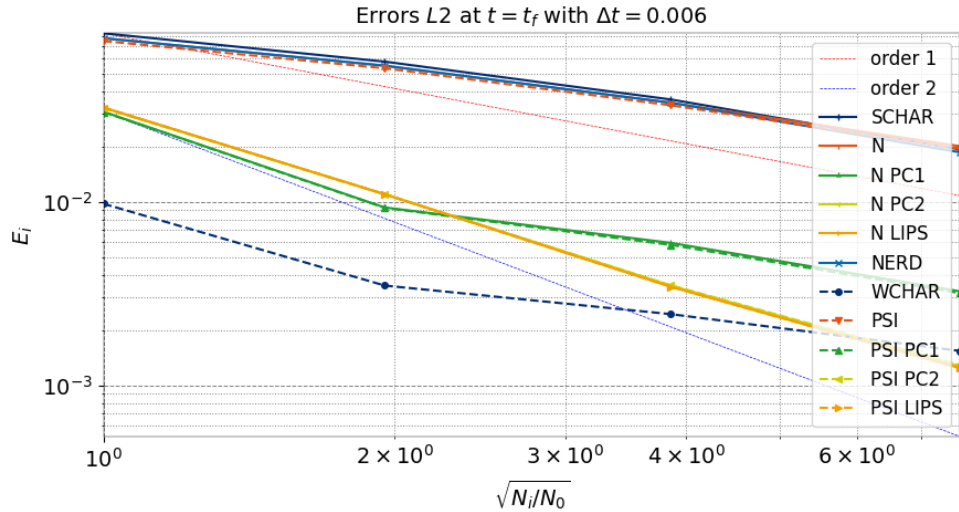
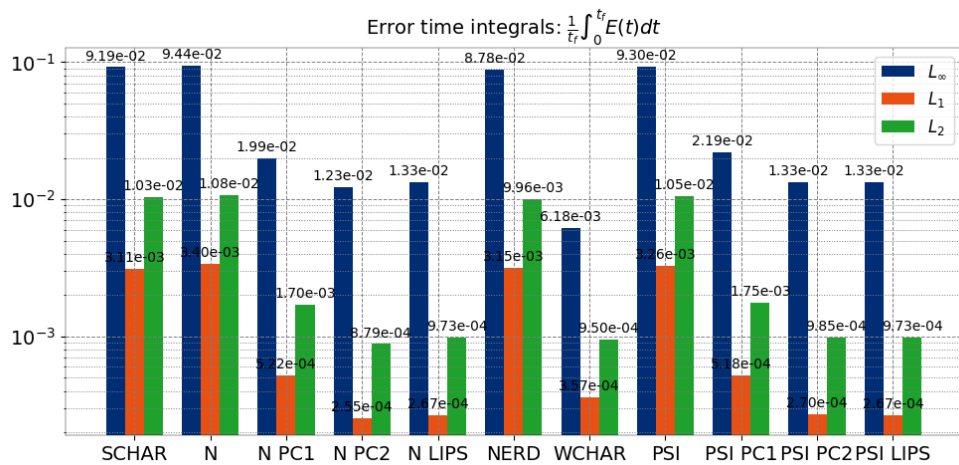
Figure 13.9: Mesh convergence in  $L^2$  norm.

Figure 13.10: Error norms integrated over time for the finest mesh.

## 13.4 Conclusion

TELEMAC-2D is able to model passive scalar transport problems in shallow water flows.

## 14. Diffusion of tracers in 2D (cone\_diffusion)

### 14.1 Purpose

This test shows the performance of the finite volume diffusion schemes of TELEMAC-2D for passive scalar in a time dependent case. It shows the diffusion of tracers in 2D in a rectangular domain with different meshes.

### 14.2 Description

#### 14.2.1 Geometry and mesh

The dimensions of the domain are  $[20 \times 20] \text{ m}^2$ . Three meshes are used to compare their impact on the results depending on the numerical scheme used. The meshes are plotted in Figure 14.2.

#### 14.2.2 Initial condition

The water depth is constant in time and in space, equal to 1 m. The velocity is constant and equal to 0 m/s. Two tracers are defined in the domain for which initial conditions are a Gaussian and a Crenel.

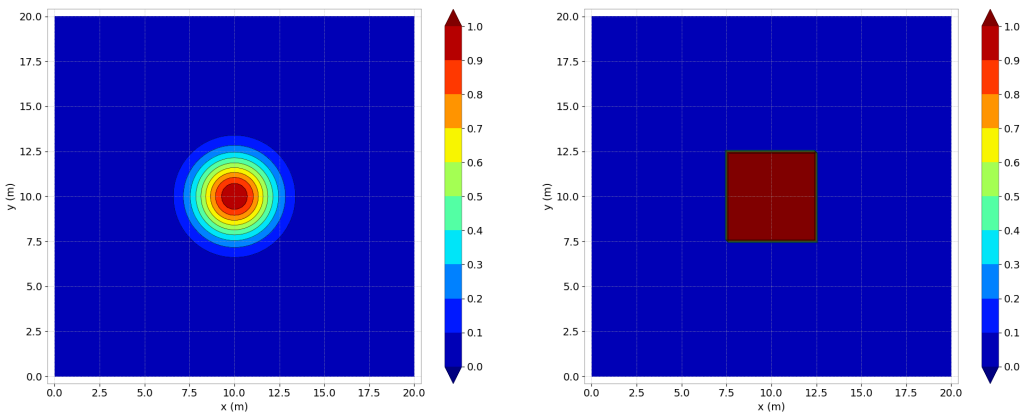


Figure 14.1: Initial conditions for the two tracers.

#### 14.2.3 Boundary conditions

All the tests are carried out with Neumann boundary conditions on the walls.

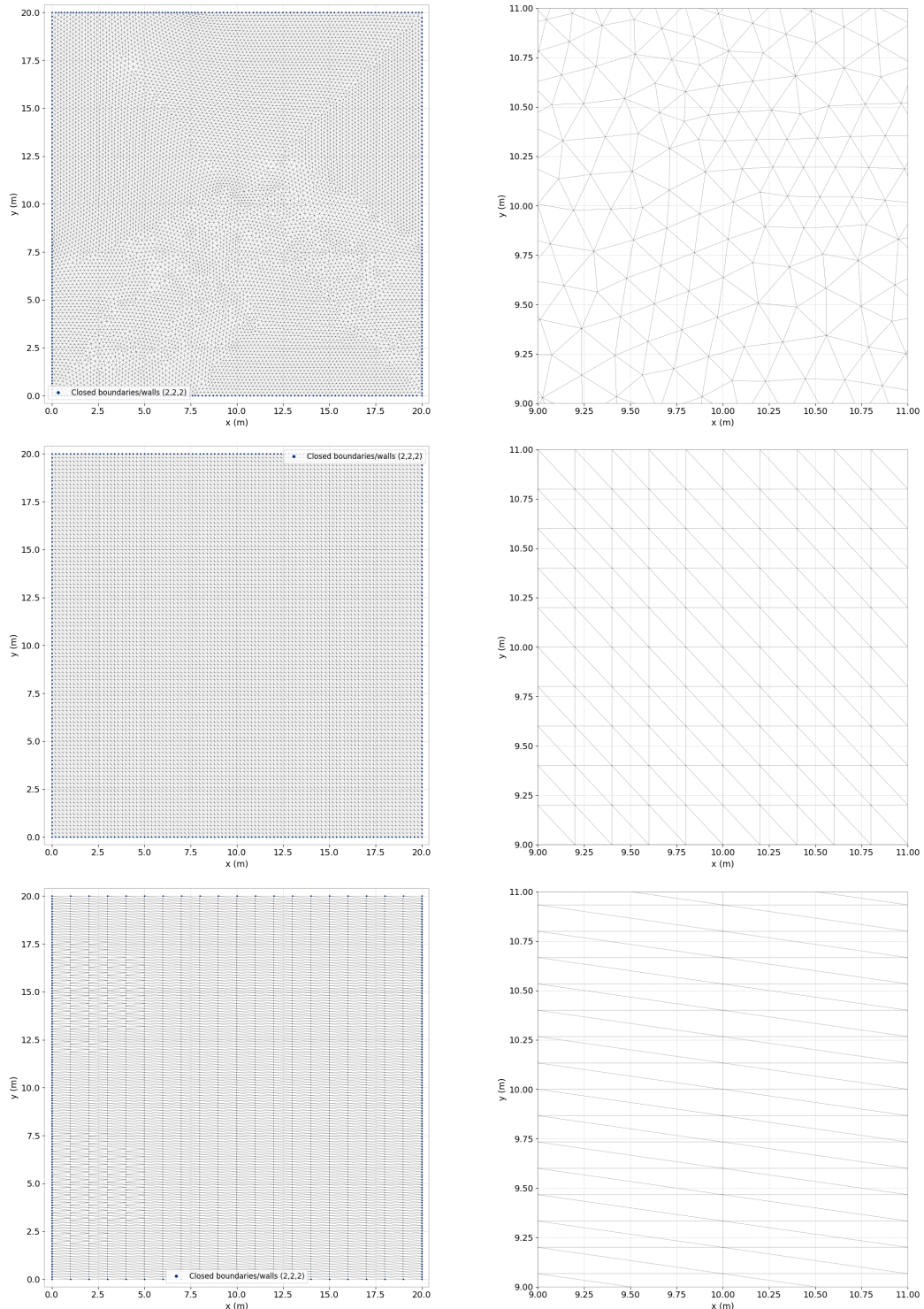


Figure 14.2: 2D domain and unstructured, regular, distorted meshes (from top to bottom) with zoom view (right).

#### 14.2.4 Physical parameters

Tracer diffusion is activated and the following keywords are set:

- DIFFUSION OF TRACERS = TRUE,

- COEFFICIENT FOR DIFFUSION OF TRACERS = 0.1;0.1.

The stability of the explicit finite volume diffusion schemes is garantied by choosing:

- DESIRED FOURIER NUMBER = 0.9.

### 14.2.5 Numerical parameters

The simulation time is set to 10 s. For tracers diffusion, all numerical schemes available in TELEMAC-2D finite volume solver are tested i.e. the TPF (Two Point Flux) scheme, the RTPF (Reconstructed Two Point Flux) scheme, the explicit P1 finite element scheme with mass lumping, designed to work alongside finite volume hyperbolic solvers (noted here HEFE for Hybrid Explicit Finite Element). The schemes are selected via the keyword FINITE VOLUME SCHEME FOR TRACER DIFFUSION. Additionally the standard implicit finite element method of TELEMAC-2D is computed for the purpose of comparison.

## 14.3 Results

### 14.3.1 Computation time

Simulation times for each of these cases with sequential and parallel runs (using 4 processors) are shown in Figure 14.3.

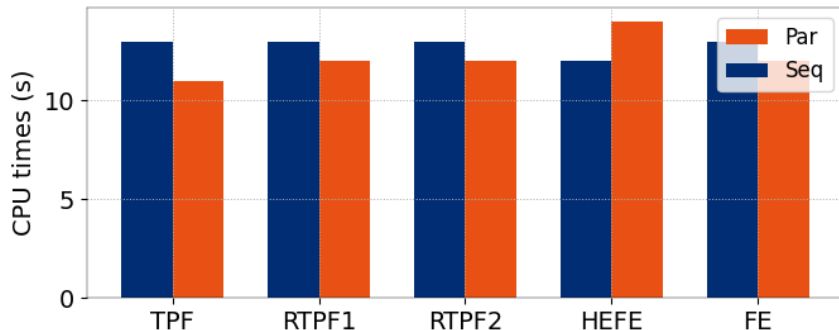


Figure 14.3: CPU times.

### 14.3.2 Comparison of diffusion schemes

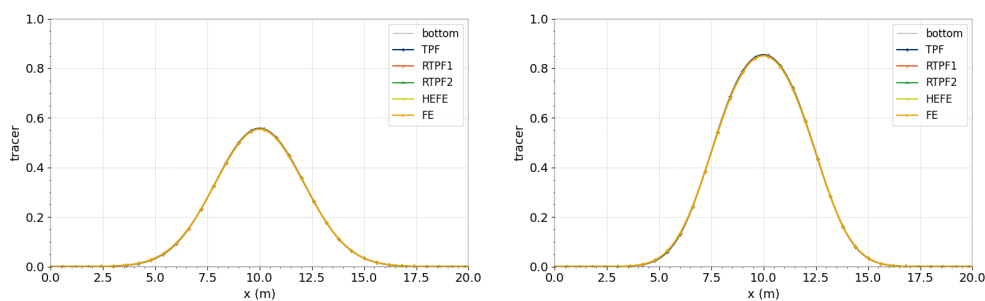


Figure 14.4: Results at final time in the longitudinal centerline of the domain for the two tracers in the case of the first mesh.

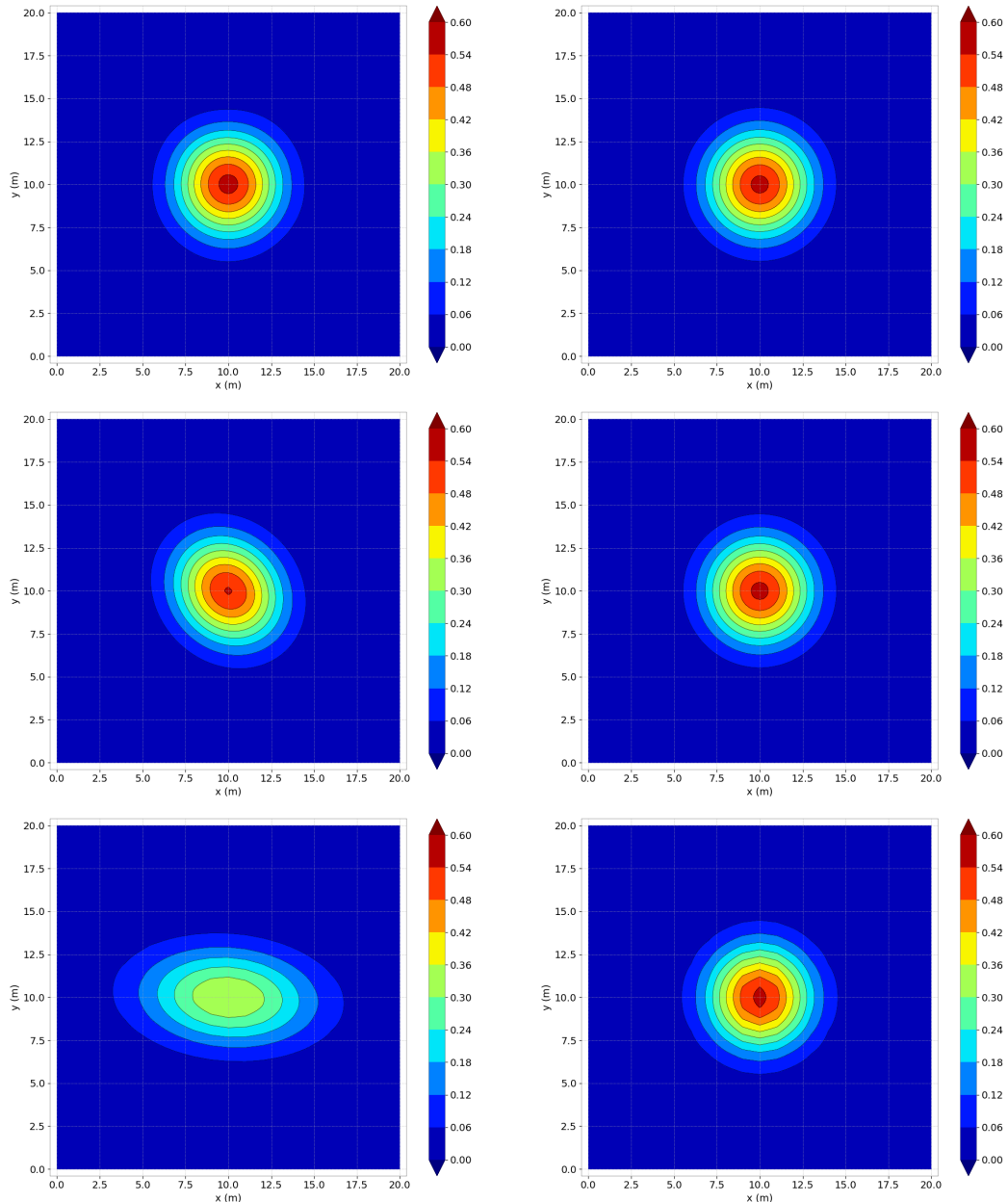


Figure 14.5: TPF (left) and RTPF (right) schemes for the unstructured, regular, distorted meshes (from top to bottom).

## 14.4 Conclusion

TELEMAC-2D is able to model passive scalar diffusion problems in shallow water flows in 2D with finite volume diffusion schemes.

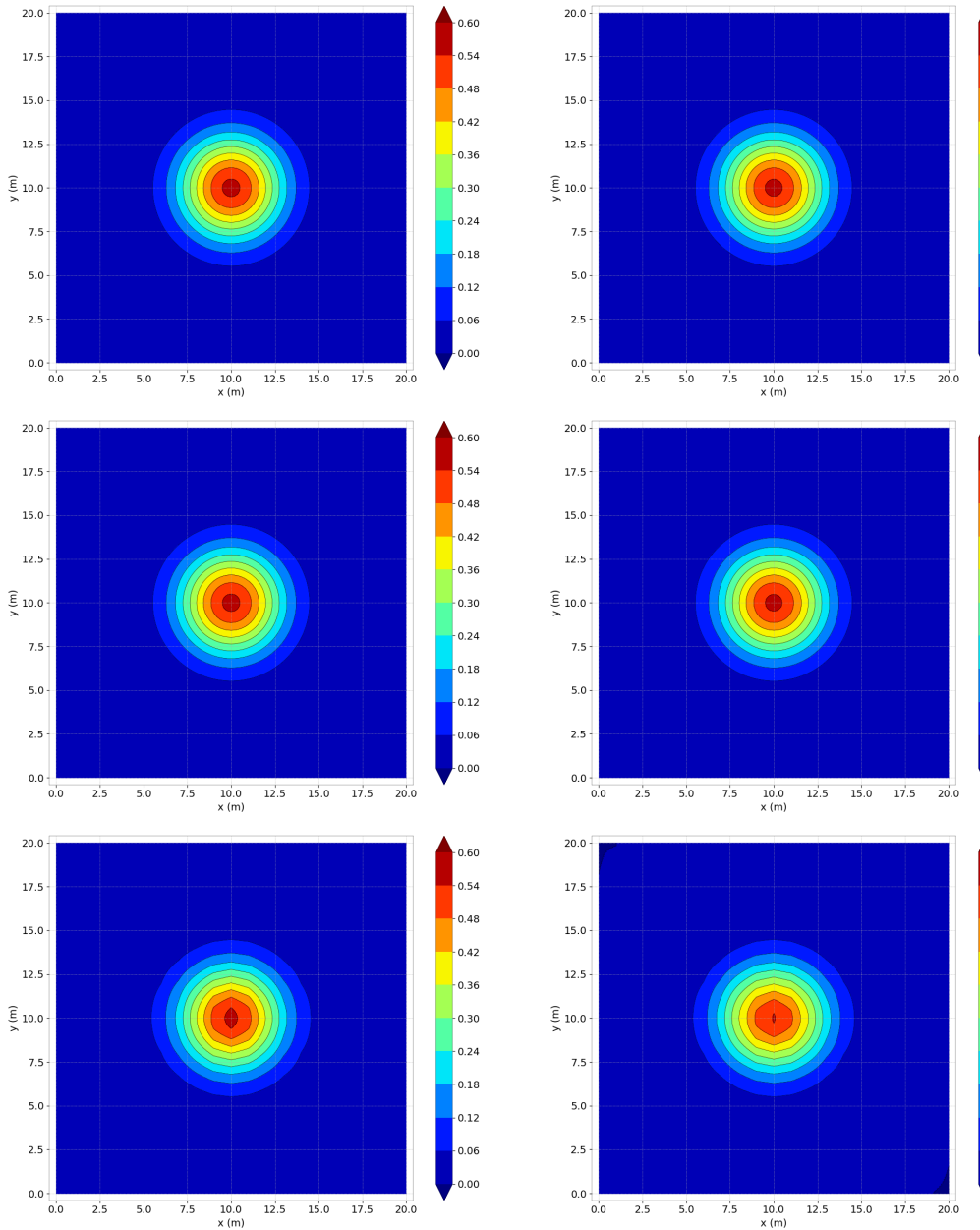


Figure 14.6: HEFE (left) and FE (right) schemes for the unstructured, regular, distorted meshes (from top to bottom).

# 15. Flow at a river confluence (confluence)

## 15.1 Purpose

To demonstrate that TELEMAC-2D can model the flow that occurs at a river confluence. The model represents the junction between two rectilinear laboratory channels with rectangular cross-sections and constant slope.

## 15.2 Description

### 15.2.1 Geometry and Mesh

The main channel is  $10.8 \text{ m} \times 0.8 \text{ m}$  and the influent  $3.2 \text{ m} \times 0.5 \text{ m}$ . The mesh is composed of 6,168 triangular elements and 3,303 nodes. Maximum size range: from 0.03 to 0.1 m. The mesh is refined near the confluence as shown in Figure 15.1.

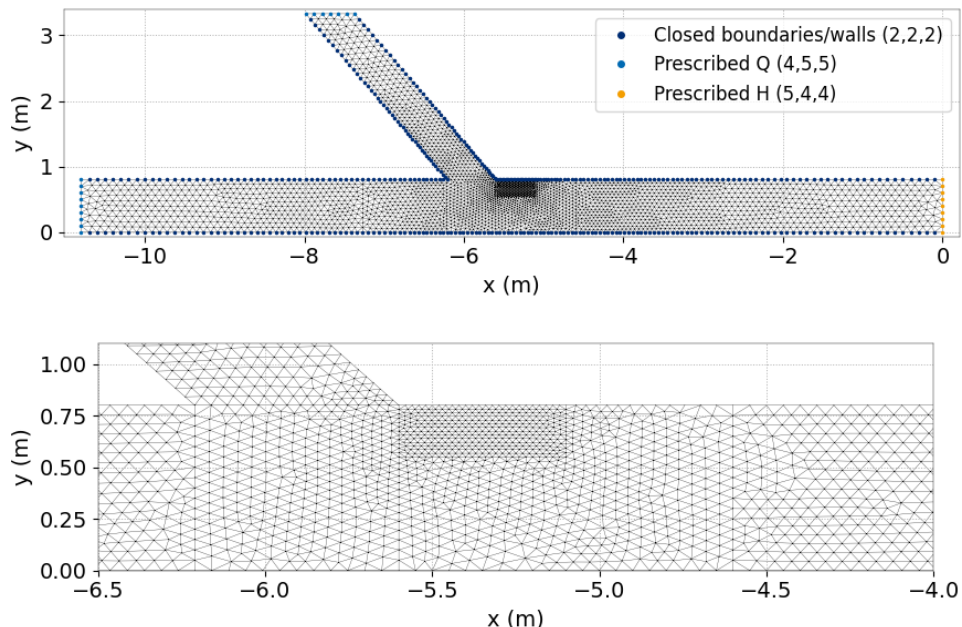


Figure 15.1: Mesh.

### 15.2.2 Bathymetry

The main channel is 0.8 m broad whereas its influent is 0.5 m broad. Both have a slope of  $10^{-3}$  m/m. The two channels join with an angle of  $55^\circ$ . The bathymetry is shown in Figure 15.2.

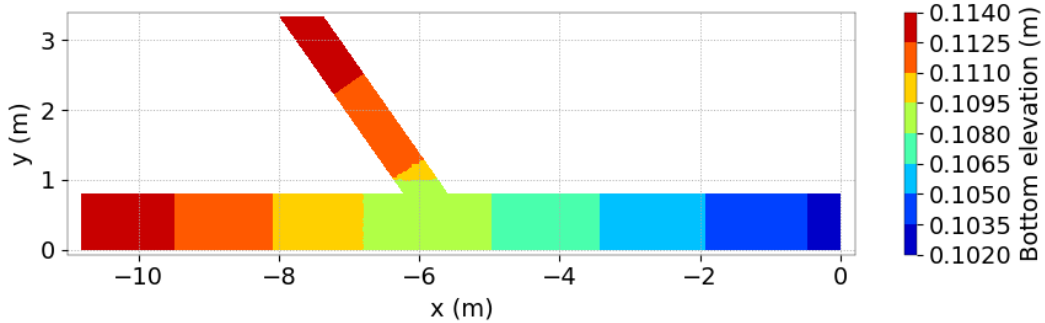


Figure 15.2: Bathymetry.

### 15.2.3 Initial condition

At initial time, there is no velocity in the channel and the free surface at rest is 0.2852 m.

### 15.2.4 Boundary Conditions

Boundary conditions in the main channel are defined by:

- channel inlet:  $Q = 0.07 \text{ m}^3/\text{s}$ ,
- channel outlet:  $H = 0.2852 \text{ m}$ .

At the entrance of the influent channel, a constant discharge of  $Q = 0.035 \text{ m}^3/\text{s}$  is imposed. Lateral boundaries are solid walls with slip condition in the channel.

### 15.2.5 Physical parameters

At the bottom, a Strickler formula with a friction coefficient of  $62 \text{ m}^{1/3}/\text{s}$  is set. Turbulence is modeled by a constant viscosity equal to  $10^{-3} \text{ m}^2/\text{s}$ .

### 15.2.6 Numerical parameters

Duration of the simulation is set to 100 s with a constant time step of 0.1 s.

Numerical scheme parameters are the following:

- Type of advection:
  - Characteristics on velocities (scheme #1),
  - Conservative + modified SUPG on depth (mandatory scheme).
- Type of element:
  - Linear triangle (P1) for  $h$  and for velocities
- Solver : Conjugate gradient,
- Solver accuracy:  $10^{-10}$
- Implicitation for depth and for velocity: 1.0.

## 15.3 Results

Initially the water level is horizontal. In the main channel and in the lateral channel, the free surface increases with time. At the end of the calculation the water surface profile is constant in time downstream and upstream from the confluence which shows that the computation has converged. The water depths in both channels (upstream and downstream) tend to be uniform. The water level upstream from the confluence is 0.30 m higher than the water level downstream.

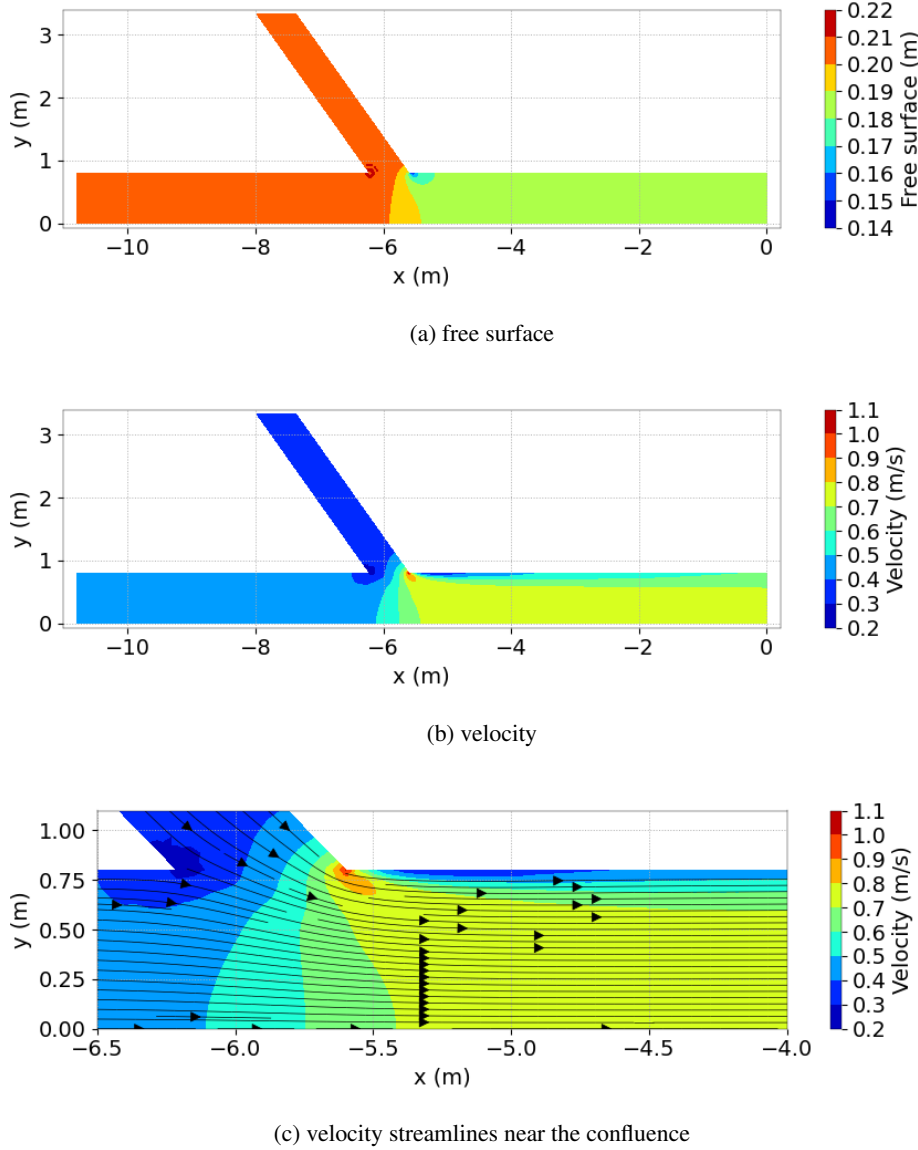


Figure 15.3: Results.

Close to the confluence, the water surface is rapidly varying. The velocity field is regular in the whole domain (see Figure 15.3). No back eddy is computed at the junction of the two rivers with the turbulence model used in this test case despite mesh refinement in this area; such back eddy has been observed on physical model experiments (see ref. [11]).

## 15.4 Conclusions

TELEMAC-2D reproduces appropriately free surface variations at a river confluence. However, in order to simulate in detail the flow pattern in such conditions, more sophisticated turbulence model should be used (see e.g: test case called “cavity”).

## 16. Propagation of a wave over a conical island (conical\_island)

### 16.1 Purpose

To compare TELEMAC-2D simulation with an experiment by Costas E Synolaki [4].

### 16.2 Description

#### 16.2.1 Geometry and mesh

Size of the model: rectangle (25 m × 30 m)

Water depth:  $h = 0.32$  m

Figure 16.1 shows the geometry of the study.

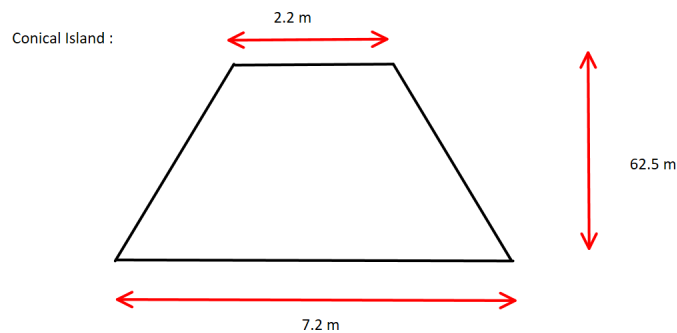


Figure 16.1: Geometry of the study.

- Nodes: 4,995

- Elements: 9,741

Figure 16.2 displays the mesh.

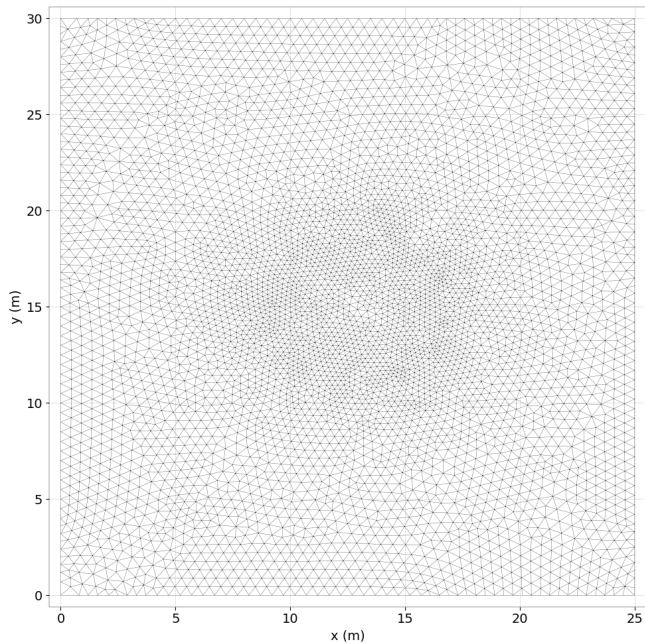


Figure 16.2: Mesh of the study.

Figure 16.3 displays the bathymetry.

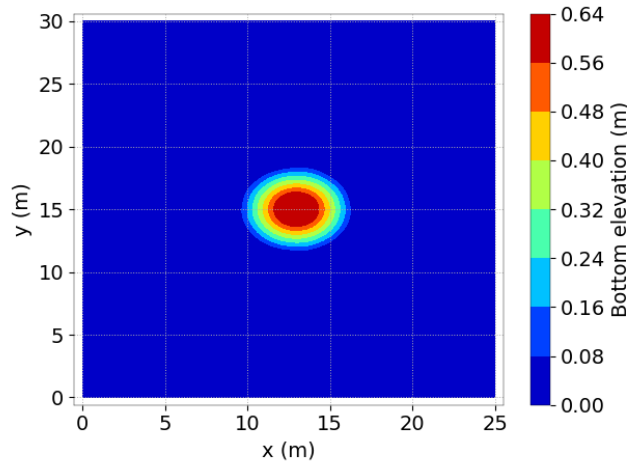


Figure 16.3: Bathymetry of the study.

### 16.2.2 Boundaries

Figure 16.4 shows what types of boundaries are used for this study.

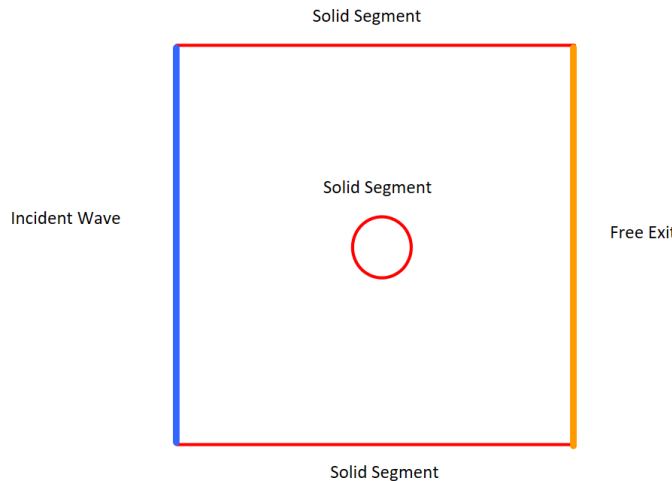


Figure 16.4: Boundaries of the study.

Equation for the free surface:  $\eta(t) = h + H \cdot \operatorname{sech}^2(\sqrt{(3H/(4h^3)) \cdot ct - X_1})$  with  $H/h = 0.045$

Bottom:

- Bottom Friction: Chézy's formula,
- Friction Coefficient:  $100 \text{ m}^{1/2}/\text{s}$ .

### 16.2.3 Physical Parameters

Turbulence: Constant viscosity equal to zero.

### 16.2.4 Numerical parameters

- Type of element: P1 triangle for  $h$  and for velocity
- Finite volume scheme: Kinetic order 2
- Desired Courant number: 0.8
- Option for liquid boundaries: Thompson

Time Date:

- Time step 0.05 s,
- Simulation duration 20 s.

## 16.3 Results

We compare the model and the analytical solution free surface at gauges 6, 9, 16 and 22.

Figure 16.5 displays the experiment we are comparing to.

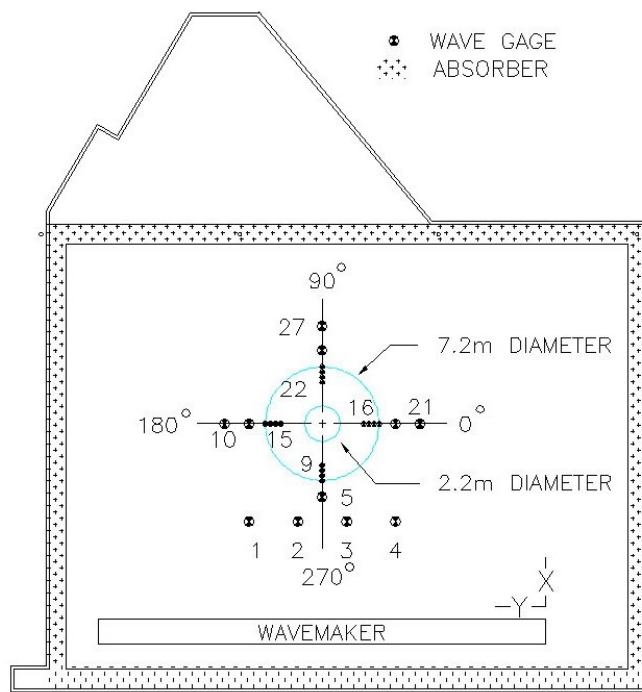


Figure 16.5: Boundaries of the study.

Figure 16.6 shows comparison between experimental values and the simulation at specific points.

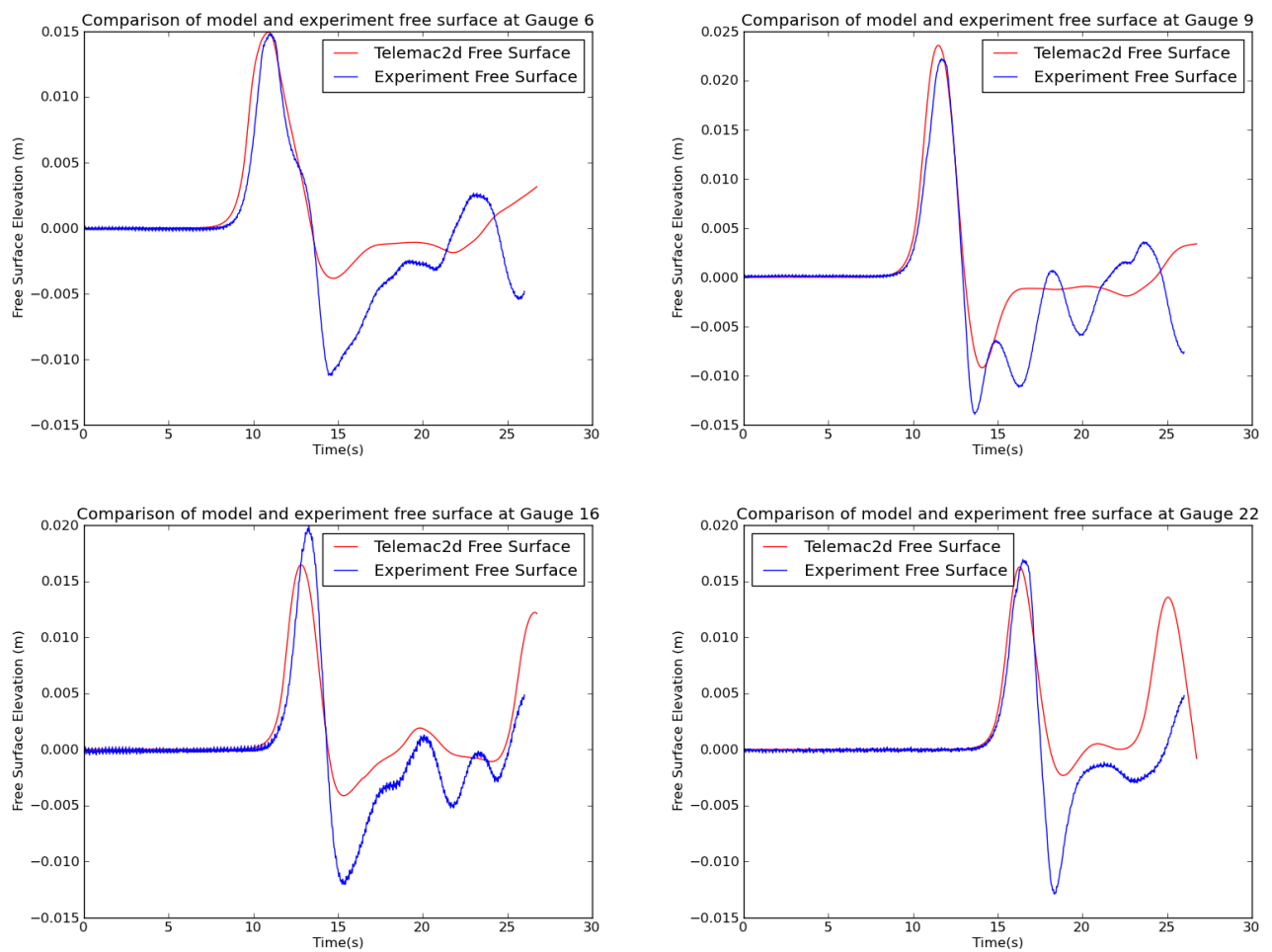


Figure 16.6: Comparison with experimental data at the some gauges.

## 17. convergence

This test shows the old fashion to carry out convergence studies.

It is now recommended to use Python scripts for such studies. See for example vnv.py scripts with \_convergence suffix in bump, cone, flume\_tracer, thacker or tracer\_diffusion\_convergence.

## 18. Transient flood flow in the valley of river Culm (culm)

### 18.1 Purpose

To illustrate that TELEMAC-2D is capable of simulating the real inundation of a flood plain. Also to show the evolution in time of the water surface and velocity patterns in the flood plain.

#### 18.1.1 Approach

This test case represents the plain of the river Culm (Devon, UK) over a 11 km reach. The river is meandering in its valley. A narrowing concentrates flow in the middle of the reach represented. The main channel is approximately 19 m wide. The downstream elevation and the upstream discharge prescribed vary in time to simulate one flood of the river. Field data concerning discharge and flooded areas were available for this event.

### 18.2 Description

#### 18.2.1 Geometry and mesh

The size of the model river is approximately 10 km with water depth at rest = 0 m. The mesh is unstructured. It is denser in the bed of the river than in the flood plain. Triangles are elongated in the direction of flow:

- 2,019 triangular elements,
- 1,130 nodes,
- Maximum size range: from 18 to 258 m.

#### 18.2.2 Boundaries

Initially:

- River entrance:  $Q = 28.32 \text{ m}^3/\text{s}$  imposed,
- River outlet:  $H = 23.77 \text{ m}$  imposed.

During the simulation, the discharge at the entrance and the water level at the outlet are varying with time and prescribed by the formatted data files.

The lateral boundaries are solid walls with slip condition in the domain.

Bottom: Strickler formula with friction coefficient =  $30 \text{ m}^{1/3}/\text{s}$ .

The mesh and the topography are shown in Figures 18.1 and 18.2.

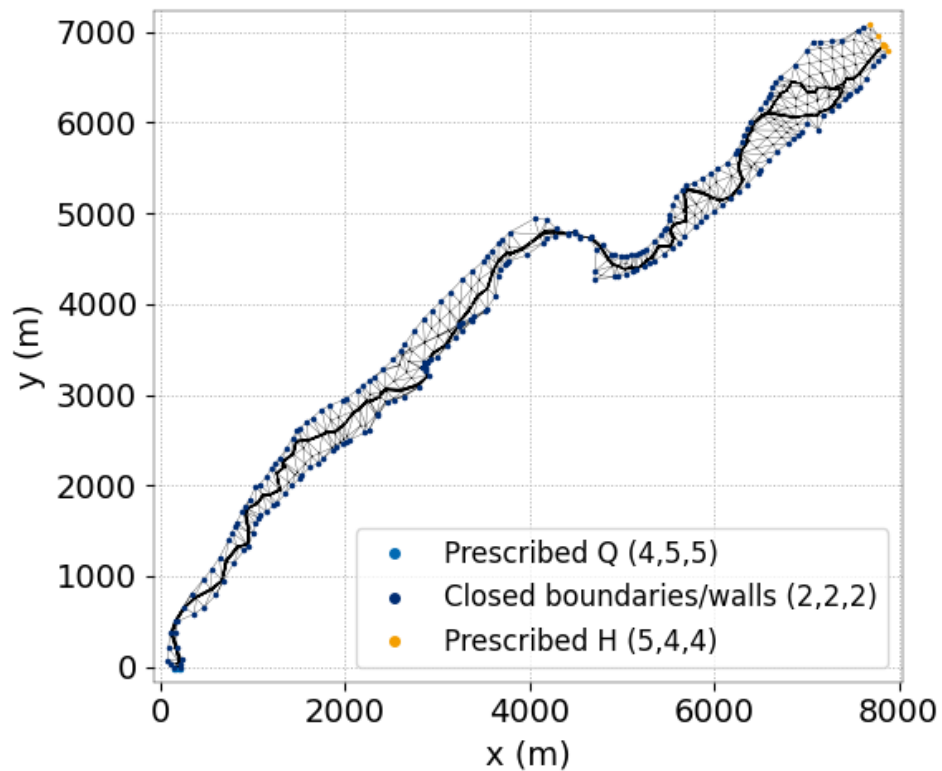


Figure 18.1: 2D-mesh of the culm case.

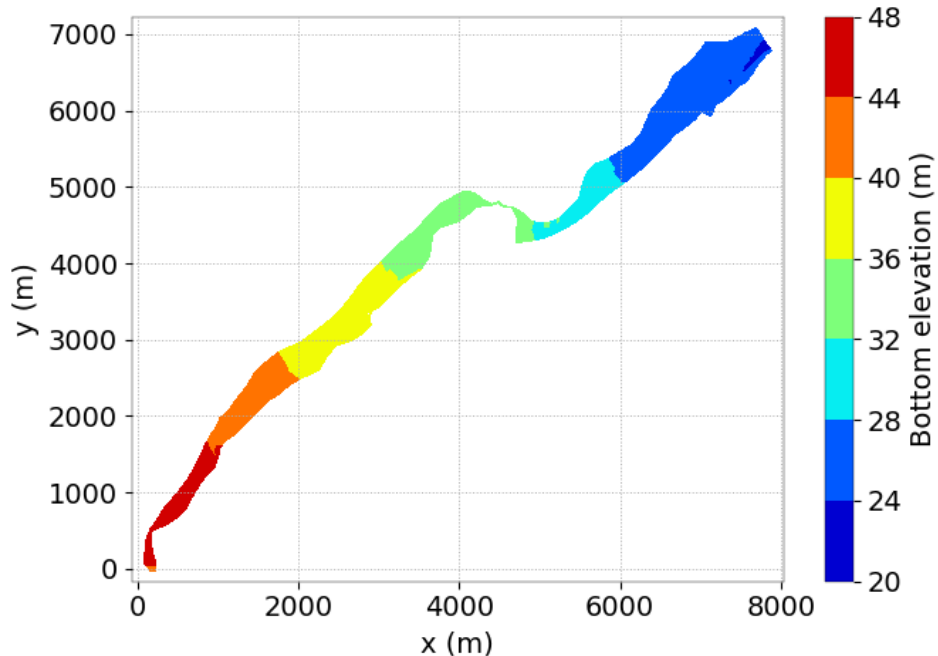


Figure 18.2: Bathymetry of the culm case.

### 18.2.3 Physical parameters

The model of turbulence is constant viscosity with velocity diffusivity =  $2 \text{ m}^2/\text{s}$ .

### 18.2.4 Numerical parameters

Type of advection:

- Methods of characteristics on velocities (scheme #1),
- Conservative + modified SUPG on depth (mandatory scheme).

The type of element is linear triangle (P1) for  $h$  and for velocities.

- Implicitation for depth and velocities = 1,
- Solver: Conjugate gradient with solver accuracy  $10^{-4}$ ,
- Tidal flats,
- Time step = 2 s,
- Simulation duration = 54,000 s (= 15 h).

## 18.3 Results

The water profile in the river varies according to the flood conditions prescribed at the boundaries (water elevation downstream and discharge upstream). Flooding of the plain occurs during the simulation. At the peak of the inundation, the water depth is approximately equal to 0.40 m in the plain close to the river.

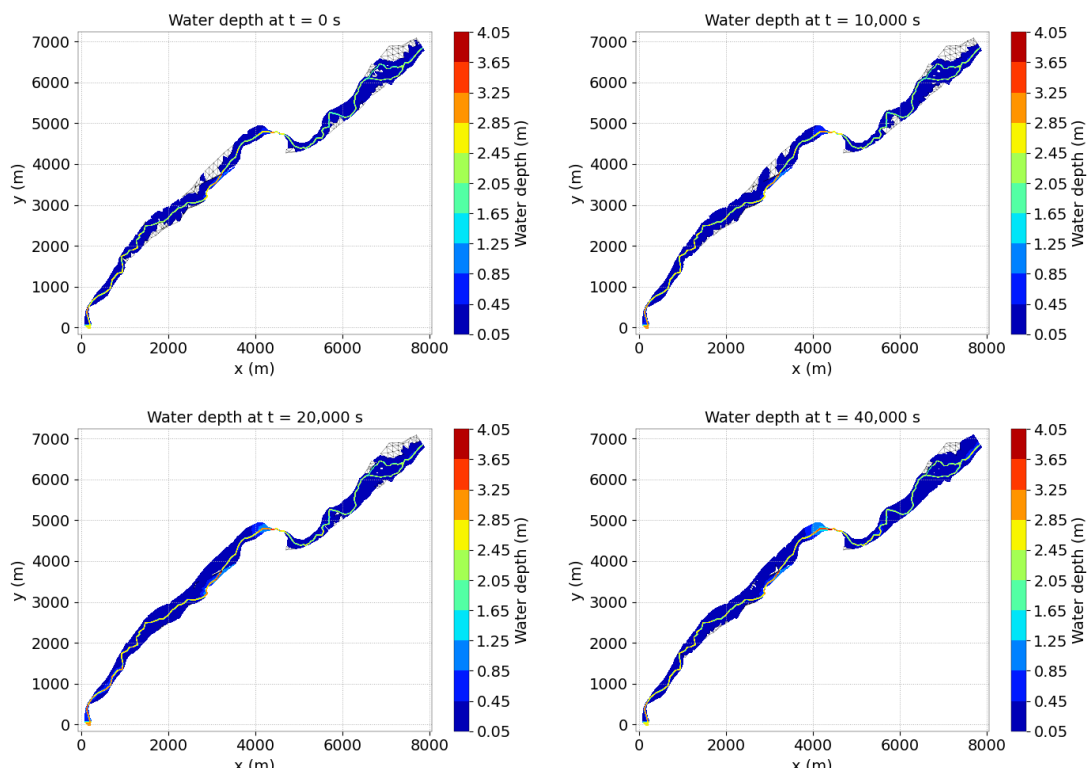


Figure 18.3: Water depth at different times.

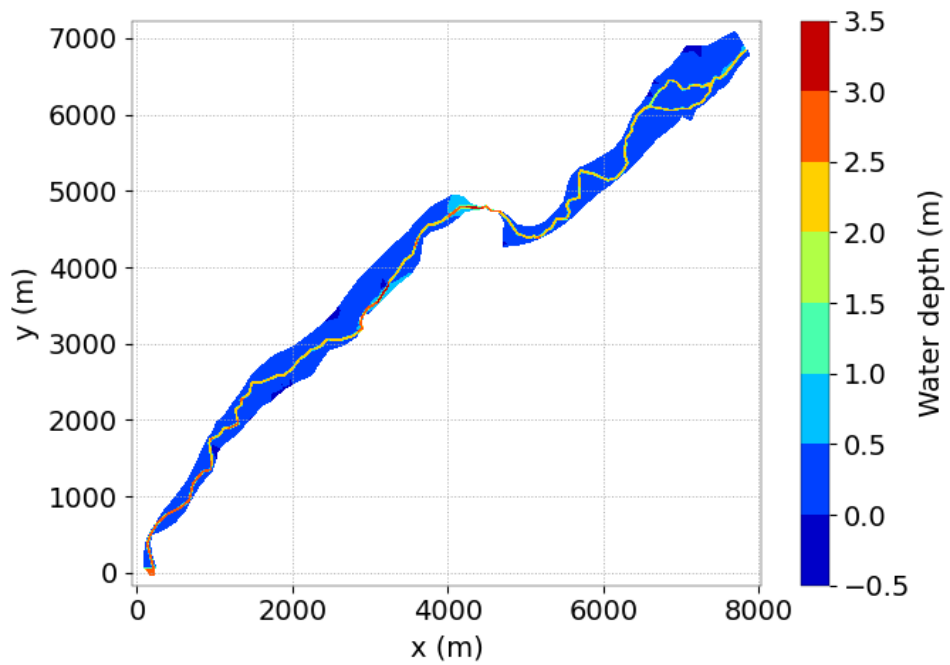


Figure 18.4: Water depth at final time.

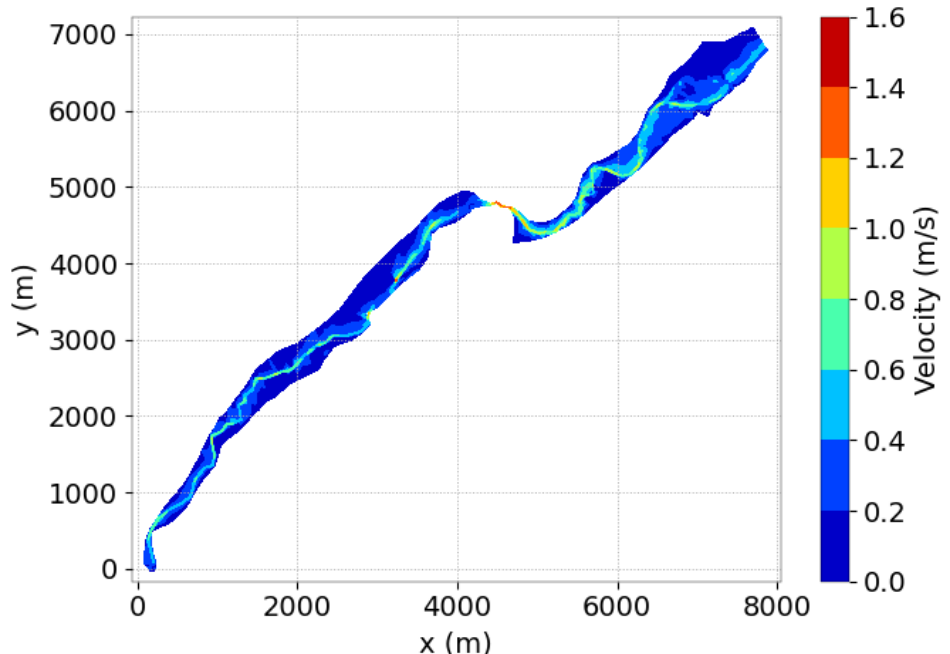


Figure 18.5: Velocity at final time.

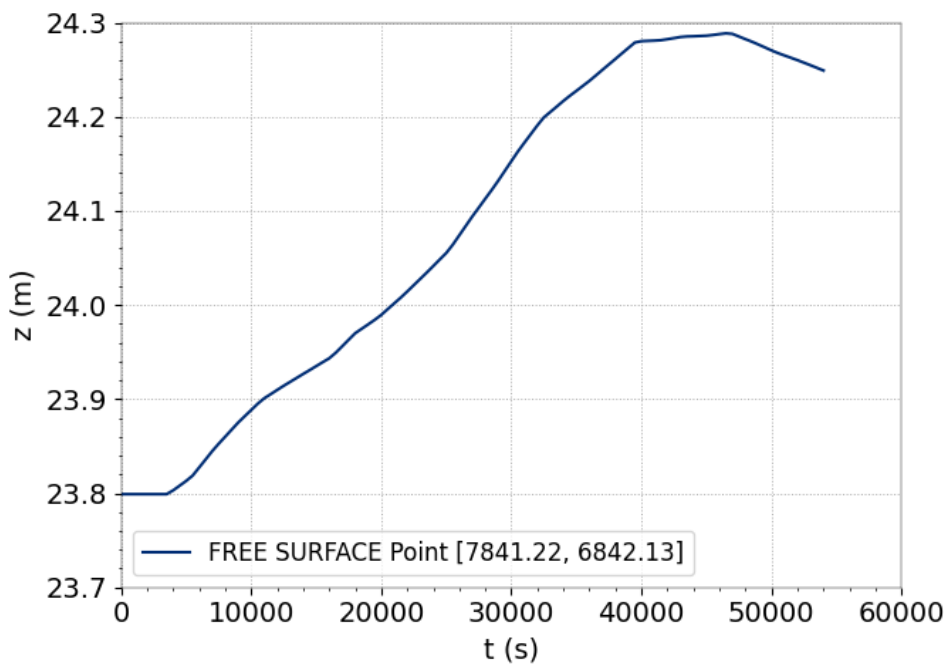


Figure 18.6: Free surface at point (7841.22 ; 6842.13).

#### 18.4 Conclusion

TELEMAC-2D can simulate the flow resulting from the inundation of a river valley by natural floods.

# 19. Dambreak: Ritter and Stoker

## 19.1 Purpose

The purpose of this case is to demonstrate that the TELEMAC-2D solution is able to simulate the propagation of a wave due to a dam break. We compare TELEMAC-2D with two classical analytical solutions: Ritter's solution and Stoker's solution.

## 19.2 Description

### 19.2.1 Geometry and mesh

We consider a channel on length  $L = 16$  m and width  $l = 0.45$  m with a flat bottom and with no friction.

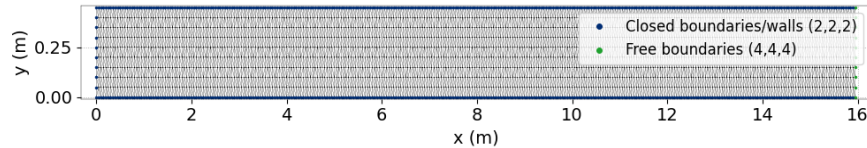


Figure 19.1: Mesh of the channel.

### 19.2.2 Initial conditions

Let us define the abscissa of the dam by  $x_d$ . The initial condition is given by a 1D Riemann problem:

**Dry case:**

$$h(x) = \begin{cases} h_l > 0 & \text{for } 0 \leq x \leq x_d \\ h_r = 0 & \text{for } x_d < x \leq L \end{cases} \quad (19.1)$$

with  $h_l \geq h_r$  and zero velocity in the channel.

**Wet case:**

$$h(x) = \begin{cases} h_l & \text{for } 0 \leq x \leq x_d \\ h_r & \text{for } x_d < x \leq L \end{cases} \quad (19.2)$$

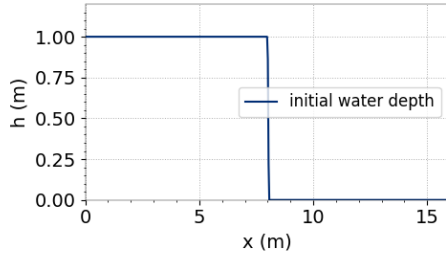


Figure 19.2: Initial condition for Ritter.

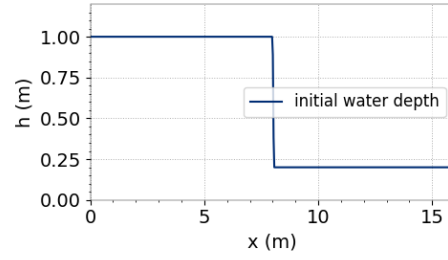


Figure 19.3: Initial condition for Stoker.

### 19.2.3 Analytical solutions

Given the 2 Riemann problems defined as initial conditions, the analytical solution is obtained with characteristics method and is given by:

#### Dry case: Ritter's solution

$$h(x, t) = \begin{cases} h_l & \text{if } x \leq x_A(t) \\ \frac{4}{9g} \left( \sqrt{gh_l} - \frac{x - x_0}{2t} \right)^2 & \text{if } x_A(t) \leq x \leq x_B(t) \\ 0 & \text{if } x_B(t) \leq x \end{cases} \quad (19.3)$$

$$u(x, t) = \begin{cases} 0 & \text{if } x \leq x_A(t) \\ \frac{2}{3} \left( \frac{x - x_0}{t} + \sqrt{gh_l} \right) & \text{if } x_A(t) \leq x \leq x_B(t) \\ 0 & \text{if } x_B(t) \leq x \end{cases} \quad (19.4)$$

$$\begin{cases} x_A(t) = x_0 - t\sqrt{gh_l} \\ x_B(t) = x_0 + 2t\sqrt{gh_l} \end{cases} \quad (19.5)$$

#### Wet case: Stoker's solution

$$h(x, t) = \begin{cases} h_l & \text{if } x \leq x_A(t) \\ \frac{4}{9g} \left( \sqrt{gh_l} - \frac{x - x_0}{2t} \right)^2 & \text{if } x_A(t) \leq x \leq x_B(t) \\ \frac{c_m^2}{9} & \text{if } x_B(t) \leq x \leq x_C(t) \\ h_r & \text{if } x_C(t) \leq x \end{cases} \quad (19.6)$$

$$u(x, t) = \begin{cases} 0 & \text{if } x \leq x_A(t) \\ \frac{2}{3} \left( \frac{x - x_0}{t} + \sqrt{gh_l} \right) & \text{if } x_A(t) \leq x \leq x_B(t) \\ 2(\sqrt{gh_l} - c_m) & \text{if } x_B(t) \leq x \leq x_C(t) \\ 0 & \text{if } x_C(t) \leq x \end{cases} \quad (19.7)$$

$$\text{with :} \quad \begin{cases} x_A(t) = x_0 - t\sqrt{gh_l} \\ x_B(t) = x_0 + t(2\sqrt{gh_l} - 3c_m) \\ x_C(t) = x_0 + t \left( \frac{2c_m^2(\sqrt{gh_l} - c_m)}{c_m^2 - gh_r} \right) \end{cases} \quad (19.8)$$

$c_m$  being solution of  $-8gh_r c_m^2 (\sqrt{gh_l} - c_m)^2 + (c_m^2 - gh_r)^2 (c_m^2 + gh - r)$ .

### 19.2.4 Boundary conditions

Boundary conditions are defined by no slip walls on the entry and channel sides and torrential outflow on the outlet boundary with free water depth and velocity.

### 19.2.5 Physical parameters

The molecular viscosity is set as constant and equal to  $0 \text{ m}^2/\text{s}$  (VELOCITY DIFFUSION = 0) and no friction is set to the bottom.

### 19.2.6 Numerical parameters

For this test case, duration is set to 2.5 s for the Ritter case and 1.5 s for the Stocker case. Several numerical schemes of advection for velocities are confronted. The solver used is the conjugate gradient with an accuracy of  $10^{-8}$ . The parameters specific to each case are summed up in Table 19.1.

| Case | Name | Equations       | Advection scheme for velocities | Time-step / Desired Courant number |
|------|------|-----------------|---------------------------------|------------------------------------|
| 1    | CHAR | Saint-Venant FE | Characteristics                 | 0.0025 s / -                       |
| 2    | NERD | Saint-Venant FE | Edge-based n-scheme             | 0.0025 s / -                       |
| 3    | ERIA | Saint-Venant FE | ERIA scheme                     | 0.0025 s / -                       |
| 4    | HLLC | Saint-Venant FV | HLLC order 1                    | - / 0.8                            |
| 5    | KIN1 | Saint-Venant FV | Kinetic order 1                 | - / 0.8                            |
| 6    | KIN2 | Saint-Venant FV | Kinetic order 2                 | - / 0.8                            |

Table 19.1: List of the simulation parameters used for the six cases tested in the Ritter and Stokes cases.

## 19.3 Results for Ritter

### 19.3.1 Computation time

Simulation times for each of these cases with sequential and parallel runs (using 4 processors) are shown in Figure 19.4<sup>1</sup>.

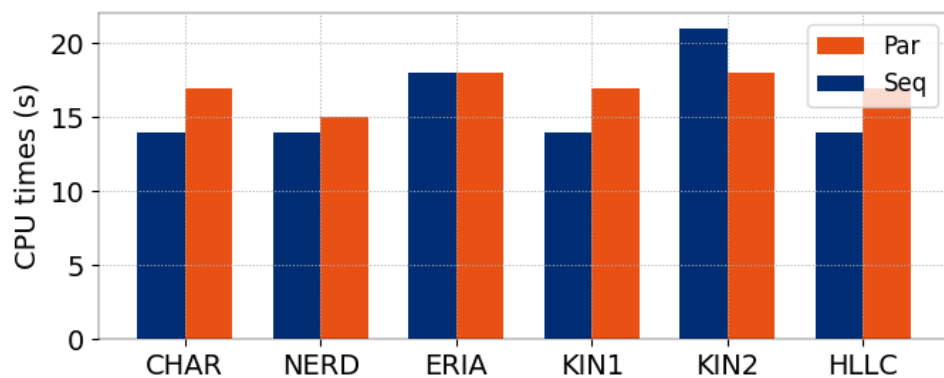


Figure 19.4: CPU times.

<sup>1</sup>Keep in mind that these times are specific to the validation run and the type of processors that were used for this purpose.

### 19.3.2 First observation

Figure 19.5 illustrates the result obtained for water depth and velocity after 0.5 s of simulation with the Kinetic finite volume scheme. The rarefaction wave is clearly visible and well captured as well as the moving wet/dry transition. In Figures 19.6 and 19.7, water depth and velocity are presented in the 2D plane.

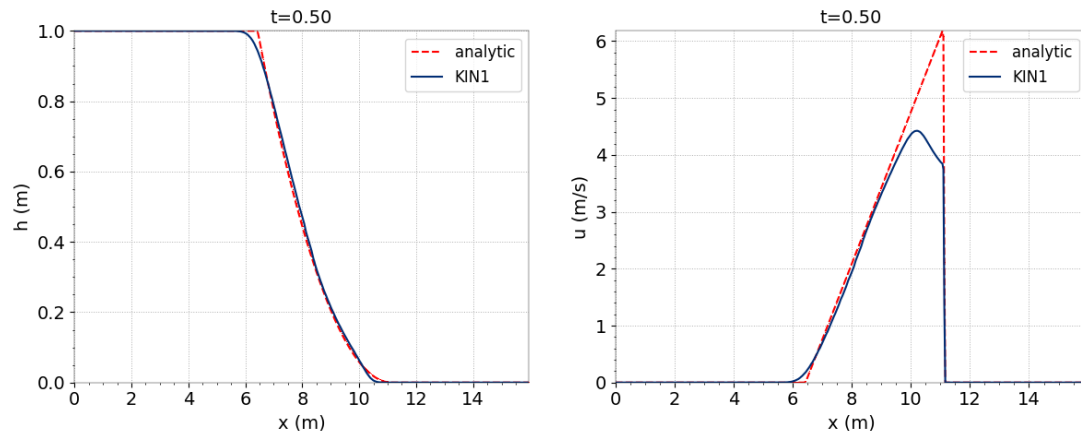


Figure 19.5: Water depth and velocity with the Kinetic scheme.

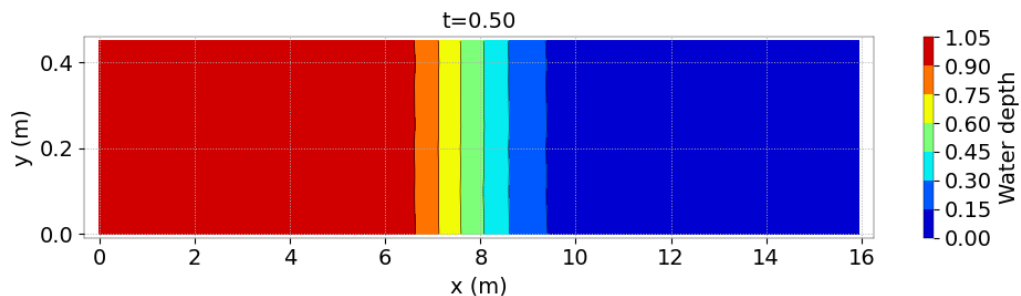


Figure 19.6: Water depth in 2D with the Kinetic scheme.

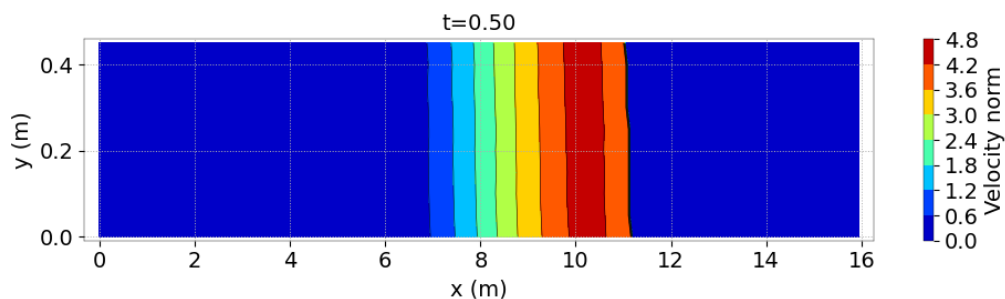


Figure 19.7: Velocity norm in 2D with the Kinetic scheme.

### 19.3.3 Comparison of schemes

The results obtained with the different numerical schemes are compared to the analytical solution for both water depth and velocity. Comparisons are shown in Figure 19.8.

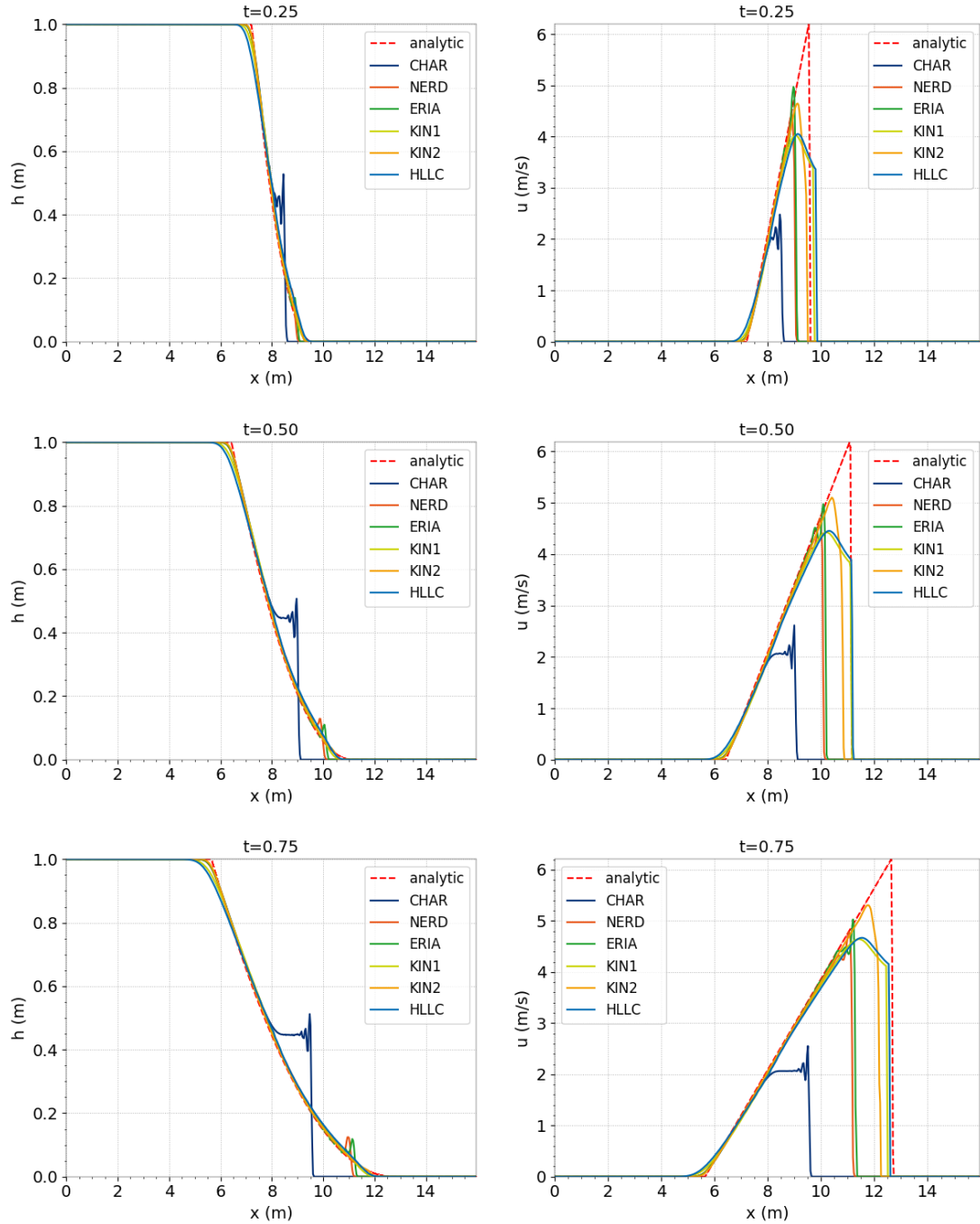


Figure 19.8: Comparison of water depth and velocity with analytical solution.

Kinetic and HLLC schemes are able to track the rarefaction wave with a good precision and are capable of handling wet/dry transition smoothly. NERD and ERIA are also able to track the rarefaction wave schemes but exhibit oscillations on the wet/dry transition. Finally characteristics are not capable to reproduce the analytical solution.

#### 19.3.4 Accuracy

For a more quantitative comparison of schemes, the  $L^1$ ,  $L^2$  and  $L^\infty$  error norms of the water depth and velocity are calculated at each time step for each scheme.  $L^2$  errors time series and

time integrated  $L^1$ ,  $L^2$  and  $L^\infty$  errors are presented in Figures 19.9, 19.10 and 19.11 for  $H$ ,  $U$  and  $V$  respectively.

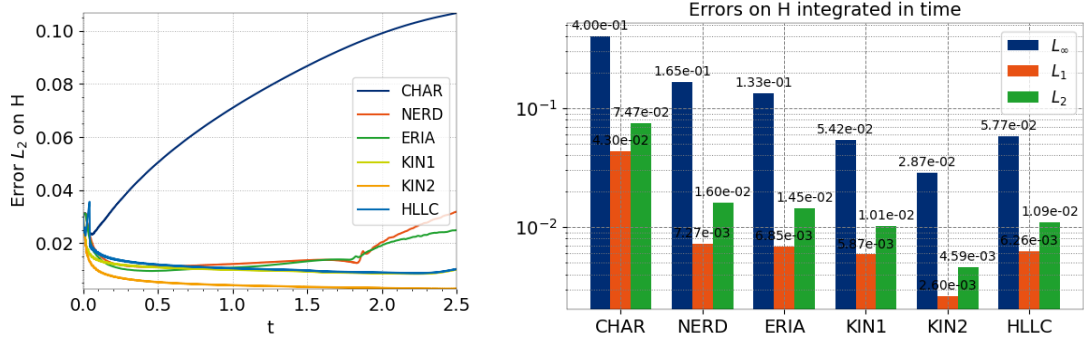


Figure 19.9: Error on  $H$ : timeseries (left) and integrated over time (right).

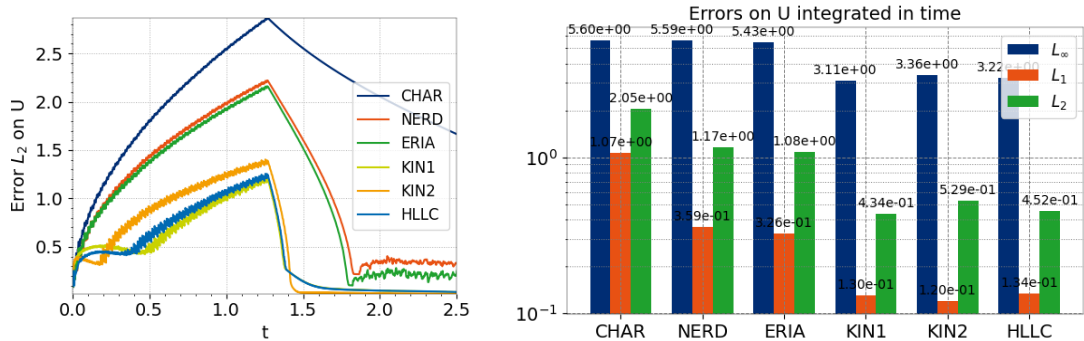


Figure 19.10: Error on  $U$ : timeseries (left) and integrated over time (right).

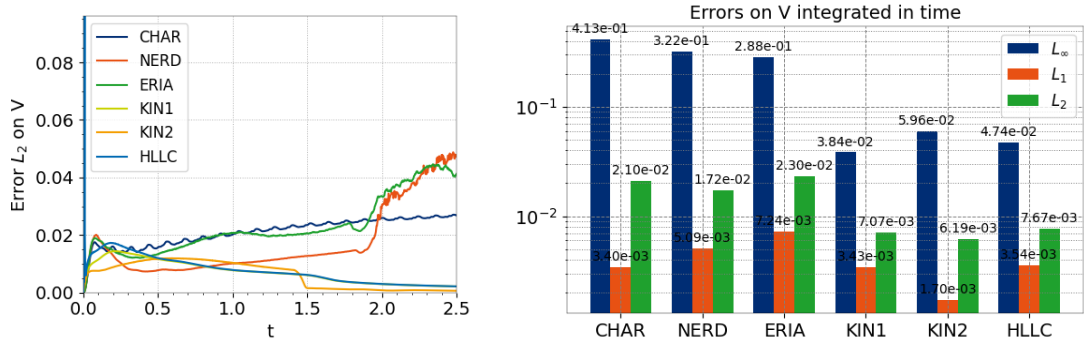


Figure 19.11: Error on  $V$ : timeseries (left) and integrated over time (right).

For water depth, first order kinetic scheme, HLLC, NERD and ERIA exhibit similar errors but kinetic and HLLC are more precise on velocity. Finally the time integrated errors show that Kinetic schemes and HLLC are the most precise schemes, especially the second order kinetic scheme. This is to be put in perspective with CPU time presented previously in Figure 19.4.

### 19.3.5 Positivity of the water depth

The minimum values of the water depth are checked during the whole simulation. Results are shown in Figure 19.12.

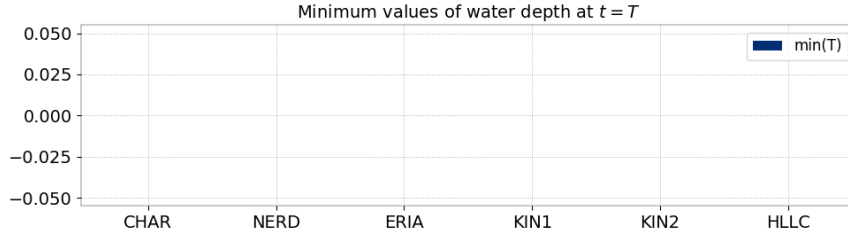


Figure 19.12: Minimum values of water depths for the Ritter test case.

No negative values are recorded, which shows that the positivity is fulfilled. In the case of finite volume schemes, positivity is ensured without additionnal treatment. With finite element schemes, the positivity is ensured with a treatment of negative depths during simulation (TREATMENT OF NEGATIVE DEPTHS = 2 for characteristics and NERD and 3 for ERIA scheme).

### 19.3.6 Mass balance

Mass conservation can be checked by calculating the mass in the domain during time. The lost mass is calculated as  $M_{initial} - M_{final}$ . The evolution of mass for each of the schemes is shown in Figure 19.13.

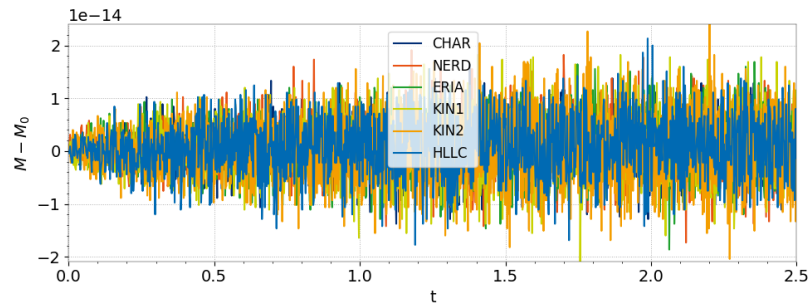


Figure 19.13: Mass loss for the tested schemes on the Ritter test case.

### 19.3.7 Energy balance

In this section, the evolution of the mean energy is checked. In fact, for the Saint-Venant equations, the quantity  $h \frac{\|U\|^2}{2} + g \frac{h^2}{2}$ , called mean or integrated energy, is conserved, where  $\|U\|$  is the Saint-Venant depth averaged velocity magnitude. The following quantities are studied:

- Integrated potential energy  $E_p = \int \int_{\Omega_{xy}} \rho_{water} g \frac{h^2}{2} dx dy$  where  $\Omega_{xy}$  is the 2D domain of simulation: Figure 19.14,
- Integrated kinetic energy  $E_c = \int \int_{\Omega_{xy}} \rho_{water} h \frac{\|U\|^2}{2} dx dy$ : Figure 19.15,
- Integrated mechanical energy  $E_m = E_p + E_c$ : Figure 19.16.

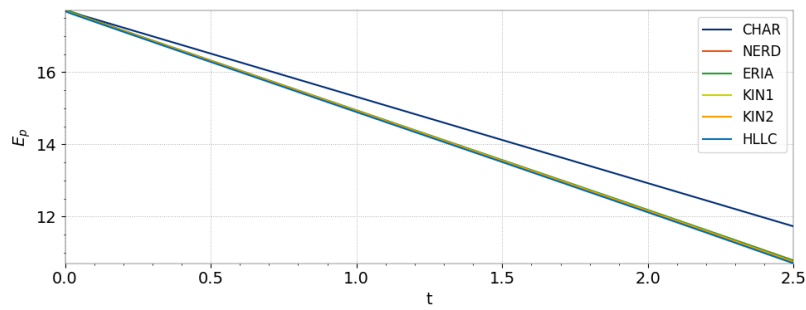


Figure 19.14: Evolution of the potential energy for the tested schemes on the Ritter test case.

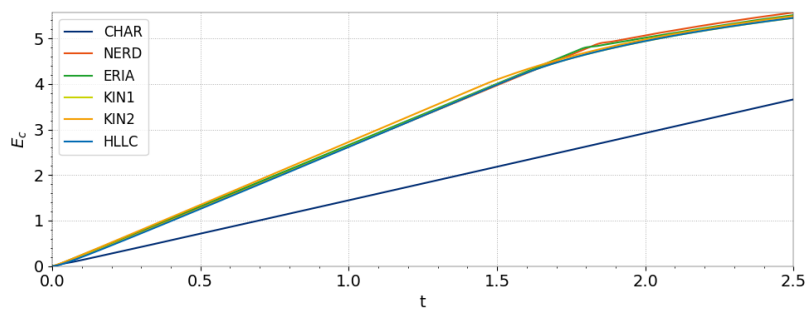


Figure 19.15: Evolution of the kinetic energy for the tested schemes on the Ritter test case.

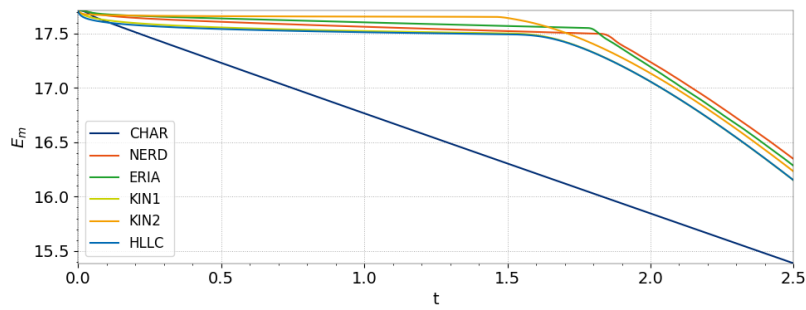


Figure 19.16: Evolution of the mechanical energy for the tested schemes on the Ritter test case.

## 19.4 Results for Stoker

### 19.4.1 Computation time

Simulation times for each of these cases with sequential and parallel runs (using 4 processors) are shown in Figure 19.17<sup>2</sup>.

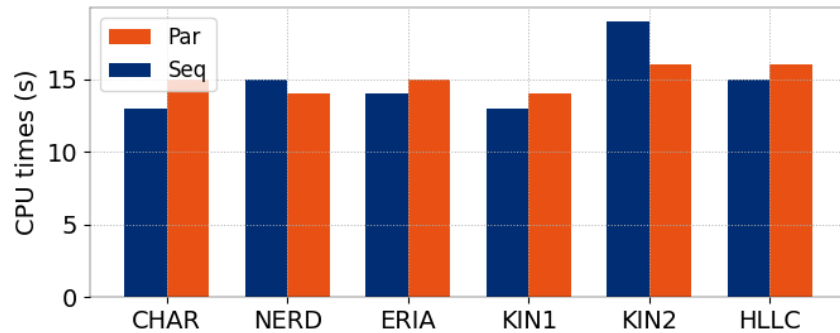


Figure 19.17: CPU times.

### 19.4.2 First observation

Figure 19.5 illustrates the result obtained for water depth and velocity after 0.5 s of simulation with the Kinetic finite volume scheme. The left going rarefaction wave and the right going shock are clearly visible and well captured by the Kinetic scheme.

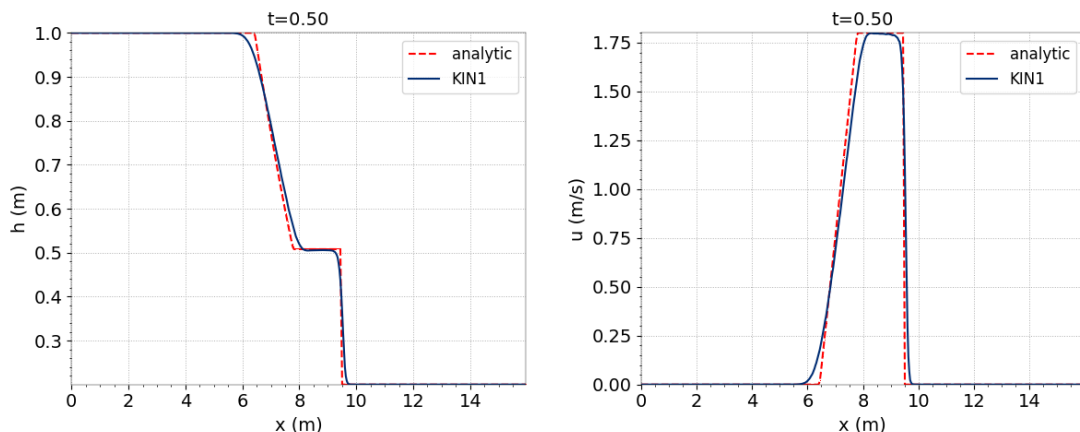


Figure 19.18: Water depth and velocity with the Kinetic scheme.

### 19.4.3 Comparison of schemes

The results obtained with the different numerical schemes are compared to the analytical solution for both water depth and velocity. Comparisons are shown in Figure 19.19.

---

<sup>2</sup>Keep in mind that these times are specific to the validation run and the type of processors that were used for this purpose.

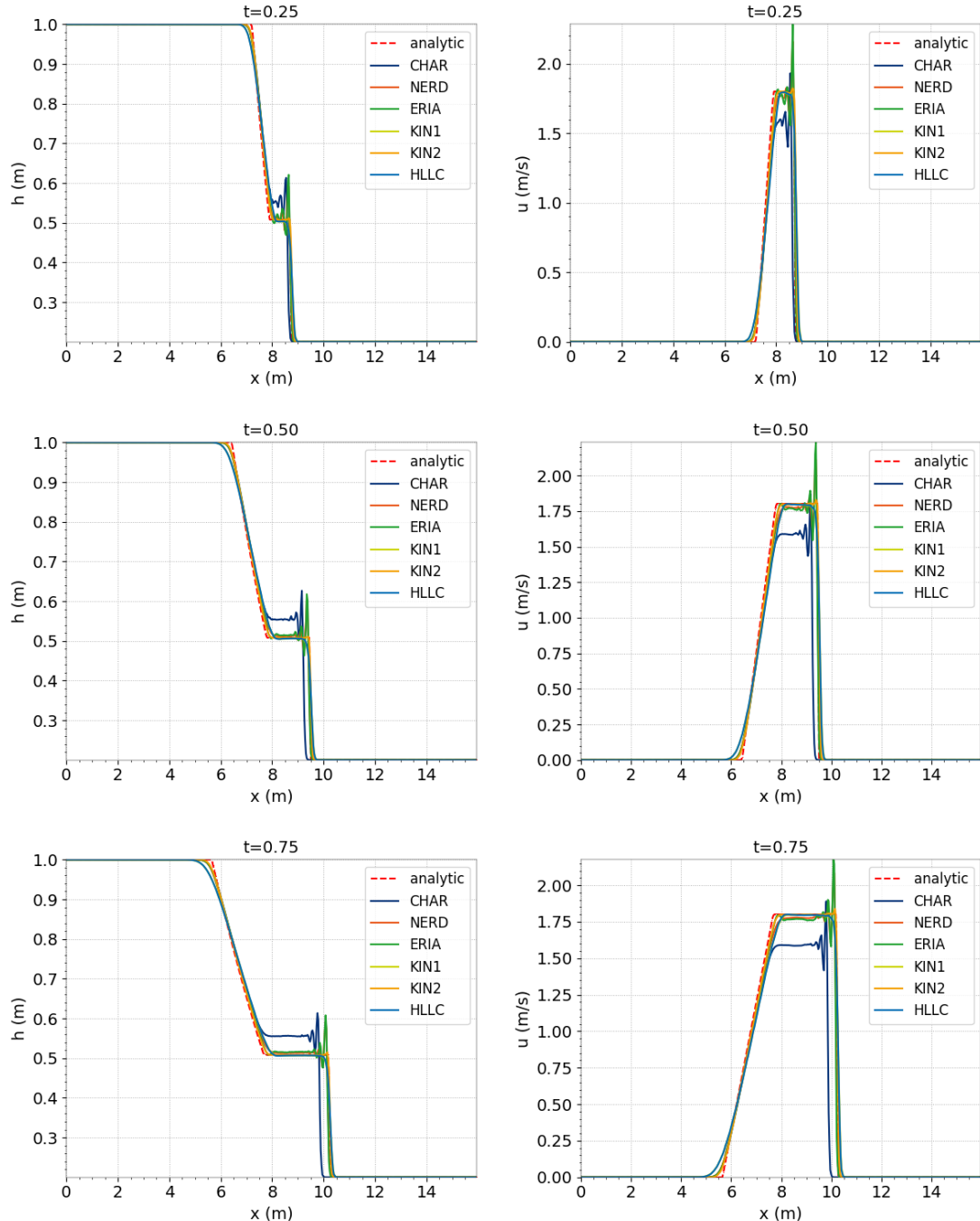


Figure 19.19: Comparison of water depth and velocity with analytical solution.

Kinetic and HLLC schemes are able to track the rarefaction wave and the shock with a good precision. Characteristics, NERD and ERIA schemes exhibit numerical oscillations on the shock. The worst results are obtained with the characteristics which is not capable of reproducing the analytical solution both in terms of water levels and velocity.

#### 19.4.4 Accuracy

For a more quantitative comparison of schemes, the  $L^1$ ,  $L^2$  and  $L^\infty$  error norms of the water depth and velocity are calculated at each time step for each scheme.  $L^2$  errors time series and

time integrated  $L^1$ ,  $L^2$  and  $L^\infty$  errors are presented in Figures 19.20, 19.21 and 19.22 for  $H$ ,  $U$  and  $V$  respectively.

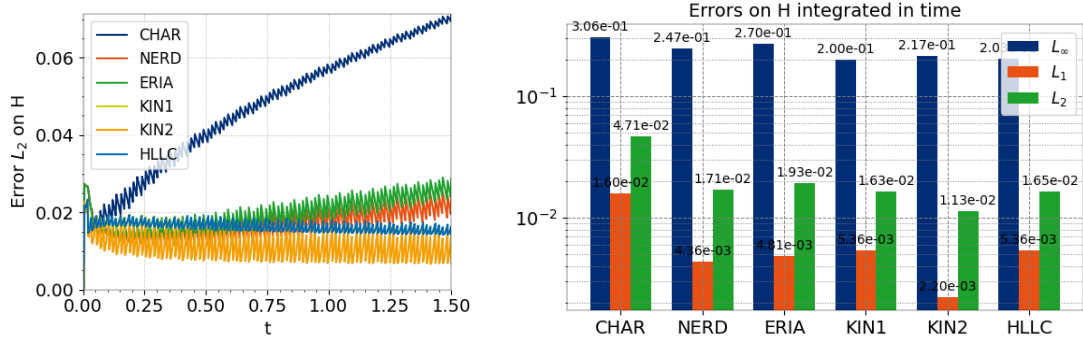


Figure 19.20: Error on  $H$ : timeseries (left) and integrated over time (right).

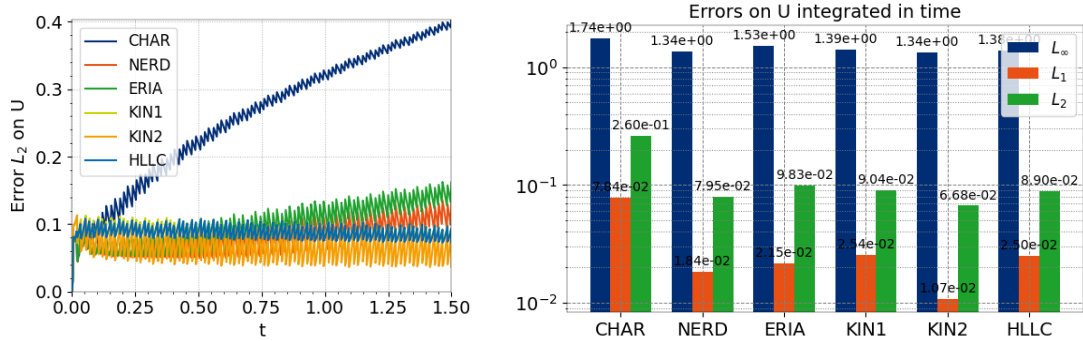


Figure 19.21: Error on  $U$ : timeseries (left) and integrated over time (right).

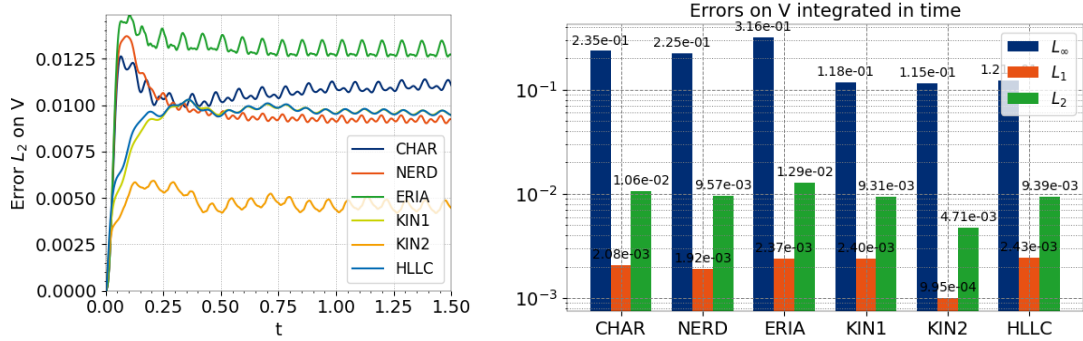


Figure 19.22: Error on  $V$ : timeseries (left) and integrated over time (right).

#### 19.4.5 Positivity of the water depth

The minimum values of the water depth are checked during the whole simulation. Results are shown in Figure 19.23.

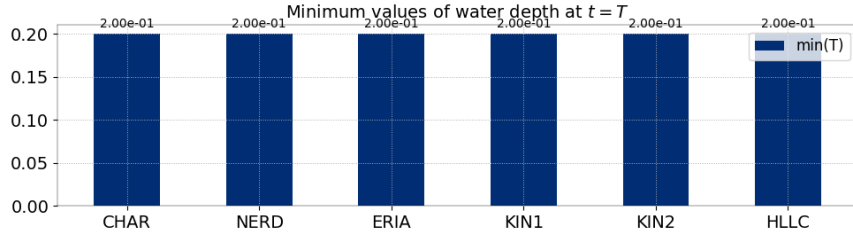


Figure 19.23: Minimum values of water depths after one rotation of the cone.

No negative values are recorded, which shows that the positivity is fulfilled. In the case of finite volume schemes, positivity is ensured without additional treatment. With finite element schemes the positivity is ensured with a treatment of negative depths during simulation (TREATMENT OF NEGATIVE DEPTHS = 2 for characteristics and NERD and 3 for ERIA scheme).

#### 19.4.6 Mass balance

Mass conservation can be checked by calculating the mass in the domain during time. The lost mass is calculated as  $M_{initial} - M_{final}$ . The evolution of mass for each of the schemes is shown in Figure 19.24.

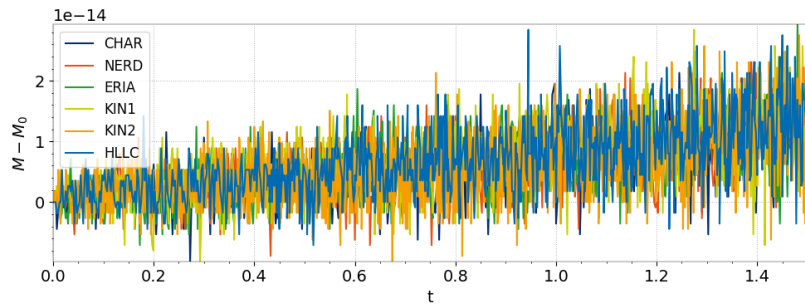


Figure 19.24: Mass loss for the tested schemes on the Stoker test case.

#### 19.4.7 Energy balance

In this section, the evolution of the mean energy is checked. In fact, for the Saint-Venant equations, the quantity  $h \frac{\|U\|^2}{2} + g \frac{h^2}{2}$ , called mean or integrated energy, is conserved, where  $\|U\|$  is the Saint-Venant depth averaged velocity magnitude. The following quantities are studied:

- Integrated potential energy  $E_p = \int \int_{\Omega_{xy}} \rho_{water} g \frac{h^2}{2} dx dy$  where  $\Omega_{xy}$  is the 2D domain of simulation: Figure 19.25,
- Integrated kinetic energy  $E_c = \int \int_{\Omega_{xy}} \rho_{water} h \frac{\|U\|^2}{2} dx dy$ : Figure 19.26,
- Integrated mechanical energy  $E_m = E_p + E_c$ : Figure 19.27.

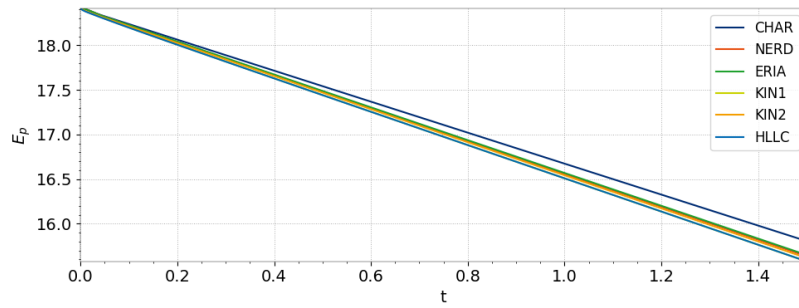


Figure 19.25: Evolution of the potential energy for the tested schemes on the Stoker test case.

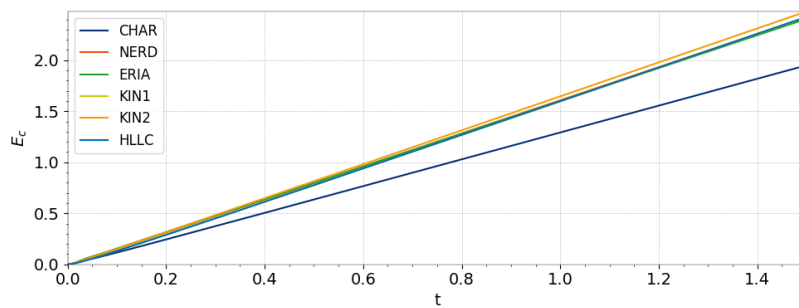


Figure 19.26: Evolution of the kinetic energy for the tested schemes on the Stoker test case.

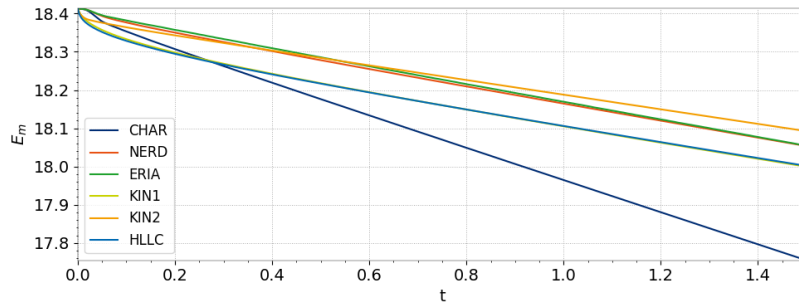


Figure 19.27: Evolution of the mechanical energy for the tested schemes on the Stoker test case.

## 19.5 Conclusions

With the tested dambreak cases, we have shown that TELEMAC-2D is able to reproduce the propagation of rarefaction and shock waves in good accordance with analytical solutions.

## 19.6 Reference

- J. J. Stoker, Water Waves: The Mathematical Theory with Applications, Interscience, 1957.
- Ritter, A. (1892). "Die Fortpflanzung der Wasserwellen." Vereine Deutscher Ingenieure Zeitschrift, Vol. 36, No. 2, 33, 13 Aug., pp. 947-954 (in German).

## 20. One way chaining with DELWAQ (delwaq)

### 20.1 Description

This test demonstrates the ability of TELEMAC-2D to be chained with DELWAQ, the water quality software from Deltares. This is a one way-chaining by files.

A 20 m wide and 28.5 m long prismatic channel with trapezoidal cross-section contains bridge-like obstacles in one cross-section made of two abutments and two circular 4 m diameter piles (see Figure 20.1).

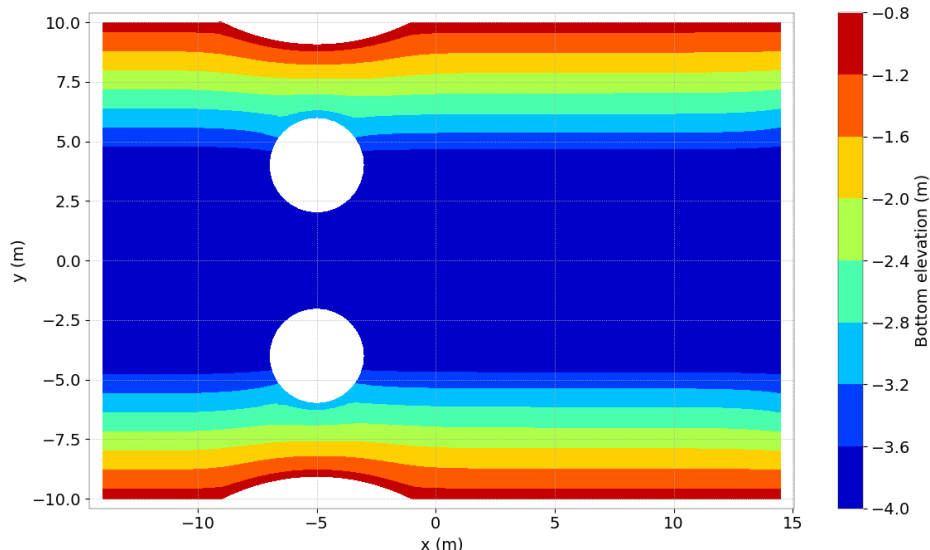


Figure 20.1: Bottom elevation.

The flow resulting from steady state boundary conditions is studied. The deepest water depth is 4 m. The hydrodynamic part is similar to the pildepon test case. The tracer used is salinity.

#### 20.1.1 Initial and boundary conditions

The computation is initialised with a constant elevation equal to 0 m, no velocity and a uniform salinity at 0.

The boundary conditions are:

- For the solid walls, a slip condition on channel banks is used for the velocities,
- On the bottom, a Strickler law with friction coefficient equal to  $40 \text{ m}^{1/3}/\text{s}$  is prescribed,
- Upstream a flowrate equal to  $62 \text{ m}^3/\text{s}$  is prescribed, linearly increasing from 0 to  $62 \text{ m}^3/\text{s}$  during the first 10 s. Salinity of 1 g/L is prescribed only along only 3 m of the liquid boundary (See Figure 20.2 for salinity after 1 s),
- Downstream the water level is equal to 0 m.

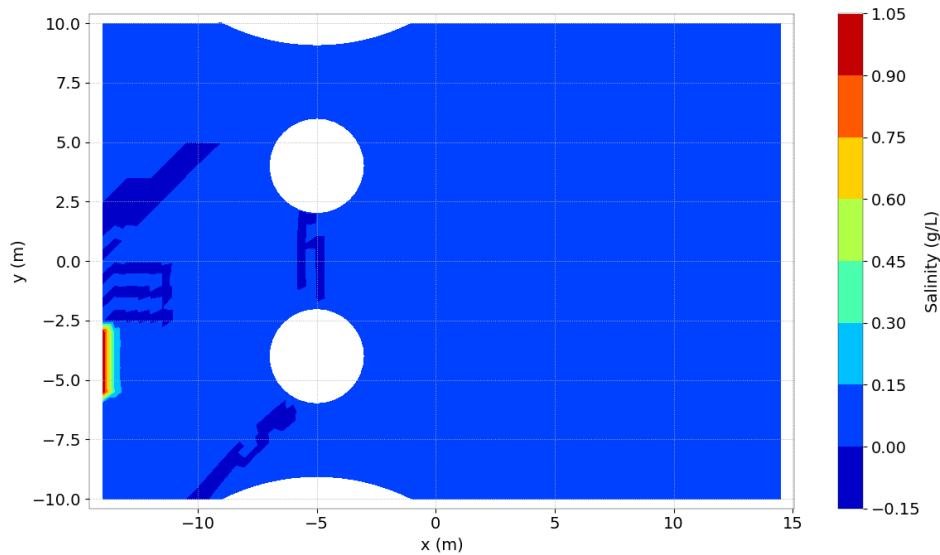


Figure 20.2: Salinity at the surface after 2 s.

### 20.1.2 Mesh and numerical parameters

The 2D mesh (Figure 20.3) is made of 4,304 triangular elements (2,280 nodes).

The time step is 0.2 s for a simulated period of 80 s.

To solve the advection, the characteristics (scheme 1) and N scheme (scheme 4) are respectively used for the velocities and tracers. The conjugate gradient is used for solving the propagation step (option 1) and the implicitation coefficients for depth and velocities are respectively equal to 0.6 and 1.

### 20.1.3 Physical parameters

A constant horizontal viscosity for velocity equal to  $0.005 \text{ m}^2/\text{s}$  is chosen. No diffusion is done for tracer salinity.

## 20.2 Results

Figure 20.4 shows the free surface elevation at the end of the computation.

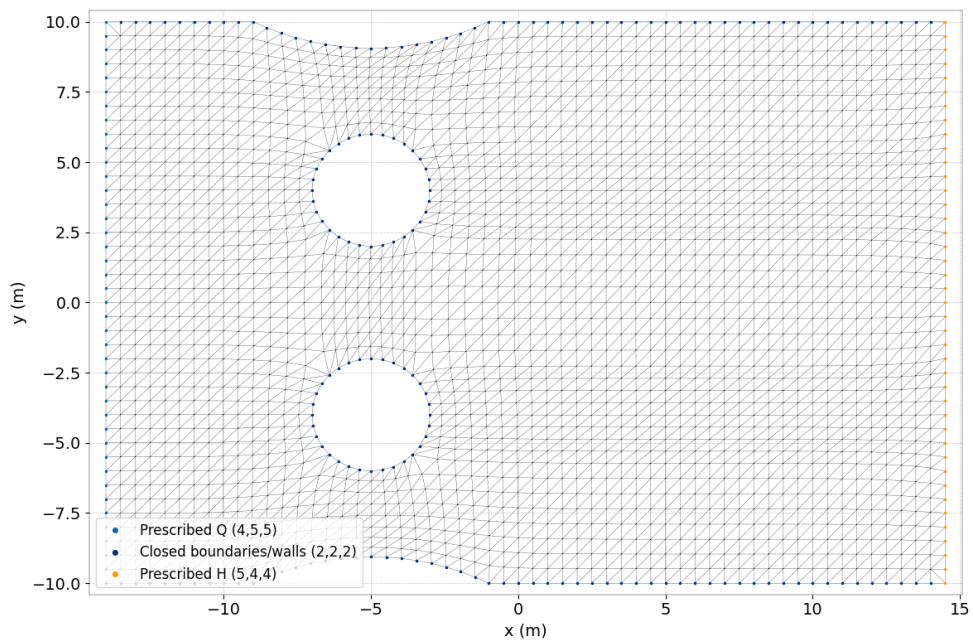


Figure 20.3: Horizontal mesh.

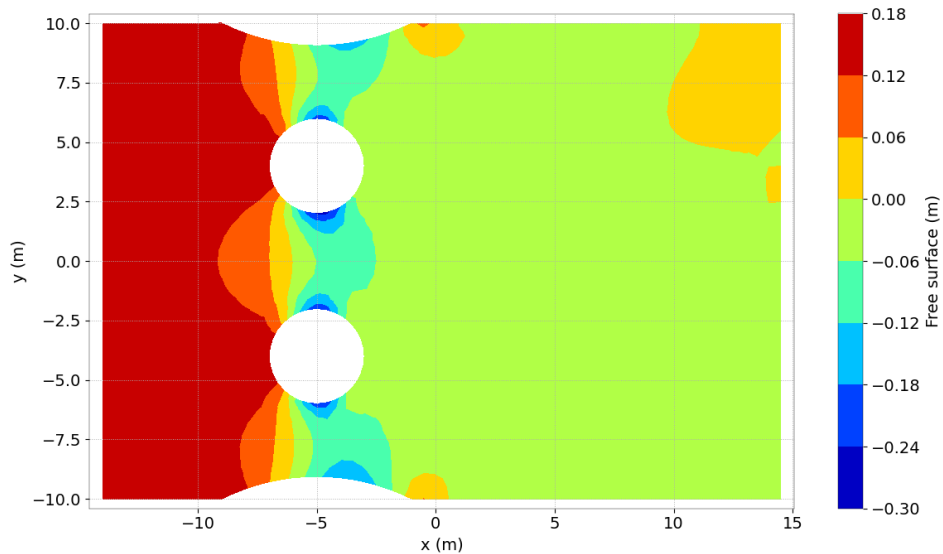


Figure 20.4: Free surface at final time step.

Figure 20.5 shows the magnitude of velocity at the end of the computation.

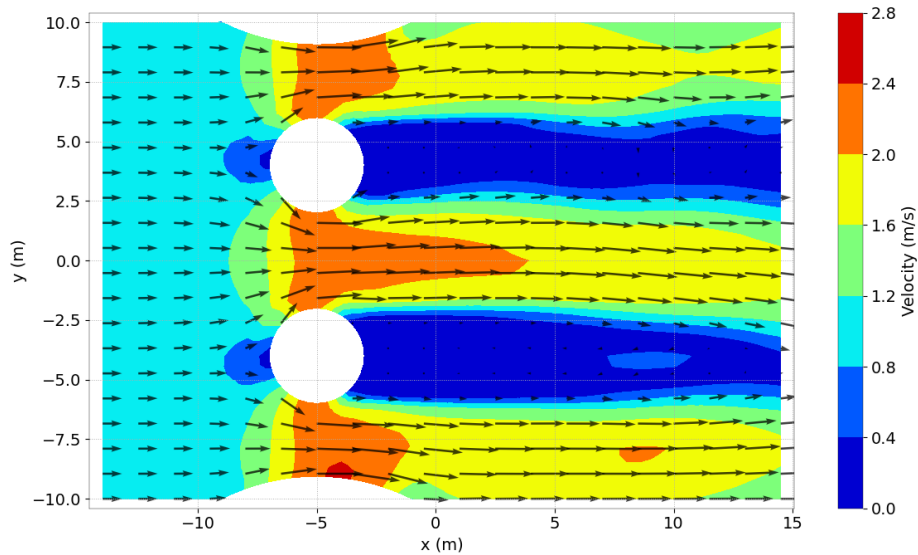


Figure 20.5: Velocity magnitude at the surface at final time step.

If running DELWAQ with the DELWAQ result files written by TELEMAC-2D, the velocity results are similar with both codes.

Figure 20.6 shows the salinity at the end of the computation.

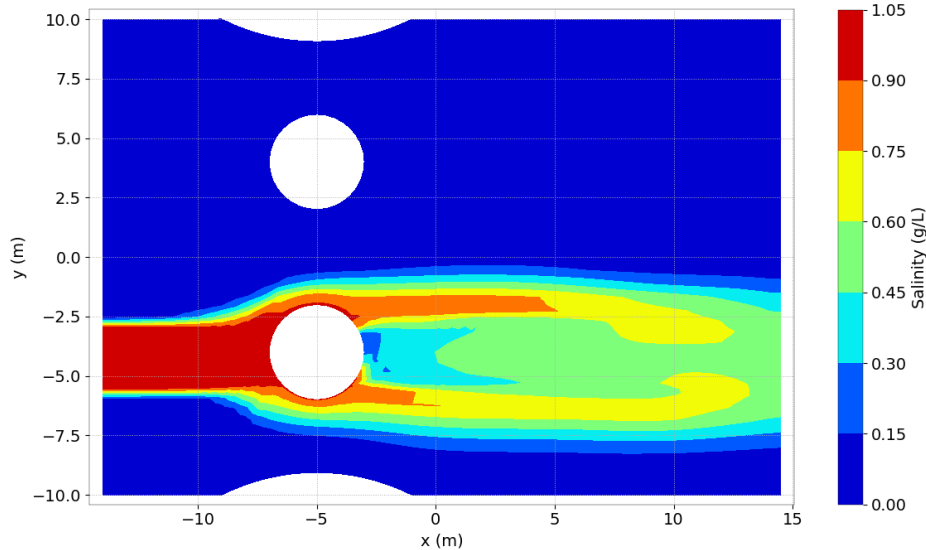


Figure 20.6: Salinity at the surface at final time step.

### 20.3 Conclusion

TELEMAC-2D can be used to chain with DELWAQ.

# 21. Flow over a breakwater (digue)

## 21.1 Purpose

This test case is to demonstrate the capability of TELEMAC-2D to model a situation with a very steep bed thanks to a refined mesh. Two pools are located downstream of the breakwater. They induce flow regime transitions from super-critical to sub-critical flow.

### 21.1.1 Approach

The computational domain is a rectangle with flat bottom and initially dry bed in which a 4 m high breakwater with trapezoidal cross-section splits the domain into two zones. Water is introduced in the area on the one side of the breakwater until this one overflows. The area protected by the breakwater, which includes two pools, is suddenly flooded. See Figure 21.1 for the initial conditions and Figure 21.2 for free surface profile.

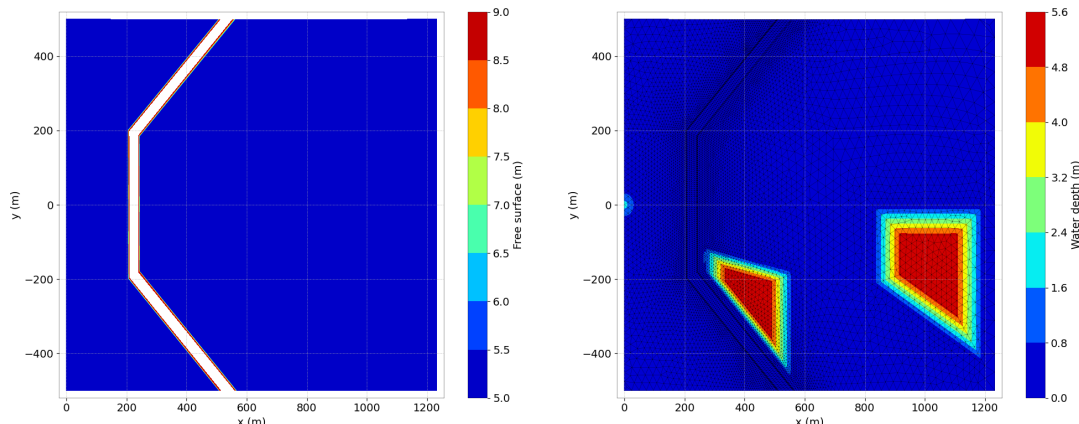


Figure 21.1: Initial conditions for free surface and water depth.

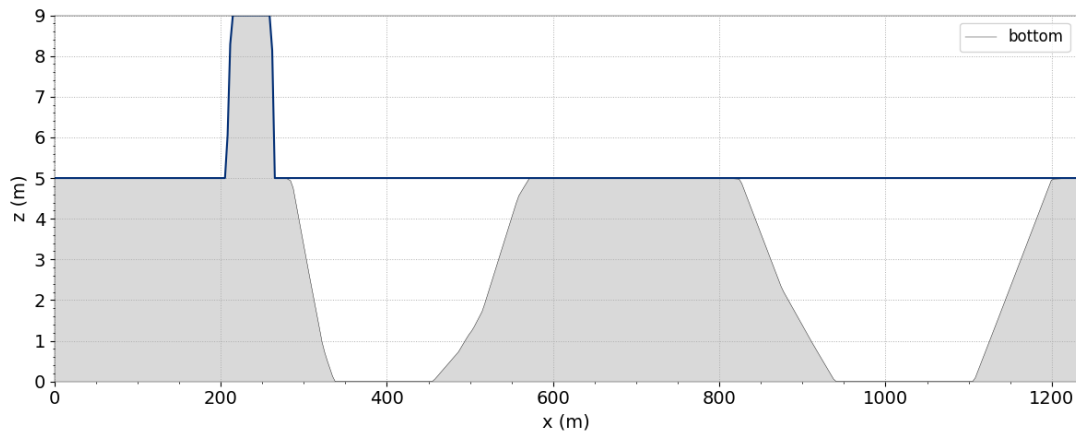


Figure 21.2: Free surface profile along (0 ; -200) and (1,250 ; -200).

## 21.2 Description

### 21.2.1 Geometry and mesh

The computational domain is a 1,232.5 m × 1,000 m rectangular channel. A triangular non-structured mesh is constructed on this domain and refined near the breakwater. It has the following characteristics:

- 19,202 triangular elements,
- 9,734 nodes.

Maximum size range: from 3 to 37 m.

Water depth at rest = 5 m.

### 21.2.2 Boundaries

- Domain entrance: free depth and discharges imposed at 100 m<sup>3</sup>/s,
- Domain outlet: free depth and Thompson conditions,
- Lateral boundaries: solid walls with slip condition.

Bottom: Strickler formula with friction coefficient = 55 m<sup>1/3</sup>/s.

The mesh and the topography are shown in Figure 21.3.

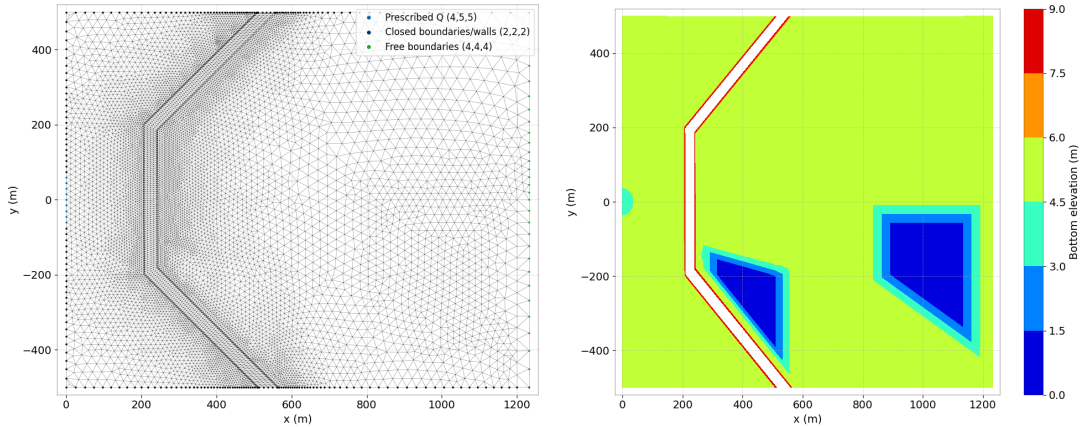


Figure 21.3: Horizontal mesh and bathymetry.

### 21.2.3 Physical parameters

The model of turbulence is constant viscosity with velocity diffusivity =  $2 \text{ m}^2/\text{s}$ .

### 21.2.4 Numerical parameters

Type of advection:

- Methods of characteristics on velocities (scheme #1),
- Conservative + modified SUPG on depth (mandatory scheme)

The type of element is linear triangle (P1) for  $h$  and for velocities.

- Implicitation for velocities = 0.55 (default value),
- Implicitation for depth = 1.0,
- Solver: Conjugate gradient with solver accuracy =  $10^{-6}$ ,
- Time step = 2 s,
- Simulation duration = 14,000 s (a little bit less than 4 h).

## 21.3 Results

Even though the slopes of the breakwater are steep, progressive flooding of the breakwater and overflowing with mixed super-critical/sub-critical flow conditions are reproduced as expected. The time when overflowing occurs is 12,000 s (see Figures 21.4 and 21.5).

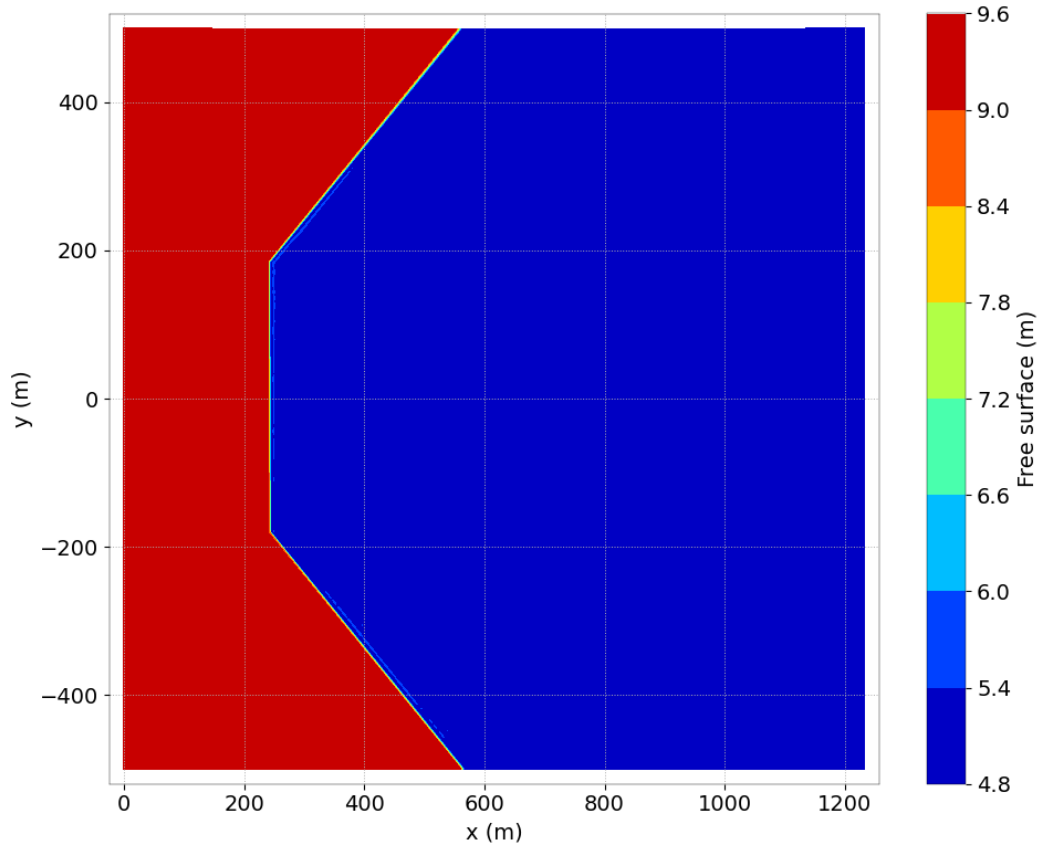


Figure 21.4: Free surface at final time.

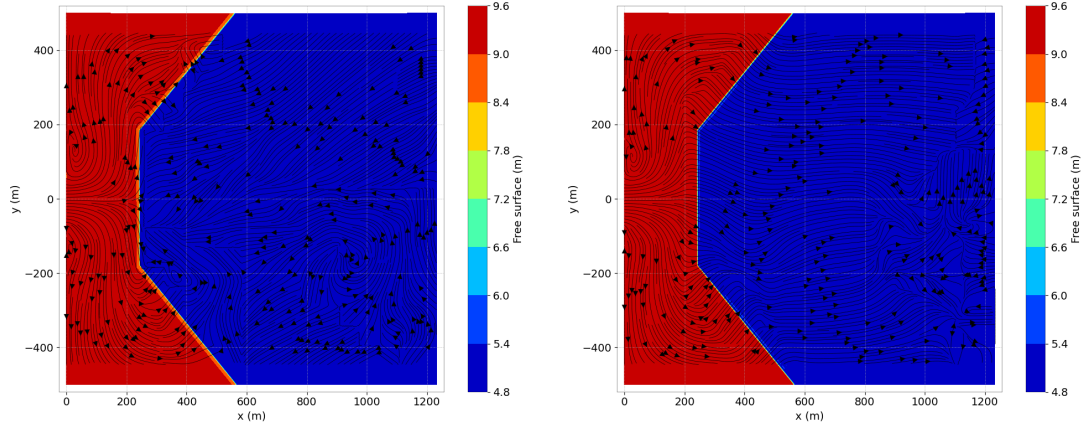


Figure 21.5: Free surface and streamlines at 12,000 s and 14,000 s.

## 21.4 Conclusions

TELEMAC-2D is capable of simulating the flooding of a breakwater including the different flow regimes and regime transitions it induces provided that the mesh is sufficiently refined. Hydrodynamics are appropriately reproduced at each stage of the flooding event (free overfall or flooded breakwater).

## 22. donau

### 22.1 Purpose

This test case shows a real case application in order to test zonal friction values given by a table. The test case exists since at least release v5p5 but was modified for release v8p2 in order to take into account lateral boundary friction and to compare the results to measurements.

### 22.2 Description

#### 22.2.1 Geometry and mesh

The model area is a 7.7 km stretch of the Danube River near Deggendorf in Germany. In the grid, several regulation structures (groyne, longitudinal dams) and bridge piers are integrated using node distances up to 60 cm while the mean node distances are about 6 m in the main channel and about 20 m at the floodplains. The grid contains 47,543 nodes and 93,209 elements and can be seen in Figure 22.1. The bathymetry is shown in Figure 22.2. The flow direction is from left to right.

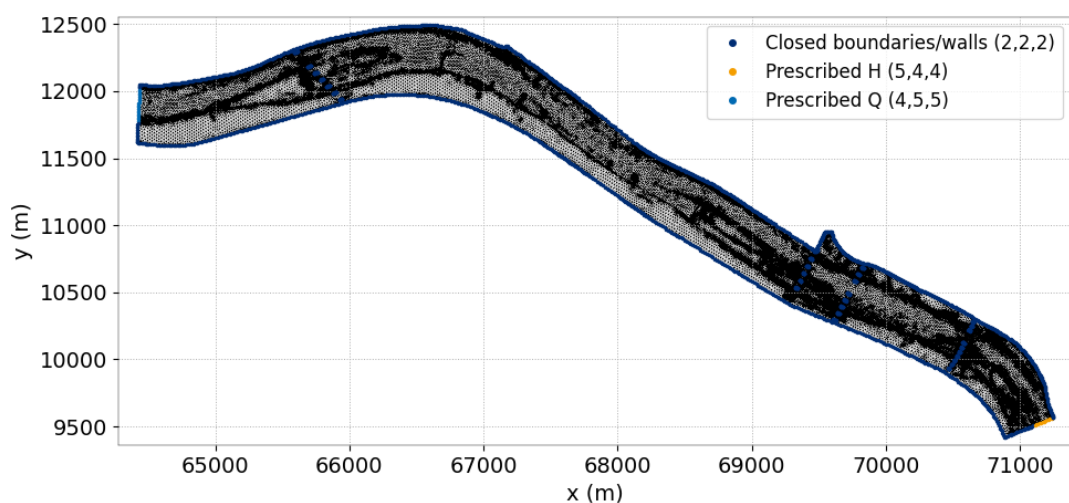


Figure 22.1: Mesh and boundary conditions.

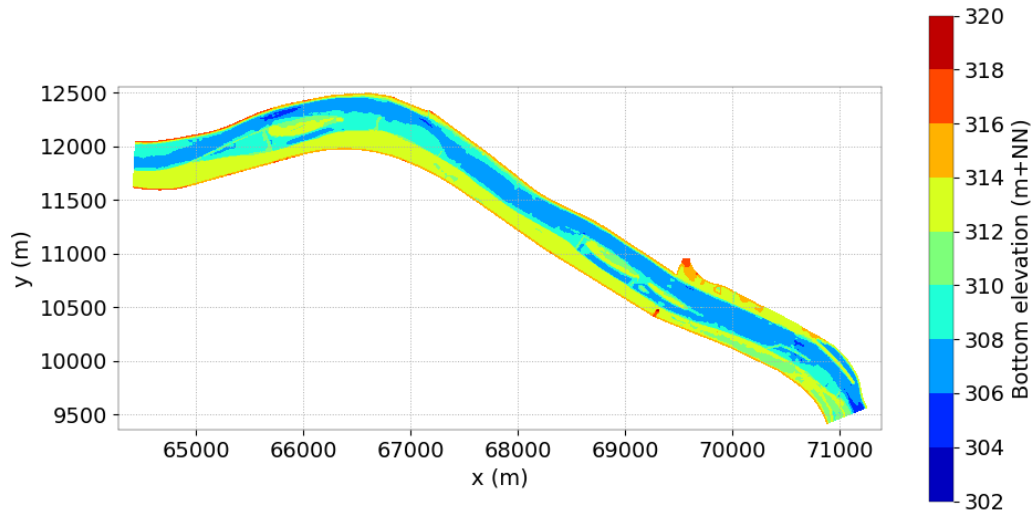


Figure 22.2: Bathymetry.

### 22.2.2 Initial condition

The initial conditions for velocities and water depths are read from the PREVIOUS COMPUTATION FILE. With this, the simulation starts from a fully developed flow with steady state conditions. The initial water levels and scalar velocities are printed in Figures 22.3 and 22.4.

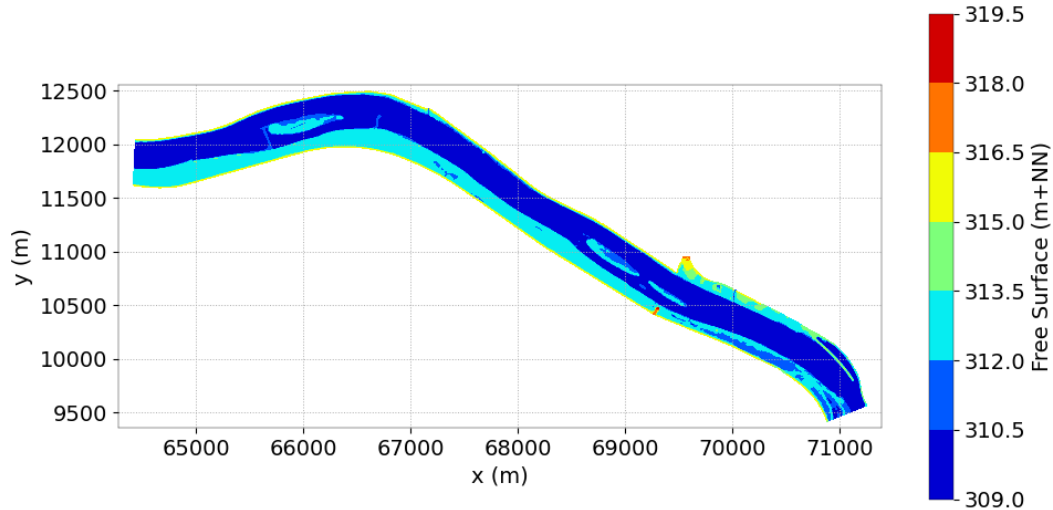


Figure 22.3: Initial water levels.

### 22.2.3 Boundary conditions

The boundary conditions are chosen according low water conditions in September 1999. At the inlet, the discharge of  $218 \text{ m}^3/\text{s}$  is imposed only at the main channel. At the outlet, the water depth is fixed to  $309.205 \text{ m+NN}$ .

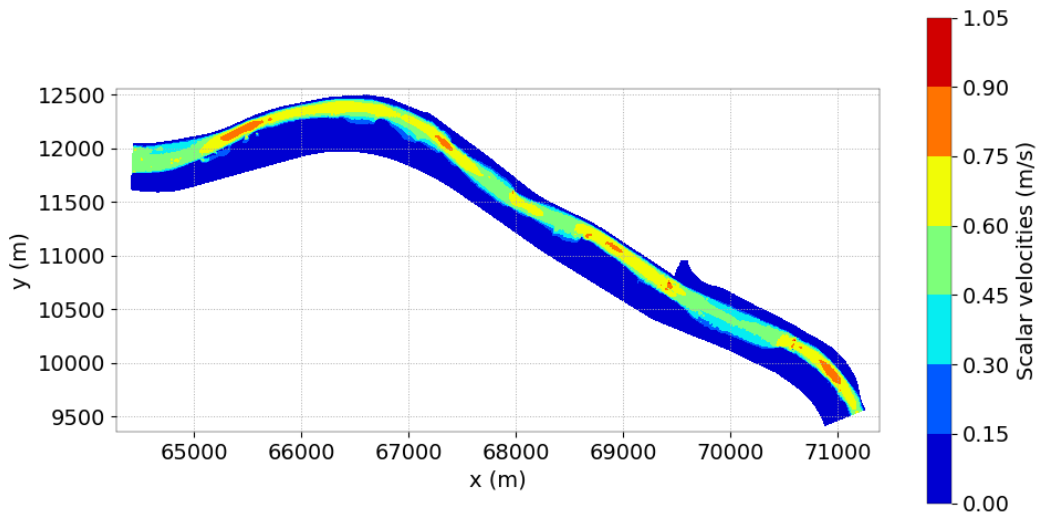


Figure 22.4: Initial scalar velocities.

#### 22.2.4 Physical parameters

Seven different friction domains are distinguished. They are marked with friction IDs given in the ZONES FILE so that the roughness laws and corresponding parameters can be chosen easily in the FRICTION DATA FILE. The values are given in Table 22.1. The distribution of the roughness coefficients can be seen in Figure 22.5.

| Friction domain       | friction law | parameter (m) | friction ID |
|-----------------------|--------------|---------------|-------------|
| main channel          | Nikuradse    | 0.025         | 99999024    |
| groyne fields         | Nikuradse    | 0.15          | 99999150    |
| regulation structures | Nikuradse    | 0.3           | 99999300    |
| site                  | Nikuradse    | 0.5           | 99999500    |
| fields                | Nikuradse    | 0.1           | 99999100    |
| forest                | Nikuradse    | 1             | 99999001    |
| buildings             | Nikuradse    | 10            | 99999010    |

Table 22.1: Friction law and parameter for the different friction domains.

As this is a long existing example, the Nikuradse law is used for all friction domains. With low water levels at the floodplains, the restriction that the equivalent sand roughness should not be higher than 50 % of the water depth will not be fulfilled. For the forest, buildings and maybe also for the site, it would be better to choose a vegetation law.

The Elder turbulence model is chosen and the molecular viscosity is set to its physical value  $10^{-6} \text{ m}^2/\text{s}$ .

Four bridges cross the modelled river stretch. The areas of the bridge piers is cut from the grid (see Figure 22.6). The friction for the lateral boundaries is set in the steering file. The Nikuradse friction law is used LAW OF FRICTION ON LATERAL BOUNDARIES = 5 with an equivalent sand roughness of 1 cm for concrete ROUGHNESS COEFFICIENT OF BOUNDARIES = 0.01. For the third bridge pier of the second bridge in flow direction, the roughness coefficient is increased to 5.0 m. This is done in the BOUNDARY CONDITIONS FILE giving the values in the 7th column. This artificial high value is chosen in order to see significant differences in the flow field around the third and fourth bridge pier.

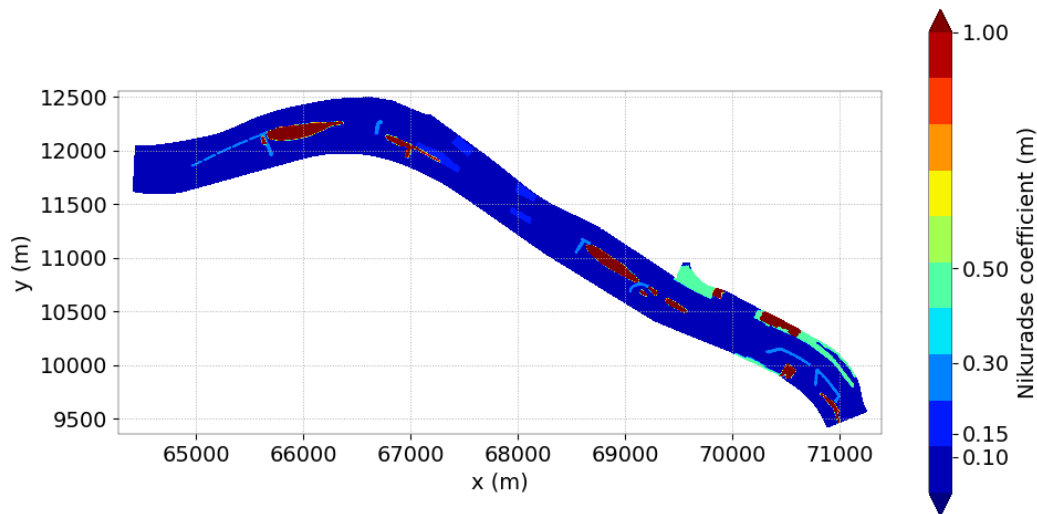


Figure 22.5: Distribution of the roughness parameters.

### 22.2.5 Numerical parameters

10 min are simulated with a time step of 0.5 s. Figure 22.7 shows the evolution of the inlet and outlet fluxes which equals at the end of the simulation time. The characteristics are used for the advection scheme. The GMRES solver with a solver accuracy of  $10^{-6}$  is applied. Implicit conditions are set for depth and semi-implicit conditions for the velocities (with 0.55 value). The classic discretisation of the equations is applied.

## 22.3 Results

A comparison along the main channel between the measured water levels and the simulated ones for both configurations is presented in Figure 22.8. The simulated water levels are in a very good agreement to the measurement.

The increased roughness at the third bridge pier in Figure 22.9 leads to smaller velocities. The third and the fourth bridge pier both stand in the main channel and would have a very similar velocity distribution. Due to the different roughness coefficients, the velocities are smaller at the third bridge pier (numbering from north to south).

## 22.4 Conclusion

The example shows a successful simulation of low water steady state conditions with tidal flats. The influence of sidewall friction is shown by the comparison of the flow field downstream of two bridge piers with different sidewall frictions. The roughness coefficients can easily be modified in the roughness table because of the use of roughness zones.

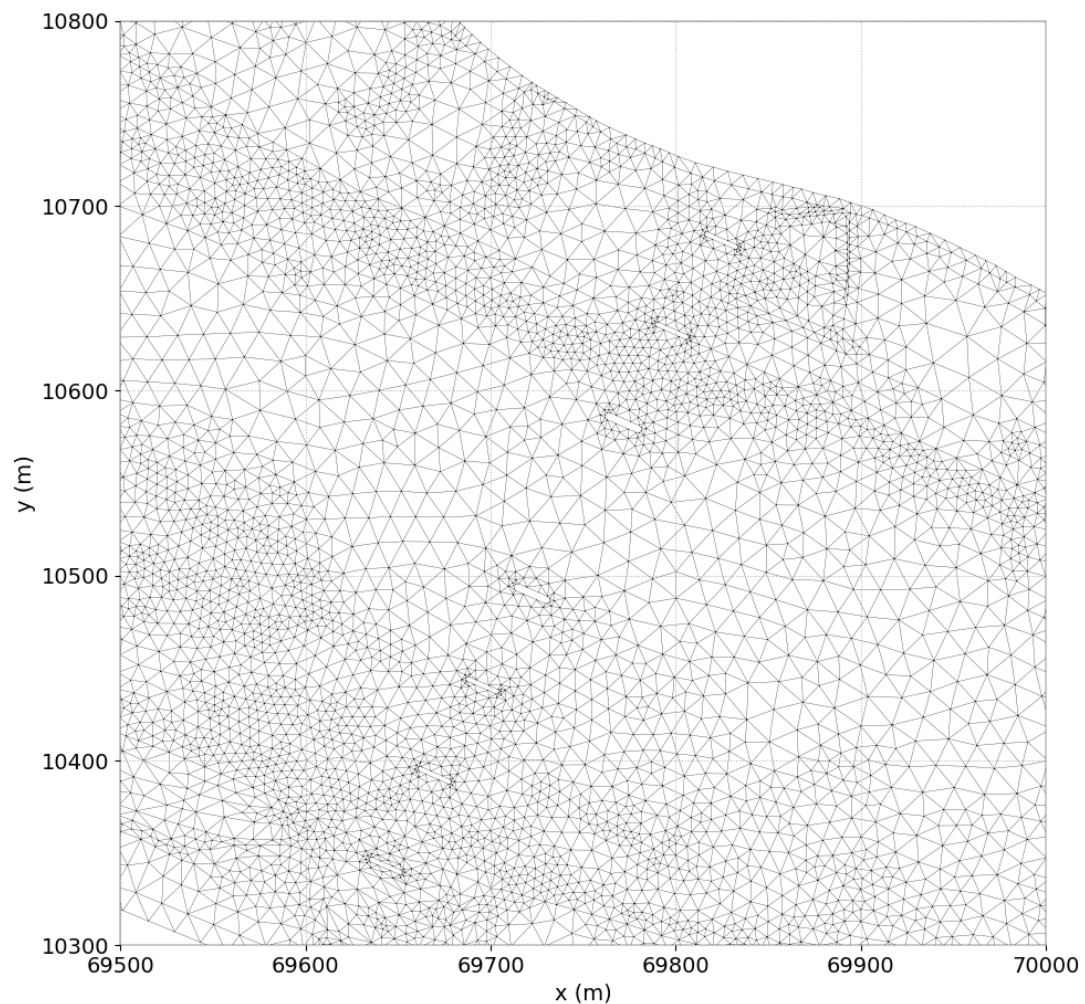


Figure 22.6: Grid part with bridge piers.

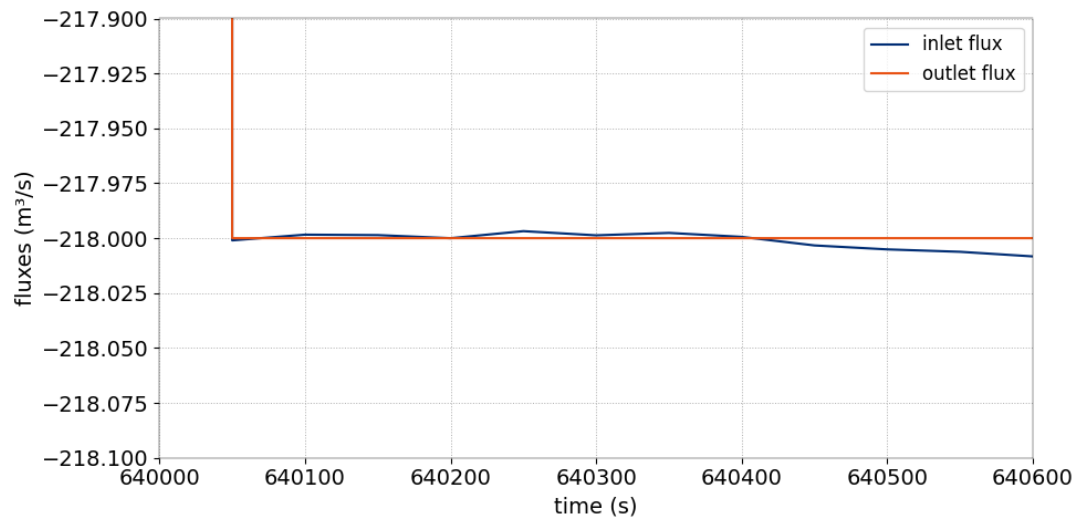


Figure 22.7: Evolution of inlet and outlet fluxes.

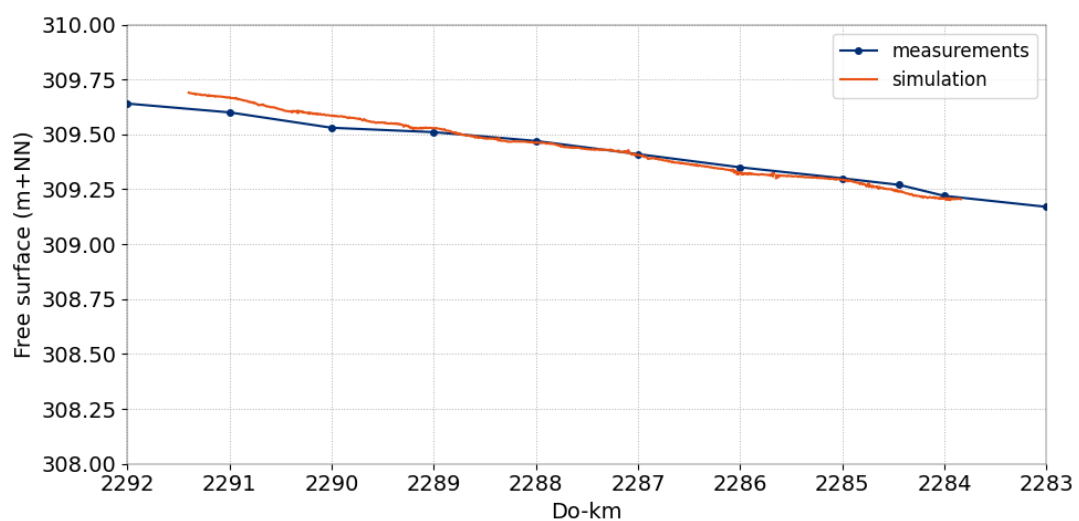


Figure 22.8: Comparison of measured and simulated final water levels.

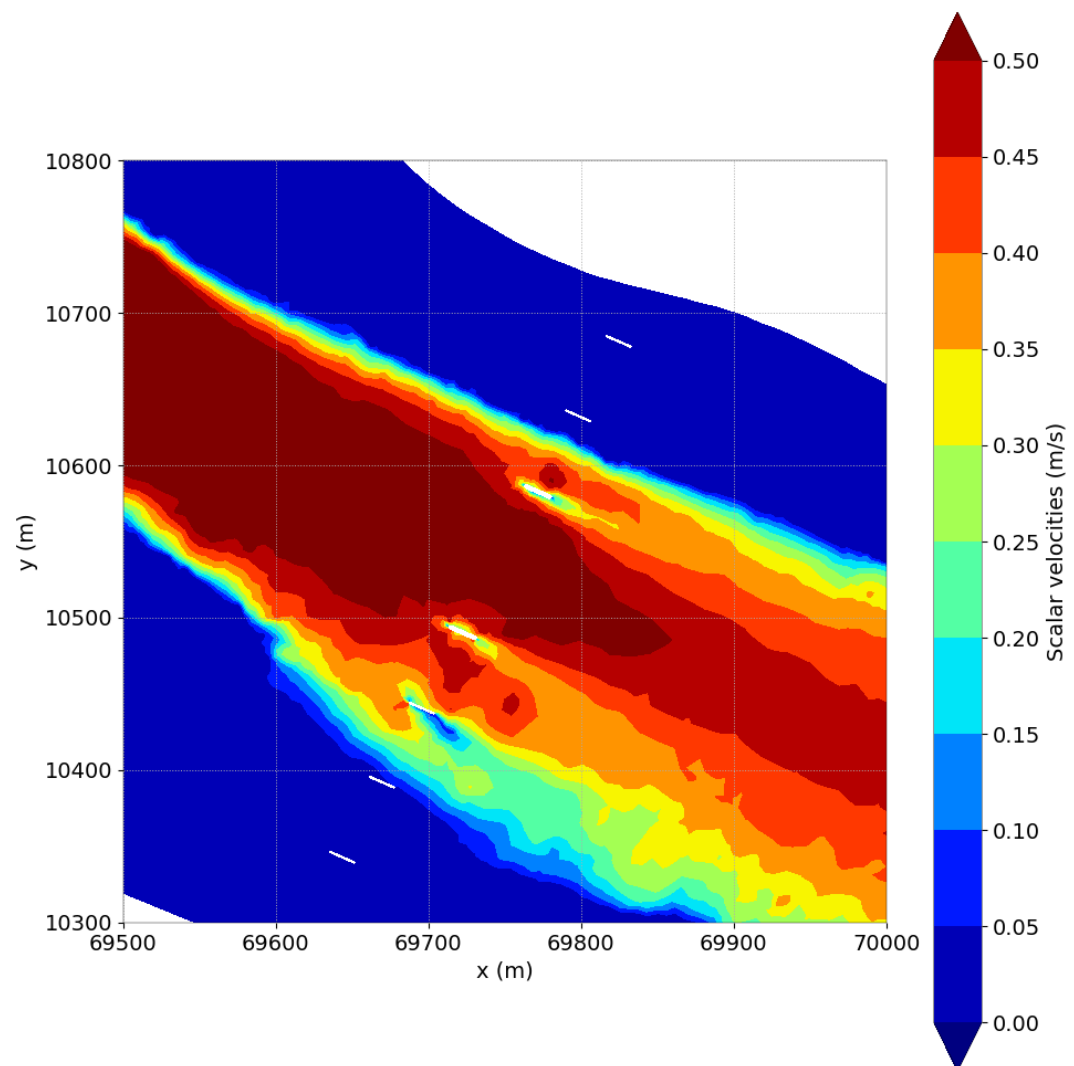


Figure 22.9: Scalar velocities around bridge piers.

# 23. Drag force in a channel (dragforce)

## 23.1 Description

This example checks that TELEMAC-2D is able to represent a drag force and porosity.

The configuration is a straight channel 200 m long and 40 m wide with a flat horizontal bottom without slope.

### 23.1.1 Initial and boundary conditions

The computation is initialised with a constant elevation equal to 4 m and a constant velocity along  $x$  equal to 0.625 m/s.

The boundary conditions are:

- For the solid walls, a slip condition on channel banks is used for the velocities,
- On the bottom, a Strickler law with friction coefficient equal to  $40 \text{ m}^{1/3}/\text{s}$  is prescribed,
- Upstream a flowrate equal to  $100 \text{ m}^3/\text{s}$  is prescribed,
- Downstream the water level is equal to 4 m.

### 23.1.2 Mesh and numerical parameters

The mesh (Figure 23.1) is made of 7,334 triangular elements (3,740 nodes). It is particularly refined around where the drag force and porosity are applied.

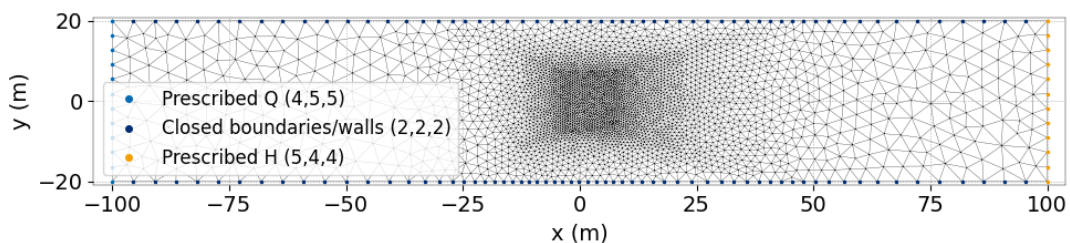


Figure 23.1: Horizontal mesh.

The time step is 0.2 s for a simulated period of 2,000 s.

To solve the advection, the method of characteristics is used for the velocities (scheme 1). The conjugate gradient is used for solving the propagation step (option 1) and the implicitation coefficients for depth and velocities are respectively equal to 1 and 0.6.

### 23.1.3 Physical parameters

The  $k - \varepsilon$  model is used for turbulence modelling. The drag force is activated by setting the keyword VERTICAL STRUCTURES = YES. The default treatment implemented in the DRAGFO subroutine is used in this example but it can be changed if needed.

In addition, porosity is applied by setting TIDAL FLATS = YES (default value) + OPTION FOR THE TREATMENT OF TIDAL FLATS = 3 and by implementing the user subroutine USER\_CORPOR:

$$\left\{ \begin{array}{ll} \text{if } -10 \leq x \leq 10, & \text{porosity} = \frac{19}{20}, \\ \text{if } x < -10, & \text{porosity} = \frac{19}{20} - \frac{1}{20} \frac{x+10}{10}, \\ \text{if } x > 10, & \text{porosity} = \frac{19}{20} + \frac{1}{20} \frac{x-10}{10}. \end{array} \right.$$

## 23.2 Results

The flow establishes a steady flow where the free surface is lightly higher at the entrance and lightly drops (less than 1 cm) after the area where the drag force and porosity are applied (see Figure 23.2). The flow accelerates where porosity and drag force are applied and then retrieves quite similar velocity after.

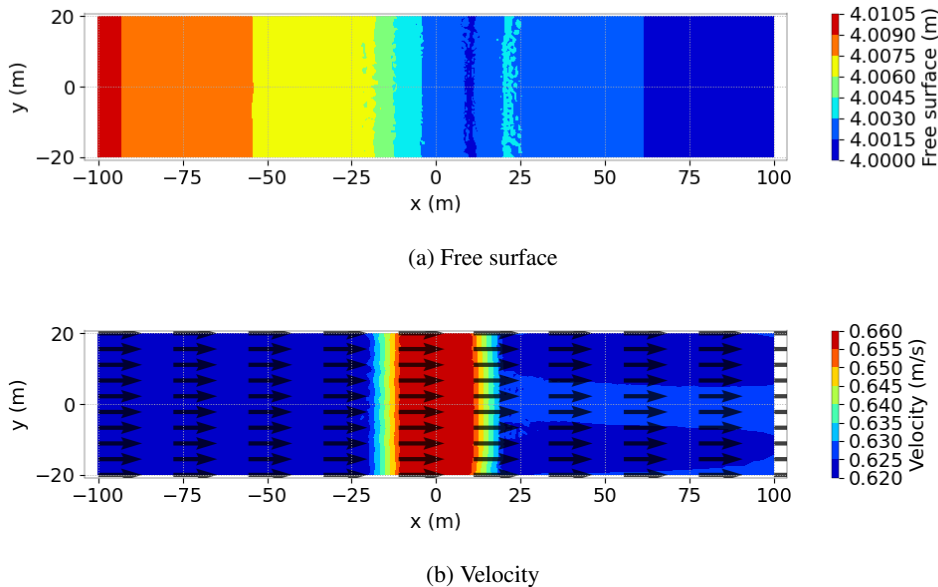


Figure 23.2: Results.

### 23.3 Conclusions

TELEMAC-2D is capable to model drag forces and porosity.

## 24. Parameter estimation (estimation)

### 24.1 Description

This example shows how to use parameter estimation with TELEMAC-2D.

The configuration is a straight channel 500 m long and 100 m wide with a flat bottom.

#### 24.1.1 Initial and boundary conditions

The computation is initialised with a constant elevation equal to 5 m and horizontal velocity along  $x$  equal to 1 m/s.

The boundary conditions are:

- For the solid walls, a slip condition on channel banks is used for the velocities,
- On the bottom, a Strickler law is prescribed,
- Upstream a flowrate equal to 50 m<sup>3</sup>/s is prescribed, linearly increasing from 1 to 50 m<sup>3</sup>/s during the first 20 s,
- Downstream the water level is suggested to be equal to 0.5 m.

#### 24.1.2 Mesh and numerical parameters

The mesh is made of 551 triangular elements (319 nodes), see Figure 24.1.

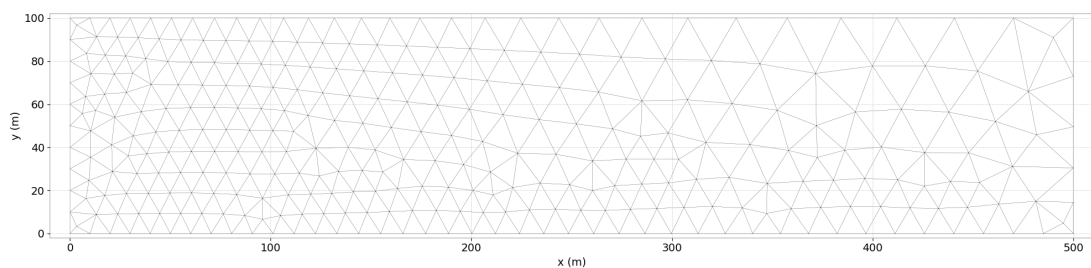


Figure 24.1: Horizontal mesh.

The time step is 2 s.

To solve the advection, the NERD scheme (= 13) is used for the velocities. The GMRES method is used for solving the propagation step (option 1) and the implicitation coefficients for

depth and velocities are let to default values. To use the parameter estimation mode, primitive equations are mandatory (TREATMENT OF THE LINEAR SYSTEM = 1) which is not the default option (= wave equation with TREATMENT OF THE LINEAR SYSTEM = 2). Please read the TELEMAC-2D user manual to know how to use specific keywords for parameter estimation feature.

#### 24.1.3 Physical parameters

No diffusion is chosen for this computation (constant horizontal viscosity for velocity equal to 0. m<sup>2</sup>/s).

### 24.2 Conclusions

This example shows how parameter estimation can be used with TELEMAC-2D.

# 25. Particle transport (flotteurs)

## 25.1 Description

This example checks that TELEMAC-2D is able to model particles transport with drogues. The configuration is a section of river (around 1,700 m long and 300 m wide) with realistic bottom. The geometric data include a groyne in the transversal direction and an island (see Figure 25.1).

### 25.1.1 Initial and boundary conditions

There are 2 computations:

- The first computation (with t2d\_flotteurs\_v1p0.cas steering file) writes the r2d\_flotteurs\_v1p0.slf file and is initialised with a constant elevation equal to 265 m and no velocity,
- The second computation (with t2d\_flotteurs\_v2p0.cas steering file) is a continued computation with drogues from the result file of the first computation.

The boundary conditions are:

- For the solid walls, a slip condition on channel banks is used for the velocities,
- On the bottom, a Strickler law with friction coefficient equal to  $55 \text{ m}^{1/3}/\text{s}$  is prescribed,
- Upstream a flowrate equal to  $500 \text{ m}^3/\text{s}$  is prescribed (linearly increasing from 0 to  $500 \text{ m}^3/\text{s}$  during the first half hour) for the first computation and always to  $700 \text{ m}^3/\text{s}$  for the second computation. The velocity profile is given in the boundary conditions file along this liquid boundary for the first computation and is a constant normal profile for the second one,
- Downstream the water level is equal to 265 m.

Drogues are released every 10 time steps until the 600<sup>th</sup> time step (= 3,000 s). Thus a maximum of 61 drogues are released, each time at  $x = -200 \text{ m}$ .

### 25.1.2 Mesh and numerical parameters

The mesh (Figure 25.1) is made of 3,780 triangular elements (2,039 nodes). It is refined around the island and in front of the groyne.

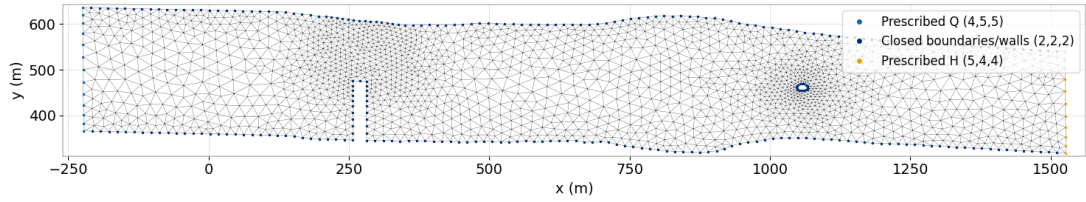


Figure 25.1: Horizontal mesh.

The time step is 5 s for a simulated period of 15 h ( $= 54,000$  s) for the first computation and 2 h ( $= 7,200$  s) for the second computation.

To solve the advection, the method of characteristics is used for the velocities (scheme 1). The GMRES is used for solving the propagation step (option 7).

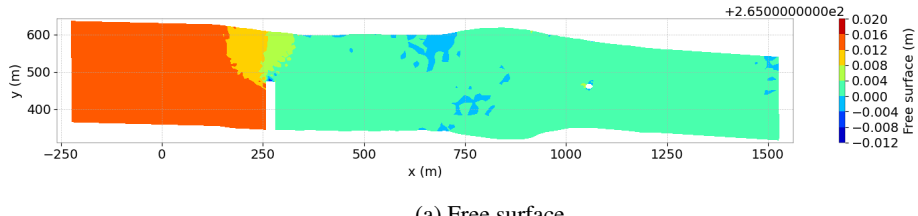
For the second computation only, a maximum of 100 drogues are released and control sections are calculated between two couples of nodes.

### 25.1.3 Physical parameters

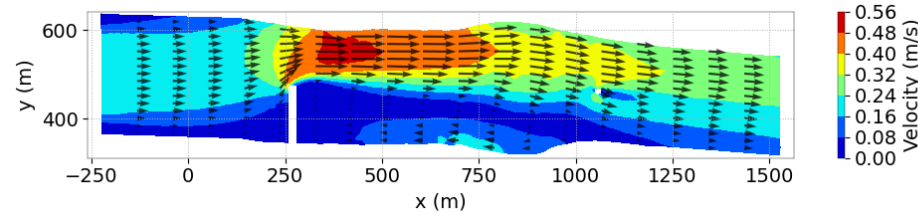
Turbulence is modelled by a constant viscosity equal to  $10^{-2}$  m<sup>2</sup>/s.

## 25.2 Results

In the first computation, the flow establishes a steady flow where the free surface is lightly higher before the groyne than after (see Figure 25.2). The flow accelerates in front of the groyne due to the restriction of section. A recirculation appears just after the groyne.



(a) Free surface



(b) Velocity

Figure 25.2: Results.

The same remarks can be done for the second computation (see Figure 25.3). The velocities are bigger in the second computation than in the first due to the bigger inlet flowrate ( $700$  m<sup>3</sup>/s compared to  $500$  m<sup>3</sup>/s).

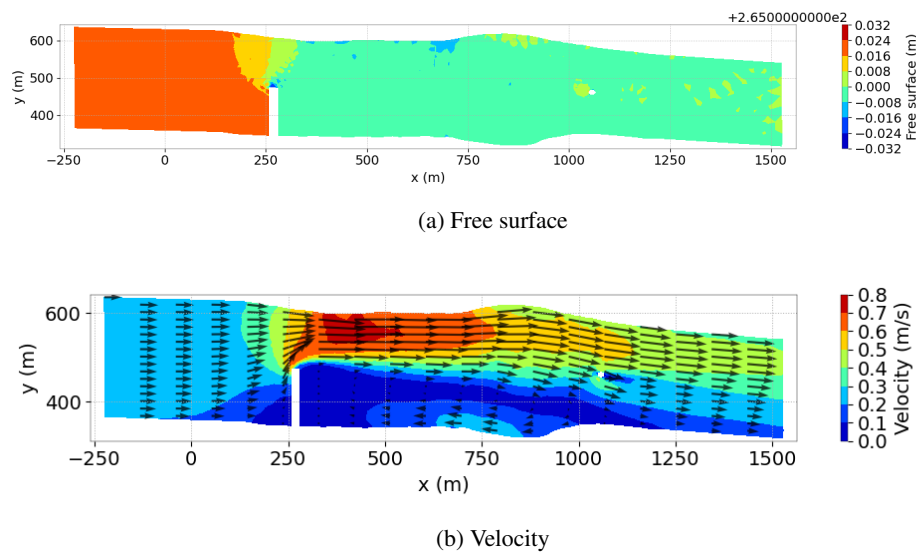


Figure 25.3: Results.

## 26. Flume with tracers (flume\_tracer)

### 26.1 Purpose

This test shows the performance of the finite volume advection schemes of TELEMAC-2D for passive scalar transport in a time dependent case. It shows the advection of a tracer (or any other passive scalar) in a flume with flat frictionless bottom.

### 26.2 Description

#### 26.2.1 Geometry and mesh

The dimensions of the domain are  $[2 \times 20]$  m<sup>2</sup>. The mesh is made from a regular grid from which all squares are cut in half. The number of elements and points in the mesh are 729 and 1,280 respectively.

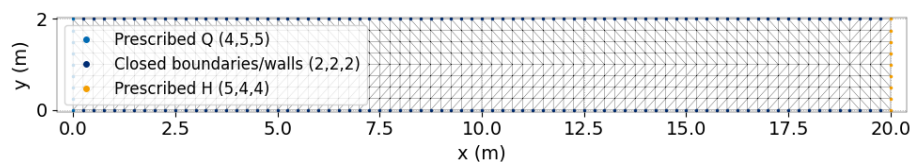


Figure 26.1: 2D domain and mesh of the flume\_tracer test case.

#### 26.2.2 Initial condition

The water depth is constant in time and in space, equal to 1 m. The streamwise velocity  $u$  is constant and equal to 1 m/s. Two tracers are defined in the domain. Their initial values are taken from analytical solution at time  $t = 0$ .

#### 26.2.3 Analytical solution

The first tracer is described by a Gaussian function and the second is defined by a crenel. The analytical solution for both tracers  $T_1$  and  $T_2$  are given by:

$$T_1(x, y, t) = e^{-\frac{1}{2}(x-x_0(t))^2}$$

and

$$T_2(x, y, t) = \begin{cases} 1 & \text{if } x_1(t) \leq x \leq x_2(t) \\ 0 & \text{else} \end{cases}$$

with

$$\begin{cases} x_0(t) = 5 + u * t \\ x_1(t) = 2.5 + u * t \\ x_2(t) = 7.5 + u * t \end{cases}$$

#### 26.2.4 Physical parameters

No bottom friction is imposed and diffusivity of tracer is set to zero.

#### 26.2.5 Numerical parameters

The simulation time is set to 7.5 s. For tracers advection, most numerical schemes available in TELEMAC-2D finite volume solver are tested. First order schemes results are very similar for passive scalar transport so only Roe, Kinetic and HLLC are tested. Second order reconstructions are tested for Kinetic and HLLC schemes. We also test different flux limitors on tracer i.e. Minmod (MM), Van Albada (VA) and monotonized central (MC) limitors. All limitors are tested with Kinetic scheme. Since HLLC and Kinetic give very similar results only MC limitor is tested with HLLC.

### 26.3 Results

#### 26.3.1 Computation time

Simulation times for each of these cases with sequential and parallel runs (using 4 processors) are shown in Figure 26.2

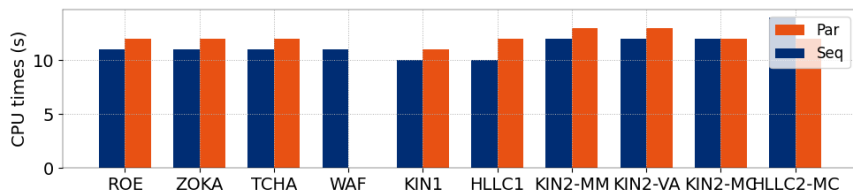


Figure 26.2: CPU times.

#### 26.3.2 Comparison of schemes

One dimensional profiles are extracted from slice plane ( $x, y = 1, z$ ) at final time in Figure 26.3.

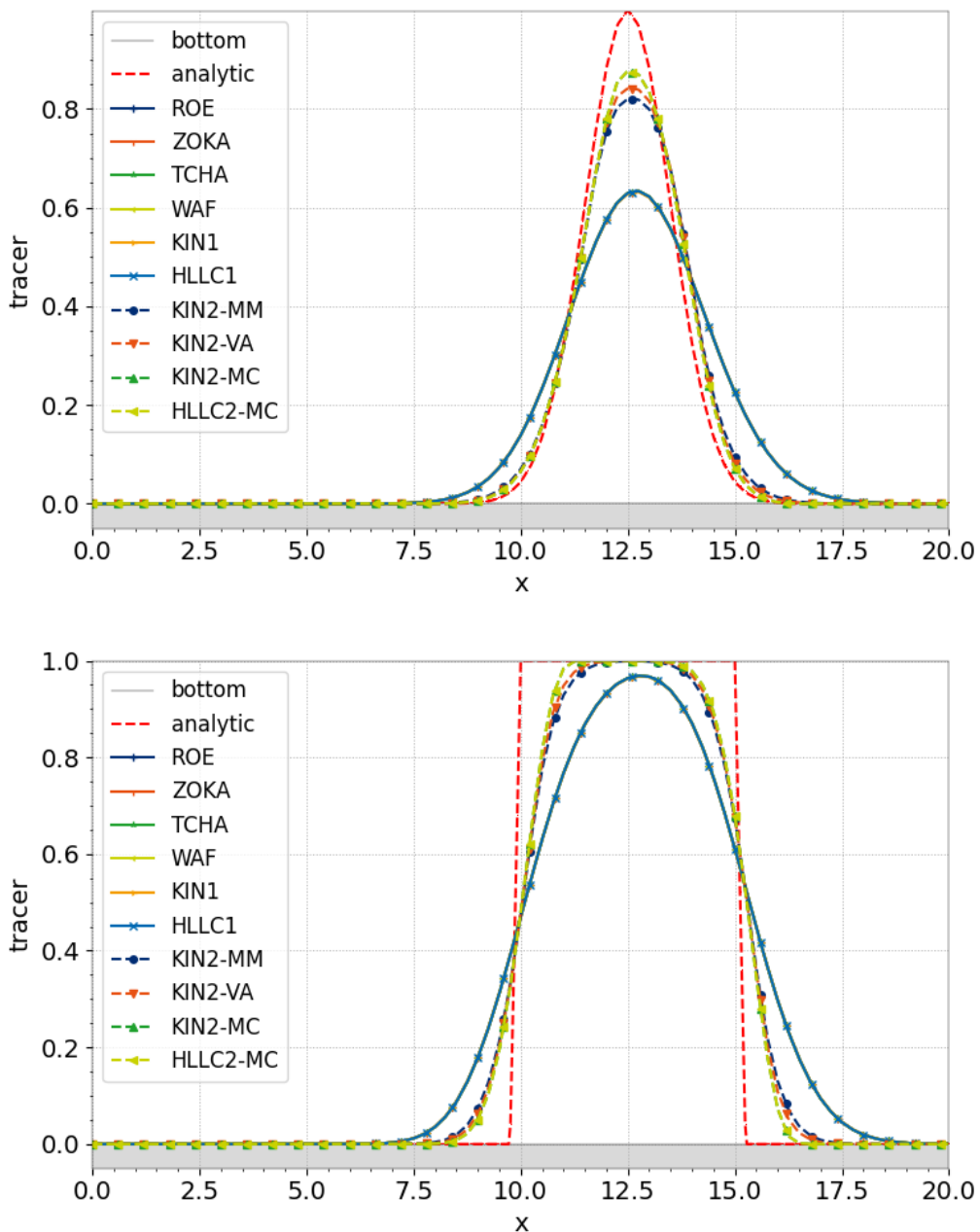


Figure 26.3: 1D solution along slice plane  $(x, z)$ ,  $y = 1$  at  $t = 7.5$  s for  $T_1$  (up) and  $T_2$  (down).

### 26.3.3 Convergence

To assess the accuracy of the schemes, computation of error on one mesh is not sufficient. In this section a mesh convergence is carried out for each numerical scheme. From a starting mesh, we divide by 4 each triangle recursively to generate new meshes. The first 4 meshes used in the convergence study are presented in Figure 26.4.

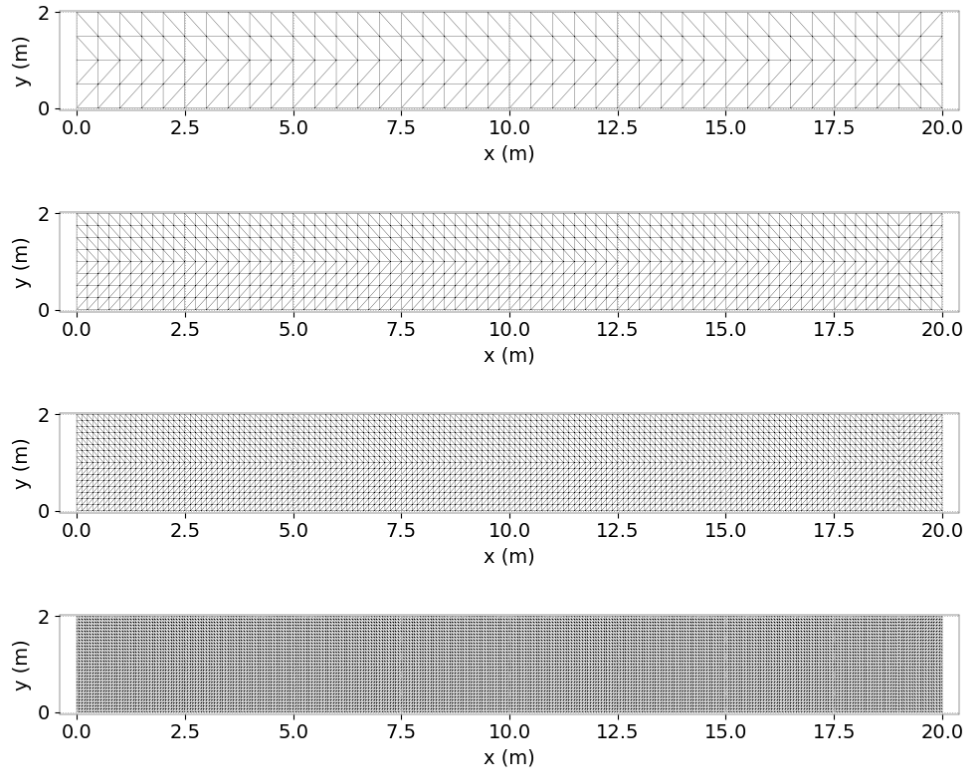


Figure 26.4: 2D Mesh used in flume\_tracer mesh convergence.

Convergence slopes of error in  $L^1$ ,  $L^2$  and  $L^\infty$  norm at final time are plotted for each numerical scheme in Figure 26.5.

Convergence slopes in  $L^2$  norm are compared in Figure 26.6. Errors on the finest mesh are presented in Figure 26.7.

## 26.4 Conclusion

TELEMAC-2D is able to model passive scalar transport problems in shallow water flows.

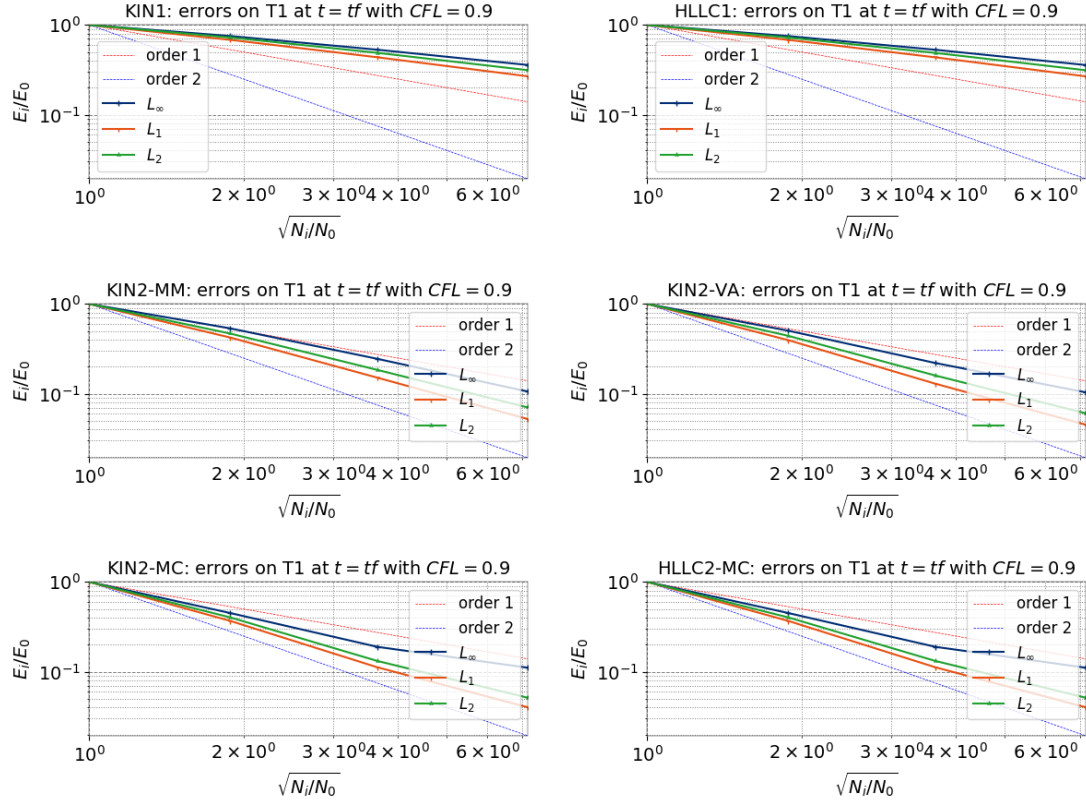
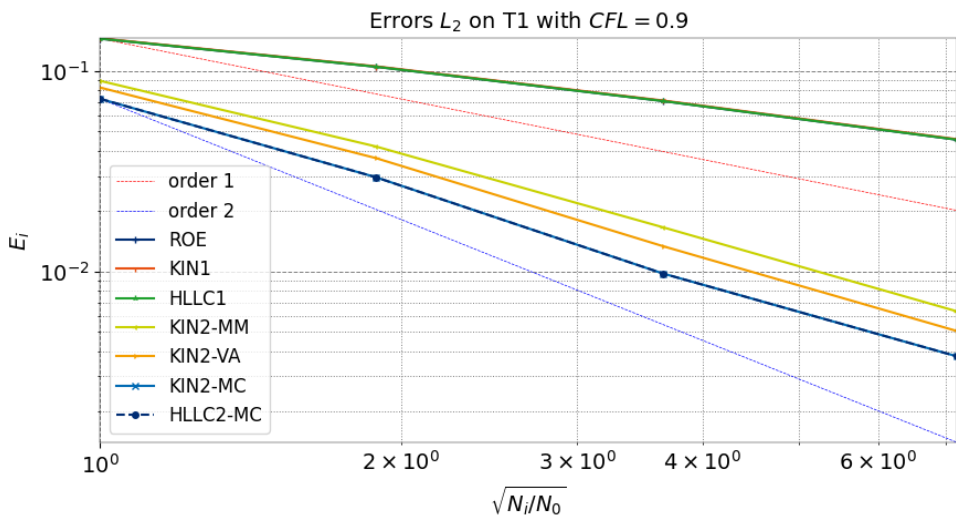
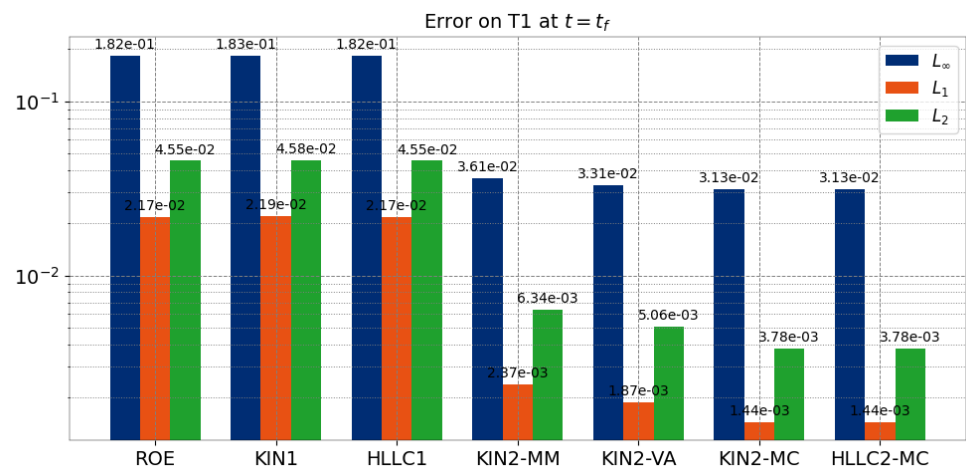


Figure 26.5: Mesh convergence of numerical schemes.

Figure 26.6: Mesh convergence in  $L^2$  norm.

Figure 26.7: Mesh convergence in  $L^2$  norm.

## 27. Flow in a channel with slope and friction (friction)

### 27.1 Description

This example shows that TELEMAC-2D is able to simulate a flow in a channel with mild slope and friction.

The configuration is a straight channel 410 km long and 450 m wide with a mild slope ( $z = -1.8536585365 \cdot 10^{-5}x - 4$ ), see Figure 27.1.

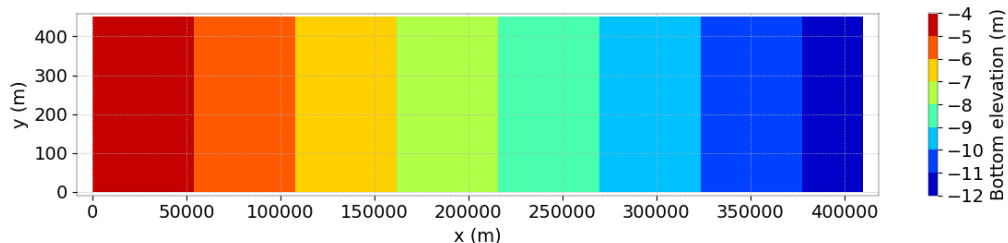


Figure 27.1: Bottom elevation.

#### 27.1.1 Initial and boundary conditions

The computation is initialised with a constant elevation equal to -9 m and no velocity.

The boundary conditions are:

- For the solid walls, a slip condition on channel banks is used for the velocities,
- On the bottom, a Strickler law with friction coefficient equal to  $70 \text{ m}^{1/3}/\text{s}$  is prescribed,
- Upstream a flowrate equal to  $6,000 \text{ m}^3/\text{s}$  is prescribed,
- Downstream the water level is suggested to be equal to 0 m.

Boundary conditions types can be seen in Figure 27.2.

#### 27.1.2 Mesh and numerical parameters

The mesh is made of 10,524 triangular elements (7,317 nodes), see zooms around inlet and outlet of the mesh in Figures 27.3 and 27.4.

The simulated period is 55,000 s (around 15 h 17 min).

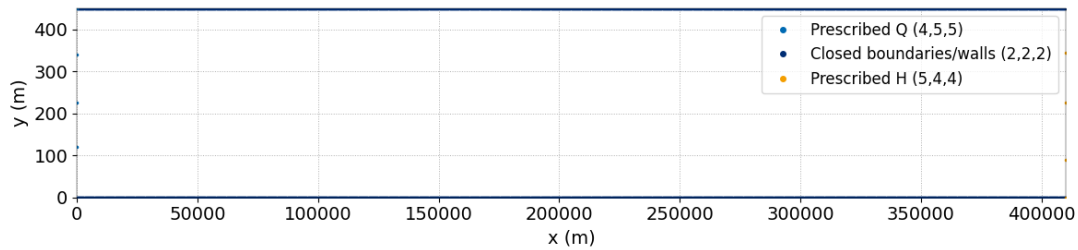


Figure 27.2: Boundary conditions types.

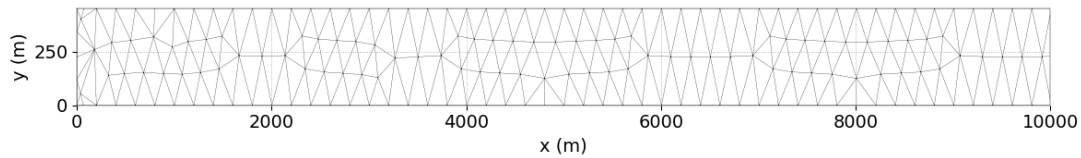


Figure 27.3: Zoom of the mesh at the inlet.

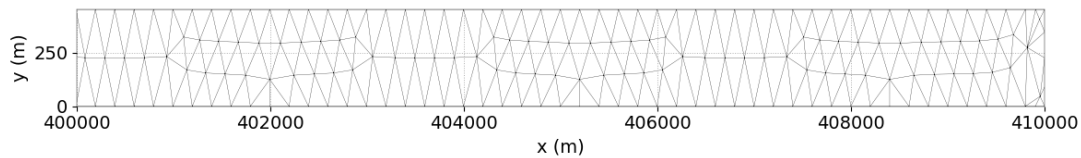


Figure 27.4: Zoom of the mesh at the outlet.

To solve the advection, the HLLC finite volume scheme is used with a desired Courant number equal to 0.8.

### 27.1.3 Physical parameters

No diffusion is chosen for this computation (constant horizontal viscosity for velocity equal to 0.  $\text{m}^2/\text{s}$ ).

## 27.2 Results

The flow establishes a steady flow, see Figures 27.5 and 27.6.

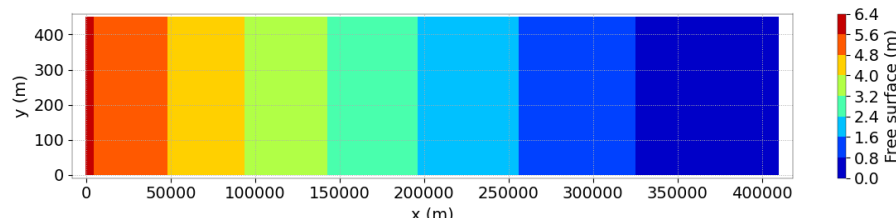


Figure 27.5: Free surface elevation at final time step.

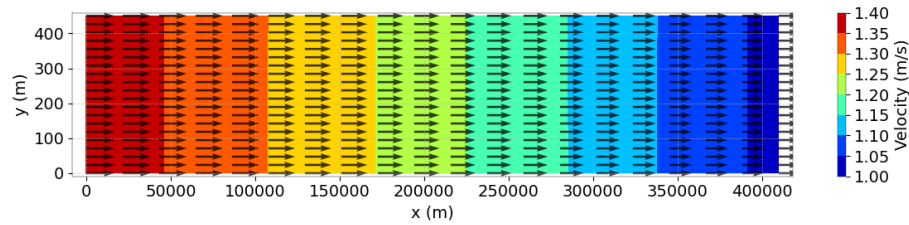


Figure 27.6: Magnitude of velocity at final time step with vectors.

### 27.3 Conclusions

This example shows that TELEMAC-2D is able to simulate a flow in a channel with mild slope and friction.

## 28. Gaussian water surface (gouttedo)

### 28.1 Purpose

To demonstrate that the TELEMAC-2D solution is not polarised because it can simulate the circular spreading of a wave. Two types of boundary conditions are tested, solid walls and Thompson. The first case shows that the no-flow condition is satisfied on solid boundaries and that the solution remains symmetric after reflection of the circular wave on the boundaries. The second case shows that Thompson boundary condition in TELEMAC-2D makes it possible to simulate the propagation of a circular wave out of the domain without spurious reflections on the open boundaries.

### 28.2 Description of the problem

#### 28.2.1 Geometry and mesh

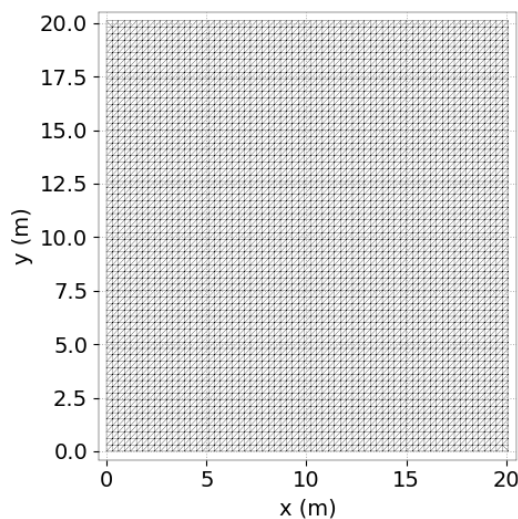


Figure 28.1: Mesh.

The domain is square with a size of  $20.1 \text{ m} \times 20.1 \text{ m}$  with a flat bottom. The domain is meshed with 8,978 triangular elements and 4,624 nodes. Triangles are obtained by dividing rectangular

elements on their diagonals. The mean size of obtained triangles is about 0.3 m (see Figure 28.1).

### 28.2.2 Initial conditions

The fluid is initially at rest with a Gaussian free surface in the centre of a square domain (see Figure 28.2). Water depth is given by  $H = 2.4 \left( 1.0 + \exp \left( \frac{-[(x-10.05) + (y-10.05)^2]}{4} \right) \right)$

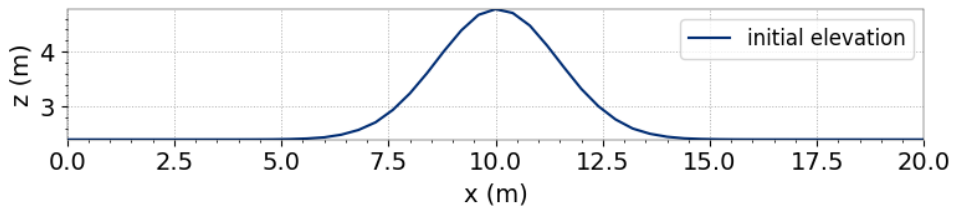


Figure 28.2: Gouttedo case: initial elevation.

### 28.2.3 Boundary conditions

Two cases are considered:

- Boundaries are considered as solid walls with perfect slip conditions (condition 2 2 2),
- The Thompson boundary conditions are applied for open boundaries (condition 4 4 4).

### 28.2.4 Physical parameters

The physical parameters used for this case are the following:

- Friction: Strickler formula with  $k_s = 40 \text{ m}^{1/3}/\text{s}$  for the solid wall case and no friction for the open case,
- Turbulence: Constant viscosity equal to zero.

### 28.2.5 Numerical parameters

- Type of advection: centred semi-implicit scheme + SUPG upwinding on velocities (2 = SUPG) for the solid wall case and characteristics for the open boundary case,
- Type of advection: conservative + modified SUPG on depth (mandatory scheme),
- Type of element: Linear triangle (P1) for  $h$  and velocities,
- Solver: GMRES with an accuracy  $= 10^{-4}$  for the solid wall case and conjugate gradient with an accuracy  $= 10^{-6}$  for the open case,
- Time step: 0.04 s,
- Simulation time: 4 s.

### 28.3 Results with solid walls

The wave spreads circularly around the initial water surface peak elevation. When it reaches the boundaries, reflection occurs. Interaction between reflected waves issuing from the four walls can be observed after time 2.4 s (cf. Figure 28.3).

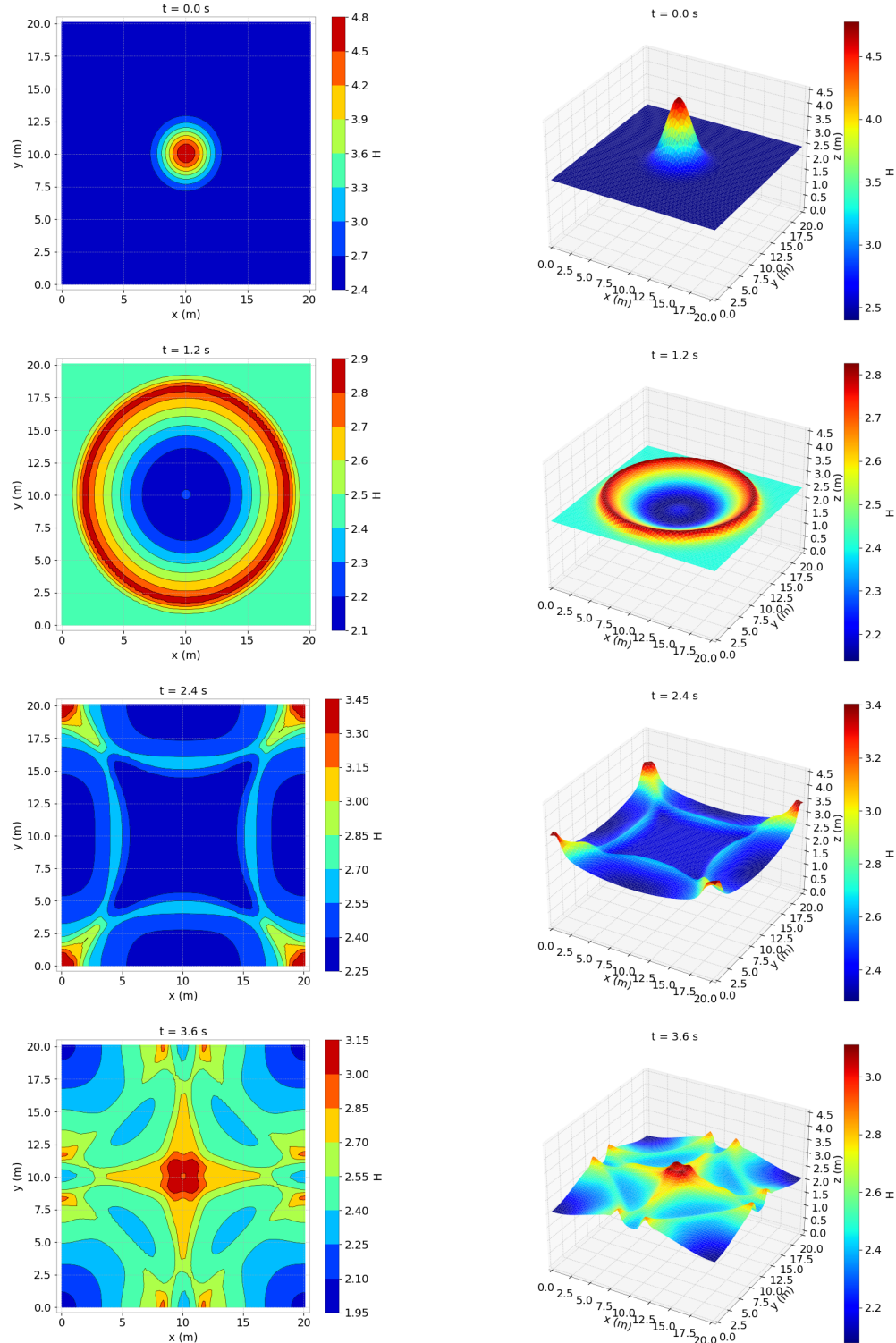


Figure 28.3: Evolution of free surface with solid boundary conditions.

**28.4 Results with Thompson boundary conditions**

The wave spreads circularly around the initial water surface peak elevation. The velocity field is radial. No reflection occurs on the open boundaries (cf. Figure 28.4). The initial volume of water in the domain is  $999.784 \text{ m}^3$ . The volume that left the domain is  $27.83 \text{ m}^3$ . The total volume of water numerically lost is  $0.11 \times 10^{-4} \text{ m}^3$ , i.e. 0,000001 %.

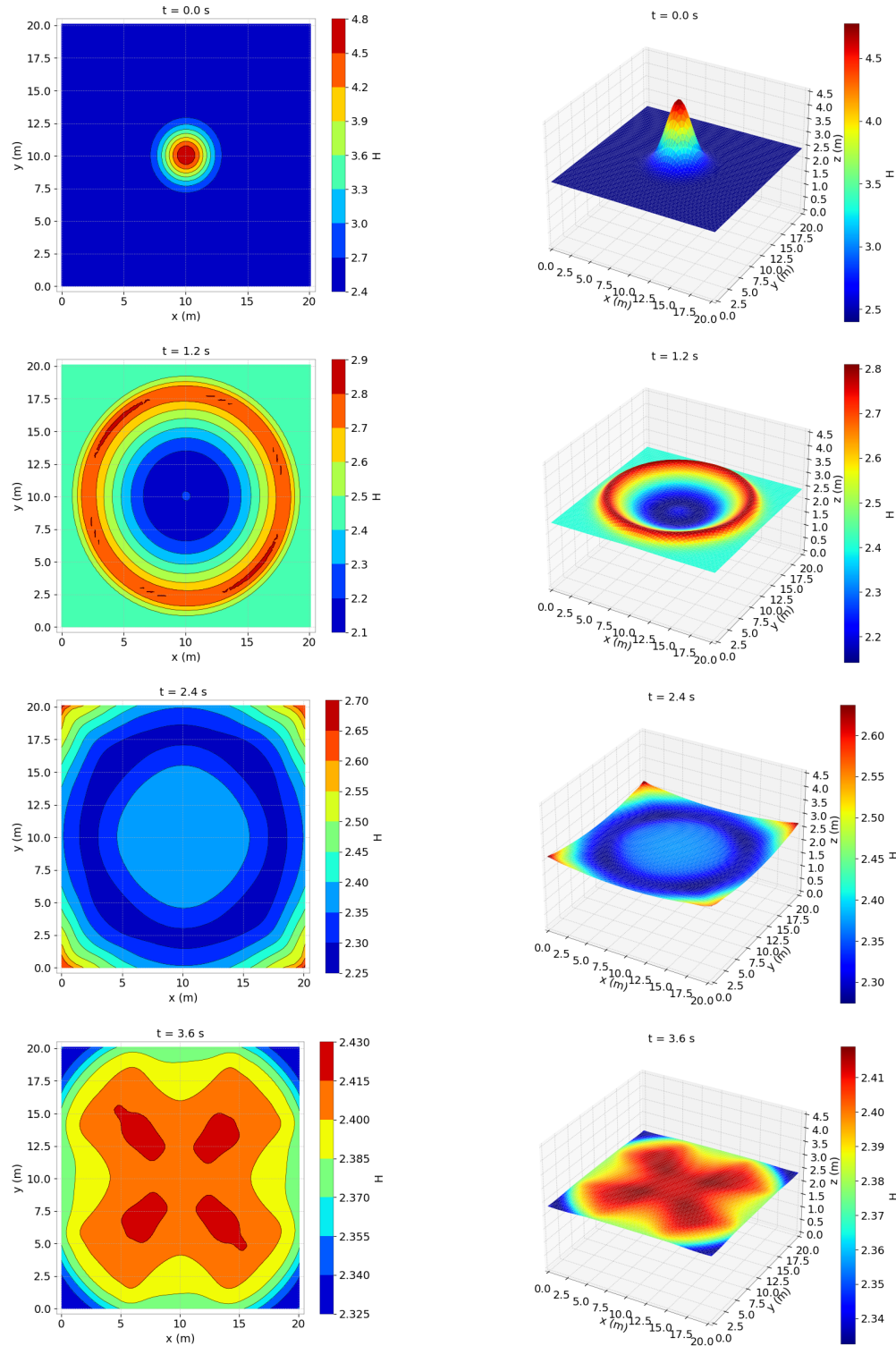


Figure 28.4: Evolution of free surface with Thompson boundary conditions.

Long wave celerity is  $4.85 \text{ m.s}^{-1}$  for  $h = 2.40 \text{ m}$  and  $6.86 \text{ m.s}^{-1}$  for  $h = 4.80 \text{ m}$ , which means the peak of the wave should reach the boundary after 1.46 to 2 s in the long wave hypothesis. The computed value is 1.6 s.

## 28.5 Conclusions

Even though the mesh is polarised (along the  $x$  and  $y$  directions and the main diagonal), the solution is not. Solid boundaries are treated properly: no bias occurs in the reflected wave and water mass is conserved. With Thompson boundary conditions, no parasite reflection waves are visible.

## 29. init

### 29.1 Description

This example checks some features available in TELEMAC-2D:

- sources by nodes,
- sources by regions,
- kinetic schemes.

The configuration is the same for the 6 computations: a section of river (around 1,700 m long and 300 m wide) with realistic bottom. The geometric data include a groyne in the transversal direction and an island (see Figure 29.1).

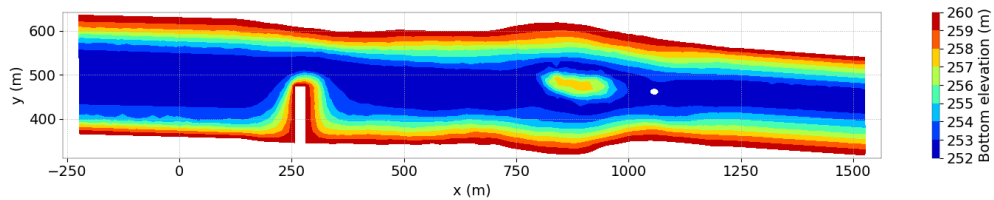


Figure 29.1: Bottom elevation.

#### 29.1.1 Initial and boundary conditions

There are 6 computations:

- The first computation (with t2d\_init.cas steering file), for which the computation is initialised with a constant elevation equal to 265 m and no velocity,
- The second computation (with t2d\_init\_cin.cas steering file), for which the computation is initialised with a constant elevation equal to 265 m and no velocity,
- The third computation (with t2d\_init\_cin\_source\_by\_reg.cas steering file), for which the computation is initialised with a constant elevation equal to 265 m and no velocity,
- The fourth computation (with t2d\_init-no-water.cas steering file) which is initialised with a special treatment: water depth equal to 0 m everywhere except along the inlet boundary where elevation is equal to 260 m, and no velocity,

- The fifth computation (with t2d\_init-restart.cas steering file) is a restart computation,
- The sixth computation (with t2d\_init-restart\_source\_by\_reg.cas steering file) is a restart computation.

The boundary conditions are:

- For the solid walls, a slip condition on channel banks is used for the velocities,
- On the bottom, a Strickler law with friction coefficient equal to 50 or  $55 \text{ m}^{1/3}/\text{s}$  is prescribed depending on the computation,
- Upstream a flowrate equal to  $750 \text{ m}^3/\text{s}$  is prescribed (linearly increasing from 0 to  $750 \text{ m}^3/\text{s}$  during the first hour),
- Downstream the water level is equal to 265 m for most of the computations except no-water computation for which it is let free.

### 29.1.2 Mesh and numerical parameters

The mesh (Figure 29.2) is made of 3,780 triangular elements (2,039 nodes). It is refined around the island and in front of the groyne.

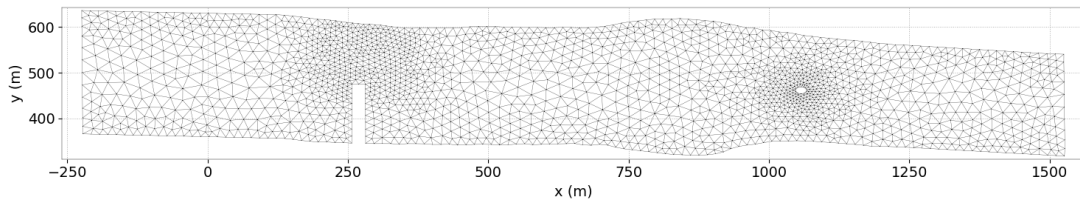


Figure 29.2: Horizontal mesh.

The simulated period is 500 s for most of the computations, except the restart computations which simulate 3 h.

The time step is 2.5 s (for the Finite Elements computations). Variable time step is used with a desired Courant number equal to 0.9 for the Kinetic computations.

For Finite Elements computations, to solve the advection:

- the method of characteristics is used for the velocities (scheme 1),
- the PSI scheme is used for tracers for restart computations,
- the SUPG scheme is used for the  $k - \varepsilon$  variables for the t2d\_init.cas computation.

The GMRES is used for solving the propagation step (option 7) and diffusion of tracer when tracer is modelled.

2nd order Kinetic scheme is used to solve the kinetic computations with desired Courant number equal to 0.9.

### 29.1.3 Physical parameters

Except for the t2d\_init.cas computation, turbulence is modelled by a constant viscosity. It is equal to  $10^{-2} \text{ m}^2/\text{s}$  for the restart computations,  $1 \text{ m}^2/\text{s}$  for the no-water computation, and no diffusion for the kinetic computations. The  $k - \varepsilon$  model is used for the t2d\_init.cas computation.

One tracer transport is modelled with the kinetic and the restart computations, with one source point or sources defined by regions (defined by a polygon, in that case with the keyword SOURCE REGIONS DATA FILE). For kinetic computations, the source term is multiplied by a Dirac function (TYPE OF SOURCES = 2 which is recommended when the number of sources is big) whereas for restart computations, the source term is multiplied by a finite element basis (= 1, which is the default choice). For restart computations, no diffusion for tracers is considered.

During the restart computations, tracer is released during 2 periods of time, between 1,800 s and 3,600 s but also between 4,800 s and 7,200 s.

Porosity is used (OPTION FOR THE TREATMENT OF TIDAL FLATS = 3) for the no-water computation.

## 29.2 Results

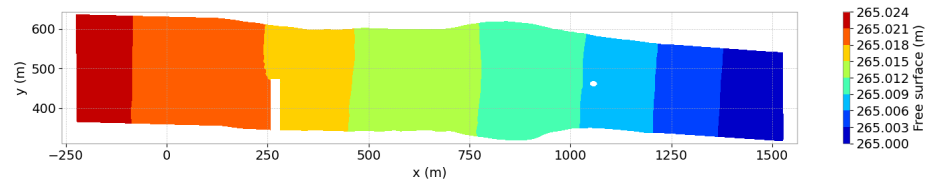


Figure 29.3: Free surface elevation at final time step ( $k - \varepsilon$ ).

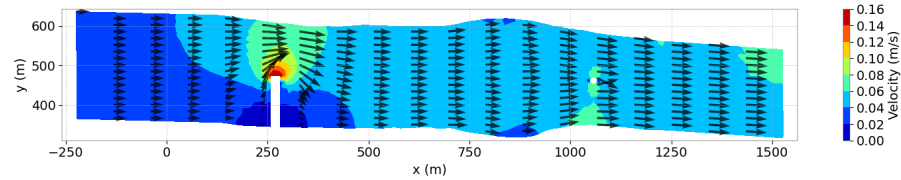


Figure 29.4: Magnitude of velocity at final time step with vectors ( $k - \varepsilon$ ).

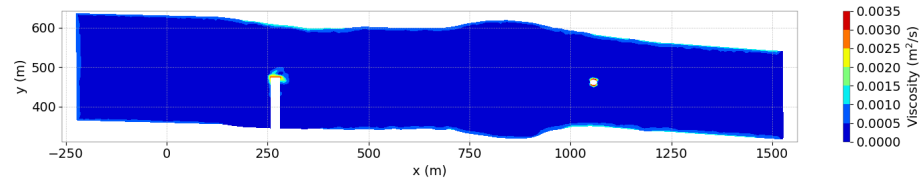


Figure 29.5: Viscosity at final time step with vectors ( $k - \varepsilon$ ).

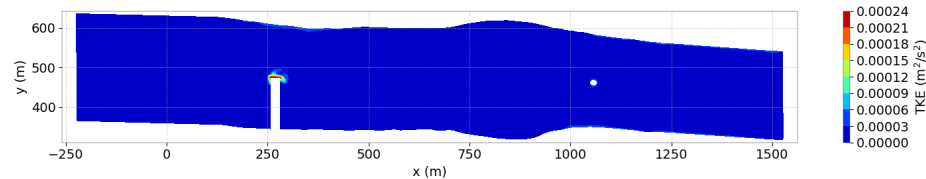


Figure 29.6: Turbulent Kinetic Energy at final time step with vectors ( $k - \varepsilon$ ).

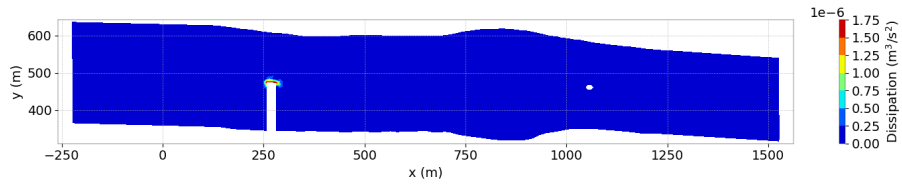


Figure 29.7: Dissipation at final time step with vectors ( $k - \varepsilon$ ).

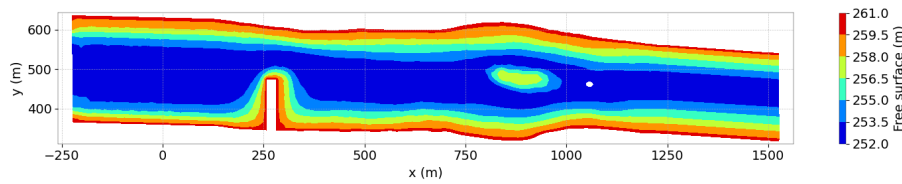


Figure 29.8: Free surface elevation at final time step (no water).

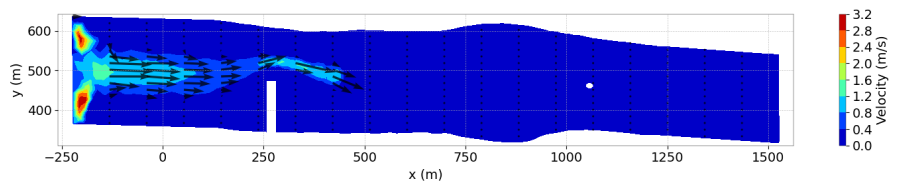


Figure 29.9: Magnitude of velocity at final time step with vectors (no water).

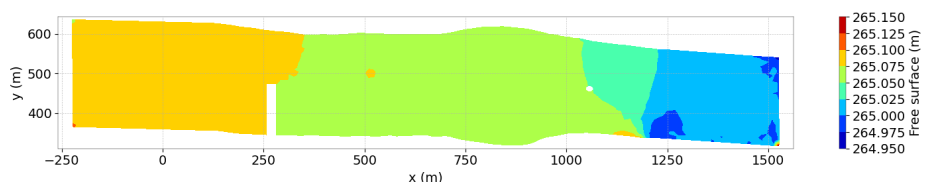


Figure 29.10: Free surface elevation at final time step (kinetic with sources by points).

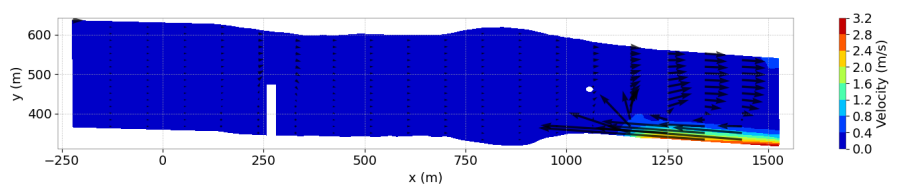


Figure 29.11: Magnitude of velocity at final time step with vectors (kinetic with sources by points).

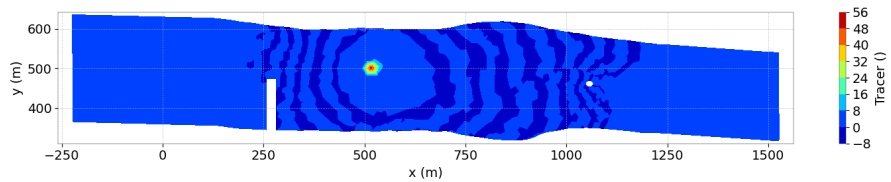


Figure 29.12: Tracer at final time step (kinetic with sources by points).

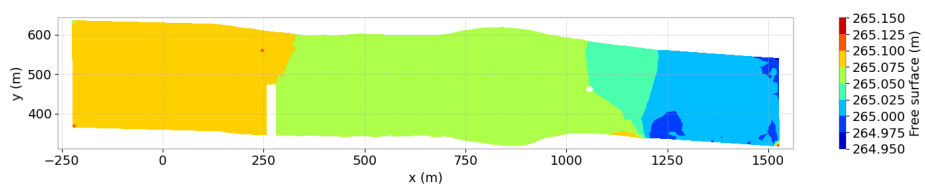


Figure 29.13: Free surface elevation at final time step (kinetic with sources by regions).

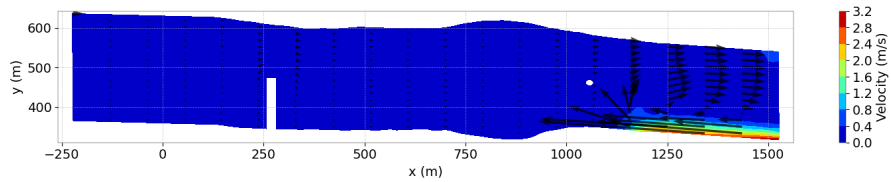


Figure 29.14: Magnitude of velocity at final time step with vectors (kinetic with sources by regions).

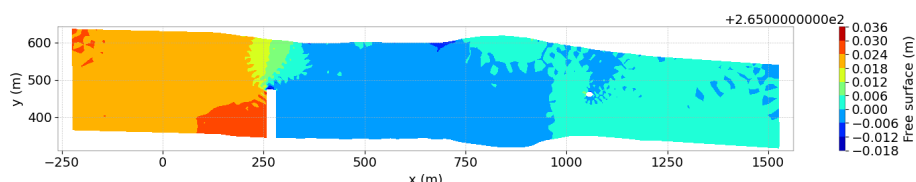


Figure 29.15: Free surface elevation at final time step (restart with sources by points).

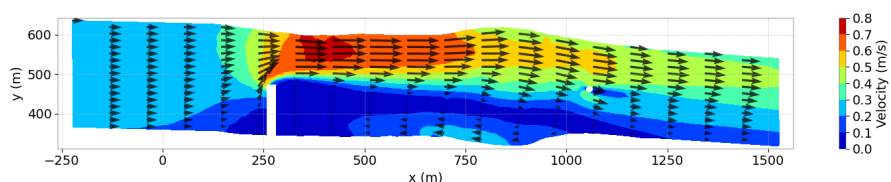


Figure 29.16: Magnitude of velocity at final time step with vectors (restart with sources by points).

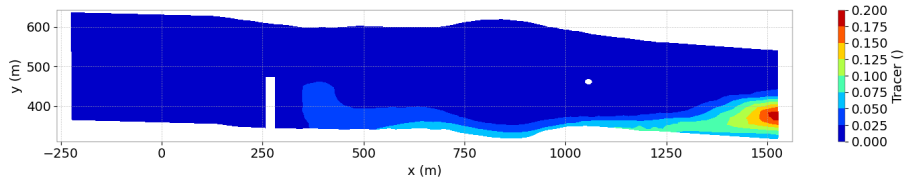


Figure 29.17: Tracer at final time step (restart with sources by points).

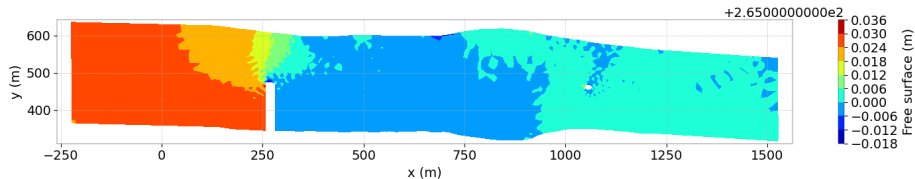


Figure 29.18: Free surface elevation at final time step (restart with sources by regions).

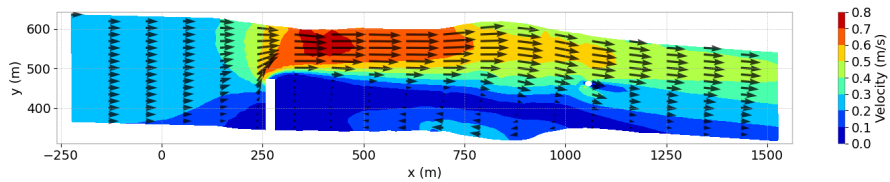


Figure 29.19: Magnitude of velocity at final time step with vectors (restart with sources by regions).

## 30. Transformation of the M2 tide constituent along the western European Continental shelf (m2wave)

### 30.1 Purpose

This test case computes the transformation of the main tide constituent (M2 - semi-diurnal moon generated wave) occurring along the western Europe continental margin.

### 30.2 Description

#### 30.2.1 Approach

The model extends from the Iberian Peninsula up to South England. The whole continental margin of the Atlantic coasts of France is represented as well as the Southern part of the North Sea. The model is forced by the M2 tide component. 4 tide cycles are simulated.

#### 30.2.2 Geometry and mesh

Size of the model: 520 km × 950 km.

The mesh is denser near the coastline than along the open Atlantic boundaries. However, the mesh is not refined along the slope of the continental shelf in the present model (following studies have shown that this refinement was important for the overall quality of results).

- 9,414 triangular elements,
- 5,007 nodes,
- Maximum size range: from 10 to 50 km.

#### 30.2.3 Boundaries

- Ocean open boundaries:  $h$  imposed with the tide,
- Coastline: solid walls with slip condition.

#### 30.2.4 Bottom

Chézy formula with friction coefficient = 40 m<sup>2</sup>/s.

Mesh and topography are shown in Figures 30.1 and 30.2.

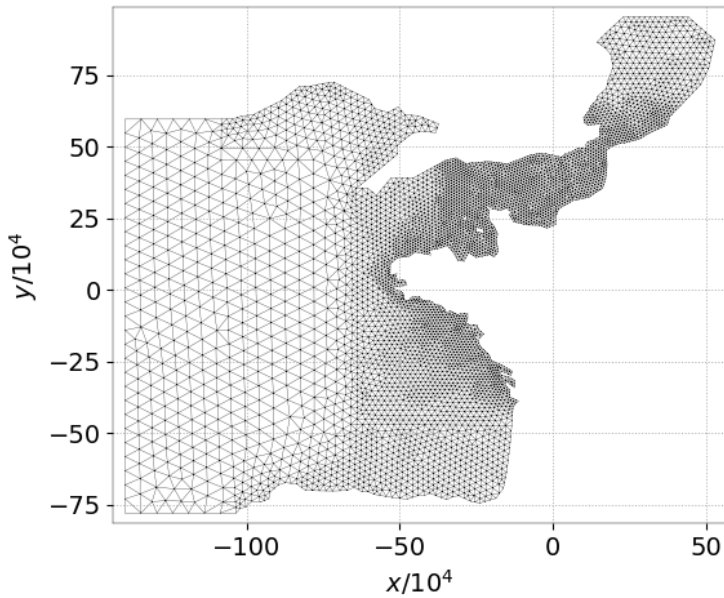


Figure 30.1: Mesh of the m2wave case.

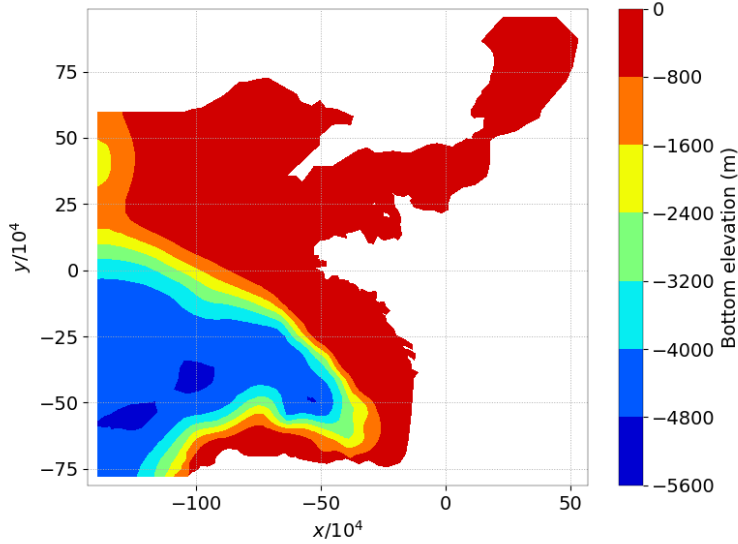


Figure 30.2: Bathymetry of the m2wave case.

### 30.2.5 Numerical parameters

- No advection of  $U$  and  $V$ , Conservative + modified SUPG on depth (mandatory scheme),
- Elements : Quasi-bubble triangle for velocities, Linear triangle (P1) for  $H$ ,
- Implicitation for depth and for velocity = 0.55,
- GMRES Solver, with Solver accuracy =  $10^{-3}$ ,
- INITIAL GUESS FOR  $U = 2$ ,

- SUPG option: Upwinding equal to 1 for velocity and depth,

- Coriolis and spherical coordinates,

- Time step = 150 s,

- Simulation duration = 178,800 s (a little bit less than 50 h).

### 30.3 Results

The resulting amplitude and phase of the M2 tide component are shown in Figures 30.3 and 30.4.

More accurate results were found in a subsequent model with a finer mesh along the continental shelf and along the coastline. More tidal constituents were also taken into account. Inclusion of the tide generating potential in basic equations of TELEMAC-2D further improved the results.

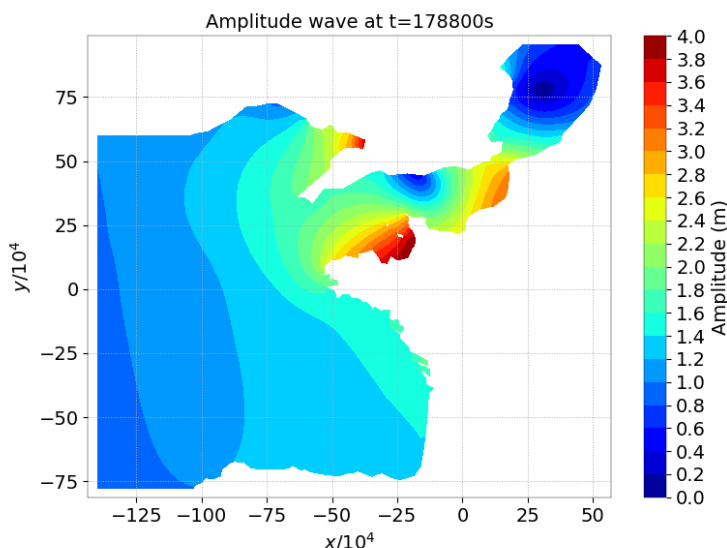


Figure 30.3: M2 amplitude at  $t = 178,800$  s.

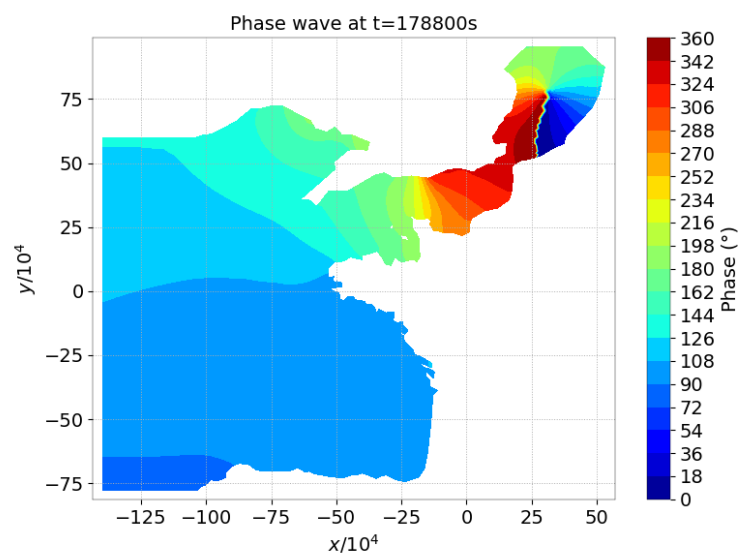


Figure 30.4: M2 phase at  $t = 178,800$  s.

# 31. Malpasset dambreak (malpasset)

## 31.1 Purpose

This test illustrates that TELEMAC-2D is able to simulate a real dam break flow on an initially dry domain. It also shows the propagation of the wave front and the evolution of the water surface and velocities in the valley downstream. It was used as a test case in the program ESPRIT for the european projet project PCECOWATER (Parallel Computing of Environment COastal and lake shallow WATER dynamics).

## 31.2 Description

This case is the simulation of the propagation of the wave following the break of the Malpasset dam (South-East of France). The accident occurred in December 1959. The model represents the reservoir upstream from the dam and the valley and flood plain downstream.

The simulation is performed using the treatment of negative depths introduced since release 7.0 of TELEMAC-2D. The historical simulation using the method of characteristics (named CHAR) has been kept. Nevertheless, the recommended numerical approach for such applications is any finite volume scheme or the NERD scheme for finite element method.

### 31.2.1 Geometry and mesh

The entire valley is approximately 18 km long and between 200 m (valley) and 7 km wide (flood plain). The complete study is described in details in [12]. The dam is modelled by a straight line between the points of coordinates (4,701.18 m ; 4,143.10 m) and (4,655.50 m ; 4,392.10 m). Its location is shown in Figure 31.2. The size of the model is approximately 17 km × 9 km. A triangular mesh is built on this domain and is refined in the river valley (downstream from the dam) and on the banks. Two meshes are tested:

- **Regular mesh (Figure 31.1 - a):** which contains 26,000 triangular elements and 13,541 nodes with a maximum size ranging from 17 to 313 m.
- **Fine mesh (Figure 31.1 - b):** which contains 104,000 triangular elements and 53,081 nodes with a maximum size ranging from 8.5 to 156.5 m.

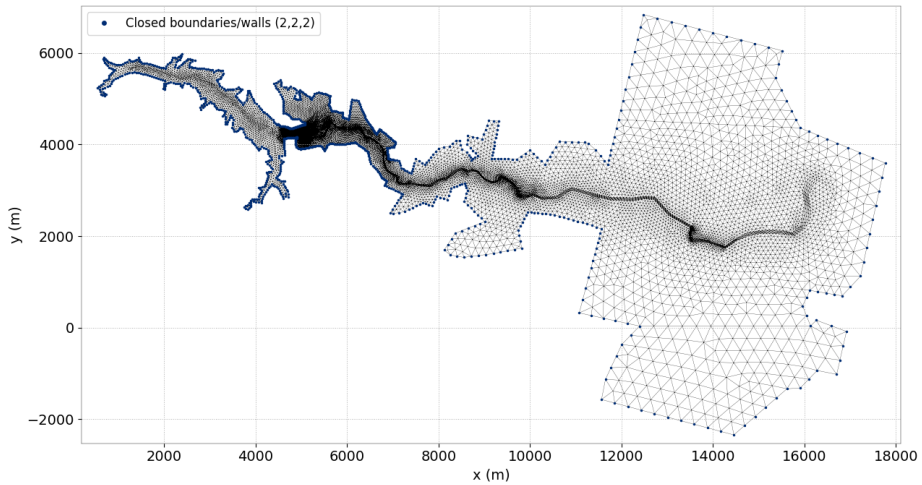
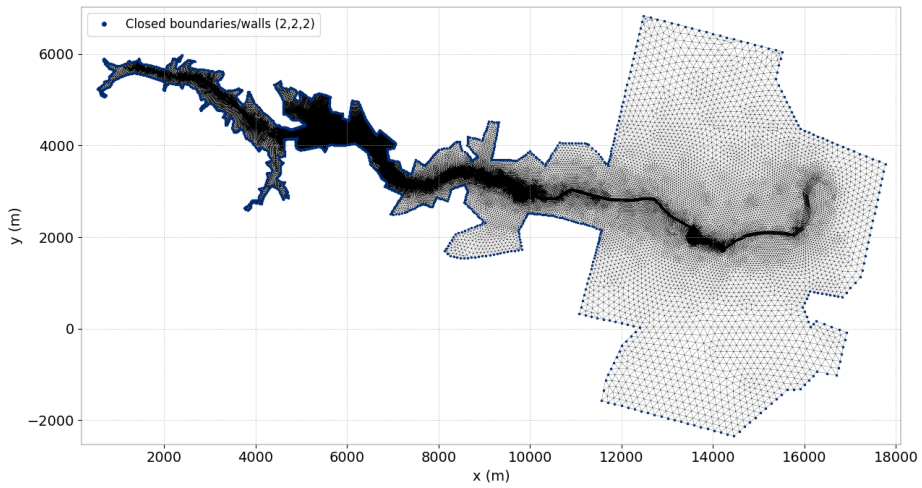
**a - Regular mesh****b - Fine mesh**

Figure 31.1: Malpasset case meshes.

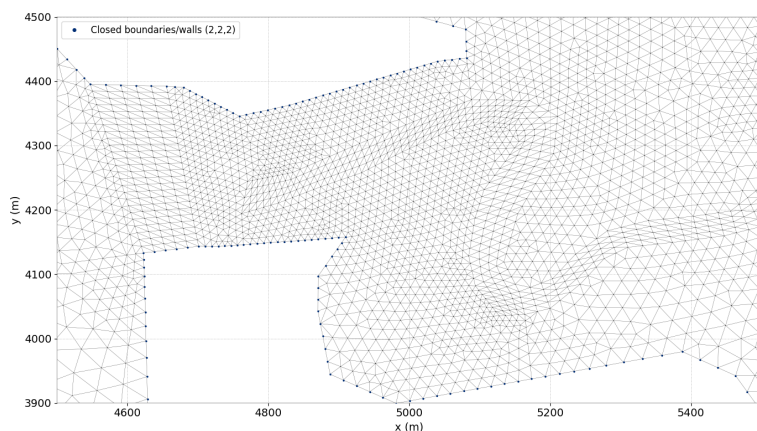


Figure 31.2: Dam location on the malpasset case.

### 31.2.2 Bathymetry

Old maps have been used to deduce the topography of the domain (Figure 31.3). In fact, the topography after the accident could not be used because of the dramatic changes that occurred. Therefore, the IGN map of Saint-Tropez, Number 3, of year 1931, was used.

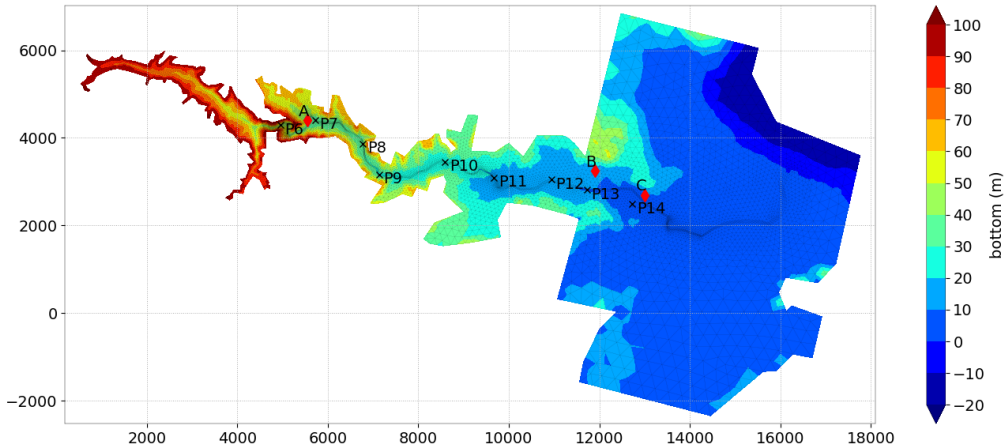


Figure 31.3: Bottom levels in the domain and reference points.

### 31.2.3 Reference data

In order to evaluate the precision of the numerical schemes, the results are compared to data obtained from: a physical model (see [12]) (Non-distorted, 1/400 scale) that was built in LNHE in 1964 (Gauges P6 to P14) and three electric transformers were destroyed by the wave and the times of electric shutdown were precisely recorded (Points A, B and C). The locations of these observation points are shown in Figure 31.3. The data used for verification are the following:

- Recorded time from A (5,550 m ; 4,400 m) to B (11,900 m ; 3,250 m): 1,140 s,
- Recorded time from A to C (13,000 m ; 2,700 m): 1,320 s,
- Maximum free surface elevations obtained from gauges. The values are converted to water depths (by deducing the bathymetry values) and summed up in Table 31.1.

| Point Name | x-coordinate | y-coordinate | Distance to dam | Measured Max water depth |
|------------|--------------|--------------|-----------------|--------------------------|
| P6         | 4,947        | 4,289        | 336             | 40.3                     |
| P7         | 5,717        | 4,407        | 1,320           | 14.6                     |
| P8         | 6,775        | 3,869        | 2,160           | 24.0                     |
| P9         | 7,128        | 3,162        | 3,420           | 12.8                     |
| P10        | 8,585        | 3,443        | 4,840           | 11.8                     |
| P11        | 9,674        | 3,085        | 6,000           | 8.3                      |
| P12        | 10,939       | 3,044        | 7,220           | 10.1                     |
| P13        | 11,724       | 2,810        | 7,980           | 6.8                      |
| P14        | 12,723       | 2,485        | 8,960           | 5.4                      |

Table 31.1: Maximum values of water depth on measurement points for the malpasset case (everything in m).

### 31.2.4 Initial conditions

At the beginning of the simulation, the dam is assumed undamaged and the reservoir is full. There is no water in the downstream valley, and no velocity in all the domain.

### 31.2.5 Boundary conditions

The boundaries are solid everywhere and the channel banks considered as solid walls. There is no friction on the solid walls. The bottom is considered as a solid boundary with roughness. The Strickler formula with friction coefficient =  $30 \text{ m}^{1/3}/\text{s}$  is used.

### 31.2.6 Physical parameters

The characteristics of the case are the following:

- Observed mean wave velocity  $U_0 = 27 \text{ km.h}^{-1} = 7.5 \text{ m.s}^{-1}$ ,
- Initial water depth upstream of the dam  $H_0 = 55 \text{ m}$ ,
- Total duration of the event  $T = 4,000 \text{ s}$ ,
- Valley length  $L = 18 \text{ km}$ ,
- Maximum valley width  $l_M = 7 \text{ km}$ ,
- Reynolds Number  $R_e = \frac{U_0 \times H_0}{\nu} = 4.12 \times 10^8$  where  $\nu$  is the kinematic viscosity of water,
- Froude Number  $F_r = \frac{U_0}{\sqrt{g \times H_0}} = 0.32$  where  $g$  is the gravity acceleration.

In the simulations, the Coriolis force and the wind effect are not taken into account. Besides, the viscosity is set as constant and equal to  $1 \text{ m}^2/\text{s}$  on horizontal directions.

### 31.2.7 Numerical parameters

Duration of the simulation is set to 4,000 s. The use of coupled primitive equations (TREATMENT OF THE LINEAR SYSTEM = 1) is compared to the wave equation (TREATMENT OF THE LINEAR SYSTEM = 2). Initial and boundary conditions remain the same for all the cases, and are described in the first two sections. The solver accuracy used for the resolution of the linear system is of  $10^{-8}$  and with a maximum number of iterations equal to 200 for every finite element case. The solver used for the resolution of the linear system is the conjugate gradient for most of the finite element cases except with the primitive equations for which GMRES is necessary. For finite element cases, when using the wave equation, the type of element are linear for velocities and water depth whereas when using primitive equations the type of Element are quasi-bubble for velocities and linear for water depth. Quasi-bubble elements are used to avoid oscillations due to a violated inf-sup condition. The simulation parameters specific to each case are summed up in Table 31.2.

| Name | Mesh    | Equations       | Advection scheme for velocities | Time-step / Desired CFL |
|------|---------|-----------------|---------------------------------|-------------------------|
| ERIA | Regular | Wave Eq. FE     | ERIA scheme                     | 0.5 s / -               |
| NERD | Regular | Wave Eq. FE     | Edge-based n-scheme             | 0.5 s / -               |
| CHAR | Regular | Wave Eq. FE     | Characteristics                 | 0.5 s / -               |
| PRIM | Regular | Saint-Venant FE | Characteristics                 | 0.5 s / -               |
| KIN1 | Regular | Saint-Venant FV | Kinetic order 1                 | - / 0.9                 |
| HLLC | Regular | Saint-Venant FV | HLLC order 1                    | - / 0.9                 |
| FINE | Fine    | Saint-Venant FV | Kinetic order 1                 | - / 0.9                 |

Table 31.2: List of the simulation parameters used for the different cases tested.

### 31.3 Results

#### 31.3.1 First observations - regular mesh

Figure 31.4 illustrates the progression of the flood wave after the dam break. The propagation of the wave front is very fast. The water depth increases rapidly in the valley downstream from the dam location. The wave spreads in the plain when arriving to the sea.

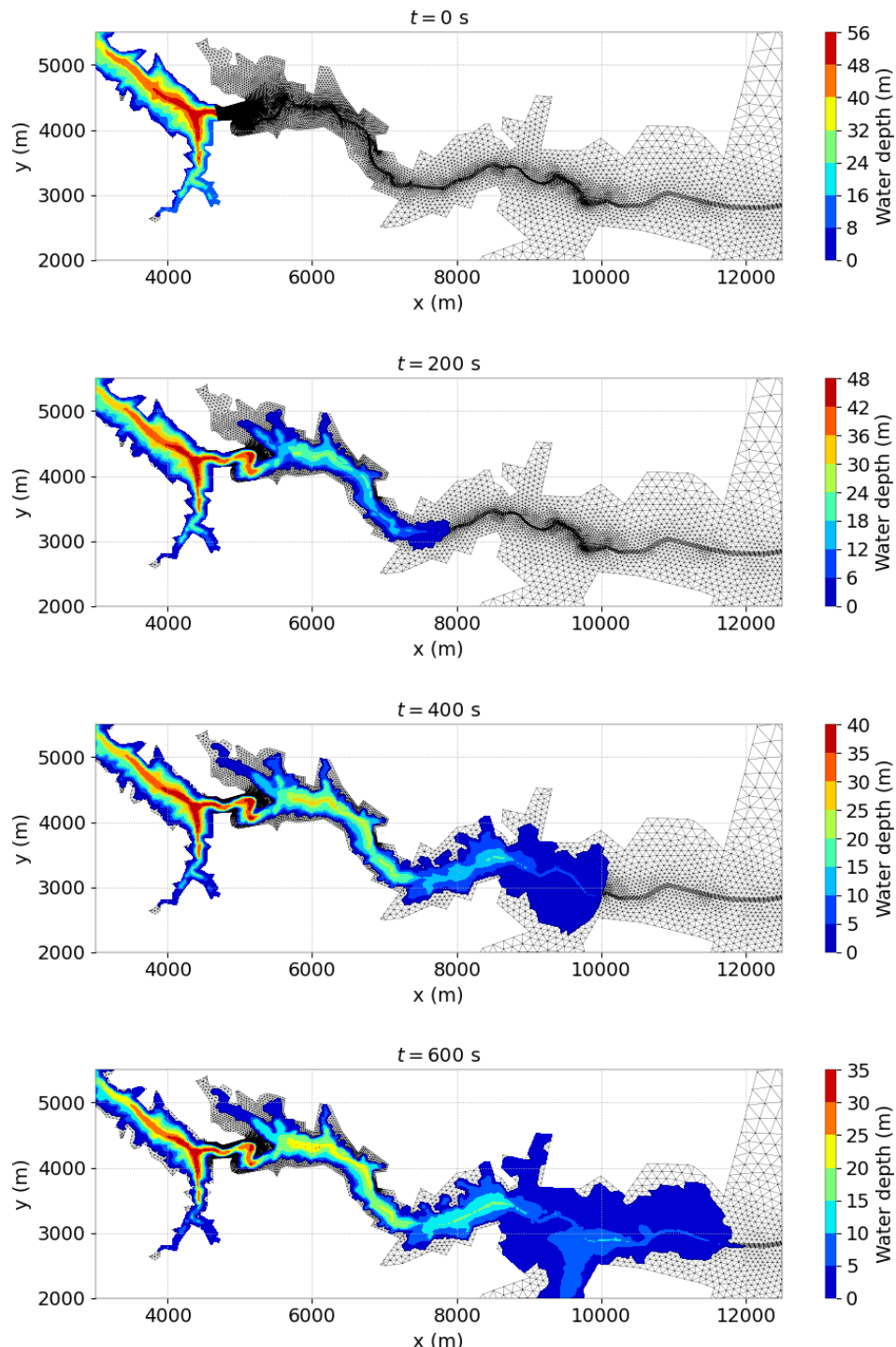


Figure 31.4: Evolution of the water depth with the KIN1 scheme.

### 31.3.2 First observations - fine mesh

Figure 31.5 illustrates the progression of the flood wave after the dam break on the fine mesh with the KIN1 scheme.

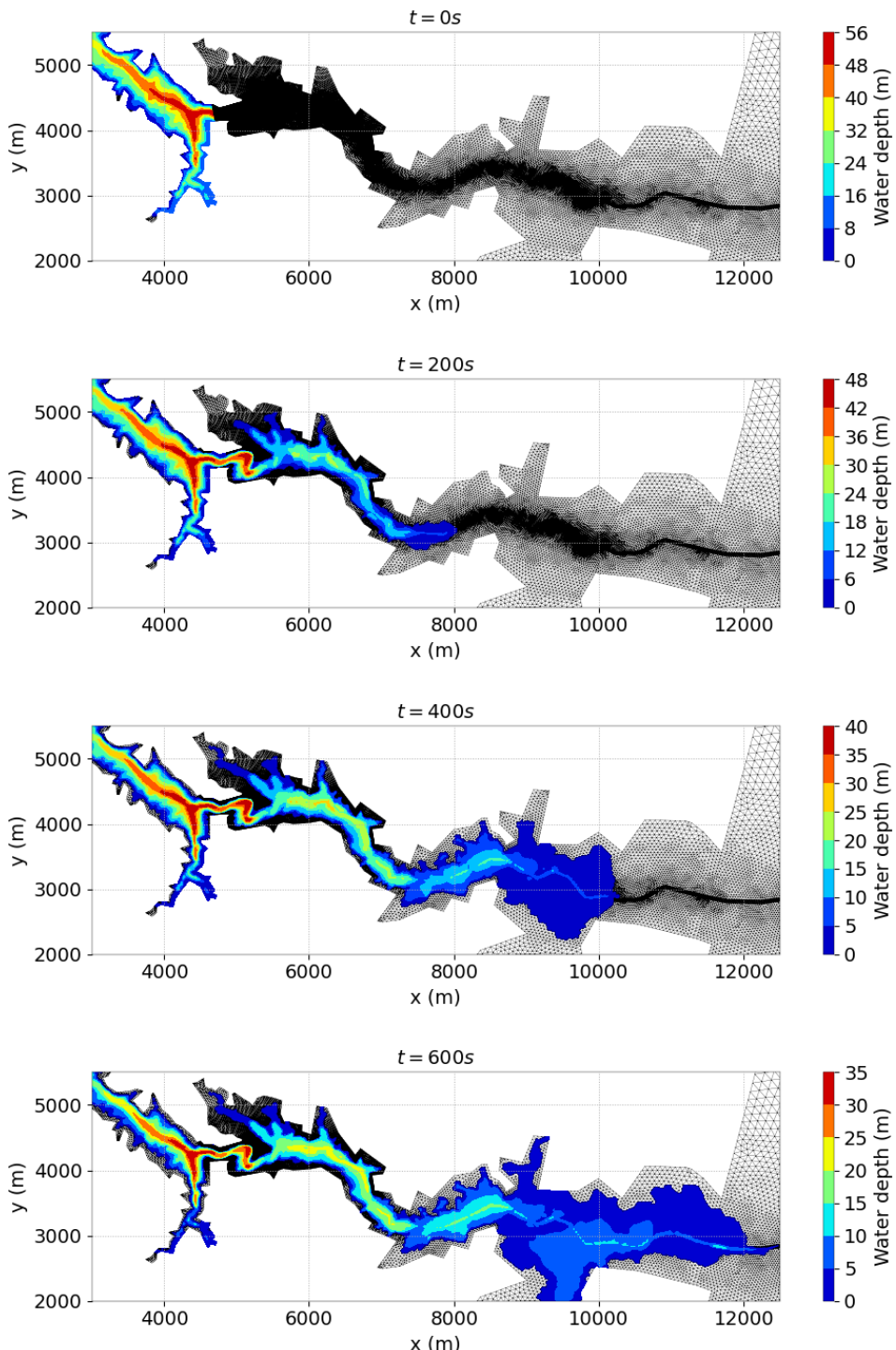


Figure 31.5: Evolution of the water depth with the KIN1 scheme on fine mesh.

### 31.3.3 Computation time

Simulation times for each of these cases with sequential and parallel runs (using 4 processors) are shown in Figure 31.6<sup>1</sup>.

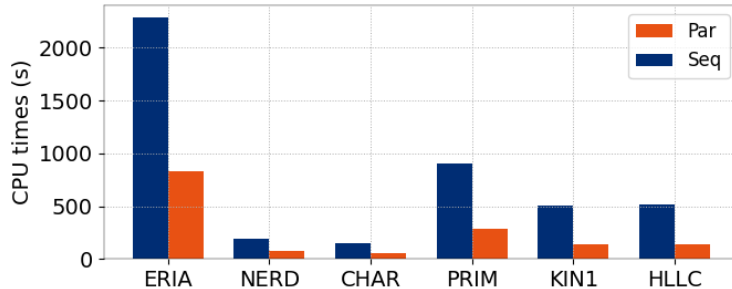


Figure 31.6: CPU times.

### 31.3.4 Comparison of schemes

In Figures 31.7 and 31.8, water depth is plotted after 400 s of simulation. Depending on the system of equation and on the method of resolution, wave propagates at different speeds.

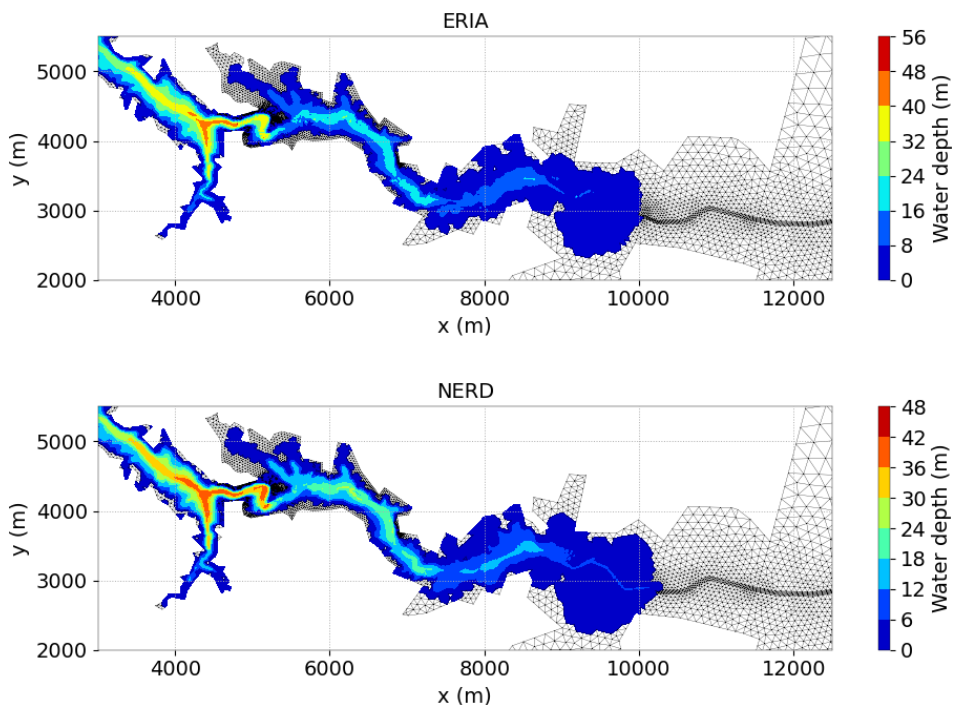


Figure 31.7: Water depth at  $t = 400$  s for different cases of the malpasset example.

---

<sup>1</sup>Keep in mind that these times are specific to the validation run and the type of processors that were used for this purpose.

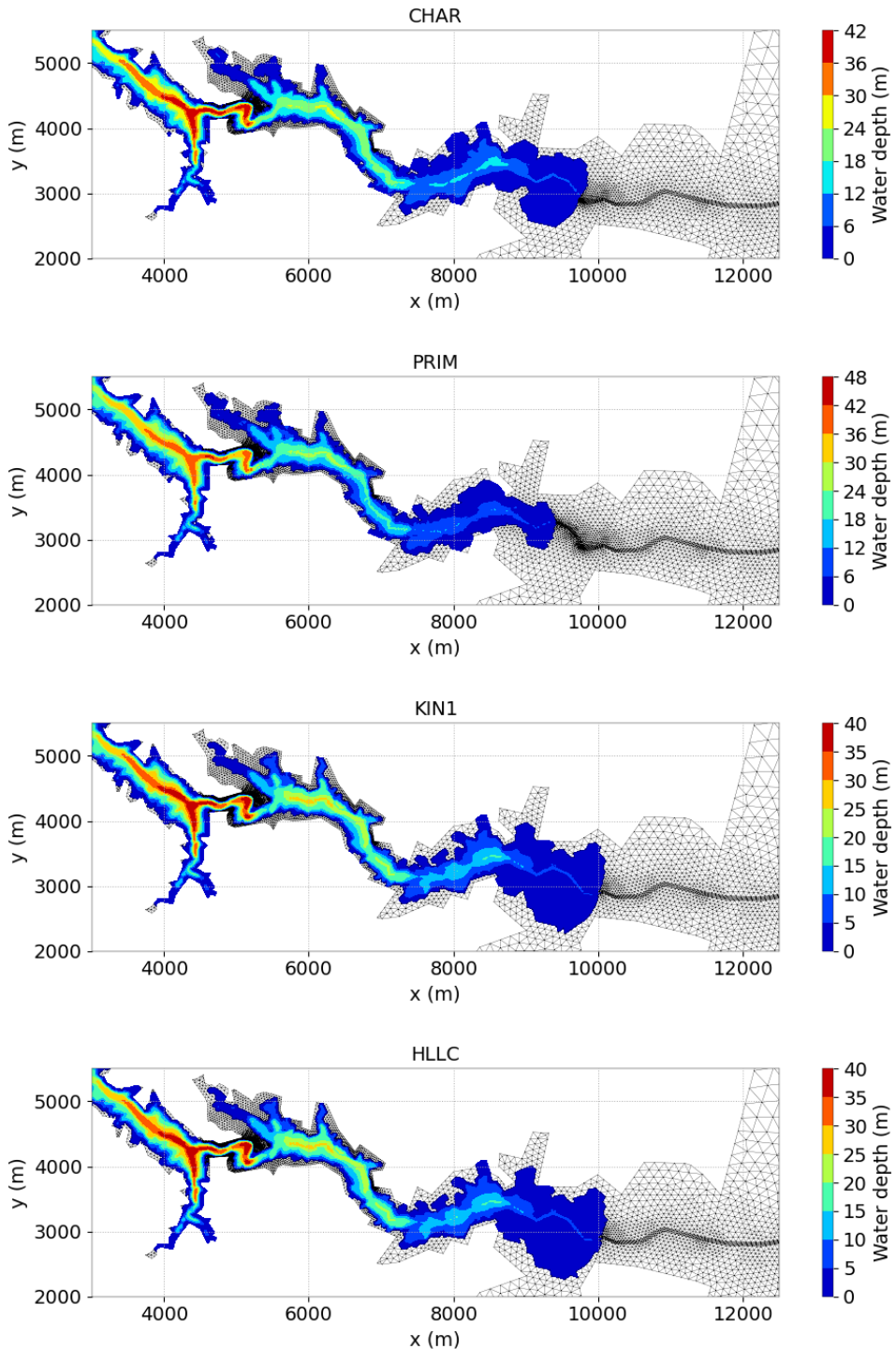


Figure 31.8: Water depth at  $t = 400$  s for different cases of the malpasset example.

In Figures 31.9, the velocity field after 100 s of simulation is presented in the vicinity of the dam. Contrary to the TELEMAC-2D validation manual in release v8.1, with the wave equation option and P1-P1 discretization, there are less visible numerical oscillations on both water depth and velocity by using a smaller time step (0.5 s rather than 1 s) and MAXIMUM NUMBER OF ITERATIONS FOR ADVECTION SCHEMES so that this maximum number is not reached lead to no spurious oscillation. Using primitive equation with quasi bubble elements on velocity

allows to also obtain correct results, at a higher cost. However numerical oscillations are still visible.

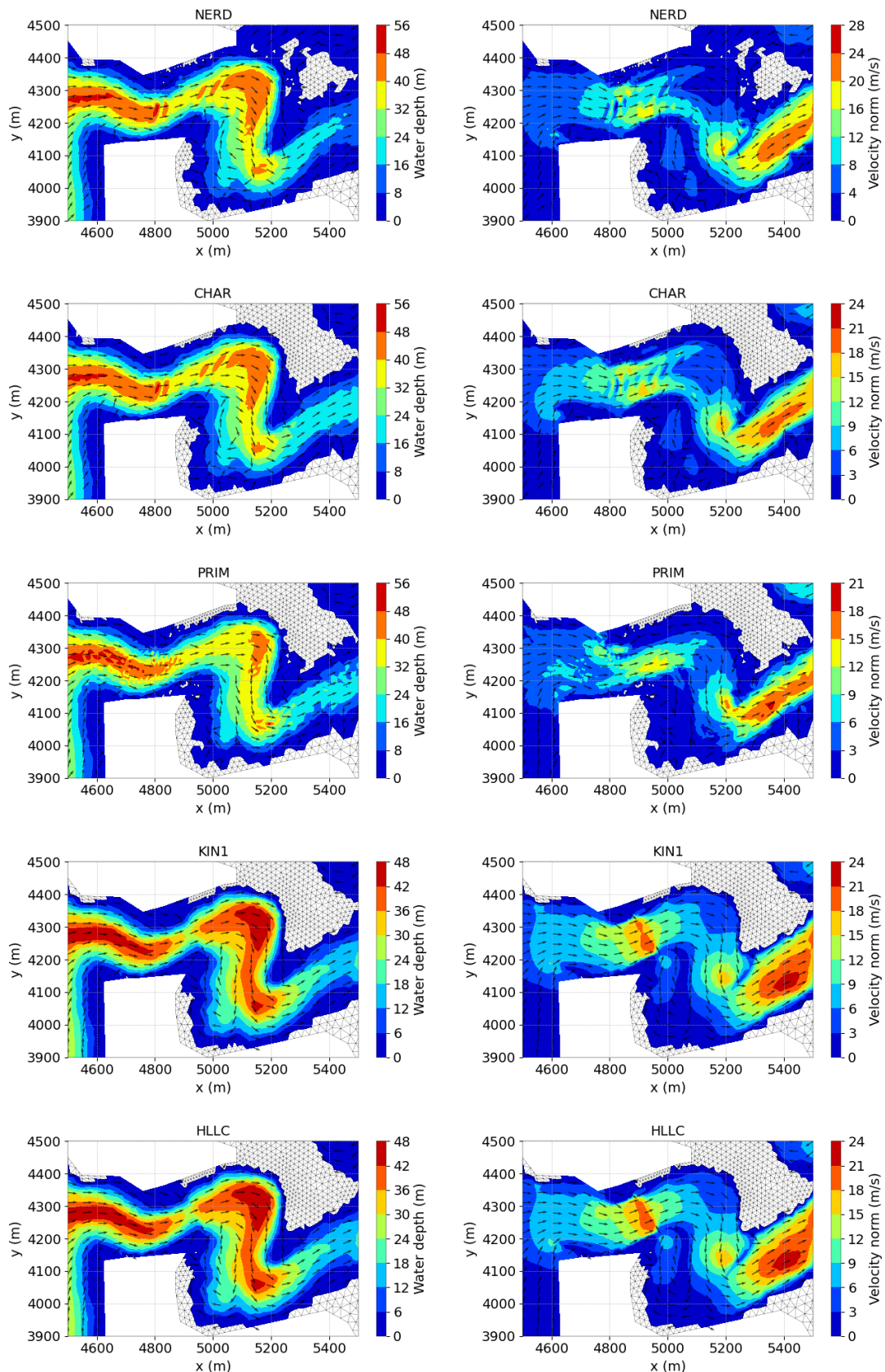


Figure 31.9: Water depth (left) and velocities (right) after 100 s on the malpasset case.

### 31.3.5 Accuracy of the water depth

The maximum values of water depth are extracted for each gauge for all the schemes and compared to reference data in Figure 31.10.

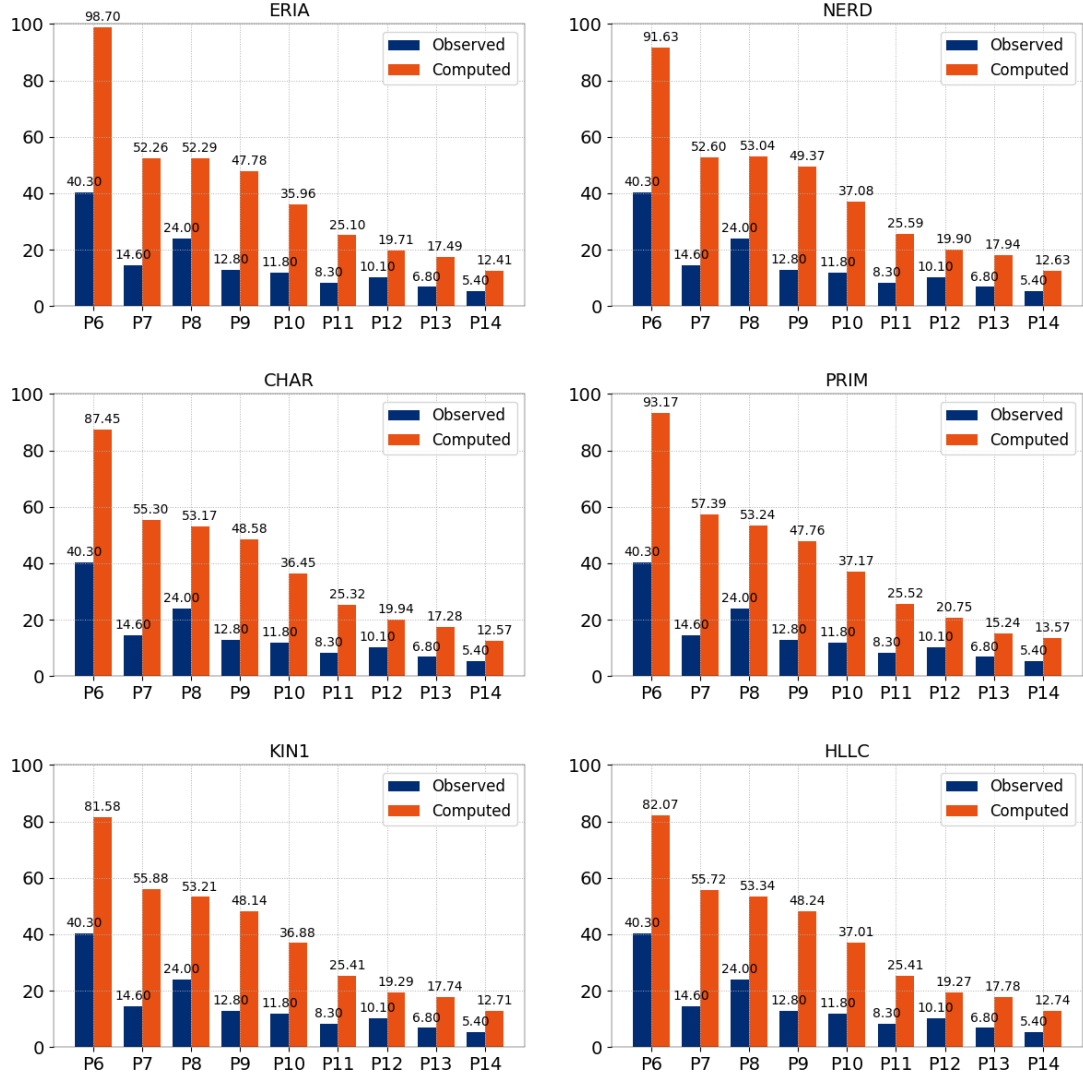


Figure 31.10: Comparison of maximum water depth recorded to lab data at different locations.

Every scheme gives rather the same results for this criterion. However, for all the schemes the numerical results are far from observations. The following interpretation can be found in reference [12].

« The discrepancies on the free surface elevation at the nine gauges, between 1-D and 2-D solutions, and the physical model, remain large and are questionable. However, the results are good as soon as the wave reaches the floodplain, the difference at gauge 14 being 14 cm with a total depth of 5.4 m. It is clear from the sensitivity study done with TELEMAC-2D that the differences are not entirely due to an inaccurate solution of the Shallow water equations. As a matter of fact, numerical and physical parameters have little influence on the maximum free surface elevation, but not in a range that would allow a possible perfect match. Several other factors could be responsible for the error such as:

- the physical model itself, because a 1/400 scale gives a 4m difference for a 1cm error on measurements;
- the Shallow Water equations are an approximation and their assumptions, such as the hydrostatics pressure, cannot be fully verified in this case - a test with Boussinesq or Serre equations would be of the utmost interest to clarify this point;
- the dam failure scenario, which was probably not absolutely instantaneous;
- the debris flow and sediment transport, which was not taken into account in this study»

### 31.3.6 Accuracy of the wave propagation

Next, the wave propagation time computed with TELEMAC-2D is compared to reference data in Figure 31.11. Globally, the estimated propagation time is lower than the observed one. Furthermore, be it for the A-C or the A-B transit, the differences remain low. The most satisfying results are the ones observed for the KIN1, HLLC and ERIA schemes. But characteristics and NERD results are OK.

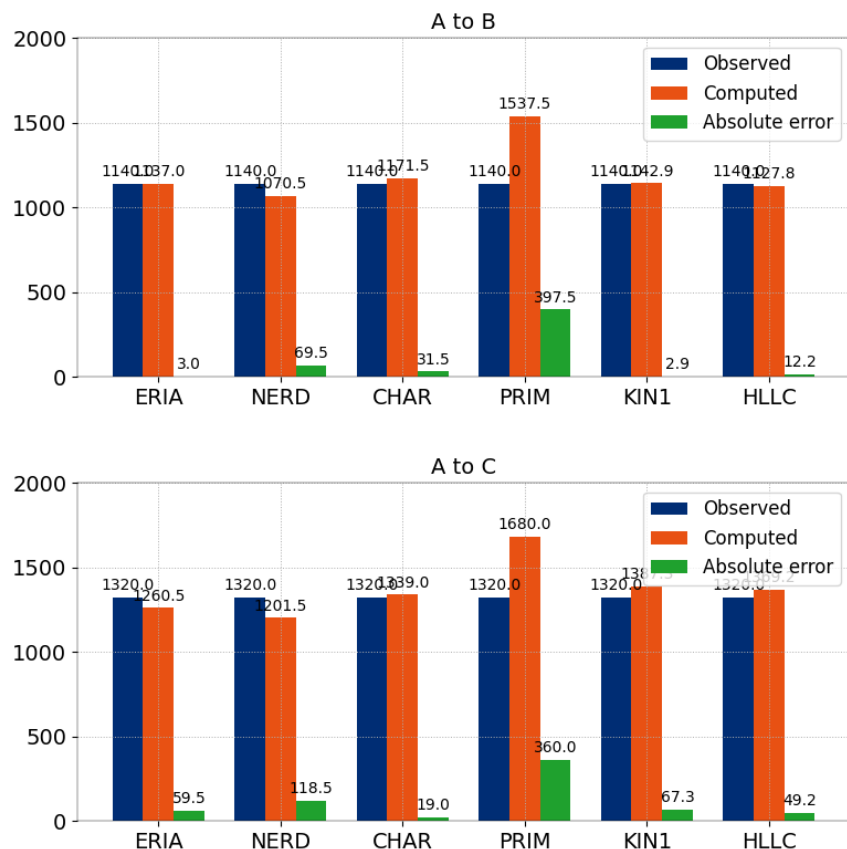


Figure 31.11: Comparison of propagation time delta between A and B (up) and A and C (down).

### 31.3.7 Comparison on profiles

Here, the schemes are compared on profiles upstream (Figure 31.12) and downstream (Figure 31.13) of the dam. The locations of these profiles are the following:

- Upstream of the dam: (4,634.0; 4,132.84) to (4,589.81; 4,393.22),
- Downstream of the dam: (4,884.95; 4,161.82) to (4,846.39; 4,362.44).

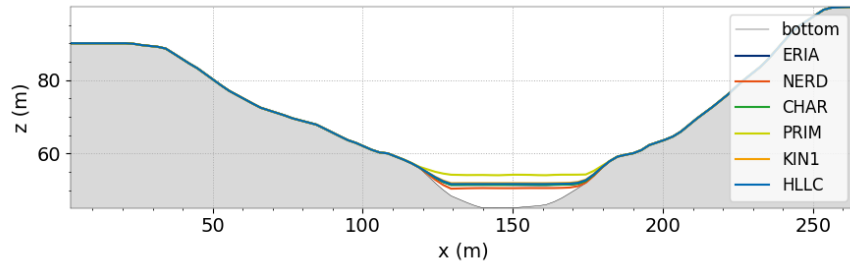


Figure 31.12: Profiles of water depth upstream of the dam at last iteration of the malpasset case.

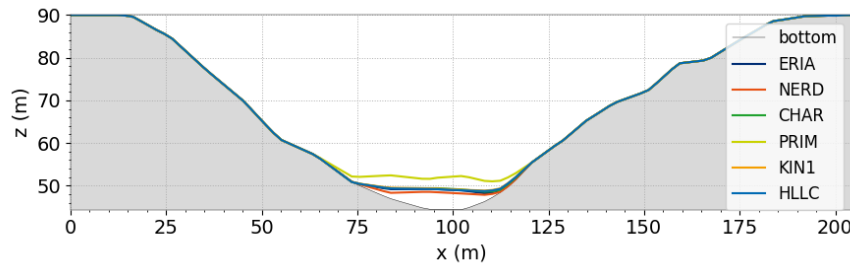


Figure 31.13: Profiles of water depth downstream of the dam at last iteration of the malpasset case.

Except coupled primitive equations, every other scheme gives rather the same results for this criterion.

### 31.3.8 Positivity of the water depth

The positivity of the used schemes can be checked for all cases. In order to achieve this, the minimum value of the water depth during the whole simulation, and on all the points of the mesh, is transcribed in Figure 31.14. In the case of finite volume schemes, positivity is ensured without additional treatment. With finite element schemes, the positivity is ensured with a treatment of negative depths during simulation (TREATMENT OF NEGATIVE DEPTHS = 2 for characteristics + NERD schemes and 3 for ERIA scheme).

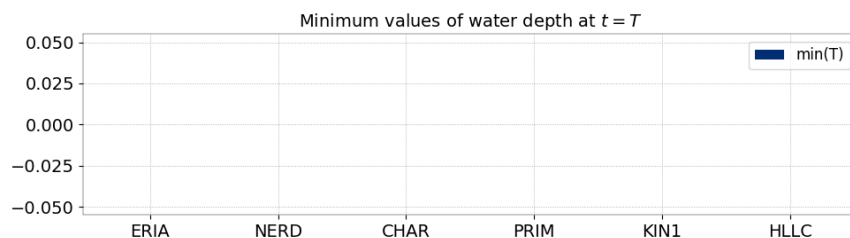


Figure 31.14: Minimum values of water depths.

### 31.3.9 Mass conservation

Mass conservation can be checked by calculating the volume in the domain during time (as the density is constant in time and space). The lost volume is calculated as  $V_{initial} - V_{final}$ . Figure 31.15 shows that all used schemes are mass conservative. Mass is conserved for sequential runs as well as parallel ones.

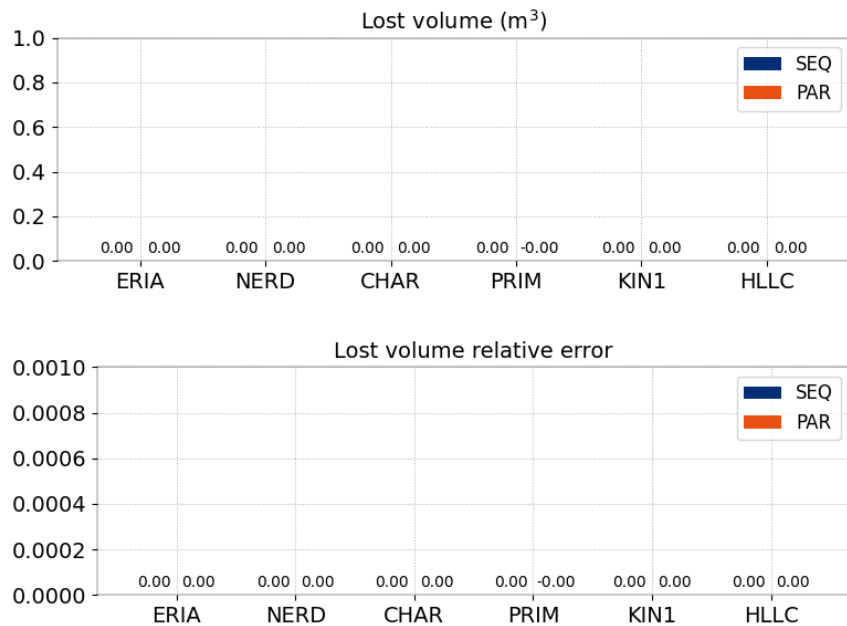


Figure 31.15: Lost volume during simulation.

## 31.4 Conclusion

TELEMAC-2D is capable of simulating the propagation of a dam break wave in a river valley initially dry.

## 32. Tidal flow in the Mersey estuary (mersey)

### 32.1 Purpose

To illustrate that TELEMAC-2D is capable of simulating the hydrodynamics (tidal currents and water elevations) in an estuarial zone due to long period tidal wave forcing, with the covering/uncovering of tidal flats.

#### 32.1.1 Approach

This case simulates the flow in the Mersey estuary on the west coast of England. Tide hydrodynamics in this area is complex, with large tidal range (up to 9 m on spring tide), extensive intertidal areas and an unusual tide curve: in the upper reaches of the estuary, the tide ebbs for a large proportion of the tidal period, and then floods very rapidly. A sinusoidal water elevation is prescribed at the maritime open boundary to simulate a mean spring tide wave. The river discharge is neglected at the upstream end of the model.

### 32.2 Description

#### 32.2.1 Geometry and mesh

The size of the domain is around 40 km × 33 km.

Water depth at rest = 9.2 m.

The mesh is dense in the river and at the mouth.

- 4,490 triangular elements,
- 2,429 nodes,
- Maximum size range: from 200 to 1,500 m.

#### 32.2.2 Boundaries

- Domain entrance  $H = 5.15 + 4.05 \cos\left(\frac{\pi}{2} \frac{t}{44700}\right)$ ,
- Lateral boundaries: solid walls with slip condition.

#### 32.2.3 Bottom

Strickler formula with friction coefficient = 50 m<sup>1/3</sup>/s.

The mesh and the topography are shown in Figures 32.1 and 32.2.

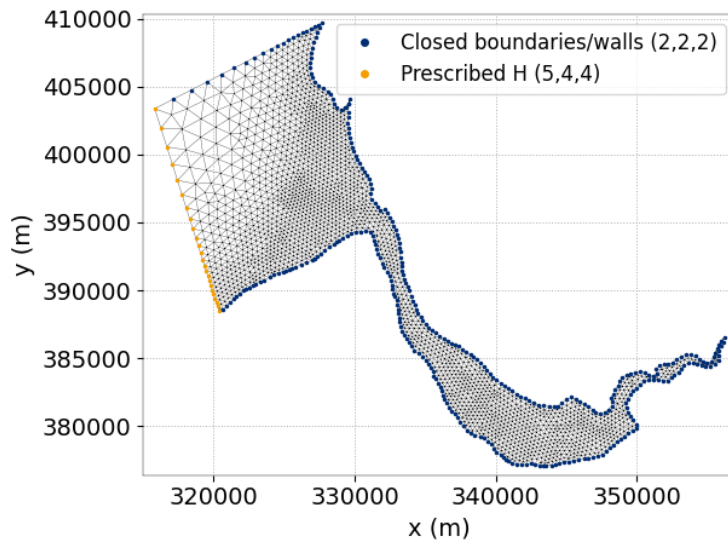


Figure 32.1: 2D-mesh of the mersey case.

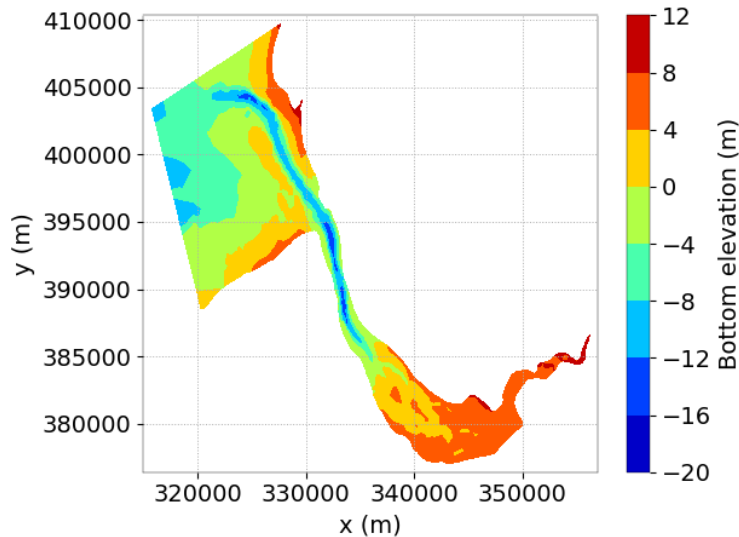


Figure 32.2: Bathymetry of the mersey case.

### 32.2.4 Physical parameters

The model of turbulence is constant viscosity with velocity diffusivity equal to  $0.2 \text{ m}^2/\text{s}$ .

### 32.2.5 Numerical parameters

Type of advection:

- Methods of characteristics on velocities (scheme #1),
- Conservative + modified SUPG on depth (mandatory scheme).

The type of element is linear triangle (P1) for  $h$  and quasi bubble triangle for velocities.

- Implicitation for depth and velocities = 0.6,
- Solver: Conjugate gradient on a normal equation with solver accuracy =  $10^{-3}$ ,
- BOTTOM SMOOTHINGS = 1,
- Time step = 50 s,
- Simulation duration = 44,700 s (a little bit more than 12 h and a half).

### 32.3 Results

The total volume lost is  $0.2 \times 10^{-2} \text{ m}^3$ , in comparison to the initial volume in the domain ( $0.289417 \times 10^{10} \text{ m}^3$ ). The error represents  $7 \times 10^{-13}$  which is the machine precision. The final balance of water volume is excellent.

Figures 32.3 and 32.4 show the water depths at high tide and low tide in the domain. Tidal flats are represented.

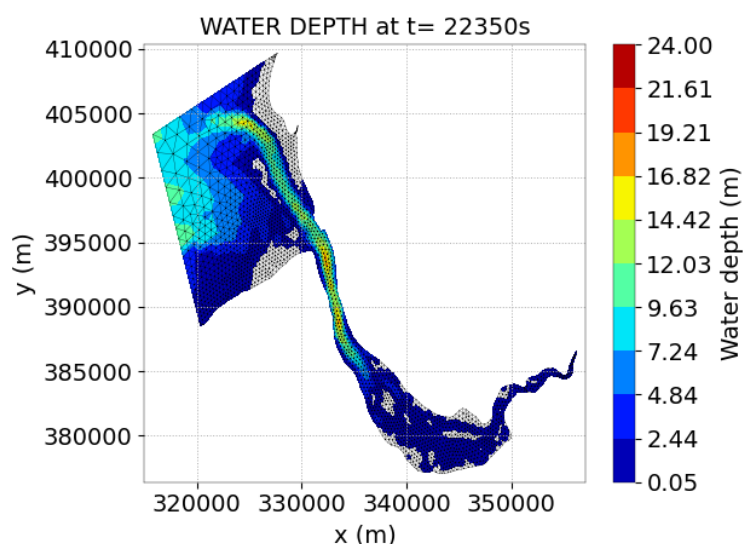


Figure 32.3: Water depth at  $t = 22,350$  s.

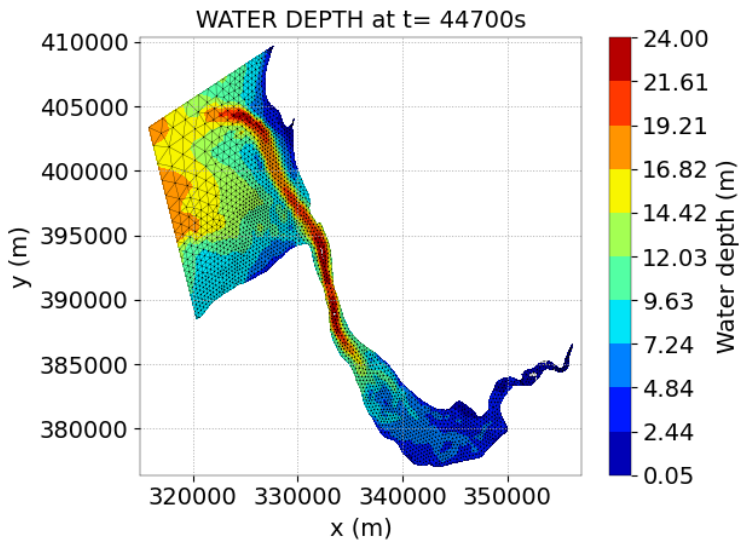


Figure 32.4: Water depth at  $t = 44,700$  s.

Figure 32.5 shows the evolutions of the free surface elevation at four different points:

- at the open boundary (1), where the tide is regular and symmetric,
- at the mouth of the Mersey river (2), where a small asymmetry of the curve and a drift in time is observed,
- in the estuary (3 and 4), where the tide is very asymmetric and a significant drift in time occurs.

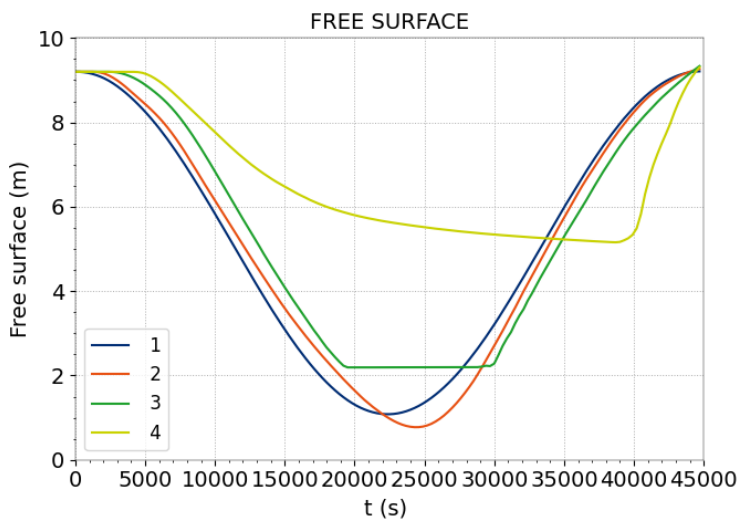


Figure 32.5: Free surface at points (318,021 ; 400,340), (331,444 ; 395,025), (337,922 ; 383,132) and (348,256 ; 380,434).

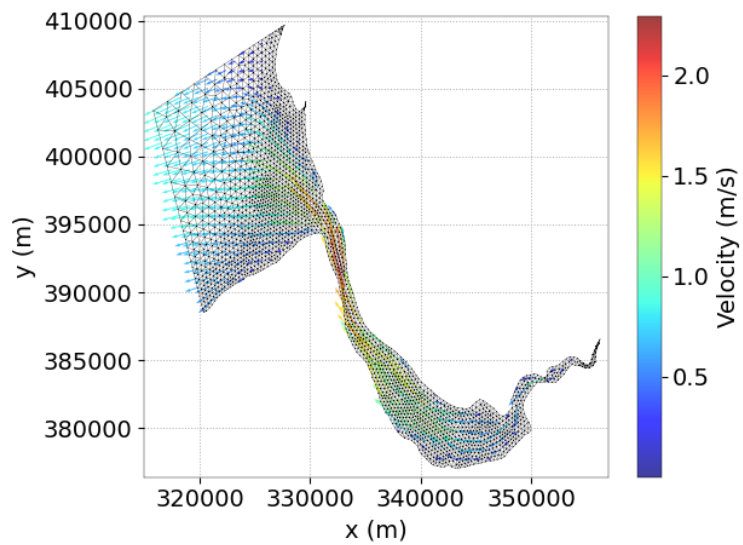


Figure 32.6: Velocity at  $t = 11,200$  s.

## 33. Monai Valley experiment (monai\_valley)

### 33.1 Purpose

This test case redoess the monai valley experiment from Costas E Synolakis (p.45, 3.4) [4].

### 33.2 Description

The configuration is a 5.5 m long and 3.4 m wide rectangle.

#### 33.2.1 Mesh and geometry

The mesh is made of 25,553 elements and 12,989 nodes (see Figure 33.1).

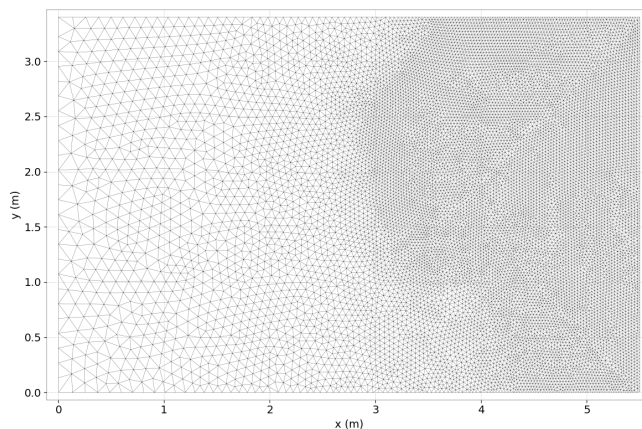


Figure 33.1: Mesh of the study.

Figure 33.2 shows the bathymetry of the study.

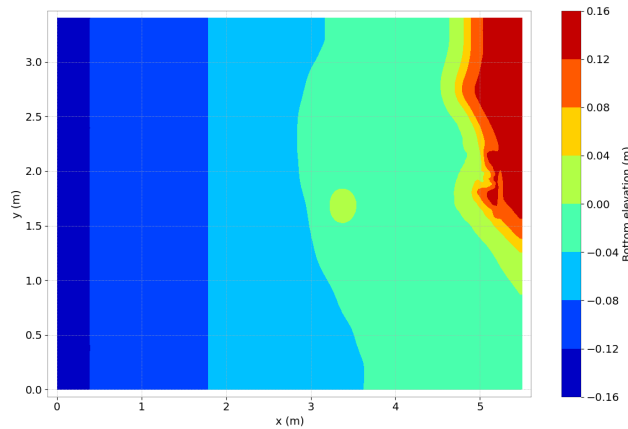


Figure 33.2: Bathymetry of the study.

### 33.2.2 Boundary

Figure 33.3 shows the boundaries of the study and the incident wave.

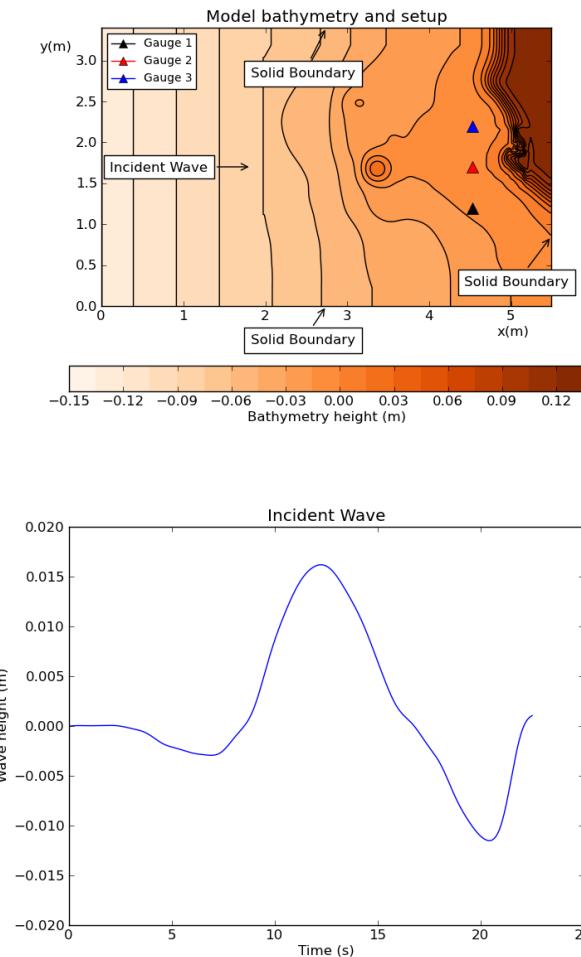


Figure 33.3: Boundaries of the study.

Chézy's friction law is used for the bottom with a friction coefficient equal to  $180 \text{ m}^{1/2}/\text{s}$ .

### 33.2.3 Physical parameters

Constant viscosity equal to  $0 \text{ m}^2/\text{s}$  is used as turbulence model.

### 33.2.4 Numerical parameters

- Type of element: P1 triangle for  $h$  and for velocity,
- Solver: GMRES,
- Accuracy:  $10^{-6}$ ,
- Finite volume scheme: Kinetic order 2.

Time data:

- Desired Courant number = 0.9,
- Simulation duration: 22.5 s.

## 33.3 Results

Figure 33.4 shows the velocity vectors.

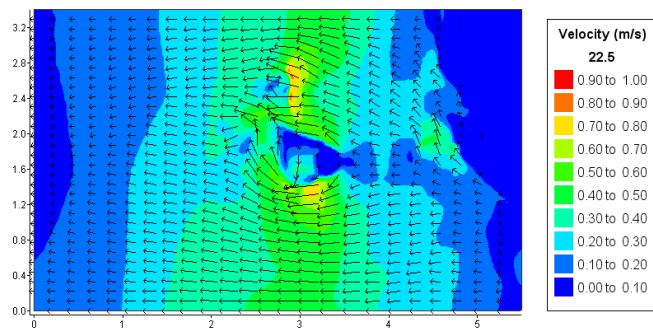
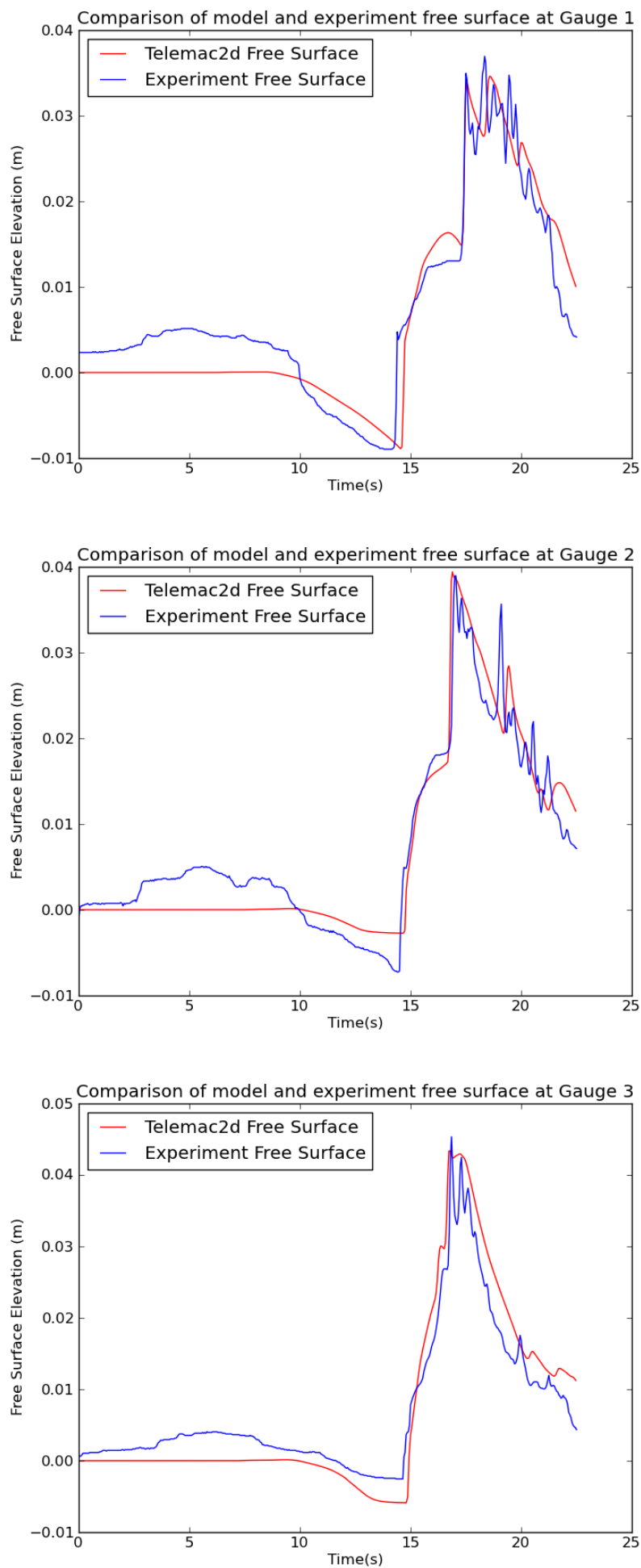


Figure 33.4: Velocity vectors over the free surface.

We compare the model and experiment free surface at gauges 1,2 and 3.

Figure 33.5 shows the comparison with the benchmark data.



## 34. Non-Newtonian model (nn\_newt)

### 34.1 Purpose

The purpose of this test case is to validate the implementation of the non-Newtonian module. This test case and documentation is taken from [21].

### 34.2 Theoretical background

The non-Newtonian fluid behaviour is modeled by an additional friction source term in the fluid. This term is treated with a semi-implicit approach in the finite volume framework.

#### 34.2.1 Bingham model

With  $\tau$  the viscous shear stress of the fluid, the Bingham model reads:

$$\tau = \begin{cases} 0 & \text{if } \tau < \tau_y \\ \tau_y + \mu \dot{\gamma} & \text{else} \end{cases}, \quad (34.1)$$

where  $\mu$  is the fluid's dynamic viscosity [Pa·s],  $\dot{\gamma}$  is the shear rate [ $s^{-1}$ ] and  $\tau_y$  is the fluid's yield stress [Pa].  $\dot{\gamma}$  can be expressed as:

$$\dot{\gamma} = \frac{KU}{8h}, \quad (34.2)$$

with  $U$  the depth-averaged flow velocity [m/s],  $h$  the water depth [m] and  $K$  a resistance parameter for laminar flow [-]. Its value lies in the range 24-108 for smooth surfaces (concrete, asphalt) but can increase significantly with irregular geometry and roughness (highest values of approximatively 50,000). When modelling turbulent flows, the lowest and default value of 24 is recommended [21].

Even though the Bingham model's mathematical expression is relatively simple, the discontinuity generated by the yield stress parameter at very low shear rates is a disadvantage and can lead to numerical instabilities. To solve this issue, several solution methods have been proposed in the literature, aiming at replacing the discontinuity by a continuous relationship between shear stress and shear rate.

#### Exponential regularization

This method is based on the exponential regularization method proposed by [24]. An exponential term is added to the yield stress parameter making it possible to introduce a continuous relationship for low shear rates:

$$\tau = \tau_y(1 - e^{-m\dot{\gamma}}) + \mu\dot{\gamma}, \quad (34.3)$$

with  $m$  a so-called regularization parameter [s] used to control the exponential growth of shear stress for low shear rates and set to 1,000 in the model.

### Effective viscosity

This method is based on the effective viscosity concept by rewriting the Bingham model as:

$$\tau = \mu_{eff}\dot{\gamma}, \quad (34.4)$$

with  $\mu_{eff}$  the effective viscosity [Pa·s], defined by:

$$\mu_{eff} = \frac{\mu_0 + \mu K_B \dot{\gamma}}{1 + K_B \dot{\gamma}}, \quad (34.5)$$

with  $K_B = \frac{\mu_0}{\tau_y}$  and  $\mu_0 = 10^3 \mu$ .

### Cubic equation

This method is based on a cubic equation for the non-Newtonian shear stress that is obtained from the integration of the classical Bingham equation for laminar flow in a wide open channel, and then solving for the depth-averaged flow velocity as proposed by [26]. The resulting cubic equation reads:

$$2\tau^3 - 3\tau^2 \left( \tau_y + 2\mu \frac{U}{h} \right) + \tau_y^3 = 0. \quad (34.6)$$

It is solved by keeping the positive root closest from the theoretical value of  $\tau$  defined by (34.1).

#### 34.2.2 Herschel-Bulkley model

The equation of the Herschel-Bulkley model reads:

$$\tau = \begin{cases} 0 & \text{if } \tau < \tau_y \\ \tau_y + K_{HB} \dot{\gamma}^n & \text{else} \end{cases}. \quad (34.7)$$

The Herschel-Bulkley model has been implemented using the exponential regularization method also used for the Bingham model:

$$\tau = \tau_y(1 - e^{-m\dot{\gamma}}) + K_{HB} \dot{\gamma}^n. \quad (34.8)$$

#### 34.2.3 Pseudo biphasic model

The principle of this formulation is to determine the fluid density and the rheological parameters (yield stress and dynamic viscosity) from the local sediment volumetric concentration  $C_v$  [-]. The type of fluid can therefore be defined by the local sediment volumetric concentration  $C_v$ . This concentration is to be defined by the user in a passive tracer (with initial and boundary conditions). The local fluid's bulk density is then computed as:

$$\rho = \rho_w + (\rho_s - \rho_w)C_v, \quad (34.9)$$

with  $\rho_w$  the water density [ $\text{kg}/\text{m}^3$ ] and  $\rho_s$  the sediment specific density (grains) [ $\text{kg}/\text{m}^3$ ].

Empirical relationships have been proposed to express the yield stress and the dynamic viscosity as functions of the sediment volumetric concentration  $C_v$  [17]:

$$\tau_y = a 10^{b C_v}, \quad (34.10)$$

$$\mu = c10^{dC_v}. \quad (34.11)$$

The values of the coefficients  $a$ ,  $b$ ,  $c$  and  $d$  are mainly function of the nature and percentage of fine particles in the mixture. Experimental values have been proposed in the literature [17].

### 34.3 Dambreak test case

#### 34.3.1 Description

The one-dimensional dam break case presented in [13] is used to test the implemented non-Newtonian models for such applications. The dam break case corresponds to the instantaneous release of a non-Newtonian fluid.

#### 34.3.2 Theoretical solution

The theoretical solution of this case provided by [22] and based on the assumption that the flow profile after reaching equilibrium is parabolic, gives a front location of  $x = 1,896$  m counted from  $x = 0$  m, which corresponds to a runout distance of 1,591 m counted from the dam location ( $x = 305$  m).

#### 34.3.3 Geometry and mesh

This case was simulated using a two-dimensional triangular mesh with an element size of 3 m in both  $x$  and  $y$  directions. The model is 3,000 m long in the  $x$  direction and 12 m wide in the  $y$  direction. Figure 34.1 presents the mesh used and the domain.

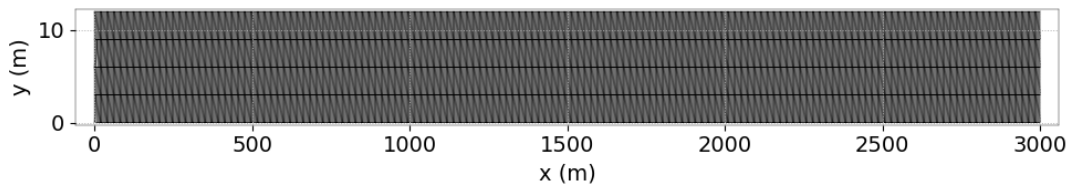


Figure 34.1: Mesh of the channel.

#### 34.3.4 Initial and boundary conditions

The initial condition is defined by a volume of 305 m in length (in the  $x$  direction) and 30.5 m in height on a flat and dry bottom. Figure 34.2 shows the mixture depth at the initial time.

#### 34.3.5 Physical parameters

The fluid properties are a fluid density  $\rho = 1,835$  kg/m<sup>3</sup>, a yield stress  $\tau_y = 1,500$  Pa and a dynamic viscosity  $\mu = 100$  Pa·s. Bottom friction has been simulated with a Strickler coefficient of  $70$  m<sup>1/3</sup>/s to mimic the smooth and plane bottom.

#### 34.3.6 Numerical parameters

The simulations have been performed with the Bingham model for the three options implemented and the Herschel-bulkley model using the HLLC finite volume scheme (FINITE VOLUME SCHEME = 5).

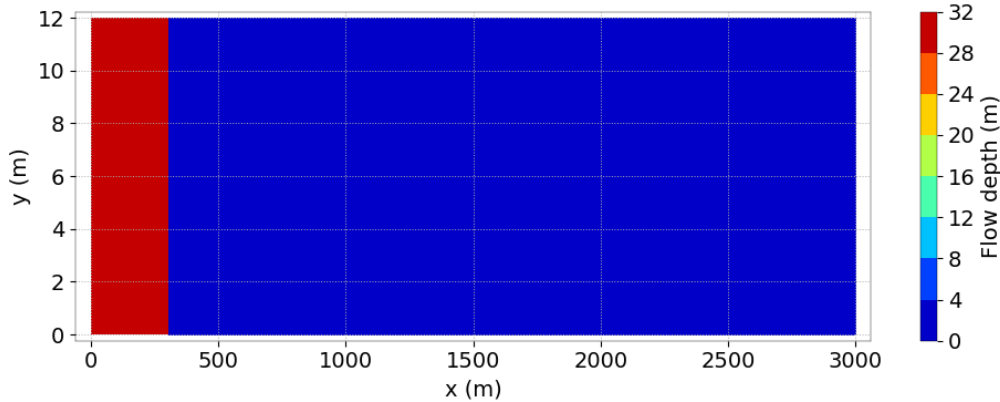


Figure 34.2: Initial mixture depth.

### 34.3.7 Results

The results are presented in Figure 34.3 as flow profiles extracted along the longitudinal axis (defined by  $y = 6 \text{ m}$ ) once the fluid has reached a pseudo-equilibrium state, which occurs after approximatively three minutes. The flow profiles corresponding to the three different Bingham options implemented are compared with the analytical solution from [22].

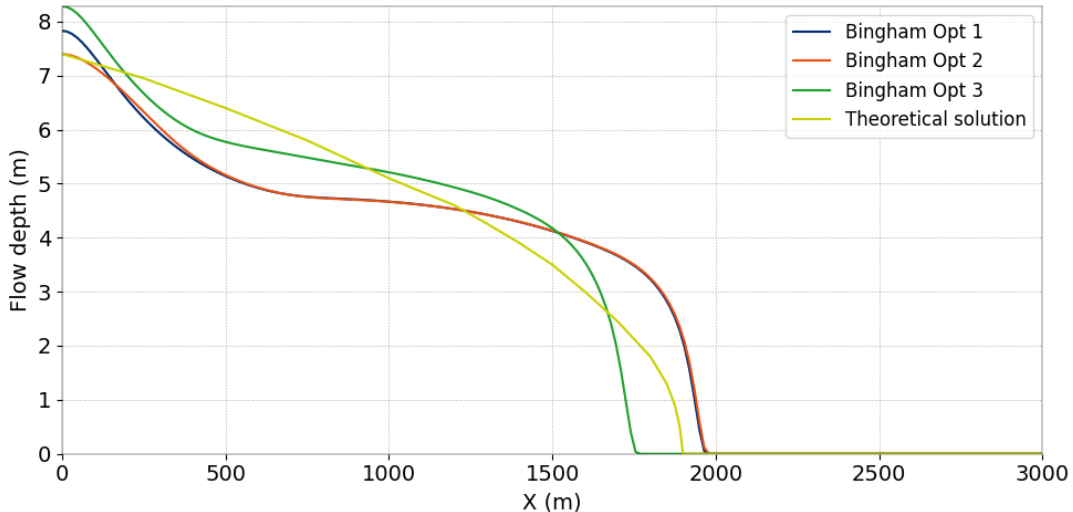


Figure 34.3: Flow profile after 180 s for the three Bingham options.

This dam break case has also been simulated with the Herschel-Bulkley model in which the consistency parameter  $K_{HB}$  was taken equal to the dynamic viscosity used in the Bingham simulations. Two simulations were performed with power-law index values of  $n = 0.5$  and  $n = 1.5$ . The results are compared in Figure 34.4 qualitatively with the Bingham Option 1 for the flow profiles corresponding to the pseudo-equilibrium state (after 3 minutes of simulation).

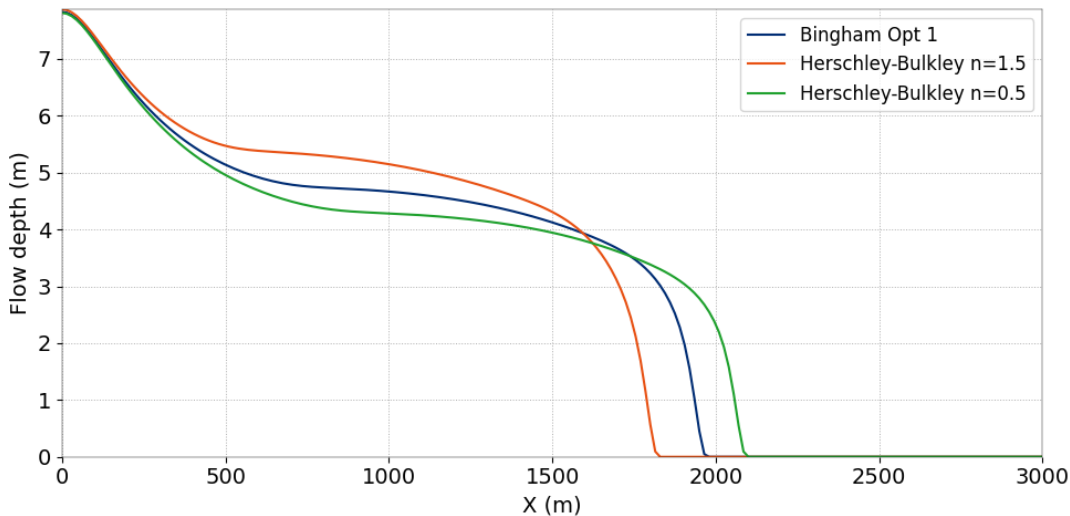


Figure 34.4: Flow profile after 180 s for the first Bingham option and the Herschley-Bulkley model with  $n = 0.5$  and  $n = 1.5$ .

## 34.4 Pseudo biphasic

### 34.4.1 Description

To illustrate the pseudo-biphasic, variable-density formulation, a simple test case is used. The computational domain is composed of a mean channel reach and of a side channel discharging into the main channel with a 90-degree angle.

### 34.4.2 Geometry and mesh

The main channel is 90 m long and the side channel is 21 m long. Both channels are 10 m wide. The bathymetry is defined as a constant level in all the model. The computational mesh is composed of triangles with an edge side of approximatively 1 m. Figure 34.5 presents the mesh used and the domain.

### 34.4.3 Initial and boundary conditions

Two inflow boundaries are defined at the upstream end of both channels. One outflow boundary is defined at the downstream end of the main channel with a flow depth of 1 m. Inflow of the non-Newtonian fluid is applied at the upstream end of the side channel by prescribing a discharge of 4 m<sup>3</sup>/s and a sediment volumetric concentration  $C_v$  of 0.5 through a passive tracer. At the inflow boundary, the fluid's bulk density is  $\rho = 2,000 \text{ kg/m}^3$ . Inflow of Newtonian fluid is applied at the upstream end of the main channel by prescribing a discharge of 2 m<sup>3</sup>/s and a nil sediment volumetric concentration through a passive tracer.

### 34.4.4 Physical parameters

The non-Newtonian fluid density is computed by the model based on a sediment specific density  $\rho_s = 3,000 \text{ kg/m}^3$  and the specified sediment volumetric concentration  $C_v$ . The Newtonian fluid density is set to  $\rho_w = 1,000 \text{ kg/m}^3$ . The non-Newtonian parameters, yield stress and dynamic viscosity, are computed by the model with power laws (34.10) and (34.11) based on the local sediment volumetric concentration  $C_v$ , with the following coefficients:  $a = 0.025$ ,  $b = 8.0$ ,  $c = 0.001$ ,  $d = 8.0$ . For the non-Newtonian fluid defined with  $C_v = 0.5$ , those coefficients yield a yield stress and dynamic viscosity of 250 Pa and 10 Pa·s, respectively while the Newtonian fluid

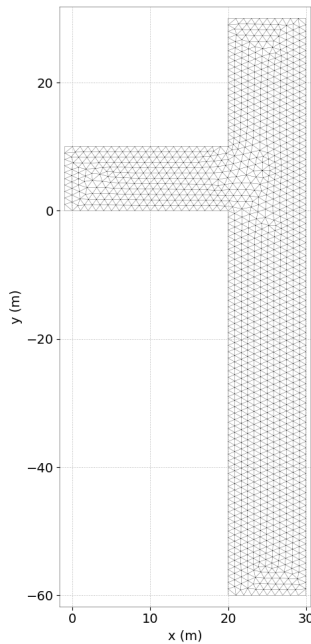


Figure 34.5: Mesh of the channel.

( $C_v = 0$ ) is consequently described with a yield stress and dynamic viscosity of 0.025 Pa and 0.001 Pa·s, respectively, which is a reasonable approximation.

Bottom friction has been simulated with a Strickler coefficient of  $70 \text{ m}^{1/3}/\text{s}$ .

#### 34.4.5 Numerical parameters

The simulations have been performed with the first option of the Bingham model using the HLLC finite volume scheme (FINITE VOLUME SCHEME = 5).

#### 34.4.6 Results

Figure 34.6 presents the steady state conditions for the flow depth, sediment volumic concentration, fluid density, yield stress and dynamic viscosity.

### 34.5 Conclusion

The model is able to properly reproduce non-Newtonian Bingham type of flows. It is also possible to simulate mixture with water with a simplified model.

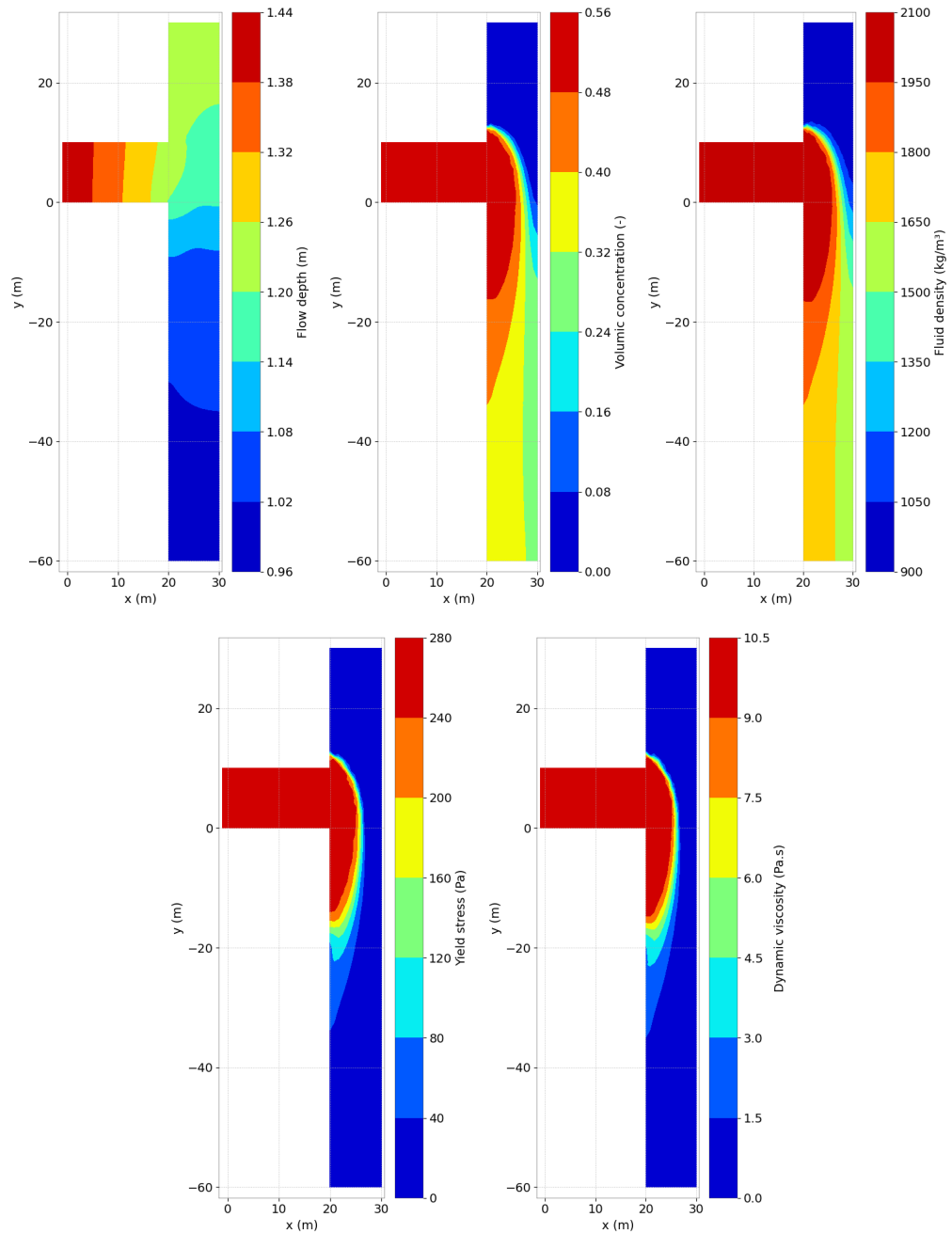


Figure 34.6: Results of the model.

## 35. Tsunami generation with the Okada model (okada)

### 35.1 Purpose

The Okada model [23] has been implemented in TELEMAC-2D to simulate the free surface displacement due to underwater earthquake. The Okada model is based on a number of parameters characterising the fault displacement, each parameter being given in the steering file by the user. An illustration of the definition of each parameter is shown in Figure 35.1.

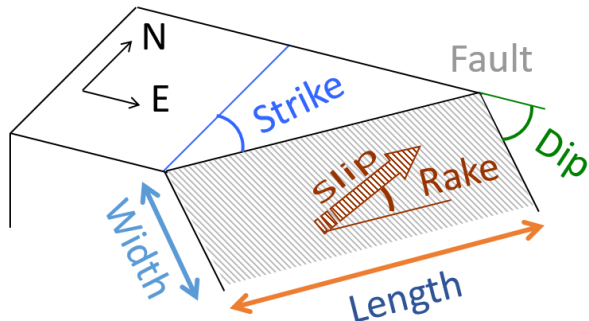


Figure 35.1: Scheme of Okada model.

This test case demonstrates the ability of TELEMAC-2D to generate a tsunami and to propagate it through open boundary conditions without parasite reflexions.

### 35.2 Description

For illustrative purposes we consider a square domain of 600 km within which the tsunami wave will be developed as an initial free surface condition. The tsunami wave will then fall on itself and propagate out of the domain.

#### 35.2.1 Geometry and Mesh

The area is 600 km long by 600 km wide and 5 km deep. The channel bottom is placed at  $z = -5,000$  m. The edge length of the mesh is uniform, set at about 10 km.

#### 35.2.2 Parameters

The Okada model is activated with the set of keywords:

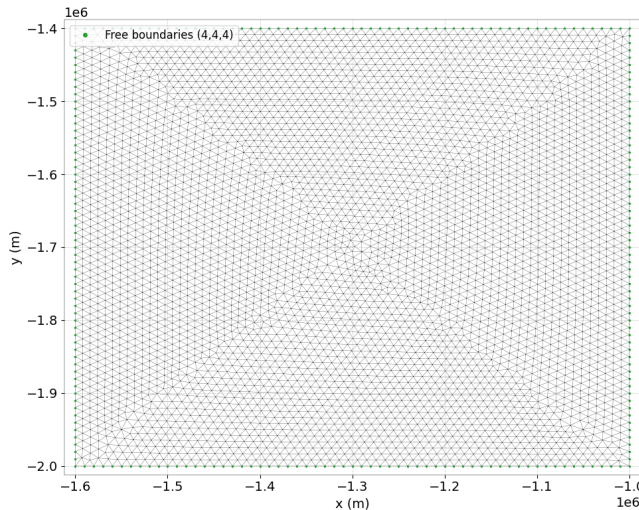


Figure 35.2: Mesh of the domain.

- OPTION FOR TSUNAMI GENERATION = 1,
- PHYSICAL CHARACTERISTICS OF THE TSUNAMI =  
100.;210000.;75000.;13.6;81.;41.;110.;37.;-11.5;3.

See the TELEMAC-2D user manual for a description of the keywords in reference to the tsunami characteristics.

### 35.3 Results

Figures 35.3 and 35.4 show that the initial tsunami wave is set at the start of the simulation ( $t = 0$  s) and then falls on itself ( $t = 10$  min) and out of the computation domain computation ( $t = 20$  min).

### 35.4 Conclusion

This test case demonstrates the ability of TELEMAC-2D to generate a tsunami and to propagate it through open boundary conditions without parasite reflexions.

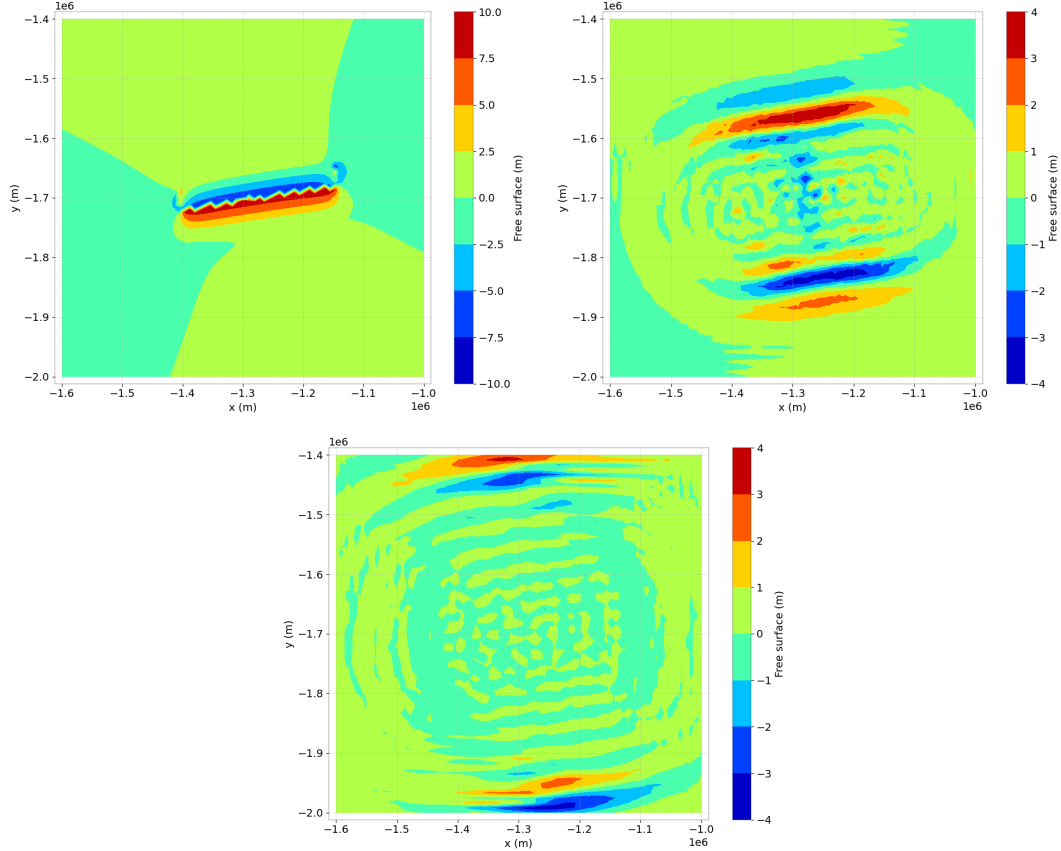


Figure 35.3: Free Surface at time 0, 10 and 20 min.

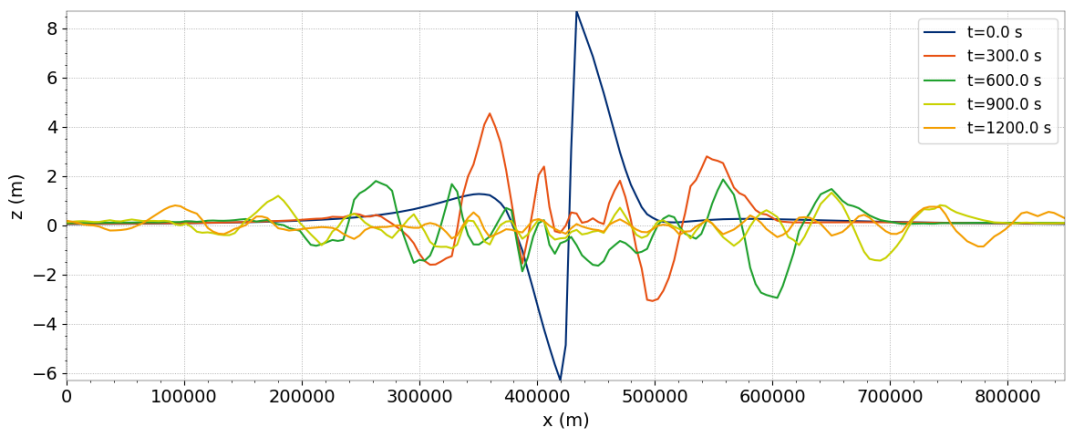


Figure 35.4: Profile of the free surface on the diagonal at time 0, 5, 10, 15 and 20 min.

## 36. Flow in a channel with 2 bridge piers (pildepon)

### 36.1 Purpose

This test case shows that TELEMAC-2D is able to represent the impact of an obstacle on a channel flow. It simulates a laminar and very viscous flow in a channel with two cylindrical piers. The effect of the flow on the piers is assessed with the computation of the Strouhal number.

### 36.2 Description

#### 36.2.1 Geometry

The channel is 28.5 m long and 20 m wide ( $L = 28.5$  m and  $H = 20$  m) with two bridge piers located at  $P_1 = (-5, 4)$ ,  $P_2 = (-5, -4)$  and a diameter  $D$  of 4 m. The geometry is shown in Figure 36.1.

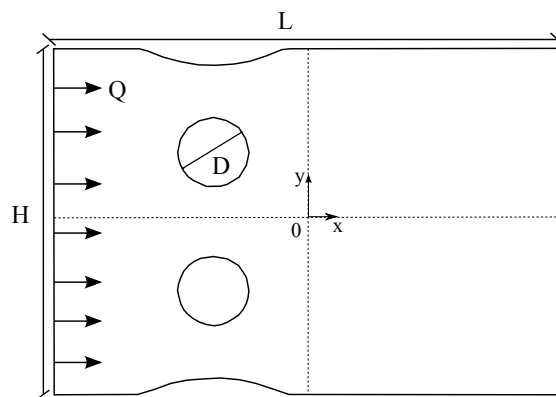


Figure 36.1: Geometry of the pildepon test case.

#### 36.2.2 Mesh and Bathymetry

The computational domain is made up by 4,304 triangular elements and 2,280 nodes and it is shown in Figure 36.2. The section is trapezoidal (see the bottom in Figure 36.2) and the minimum value of the bottom elevation is equal to -4 m in the main channel.

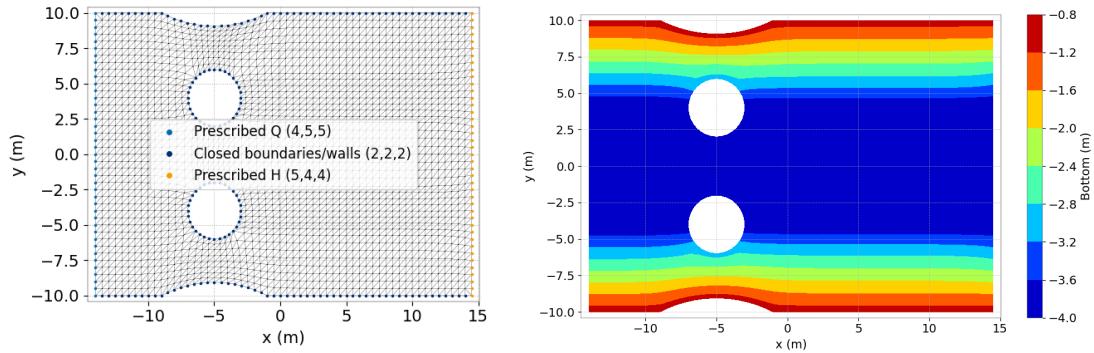


Figure 36.2: Mesh and bathymetry of the pildepon test case.

### 36.2.3 Initial condition

Initially, water elevation is set to zero as well as velocity.

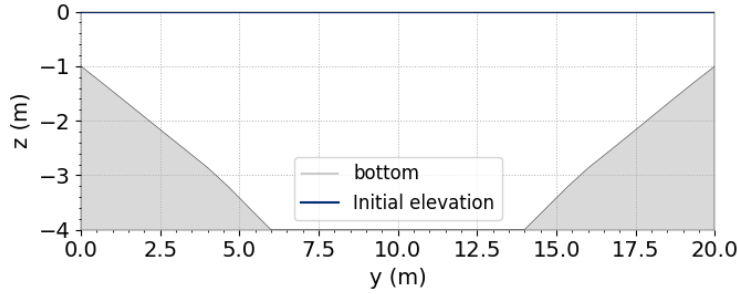


Figure 36.3: Bathymetry and initial free surface at the inlet of the channel.

### 36.2.4 Boundary conditions

At the inlet of the channel, we gradually impose as upstream boundary condition a flow discharge  $Q = 62 \text{ m}^3\text{s}^{-1}$ , while at the outlet a null free surface is imposed, which is also the initial condition. On the lateral walls and on the cylinder, slip boundary conditions are imposed.

### 36.2.5 Computation of the Strouhal number

For this case, neither analytical nor experimental solutions are available, but the formation of von Karman vortex is expected behind the piers. The validation is performed computing the Strouhal number for the two piers, given by the following formula:

$$St = \frac{f_{lift} D}{U}$$

where  $f_{lift}$  is the lift frequency which usually corresponds to the vortex shedding frequency,  $D$  is the diameter of the cylinder and  $U$  is the average free-stream velocity.

In order to compute the lift frequency, a FFT (Fast Fourier Transform) has been performed on the signal which describes the variation of the force with time. The force is computed as:

$$F = \int_0^l \int_0^h \rho g z \mathbf{n} dz ds,$$

where  $\rho$  is the water density,  $g$  is the acceleration of gravity and  $\mathbf{n}$  is the normal vector. The integral is performed on the cylinder with boundary  $l$  and along the vertical direction  $z$ .

Finally, in order to check the mass conservation of the advection schemes of TELEMAC-2D, a tracer is released at the inlet with the following boundary condition:

$$c(x = -13.5, y) = \begin{cases} 2 \text{ g/L} & \text{if } \frac{H}{2} - 9 \leq y \leq \frac{H}{2} - 8 \\ 1 \text{ g/L} & \text{otherwise} \end{cases}$$

A free condition is imposed at the outlet. The error on the mass is computed as follows:

$$\varepsilon_M = M_{start} + M_{in} - M_{end},$$

$M_{start} = \int_{\Omega} (hc)^n d\Omega$  is the mass at the beginning of the simulation,  $M_{end} = \int_{\Omega} (hc)^{n+1} d\Omega$  is the mass at the end of the simulation,  $M_{in} = \int_{\Gamma} h c \mathbf{u} \cdot \mathbf{n} d\Gamma$  is the mass introduced (and leaved) by the boundaries; where  $\Omega$  is the computational domain and  $\Gamma$  is its boundary. The relative error is computed as:

$$\varepsilon_{rel} = \frac{\varepsilon_M}{\max(|M_{start}|, |M_{in}|, |M_{end}|)}.$$

### 36.2.6 Physical parameters

The bottom friction is described by the Strickler law with a coefficient equal to  $k_s = 40 \text{ m}^{1/3}/\text{s}$ . The fluid considered presents a kinematic viscosity  $\nu = 0.021 \text{ m}^2/\text{s}$ . The average flow velocity in the upstream undisturbed field is about  $U = 0.95 \text{ m/s}$ . Taking into account the diameter of the cylindrical pier, the Reynolds number is  $Re = UD/\nu = 180$ .

### 36.2.7 Numerical parameters

To perform an appropriate analysis on several cycles, the simulation time is set to 1,200 s (= 20 min). Three different numerical configurations are tested with the following parameters:

| Case | Equations       | Advection scheme for $U$ | Element for $H/U$ | Solver | Time step / Desired CFL |
|------|-----------------|--------------------------|-------------------|--------|-------------------------|
| A    | Wave Eq. FE     | Characteristics          | P1/P1             | CG     | 0.1 s / -               |
| B    | Saint-Venant FE | Characteristics          | P1/P2             | GMRES  | 0.1 s / -               |
| C    | Saint-Venant FV | Kinetic order 2          | -                 | -      | - / 0.9                 |

Table 36.1: List of the simulation parameters used for the six cases tested in the pildepon example.

For finite element schemes the treatment of the linear system is set to wave equation (TREATMENT OF THE LINEAR SYSTEM = 2) and the solver accuracy is set to  $10^{-5}$ . For the tracer, all the advection schemes of TELEMAC-2D are tested in the configuration A. In the case of the predictor-corrector schemes, the number of corrections is set to 5; for the LIPS schemes, the number of sub-steps is equal to 10 and the accuracy for diffusion of tracers is set to  $10^{-10}$ . It is important to note that the last parameter is used even if the keyword DIFFUSION OF TRACERS is set to NO. Indeed, when using the LIPS schemes, a linear system has to be solved and this parameter defines the accuracy of the solver.

## 36.3 Results

### 36.3.1 First observation

The velocity norm iso-contour map is presented at initial time and final time in Figure 36.4.

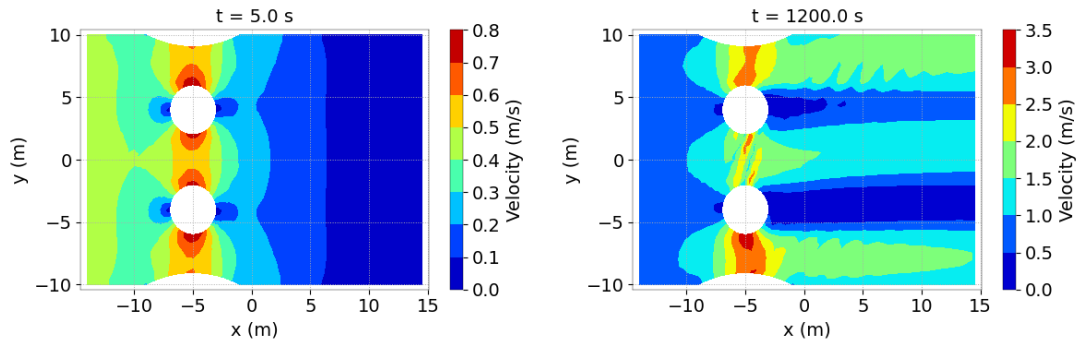


Figure 36.4: Velocity norm at the beginning and at the end of the simulation.

### 36.3.2 Comparison of numerical schemes

Comparison of free surface and velocity are presented in Figure 36.5 at  $t = 1000$  s.

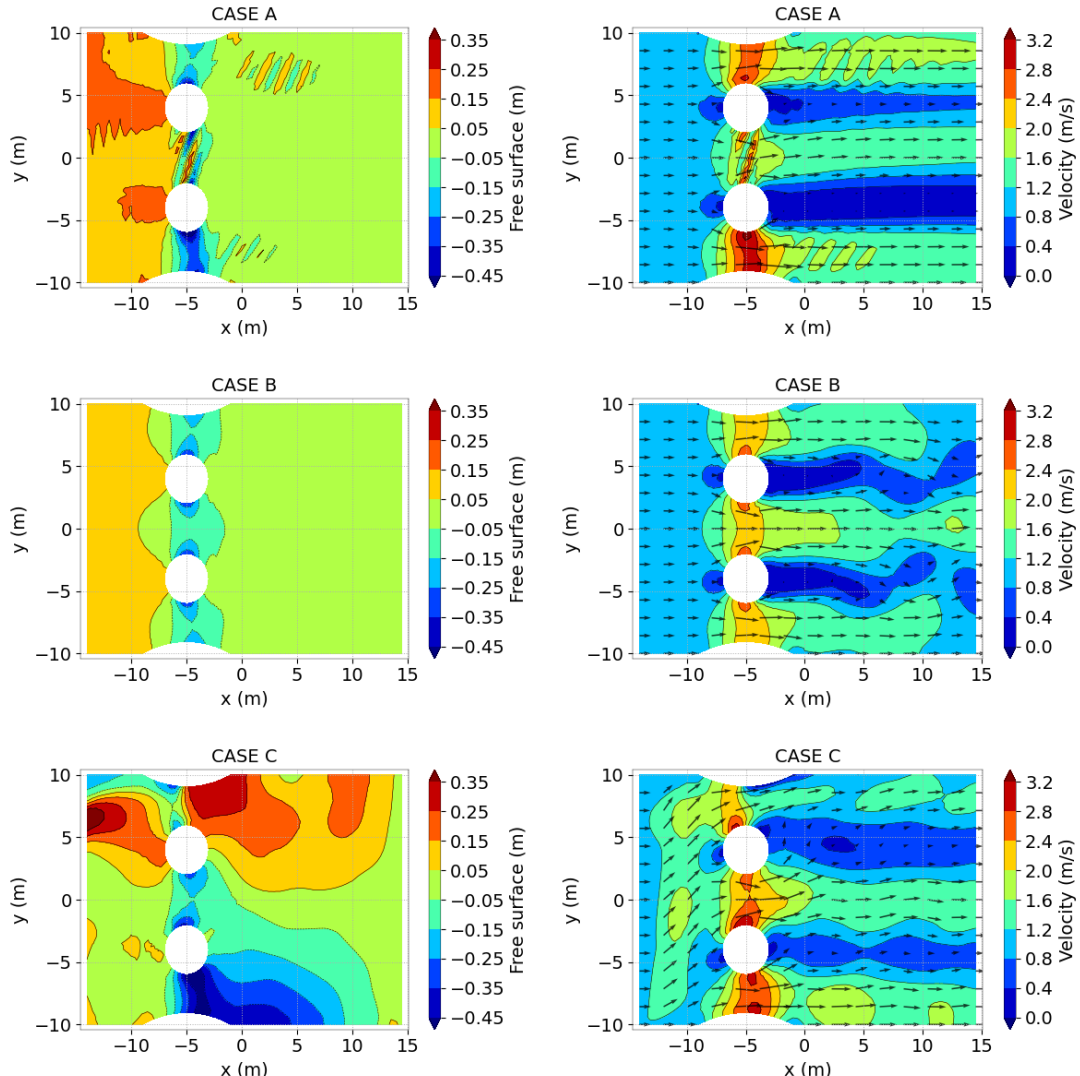


Figure 36.5: Free surface (left) and velocity norm (right) at  $t = 1,000$  s.

### 36.3.3 Computation of the Strouhal number

In Figures 36.6, 36.7 and 36.8 are plotted the fast Fourier transforms of the lift force for each cases considered in subsection 36.2.7.

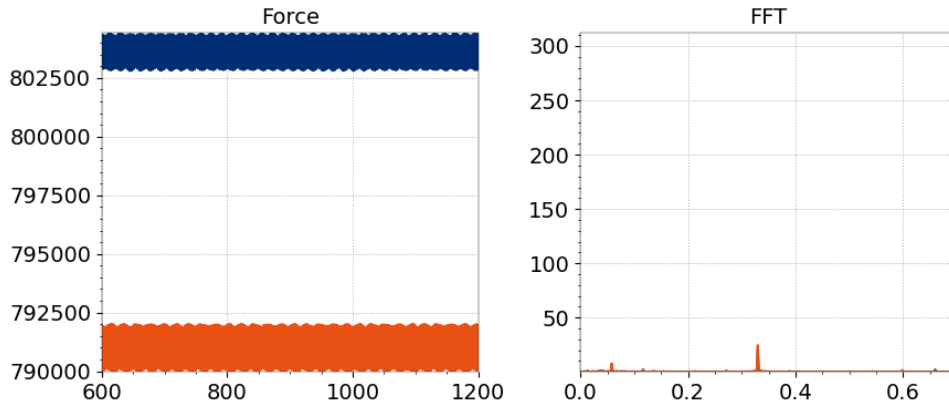


Figure 36.6: Fast Fourier transform of the lift force on the piers in case A.

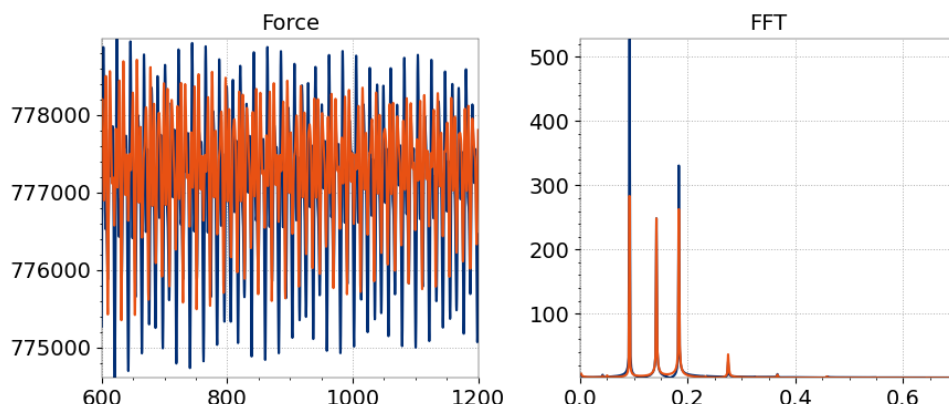


Figure 36.7: Fast Fourier transform of the lift force on the piers in case B.

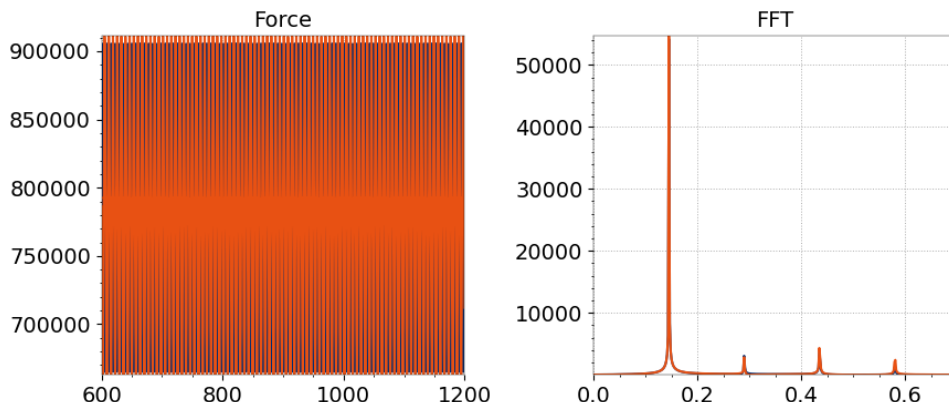


Figure 36.8: Fast Fourier transform of the lift force on the piers in case C.

The Strouhal number obtained for the different numerical configurations are presented in the following table:

|        | Strouhal for upper pier | Strouhal for lower pier |
|--------|-------------------------|-------------------------|
| CASE A | 9.784                   | 9.784                   |
| CASE B | 0.347                   | 0.347                   |
| CASE C | 0.549                   | 0.549                   |

Table 36.2: Pildepon test case: Strouhal number for the upper and lower piers according to the different numerical configurations.

### 36.3.4 Mass balance

The mass balance at the end of the simulation according to the different advection schemes are presented in the following table:

|              | $M_{\text{start}}$ | $M_{\text{end}}$ | $M_{\text{in}}$ | $\epsilon_M$   | $\epsilon_{\text{rel}}$ |
|--------------|--------------------|------------------|-----------------|----------------|-------------------------|
| Strong Char. | 1637.919           | 1791.128         | 547.5568        | 394.3479       | 0.2201673               |
| N            | 1637.919           | 1796.107         | 158.1877        | -0.7548806E-10 | -0.4202872E-13          |
| N PC1        | 1637.919           | 1789.708         | 151.7889        | -0.4279786E-07 | -0.2391332E-10          |
| N PC2        | 1637.919           | 1789.661         | 151.7418        | -0.3501100E-07 | -0.1956292E-10          |
| PSI          | 1637.919           | 1789.332         | 151.4133        | -0.7078143E-09 | -0.3955745E-12          |
| PSI PC1      | 1637.919           | 1789.721         | 151.8023        | -0.1059561E-09 | -0.5920259E-13          |
| PSI PC2      | 1637.919           | 1789.362         | 151.4428        | -0.1820922E-07 | -0.1017638E-10          |
| PSI LIPS     | 1637.919           | 1789.315         | 151.3960        | -0.2036768E-07 | -0.1138295E-10          |
| NERD         | 1637.919           | 1796.107         | 158.1878        | -0.2955858E-11 | -0.1645703E-14          |

Table 36.3: Pildepon test case: mass balance for the different advection schemes.

It can be noted that only the characteristics are not mass conservative.

## 37. Infiltration with the SCS-Curve Number runoff model (pluie)

### 37.1 Purpose

The aim of this test case is to check the implementation of the SCS-Curve Number infiltration model.

### 37.2 Theoretical background

This test case is extracted from [20]. The method described below is directly taken from this paper.

Curve Number runoff model, also known as the SCS Method of Abstractions, has been developed from 1954 by USA's Soil Conservation Service (SCS). This method, which is widely used in the world, aims at computing abstractions from storm rainfall using a spatially and temporally lumped infiltration loss model. It gives best results in agricultural watersheds with negligible baseflow [27].

The aim of runoff modelling is to assess the hydrologic abstractions  $F$  which are composed of (i) interception storage (vegetation foliage...), (ii) surface storage, (iii) infiltration, (iv) evaporation and (v) evapotranspiration. For short-term storm modelling, which is the Curve Number runoff model's field of application, abstractions due to infiltration are largely predominant over other forms which are then disregarded.

The total rain  $R_t$  can be divided in the following terms  $R_t = R_n + I_i + I_h$ , with  $R_n$  the net rainfall contributing to the runoff,  $I_i$  the initial abstraction and  $I_h$  the hydrological abstraction. The aim of this model is to estimate the total infiltration  $I_t = I_i + I_h$ , to deduce the net rainfall contributing to the runoff with  $R_n = R_t - I_t$ .

$R_n$  can be written as:

$$R_n = \begin{cases} \frac{(R_t - I_i)^2}{R_t - I_i + S} & \text{if } R_t > I_i \\ 0 & \text{else} \end{cases} \quad (37.1)$$

where:

$$I_i = \lambda S \quad (37.2)$$

with  $\lambda$  the initial abstraction ratio, set to 0.2, and:

$$S = 25.4 \left( \frac{1000}{CN} - 10 \right) \quad (37.3)$$

the potential maximal retention.  $CN$  is the Curve Number representing the calibration variable of the model. Its value can be spatially distributed and has been defined for different types of land use classes and for four different hydrological soil groups: Group A (deep sands, deep loess and aggregated silts), Group B (shallow loess, sandy loams), Group C (clay loams, shallow sandy loams, soils low in organic content and soils usually high in clay) and Group D (soils that swell significantly when wet, heavy plastic clays and certain saline soils) and for three type of hydrologic surface condition of native pasture (poor, fair, and good).

### 37.3 Description

Three examples are provided with (i) a classic rainfall defined by a constant rainfall intensity without runoff model, (ii) a classic rainfall defined by a constant rainfall intensity with Curve Number runoff model using  $CN$  values interpolated from a set of points provided in a formatted data file and (iii) a rainfall defined by a hyetograph read from a formatted data file with Curve Number runoff model using  $CN$  values stocked in the geometry file as an additional variable.

#### 37.3.1 Geometry and mesh

The model geometry is a square with a side length of 100 meters composed of 5412 triangular elements. The computational domain is divided in four parts with  $CN$  values of 80, 85, 90 and 95. Figure 37.1 presents the mesh.

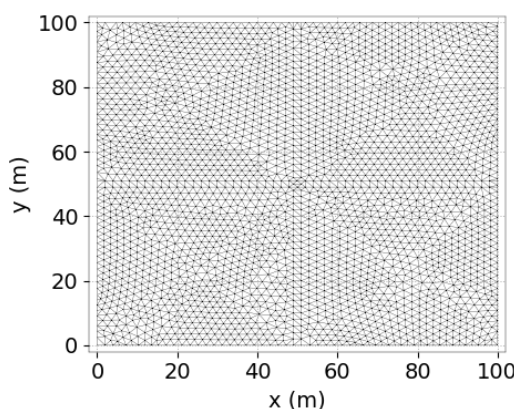


Figure 37.1: Mesh of the channel.

#### 37.3.2 Bathymetry

The bottom is flat in this test case.

#### 37.3.3 Initial and boundary conditions

The initial condition is a zero water depth, and there is no open boundary.

#### 37.3.4 Physical parameters

The classic rainfall is defined using the existing keyword RAIN OR EVAPORATION IN MM PER DAY = 100.0 and for a duration of 6 hours (DURATION OF RAIN OR EVAPORATION IN HOURS = 6.0) so that the total rainfall depth is 25 mm. The hyetograph defined in the last example has an irregular time distribution but has the same total rainfall depth. All the examples are run over a simulation period of 8 hours with a time-step of 200 seconds.

The Curve Number runoff model is used with default settings (ANTECEDENT MOISTURE CONDITIONS = 2 and OPTION FOR INITIAL ABSTRACTION RATIO = 1).

## 37.4 Results

Figure 37.2 shows the results at the final time step for the 3 simulations.

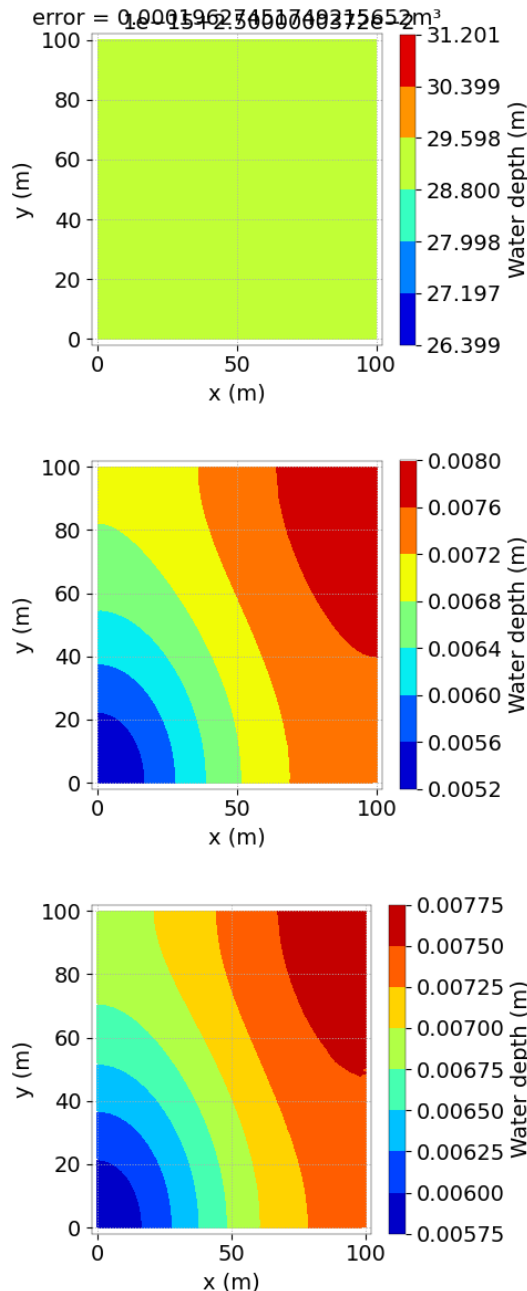


Figure 37.2: Water depth at the final time step and volume balance for all test cases.

## 37.5 Conclusion

TELEMAC-2D is able to simulate the infiltration with the SCS-Curve Number runoff model.

## 38. Porosity (porosité)

### 38.1 Description

This example checks that TELEMAC-2D is able to represent porosity.

The configuration is a straight channel 300 m long and 40 m wide with a flat horizontal bottom without slope.

#### 38.1.1 Initial and boundary conditions

The computation is initialised with a constant elevation equal to 5 m and no velocity.

The boundary conditions are:

- For the solid walls, a slip condition on channel banks is used for the velocities,
- On the bottom, a Strickler law with friction coefficient equal to  $40 \text{ m}^{1/3}/\text{s}$  is prescribed,
- Upstream a flowrate equal to  $100 \text{ m}^3/\text{s}$  is prescribed,
- Downstream the water level is equal to 5 m.

#### 38.1.2 Mesh and numerical parameters

The mesh (Figure 38.1) is made of 10,508 triangular elements (5,354 nodes). It is particularly refined around  $x = 0 \text{ m}$ .

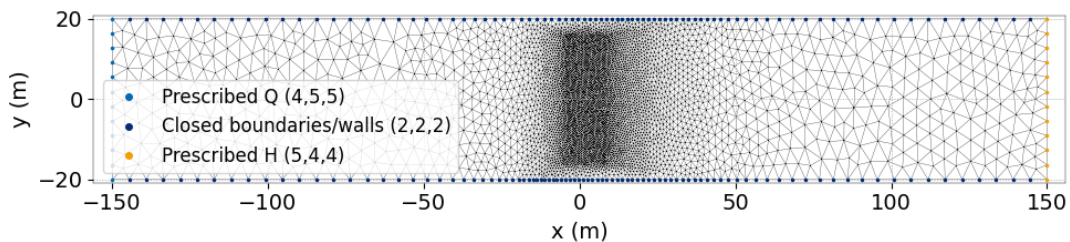


Figure 38.1: Horizontal mesh.

The time step is 0.2 s for a simulated period of 5,000 s.

To solve the advection, the method of characteristics is used for the velocities (scheme 1). The conjugate gradient is used for solving the propagation step (option 1) and the implicitation coefficients for depth and velocities are respectively equal to 1 and 0.6.

### 38.1.3 Physical parameters

The turbulent viscosity is constant with velocity diffusivity equal to 0.1 m<sup>2</sup>/s.

Porosity is applied by setting TIDAL FLATS = YES (default value) + OPTION FOR THE TREATMENT OF TIDAL FLATS = 3 and by implementing the user subroutine **USER\_CORPOR**:

$$\text{porosity} = \begin{cases} \frac{1}{2} \left( 1 + \frac{|x|}{50} \right) & \text{if } -50 \leq x \leq 50, \\ 1 & \text{otherwise.} \end{cases}$$

## 38.2 Results

The flow establishes a steady flow where the free surface is lightly higher at the entrance and significantly drops where porosity is applied, up to 5 cm (see Figure 38.2). Thus we can see that at the locations where porosity is lower than 1, water depth decreases, what is expected by the porosity feature (read the TELEMAC-2D user manual to know more about it). The flow accelerates up to twice where porosity is applied and then retrieves quite similar velocity after (see Figure 38.3).

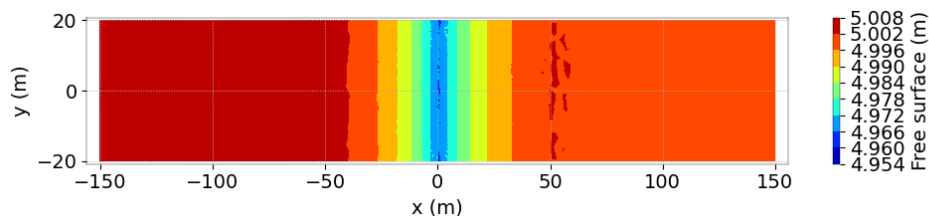


Figure 38.2: Free surface at final time step.

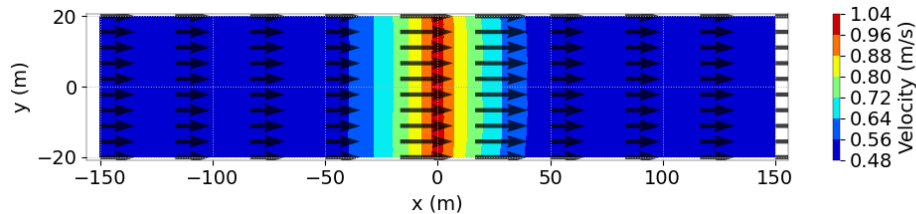


Figure 38.3: Velocity at final time step.

## 38.3 Conclusions

TELEMAC-2D is capable to model porosity.

## 39. Rain runoff and hydrostatic reconstruction (rain\_runoff)

### 39.1 Purpose

The purpose of this test case is to validate the implementation of the hydrostatic reconstruction modification proposed by [3]. This option is used by activating the keyword `OPTION OF THE HYDROSTATIC RECONSTRUCTION = 2` for kinetic, HLLC and WAF finite volume schemes. As several authors have highlighted a limitation in the formulation of the classical hydrostatic reconstruction [6], this option allows a correction to be made to the hydrostatic reconstruction only at the point where it fails, i.e. when:

$$\frac{h}{\Delta z} < 1, \quad (39.1)$$

where  $h$  is the water depth and  $\Delta z = \Delta x \partial_x z$  the difference of elevation between two neighboring nodes.

To reproduce these conditions, a rain induced runoff test case with a straight channel that can have three different slopes, on which an analytical solution and experimental data on the outflow is available, is used.

### 39.2 Description

#### 39.2.1 Analytical solution

An analytical solution can be calculated to represent the hydrograph at the channel outlet, proposed by [5]. This solution is only available for the rise of the hydrograph and the plateau, i.e. when the equilibrium state is reached and the amount of rain falling on the domain is equal to the outflow at the channel outlet. The amplitude of this plateau is given by:

$$q_{out} = R.A, \quad (39.2)$$

where  $R$  is the rain intensity and  $A$  the channel area.

The rise of the hydrograph is described by:

$$\partial_t q_{out} = -gh(S_0 + S_f), \quad (39.3)$$

where  $g$  is the gravity constant,  $S_0$  the slope of the channel and  $S_f$  the friction slope which depends on the chosen friction law (see 39.2.6). Then, with the semi-implicit like treatment of the friction term, one can write the exact solution of the hydrograph as:

$$q_{out}^{t+1} = \frac{q_{out}^t + \Delta t \cdot g \cdot R \cdot S_0 \cdot T}{1 + S_f}, \quad (39.4)$$

with  $\Delta t$  a time step chosen for the analytical solution and  $T$  the total time.

Finally, to select if one is on the plateau or the rise, one just has to select the minimum  $q_{out}$  value computed with the two formulae.

### 39.2.2 Experimental data

Experimental data of the outlet discharge are also available in this test case. Indeed, [19] provides data from a laboratory flume which is 4.04 m long and 0.115 m wide. The water leaving the channel is weighed every second to determine the output quantity for 2 %, 5 % and 25 % slopes.

### 39.2.3 Geometry and mesh

The channel is 1 m wide and 5 m long. The mesh is regular along the channel. It is made up with triangles following the channel slopes. It is composed of 2,000 triangular elements (1,061 nodes) and the size of triangles is about 10 cm (see Figure 39.1).

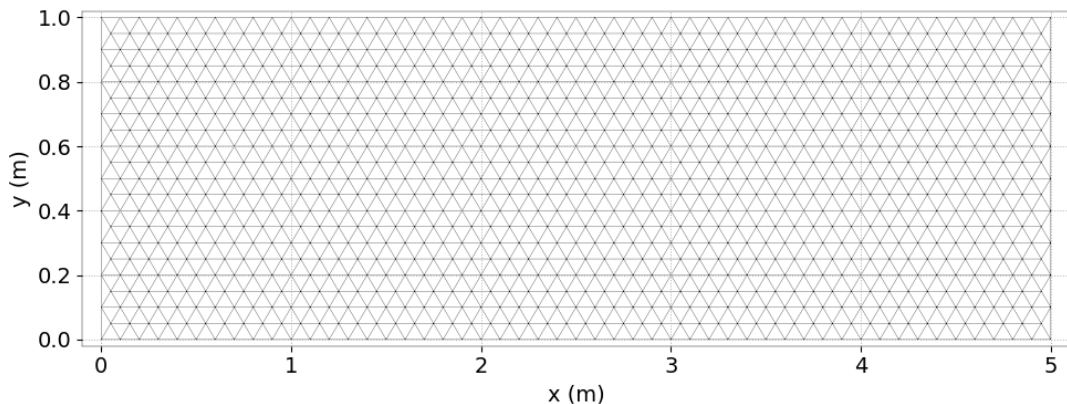


Figure 39.1: Mesh of the channel.

### 39.2.4 Bathymetry

The elevation of the bottom follows a slope defined for each geometry. There are three different slopes studied: 2 %, 5 % and 25 %. The slope is in the  $x$ -direction and the maximum elevation is for  $x = 0$  m and is 0 m. Figure 39.2 shows the bottom elevation for each slope considered.

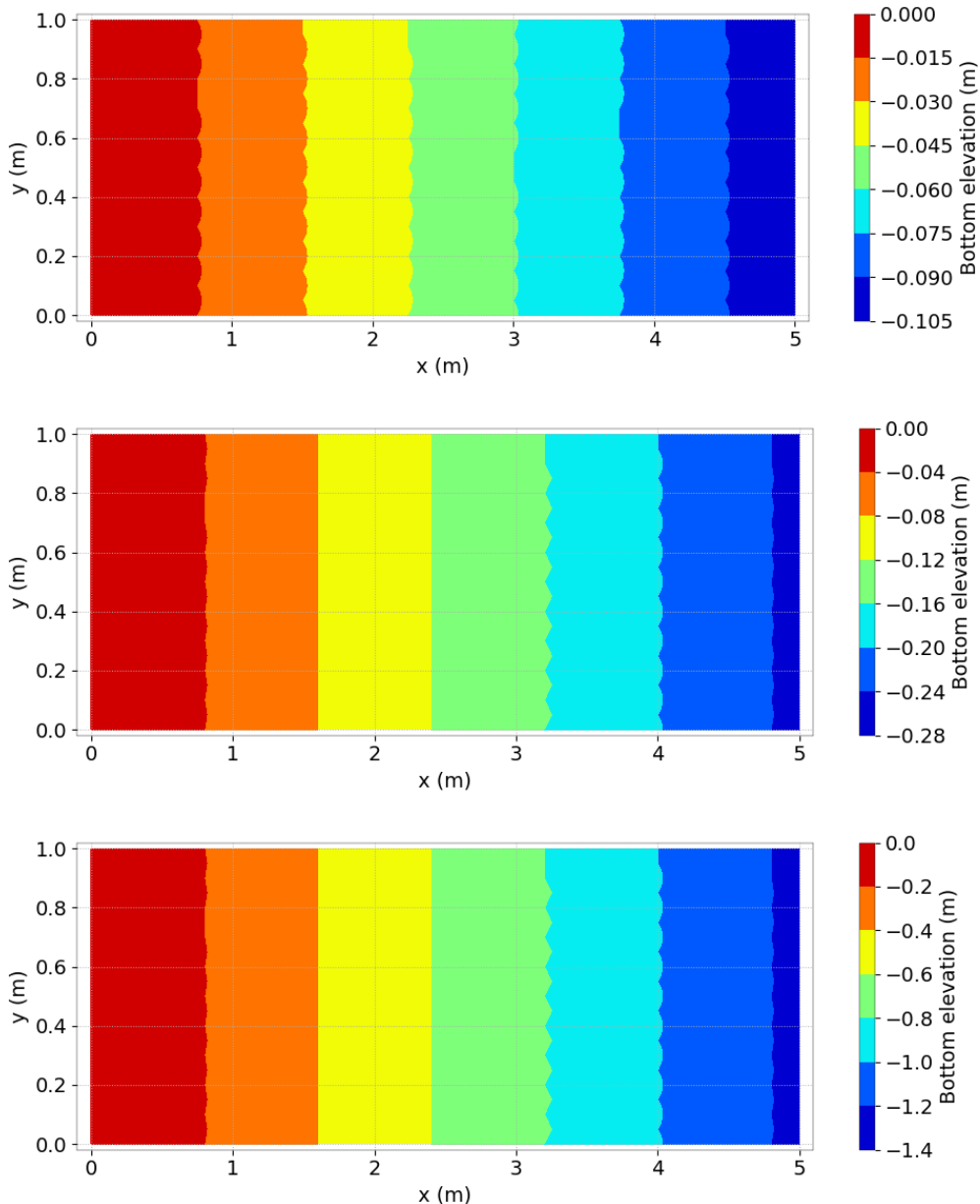


Figure 39.2: Bathymetry in the channel.

### 39.2.5 Initial and boundary conditions

The initial conditions are zero water depth everywhere.

The boundary conditions are defined as in Figure 39.3.

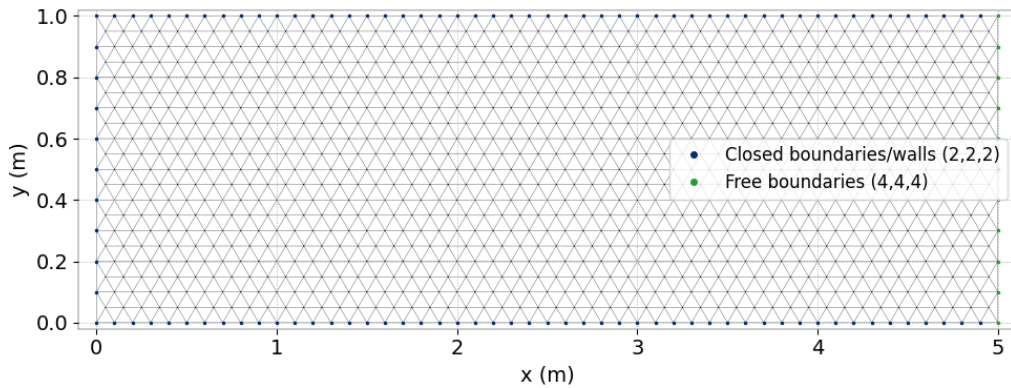


Figure 39.3: Boundaries conditions in the channel.

### 39.2.6 Physical parameters

The Poiseuille friction law is used, programmed in the user Fortran subroutine **SOURCE\_MOMENT**. This law writes:

$$S_f = \frac{3\mu u}{gh^2}, \quad (39.5)$$

with  $\mu$  the water kinematic viscosity set at  $10^{-6}$  m<sup>2</sup>/s and  $u$  the norm of the velocity.

The rain intensity is variable in time and space. The rain intensity is constant during the 610 first seconds with a value of 25.83 mm/h. It then stops to observe the decreasing of the hydrograph. When the rain is activated, it is only applied on the 4.04 m downstream the channel to reproduce the length of the laboratory case [19]. This has been programmed in the **USER\_RAIN** user subroutine.

The total time of the simulation is 1,000 s.

### 39.2.7 Numerical parameters

The test case is run with a maximum time step of 0.1 s and a desired Courant number of 0.9. The first order Kinetic scheme is used with both of the hydrostatic reconstruction options.

## 39.3 Results

Figure 39.4 shows the outlet discharge for both hydrostatic reconstruction methods compared to analytical solution and experimental data. The [3] scheme allows an improvement of the results, in particular for very steep slopes. The outlet discharge has been computed with a flux computation 1 cm above the downstream boundary, and the mass source term is obtained in the TELEMAC-2D listing.

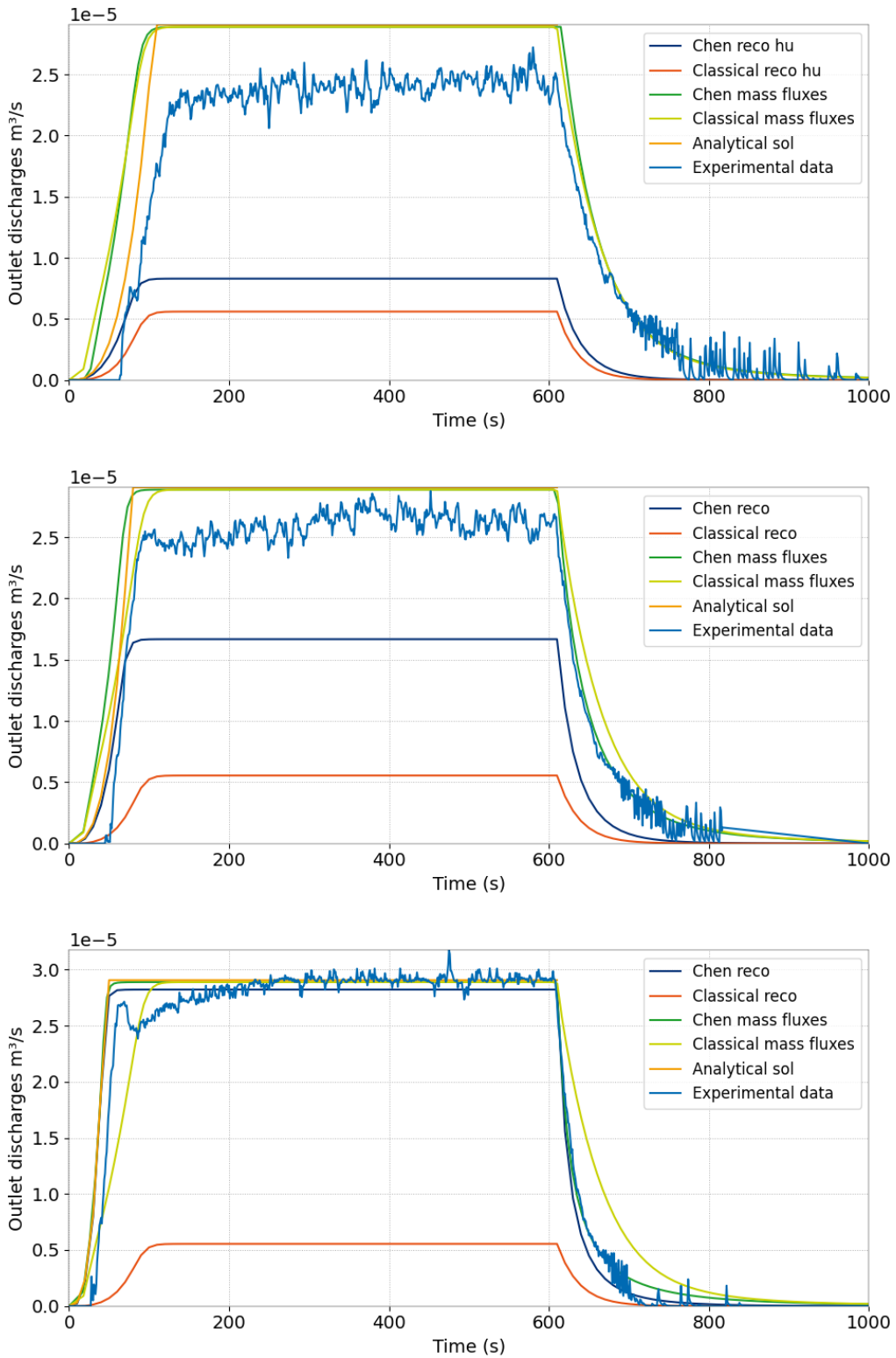


Figure 39.4: Outlet discharge for each slope vs analytical solution and experimental data.

# 40. riogrande

## 40.1 Description

The configuration is a part of river (around 6 km long) with schematic bathymetry defined by sections depending on ordinate  $y$  (affine function with respect to  $y$ , see Figure 40.1).

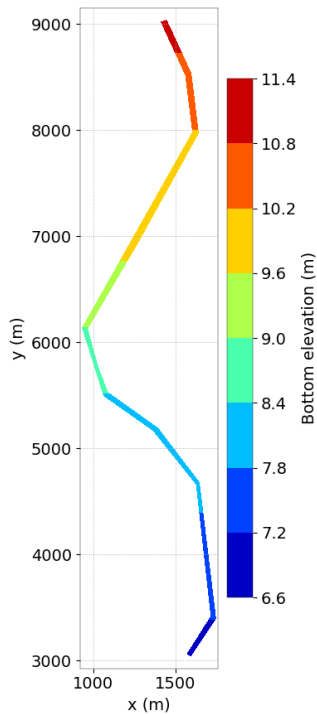


Figure 40.1: Bottom elevation.

### 40.1.1 Initial and boundary conditions

The computation is initialised with a constant elevation equal to 13 m, a constant velocity along  $x$  equal to  $\frac{0.25}{0.6 \times 1.1}$ .

The boundary conditions are:

- For the solid walls, a slip condition on channel banks is used for the velocities,

- On the bottom, a Chézy law with friction coefficient equal to  $55 \text{ m}^{1/2}/\text{s}$  is prescribed,
- Upstream a flowrate is prescribed, linearly increasing from 0 to final flowrate during the simulation. A velocity profile proportional to the square root of depth (option 4) is used to prevent from potential dry segments along the liquid boundary,
- Downstream the water level is also linearly increasing from 0 to final surface level during the simulation.

#### 40.1.2 Mesh and numerical parameters

The mesh (see Figure 40.2) is made of 8,268 triangular elements (4,989 nodes).

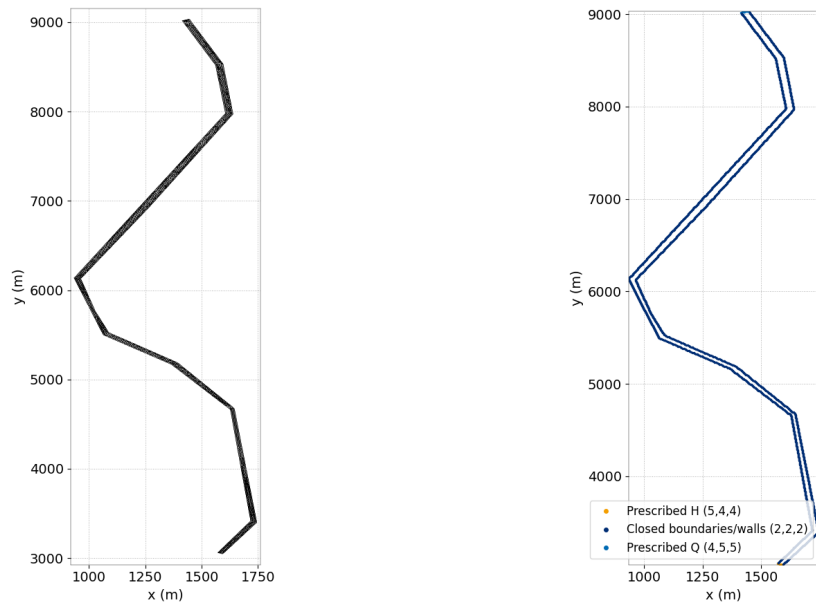


Figure 40.2: Mesh and boundary conditions types.

Zooms around inlet and outlet of the mesh can be seen in Figure 40.3.

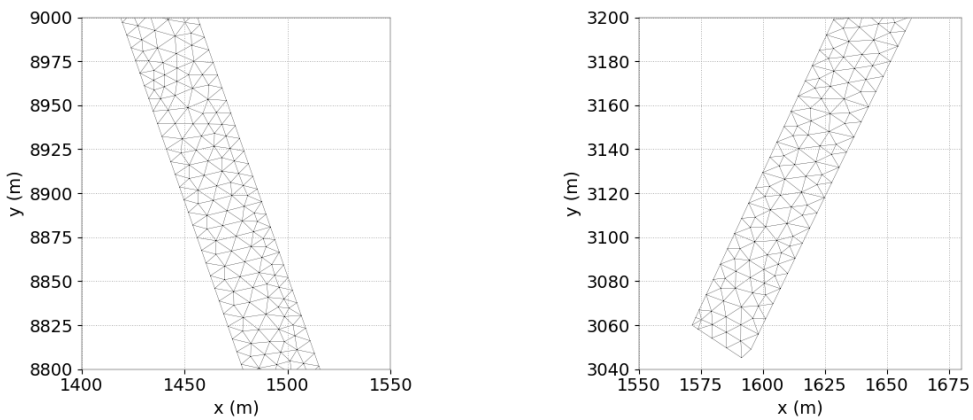


Figure 40.3: Zoom of the mesh at the inlet and the outlet.

The time step is 5 s for a simulated period of 25,000 s (a little bit less than 7 h).

To solve the advection, the characteristics is used for the velocities. The conjugate gradient is used for solving the propagation step (option 1) and the implicitation coefficients for depth and velocities are respectively equal to 1. and 0.55 (= default value).

#### 40.1.3 Physical parameters

A constant horizontal viscosity for velocity equal to  $0.0001 \text{ m}^2/\text{s}$  is chosen.

### 40.2 Results

Figure 40.4 shows the free surface elevation and velocity magnitude at the end of the computation.

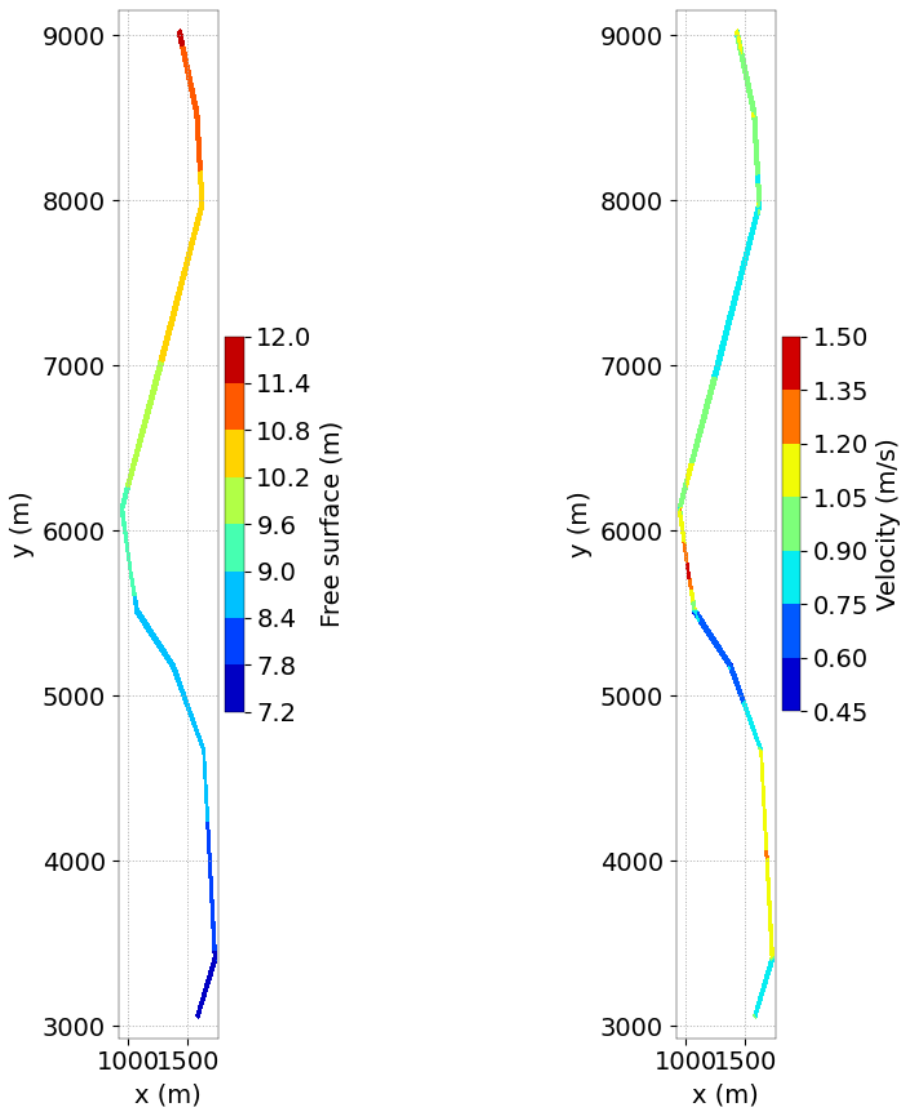


Figure 40.4: Free surface and velocity magnitude at final time step.

### 40.3 Conclusion

TELEMAC-2D can be used to model river flows.

## 41. Oil spill artificial river experiments (riv\_art)

### 41.1 Purpose

An artificial river test campaign was conducted by Veolia Environnement Recherche et Innovation in order to observe the capacity of oil spill pollutant to dissolve PAHs (Polycyclic Aromatic Hydrocarbons). The UBA (Umweltbundesamt German Federal Agency for the Environment) has on its site 16 identical systems of artificial rivers with each 100 m in circumference. Among these rivers called FSA (acronym for Fliess und StillgewässersimulationsAnlage: simulator rivers and lakes), eight are located outdoors. A water flow is generated in these rivers with a screw pump. A system for continuous measurement of physical parameters river is installed for each river, and there is one weather station. For the purpose of the experiment set up, two rivers were linked together to increase the installation length and sinuosity (Figure 41.1).

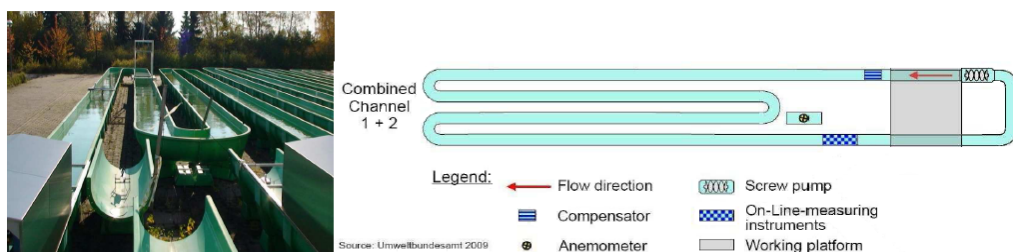


Figure 41.1: Artificial river sketch.

The release of the hydrocarbon is achieved through a ring on water surface, the pollutant is injected inside it. Then, the ring is removed to allow the pollutant transport (Figure 41.2). To observe the evolution of the concentration of dissolved PAHs, a fluorescence probe is used. Every morning a sample called "white" is made to know the initial concentration of PAHs already present in the channel. When the signal (%) is approximately on the peak, a water sample is taken during 30 seconds using an automatic device located with the probe. The samples are then sent to the CEDRE for the analysis of dissolved concentrations of PAHs in samples. For each sample, there is therefore a concentration of total PAHs (ng/L) and a probe signal (%).

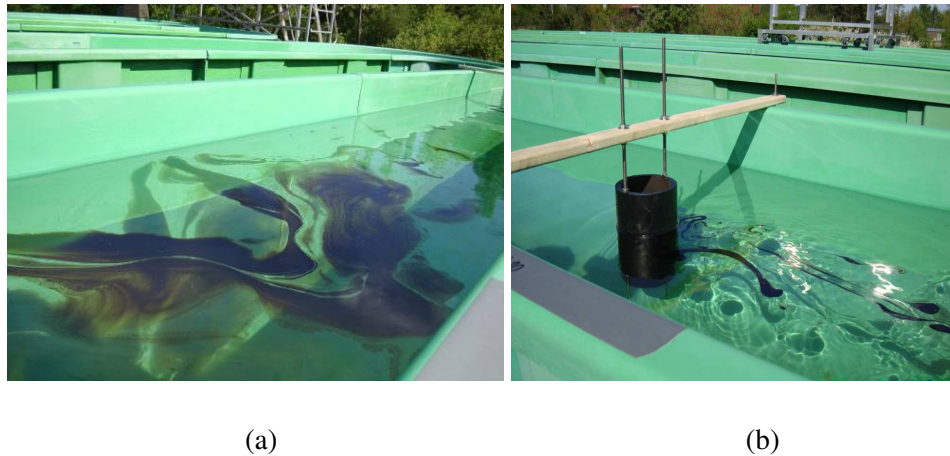


Figure 41.2: Oil spill in artificial river without and with obstacles respectively (a) and (b).

## 41.2 Description

The finite element mesh consists of 23,234 nodes and about 43,000 triangles of average size 0.08 m (Figure 41.3). The flow velocity and surface elevation are imposed respectively on inflow and outflow boundary conditions. For shoreline nodes, solid wall conditions are considered.

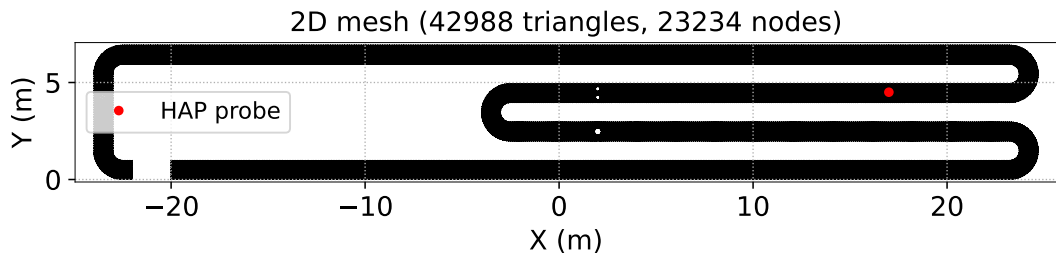


Figure 41.3: Mesh.

In the simulation, a kerosene spill which occurs in the first artificial river curve is considered. A volume of  $2 \times 10^{-5} \text{ m}^3$  has been spilled into the channel. The flow velocity is imposed to 0.1 m/s on inflow boundary and obstacles are in the channel (Figure 41.2 b).

## 41.3 Result

In the simulation result, the particles represent the oil surface slick whereas the eulerian tracer represents the dissolved petroleum in the water column. The numerical and experiment concentrations are shown in Figure 41.4.

The dissolved hydrocarbons concentration in the water column has the same order of magnitude and compares well with experiments. However, there is a delay (about 160 s) between the model results and the experimental expected values. This lag can be explained by the outdoor conditions which cannot be modelled, such as gusts of wind.

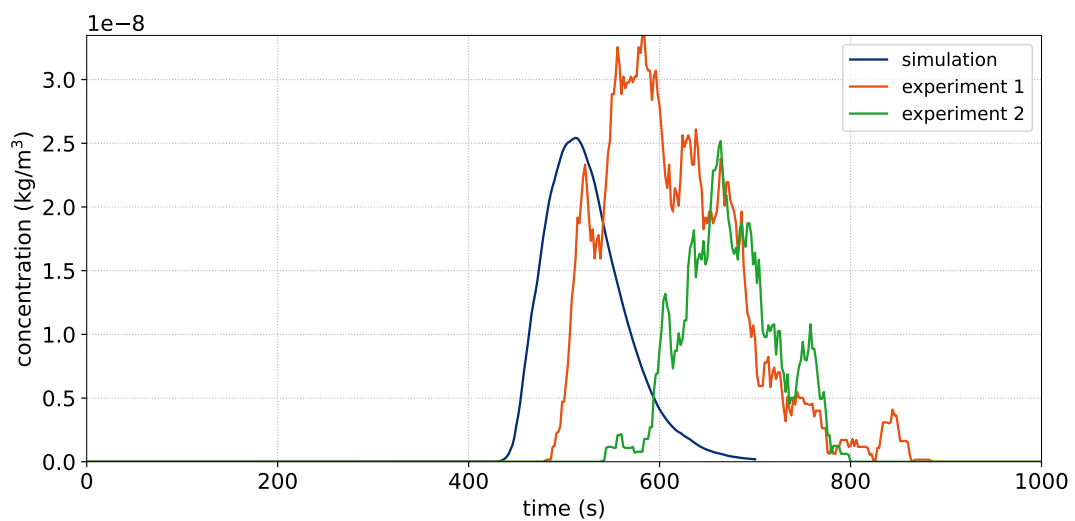


Figure 41.4: Kerosene concentration in the water column.

## 42. Secondary flow correction (securrents)

### 42.1 Purpose

The secondary flow correction proposed by Bernard and Schneider [1, 8] and implemented in TELEMAC-2D has been tested on experimental data from the Riprap Test Facility conducted at the Waterway Experiment Station of the U.S. Army Engineer Waterways Experimental Station [1].

### 42.2 Description

The channel presents four bends and two reversals in curvature, with  $L = 274$  m long and  $B = 3.63$  m wide with a bed slope of 2.16 per thousand and 2H:1V bank side slopes (Figure 42.1).

IMAGE NOT  
FOUND

.../img/Bottom.png is missing

Figure 42.1: Bottom elevation.

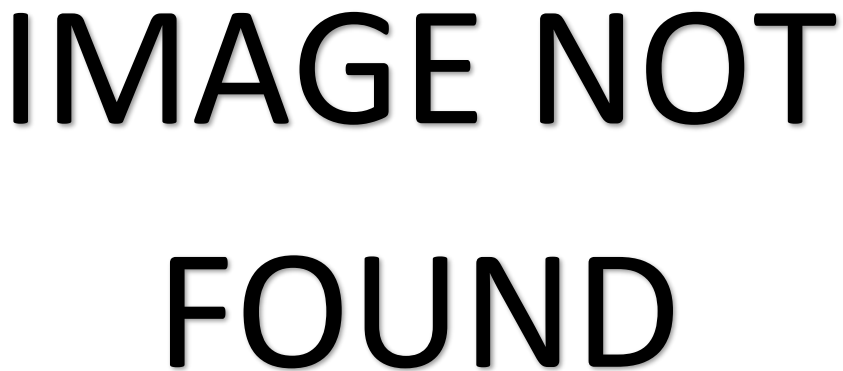
### 42.2.1 Boundary Conditions

Numerical simulations were performed with a constant discharge  $q_{in} = 4.2475 \text{ m}^3/\text{s}$  at inlet and mean flow depth  $h_{out} = 0.9 \text{ m}$  at outlet.

The channel bed has been treated as rigid, with the friction coefficient  $C_f$  specified with the Manning relation with a roughness coefficient  $n = 0.024 \text{ s/m}^{-1/3}$ .

### 42.2.2 Mesh and numerical/physical parameters

The computational domain has been discretized with a non-structured triangular finite element mesh with a total of 25,577 elements and 13,340 nodes, with mean element size of 0.4 m (Figure 42.2). The discretization of the banks was done with 5 elements on each side of the channel.



.../img/Mesh.png is missing

Figure 42.2: Horizontal mesh.

The numerical experience was run for  $\approx 5 \text{ min}$  until the equilibrium stage was reached, with a time step  $\Delta t = 0.1 \text{ s}$ .

The secondary flow correction coefficients were set to  $A_s = 7.071$  and  $D_s = 0.5$ .

Keywords and printout variables used for this test case are given below.

#### Keywords

- SECONDARY CURRENTS = YES,
- PRODUCTION COEFFICIENT FOR SECONDARY CURRENTS = 7.071,
- DISSIPATION COEFFICIENT FOR SECONDARY CURRENTS = 0.5.

#### Printout variables

- 1/R: The reverse of local radius:  $1/r_{sec}$ ,
- OMEGA: Flow vorticity:  $\Omega$ ,
- TAU\_S: Streamwise stresses:  $\tau_s$ .

## 42.3 Results

Free surface elevation and velocity magnitude at the end of the simulation can be seen in Figures 42.3 and 42.4.

IMAGE NOT  
FOUND

../img/FreeSurface.png is missing

Figure 42.3: Free surface elevation at final time.

IMAGE NOT  
FOUND

../img/Velocity.png is missing

Figure 42.4: Velocity magnitude at final time.

# 43. Seiche

## 43.1 Purpose

Seiches are resonant oscillations, or ‘normal modes’, of lakes and coastal waters; that is, they are standing waves with unique frequencies, imposed by the dimensions of the basins in which they occur. Water moves back and forth across the basin in a periodic oscillation, alternately raising and lowering sea level at the basin sides. Sea level pivots are ‘node’ at which the sea level never changes. Currents are maximum beneath the node when the sea level is horizontal, and they vanish when the sea level is at its extremes.

The purpose of this test case is to show that TELEMAC-2D compares well against the analytical solution of the linearised shallow water equations, in a physical domain close to the linearising assumptions.

At this stage, only the results of the TELEMAC system are presented. The comparison against the analytical solution will be added later.

## 43.2 Description

For illustrative purposes we consider a rectangle domain, or flume, 200 m long and 1.8 m wide – for all intent and purposes, this test case can be considered as a 1D test case.

The channel bottom is placed at  $z = 0$  m.

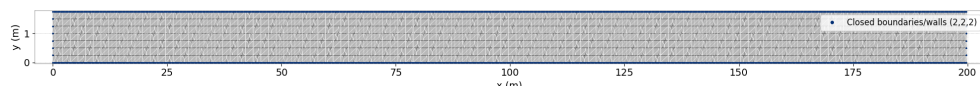


Figure 43.1: Mesh of the domain.

The edge length of the mesh is uniform, set at about 0.3 m. It was built as a triangulation of a regular mesh of cell size of 0.25 m.

### 43.2.1 Initial conditions

The initial free surface elevation is set through the subroutine **USER\_CONDIN\_H** as follows:

$$H = H_o + A \cos\left(\frac{2\pi X}{L}\right), \quad (43.1)$$

where  $L$  is the length of the flume (200 m),  $H_o$  is the water depth at the equilibrium (10 m) and  $A$  is the initial seiche amplitude (chosen as 0.01 m, which is small compared to  $H_o$ ).

### 43.3 Reference

Analytical solution of the linearised shallow water equation...

### 43.4 Results

Figure 43.2 shows the free surface at the end of the simulation.

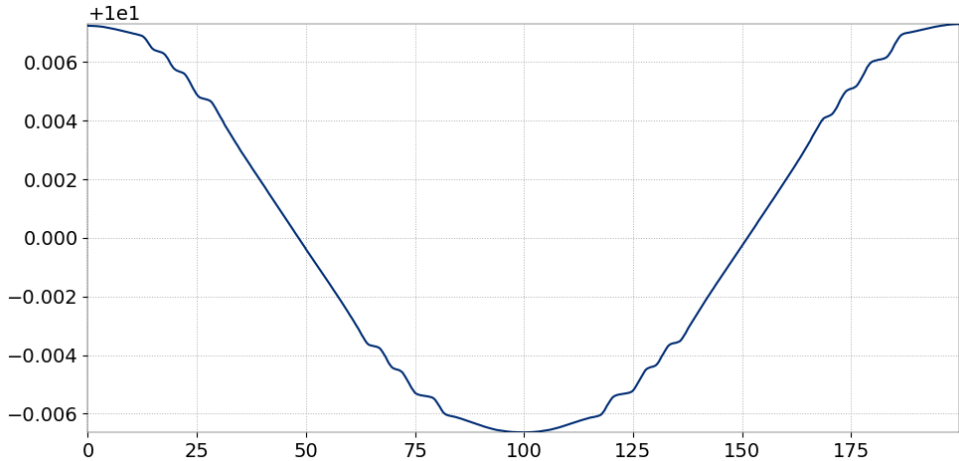


Figure 43.2: Free surface at time 300 s.

### 43.5 Conclusion

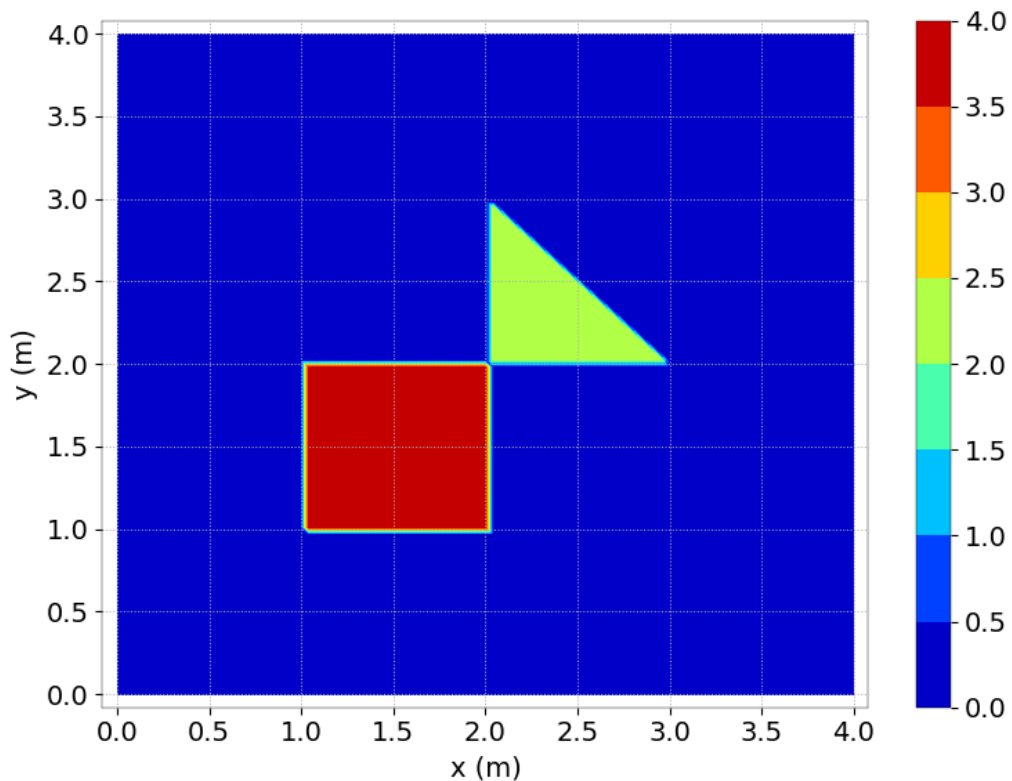
Without a comparison against an analytical solution, all we have demonstrated at this stage is that TELEMAC-2D conserves energy, as the water keeps sloshing without attenuations of the amplitude of the seiche – and this is already a interesting result.

## 44. Shape file to define bathymetry (shapeTXT)

### 44.1 Purpose

This is an example of the use of a text file coming from a shapefile to define a specific bathymetry in some areas. For an example of the construction of the text file from a shapefile containing polygons, one can see the notebook *shape\_file\_reader.ipynb*. The file *shape.txt* defines a square and a triangle that are read by **user\_corfon** subroutine. The bathymetry is set to 3.9 m in the square and 2 m in the triangle.

### 44.2 Results



## 45. Wave refraction and diffraction around a circular island (shoal)

### 45.1 Purpose

This case models refraction around a circular island [18]. This process is extremely important as tsunami waves travel a long way and is subject to diffraction around islands, headlands etc., and is subject to refraction wherever there are significant variations of water depth.

### 45.2 Description

This case is the analytical solution for a wave train travelling over a circular island, which vertical cross-section is shown in Figure 45.1.

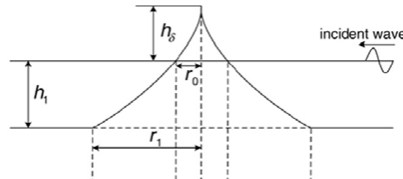


Figure 45.1: Vertical cross-section through circular island.

This is a case where refraction and diffraction of a wave both occur.

#### 45.2.1 Numerical and physical parameters

TELEMAC-2D is run using the wave equation formulation and no bed friction or viscosity. Thompson boundary condition is used so waves could pass out from the modelled domain. The implicitation coefficients are taken as 0.501 (the model is second order accurate if implicitation = 0.5, but on the edge of instability as the scheme is unstable if implicitation < 0.5) and the free surface gradient compatibility is taken as 0.9 (recommended value).

### 45.3 Results

The model is compared with the analytical solution by contouring the wave amplitude (Figure 45.3) to compare with the analytical solution (Figure 45.2). These figures are for a profile in which the depth varies as the 2/3 power of the radius as shown in Figure 45.1.

It can be seen that the wave height pattern is well reproduced for this situation.

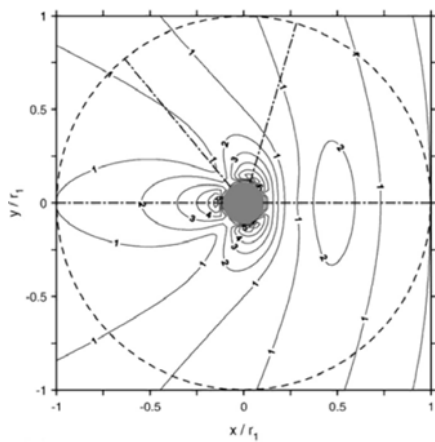


Figure 45.2: Wave amplitude contours for a circular island with  $r_1 = 9r_0$ ,  $r_0 = 10$  km,  $h_1 = 4$  km. Analytical solution.

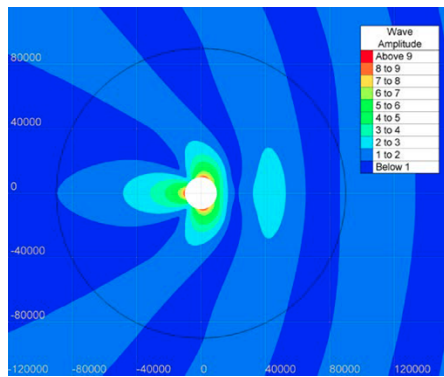


Figure 45.3: Wave amplitude contours for a circular island with  $r_1 = 9r_0$ ,  $r_0 = 10$  km,  $h_1 = 4$  km. Model solution.

Free surface elevation at the end of the simulation can be seen in Figures 45.4 and 45.5 (the latter is a zoom around the circular island).

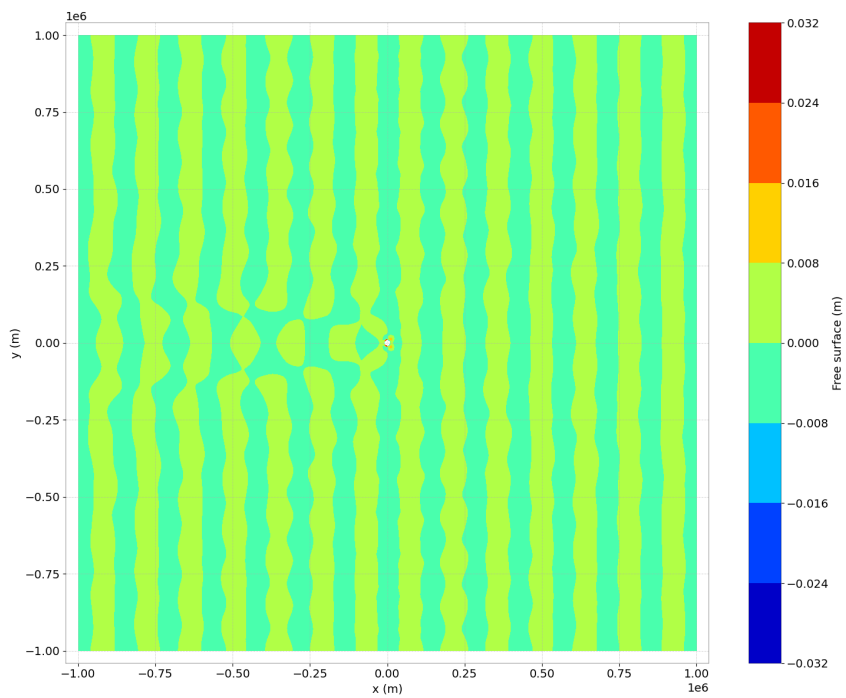


Figure 45.4: Free surface elevation at final time.

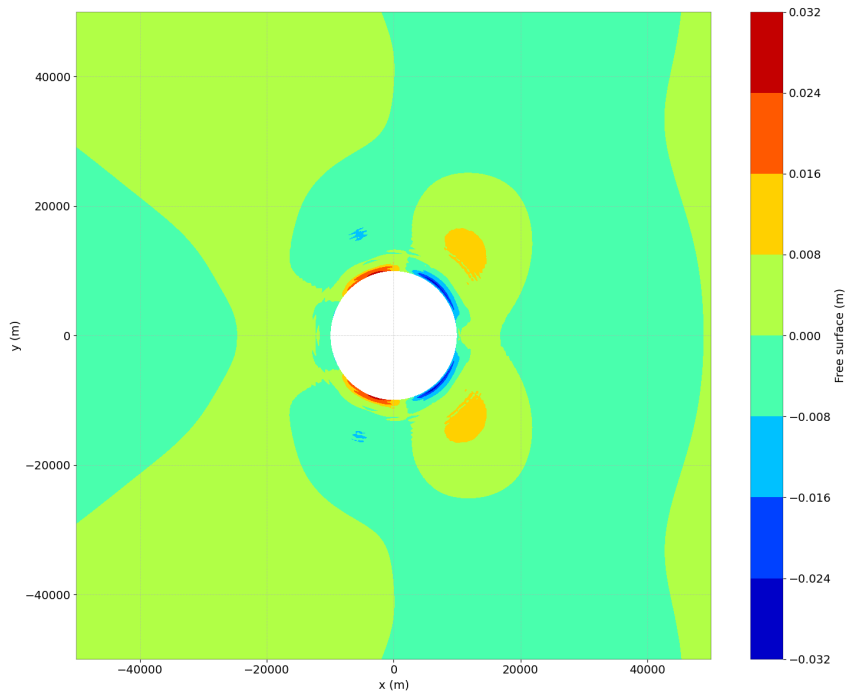


Figure 45.5: Free surface elevation at final time (zoom around the island).

## 46. Culvert modelling (siphon)

### 46.1 Purpose

To demonstrate that TELEMAC-2D can solve the flow in a culvert considered as an internal singularity, under the form of a couple of source and sink nodes. Also to show that TELEMAC-2D can compute tracer dispersion.

### 46.2 Description

Two square tanks are connected hydraulically by a culvert. The culvert is represented by a couple of source / sink nodes, one in each tank. The water level and the tracer concentration are initially higher in the left tank.

#### 46.2.1 Geometry and mesh

- Two identical square tanks are located 100 m apart,
- The dimension of each square tank is 200 m × 200 m,
- The water depth at rest is 4 m in the left tank, and 2 m in the right tank.

The mesh is regular. It is made up with squares split into 2 triangles.

- 1,600 triangular elements,
- 882 nodes,
- Maximum size range:  $\sqrt{200} = 14.14$  m.

#### 46.2.2 Boundaries

- Solid walls with slip condition in the domain.

Bottom:

- Strickler formula with friction coefficient =  $20 \text{ m}^{1/3}/\text{s}$ .

#### 46.2.3 Physical Parameters

Turbulence: Model of constant viscosity with velocity diffusivity =  $1 \text{ m}^2/\text{s}$ .

#### 46.2.4 Numerical Parameters

Type of advection:

- Characteristics on velocities (scheme #1),
- Conservative + modified SUPG on depth (mandatory),
- Centred semi-implicit scheme + SUPG decentring on tracer (scheme #2).

Type of element:

- Quasi-bubble triangle for velocities,
- Linear triangle P1 for  $h$ .
- GMRES solver,
- Accuracy =  $10^{-8}$ .

Tracer:

- Initial concentrations: 100 % in the left square, and 50 % in the right square,
- Co-ordinates of source / sink nodes: left = (100;100) and right = (400;100),
- No water discharge of sources,
- GMRES solver.

Time data:

- Time step = 2.5 s,
- Simulation duration = 600 s.

Mesh and initial state are shown in Figure 46.1.

### 46.3 Results

The water flows from the left tank to the right tank through the culvert. The water level decreases regularly in the left tank and increases regularly in the right tank (Figure 46.3). Simultaneously, a spot of tracer with concentration 100 arrives in the right tank and disperses.

In the left tank, the culvert is vertical. Therefore, the flow is regular and symmetric around the sink node. In the right tank, the culvert is horizontal in the direction of  $y$ -axis. Therefore, the flow takes this direction from the source node and the velocity field forms two eddies around the source (Figure 46.6).

Water mass and tracer mass are conserved: no water mass is lost whereas the cumulated loss of tracer mass at the end of the simulation is below 0.9 % of the initial mass.

### 46.4 Conclusions

TELEMAC-2D can be used for the treatment of an internal singularity, such as a culvert, and also for the treatment of dispersion by currents and diffusion of a tracer.

### 46.5 Figures

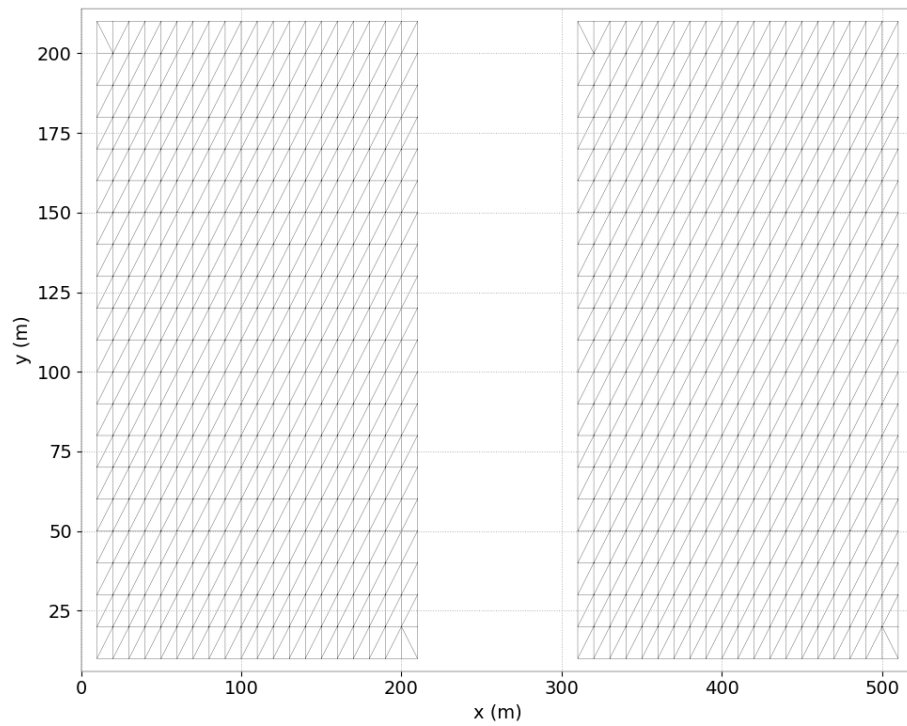


Figure 46.1: Mesh of the domain.

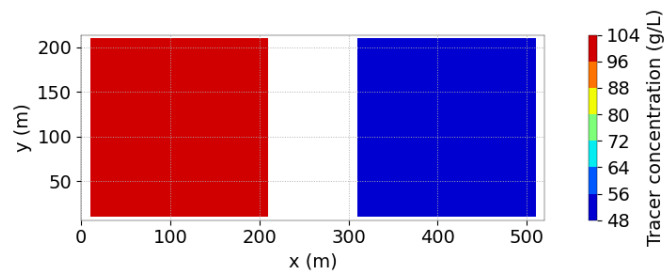


Figure 46.2: Initial state.

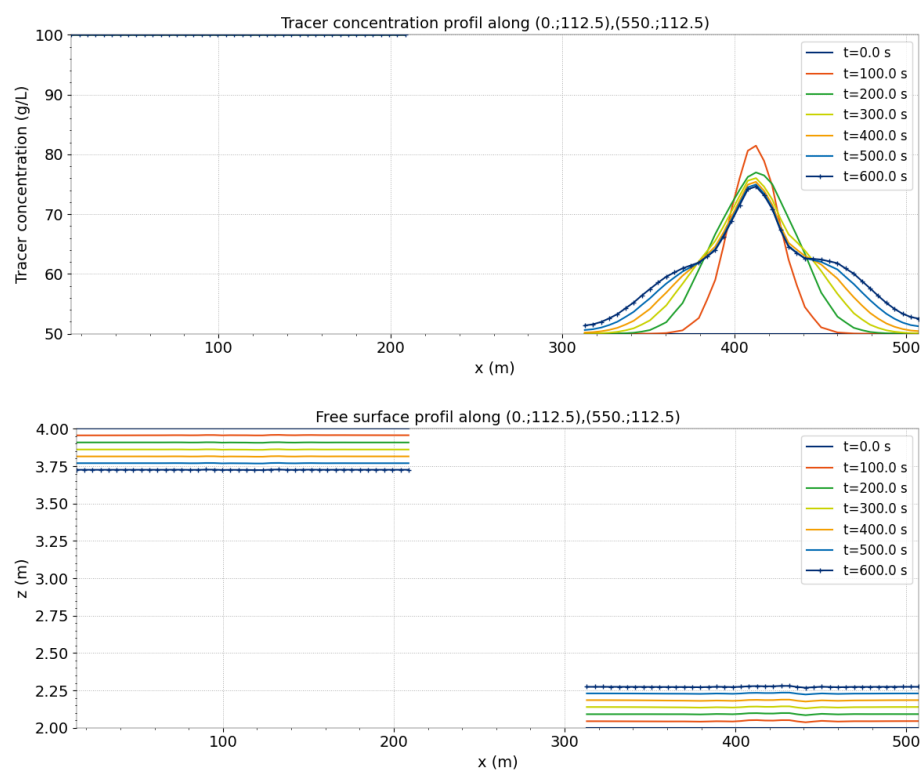


Figure 46.3: Evolution of the tracer concentration, and evolution of the free surface elevation in time in both tanks.

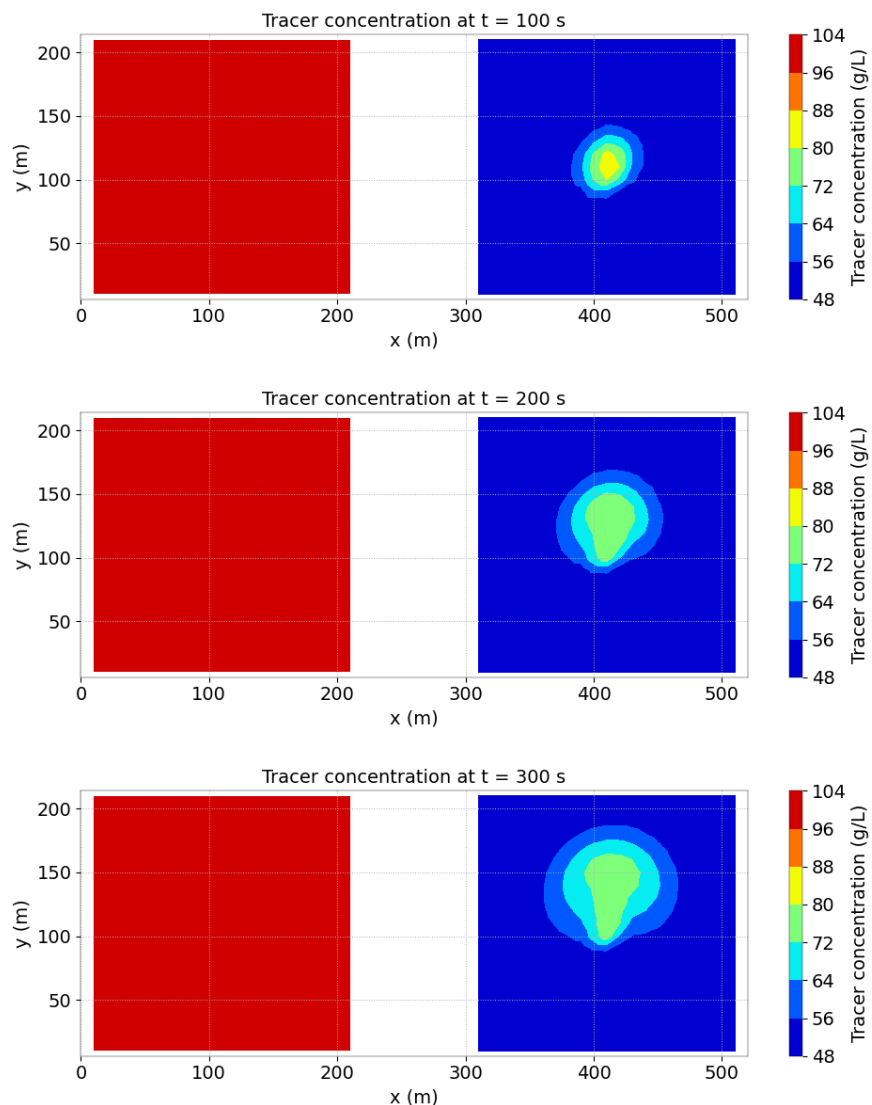


Figure 46.4: Evolution of the tracer concentration in time in both tanks.

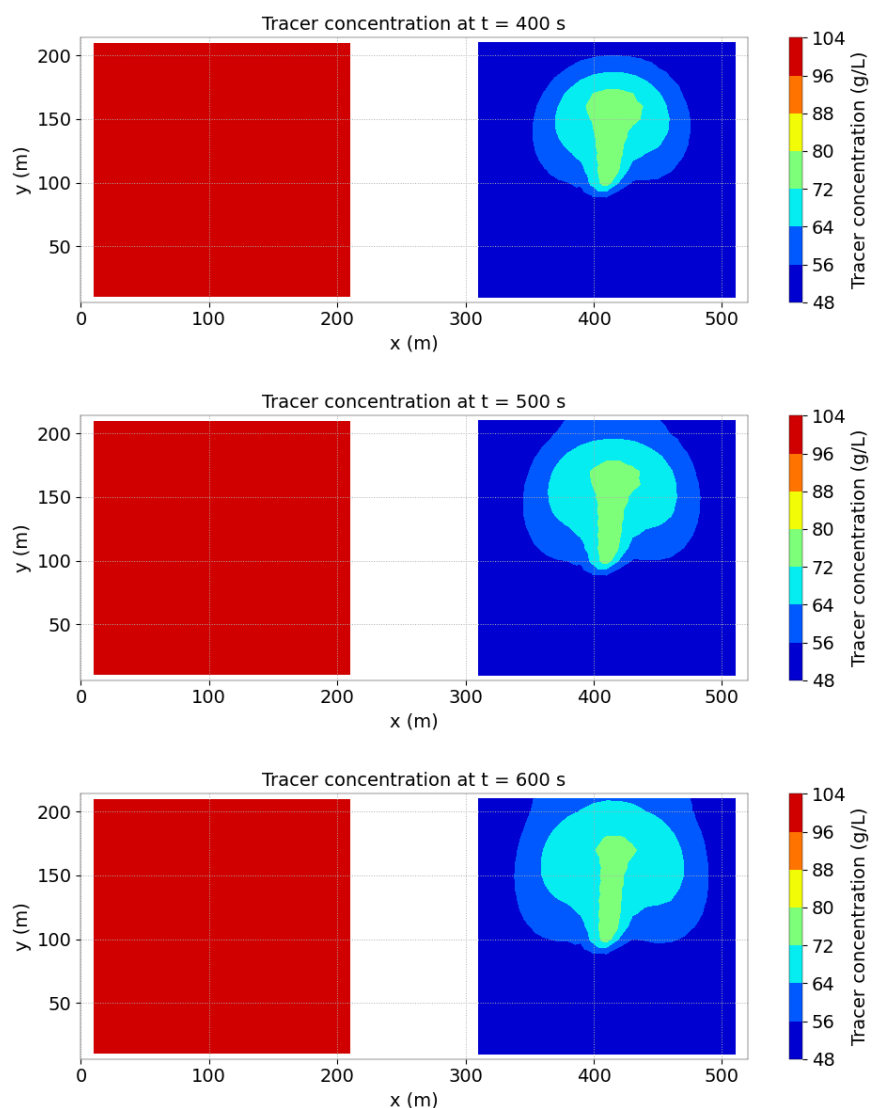


Figure 46.5: Evolution of the tracer concentration in time in both tanks.

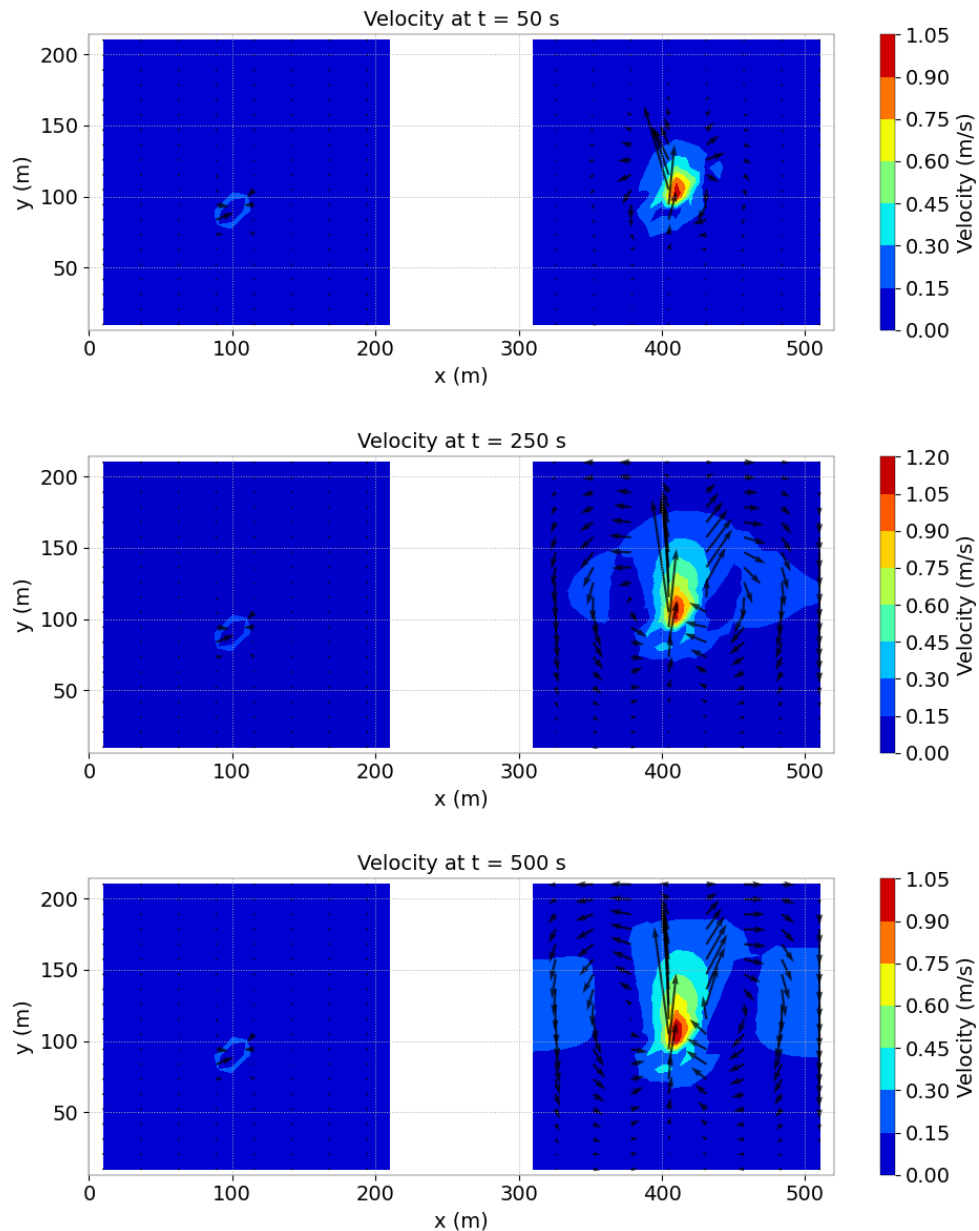


Figure 46.6: Evolution of velocity field in time in both tanks.

## 47. swash\_solution

### 47.1 Description

The configuration is a 8 m long and 0.5 m wide rectangle.

#### 47.1.1 Geometry and mesh

The mesh is made of 7,317 elements and 3,908 nodes (see Figure 47.1).

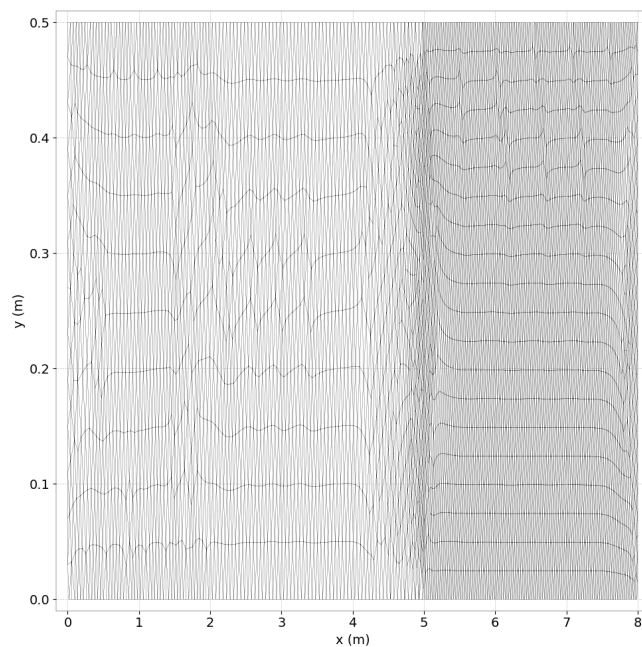


Figure 47.1: Mesh of the study.

Figure 47.2 displays the bathymetry.

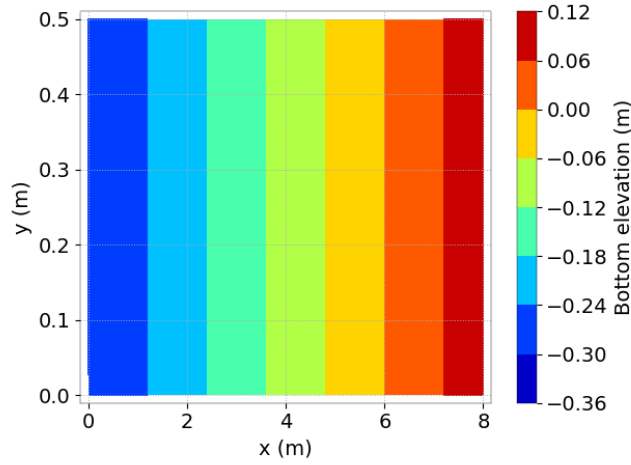


Figure 47.2: Bathymetry of the study.

### 47.1.2 Boundaries

Figure 47.3 shows the boundaries of the study.



Figure 47.3: Boundaries of the study.

Wave generated for  $x > 6$  m:

$$H(x) = \frac{x}{20} + \frac{0.05}{\cos(\arctan(0.05))} \quad (47.1)$$

Bottom: No bottom friction

### 47.1.3 Physical parameters

Turbulence: Constant viscosity equal to zero

### 47.1.4 Numerical parameters

- Type of element: P1 triangle for  $h$  and for velocity,
- Type of advection: Implicit N scheme on non conservative equation + SUPG decentring on velocities PSI distributive scheme, mass-conservative + modified SUPG on depth,
- Solver: GMRES,
- Accuracy:  $10^{-4}$ ,
- Finite volume scheme: Kinetic order 2,
- Implicitation for depth: 1,

- Implicitation for velocity: 0.6.

Time data:

- Desired Courant number = 0.8,
- Simulation duration: 12 s.

## 47.2 Results

Figure 47.4 shows the velocity vectors.

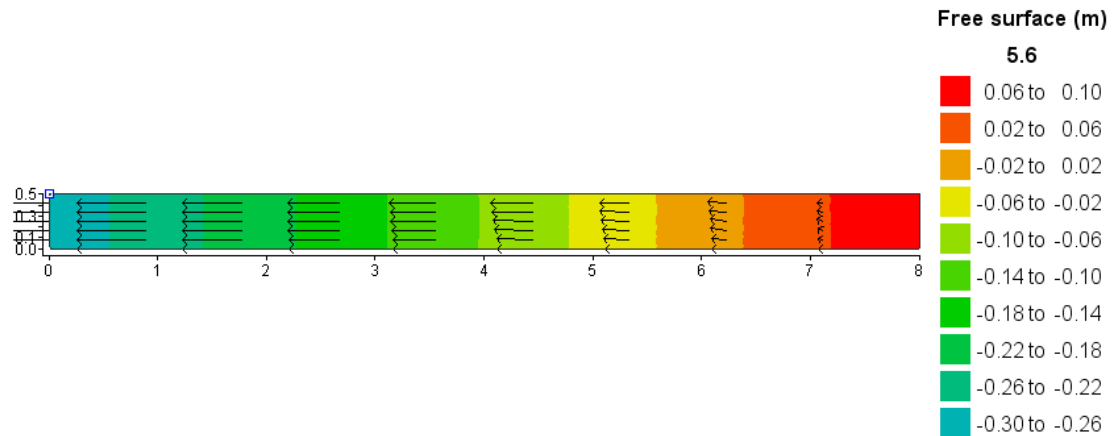


Figure 47.4: Velocity vectors and free surface.

We then compare the model and the analytical solution free surface.

Figure 47.5 shows the comparison for the free surface.

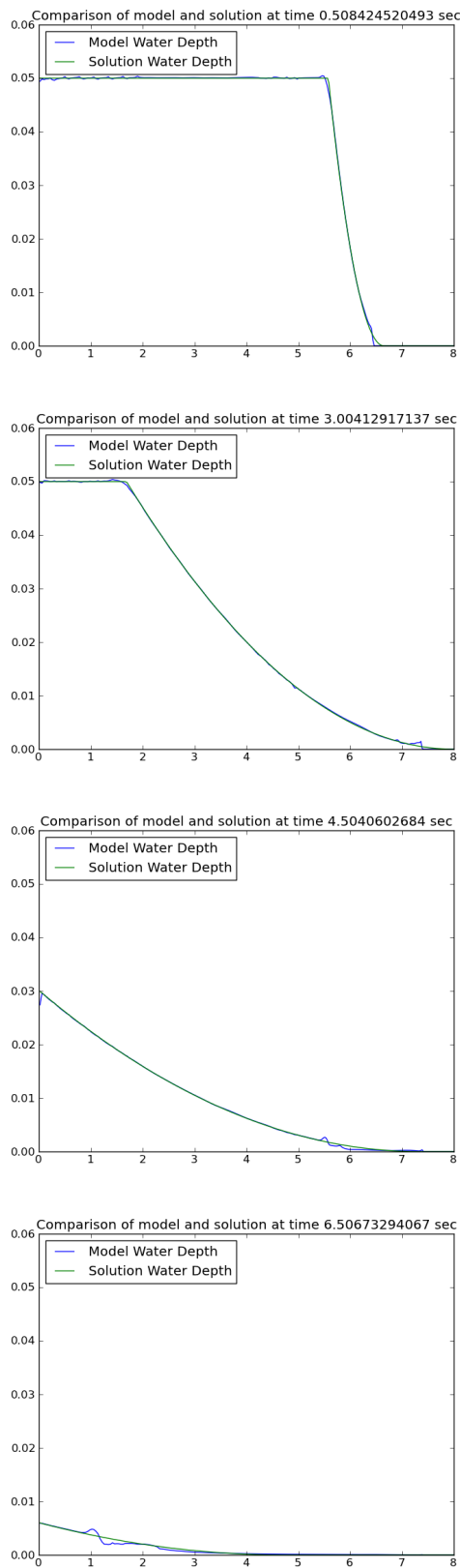


Figure 47.5: Comparison of the results.

Figure 47.6 shows the comparison for the velocity.

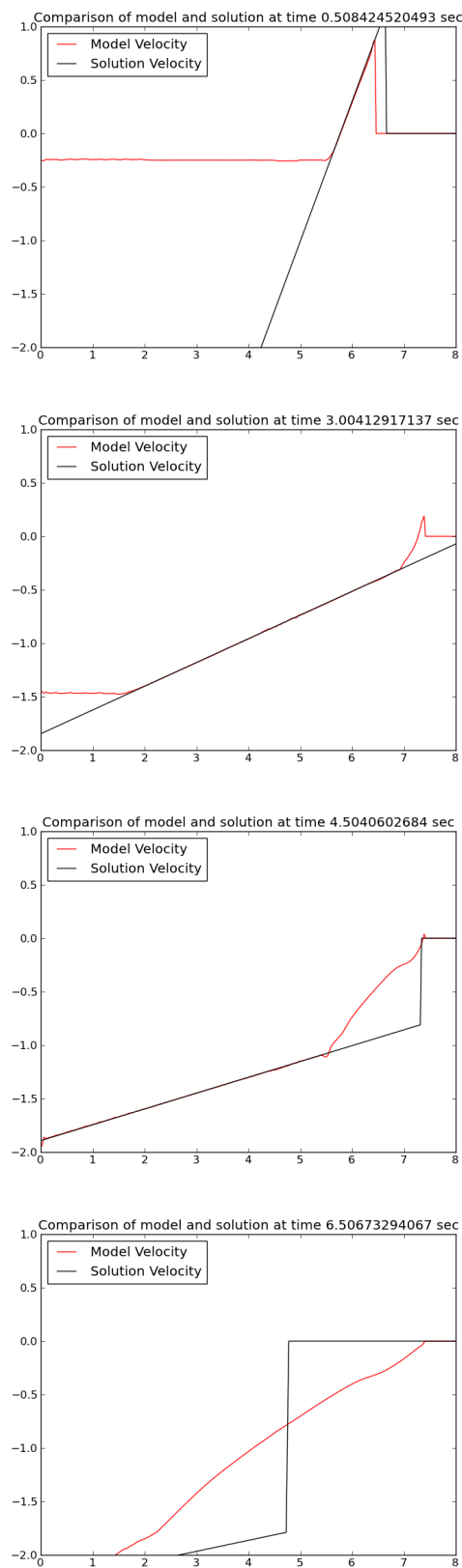


Figure 47.6: Comparison of the results for the velocity.

## 48. Solitary wave run-up (tests\_channel)

### 48.1 Purpose

This project aims to simulate the solitary wave run-up tests described in Synolakis in 1986 [28] and in 1987 [29] using a range of numerical models. Those tests were performed in a wave flume with a model beach of slope 1:19.85. Solitary waves were generated at a distance of 14.68 m from the toe of the model beach.

A similarly sized domain will be created using a numerical model. Solitary waves be generated at the boundary, allowed to propagate through the domain and run-up will be extracted. The extracted values of run-up can then be compared to the physical modelling data and assessment made of the model accuracy.

### 48.2 Description

The configuration is a 50 m long and 1 m large channel.

#### 48.2.1 Geometry and mesh

Figure 48.1 shows the geometry of the study.

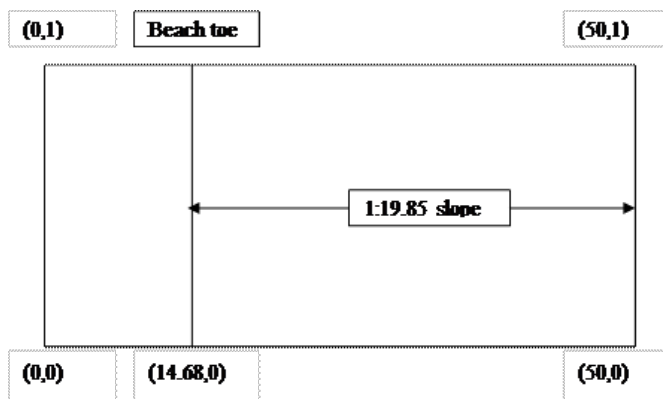


Figure 48.1: Geometry of the study.

The mesh is made of 20,000 regular triangles and 11,011 nodes (see Figure 48.2).

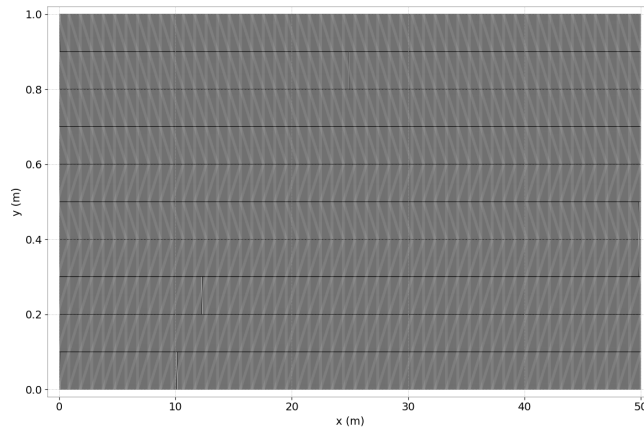


Figure 48.2: Mesh of the study.

Figure 48.3 shows the bathymetry of the study.

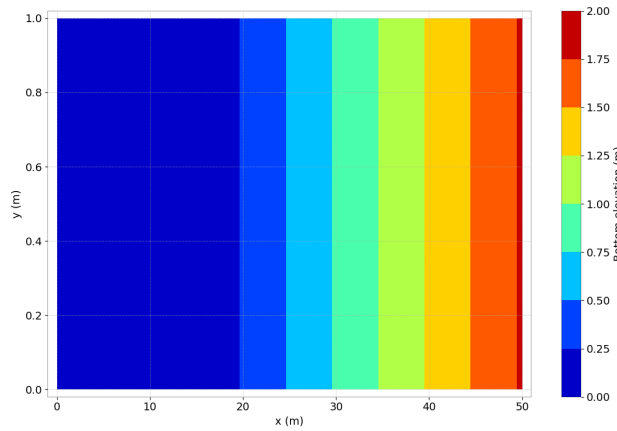


Figure 48.3: Bathymetry of the study.

### 48.2.2 Boundaries

Solid Wall all around.

Solitary wave :

$$\eta(0, t) = H \operatorname{sech}^2(\gamma c(t - T_1)) \text{ with } \gamma = \left(\frac{3H}{4d^3}\right) \text{ and } c = \sqrt{gd} \left(1 + \frac{H}{2d} - \frac{3H^2}{20d^2}\right)$$

Figure 48.4 gives a list of parameters of the simulations.

### 48.2.3 Numerical parameters

#### 48.3 Results

The results obtained with TELEMAC-2D simulation and Synolakis for cases 1, 2 and 3 are presented in Table 1. The TELEMAC-2D wave run up results versus the physical model results are presented in the scatter plot with the empirical relationships obtained by Synolakis displayed for reference.

##### 48.3.1 Case 1

It can be seen, from Table 48.1 and Figure 3 that the maximum run-up values are in reasonable agreement with the values obtained by Synolakis. The finite volume (with friction) and hybrid solution methods are in excellent agreement with the experimental value.

| Runs                           |        | Case 1 |   |   |   |   |   | Case 2 |   |   |   |   |   | Case 3 |   |   |   |   |
|--------------------------------|--------|--------|---|---|---|---|---|--------|---|---|---|---|---|--------|---|---|---|---|
|                                |        | 1      | 2 | 3 | 4 | 5 | 6 | 1      | 2 | 3 | 4 | 5 | 6 | 1      | 2 | 3 | 4 | 5 |
| Solitary waves                 | 0.0185 | X      | X | X | X | X | X |        |   |   |   |   |   |        |   |   |   |   |
| Conditions                     | 0.0390 |        |   |   |   |   |   | X      | X | X | X | X | X |        |   |   |   |   |
| H/d =                          | 0.2860 |        |   |   |   |   |   |        |   |   |   |   |   | X      | X | X | X | X |
| Friction                       | none   | X      | X | X |   |   |   | X      | X | X |   |   |   | X      | X | X | X | X |
| Chezy                          | Chezy  |        |   |   | X | X | % |        | % | % | X | X | % |        |   |   |   | X |
|                                | 0.001  | %      | % | % | X | X | % | %      | % | % | X | X | % | %      | % | % | % | X |
| Finite element solution method |        | X      |   |   |   |   |   | X      |   |   |   |   |   | X      |   |   |   |   |
| Finite volume solution method  |        |        | X |   |   |   |   |        | X |   |   |   |   |        | X |   |   |   |
| Boussinesq solution method     |        |        |   | X |   |   |   |        |   | X |   |   |   |        |   | X |   |   |
| Hybrid Boussinesq Part         |        |        |   |   | X |   |   |        |   |   | X |   |   |        |   |   | X |   |
| Hybrid Finite volume part      |        |        |   |   |   | X |   |        |   |   |   | X |   |        |   |   |   | X |
| Time step                      | 0.1    |        | X | X | X |   |   |        | X | X | X |   |   |        | X | X | X | X |
|                                | 0.05   | X      | X | X | X |   |   | X      |   | X |   | X |   | X      | X | X | X |   |
|                                | 0.035  |        |   |   | X |   |   |        |   |   |   | X |   |        |   |   |   |   |
| Duration                       | 60     | X      | X | X | X |   |   | X      | X | X | X |   |   | X      | X | X | X |   |
|                                | 38     |        |   |   |   | X |   |        |   |   |   | X |   |        |   |   |   |   |
|                                | 21     |        |   |   |   |   | X |        |   |   |   |   | X |        |   |   |   |   |
|                                | 40     |        |   |   |   |   |   |        |   |   |   |   |   |        |   |   |   | X |
| Implications                   | 0.53   |        |   |   |   |   |   |        |   |   |   |   |   |        |   | X | X |   |

Figure 48.4: List of parameters.

|   | Case         | Wave Run-up (R/d) |       |            |                       |  |        |
|---|--------------|-------------------|-------|------------|-----------------------|--|--------|
|   | Synolakis    | FE                | FV    | Boussinesq | FV with $C_f = 0.001$ |  | Hybrid |
| 1 | 0.076, 0.078 | 0.068             | 0.084 | 0.068      | 0.077                 |  | 0.076  |
| 2 | 0.162        | 0.103             | 0.199 | 0.107      | 0.155                 |  | 0.156  |
| 3 | 0.513        | 0.148             | 0.497 | 0.135      | -                     |  | 0.535  |

Table 48.1: Maximum run-up (experiments and simulations).

Figure 48.5 shows the comparison with the benchmark data.

### 48.3.2 Case 2

The results in this case follow a broadly similar pattern to that obtained for Case 1, presented above. Again a hybrid solution method is essential to model accurately all phases of the wave profile development.

### 48.3.3 Case 3

Figure 48.6 shows the results for the case 3.

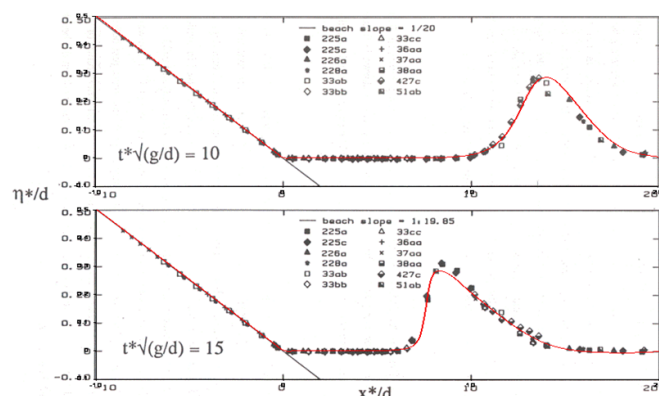


Figure 48.6: Velocity vectors over the free surface.

Figure 48.7 shows the results for the case 3.

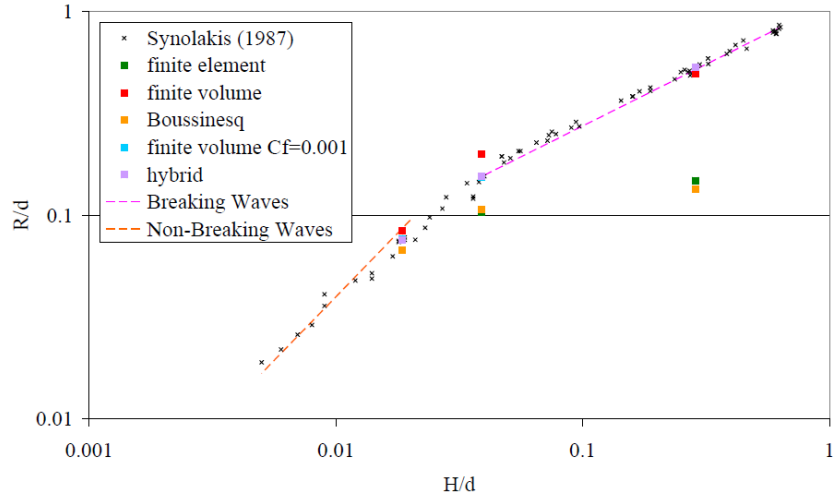


Figure 3 TELEMAC2D simulated maximum run-up values

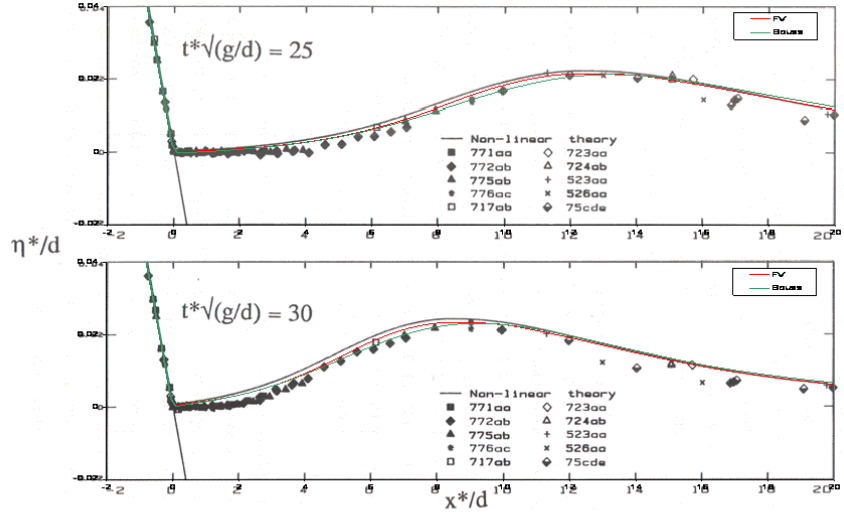


Figure 4 Boussinesq and finite volume profiles as wave approaches model beach

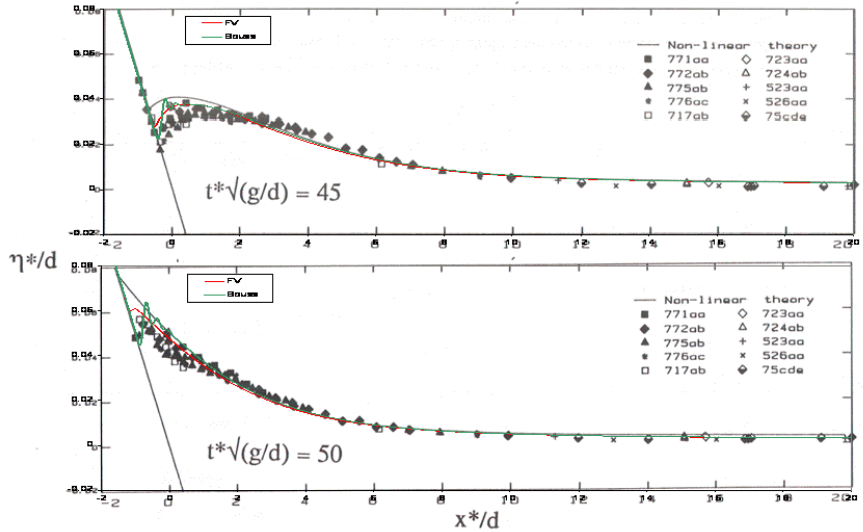


Figure 5 Boussinesq and finite volume profiles during wave run-up

Figure 48.5: Comparison with the benchmark data.

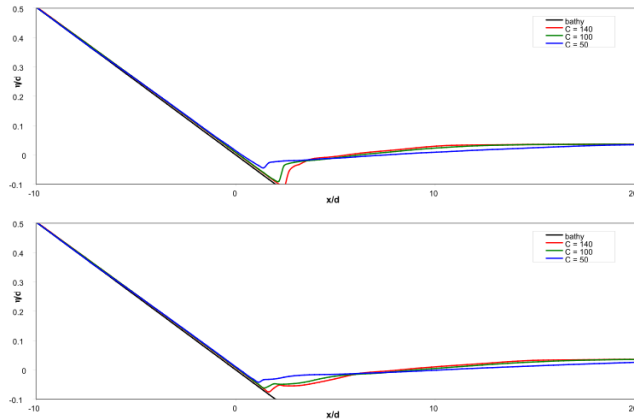


Figure 48.7: Chézy friction factors of 140, 100 and 50 (which correspond to  $C_f$  values of 0.001, 0.002 and 0.008 respectively).

Chézy friction factors of 140, 100 and 50  $\text{m}^{1/2}/\text{s}$  (which correspond to  $C_f$  values of 0.001, 0.002 and 0.008 respectively).

The inadequacy of the finite element and Boussinesq solution methods for this case is clear from inspection of Table 48.1 and Figure 3. The finite volume method appears to perform better (from consideration of the run-up value alone) but, on closer inspection of the wave propagation, it can be seen that the wave shape was not adequately maintained, deforming significantly from the input profile before reaching the beach slope. All three solving methods result in a dramatic reduction in the peak wave height before the wave reaches the beach slope.

The hybrid method performed better, with a good representation of the wave approach and run-up. The wave run-down was less well modelled, with the thickness of the fluid layer being badly reproduced. It was theorised that the friction factor used is not large enough and so a sensitivity study was performed using Chézy friction factors. It was found however that increasing the friction factor had very little impact on the thickness of the fluid layer in the wave run-down phase, and reduced the magnitude of the hydraulic jump attained as the wave ran down the slope.

#### 48.4 Conclusion

Only hybrid method can capture the development of the wave on the flat bed and model beach and match the maximum run-up:

- Point of wave breaking needs to be decided a posteriori,
- Tuning of the numerical Boussinesq solution method is required to propagate large waves,
- Friction is crucial to limit run-up.

## 49. Wet and dry moving transitions (thacker)

### 49.1 Purpose

Thacker test cases illustrate that TELEMAC-2D is able to simulate wet/dry moving transitions (comings and goings) over a variable slope. It is also useful to check the numerical diffusion and mass conservation, as the water height is periodic in time.

### 49.2 Description

#### 49.2.1 Thacker analytical solutions

##### Rotation of a planar surface in a parabolic bowl

This Thacker solution consists of a planar surface rotating in a paraboloid reservoir without friction for which analytical solution exists in the bibliography. The free surface has a periodic motion and remains planar in time. The bathymetry of the paraboloid reservoir is defined on a square domain of width  $L$ , as follows:

$$z(r) = -H_0 \left( 1 - \frac{r^2}{a^2} \right), \quad (49.1)$$

Where  $r(x,y) = \sqrt{(x-L/2)^2 + (y-L/2)^2}$  for each  $(x,y)$  in  $[0;L] \times [0;L]$ . The bathymetry is illustrated in Figure 49.1. For the defined bathymetry, the analytical solution of the studied case is given by:

$$\begin{cases} h(x,y,t) = \frac{\eta H_0}{a^2} \left( 2 \left( x - \frac{L}{2} \right) \cos(\omega t) + 2 \left( y - \frac{L}{2} \right) \sin(\omega t) - \eta \right) - z(x,y) \\ u(x,y,t) = -\eta \omega \sin(\omega t) = -U_0 \sin(\omega t) \\ v(x,y,t) = \eta \omega \cos(\omega t) = U_0 \cos(\omega t) \end{cases} \quad (49.2)$$

where  $H_0$  is the water depth at the central point of the domain for a zero elevation,  $a$  is the distance from the central point to the zero elevation of the shoreline and  $\eta$  is a parameter. In our specific case, we choose  $L = 4$  m,  $H_0 = 0.1$  m,  $a = 1$  m and  $\eta = 0.5$  m. The angular frequency  $\omega$  can therefore be calculated as  $\omega = \sqrt{2gH_0}/a = 1.4 \text{ rad.s}^{-1}$ , and the period of the free surface evolution is consequently  $T = \frac{2\pi}{\omega} = 4.49$  s. Furthermore, the amplitude of the flow velocity is  $U_0 = \eta \omega = 0.70 \text{ m.s}^{-1}$ .

### Oscillation of a radially symmetrical paraboloid

This second analytical solution of Thacker presented in this test case consists of an oscillating paraboloid surface radially symmetrical without friction. The bathymetry is the same as the planar thacker solution and the analytical solution is given by:

$$\begin{cases} h(r,t) = H_0 \left( \frac{\sqrt{1-A^2}}{1-A \cos(\omega t)} - 1 - \frac{r^2}{a^2} \left( \frac{1-A^2}{(1-A \cos(\omega t))^2} - 1 \right) \right) - z(r) \\ u(x,y,t) = \frac{1}{1-A \cos(\omega t)} \left( \frac{1}{2} \omega \left( x - \frac{L}{2} \right) A \sin(\omega t) \right) \\ v(x,y,t) = \frac{1}{1-A \cos(\omega t)} \left( \frac{1}{2} \omega \left( y - \frac{L}{2} \right) A \sin(\omega t) \right) \end{cases} \quad (49.3)$$

where  $H_0$  is the water depth at the central point of the domain for a zero elevation,  $a$  is the distance from the central point to the zero elevation of the shoreline and  $r_0$  is the distance from the central point to the point where shoreline is initially located and  $A = (a^2 - r_0^2)/(a^2 + r_0^2)$ . In our specific case, we choose  $L = 4$  m,  $H_0 = 0.1$  m,  $a = 1$  m and  $r_0 = 0.5$  m. The angular frequency  $\omega$  can therefore be calculated as  $\omega = \sqrt{8gH_0/a} = 2.80$  rad, and the period of the free surface evolution is consequently  $T = \frac{2\pi}{\omega} = 2.24$  s.

#### 49.2.2 Geometry, mesh and bathymetry

The computational domain is a  $4 \text{ m} \times 4 \text{ m}$  square. A triangular regular mesh is constructed with 19,800 triangular elements and 10,100 nodes (see Figure 49.1):

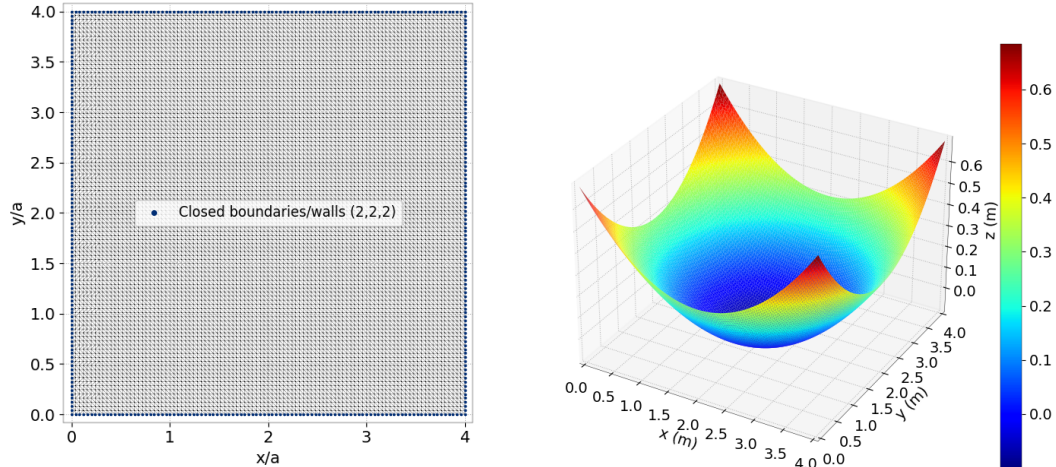


Figure 49.1: 2D-mesh (left) and bathymetry (right) of the Thacker case.

#### 49.2.3 Initial conditions

The water depth and velocities are initialized at time  $t = 0.0$  s with the analytical solution (Eq. 49.2) and (Eq. 49.3) depending on the test case.

#### 49.2.4 Boundary conditions

The boundaries are solid walls everywhere. There is no friction on the solid walls.

#### 49.2.5 Physical parameters

The molecular viscosity is set as constant and equal to  $0 \text{ m}^2/\text{s}$  (VELOCITY DIFFUSION = 0.) and no friction is set to the bottom.

### 49.2.6 Numerical parameters

For this test case, duration is set to 10 s and several numerical schemes of advection for velocities are confronted. The solver used is the conjugate gradient with an accuracy of  $10^{-8}$ . For finite element schemes the treatment of the linear system is set to wave equation (TREATMENT OF THE LINEAR SYSTEM = 2). The parameters specific to each case are summed up in Table 49.1.

| Case | Name | Equations       | Advection scheme for velocities | Time-step / Desired Courant number |
|------|------|-----------------|---------------------------------|------------------------------------|
| 1    | CHAR | Wave Eq. FE     | Characteristics                 | 0.005 s / -                        |
| 2    | NERD | Wave Eq. FE     | Edge-based n-scheme             | 0.005 s / -                        |
| 3    | ERIA | Wave Eq. FE     | ERIA scheme                     | 0.005 s / -                        |
| 4    | HLLC | Saint-Venant FV | HLLC order 1                    | - / 0.8                            |
| 5    | KIN1 | Saint-Venant FV | Kinetic order 1                 | - / 0.8                            |
| 6    | WAF  | Saint-Venant FV | WAF                             | - / 0.8                            |

Table 49.1: List of the simulation parameters used for the six cases tested in the Thacker example.

## 49.3 Results - Rotation of a planar surface in a parabolic bowl

### 49.3.1 First observation

The water planar surface moves anticlockwise. Evolution of water depth and velocity during one rotation is illustrated in Figures 49.2 and 49.3.

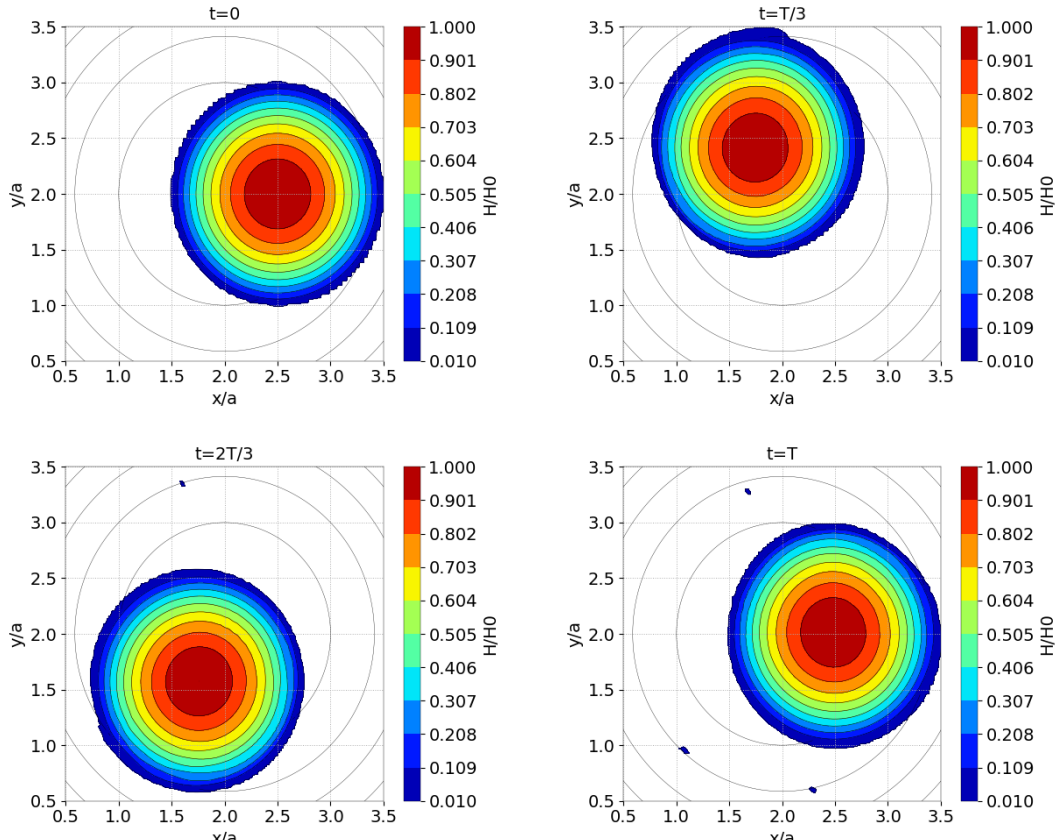


Figure 49.2: Water depth for one rotation of the Thacker case with NERD scheme.

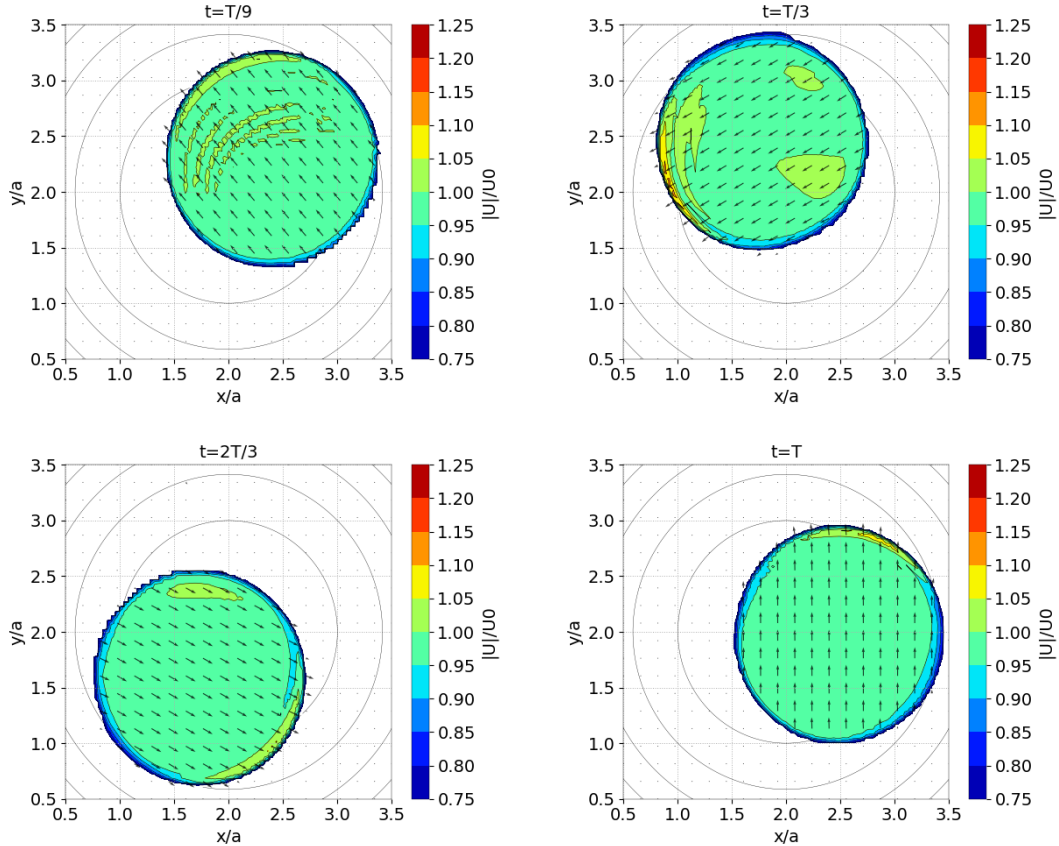


Figure 49.3: Velocity norm and vector field of the Thacker case with NERD scheme.

#### 49.3.2 Computation time

Simulation times for each of these cases with sequential and parallel runs (using 4 processors) are shown in Figure 49.4<sup>1</sup>. The WAF case is run only in scalar mode because the parallel version is not implemented yet.

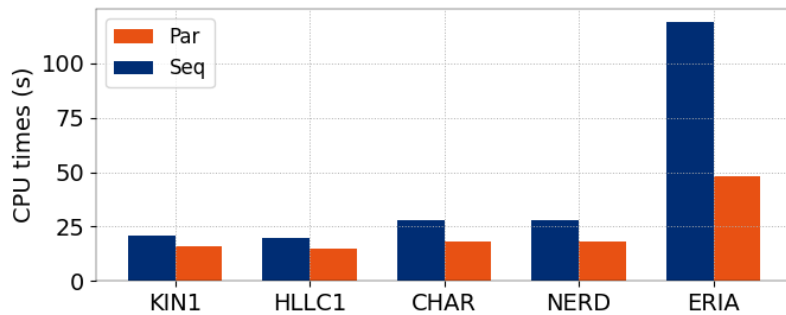


Figure 49.4: CPU times.

In general, the finite-volume schemes are much faster than the finite-element ones with the chosen parameters. This is to be put in perspective with the better accuracy of the NERD and ERIA schemes, which actually perform sub-iterations during each time-step. This performance

<sup>1</sup>Keep in mind that these times are specific to the validation run and the type of processors that were used for this purpose.

comparison is thus biased and should be interpreted carefully. In the example we did not seek the best accuracy for each scheme, which would have provided us with a different performance result. The NERD scheme is faster than the ERIA scheme, which is expected since ERIA is a more elaborate version of NERD that provides better accuracy.

### 49.3.3 Comparison of schemes

In order to evaluate the accuracy of the tested advection schemes, the results are compared to the analytical solution (49.2). A first visual comparison in time can be found in Figure 49.5. The analytical solution is represented by the light red coloured area.

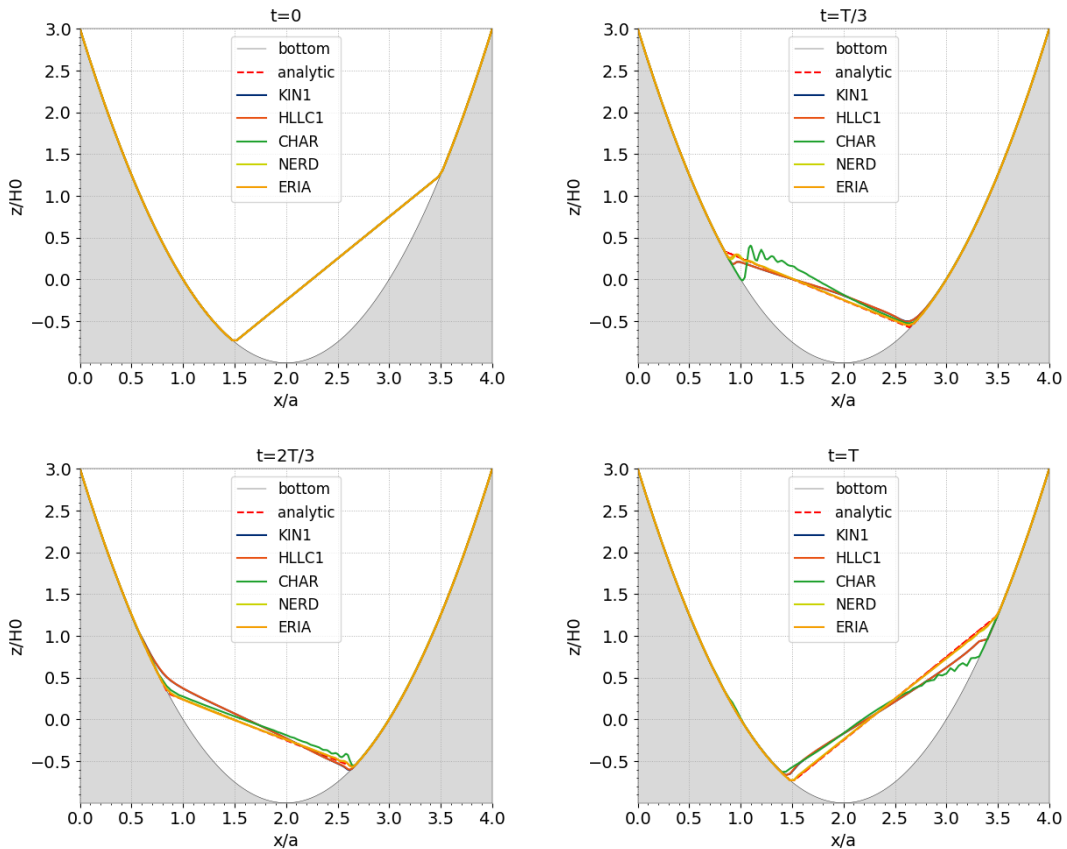


Figure 49.5: Comparison of free surface with analytical values on the Thacker case.

In Figures 49.6 and 49.7 some comparisons of water depth and velocity field are presented. Elements where water depth is lower than 1 mm have been masked.

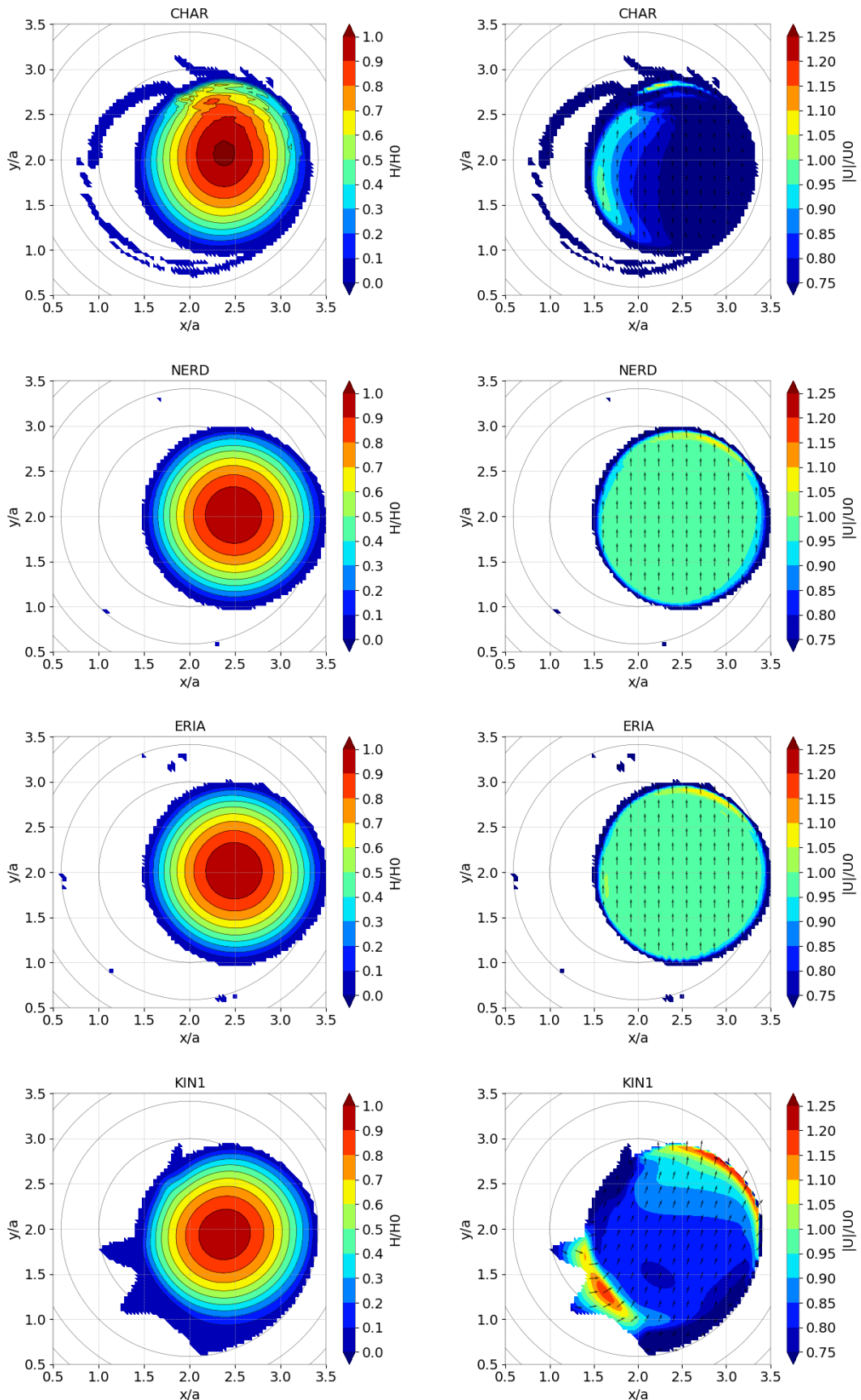


Figure 49.6: Comparison of water depth and velocity after one rotation.

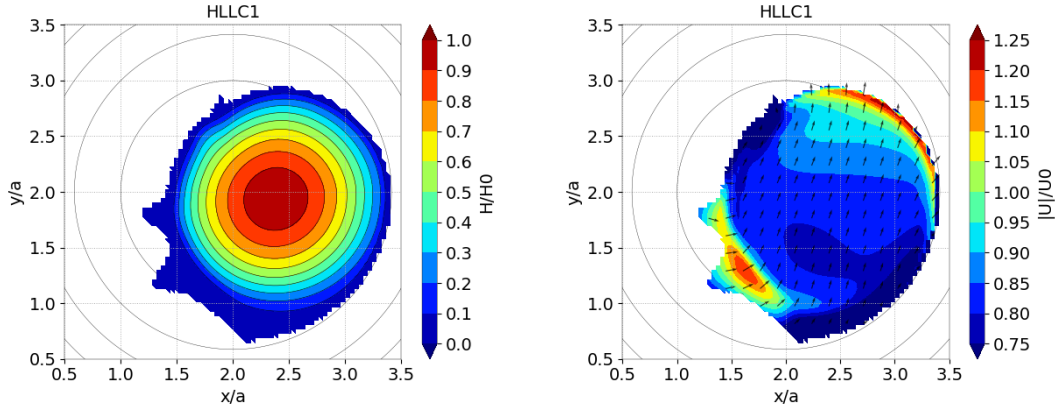
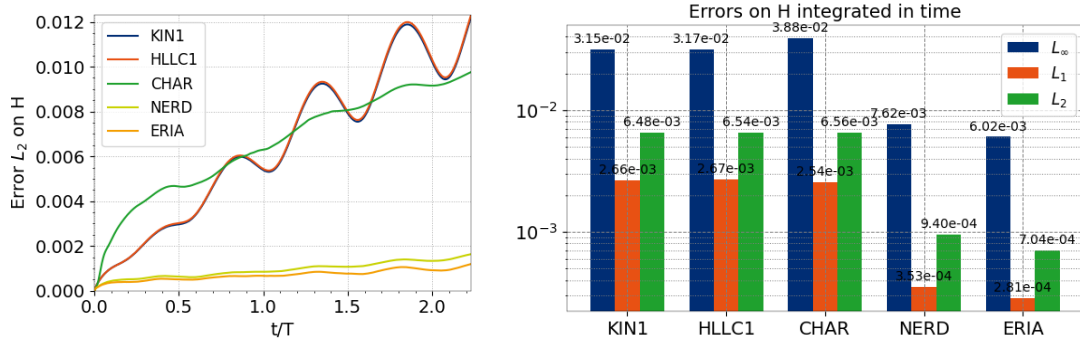
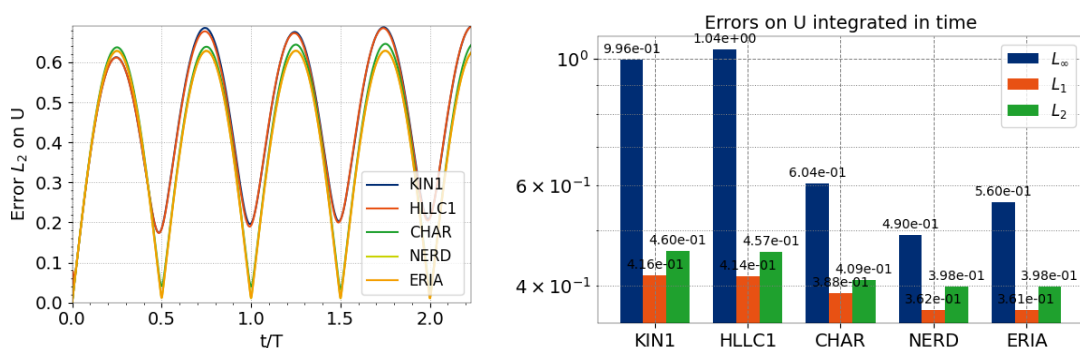


Figure 49.7: Comparison of water depth and velocity after one rotation.

#### 49.3.4 Accuracy

For a more quantitative comparison of schemes, the  $L^1$ ,  $L^2$  and  $L^\infty$  error norms of the water depth and velocity are calculated at each time step for each scheme.  $L^2$  errors time series and time integrated  $L^1$ ,  $L^2$  and  $L^\infty$  errors are presented in Figures 49.8, 49.9 and 49.10 for  $H$ ,  $U$  and  $V$  respectively.

Figure 49.8: Error on  $H$ : timeseries (left) and integrated over time (right).Figure 49.9: Error on  $U$ : timeseries (left) and integrated over time (right).

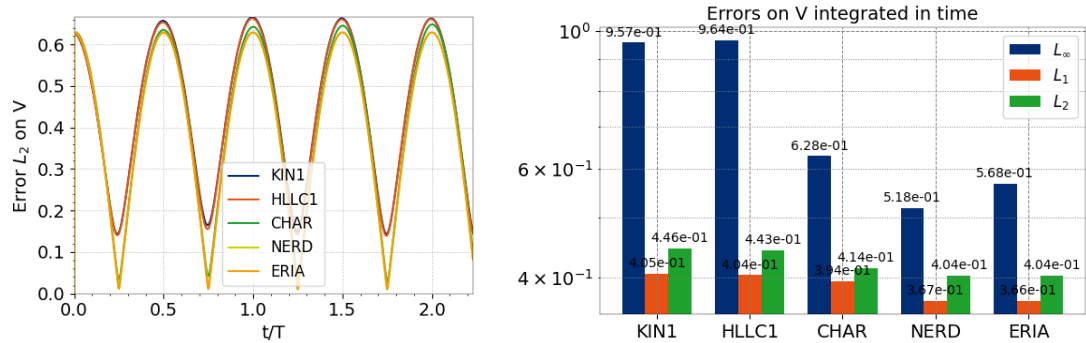


Figure 49.10: Error on  $V$ : timeseries (left) and integrated over time (right).

CHAR scheme is the least accurate for this example with the chosen time step size. Numerical diffusion is also noticeable for WAF, HLLC and KIN1 schemes, and a phase difference appears between their results and the analytical solution. NERD and ERIA are in good agreement with the analytical solution, keeping in mind that to reach that accuracy they actually perform sub-iterations.

#### 49.3.5 Positivity of water depth

The minimum value of the water depth are checked after one rotation. Results are shown in Figure 49.11. No negative values are recorded, which shows that the positivity is fulfilled. In the case of finite volume schemes, positivity is ensured without additional treatment. With finite element schemes the positivity is ensured with a treatment of negative depths during simulation (TREATMENT OF NEGATIVE DEPTHS = 2 for characteristics and NERD and 3 for ERIA scheme).

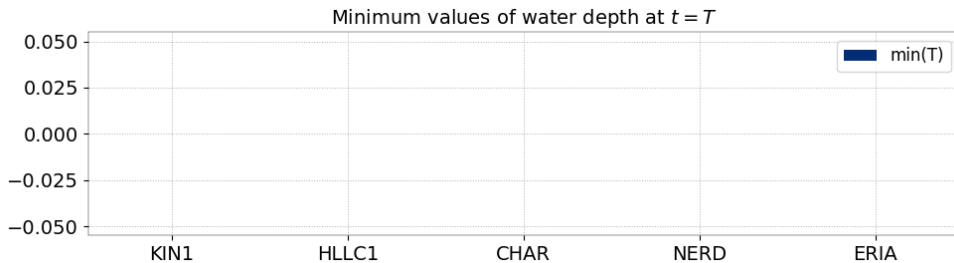


Figure 49.11: Minimum values of water depths after one rotation.

#### 49.3.6 Mass balance

Mass conservation can be checked by calculating the mass in the domain during time. The lost mass is calculated as  $M_{initial} - M_{final}$ . The evolution of mass for each of the schemes is shown in Figure 49.12. All the schemes provide a satisfying mass conservation.

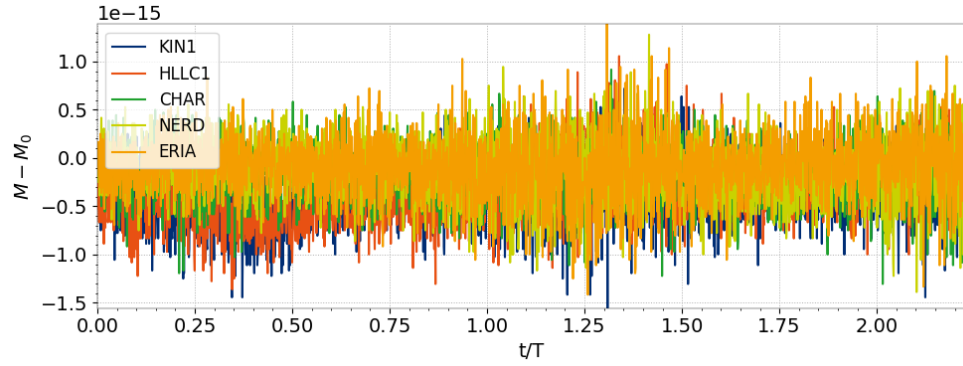


Figure 49.12: Mass loss for the tested schemes on the Thacker case.

#### 49.3.7 Energy balance

In this section, the conservation of the mean energy is checked. In fact, for the Saint-Venant equations, the quantity  $h \frac{\|U\|^2}{2} + g \frac{h^2}{2}$ , called mean or integrated energy, is conserved, where  $\|U\|$  is the Saint-Venant depth averaged velocity magnitude. The following quantities are studied:

- Integrated potential energy  $E_p = \int \int_{\Omega_{xy}} \rho_{water} g \frac{h^2}{2} dx dy$  where  $\Omega_{xy}$  is the 2D domain of simulation: Figure 49.13,
- Integrated kinetic energy  $E_c = \int \int_{\Omega_{xy}} \rho_{water} h \frac{\|U\|^2}{2} dx dy$ : Figure 49.14,
- Integrated mechanical energy  $E_m = E_p + E_c$ : Figure 49.15.

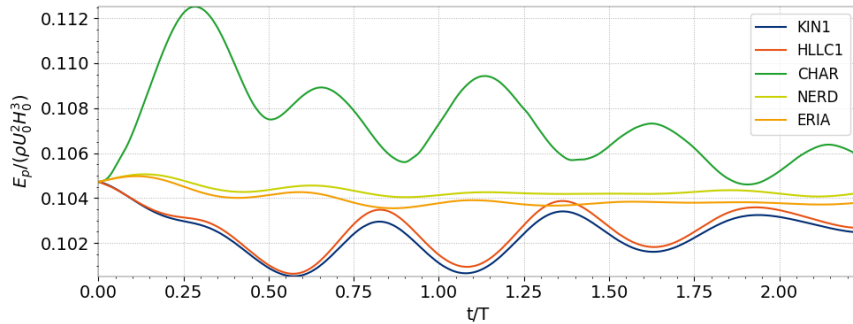


Figure 49.13: Evolution of kinetic energy for the tested schemes on the Thacker case.

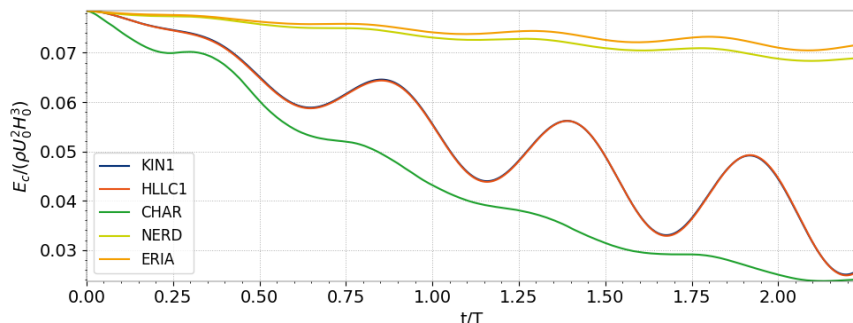


Figure 49.14: Evolution of kinetic energy for the tested schemes on the Thacker case.

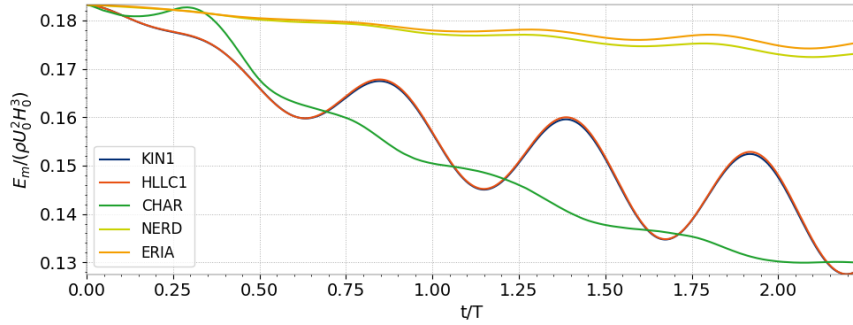


Figure 49.15: Evolution of mechanical energy for the tested schemes on the Thacker case.

The ERIA and NERD schemes seem to provide the best results. In fact, the mean energy (also called integrated, total, mechanical) is almost stable in time. But overall, all schemes included, no energy creation is observed and the mean energy in time stays lower than the initial one during the whole simulation.

#### 49.3.8 Convergence

To assess the accuracy of the schemes, computation of error on one mesh is not sufficient. In this section a mesh convergence is carried out for each numerical scheme. From a starting mesh with 121 nodes and 200 elements we divide by 4 each triangles recursively to generate new meshes. The first and last meshes used in the convergence study are presented in Figure 49.16.

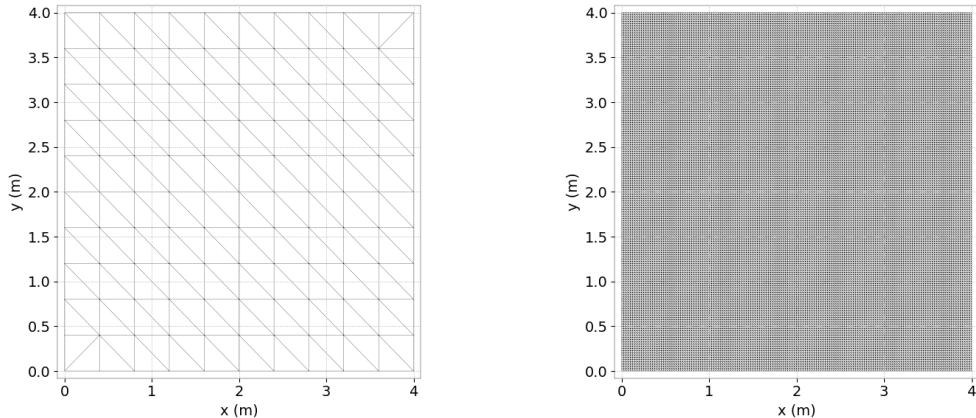
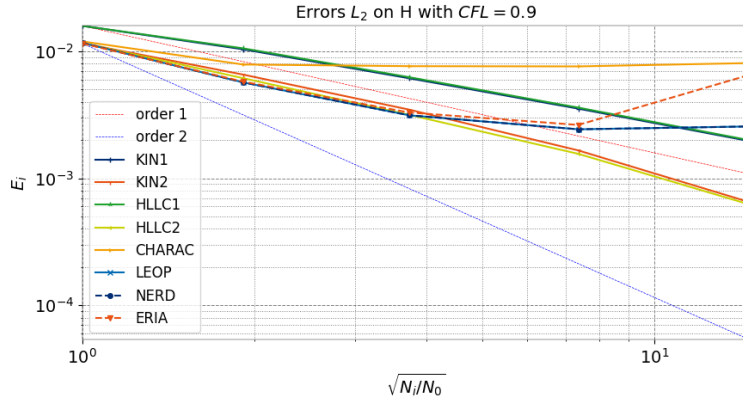
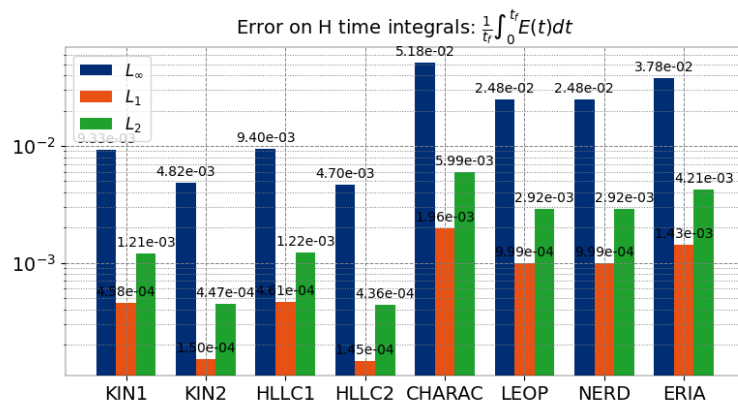


Figure 49.16: First and last meshes used in Thacker mesh convergence.

Final time is set to  $t_f = T/2$ . With decreasing space step we adjust time step to ensure a constant CFL for each mesh increment. In this section two additional numerical schemes are tested i.e. edge by edge implementation of Leo Potsma scheme (noted LEOP, scheme number 13) and second order in space kinetic scheme (noted KIN2).

Figure 49.17:  $H$  convergence in  $L^2$  norm.Figure 49.18:  $H$  time integrated errors on finest mesh.

Convergence slopes of time integrated error of  $H$  in  $L^2$  norm are compared in Figure 49.17. Time integrated errors on  $H$  on the finest mesh are presented in Figure 49.18. Convergence slopes of error in  $L^1$ ,  $L^2$  and  $L^\infty$  norm at final time are plotted for each numerical scheme in Figure 49.19.

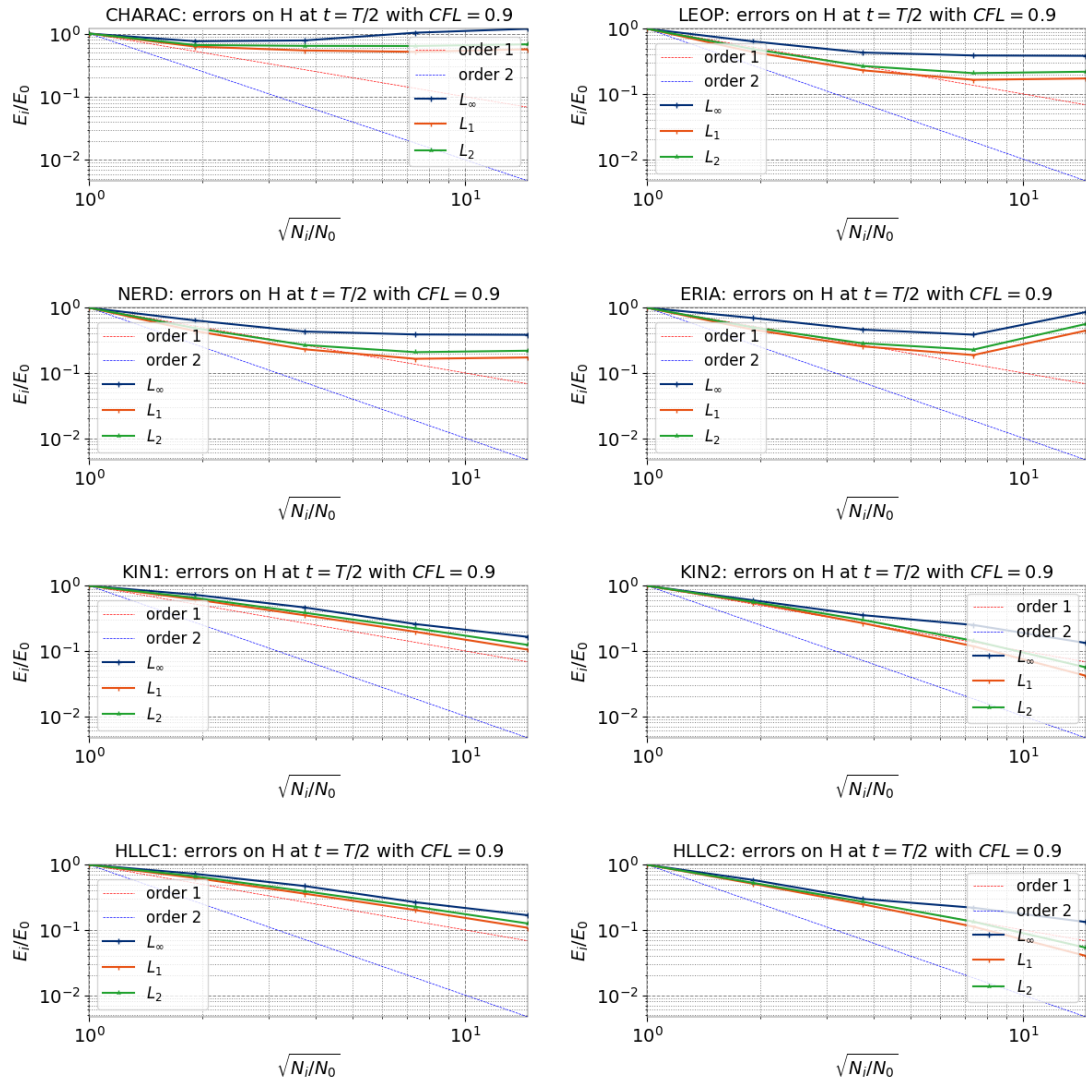


Figure 49.19:  $H$  convergence with different numerical schemes.

Finite volume schemes converge with a order of convergence near one for first order kinetic, HLLC and WAF and slightly steeper than one for second order kinetic scheme. For finite element schemes, CHAR scheme does not convergence whereas LEOP, NERD and ERIA schemes exhibit a slope of convergence comprised between one and two.

## 49.4 Results - Oscillation of a radially symmetrical paraboloid

### 49.4.1 Computation time

Simulation times for each of these cases with sequential and parallel runs (using 4 processors) are shown in Figure 49.20.

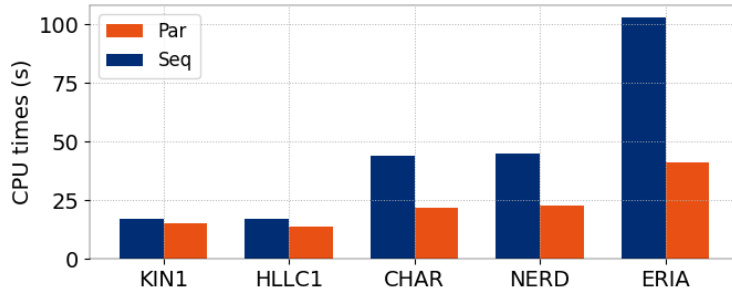


Figure 49.20: CPU times.

### 49.4.2 Comparison of schemes

In order to evaluate the accuracy of the tested advection schemes, the results are compared to the analytical solution (49.3). A first visual comparison in time can be found in Figure 49.21. The analytical solution is represented by the light blue coloured area. In Figures 49.22 and 49.23 some comparisons of water depth and velocity field are presented. Elements where water depth is inferior to 1 mm have been masked.

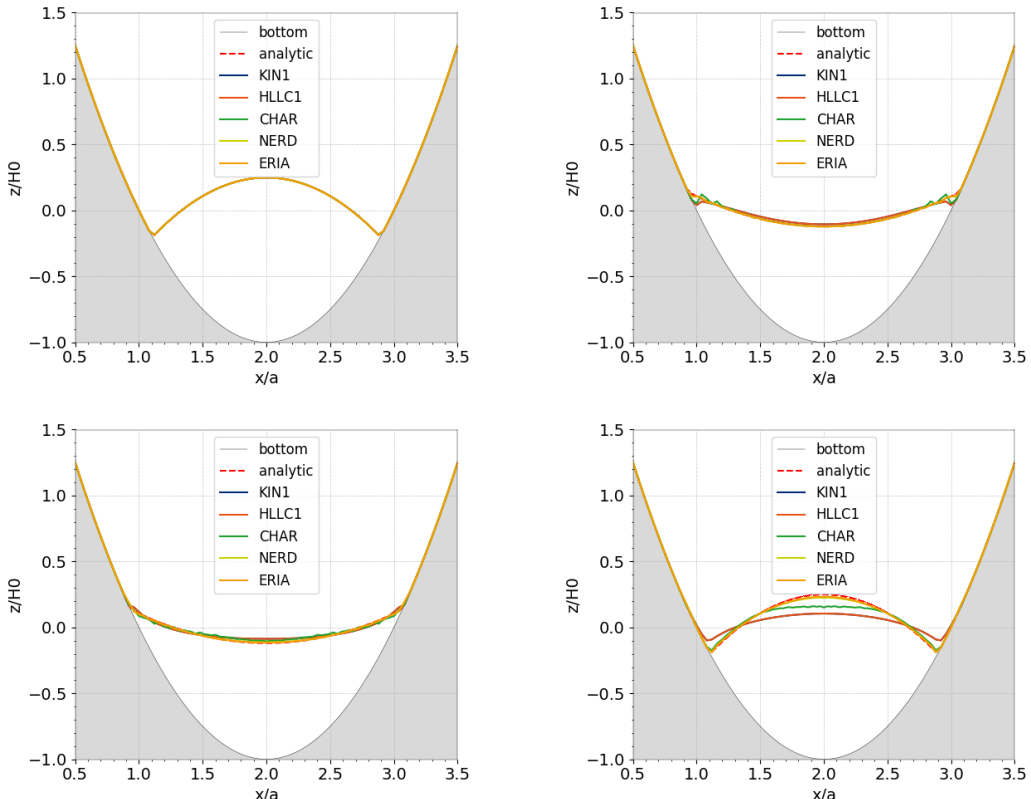


Figure 49.21: Comparison of free surface with analytical values on the Thacker case.

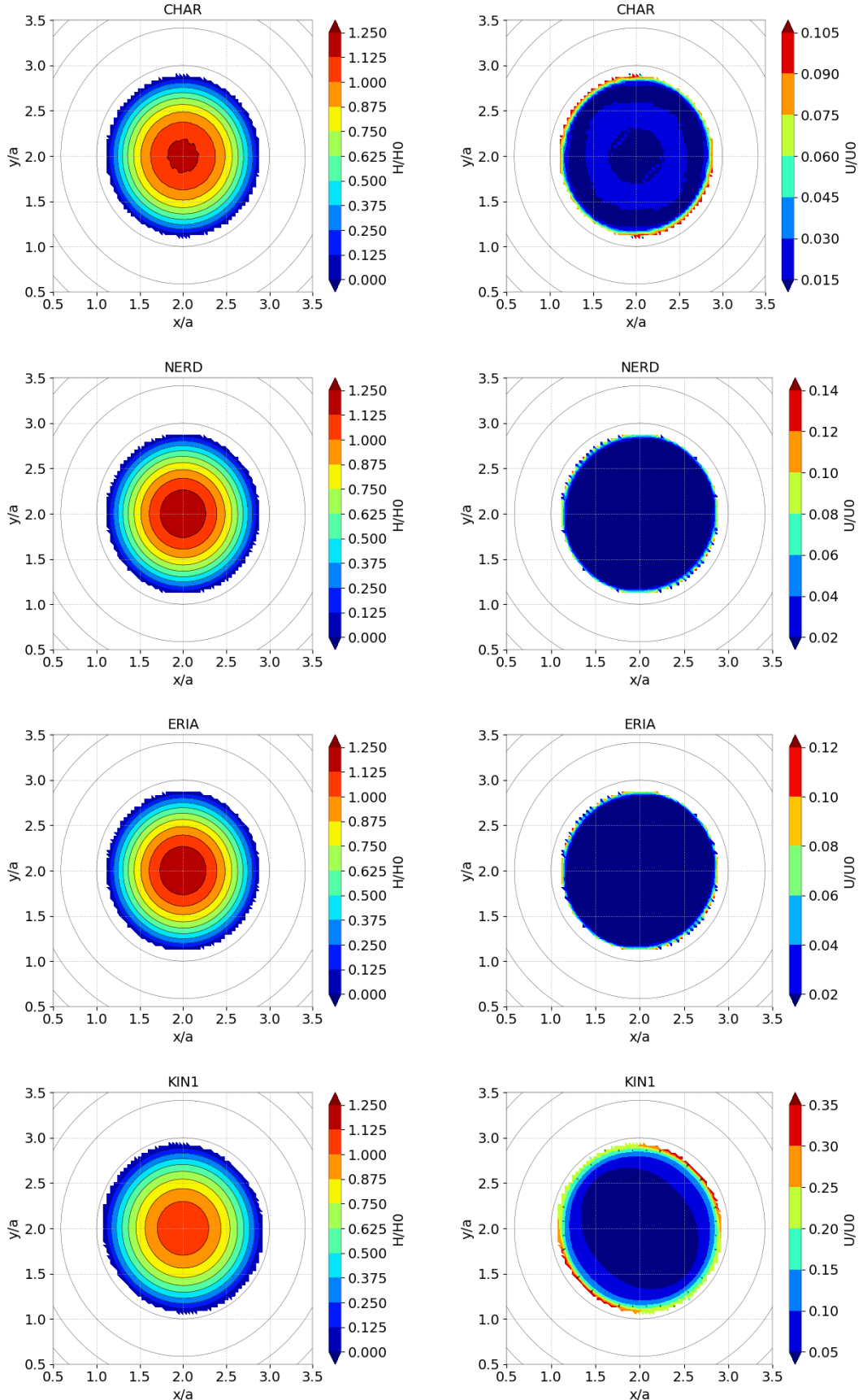


Figure 49.22: Comparison of water depth and velocity after one oscillation.

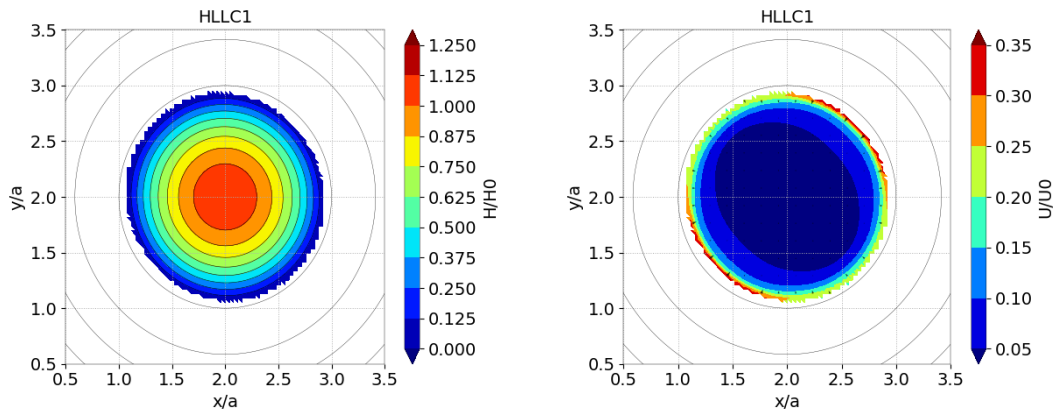


Figure 49.23: Comparison of water depth and velocity after one oscillation.

## 49.5 Conclusion

TELEMAC-2D is capable of simulating the wet/dry moving transitions with good accuracy and conservation of mass, energy and positivity of the water depth.

## 50. Propagation of tide prescribed by boundary conditions (tide)

### 50.1 Purpose

This test demonstrates the availability of TELEMAC-2D to model the propagation of tide in a maritime domain by computing tidal boundary conditions. A coastal area located in the English Channel off the coast of Brittany (in France) close to the real location of the Paimpol-Bréhat tidal farm is modelled to simulate the tide and the tidal currents over this area. Time and space varying boundary conditions are prescribed over liquid boundaries.

### 50.2 Description

#### 50.2.1 Geometry and Mesh

The geometry of the domain is almost a rectangle with the French coasts on one side (22 km  $\times$  24 km). The triangular mesh is composed of 4,385 triangular elements and 2,386 nodes (see Figure 50.1).

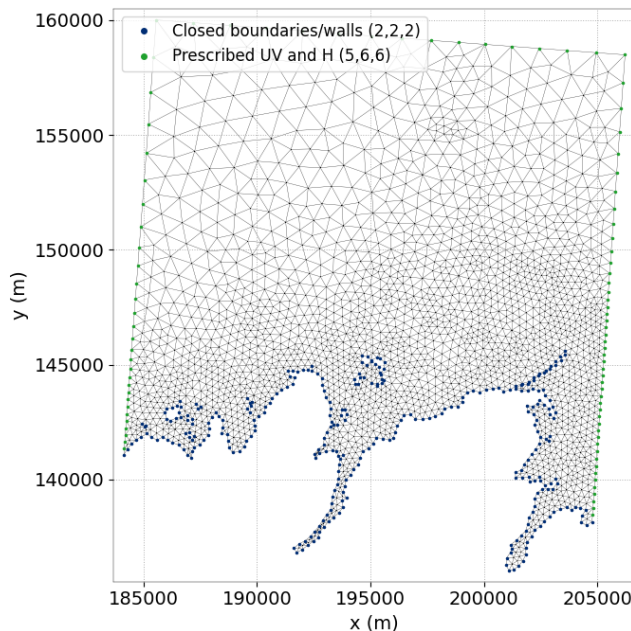


Figure 50.1: Mesh.

### 50.2.2 Bathymetry

A real bathymetry of the area bought from the SHOM (French Navy Hydrographic and Oceanographic Service) is used. ©Copyright 2007 SHOM. Produced with the permission of SHOM. Contract number 67/2007

### 50.2.3 Initial conditions

Initial conditions are defined by a constant elevation and no velocity.

### 50.2.4 Boundary conditions

Several databases of harmonic constants are interfaced with TELEMAC-2D:

- The JMJ database resulting from the LNH Atlantic coast TELEMAC model by Jean-Marc JANIN,
- The global TPXO database and its regional and local variants from the Oregon State University (OSU),
- The regional North-East Atlantic atlas (NEA) and the global atlas FES (e.g. FES2004 or FES2012...) coming from the works of Laboratoire d'Etudes en Géophysique et Océanographie Spatiales (LEGOS),
- The PREVIMER atlases.

In the tide test case, the JMJ database and the NEA prior atlas are used as examples. A TPXO-like example is also provided as an example but the user has to download the local solution available on the OSU website: <http://volkov.oce.orst.edu/tides/region.html>. Elevation and horizontal velocity boundary conditions are computed by TELEMAC-2D from an harmonic constants database (JMJ from LNH or NEA prior from LEGOS). If a tidal solution from OSU has been downloaded (e.g. TPXO, European Shelf), it can be used to compute elevation and horizontal velocity boundary conditions as well.

### 50.2.5 Physical parameters

Horizontal viscosity for velocity:  $10^{-6} \text{ m}^2/\text{s}$

Coriolis: yes (constant coefficient over the domain =  $1.10 \times 10^{-4} \text{ rad/s}$ )

No wind, no atmospheric pressure, no surge and nor waves

### 50.2.6 Numerical parameters

Time step: 60 s

Simulation duration: 90,000 s = 25 h

Advection for velocities: Characteristics method

Thompson method with calculation of characteristics for open boundary conditions

Free Surface Gradient Compatibility = 0.5 (not 0.9) to prevent on wiggles

Tidal flats with correction of Free Surface by elements, treatments to have  $h \geq 0$

### 50.2.7 Comments

If a tidal solution from OSU has been downloaded (e.g. TPXO, European Shelf), it can be used to compute initial conditions with the keyword INITIAL CONDITIONS set to TPXO SATELLITE ALTIMETRY. Thus, both initial water levels and horizontal components of velocity can be calculated and may vary in space.

## 50.3 Results

Tidal range, sea levels and tidal velocities are well reproduced compared to data coming from the SHOM or at sea measurements. In Figure 50.2 the water depth and free surface elevation at final time are shown in the case of the JMJ database. In Figure 50.3 the velocity magnitude, vectors and streamlines are plotted.

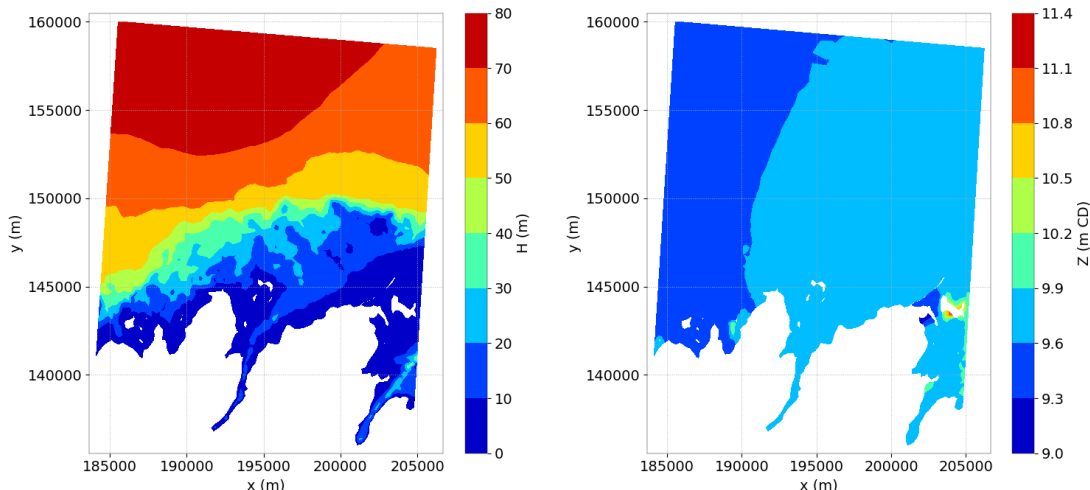


Figure 50.2: Water depth (in m) and free surface elevation (in m CD) at final time with the JMJ database.

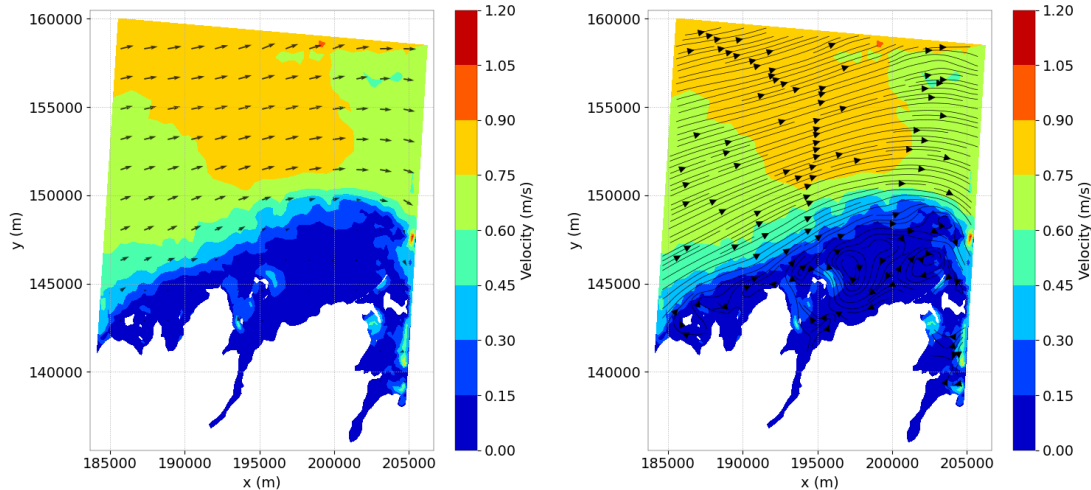


Figure 50.3: Velocity (in m/s) at final time (with vectors on the left and streamlines on the right) with the JMJ database.

## 50.4 Conclusion

TELEMAC-2D is able to model tide in coastal areas.

# 51. Diffusion of tracers (tracer\_diffusion)

## 51.1 Purpose

This test shows the performance of the finite volume diffusion schemes of TELEMAC-2D for passive scalar in a time dependent case. It shows the diffusion of a tracer (or any other passive scalar) in a flume with both Dirichlet and Neumann boundary conditions.

## 51.2 Description

### 51.2.1 Geometry and mesh

The dimensions of the domain are  $[2 \times 20]$  m<sup>2</sup>. The mesh is made from a regular grid from which all squares are cut in half.

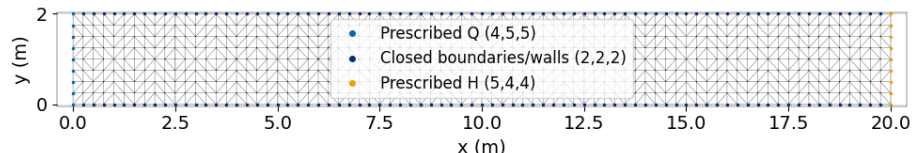


Figure 51.1: 2D domain and mesh of the tracer\_diffusion test case.

### 51.2.2 Initial condition

The water depth is constant in time and in space, equal to 1 m. The streamwise velocity  $u$  is constant and equal to 0 m/s. Two tracers are defined in the domain for which initial conditions are a Gaussian and a Crenel.

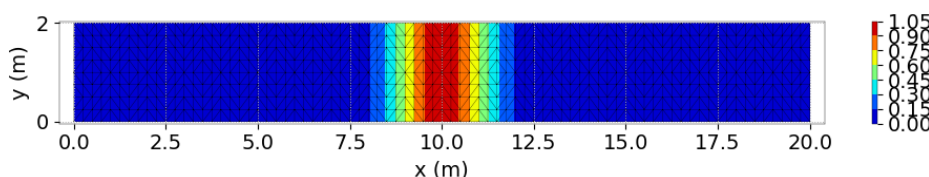


Figure 51.2: Initial condition of the first tracer.

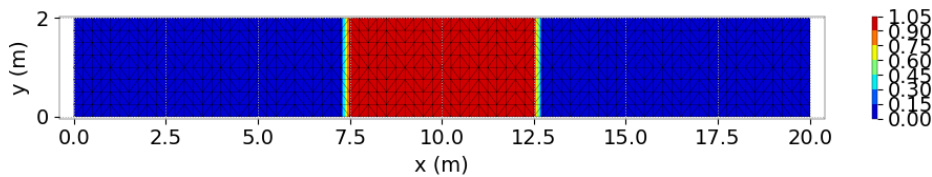


Figure 51.3: Initial condition of the second tracer.

### 51.2.3 Boundary conditions

All the tests are carried out with both Dirichlet and Neumann boundary conditions at the inlet and outlet of the domain.

### 51.2.4 Physical parameters

Tracer diffusion is activated and the following keywords are set:

- DIFFUSION OF TRACERS = TRUE,
- COEFFICIENT FOR DIFFUSION OF TRACERS = 1.;1.

The stability of the explicit finite volume diffusion schemes is guaranteed by choosing:

- DESIRED FOURIER NUMBER = 0.9.

### 51.2.5 Numerical parameters

The simulation time is set to 10 s. For tracers diffusion, all numerical schemes available in TELEMAC-2D finite volume solver are tested i.e. the TPF (Two Point Flux) scheme, the RTPF (Reconstructed Two Point Flux) scheme, the explicit P1 finite element scheme with mass lumping, designed to work alongside finite volume hyperbolic solvers (noted here HEFE for Hybrid Explicit Finite Element). The schemes are selected via the keyword FINITE VOLUME SCHEME FOR TRACER DIFFUSION. Additionally the standard implicit finite element method of TELEMAC-2D is computed for the purpose of comparison.

## 51.3 Results

### 51.3.1 Computation time

Simulation times for each of these cases with sequential and parallel runs (using 4 processors) are shown in Figure 52.3.

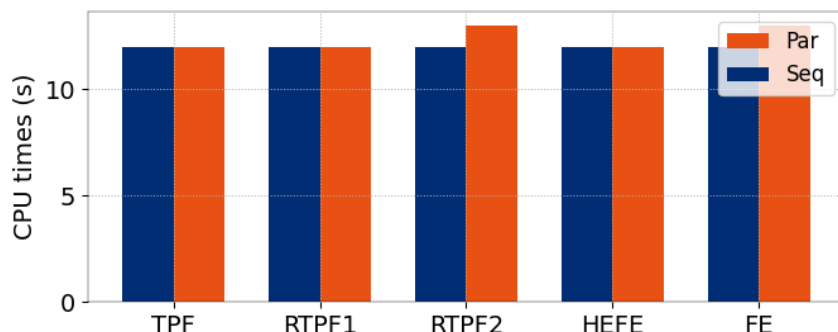


Figure 51.4: CPU times (Dirichlet conditions case).

### 51.3.2 Comparison of diffusion schemes

The evolution of both tracers are plotted against time at the centerline of the flume in Figures 51.5 and 51.6 respectively with both Dirichlet (left) and Neumann (right) boundary conditions.

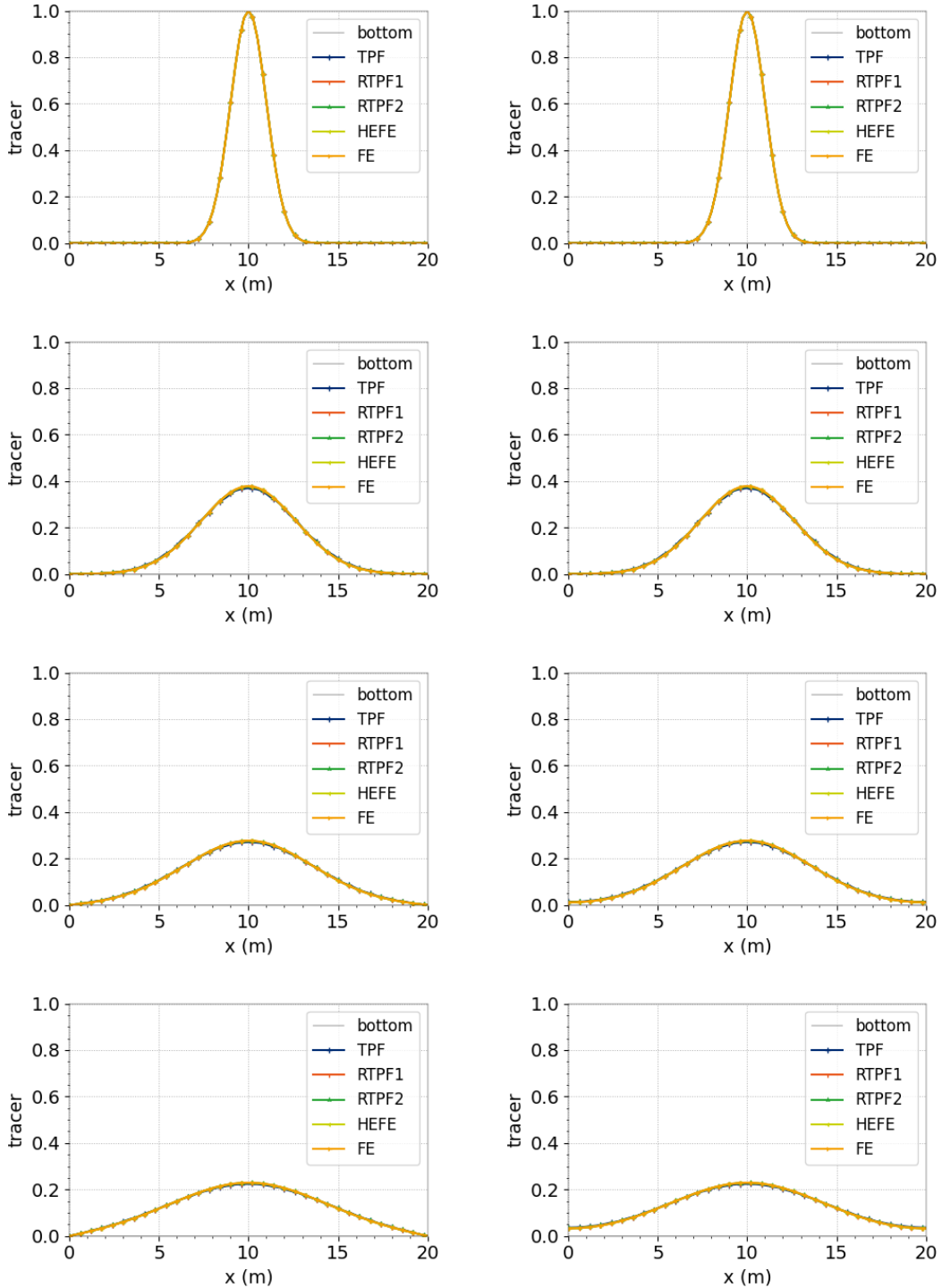


Figure 51.5: Diffusion of the first tracer with Dirichlet boundary conditions (left) and Neumann boundary conditions (right).

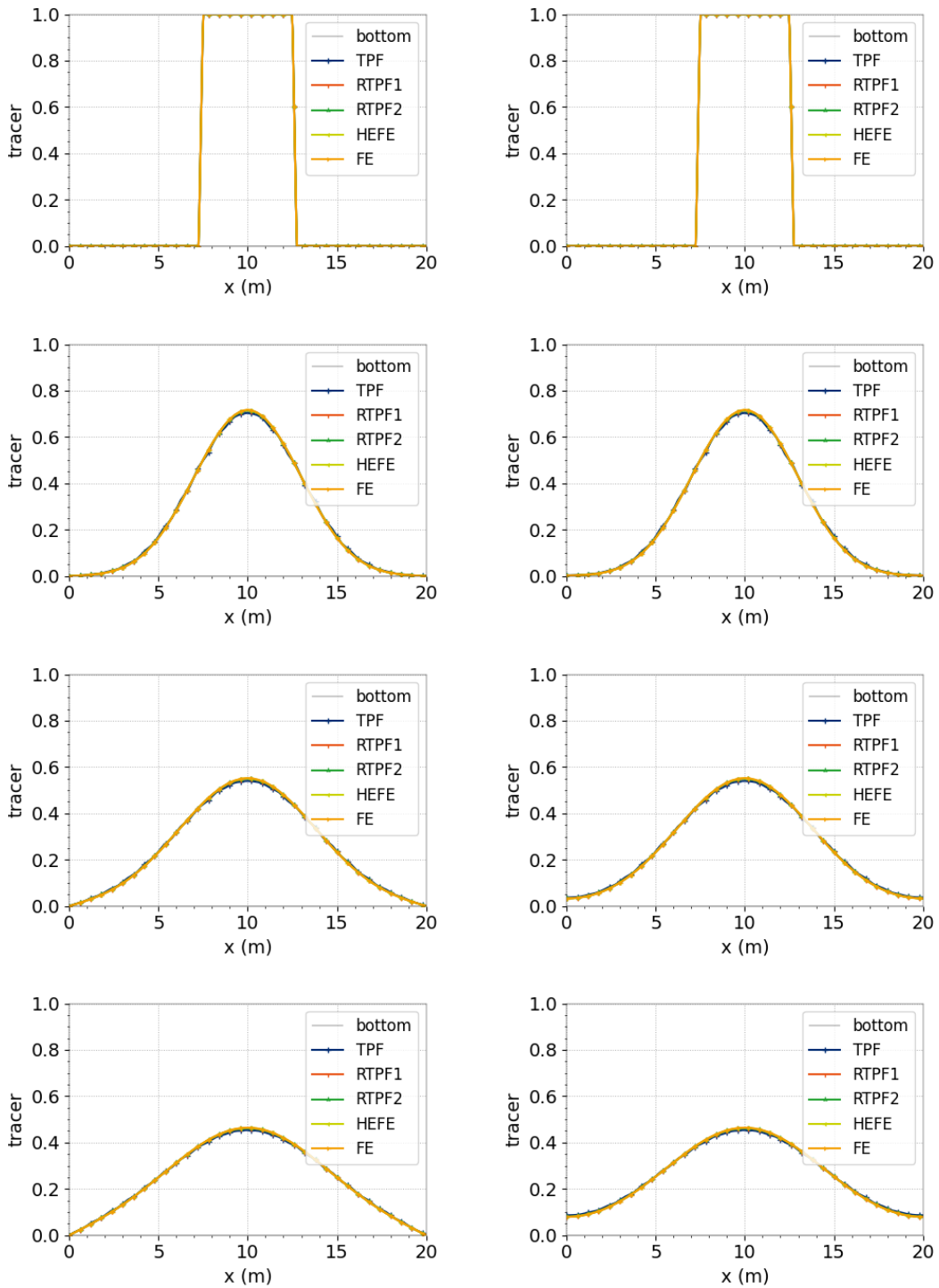


Figure 51.6: Diffusion of the second tracer with Dirichlet boundary conditions (left) and Neumann boundary conditions (right).

## 51.4 Conclusion

TELEMAC-2D is able to model passive scalar diffusion problems in shallow water flows with finite volume diffusion schemes.

## 52. Convergence study for the diffusion of tracers (tracer\_diffusion\_convergence)

### 52.1 Purpose

This test shows the performance of the finite volume diffusion schemes of TELEMAC-2D for passive scalar in a time dependent case. A convergence study is carried out using a simple 1D analytical solution.

### 52.2 Description

#### 52.2.1 Geometry and mesh

The dimensions of the domain are  $[2 \times 20]$  m<sup>2</sup>. The mesh is made from a regular grid from which all squares are cut in half.

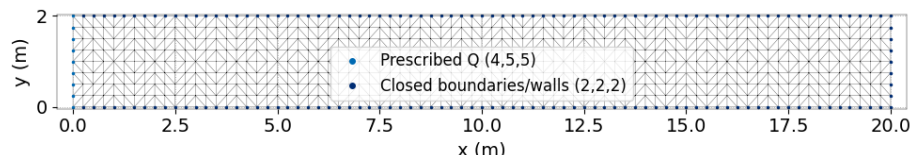


Figure 52.1: 2D domain and mesh of the flume\_tracer test case.

#### 52.2.2 Initial condition

The water depth is constant in time and in space, equal to 1 m. The streamwise velocity  $u$  is constant and equal to 0 m/s. The tracer is initially set to 1 in all the domain.

#### 52.2.3 Boundary conditions

At the begining of the test, a Dirichlet boundary condition with a tracer value of 0 is imposed on the left side boundary.

#### 52.2.4 Physical parameters

Tracer diffusion is activated and the following keywords are set:

- DIFFUSION OF TRACERS = TRUE,
- COEFFICIENT FOR DIFFUSION OF TRACERS = 1.;1.

The stability of the explicit finite volume diffusion schemes is guaranteed by choosing:

- DESIRED FOURIER NUMBER = 0.9.

### 52.2.5 Numerical parameters

The simulation time is set to 10 s. For tracers diffusion, all numerical schemes available in TELEMAC-2D finite volume solver are tested i.e. the TPF (Two Point Flux) scheme, the RTPF (Reconstructed Two Point Flux) scheme, the explicit P1 finite element scheme with mass lumping, designed to work alongside finite volume hyperbolic solvers (noted here HEFE for Hybrid Explicit Finite Element). The schemes are selected via the keyword FINITE VOLUME SCHEME FOR TRACER DIFFUSION.

## 52.3 Results

### 52.3.1 First observation

The evolution of the tracer is plotted against time at the centerline of the flume in Figure 52.2 respectively with both Dirichlet (left) and Neumann (right) boundary conditions.

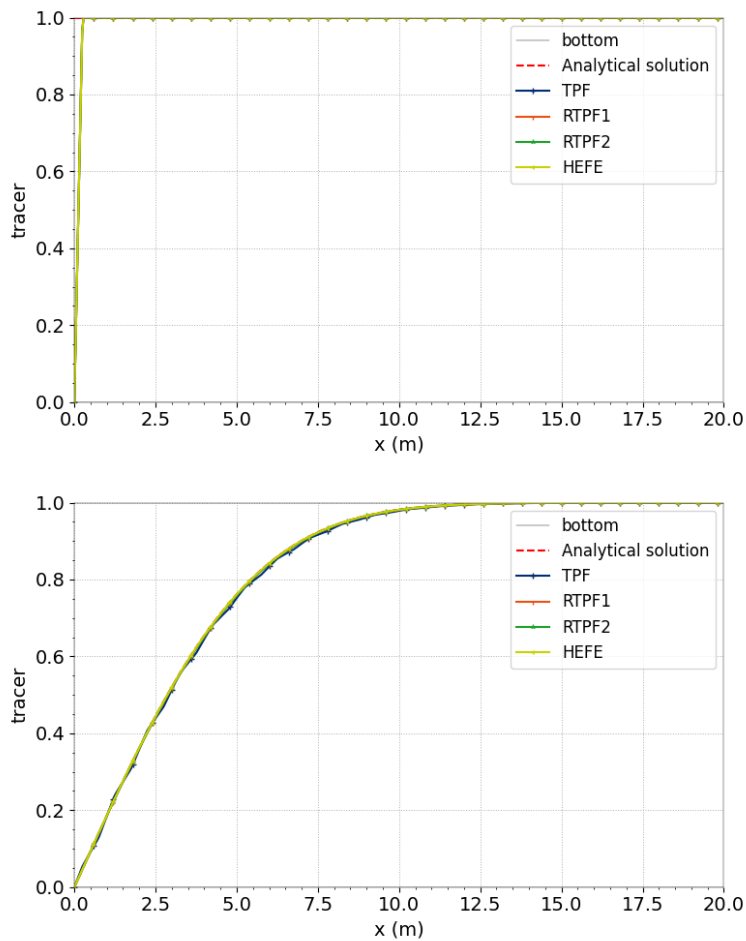


Figure 52.2: Diffusion of the tracer at the centerline of the flume (0 s, 9 s).

### 52.3.2 Computation time

Simulation times for each of these cases with sequential and parallel runs (using 4 processors) are shown in Figure 52.3.

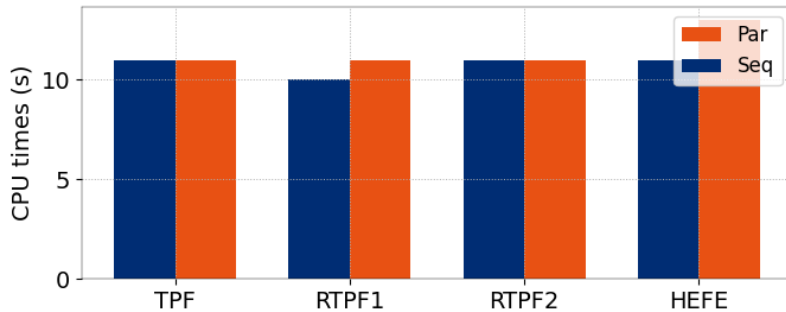


Figure 52.3: CPU times (Dirichlet conditions case).

### 52.3.3 Convergence

In this section a mesh convergence is carried out to assess the accuracy of the schemes. From a starting mesh we divide by 4 each triangles recursively to generate new meshes. The meshes used in the convergence study are presented in Figure 52.4.

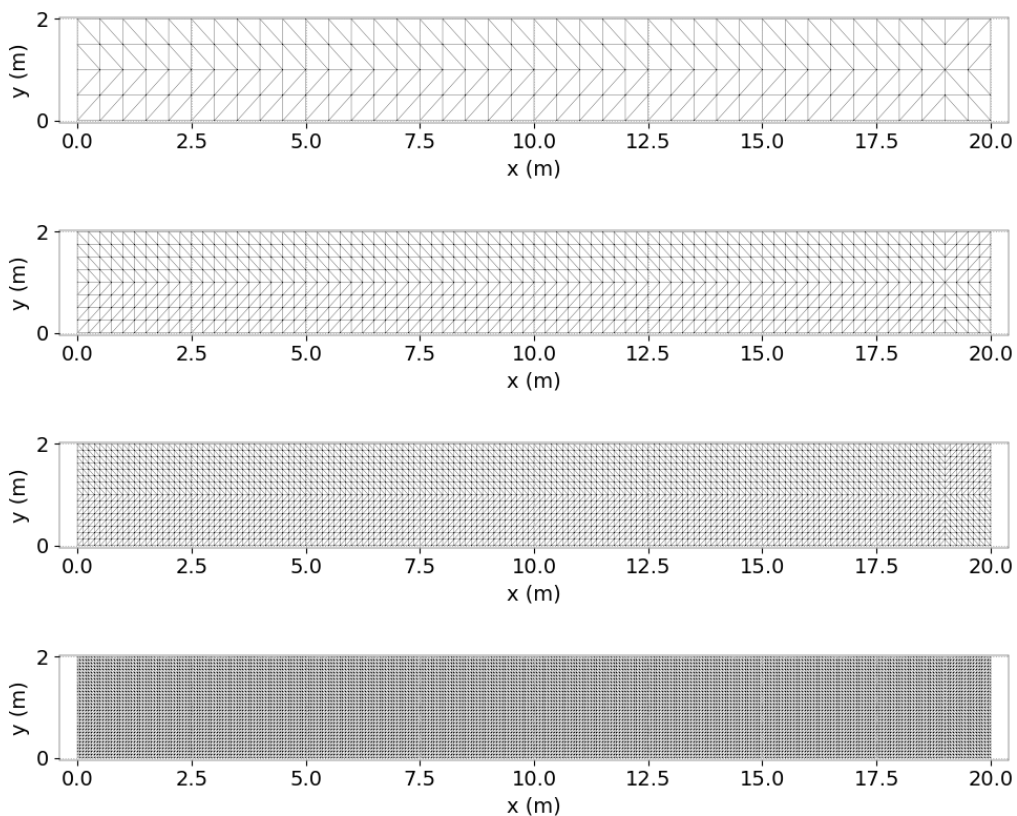


Figure 52.4: Meshes used in the mesh convergence.

With decreasing space step, we use a variable time step to ensure a constant Fourier number for each mesh increment.

Convergence errors in  $L^2$  norm are plotted in Figure 52.5 and errors at final time are compared for the finest mesh in Figure 52.6.

The results show that the TPF (Two Point Flux) finite volume scheme does not converge (this scheme is not consistent) whereas the RTPF (Reconstructed Two Point Flux) finite volume scheme gives a first order convergence rate. Finally the HEFE (explicit P1 finite element scheme with mass lumping) scheme converges with a second order convergence rate.

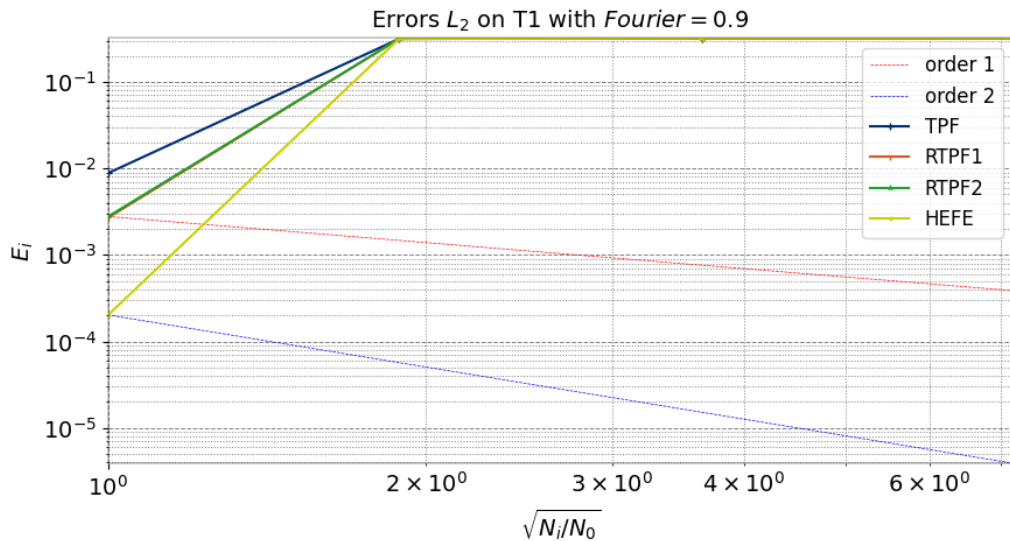


Figure 52.5: T convergence in  $L^2$  norm.

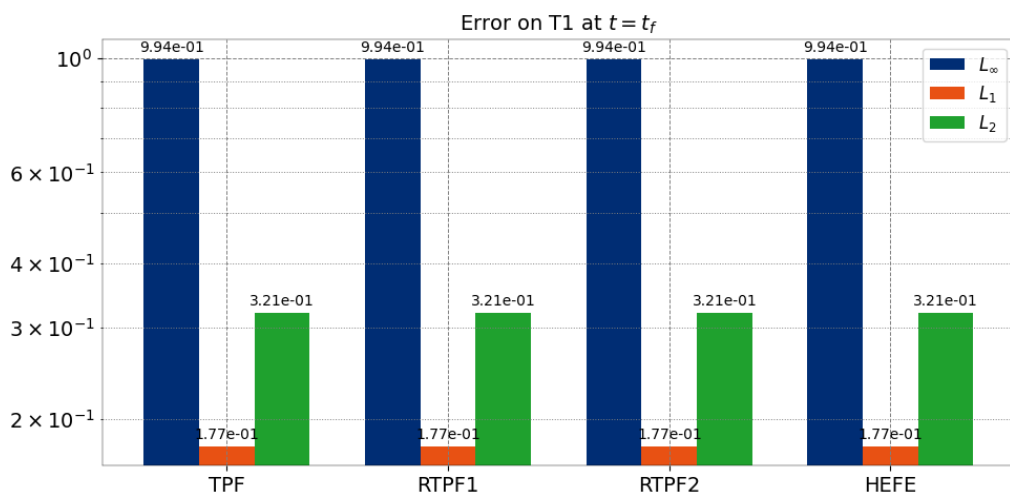


Figure 52.6: T errors at final time on the finest mesh.

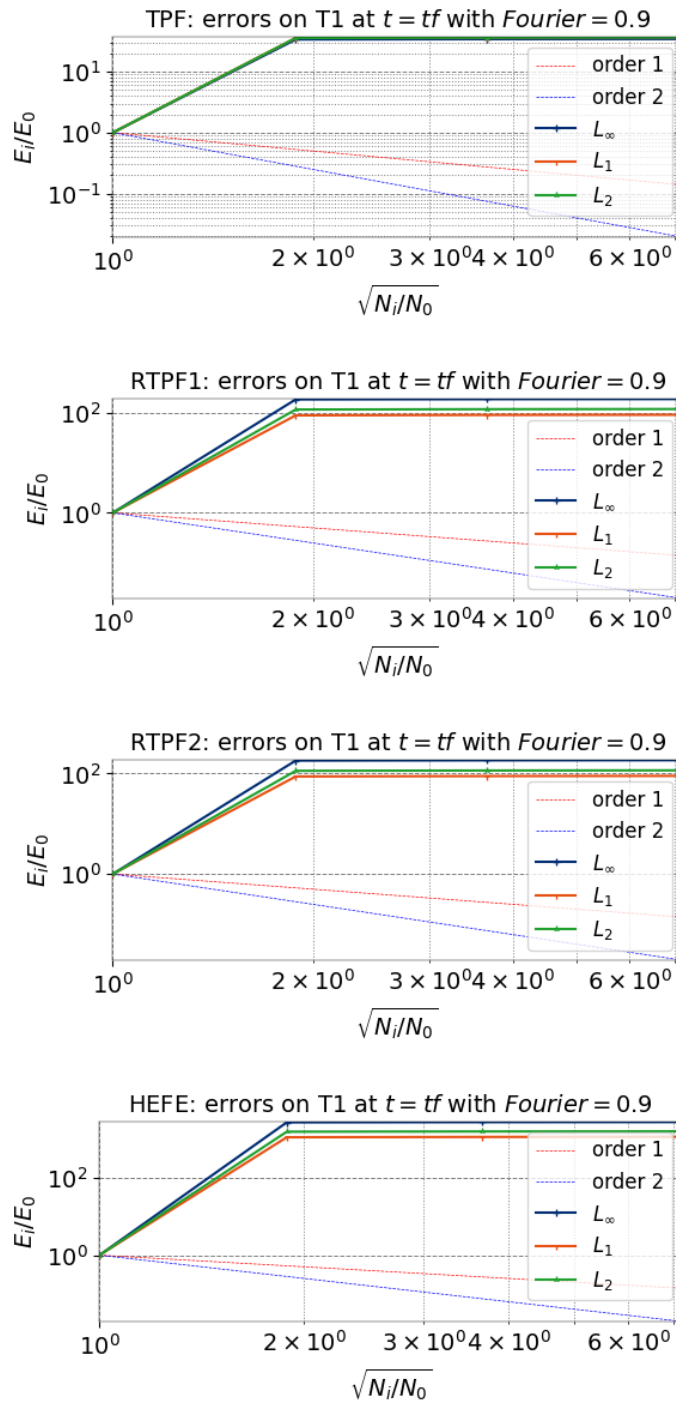


Figure 52.7: T convergence with different numerical schemes.

## 52.4 Conclusion

TELEMAC-2D is able to model passive scalar diffusion problems in shallow water flows with finite volume diffusion schemes.

## 53. triangular\_shelf

### 53.1 Purpose

To compare TELEMAC-2D simulation with a benchmark ([http://isec.nacse.org/workshop/2009\\_isec/benchmarks.html#bmark1](http://isec.nacse.org/workshop/2009_isec/benchmarks.html#bmark1)).

### 53.2 Description

The configuration is a 48.8 m long and 26.5 m wide rectangle. Water Depth is 0.78 m.

#### 53.2.1 Geometry and mesh

Figure 53.1 shows the geometry of the study.

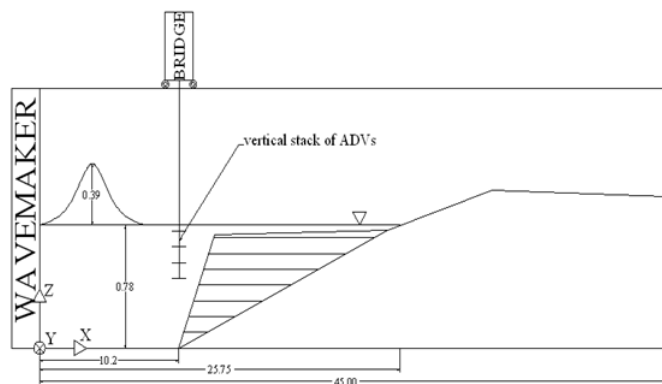


Figure 53.1: Geometry of the study.

The mesh is made of 36,874 elements and 18,720 nodes, see Figure 53.2.

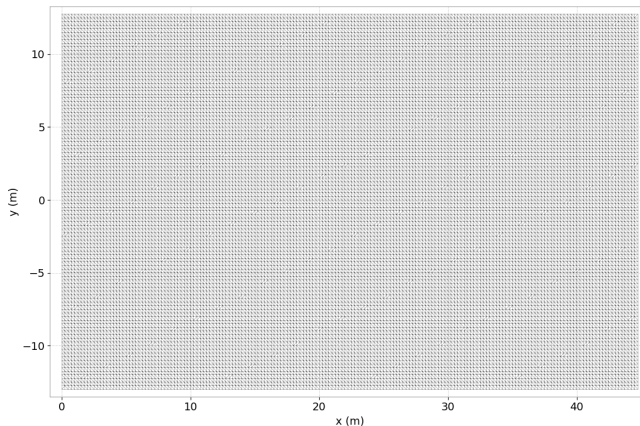


Figure 53.2: Mesh of the study.

Figure 53.3 shows the bathymetry of the study.

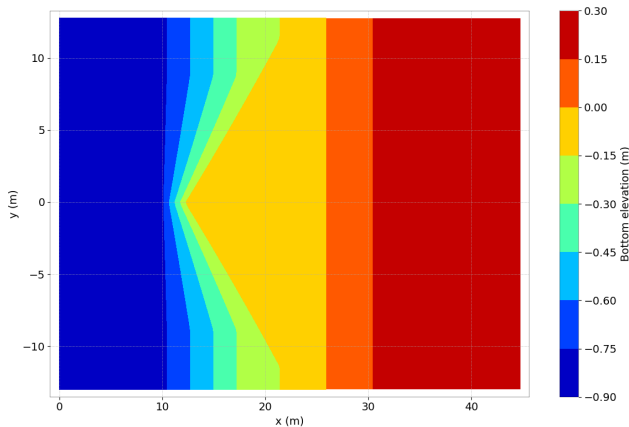


Figure 53.3: Bathymetry of the study.

### 53.2.2 Boundaries

Figure 53.4 shows the boundaries of the study.

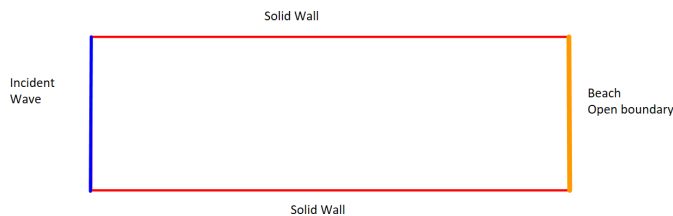


Figure 53.4: Geometry of the study.

Single solitary wave generated ( $H = 0.39$  m)  
Bottom:

- Chezy's Law,
- Friction coefficient:  $180 \text{ m}^{1/2}/\text{s}$ .

### 53.2.3 Physical parameters

Turbulence: Constant viscosity equal to zero.

### 53.2.4 Numerical parameters

- Type of element: P1 triangle for  $h$  and for velocity,
- Solver: GMRES,
- Accuracy:  $10^{-6}$ ,
- Finite volume scheme: Kinetic order 2.

|                     |                 |            |  |
|---------------------|-----------------|------------|--|
| Equations           | Saint-Venant VF | Boussinesq |  |
| Time step           | 0.05            | 0.005      |  |
| Simulation duration | 20              | 20         |  |

## 53.3 Results

We compare the model and experiment free surface at

- $X = 25$  m,
- $Y = 0$  m,
- $Y = -5$  m.

Figure 53.5 shows the velocity vectors.

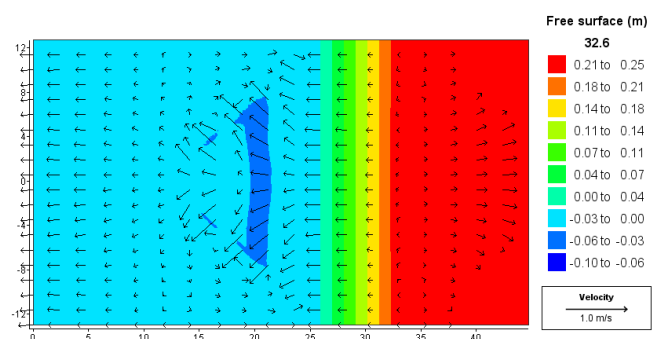


Figure 53.5: Velocity vectors over the free surface.

Figure 53.6 shows the comparison with the benchmark data.

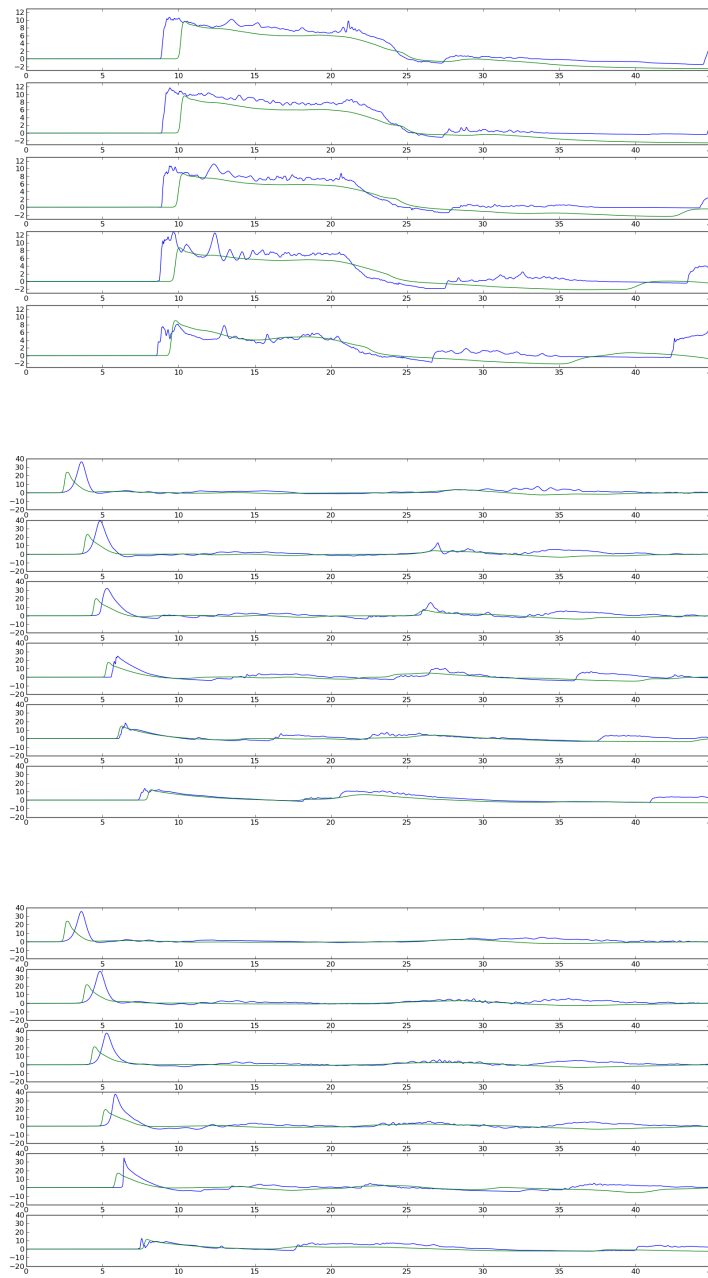


Figure 53.6: Comparaison of the results: in blue the experiment and in green the model.

## 54. Uncovering of a beach (vasque)

### 54.1 Purpose

To demonstrate that TELEMAC-2D is capable of representing the drying of a cylindrical beach presenting a pool. Also to show that TELEMAC-2D works properly when disconnected water bodies exist within the study domain.

### 54.2 Description

#### 54.2.1 Approach

A grid made of squares split into two triangles is used to represent a cylindrical beach presenting a pool. The water initially covers the entire domain (see Figure 54.1).

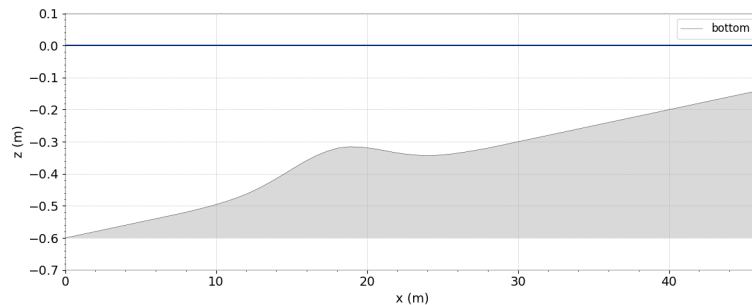


Figure 54.1: Initial free surface elevation and bottom elevation.

As the tide falls by 0.60 m, a 46 m cross-shore length of the beach is uncovered, thus leaving the pool full of water at rest.

#### 54.2.2 Geometry and mesh

- Size of the model: channel = 46 m × 9 m,
- Initial water level 0 m.

The mesh is regular. It is made up with squares split into two triangles.

- 828 triangular elements,

- 470 nodes,
- Maximum size range:  $\sqrt{2}$  m.

### 54.2.3 Boundaries

- Shoreline: solid wall with slip condition,
- Offshore boundary:  $z = \frac{0.55}{2} (\cos(\frac{2\pi}{600}t) - 1)$  imposed,
- Lateral boundaries: solid walls with slip condition in the channel.

### 54.2.4 Bottom

The bottom is defined by  $z_b = -0.6 + 0.01x + 0.1e^{-\frac{(x-19)^2}{20}}$ . The Strickler friction formula is used with friction coefficient =  $40 \text{ m}^{1/3}/\text{s}$ .

Mesh and topography are shown in Figure 54.2 and 54.3.

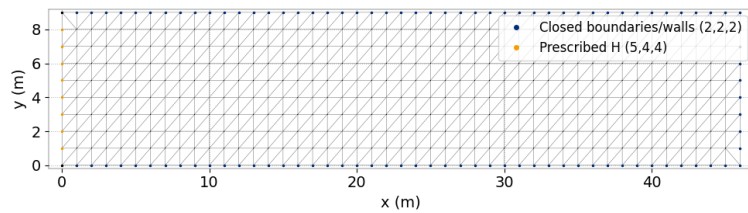


Figure 54.2: 2D-mesh of the vasque case.

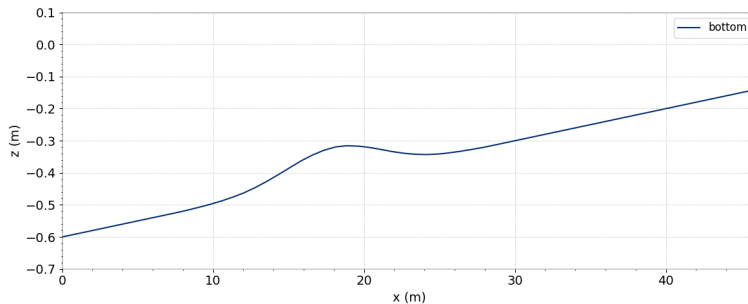


Figure 54.3: Bathymetry of the vasque case.

### 54.2.5 Physical parameters

The model of turbulence is constant viscosity with velocity diffusivity =  $10^{-2} \text{ m}^2/\text{s}$ .

### 54.2.6 Numerical parameters

Type of advection:

- Methods of characteristics on velocities (scheme #1),
- Conservative + modified SUPG on depth (mandatory scheme),
- Solver accuracy =  $10^{-4}$ ,
- Implicitation for depth and for velocity : 0.6,

- Time step = 1 s,
- Simulation duration = 300 s.

### 54.3 Results

The water level decreases regularly over the beach. At the end of the calculation, the water depth is equal to zero upstream and downstream of the pool, and the water level in the pool is completely horizontal (see Figures 54.4 and 54.5).

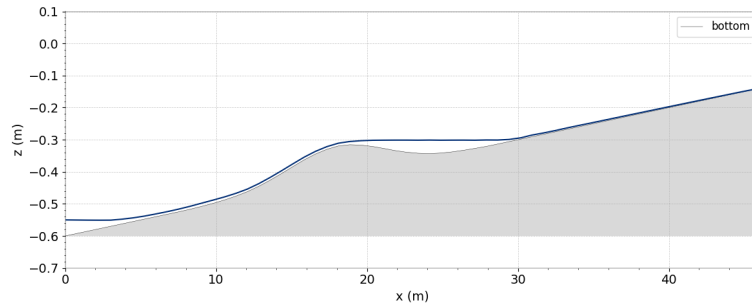


Figure 54.4: Free surface elevation at final time (= 300 s).

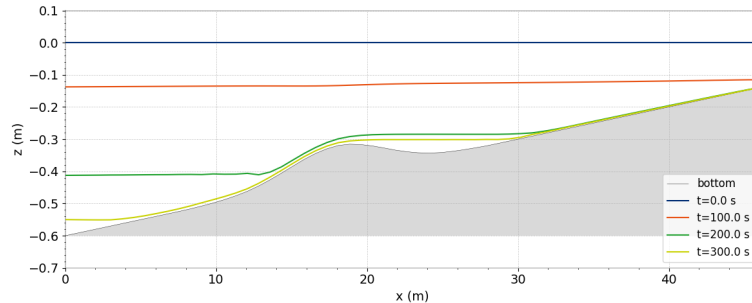


Figure 54.5: Evolution of the free surface elevation in time.

### 54.4 Conclusion

The uncovering of tidal flats is properly represented by TELEMAC-2D.

## 55. Vegetation laws (vegetation)

### 55.1 Purpose

This test case shows the capacity of TELEMAC-2D to implement vegetation approaches. In a flume with nearly normal conditions eight vegetation approaches are compared:

1. LIND (Lindner, 1982),
2. JAER (Jaervelae, 2004),
3. WHIT (Whittaker et al., 2015),
4. BAPT (Baptist et al., 2007),
5. HUTH (Huthoff et al., 2007),
6. VANV (van Velzen et al., 2003),
7. LUNE (Luhar & Nepf, 2013),
8. VAST (Vaestilae & Jaervelae, 2014).

Since not all models are capable for emerged conditions, a setup with submerged vegetation is chosen. More details to the vegetation approaches including the references to the original papers can be found e.g. [10].

### 55.2 Description

#### 55.2.1 Geometry and mesh

The 60 m long and 5 m wide flume has a slope of 0.1 per mill. The cross-section is divided into three parts, as shown in Figure 55.1: main channel (width = 1 m), sloped bank (width = 1 m, cross slope = 10 %) and floodplain (width = 3 m). The model domain is discretised with an irregular triangular mesh of 6,725 nodes and 12,798 elements (see Figure 55.2).

#### 55.2.2 Initial condition

As initial condition, a fully developed flow is read from the restart file.

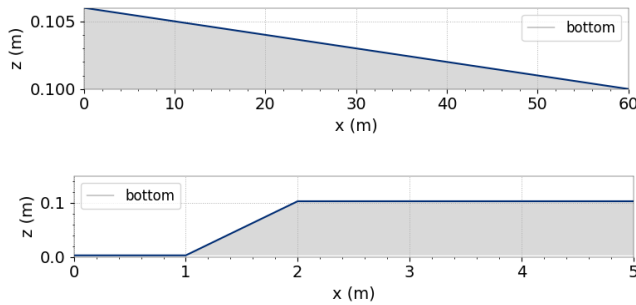


Figure 55.1: Longitudinal section and cross section of the bathymetry.

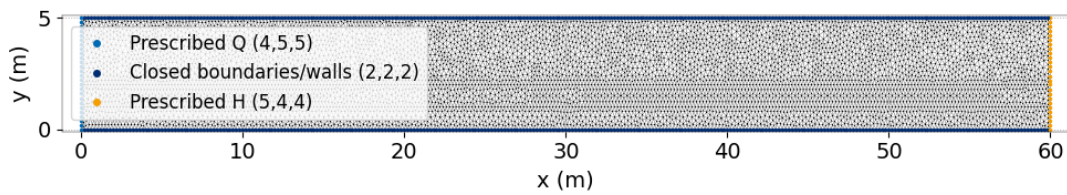


Figure 55.2: Mesh and boundary conditions of the vegetation test case.

### 55.2.3 Boundary conditions

At the flume inlet a constant discharge of 500 L/s is imposed across the full cross section. At the outlet the water depth is fixed to 47.0123 cm.

### 55.2.4 Physical parameters

The bottom friction is modelled using Nikuradse's law setting equivalent sand roughness  $k_s$  to 0.5 mm at the main channel and the banks and 3 mm at the floodplain. The lateral walls are modelled using slip conditions. The vegetation parameters for the approaches are different but tried to set as similar as possible. The following parameters are used:

- plant diameter  $D$ ,
- distance between the plants  $\Delta$ ,
- drag coefficient  $C_D$ ,
- vegetation density  $m$ ,
- friction coefficient at the top of the vegetation layer  $C_v$ ,
- plant height  $h_p$ ,
- leaf area index  $LAI$ ,
- Vogel coefficient  $\chi$ ,
- reference velocity for the Vogel coefficient  $u_{ref}$ ,
- frontal area per volume of vegetated region  $a$ ,
- frontal projected area  $A_{P0}$ ,

- flexural rigidity  $EI$ .

The used vegetation parameters are summed up in Table 55.1 and 55.2. For the VAST approach leaf area index, Vogel coefficient and reference velocity are used two times. The first values are for the foliage and the second ones are for the stem.

| Vegetation approach | $C_D$ | $D$<br>(m) | $\Delta$<br>(m) | $mD$<br>(1/m) | $Cv$ | $h_p$<br>(m) |
|---------------------|-------|------------|-----------------|---------------|------|--------------|
| 1 LIND              |       | 0.01       | 0.1             |               |      |              |
| 4 BAPT              | 1.0   |            |                 | 1.0           |      | 1.0          |
| 5 HUTH              | 1.0   |            | 0.1             | 1.0           |      | 1.0          |
| 6 VANV              | 1.0   |            |                 | 1.0           |      | 1.0          |
| 7 LUNE              | 1.0   |            |                 | 1.0           | 0.06 | 1.0          |

Table 55.1: Vegetation parameters for the approaches considering vegetation as rigid.

| Vegetation approach | $C_D$     | $LAI$       | $\chi$     | $U_{ref}$<br>(m/s) | $A_{P0}$<br>(m <sup>2</sup> ) | $EI$<br>(N/m <sup>2</sup> ) | $\Delta$<br>(m) | $h_p$<br>(m) |
|---------------------|-----------|-------------|------------|--------------------|-------------------------------|-----------------------------|-----------------|--------------|
| 2 JAER              | 0.5       | 0.1         | -0.9       | 0.1                |                               |                             |                 | 1.0          |
| 3 WHIT              | 1.0       |             | -0.9       |                    | 0.001                         | 0.0073                      | 0.1             | 1.0          |
| 8 VAST              | 0.5 / 0.5 | 0.09 / 0.01 | -0.9 / 0.0 | 0.1 / 0.1          |                               |                             |                 | 1.0          |

Table 55.2: Vegetation parameters for the approaches considering vegetation as flexible.

The density  $m$  can be calculated with the distance  $\Delta$  between the vegetation:

$$m = \frac{1}{\Delta^2}. \quad (55.1)$$

The leaf area index can be assumed by a formula of Finnigan [9] for the frontal area per volume of a vegetated region  $a$ :

$$a = \frac{D}{\Delta^2} = \frac{1}{2} \frac{LAI}{h_p}. \quad (55.2)$$

### 55.2.5 Numerical parameters

The simulation time is set to 1 h with a time step of 1 s in order to reach a steady state.

## 55.3 Results

The non-dimensional friction coefficient  $CF$  which equals a quarter of the Darcy-Weisbach friction coefficient  $CF = \frac{\lambda}{4}$  is written in the result file and displayed along the flume length in Figure 55.4. The flexible approaches (2-JAER, 3-WHIT, 8-VAST) calculate lower vegetation friction. The VAST approach is an enlargement of the JAER approach. For the flexibility parameter a distinction is made between foliage and stem. In this example the sum of the  $LAI$  for foliage and stem is according to the  $LAI$  of JAER. The only difference is the Vogel coefficient for the stem. This is set to zero which determined a rigid stem. As this is only for 10 % of the complete  $LAI$  the results are nearly the same.

The rigid approaches 4-BAPT, 5-HUTH, 6-VANV and 7-LUNE are identical for non submerged conditions. The 1-LIND approach calculates slightly higher vegetation roughnesses in this

case. If the  $C_D$  value would be set to 1.0 (like for the other approaches) instead of an iterative determination the LIND would have also the same results than the other rigid approaches. Only for the LIND approach the parallel computation is proofed.

In Figure 55.3, the simulated free surfaces along the flume length are compared. The water levels are higher if the friction coefficients are higher.

Therefore the three approaches considering the flexibility of vegetation (2-JAER, 3-WHIT, 8-VAST) forecast smaller water levels because of the lower resistance due to flexible vegetation. The approaches for the rigid parameters behave the same while the LIND approach show higher water levels according to the higher vegetation friction.

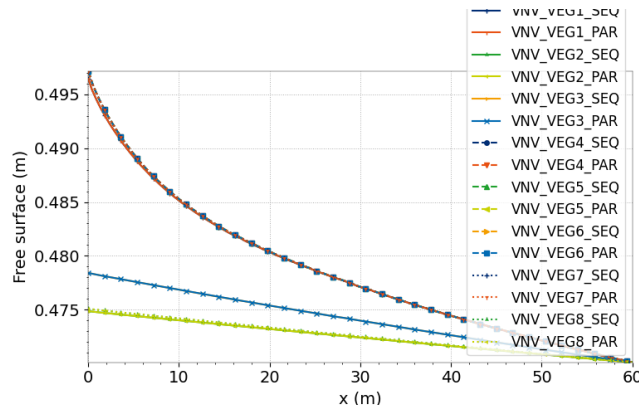


Figure 55.3: Simulated free surface along the flume length.

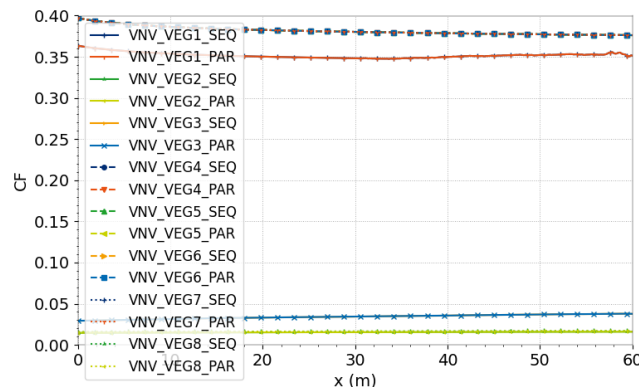


Figure 55.4: Simulated non-dimensional friction coefficient along the flume length.

## 55.4 Conclusion

For non-submerged conditions the main difference between the implemented eight approaches is the consideration of the flexibility of vegetation. Only 2-JAER, 3-WHIT and 8-VAST take flexibility into account. For manageability reasons the JAER approach is to be preferred as it has only five parameters.

From the rigid approaches 4-BAPT, 5-HUTH, 6-VANV and 7-LUNE are identical for non-submerged conditions.

The drag coefficient will be determined iteratively for the 1-LIND approach. Previous experiences showed that the iteratively estimated drag coefficient is close to the default value of 1.0 like in this example. If this is not the case it can happen that the results are not satisfying. Furthermore the iterative procedure needs up to 20 % of the simulation time. Therefore this approach is not recommended.

In order to consider the decrease of the vegetation influence for overtopped vegetation a two-layer approach like 4-BAPT, 5-HUTH, 6-VANV or 7-LUNE should be chosen. Here BAPT is recommended because only three parameters are needed and the approach is easy and the previous experiences are good.

## 56. Propagation of waves in a channel (wave)

### 56.1 Purpose

To assess the properties of TELEMAC-2D for the propagation of a long wave in a rectilinear channel without resistance effects.

### 56.2 Description

#### 56.2.1 Analytical solution

This case corresponds to the analytical solution of the shallow water equations without variation in the  $y$  direction, without diffusion and without advection, and with the assumption  $H_0 \gg H$ , where  $H$  is the water depth and  $H_0$  is the mean water depth:

$$\begin{cases} \frac{\partial H}{\partial t} + H_0 \frac{\partial U}{\partial x} = 0 \\ \frac{\partial U}{\partial t} = -g \frac{\partial H}{\partial x} = 0 \end{cases} \quad (56.1)$$

A solution to this problem is:

$$\begin{cases} H = H_0 + A \sin \left( \frac{2\pi t}{T} - \frac{2\pi x}{T\sqrt{gH_0}} \right) \\ U = A \sqrt{\frac{g}{H_0}} \sin \left( \frac{2\pi t}{T} - \frac{2\pi x}{T\sqrt{gH_0}} \right) \end{cases} \quad (56.2)$$

with  $A$  the amplitude of the wave and  $T$  its period.

In this example, a 16 m long and 0.3 m wide channel with constant depth of 10 m is considered. At the channel entrance, a sinusoidal water surface elevation is imposed, that corresponds to the analytical solution. No bed resistance occurs and the advection step of TELEMAC-2D is skipped in order to solve the system (56.1).

#### 56.2.2 Geometry and mesh

The domain is a channel with a size of 16 m  $\times$  0.3 m. The bottom is horizontal and the water depth at rest is equal to 10 m. The domain is meshed with 3,840 triangular elements and 2,247 nodes. Triangles are obtained by dividing rectangular elements on their diagonals. The mean size of obtained triangles is about 0.07 m (see Figure 56.1).

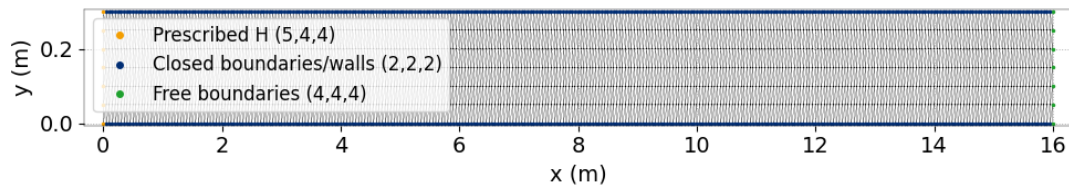


Figure 56.1: Mesh.

### 56.2.3 Initial conditions

The initial velocity is zero and the water level is horizontal, with a water depth of 10 m.

### 56.2.4 Boundary conditions

The incident water wave is imposed on the channel's entrance as follows:

$$H = 10 + 0.05 \sin\left(\frac{2\pi t}{0.5}\right) \quad (56.3)$$

so that  $H_0 = 10$  m,  $A = 0.05$  m,  $T = 0.5$  s. A free surface elevation of 10 m is imposed on channel's outlet. The Thompson boundary conditions are applied for open boundaries. The lateral boundaries are considered as solid walls with slip condition.

### 56.2.5 Physical parameters

The physical parameters used for this case are:

1. No friction (LAW OF BOTTOM FRICTION set to 0),
2. No diffusion.

### 56.2.6 Numerical parameters

1. Simulation type: propagation without advection,
2. Type of element: Linear triangle (P1) for velocities and  $h$ ,
3. Solver: GMRES (solver 7) with an accuracy of  $10^{-6}$ ,
4. Implicitation for depth and for velocity: 0.5,
5. Time Step: 0.0025 s,
6. Simulation duration: 5 s.

## 56.3 Results

The solution produced by TELEMAC-2D shows very good agreement with the exact solution (see Figures 56.2 and 56.3). The incident water wave is properly propagated in the channel.

The celerity of the wave is exactly  $c = \sqrt{g \cdot H_0}$ . The phase of the wave is correct. The amplitude of the wave is nearly the same at the channel entrance and at the outlet. A very small difference between the surface elevation computed by TELEMAC-2D and the exact solution is observed. The maximum error is lower than 3 % on the amplitude of the wave. There is no reflection of the wave on the open boundary at the outlet of the channel thanks to the Thompson boundary conditions.

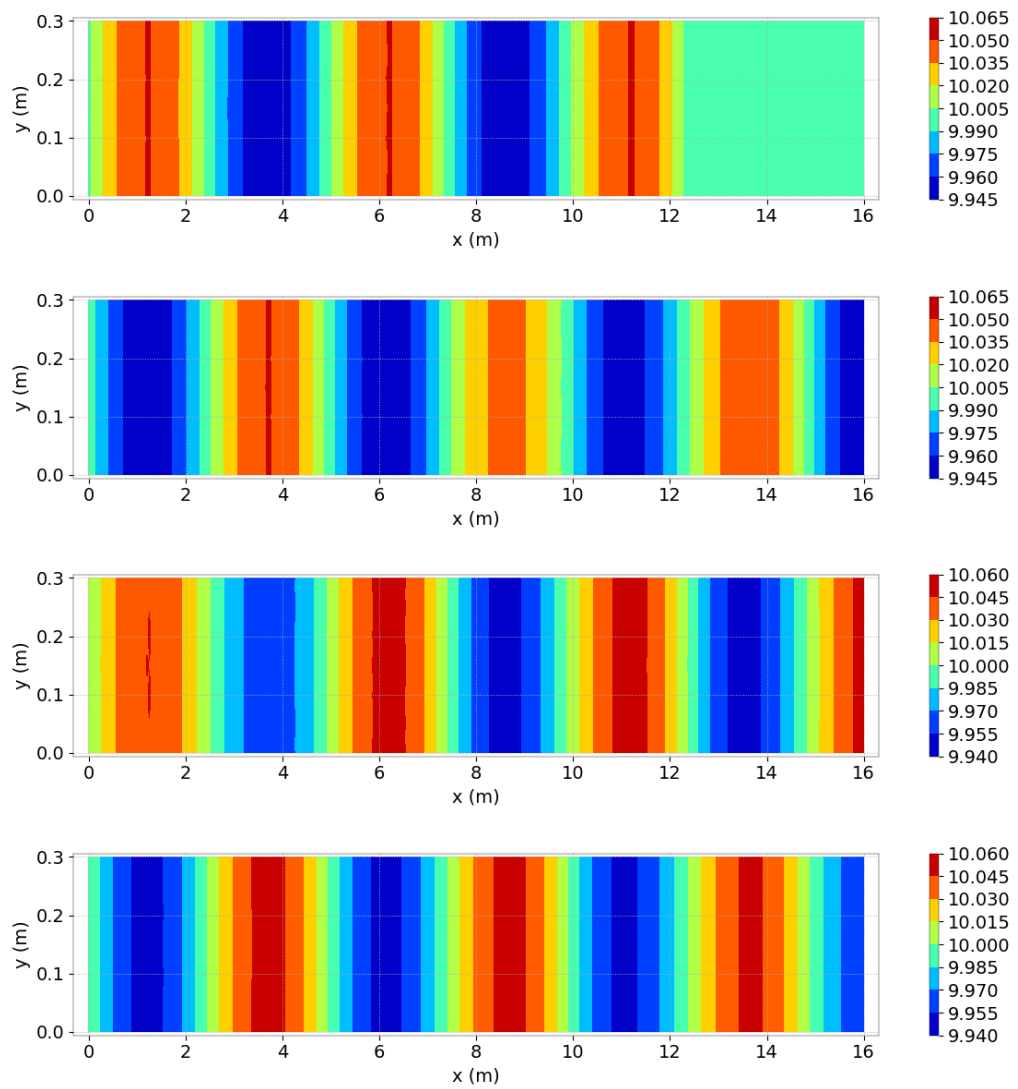


Figure 56.2: Wave example: shape of the free-surface at the times 1.25, 2.5, 3.75 and 5.0 seconds. The colors correspond span from  $H = 9.95$  m (blue) to  $H = 10.05$  m (red).

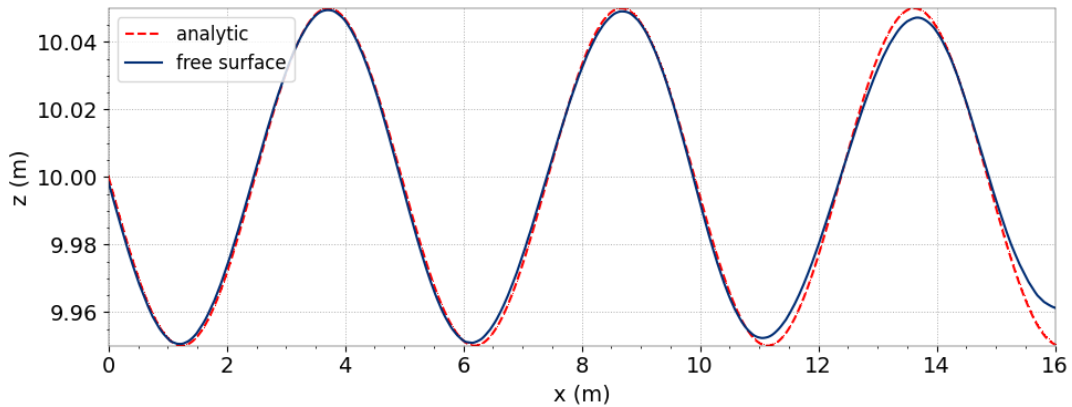


Figure 56.3: Wave example: final free-surface profile ( $t = 5$  s).

#### 56.4 Conclusions

TELEMAC-2D accurately reproduces the propagation of surface long waves in terms of celerity, phase and amplitude.

# 57. Weirs

## 57.1 Purpose

These two test cases present a flow over different sills treated as singularities. They allow to show that TELEMAC-2D is able to treat a number of flow singularities as internal boundary conditions. Moreover, they allow also to check the tracers function for this type of problem in TELEMAC-2D.

## 57.2 Description

The sills may be considered under the traditional approach made in open channel hydraulics through a relation between two superimposed open boundaries, short sills may be treated as a couple of nodes with respective source and sink terms.

This sills description, which are represented in a channel as internal singularities, was introduced in TELEMAC-2D in order to avoid the multiplication of computational nodes and associated reduction in time step when a sill is represented thanks to variations in the bathymetry. In the first version implemented in TELEMAC-2D, the weir law as traditionally used in channel hydraulics is prescribed through two boundary conditions: one upstream the weir and one downstream (with the same number of nodes upstream and downstream). Recently, a more generic solution has been implemented where the weir law is prescribed through sources points and where the description of the weir itself could be done at a smaller scale than the surrounding mesh. It should be mentioned however that both options give satisfactory results only if the flow is relatively perpendicular to the weir, which is the case in the two tests.

## 57.3 Option 1 - Horizontal weirs

### 57.3.1 Geometry and mesh

In this test case, the sills are so represented as internal singularities, as just indicated. The geometry dimensions of rectangular channel are 848 m wide and 3,522 m long. The channel is flat bottom and it is decomposed of four part reaches 848 m long. The three upstream reaches are limited at their downstream end by 3 sills with crest heights 1.8 m (upstream sill), 1.6 m and 1.4 m (downstream sill).

The mesh is regular along the domain. It is generally made up with quadrangles split into two triangles. It is irregular in the upstream reach in order to test the sensitivity on this feature of

the flow results above the sill (see Figure 57.1). It is composed of 870 triangular elements (519 nodes) and the size of triangles ranges between 53 m and 120 m.

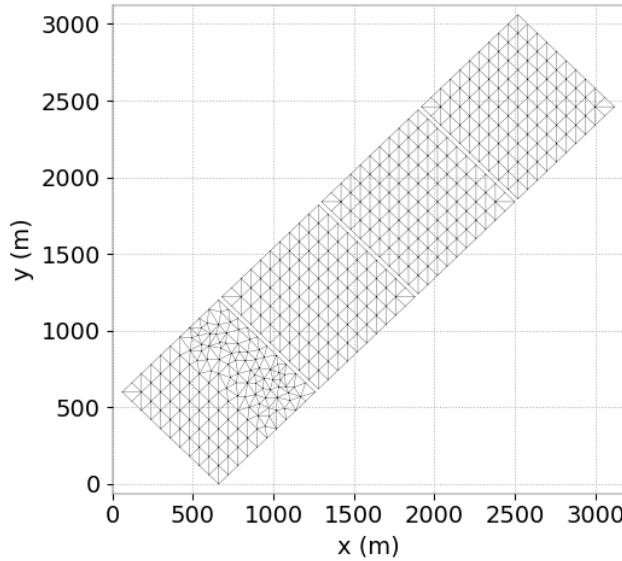


Figure 57.1: Mesh and topography of the domain.

### 57.3.2 Initial conditions

The initial conditions are a null velocity, a water depth of 1.35 m and a tracer value of 50.

### 57.3.3 Boundary conditions

The boundary conditions (Figure 57.1) are:

- At the channel entrance (lower left), the flow rate is  $Q = 600 \text{ m}^3\text{s}^{-1}$  and the tracer value is 100.
- At the channel outlet (upper left), the water depth is  $h = 1.35 \text{ m}$ .

### 57.3.4 Physical parameters

On bottom friction, the Strickler formula with friction coefficient equal to  $30 \text{ m}^{1/3}\text{s}^{-1}$  is imposed. No friction is taken into account on lateral walls. Note that the turbulent viscosity is constant and equal to  $1 \text{ m}^2\text{s}^{-1}$ .

### 57.3.5 Numerical parameters

The time step is 150 s for a period of 6,000 s. The resolution accuracy for the velocity is taken at  $10^{-10}$ . Note that for numerical resolution, GMRES (Generalized Minimal Residual Method) is used for solving the propagation step (option 7). To solve advection, the characteristics scheme (scheme 1), and the conservative scheme (scheme 5) is used respectively for the velocities and for the depth. To finish, the implicitation coefficients for depth and velocities are equal to 0.55 (default values).

The triangular elements types are linear triangles (P1, 3 values per element, the corners) for water depth and quasi-bubble triangle (4 values per element, the corners and the element center) for velocities. It should also be noted that a tracer is used. For the advection resolution, it is

used a conservative N-scheme (scheme #4) and the solver for diffusion of tracer is the conjugate gradient (option 1).

### 57.3.6 Results

As it can be seen in Figure 57.2, the velocity field remains regular laterally in the different reaches of the channel.

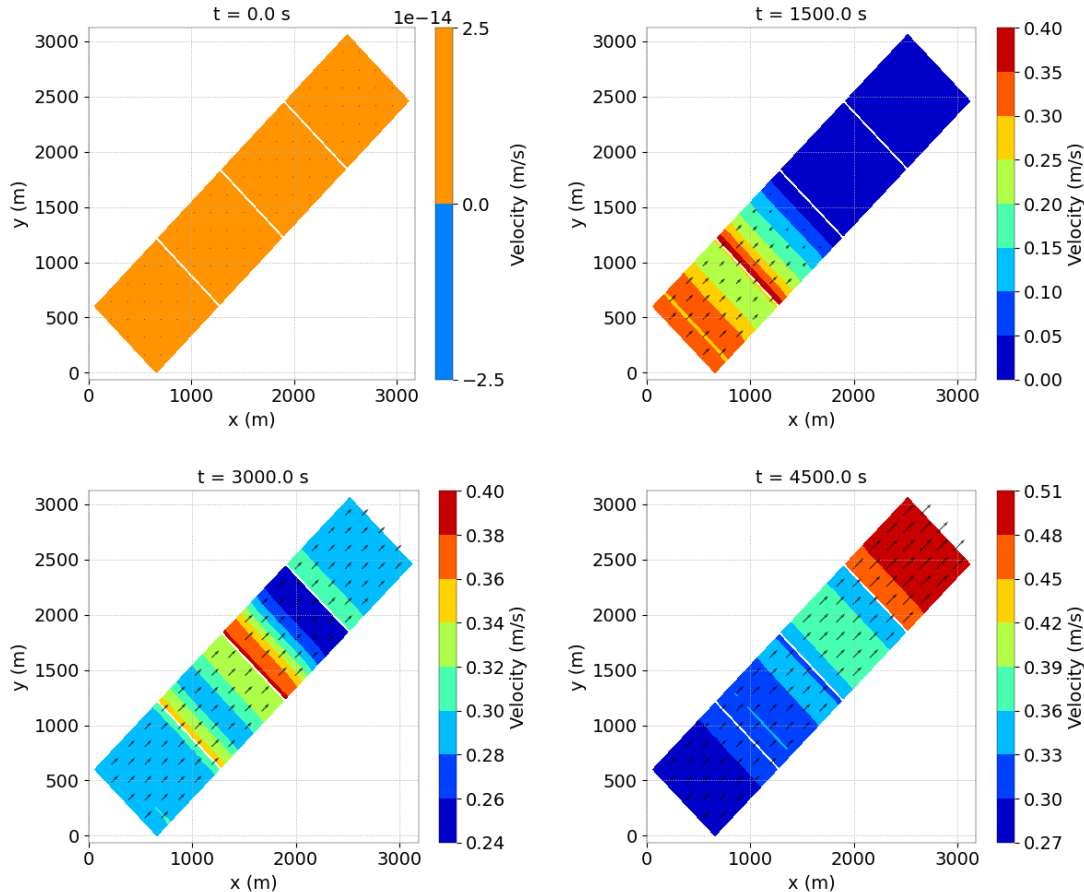


Figure 57.2: Evolution of velocity field in time.

The water level increases progressively as expected in the three upstream reaches during the simulated period (see Figure 57.3). The relations between the discharge (per unit of width) on the sill, the water levels upstream and downstream and the sill crest elevation must be respected. They are:

- Free overflow weir:

$$q = \mu \sqrt{2g} (z_{up} - z_{sill})^{3/2},$$

- Drowned weir :

$$q = \frac{2}{3\sqrt{3}} C_d \sqrt{2g} (z_{down} - z_{sill}) \sqrt{(z_{up} - z_{down})}.$$

The transition from free overflow to drowned condition is defined by:

$$z_{down} \leq z_{sill} + \frac{2}{3} (z_{up} - z_{sill}), \quad (57.1)$$

Where  $z_{up}$ ,  $z_{down}$  and  $z_{sill}$  are respectively water level upstream (m), water level downstream (m) and sill crest elevation (m).  $q$  is discharge per unit width ( $\text{m}^2.\text{s}^{-1}$ ).  $g$  is the gravitational acceleration ( $\text{m.s}^{-2}$ ).  $\mu$  is viscosity coefficient ( $\text{Pa.s}^{-1}$ ) and  $C_d$  is the discharge coefficient (usually between 0.4 and 0.5).

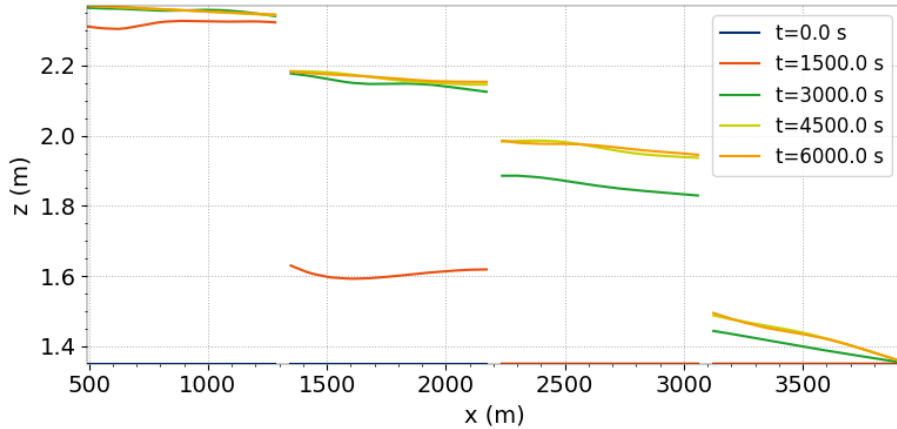


Figure 57.3: Evolution of the free surface elevation in time.

The TELEMAC-2D results respect well these relations (57.1) (Figure 57.3). Furthermore the tracer propagation is well carried out through internal singularities (Figure 57.4).

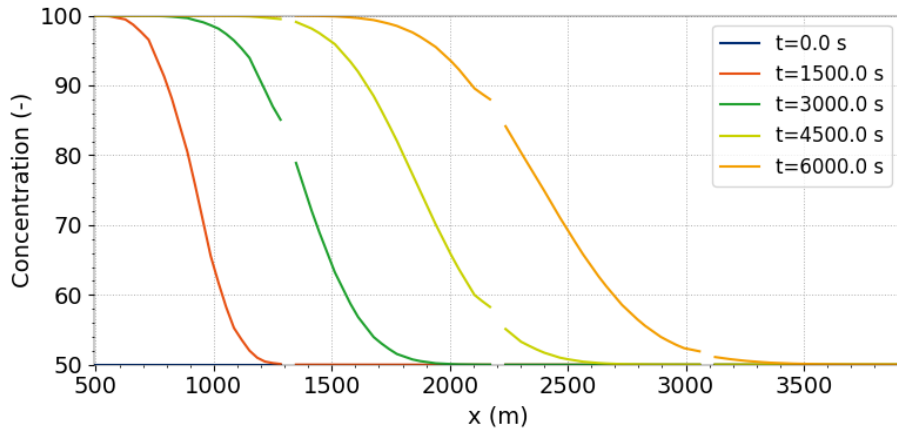


Figure 57.4: Evolution of the tracer in time.

## 57.4 Option 2 - Generic weirs

### 57.4.1 Geometry and mesh

In this second test case, the sills are also represented as internal singularities, but with different shape, along profile and number of points.

The geometry is composed by 6 different squares  $1,000 \text{ m} \times 1,000 \text{ m}$ . The mesh of each square is irregular with mean size equal to 50 m (domain 4), 100 m (domain 1, 3 and 5) and 200 m (domain 2 and 6) (see Figure 57.5).

There are 5 weirs between those 6 small domains (see Figure 57.6).

The global mesh is composed of 1,702 triangular elements (977 nodes).

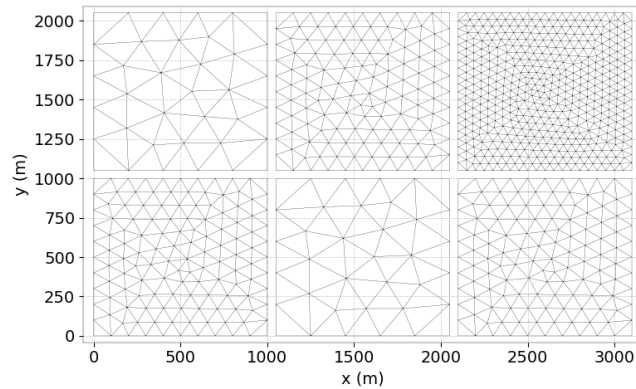


Figure 57.5: Mesh of the domain.

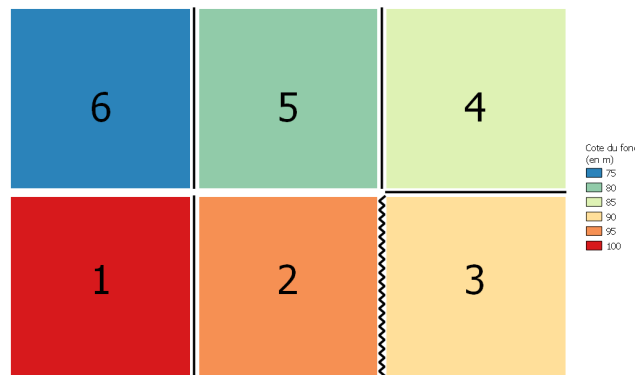
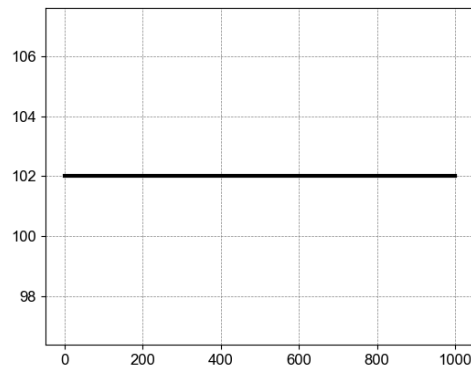


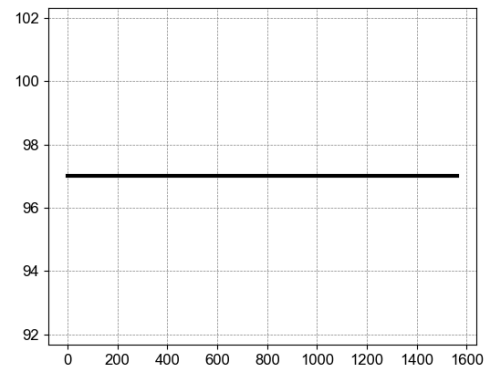
Figure 57.6: Topography of the domain with weirs position.

Those 5 weirs have different shapes (see Figure 57.7):

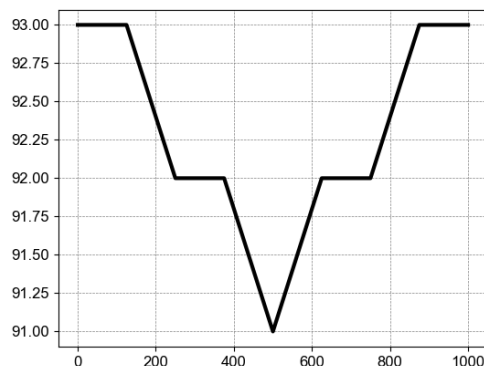
- Simple horizontal shape between domain 1 and 2,
- Horizontal shape but with a zigzag trace between domain 2 and 3 that leads to a longer weir,
- V shape between domain 3 and 4,
- Horizontal shape with 2 slots between domain 4 and 5,
- Free Shape between domain 5 and 6.



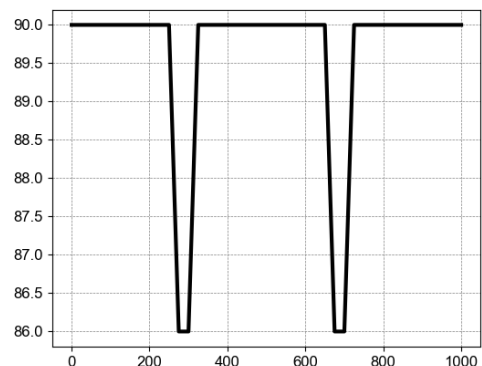
a: Profile of weirs between 1 and 2



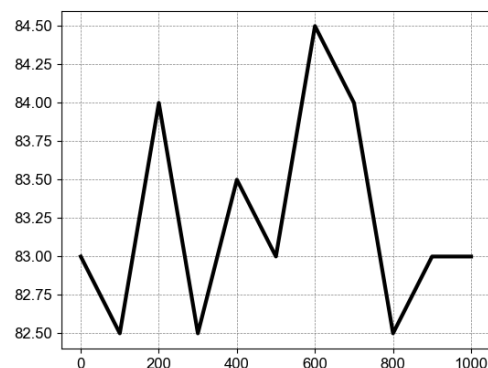
b: Profile of weirs between 2 and 3



c: Profile of weirs between 3 and 4



d: Profile of weirs between 4 and 5



e: Profile of weirs between 5 and 6

Figure 57.7: Profile of weirs.

#### 57.4.2 Initial conditions

The initial conditions are a null velocity, null concentration tracer, a water depth of 1 m in domain 1 and 6 and 0.1 m in other domain.

#### 57.4.3 Boundary conditions

The boundary conditions are:

- At the domain 1 entrance (left side), the flow rate starts from  $Q = 0 \text{ m}^3\text{s}^{-1}$  and increases to  $Q = 500 \text{ m}^3\text{s}^{-1}$  during the 200 first seconds and remain to this value after that. The tracer value is 100.
- At the channel outlet, the water depth is  $h = 1\text{m}$ .

#### 57.4.4 Physical parameters

On bottom friction, the Strickler formula with friction coefficient equal to  $50 \text{ m}^{1/3}\text{s}^{-1}$  is imposed. No friction is taken into account on lateral walls. For turbulence, the default parameters are used.

#### 57.4.5 Numerical parameters

The time step is 10 s for a period of 43,200 s (= 12 h). All other numerical parameters are let at theirs default value.

#### 57.4.6 Results

As it can be seen in Figure 57.8, the velocity field remains regular laterally between the 3 first domains. Between domain 3 and 4, the flow shows a concentration in the center due to the V shape and between 4 and 5, the flow is splitted in 2 according to the slots. Over the last weir, the flow is irregular but smoothed by the large cell sized of the domain...

The final discharge for each weirs is presented in the following table. The test case is supposed to reach steady state at the end of simulation so we should obtain the same discharge as imposed upstream ( $Q = 500 \text{ m}^3\text{s}^{-1}$ ).

| Weir number | Discharge  |
|-------------|------------|
| 1           | 500.000000 |
| 2           | 500.000000 |
| 3           | 499.999994 |
| 4           | 499.973884 |
| 5           | 499.961762 |

Table 57.1: Weirs2 test case: final discharge over weirs.

The evolution of piece-wise discharge (the discharge on each elemental part of the weir) can be seen in Figure 57.9.

- For weirs 1 and 2, which are horizontal, that the piece-wise discharge is the same for each element of the weir,
- For weirs 3, the highest discharge is located in the middle part of the weir and the discharge is 0 on the lateral part,
- For weir 4, only the element in the slot have a positive discharge,

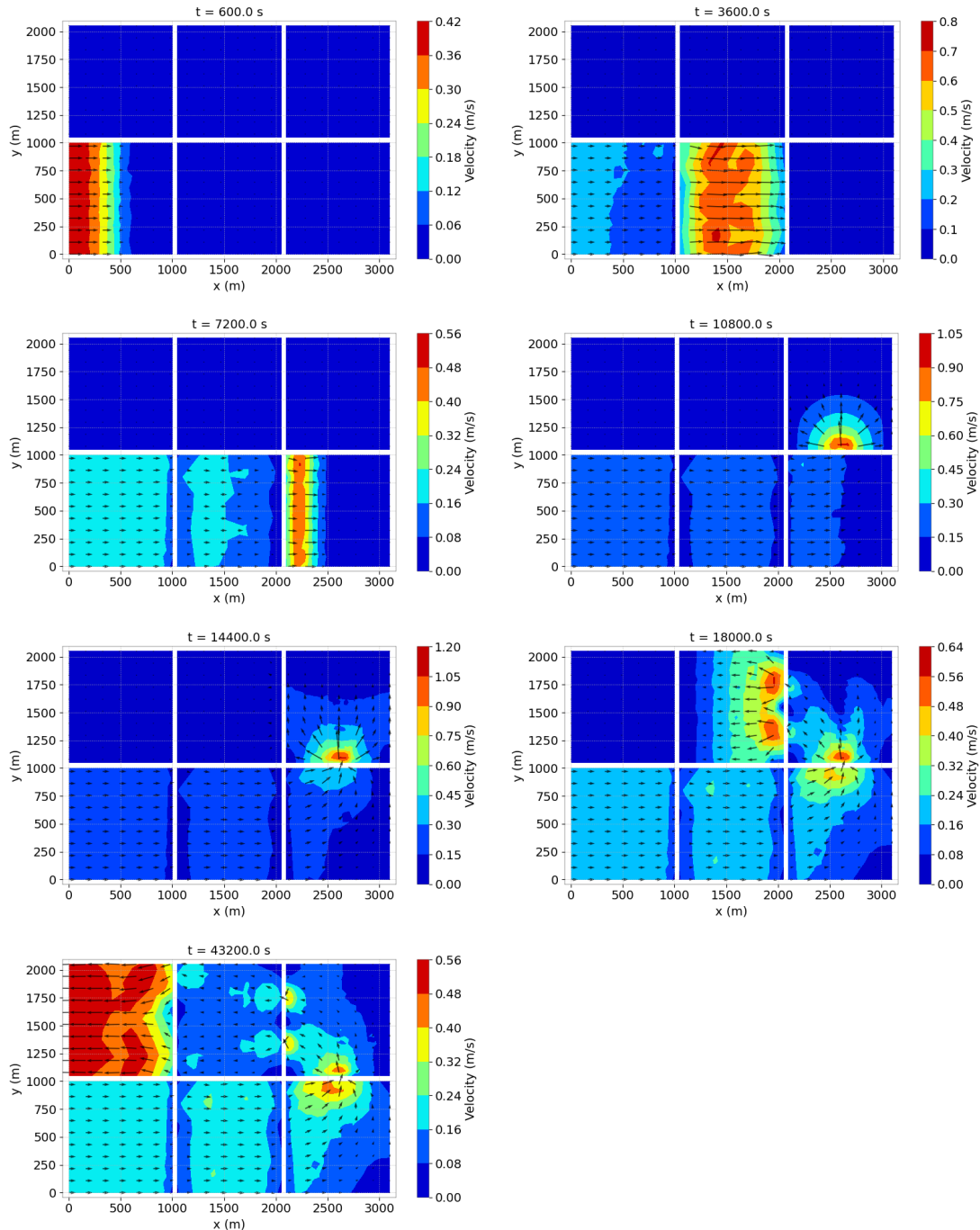


Figure 57.8: Evolution of velocity field in time.

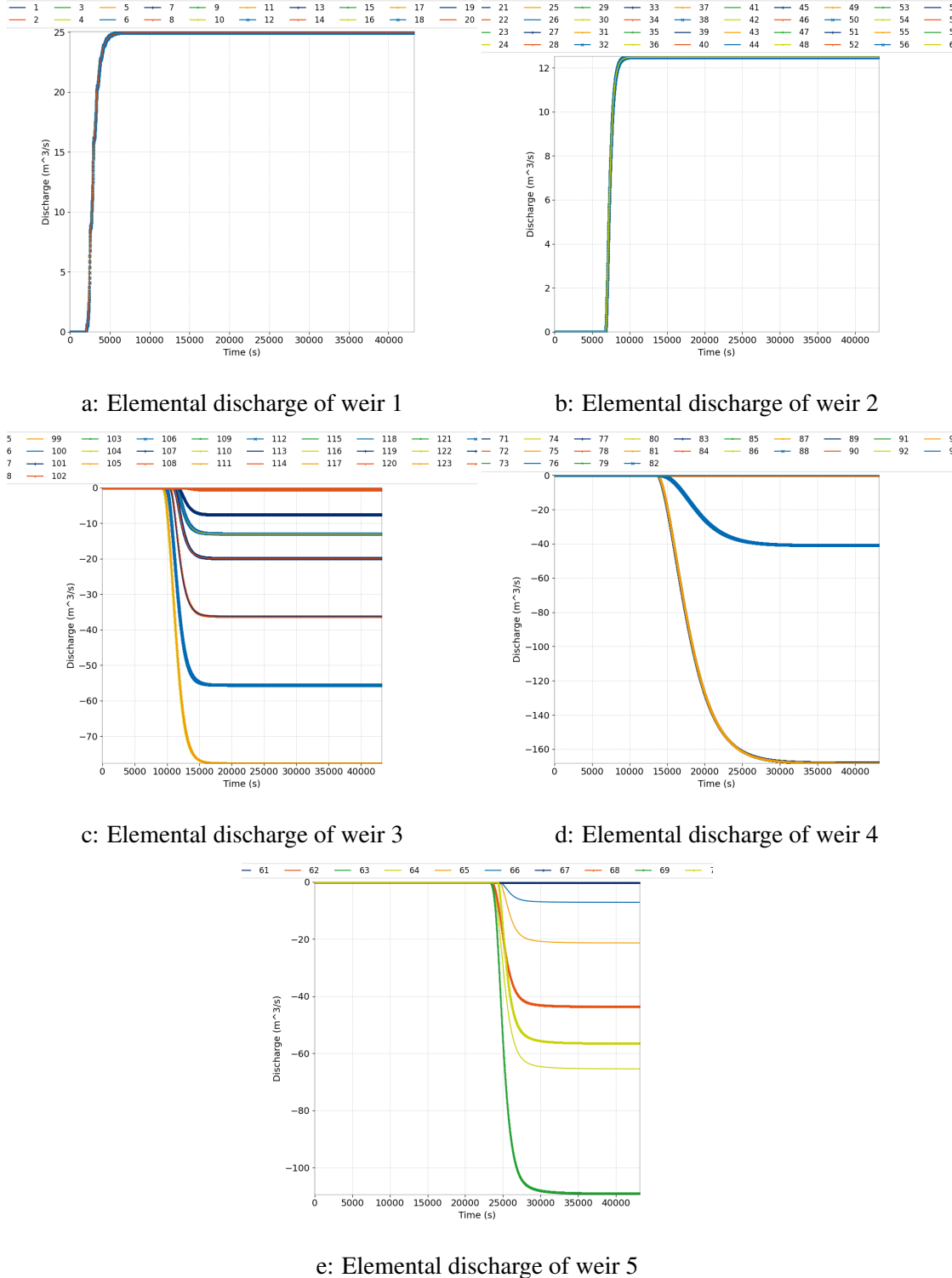


Figure 57.9: Evolution of discharge per elemental part of each weir.

- For weir 5, the discharge could be linked to the shape of the weir.

The water level increases progressively as expected in the different domains during the simulated period (see Figure 57.10). Like in Option 1, the relations (57.1) are respected.

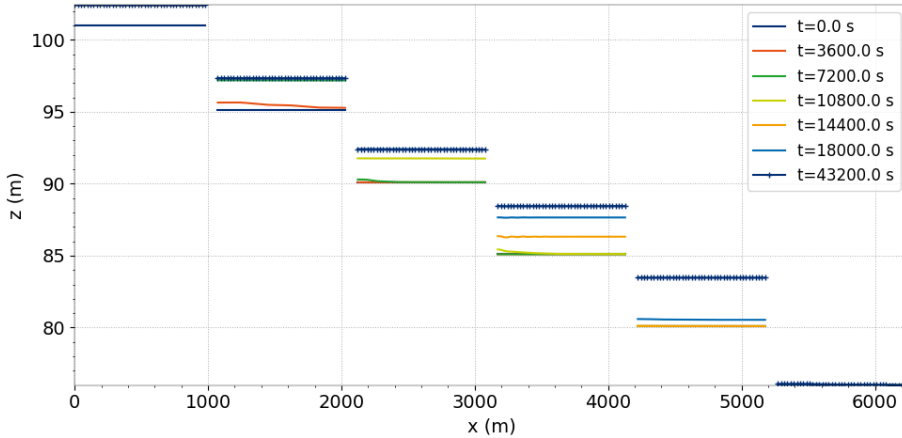


Figure 57.10: Evolution of the free surface elevation in time.

The tracer propagation is also well carried out through internal singularities (Figure 57.11).

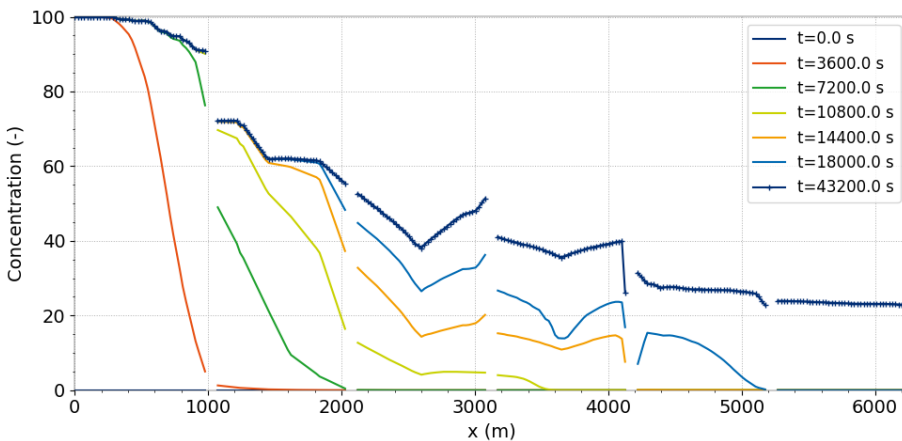


Figure 57.11: Evolution of the tracer in time.

## 57.5 Conclusion

To conclude, TELEMAC-2D computes adequately weir flows as given by analytical hydraulic laws. This type of flow is represented as an internal singularity in the model. These internal singularity could be described with 2 different options:

- Option 1, the weir law as traditionally used in channel hydraulics is prescribed through boundary conditions. This option requires the same number of nodes upstream and downstream and the weir should be horizontal,
- Option 2, the weir law is prescribed through sources points located on the upstream and downstream boundary. The description of the weir itself could be done at a smaller scale than the surrounding mesh without any constraint on its level.

# 58. wesel

## 58.1 Purpose

This test case shows a real case application with tidal flats and very large time steps. It was made for comparison with the program UnTRIM from Prof. Casulli (University of Trento) and was provided before release v5p5. The mesh is compatible with UnTRIM meshes which have restrictions according the orthogonality.

Since release 6.2, newer numerical options are tested in t2d\_wesel\_pos.cas for the treatment of tidal flats.

## 58.2 Description

### 58.2.1 Geometry and mesh

The model area is a 9 km stretch of Lower Rhine River near the towns of Wesel and Xanten (Rh-km 812.5 - 821.5). The resolution is very coarse with mean node distances of about 6 m in the main channel and about 30 m at the floodplains. The grid contains 9,064 nodes and 17,340 elements and can be seen in Figure 58.1. The mesh is compatible to UnTRIM meshes which means that the center of each triangle is inside the triangle. The bathymetry is shown in the Figure 58.2.

### 58.2.2 Initial condition

The initialising of the water level is done with the subroutine **SURFINI** called by **USER\_CONDIN\_H**. From water level measurements in m+NN at low water conditions in 1997 in the file fo1\_wesel.txt (FORMATTED DATA FILE 1) the initial water level is interpolated (see Figure 58.3). The coordinates are given as the left and right hectometer points. The initial velocities are set to zero.

### 58.2.3 Boundary conditions

At the inlet, the discharge is imposed across the full cross section. In order to avoid instabilities at the beginning, the discharge is increased from 0 to 1,061 m<sup>3</sup>/s in 30 min and remains constant afterwards. At the outlet, the water depth is fixed to 11.82 m+NN.

### 58.2.4 Physical parameters

For the time optimisation, constant values for the friction and the turbulence are chosen: The Nikuradse friction law is used and an uniform equivalent sand roughness of 3.5 cm is applied.

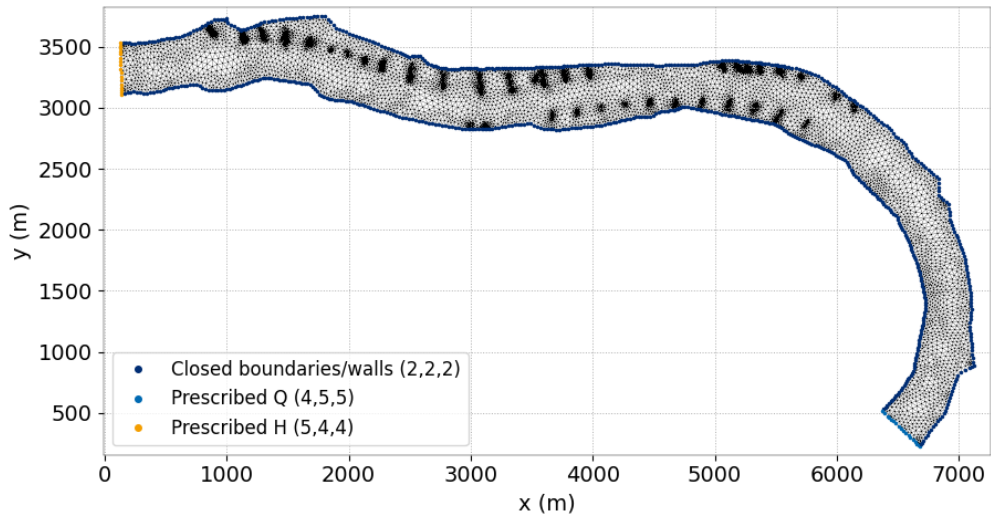


Figure 58.1: Mesh and boundary conditions.

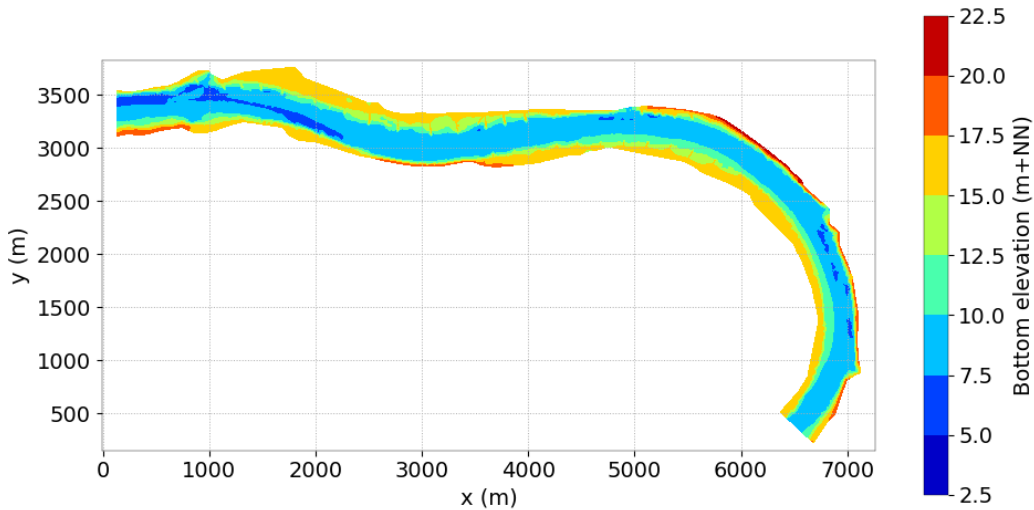


Figure 58.2: Bathymetry.

The constant turbulent viscosity is set to  $2 \text{ m}^2/\text{s}$ . This very high value stabilises the simulation. Typically values of one to two orders of magnitudes lower are applied.

### 58.2.5 Numerical parameters

12 h are simulated with a time step of 120 s to ensure steady state conditions. Figure 58.4 shows that the flux at the outlet equals the flux at the inlet for the configuration with TREATMENT OF NEGATIVE DEPTHS = 2 at the end of the simulation time. The characteristics are used for the advection type. The direct solver with a relatively low solver accuracy of  $10^{-5}$  is applied. Full implicit conditions are set for depth and velocities. The difference between both configurations consists of using a treatment for negative depth, the historical in t2d\_wesel.cas (TREATMENT OF NEGATIVE DEPTHS = 1) and using the one which always gives positive depths in t2d\_wesel\_pos.cas (TREATMENT OF NEGATIVE DEPTHS = 2).

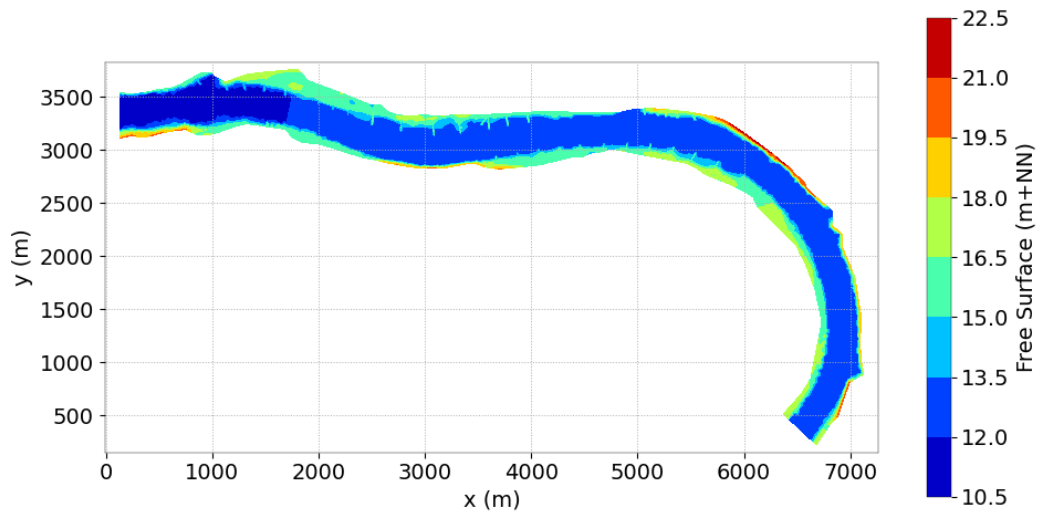


Figure 58.3: Initial water levels.

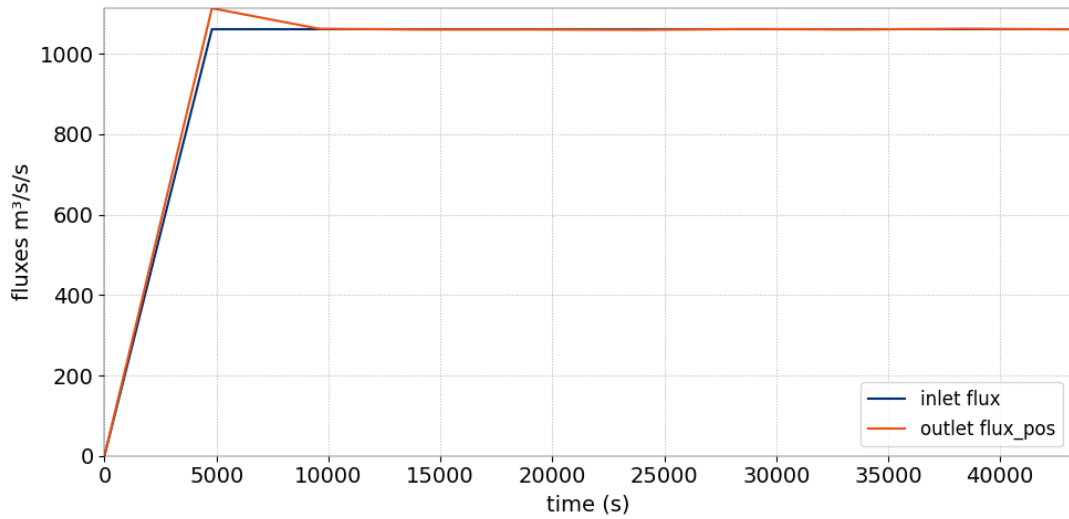


Figure 58.4: Evolution of inlet and outlet fluxes for TREATMENT OF NEGATIVE DEPTHS = 2.

### 58.3 Results

The final velocities and water levels for the configuration with TREATMENT OF NEGATIVE DEPTHS = 2 are shown in Figure 58.5 and 58.6. The differences between the initial and the final water levels are quite small as the initial water levels are calculated from the measurements. A comparison along the main channel between the measured water levels and the simulated ones for both configurations is presented in Figure 58.7. As the simulated water levels are slightly higher at the inlet, it can be assumed that the friction should be minimal decreased for a perfect agreement. The differences between the two configurations are rather small but the mass conservation is only ensured for TREATMENT OF NEGATIVE DEPTHS = 2 (compare Figure 58.4 and 58.8). The classical discretisation tends to have higher water levels which could be a hint to slightly higher numerical diffusion.

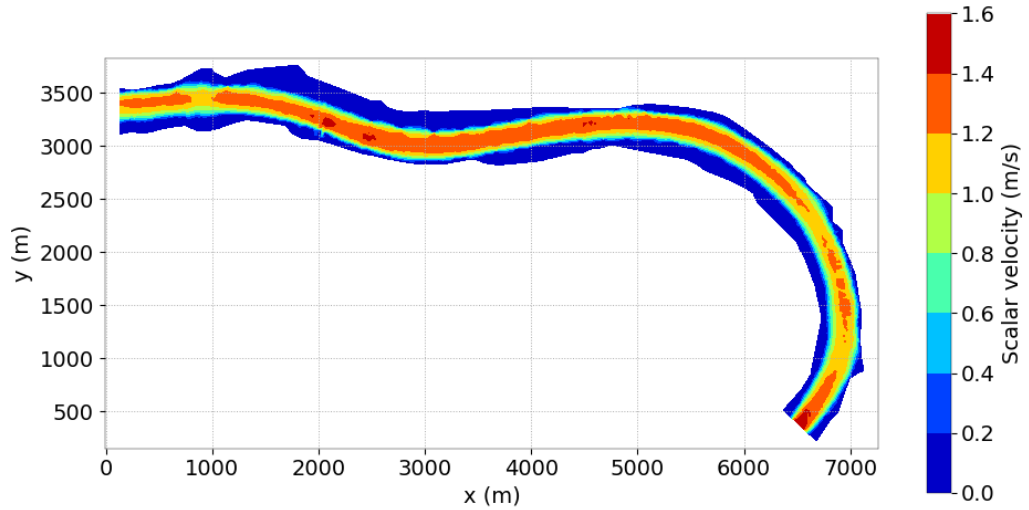


Figure 58.5: Final velocities.

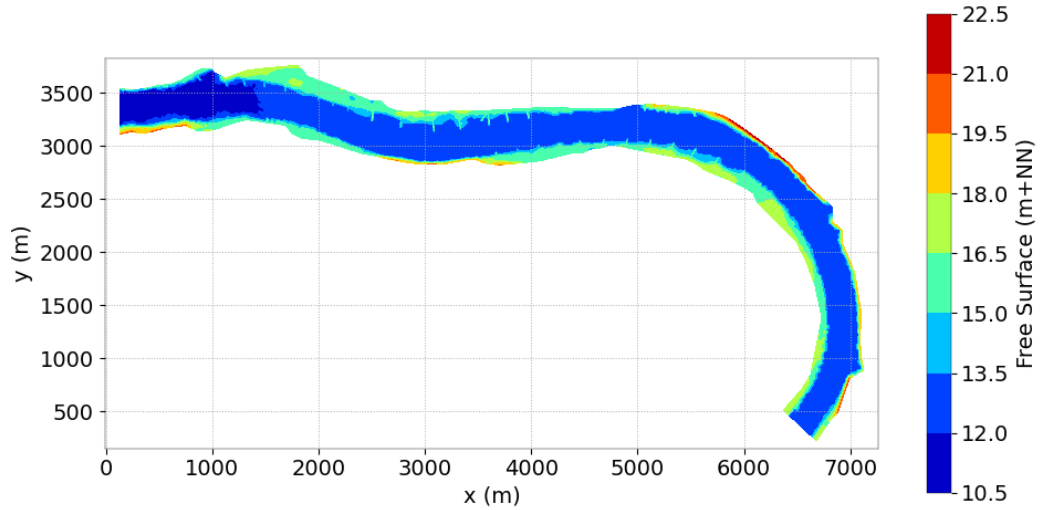


Figure 58.6: Final water levels.

## 58.4 Conclusion

The example shows a successful simulation of low water steady state conditions with tidal flats. The configuration is time optimised by using a coarse grid, a big time step, a low solver accuracy, a full implicit scheme and a high turbulent viscosity. It is recommended to use the configuration with TREATMENT OF NEGATIVE DEPTHS = 2 to ensure the mass conservation.

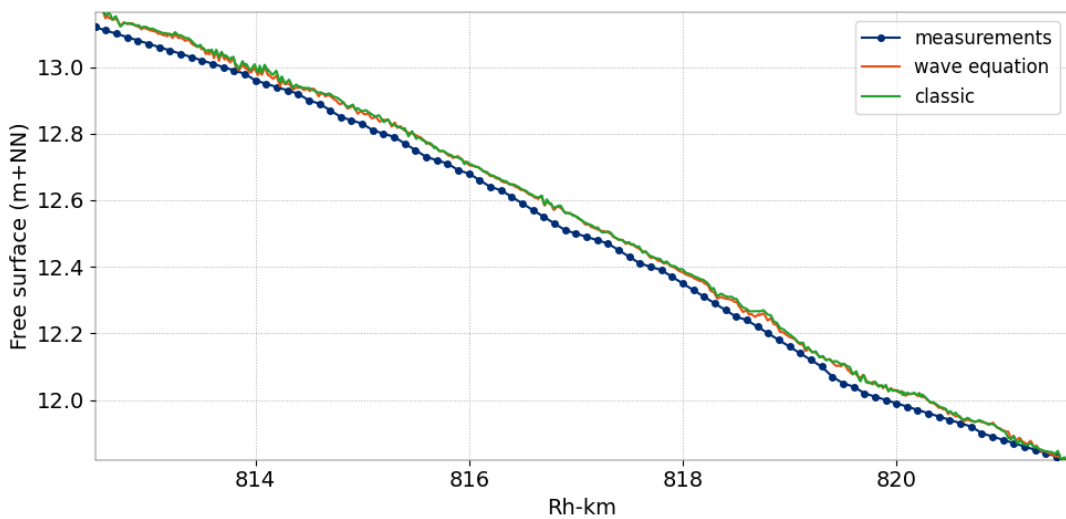


Figure 58.7: Comparison of measured and simulated final water levels with the 2 configurations and wave equation along river axis.

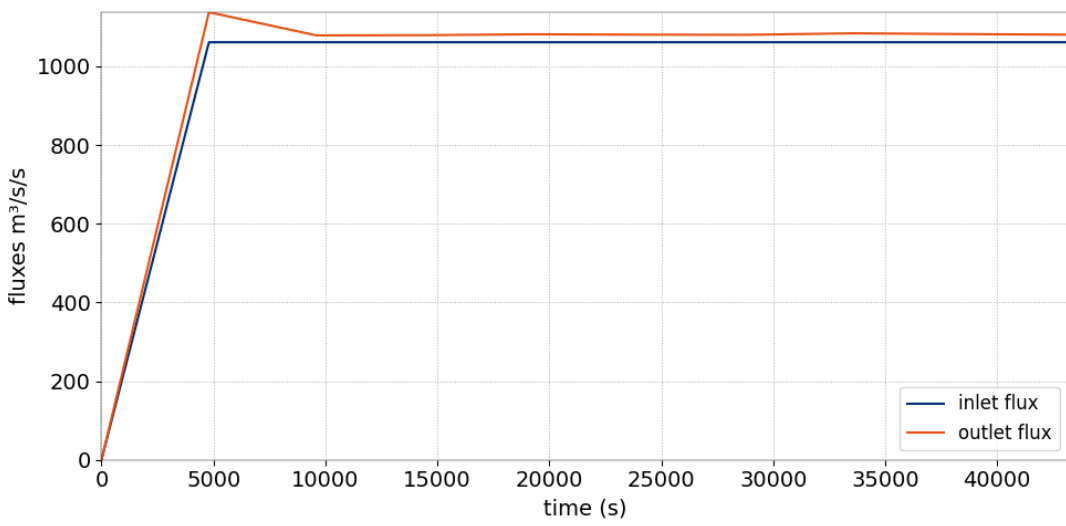


Figure 58.8: Evolution of inlet and outlet fluxes with TREATMENT OF NEGATIVE DEPTHS = 1.

## 59. Flow in a channel submitted to wind (wind)

### 59.1 Purpose

This test case presents the hydrodynamics study resulting from wind set-up in a closed rectangular basin or channel. It allows to show that TELEMAC-2D is able to correctly simulate the effect of meteorological conditions such as surface layer motion generated by the wind blowing at the water surface provided a depth integration of this process is adequate. This test case allows also to demonstrate that TELEMAC-2D produces the expected one-dimensional solution even though the grid of triangles is irregular (various sizes and orientations of triangles).

### 59.2 Description

#### 59.2.1 Analytical solution

The wind blowing on whole basin produces a surface current in the direction of the wind and a bottom current in the opposite direction. The total discharge in each cross-section is null and the wind shear stress is balanced by the slope of the induced free surface. The solution produced by TELEMAC-2D is compared with the analytical solution to this problem. The analytical solution for this problem is given by the equation:

$$H(x) = \sqrt{H_0^2 + a_{wind} \frac{2\rho_{air}}{g\rho_{eau}} ||\mathbf{Wind}||^2 x} \quad (59.1)$$

where  $||\mathbf{Wind}||^2$  is the norm of wind velocity vector.  $H_0$  is depth water on the wind entrance side (west side in this case) and  $H_L$  is depth water at the end basin within  $L$  distance (east side in this case). In addition,  $H_0$  is the solution of the following equation:

$$F(x) = \left( a_{wind} \frac{2\rho_{air}}{g\rho_{eau}} ||\mathbf{Wind}||^2 L \right)^{3/2} - x^3 - a_{wind} \frac{3\rho_{air}}{g\rho_{eau}} ||\mathbf{Wind}||^2 L \cdot x \cdot H_{initial} = 0 \quad (59.2)$$

With  $H_{initial}$  is the initial water depth equal here to 2 m. In this test case, the analytical values of water depths in basin are  $H_0 \approx 1.56431$  m and consequently  $H_L \approx 2.37947$  m.

#### 59.2.2 Geometry and mesh

This test case models the hydrodynamics behaviours due to wind blowing in a closed rectangular basin. The geometry dimensions of basin are 100 m wide and 500 m long. The basin has a flat bottom and the water depth is equal to 2 m depth. The mesh is irregular in the basin.

The mesh is shown in Figure 59.1. It is composed of 551 triangular elements (319 nodes) and the size of triangles ranges between 14 m and 24 m. The triangular elements types are linear triangles (P1, 3 values per element) for water depth and for velocities.

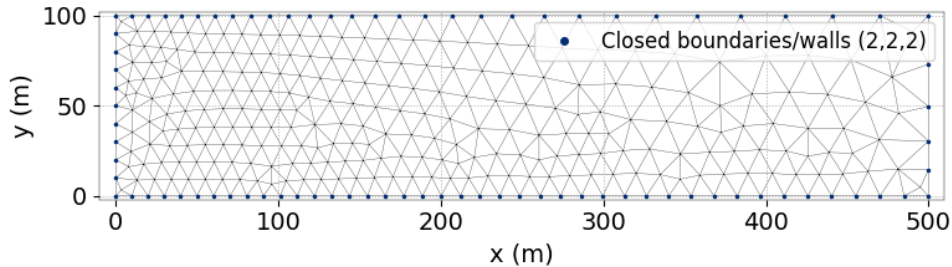


Figure 59.1: Mesh.

### 59.2.3 Initial conditions

The initial water depth is 2 m with null velocity.

### 59.2.4 Boundary conditions

The boundary conditions are:

- For the solid walls, a slip condition in the basin is used for the velocity.
- No bottom friction.
- The wind stress at the surface is imposed.

The wind conditions allowing to compute the wind stress are :

- The wind velocity is equal to 5 m.s<sup>-1</sup> (West wind; the wind is coming from the West)
- The coefficient of wind influence is  $a_{wind} \frac{\rho_{air}}{\rho_{water}} = 1.2615 \cdot 10^{-3}$  with  $\rho_{air}$ ,  $\rho_{water}$  which are respectively the air density and the water density and with  $a_{wind}$  an addimentional coefficient.

### 59.2.5 Physical parameters

The turbulent viscosity is constant with velocity diffusivity equal to 0 m<sup>2</sup>.s<sup>-1</sup>.

### 59.2.6 Numerical parameters

The time step is 10 s for a period of 100 s which is an added at initial computation of 500 s. The simulation duration is then 600 s. The resolution accuracy for the velocity is taken at 10<sup>-8</sup>. Note that a pre-computation is carried out with the precedent conditions until 500 s. For the pre-computation, the wind is applied progressively during the 4 first time step (40 s). The computation is after continued until 10 time steps. The results are so observed after 60 time step (600 s). Note that for numerical resolution, conjugate gradient on a normal equation is used for solving the propagation step (option 3). To solve advection, the characteristics scheme (scheme 1), and the conservative scheme (scheme 5) is used respectively for the velocities and for the depth. To finish, the implicitation coefficients for depth and velocities are equal to 0.5.

### 59.3 Results

The obtained TELEMAC-2D solution reproduces well the behaviour of a balance between the wind stress and the surface slope occurs. When you consider the one-dimensional solution (independent of the  $y$ -axis, Figure 59.3) as shown in Figure 59.4, the water surface elevation difference between the two extremities of this 500 m long basin is  $81.5116 \cdot 10^{-2}$  m whereas it should be  $81.5164 \cdot 10^{-2}$  m according to the analytical solution, i.e. an error of 0.006 %.

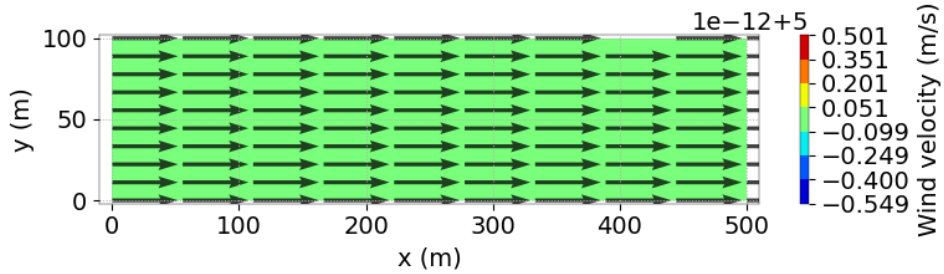


Figure 59.2: Wind velocity vector.

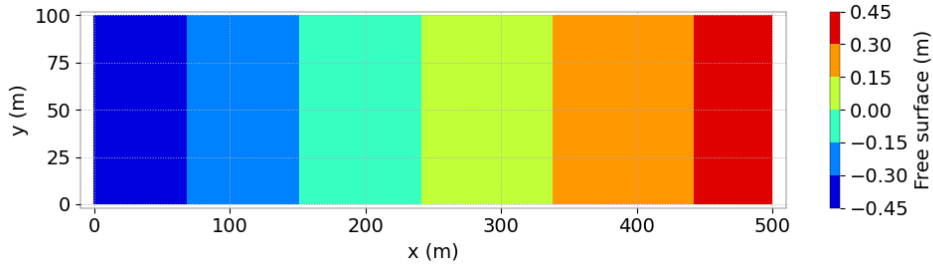


Figure 59.3: Free surface along basin.

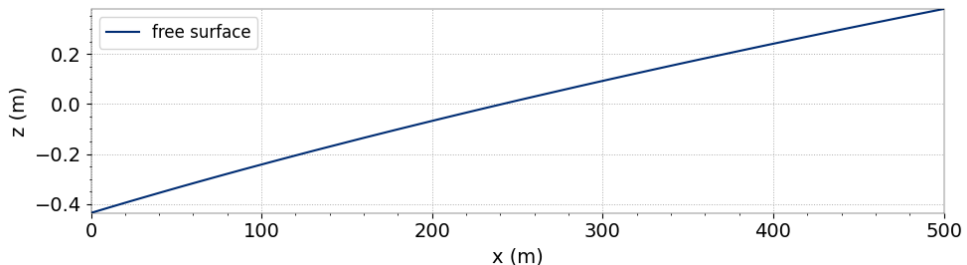


Figure 59.4: One-dimensional free surface.

### 59.4 Conclusion

TELEMAC-2D is able to compute wind generated flows on the basis of the empirical wind shear stress formulation (presented in the TELEMAC-2D User Manual). The solution computed by TELEMAC-2D in this one-dimensional test case is well independent of the computational grid characteristics although the grid meshes are very irregular.

## 60. Wind depending on time and space (wind\_txy)

### 60.1 Purpose

This test case presents the hydrodynamics study resulting from wind set-up in a closed rectangular basin or channel. Contrary to the wind example, here the wind depends on time and space (OPTION FOR WIND = 3). 2 examples are given:

- the first one uses an atmospheric data file written in ASCII,
- the second one uses an atmospheric data file written in binary.

These are examples on how to manage wind or meteo data if depending on time and space and not standardly done by TELEMAC-2D.

### 60.2 Description

#### 60.2.1 Geometry and mesh

This test case models the hydrodynamics behaviours due to wind blowing in a closed rectangular basin. The geometry dimensions of basin are 100 m wide and 500 m long. The basin has a flat bottom and the water depth is equal to 2 m depth. The mesh is irregular in the basin. The mesh is shown in Figure 60.1. It is composed of 551 triangular elements (319 nodes) and the size of triangles ranges between 14 m and 24 m.

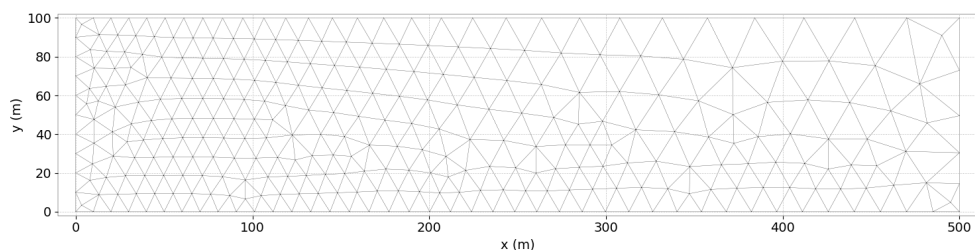


Figure 60.1: Mesh.

#### 60.2.2 Initial conditions

The computation is a continuation of the wind example with steady state with constant wind blowing on the channel.

### 60.2.3 Boundary conditions

The boundary conditions are:

- For the solid walls, a slip condition in the basin is used for the velocity,
- No bottom friction,
- The wind stress at the surface is imposed.

The wind conditions allowing to compute the wind stress are :

- The wind velocity is interpolated depending on 5 stations at coordinates (0;0), (500;0), (500;100), (0;100), (250;50) and linearly depending on time. The interpolation is implemented in the user Fortran subroutines,
- The coefficient of wind influence is  $a_{wind} \frac{\rho_{air}}{\rho_{water}} = 1.2615 \cdot 10^{-3}$  with  $\rho_{air}$ ,  $\rho_{water}$  which are respectively the air density and the water density and with  $a_{wind}$  an adimentional coefficient.

### 60.2.4 Physical parameters

The turbulent viscosity is constant with velocity diffusivity equal to 0 m<sup>2</sup>/s.

As the wind depends on time and space and there is no unique way to manage it, the treatment of wind conditions is done by changing the standard **METEO** subroutine and adding a new subroutine called **IDWM\_T2D**. Moreover, as the formats of the BINARY ATMOSPHERIC DATA FILE or the ASCII ATMOSPHERIC DATA FILE are not the one managed by the **METEO\_TELEMAC** module, the keyword FREE FORMAT FOR ATMOSPHERIC DATA FILE is activated. In the case of the BINARY ATMOSPHERIC DATA FILE, the two keywords ORIGINAL DATE OF TIME and ORIGINAL HOUR OF TIME have to be filled in.

### 60.2.5 Numerical parameters

The time step is 5 s. The simulation duration is then 100 s after the restart. For numerical resolution, conjugate gradient on a normal equation is used for solving the propagation step (option 3 = default). The characteristics scheme (scheme 1) is used to solve the advection of velocities. The implicitation coefficients for depth and velocities are equal to 0.5.

## 60.3 Results

Figures 60.2, 60.3, 60.4 show the free surface field at initial time, after 50 s and at final time (= 100 s) for the ASCII format. Figures 60.5, 60.6, 60.7 show the velocity field and streamlines at initial time, after 50 s and at final time (= 100 s) for the ASCII format. Figures 60.8, 60.9, 60.10 show the free surface field at initial time, after 50 s and at final time (= 100 s) for the binary format. Figures 60.11, 60.12, 60.13 show the velocity field and streamlines at initial time, after 50 s and at final time (= 100 s) for the binary format.

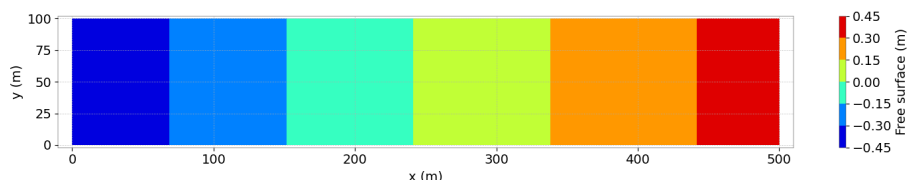


Figure 60.2: Free surface along basin at initial time step (ASCII format).

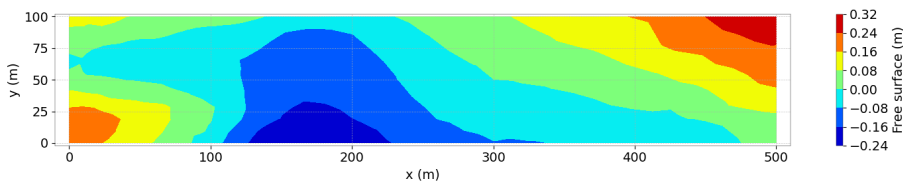


Figure 60.3: Free surface along basin at 50 s (ASCII format).

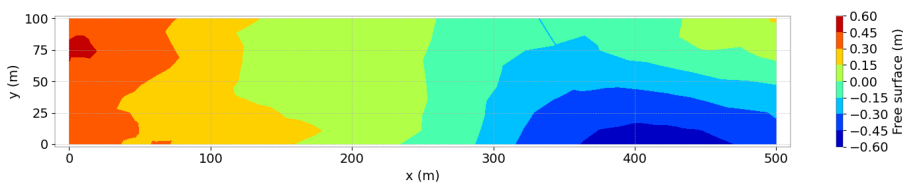


Figure 60.4: Free surface along basin at final time step (ASCII format).

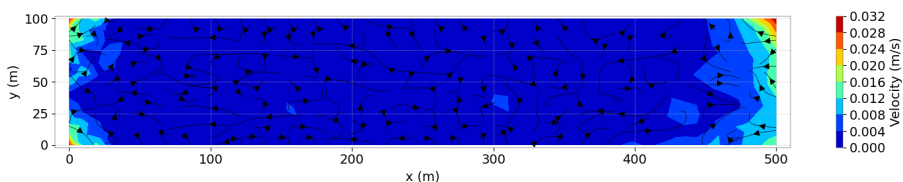


Figure 60.5: Wind velocity and streamlines at initial time step (ASCII format).

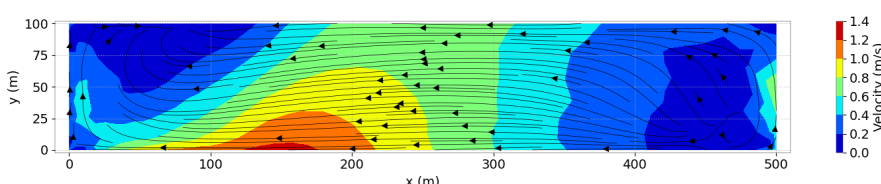


Figure 60.6: Wind velocity and streamlines at 50 s (ASCII format).

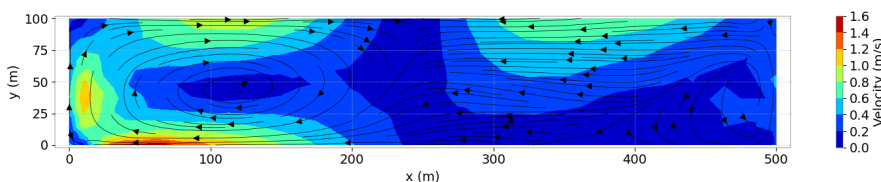


Figure 60.7: Wind velocity and streamlines at final time step (ASCII format).

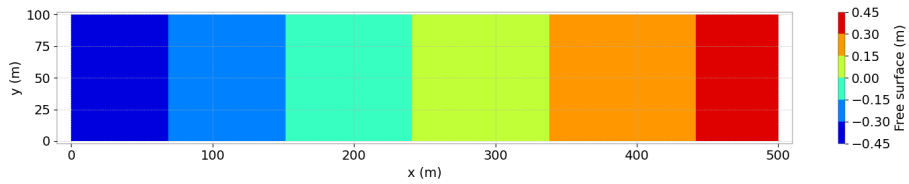


Figure 60.8: Free surface along basin at initial time step (binary format).

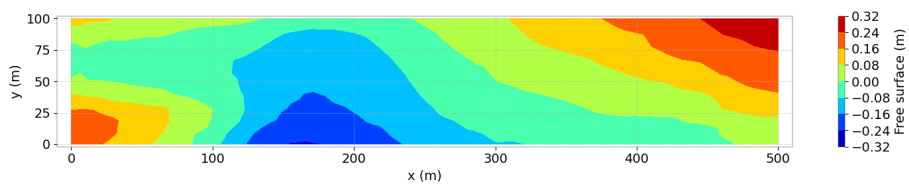


Figure 60.9: Free surface along basin at 50 s (binary format).

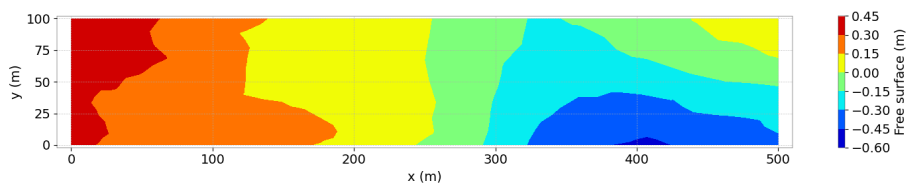


Figure 60.10: Free surface along basin at final time step (binary format).

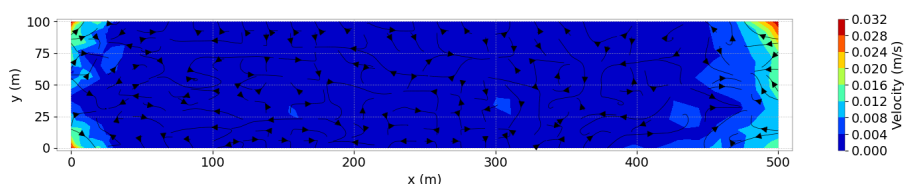


Figure 60.11: Wind velocity and streamlines at initial time step (binary format).

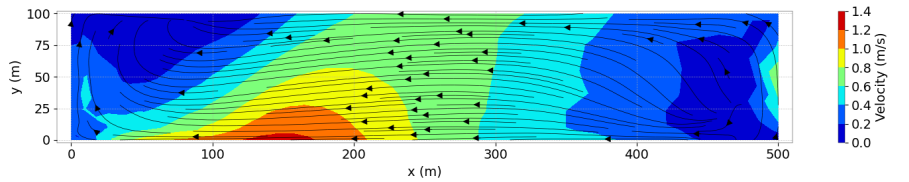


Figure 60.12: Wind velocity and streamlines at 50 s (binary format).

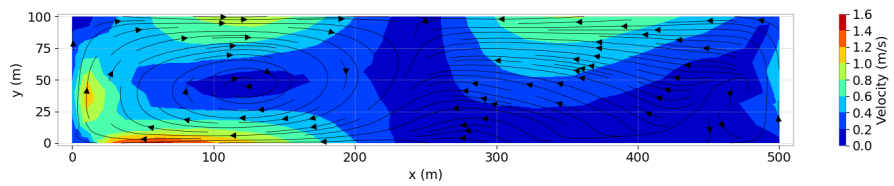


Figure 60.13: Wind velocity and streamlines at final time step (binary format).

#### 60.4 Conclusion

TELEMAC-2D is able to compute wind generated flows when depending on time and space.

- [1] Robert S Bernard and Michael L Schneider. Depth-averaged numerical modeling for curved channels. Technical report, DTIC Document, 1992.
- [2] Kranenburg C. et Stelling G. S. Bijvelds, M. *3-D numerical simulation of turbulent shallow-water flow in a square harbour*. 1997.
- [3] Guoxian Chen and Sebastian Noelle. A new hydrostatic reconstruction scheme based on subcell reconstructions. *SIAM Journal on Numerical Analysis*, 55(2):758–784, 2017.
- [4] Vasily V. Titov Utku Kanoglu Frank I. Gonzalez Costas E Synolakis, Eddie N.Bernard. Standards, criteria, nad procedures for noaa evaluation of tsunami numerical models. [http://nctr.pmel.noaa.gov/benchmark/Laboratory/Laboratory\\_ConicalIsland/index.html](http://nctr.pmel.noaa.gov/benchmark/Laboratory/Laboratory_ConicalIsland/index.html), 2007.
- [5] Olivier Delestre. *Simulation du ruissellement d'eau de pluie sur des surfaces agricoles*. PhD thesis, 2010.
- [6] Olivier Delestre, Stéphane Cordier, Frédéric Darboux, and Francois James. A limitation of the hydrostatic reconstruction technique for shallow water equations. *Comptes Rendus Mathematique*, 350(13-14):677–681, 2012.
- [7] T. D. Faure. *Unsteady flow modelling on a beach using TELEMAC-2D*. 1995.
- [8] John Finnie, Barbara Donnell, Joe Letter, and Robert S Bernard. Secondary flow correction for depth-averaged flow calculations. *Journal of Engineering Mechanics*, 125(7):848–863, 1999.
- [9] Finnigan. Turbulence in plant canopies. *Ann. Rev. Fluid Mech.*, 32(1):519–571, 2000.
- [10] F. Folke, R. Kopmann, and M. Attieh. Comparison of different vegetation models using TELEMAC-2D. In *Proceedings of the 26th TELEMAC-MASCARET User Conference 2019, 15th-17th October 2019, Toulouse–France*, 2019.
- [11] Sampath Kumar Gurram, Karam S. Karki, and Willi H. Hager. Subcritical junction flow. *Journal of Hydraulic Engineering*, 123(5):447–455, may 1997.
- [12] J-M. HERVOUET. *Hydrodynamics of free surface flows. Modelling with the finite element method*. John Wiley & Sons, Ltd, Paris, 2007.
- [13] Oldrich Hungr. A model for the runout analysis of rapid flow slides, debris flows, and avalanches. *Canadian Geotechnical Journal*, 32(4):610–623, 1995.

- [14] A. Joly. *Modelling of the transport of algae in a coastal environment using a stochastic method*. PhD thesis, 2011. URL <http://www.theses.fr/2011PEST1088>. Thèse de doctorat dirigée par Violeau, Damien Mécanique des fluides Paris Est 2011.
- [15] A. Joly, F. Moulin, D. Violeau, and D. Astruc. Diffusion in grid turbulence of isotropic macro-particles using a lagrangian stochastic method: theory and validation. *Physics of Fluids*, 24(10):1–25, 2012.
- [16] A. Joly, D. Violeau, F. Moulin, D. Astruc, and C. Kassiotis. Transport of isotropic particles in a partially obstructed channel flow. *Journal of Hydraulic Research*, 50(3):324–337, 2012.
- [17] Pierre Y Julien. *Erosion and sedimentation*. Cambridge university press, 2010.
- [18] T.-H. Jung, C. Lee, and Y.-S. Cho. Analytical solutions for long waves over a circular island. *Coastal Engineering*, 57:440–446, 2010.
- [19] Geoffroy KIRSTETTER, Jie Hu, Olivier Delestre, Frédéric Darboux, P-Y Lagrée, Stéphane Popinet, Jose-Maria Fullana, and Christophe Josserand. Modeling rain-driven overland flow: Empirical versus analytical friction terms in the shallow water approximation. *Journal of Hydrology*, 536:1–9, 2016.
- [20] P.-L. Ligier. Implementation of a rainfall-runoff model in TELEMAC-2D. In *XXIIIrd TELEMAC-MASCARET User Conference*, 2016.
- [21] P.-L. Ligier. Implementation of non-newtonian rheological models in TELEMAC-2D. In *2020 TELEMAC User Conference*, 2020.
- [22] D Naef, D Rickenmann, P Rutschmann, and BW McArdell. Comparison of flow resistance relations for debris flows using a one-dimensional finite element simulation model. 2006.
- [23] Y. Okada. Internal deformation due to shear and tensile faults in a halfspace. *Bulletin of the Seismological Society of America*, 75:1135–1154, 1985.
- [24] Tasos C Papanastasiou. Flows of materials with yield. *Journal of Rheology*, 31(5):385–404, 1987.
- [25] W. G. Penney and A. T. Price. Part i. the diffraction theory of sea waves and the shelter afforded by breakwaters. *Philosophical Transactions of the Royal Society of London. Series A, Mathematical and Physical Sciences*, 244(882):236–253, March 1952.
- [26] Dieter Rickenmann. *Bedload transport capacity of slurry flows at steep slopes*. PhD thesis, ETH Zurich, 1990.
- [27] Soil Conservation Service. National engineering handbook, section 4, hydrology, 1972.
- [28] C.E. Synolakis. The runup of long waves. *PhD Thesis, California Institute of Technology*, 1986.
- [29] C.E. Synolakis. The runup of solitary waves. *J. Fluid. Mech.*, 185, 523-545., 1987.